SEPTEMBER 2026
VOLUME 85
ISSUE
9

ANNALS OF THE RHEUMATIC DISEASES

THE EULAR JOURNAL

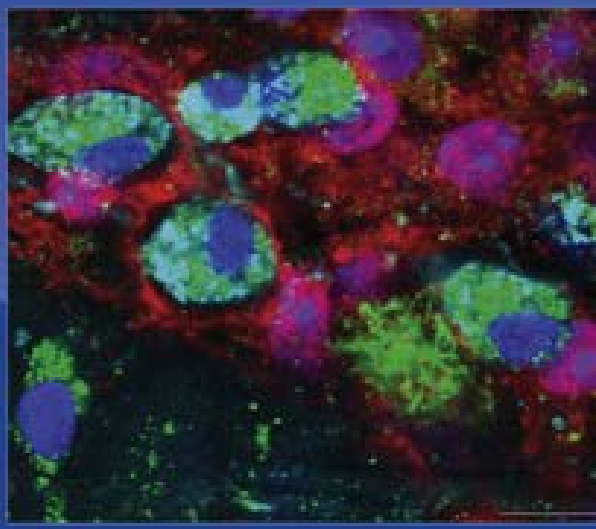

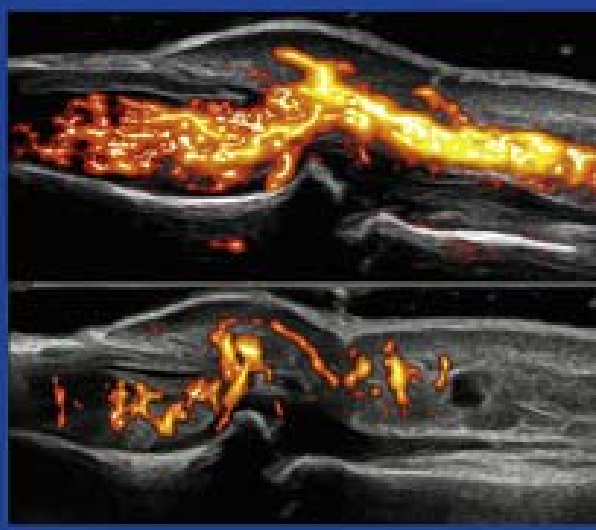

ELSEVIER

eular
EUROPEAN ALLIANCE OF ASSOCIATIONS FOR RHEUMATOLOGY

The home of innovative rheumatology research

Ann Rheum Dis 85 (2026) 1683–1693

Contents lists available at ScienceDirect

Annals of the Rheumatic Diseases

journal homepage: https://www.sciencedirect.com/journal/annals-of-the-rheumatic-diseases

Review

Chasing the target: reports from the Advances in Targeted Therapies meeting, 2025

Kevin L. Winthrop[1,*], Andreas Kerschbaumer[2,3], John D. Isaacs[4], Philip Mease[5], Xenofon Baraliakos[6], Mary K. Crow[7], Maya Buch[8], Stefan Siebert[9], Neil Basu[9], Philip Conaghan[10], Margreet Kloppenburg[11], Oliver Distler[12], Robert Landewe[13], Dana E. Orange[7,14], Kevin Wei[15], Daniel Aletaha[3], Iain B. McInnes[16], Thomas W.J. Huizinga[11], Reinhard Voll[17], Ellen M. Gravallese[18], Ferdinand C. Breedveld[11], Josef S. Smolen[3]

[1] *Oregon Health and Science University, Portland, OR, USA*
[2] *Division of Immunology and Rheumatology, Department of Medicine, Stanford University School of Medicine, Stanford, CA, USA*
[3] *Division of Rheumatology, Department of Medicine, Medical University of Vienna, Vienna, Austria*
[4] *Translational and Clinical Research Institute, Newcastle University and Musculoskeletal Unit, Newcastle Hospitals, Newcastle upon Tyne, UK*
[5] *Swedish Medical Center, University of Washington, Seattle, WA, USA*
[6] *Rheumazentrum Ruhrgebiet, Ruhr University Bochum, Herne, Germany*
[7] *Mary Kirkland Center for Lupus Research, Hospital for Special Surgery, New York, NY, USA*
[8] *Centre for Musculoskeletal Research, Division of Musculoskeletal and Dermatological Sciences, The University of Manchester, Manchester, UK*
[9] *School of Infection and Immunity, University of Glasgow, Scotland, UK*
[10] *Leeds Institute of Rheumatic and Musculoskeletal Medicine, University of Leeds and NIHR Leeds Biomechanical Research Centre, Leeds, UK*
[11] *Department of Rheumatology, University of Leiden, Leiden, Netherlands*
[12] *Department of Immunology and Rheumatology, University Hospital Zürich, Zürich, Switzerland*
[13] *Department of Rheumatology, Amsterdam University Medical Center, Heerlen, The Netherlands*
[14] *Rockefeller University, New York, NY, USA*
[15] *Division of Rheumatology, Inflammation, and Immunity, Department of Medicine, Brigham and Women's Hospital and Harvard Medical School, Boston, MA, USA*
[16] *MVLS College Office, University of Glasgow, Glasgow, UK, School of Infection, and Immunity, University of Glasgow, Glasgow, UK*
[17] *Department of Rheumatology and Clinical Immunology, University of Freiburg, Freiburg, Germany*
[18] *Brigham and Women's Hospital, Harvard Medical School, Boston, MA, USA*

ARTICLE INFO

Article history:
Received 25 November 2025
Received in revised form 26 February 2026
Accepted 17 March 2026

ABSTRACT

Objectives: This article aimed to articulate the most important unmet scientific needs in rheumatology.

Methods: At the 25th Advances in Targeted Therapies (ATT) meeting, over 100 investigators joined 6 disease-focused breakout groups (rheumatoid arthritis [RA], psoriatic arthritis [PsA], axial spondyloarthritis [axSpA], systemic lupus erythematous [SLE], systemic sclerosis [SSc], and osteoarthritis [OA]). Each group, led by a facilitator and rapporteur, mapped (i) key unmet

*Correspondence to Dr Kevin L. Winthrop, School of Public Health, 3181 SW Sam Jackson Park Rd, Mail Code GH104, Portland, OR 97239, USA.
E-mail address: Winthrop@ohsu.edu (K.L. Winthrop).
Handling editor David Pisetsky.

https://doi.org/10.1016/j.ard.2026.03.024

0003-4967/© 2026 European Alliance of Associations for Rheumatology (EULAR). Published by Elsevier B.V. All rights are reserved, including those for text and data mining, AI training, and similar technologies.

needs, (ii) promising mechanistic or therapeutic approaches, and (iii) near-term priorities for research and trials. This report synthesises the consensus highlights.
Results: Six disease-focused groups (RA, PsA, axSpA, SLE, SSc, and OA) identified convergent priorities: earlier detection and interception; validated molecular and clinical endotypes to guide therapy; strategies for immune reset and short-course induction combinations with strict safety oversight; metabolic modifiers; precision targets in axSpA and fibroblast-directed approaches in RA; phenotype-driven therapeutic development and intra-articular options in OA; and pragmatic trial designs that include pregnant persons and very early disease.
Conclusions: Across immune-mediated diseases, progress will hinge on validated endotypes, practical interception strategies, and trials that reflect real-world populations. The immediate agenda is to de-risk immune reset and induction approaches, standardise tissue and digital biomarkers, and close evidence gaps for refractory disease. Prevention—and ultimately cure—remains the horizon.

BACKGROUND

The Advances in Targeted Therapies meeting (ATT) has met annually for 25 years, typically in Europe. The gathering convenes leaders in many aspects of immune-mediated inflammatory diseases including rheumatologists/immunologists, infectologists, public health experts and epidemiologists, as well as clinical scientists from different fields of medicine. For 3.5 days, these experts deliver scientific talks with updates in their respective areas of expertise, discuss potential scientific collaborations, as well as debate and prioritise the unmet research needs in the field [1].

METHODS

On day 2 of the meeting, we divided conference participants into breakout groups according to their areas of expertise and interest. Attendees from Europe, North America, and Asia participated. The disease-specific interests groups were similar to previous years: rheumatoid arthritis (RA), psoriatic arthritis (PsA), axial spondyloarthritis (axSpA), Systemic Lupus Erythematous (SLE), systemic sclerosis (SSc), and osteoarthritis (OA). A facilitator led each group, and a rapporteur recorded the guided discussion within the areas of translational science, clinical care, and therapeutic development. This group-specific record served as the basis for each section within the current manuscript, with both facilitator and rapporteur together developing a section-specific draft for the manuscript. We asked the facilitator to guide their group in discussion regarding current unmet needs within these clinical areas. Although rapporteurs captured this dialogue, the highlighted unmet needs described herein are only a selection of those discussed.

RESULTS

Rheumatoid arthritis

Defining and characterising refractory RA

Refractory RA was highlighted by the group as a major unmet need [2]. Difficult-to-treat RA (D2T RA) is multifactorial: although many patients with RA have complicating factors (eg, comorbid chronic pain, fibromyalgia, and depression) that amplify symptom burden, others exhibit persistently active synovitis driven by ongoing inflammation despite immunosuppressive therapies targeting distinct pathways and cell types. The distinction between noninflammatory drivers vs truly refractory immune-mediated disease was felt to be one of the most critical aspects by the group. At the same time, there is a recognised need for predictive biomarkers and stratification tools to predict which patients will become refractory and to guide personalised management for this challenging subgroup. In summary, the panel emphasised refining the definition and early identification of refractory RA, acknowledging it as a heterogeneous entity requiring both multidisciplinary management and novel therapeutic strategies [3].

Identifying biomarkers of refractory RA

The timing of interventions in RA emerged as a pivotal theme. Delays in achieving disease control might predispose to develop difficult-to-treat disease. Notably, a recent multicentre study demonstrated that failure to start methotrexate within 3 months of diagnosis and prolonged corticosteroid use beyond 6 months were early predictors of later D2T RA [4], in line with findings of a very long lag period until DMARD-start in patients with refractory RA [5]. These findings reinforce the ‘window of opportunity’ concept—early, aggressive treatment can prevent the establishment of refractory disease [6]. Beyond early therapy, understanding the temporal evolution of RA at the molecular level is a growing focus. Advanced profiling techniques, including serial synovial biopsies, single-cell RNA sequencing, and spatial transcriptomics, are being applied to characterise RA disease heterogeneity over time. Such studies reveal significant cellular and molecular heterogeneity in the synovial tissue: distinct cellular communities (spanning multiple immune cell subsets and stromal cells) dominate at different disease stages [7]. These distinct RA Cell Type Abundance Phenotypes (CTAPs), represent a strategy for personalised therapy [8]. For example, molecular signals preceding a flare might prompt preemptive treatment adjustments. The group highlighted that integrating longitudinal molecular profiling data with clinical decision-making could enable truly adaptive, precision treatment in RA, adjusting therapy not just to current disease activity, but also where the patient is coming from to where the patient is headed on the disease timeline [9]. Ongoing initiatives were noted, including prospective studies following individuals from preclinical autoimmunity through disease progression, but also consortia focusing on identifying tissue and blood biomarkers to predict response to future therapies in patients with D2T, which will be crucial to validate biomarkers and novel targets for early intervention.

Further challenges arise in the context of molecular remission. For example, which joint should be biopsied if none are symptomatic? Although there is great enthusiasm for molecular phenotyping of patients using synovial biopsy, this assessment remains difficult to integrate into routine care due to concerns about indemnification, training, infrastructure, and the

immediate actionability of results. Recent advances in deep molecular profiling of formalin-fixed, paraffin-embedded (FFPE) tissue sections enable studies using historical samples, which could be informative [10]. A sufficiently large number of high-quality FFPE biopsies could facilitate machine learning (ML)/artificial intelligence (AI)-driven stratification approaches [11].

The introduction of whole-body imaging approaches, such as multiplex positive emission tomography tracers, could help address this biopsy question and revolutionise trial outcome measures [12]. These techniques, evolving in oncology, could be adapted to assess inflammation across all joints by labelling targets such as complement, fibroblast activation protein (FAP), or other immunoinflammatory markers. Molecular study data could also inform the development of novel positive emission tomography tracers for joint imaging.

ML and AI continue to develop rapidly [13], with the ability to detect complex, nonlinear patterns in large datasets that may exceed human analytical capabilities. In addition to direct clinical, biological, and genetic data, routinely collected 'metadata', such as demographics, blood counts, and biochemical tests—may contain valuable, underutilised insights. A significant challenge remains the need for high-quality, expertly curated datasets. If pharmaceutical and biotech companies agreed to pool data—such as from placebo arms of clinical trials—this could yield powerful results. Similar data-sharing models have been implemented previously, though not specifically in the context of AI [14]. Such datasets could be useful diagnostically, prognostically, or even theragnostically.

Fibroblast-targeted strategies

There is growing interest in therapies directed at the synovial stroma, particularly synovial fibroblasts, which are central drivers of chronic inflammation and joint damage in RA [15]. To date, no fibroblast-specific treatment has been approved, and current Disease Modifying anti-rheumatic drugs (DMARDs) primarily target immune cells, cytokines or cytokine-activated signal transduction pathways. The group discussed how this represents a major unmet need, especially given evidence that many refractory cases often have a fibroblast-dominated synovial tissue pathotype. Patients who experience an insufficient response to multiple biologics can exhibit a 'pauci-immune' synovial phenotype, with few infiltrating lymphocytes but an abundance of activated fibroblasts. This points to pathogenic fibroblasts as key perpetuators of disease in these cases. Recent single-cell and spatial transcriptomic studies have delineated discrete synovial fibroblast subsets in RA joints (eg, pro-inflammatory THY1$^+$ sublining fibroblasts vs tissue-destructive lining fibroblasts), providing specific targets for intervention [16]. Strategies to target fibroblasts were in focus of the discussions. One approach is to selectively deplete or modify pathogenic fibroblasts by exploiting unique surface markers—for example, FAP is being investigated as a target for imaging and directed therapies in RA synovium. Another strategy is to block critical fibroblast signalling pathways (such as cadherin-11 or Notch3, implicated in fibroblast activation and joint invasion). The group underscored that intervening at the stromal level, particularly early in disease, could disrupt the feed-forward loop of inflammation and damage [17]. Unlike broad immunosuppression, targeting fibroblasts might quell local joint pathology with fewer systemic effects, though specificity is a challenge because fibroblasts are ubiquitous in tissues. Ongoing preclinical work and early-phase trials (eg, of FAP-targeted agents or inhibitors of fibroblast survival pathways) were noted. Overall, there was optimism that fibroblast-targeted therapies will complement immune-directed therapies, especially for patients in whom immune cell–targeted drugs have proven insufficient [18].

Immune reset and combination approaches

For patients with refractory RA, the session explored more intensive therapeutic paradigms, including combination therapies and immune system 'reset' strategies. The concept of combination therapy involves hitting multiple inflammatory pathways concurrently to overcome redundancy. In practice, combining biologic DMARDs is rare due to infection risk, but emerging case reports suggest it can be effective in selected cases. The group noted that, moving forward, clinical trials could explore short-term combination induction therapy in refractory RA, with tight safety monitoring. In parallel, an even more ambitious approach is an 'immune reset'—'rebooting' the patient's immune system to a tolerant state. Autologous haematopoietic stem cell transplantation (AHSCT) was an early example, aiming to eradicate autoreactive immune cells and reconstitute a new immune repertoire. Although AHSCT achieved drug-free remission in some patients with RA, its use has been limited by procedural risks and toxicity [19]. A modern twist on immune resetting is emerging from the field of cell therapy: notably, chimeric antigen receptor (CAR) T-cell therapy. In 2022, a landmark study demonstrated that a 1-time infusion of anti-CD19 chimeric antigen receptor-T cell therapy (CAR-T)–cells (to ablate B cells) induced prolonged drug-free remission in a case series of patients with severe refractory SLE [20]. Treated individuals showed resolution of disease activity and re-emergence of naïve B cells months later, essentially achieving an autoimmune 'reset'. This striking result was discussed as proof-of-concept that resetting immunity is feasible in autoimmunity. For RA, which shares pathogenic B cell involvement (especially in seropositive RA), similar strategies could be transformative, with only a few cases being reported until now [21]. The prospect of CAR-T–cell therapy (or CAR-modified regulatory T-cells) or bispecific T-cell engagers in RA was raised, alongside antigen-specific tolerising therapies (such as peptide vaccines to induce immune tolerance to citrullinated proteins). These approaches remain experimental, but they illustrate the paradigm of aiming for sustained remission or cure in refractory RA by deep immune intervention. The experts cautioned that such approaches carry significant risks and will require careful clinical evaluation. Nonetheless, the success in lupus has galvanised interest in exploring whether difficult-to-treat RA might be overcome by therapies that reboot or retrain the immune system rather than continually suppressing it.

Advances in molecular technologies, imaging, and data science are opening new avenues for personalised management and trial design in RA. However, integration into clinical practice remains limited by workforce constraints, data interpretation challenges, and infrastructure needs. Collaborative efforts, including data sharing and investment in scalable tools, will be essential to fully realise the promise of precision rheumatology.

Psoriatic arthritis

Now that we are 25 years into the use of biologic DMARDs and targeted synthetic DMARDs in the treatment of the complex, multiclinical domain condition PsA, we are encountering an increasing number of patients who have 'tried everything' but still have evidence of active disease and/or troublesome symptoms. This is a phenomenon common across immune-mediated inflammatory disease conditions. Many of these patients have had serial treatments, often for years, with advanced

immunomodulatory drugs with different mechanisms of action (MOAs). Some have been cycling through these drugs since they first became available and are now at a juncture where they have tried at least 1 or more drugs from each MOA. Consensus-based definitions of D2T and 'Complex to Manage' (C2M) PsA have been developed [22–26], similar to the work that has been done in RA [2] and axSpA [27,28]. D2T or 'Treatment Refractory' is applied to a patient who has had adequate trials and subsequent inadequate response or intolerance to several MOAs and has active inflammation/progressive damage in relevant domains including arthritis, enthesitis, dactylitis, spondylitis, skin and/or nail disease, objectively verified by physical exam, imaging, and/or laboratory variables [26]. For this patient, there are newly approved medicines for PsA to be tried [29], or trying dual therapy with more than 1 immunomodulatory drug may be warranted. Studies of several large cohorts of patients with established PsA and axSpA have shown that between 10% and 30% of patients fall into this category and in PsA have shown that factors such as the presence of spinal disease, skin disease, and obesity increase the risk for this state [30–33]. It is these criteria that can be used by clinical trial designers for the inclusion criteria for dual or novel therapy trials, by regulatory agencies to understand the unmet need for therapies with new MOAs and dual therapy trials, and by payors to appreciate the need for more complex and costly therapy for this group of patients. C2M PsA and axSpA criteria not only subsume all patients in the D2T category but also include patients who demonstrate apparent moderate to high disease activity as measured by composite measures that include subjective elements such as pain, joint tenderness, patient global, and physical function despite lack of evidence of inflammation or progressive structural damage [26]. For example, a patient with concomitant fibromyalgia or OA may have residual pain in the absence of active PsA. Other contributing factors may be comorbidities such as obesity, cardiovascular disease, diabetes, or depression. However, as already stated in the treat-to-target recommendations almost a decade ago, 'The choice of the target and of the disease activity measure should take comorbidities, patient factors and drug-related risks into account' [34]; in other words, if certain comorbidities exist, the rheumatologist needs to think about which measure is appropriate to determine disease activity and which one is needed to assess the comorbid condition. One confounder is the inclusion of physical function into disease activity instruments, since physical function will become irreversible in long-standing disease due to joint damage and, therefore, determination of clinical remission using such scoring may be blunted by virtue of an erratic instrument [35,36]. Identification of these confounding factors and adherence to pertinent recommendations are important to avoid unnecessary switching of immunomodulatory medicines. Poor access to care and other socioeconomic and sociocultural aspects also have to be taken into account [37]. For D2T criteria, it is clear that the development of new drugs with different MOAs, such as TYK2 or TL1A inhibitors and clinical trials of dual therapy continue to be needed. In addition to trials, collecting information about dual therapy from large observational registries can be done using these standardised criteria. If confounding factors lead to the C2M state, other strategies beyond immunomodulatory therapies need to be considered and tested. For example, for concomitant nociplastic pain, improved and practical methods to identify this pain mechanism, which may respond to neuromodulatory and other modes of therapy, are needed [38]. Addressing obesity with diet and exercise, as well as weight loss drugs (trials ongoing), will likely be beneficial for C2M PsA outcomes in this group.

Current trials of therapies for PsA almost completely address the multidomain nature of the disease, with single and composite measures addressing arthritis, enthesitis, dactylitis, skin and nail disease, pain, fatigue, physical function, mental health, and quality of life [39]. However, not all clinical manifestations of psoriatic disease may respond well to the same therapeutic MOA, as is also the case in SLE and systemic sclerosis (see below). The spondylitis aspect of PsA, axial PsA (axPsA), is not reliably or accurately assessed in most clinical trials. We are now beginning to see studies devoted specifically to axPsA [40,41]. Several potentially confounding issues which may influence PsA treatment outcomes have been identified, including patient's sex [42], weight [33], concomitant nociplastic pain [43], and depression [44]. Additionally, it is now recognised that background use of weight loss medications, such as GLP-1 receptor agonists, and neuromodulatory medicines for pain, may influence treatment outcomes. These factors, and medications should be considered in stratification and other strategies to mitigate their potential confounding effect on treatment outcomes.

Accurate diagnosis of axPsA remains a problem. The axial involvement in psoriatic arthritis study, a collaborative research project between the groups of assessment and research in psoriasis and psoriatic arthritis and the assessment of spondyloarthritis international society, has completed enrollment and preliminary analysis. In over 400 patients with PsA, after careful evaluation by investigators, and then re-evaluation after central imaging reading, 27% were considered to have axPsA [45,46]. There are genetic, clinical, and imaging features that distinguish axPsA from axSpA [47]. Thus, evidence for the therapeutic effectiveness or ineffectiveness of drugs trialled in axSpA may not be equally applicable for axPsA. We encourage more specific axPsA trials such as MAXIMISE and STAR [40,41], incorporating a new definition of axPsA, to more reliably determine the effectiveness of different drugs/mechanisms in this clinical domain of PsA.

The question as to whether the transition from psoriasis alone to the appearance of concomitant PsA can be 'intercepted', ie, prevented or diminished in severity, remains open. In particular, the question as to whether achievement of remission or low disease activity in psoriasis, by 1 or more therapeutic mechanisms, can prevent the appearance of PsA is being actively pursued. There have been mixed results in observational studies regarding aggressive psoriasis treatment in preventing PsA [48,49]. An example of a prospective trial to more reliably address this question, using an IL-23 inhibitor, the PAMPA trial, is underway [50].

We expect expanding use of digitally acquired data, such as weekly or daily patient-reported measures, as well as inputs about function and motion from wearable devices, in order to provide more granular assessment in clinical trials [51]. This may also be used more commonly in clinical practice, along with support from AI, in order to track and document patient health longitudinally.

Global projections indicate there will be too few rheumatologists to face the need for rheumatology care in years to come [52]. One approach to address this gap is an increase in number of 'advanced practice practitioners' (APPs)—nurse practitioners and physician assistants—who have consultative and prescriptive authority [52,53]. APPs are an increasing part of the rheumatology workforce in the United States, but much less in other parts of the world. There needs to be increased recruitment and education of APPs, and increased acceptance in other countries, of this echelon of rheumatology clinicians to support service delivery.

Advanced therapeutic strategies in axial spondyloarthritis

AxSpA is a chronic inflammatory disease primarily affecting the sacroiliac joints and the spine. On top of nonsteroidal anti-inflammatory drugs, biological therapies such as tumor necrosis factor inhibitors and IL-17i, and targeted synthetic drugs such as Janus Kinase inhibitors, have provided relief for many patients. Recent research has unveiled novel targets that potentially promise alternative, more precise and effective interventions.

One of the most novel targets is the T-cell receptor (TCR) repertoire. A Russian study identified antibodies against TCRVβ5 as potential modulators of the immune response in axSpA [54]. These antibodies supposedly selectively influence specific T-cell subsets, which would offer a more targeted approach to treatment. In line with this, a recently reported phase 2 clinical trial, published in 2024 in Russian language only, highlighted the possible role of TCRVβ9 in the pathogenesis of axSpA [55]. A confirmatory phase 3 randomised control trial (RCT) is currently awaited.

Because of the relation between the major histocompatibility complex class I molecule HLA-B27 and axSpA, autoreactive B27-restricted CD8+ T-cell clones have been a focus of interest in axSpA research for decades. A 2022 paper by Yang et al [56] demonstrated *in vitro* the existence of these T-cells with restricted TCR repertoire and identified candidate peptides (bacterial) that could be drivers of the inflammatory processes characteristic of the disease. Their research suggests that targeting CD8+ T-cells could mitigate inflammation and prevent disease progression. However, in a recent review paper, it was noted that these B27-restricted CD8+ T-cell clones account for only a small part of the entire population supposedly deleted by the above-mentioned antibodies, and a lot of experimental work has to be done to better understand the role of such restricted CD8+ clones in driving inflammation in axSpA [57].

Beyond cellular targets, the gut microbiome may play a crucial role in axSpA. Research suggests that gut dysbiosis—an imbalance in the gut microbial community—is associated with increased disease activity and impaired physical function in patients with axSpA [58–60]. Studies have found that patients with axSpA exhibit a higher frequency of gut dysbiosis, as compared with healthy controls, with interesting correlations to disease activity measures, such as the Ankylosing Spondylitis Disease Activity Score, and measures of physical function, such as the Bath Ankylosing Spondylitis Functional Index. These findings underscore the importance of the gut-joint axis in the pathogenesis of axSpA and open up new therapeutic possibilities.

Obviously, genetic factors contribute to the development of axSpA. The HLA-B27 gene is a well-established risk factor, and its interaction with endoplasmic reticulum aminopeptidase 1 (ERAP1) has been shown to influence disease susceptibility and severity [61–63]. ERAP1 plays a pivotal role in processing peptides for presentation by major histocompatibility complex class I molecules. The contribution of certain ERAP-1 polymorphisms in affecting the peptide repertoire presented by HLA-B27 is under debate [64]. This interaction may lead to the activation of autoreactive T-cells, initiating inflammatory processes in the axial and peripheral joints. Understanding these genetic interactions may open the door to more personalised medicine approaches in axSpA treatment.

In conclusion, the evolving landscape of axSpA therapy emphasises precision medicine, targeting specific immune pathways and genetic factors. Advancements in understanding the roles of TCRVβ5, TCRVβ9, CD8+ T-cells, gut microbiota, and HLA-B27-ERAP1 interactions offer promising avenues for developing more effective and individualised treatments. As research progresses, these insights may lead to novel therapeutic strategies that may further improve patient outcomes in axSpA.

Systemic lupus erythematosus

This year's SLE-related discussions adopted a more optimistic approach. After a brief discussion around the potential for immune-reset therapy (ie, CAR-T), the group chose to consider the recent successes in the field and then reflected upon the ingredients which subserved them with the goal of motivating even greater future advances.

The shift, several years ago, of translational science towards specific SLE target discovery rather than perpetual repurposing of therapeutic agents from RA has been a major contributor to the relatively rapid growth of successful therapeutic development programmes [65,66]. Patients are only now beginning to reap the rewards of this reorientation. The investigator community now needs to devote similar energy to molecular endotyping and ultimately personalised medicine [67,68].

Another parallel factor in recent successes has been productive modifications to trial design, especially in relation to the minimisation of background glucocorticoids within protocols [69]. It is hoped that the community will now feel more confident to take the next step and aspire to support tapering protocols which aim for the complete elimination of glucocorticoids. Similarly, as familiarity grows with novel interventions and their safety profiles, it is hoped that deeper and more potent modulation of their underlying targets will be embraced with a view to enhancing efficacy, and possibly even immune reset.

It is equally important not to overlook established therapies. Mycophenolate mofetil (MMF), for example, has been an undoubted success for many and yet we still do not fully understand its molecular mechanism of action. It was recommended that studies defining the transcriptional profiles modulated by MMF in relation to clinical response could provide critical new insights into disease mechanisms and perhaps identify new therapeutic targets [70]. By harnessing such knowledge, we may derive superior drugs. However, one always has to keep in mind that concomitant glucocorticoid therapy (at different doses potentially different), let alone other treatment modalities may confound the results and, therefore, 'clean' populations should be sought for these analyses. These may also be broad in their mechanisms and ultimately inform a combinatorial targeted approach.

Regardless of the therapy, new or old, there is a consistent disconnect between patient and physician perception of what treatment success looks like. Specifically, the patient priorities of fatigue and cognitive fog are poorly managed with existing tools, often fuelling poor compliance [71]. This dimension is considered a major unmet need, and more work to understand underlying neuroimmune mechanisms may ultimately lead to new solutions which could complement existing treatment strategies.

Engagement of the rheumatology and dermatology investigator communities with regulatory authorities, along with contributions from voluntary organisations and patients, has shown progress in recognising the Cutaneous Lupus Erythematosus Disease Area and Severity Index as an outcome measure for clinical trials [72]. A similar advancement regarding measures important to patients with SLE, such as fatigue, could be similarly transformational.

Last but not least, heightened prioritisation of SLE among several industry partners has contributed greatly to the growing SLE armamentarium. Current areas in need of further progress are precision medicine biomarker discovery, paediatric trials, and inclusion of pregnant subjects and those with early disease [73–75]. These can be very feasibly addressed if the patient,

physician, academic, and industry communities continue to agilely grow their existing partnerships with the shared goal of transforming SLE outcomes.

Systemic sclerosis

This year's discussion focused on key requirements to advance therapeutics of SSc, and the discussions included 2 associated treatment paradigms.

Align trials to predominant major organ involvement: As with other Rheumatic musculoskeletal disease, a particular challenge in the management of SSc is its multiple manifestations and the heterogeneity across patient populations. This has implications for the design of trials. A point of discussion was whether the aim of treatment intervention trials should be to target all (possible) or specific major organ involvement. Heterogeneous temporal associations make it challenging to address the totality of organ involvement. Much progress has been made in the treatment landscape for SSc-pulmonary arterial hypertention and, more recently, SSc-intersitial lung disease (ILD) [76]. Consensus among the group was therefore to align trials to predominant major organ involvement, meaning SSc-ILD remains a principal focus of trials, but these should ensure other organ complications are captured in (key) secondary endpoints. This allows study of more homogeneous patient cohorts, to use US Food and Drug Administration (FDA)-approved endpoints (Forced Vital Capacity) and known pathways to approval of medications by agencies. Following this concept, SSc disease-modifying medications would then need to show clinically significant effects on several organ endpoints. Combined indices such as revised composite response index in systemic sclerosis (CRISS) were also discussed. It was noted that revised CRISS needs enrichment criteria other than, for example, ILD-enriched cohorts. Combined indices are promising but need definition of minimally clinically important difference. Performance might depend on the recruited population in each specific clinical trial. Revised CRISS is currently used in clinical trials which will allow further validation.

Target the predamage disease stage: The second paradigm discussed was stage of disease. Most clinical trials focus on early diffuse cutaneous SSc (typically, <5-7 years from the onset of the first non-Raynaud symptom of SSc) [77] to address the SSc subgroup and stage associated with the greatest risk for major organ involvement. Nevertheless, an over-riding feeling was the need to target disease at the earliest stages and not only focus once damage/fibrosis is established (eg, we do not wait for erosions in RA but have a disease activity score to identify active inflammation). To do this, we need to understand how to identify relevant (future diffuse) disease early as very early diagnosis of systemic sclerosis criteria do not enable this. Similarly, pre-stage SSc-ILD needs further study and identification of risk factors [78].

Recognise organ involvement and impact with longer disease duration: The group this year also highlighted the importance of not dismissing longer disease duration, especially with data demonstrating variable disease course and later onset ILD [79] and cardiac involvement [78].

Refine the target of treatment to reflect disease activity: The group agreed that optimal disease activity scores need to be developed to address the ability of therapies to abrogate disease activity and progression. Current activity scores often define activity as a progression in recent damage. This assumes that recent activity places patients at higher risk of ongoing activity, which is not the case in SSc [80].

The clinical trial priorities identified and associated unmet needs were:

(1) Very early, predamage SSc: this also means we need to know how to identify this stage of disease (defining disease activity in the absence of fibrosis that the very early diagnosis of systemic sclerosis criteria do not enable and similar for prestage SSc-ILD) and to recognise the sweet spot when considering risk vs benefit of targeted therapeutics.
(2) Sequencing of therapies: how and when to use predominant immune and fibrosis targeted agents was picked up from 2023 meeting discussions and remains unaddressed. Arguably, this may be relevant in mitigating development of a refractory population. It was noted that differentiating therapies as immune or fibrosis-targeting might no longer be adequate, as these targets overlap, such as with emergent therapies like nerandomilast.
(3) Post MMF, rituximab (RTX) and/or tocilizumab (TCZ) inefficacy: The group also raised the treatment gap for individuals whose disease progresses despite currently available therapeutics. This population is perhaps akin to the 'D2T' populations that have emerged in RA and PsA, although a tailored definition is warranted for SSc.

The above priorities were set against continued support of trials in limited cutaneous disease, in which there is ongoing research activity by the international community. The group emphasised that designing such trials is contingent on understanding the right trial populations and developing companion diagnostics to support a precision medicine approach. The group also acknowledged the increasing challenges in recruitment to trials now that treatments for SSc are available.

In addition to the disease stages targeted for clinical trials, the group supported development of treatments for specific manifestations of SSc with a high unmet need. SSc is associated with the greatest risk of cardiovascular involvement across the autoimmune diseases [81]. SSc-primary heart involvement has benefitted from recent consensus definitions and management strategies, but gaps in understanding of mechanisms, natural history and a lack of validated endpoints outside of Major Adverse Cardiovasular Events (MACE) limit the ability to develop specific therapeutic strategies and trials. As included in the 2023 discussion, other manifestations were discussed that associate with poor quality of life—calcinosis, gastrointestinal involvement (upper and lower gastrointestinal), and musculoskeletal involvement (including contractures). Discussion focused again on the need to appreciate the underlying mechanisms and gain a better understanding of prevalence and natural history before dedicated trials can be considered. The challenge in feasibility of trials for such manifestations was also highlighted with prevalence of, eg, calcinosis, approximately 5%, contrasting with ILD (50%). Also needed are better tools for assessment, such as joint involvement and disease activity, as simply borrowing from diseases such as RA, is not appropriate. Here, data show DAS28/similar activity measures employed in RA are likely inadequate as will be influenced by SSc skin involvement. Furthermore, the assumption that RA-targeted therapies would be effective similarly in joint involvement of other Rheumatic musculoskeletal disease including SSc, is not implicit, with notably, sc-RNA sequencing studies in SSc suggesting that synovial pathology is remarkably different from RA. An additional area highlighted was sexual/erectile dysfunction that receives little to no attention. Peripheral vasculopathy/Raynaud's Phenomenon, although almost universally

present in SSc and managed with vasodilators (CCB and PDE5i), remains suboptimally treated and associated with poor quality of life. Optimal strategies for using current therapies and development of novel treatments are needed.

Osteoarthritis

Treatment options for OA remain very limited, so unmet therapeutic need is very high for this massive global problem. Because of lack of success in clinical trials for a range of therapies, there has been increasing focus on better defining phenotypes, or more appropriately, the underpinning molecular endotypes that might enable enrichment at trial inclusion [82,83].

Current phenotypes employed in clinical trials have been very broad. Modern studies commonly use a 'pain phenotype' in that they enrol for sustained moderate to severe pain at baseline in the target joint and usually exclude widespread pain. Such inclusions have been based on historic factors that influence the responsiveness of pain outcomes, rather than targeting, for example, people with a specific type of pain, such as peripheral nociceptive pain. Also, methodological issues such as regression to the mean may influence pain measurement. A recent study applied 2 pain inclusion criteria, based on both Western Ontario and MacMaster University Osteoarthritis Index pain and average daily pain from a pretrial run-in period, as well as standard exclusions for widespread pain, and still reported substantial placebo responses [84]. Despite the limitations of current inclusion criteria, preliminary reports from this phase 2 RCT of a novel neurotrophin-3 inhibitor demonstrated analgesic efficacy compared with placebo at all 3 doses tested. Joint safety events were seen infrequently with previous neurotrophin inhibitors (antinerve growth factor therapies), but at least in the follow-up to 30 weeks after 16 weeks of treatment, there was no increased incidence of joint safety events (including rapidly progressive OA) compared with placebo [84]. Larger trials with longer follow-up will now be required.

An 'inflammatory phenotype', using magnetic resonance imaging-determined synovitis, was included in a recent RCT of methotrexate in hand OA [85]. At a dose of 20 mg weekly, this study demonstrated clinically meaningful analgesic response at 6 months, though with limited benefits on function. Another study of methotrexate (aiming for 25 mg weekly) in knee OA also demonstrated meaningful reduction in Numeric Rating Scale (NRS) pain at 6 months [86]. Synovitis was not an inclusion criterion in the latter trial, but MTX did not demonstrate a reduction in synovitis. Instead, better analgesic responses were seen in patients with elevated highly sensitive CRP (hsCRP), suggesting a systemic anti-inflammatory benefit on knee pain. Clinical trials such as this, which incorporate some exploration of mechanism of action, are essential for better phenotype or endotype delineation.

Methotrexate has broad anti-inflammatory and anticytokine actions. Targeting a single cytokine, interleukin-1, has not been considered effective in previous OA clinical trials [87]. However, an analysis from a large RCT of cardiovascular patients treated with anti-IL1 demonstrated a substantial benefit from active therapy in reducing rates of joint replacement [88]. The patients in this study had high rates of diabetes and obesity with elevated hsCRP and were treated for over 3.5 years. Another cardiovascular RCT with large patient numbers compared low-dose colchicine for over 2 years vs placebo and similarly showed a substantial reduction in joint replacement for the colchicine-treated arm [89]. Colchicine works by inhibiting the inflammasome and IL-1, but again, previous OA trials had not shown an analgesic benefit. These studies may be giving insights into an inflammatory phenotype and/or a metabolic phenotype.

Targeting IL-1 has also been the focus of novel intra-articular gene therapies, a new direction for OA therapeutics. Two such therapies aiming to provide increased expression of IL-1 receptor antagonist have recently reported preliminary phase 1 results, demonstrating acceptable safety and some evidence to support proof of principle [90,91]. Steroid pretreatment will likely be required with these therapies to improve tolerability but also vector transduction.

Obesity is a common component of metabolic syndrome. Weight loss has previously been reported to reduce OA pain, but the advent of novel weight loss therapies offers an opportunity to capitalise on their significant weight loss benefits, both systemically and at joint level. Bliddal and colleagues recently reported the results of a large RCT of the GLP-1 receptor agonist semaglutide in a large knee OA trial, where 75.4% of participants had body mass index $\geq$ 35 kg/m^2 [92]. They demonstrated substantial weight loss and clinically meaningful reduction in pain over 68 weeks.

Another agent with effects on weight, glucose production, and insulin resistance is metformin, which has also demonstrated anti-inflammatory effects. A recent RCT in knee OA randomised 107 nondiabetic overweight or obese patients to metformin or placebo and demonstrated a meaningful reduction in pain compared with placebo after 6 months of therapy [93]. Such trials indicate that targeting a 'metabolic phenotype' with weight loss and likely systemic anti-inflammatory effects will be an interesting future direction for OA management. However, more knowledge on the impact of these drugs on OA structural pathology and pain is awaited, as well as an understanding of potential side effects, including muscle loss with GLP-1 receptor agonists.

Summary

The 25th annual ATT meeting discussed and identified the most important unmet research needs in the field of rheumatology (Table 1). Novel immune reset strategies such as CAR-T −cell therapy, the potential of GLP-1 agonists as adjunctive therapy, and the further development of targeted therapies, particularly for those with advanced or refractory disease, were prominent in discussions across disease states. The need for cure or prevention of disease remains the ultimate target.

Competing interests

KLW has received research grants and/or consulting honoraria from Janssen Pfizer, AbbVie, Union Chimique Belge (UCB), Eli Lilly & Company, Galapagos, GlaxoSmithKline (GSK), Roche, Gilead, BMS, Regeneron, Sanofi, AstraZeneca, Novartis, and AnaptysBio. AK has received grants and/or consulting honoraria from AbbVie, Boehringer-Ingelheim, Eli Lilly, Galapagos, JNJ, MSD, Novartis, UCB, Pfizer, and Stada. JDI has received grants and/or consulting honoraria from Janssen, GSK, Pfizer, AbbVie, BMS, Gilead, Roche, Eli Lilly, Anaptys Bio, and Sonoma. PM has received grants and/or consulting honoraria from AbbVie, Amgen, Astra Zeneca, Biogen, BMS, Century, Cullinan, Eli Lilly, Inmagene, Janssen, Merck, Moonlake, Novartis, Oruka, Pfizer, Spyre, Sun Pharma, Takeda, and UCB. MKC is on the scientific advisory boards of AbelZeta, Aboleris, and AMPEL BioSolutions; has received consulting honoraria from BMS, GSK, Lilly, Novartis, Palleon, and Takeda; and has received a research grant

Table 1
Identified unmet research needs of high priority within rheumatoid arthritis, psoriatic arthritis, axial spondyloarthritis, systemic lupus erythematosus, systemic sclerosis, and osteoarthritis

Rheumatoid arthritis	• Better defining and treating refractory RA
	• The potential for novel targeted therapies and those involving immune reset (ie, CAR-T)
	• Predictive biomarkers for disease course and treatment response
	• Precision medicine approaches through molecular and synovial profiling
	• Novel targeted therapies, incl. fibroblast-directed strategies
Psoriatic arthritis	• Better defining difficult-to-treat and complex to manage disease states
	• Investigating potential PsA prevention in those with skin psoriasis alone
	• The potential for disease modification with GLP-1 receptor agonists
	• Development of therapies with new mechanisms and dual therapy options
	• Better recognition and management of axial PsA
	• Addressing comorbidities and modifiers (obesity, depression, and nociplastic pain)
Axial spondyloarthritis	• Further advancements in our understanding of the roles of TCRVβ5, TCRVβ9, CD8+ T-cells, gut microbiota, and HLA-B27-ERAP1
	• The need for precision medicine, with therapies better targeting these and other specific immune pathways and genetic factors
Systemic lupus erythematosus	• The need for precision medicine biomarker discovery
	• Clinical trials that incorporate paediatrics, pregnant subjects, and those with early disease
	• Evaluation of immune reset therapy in appropriate patients (ie, CAR-T)
	• Biomarker discovery and molecular endotyping for personalised care
	• Reduction and elimination of glucocorticoids in trial design
	• Addressing patient-prioritised symptoms (fatigue, cognitive and dysfunction)
Systemic sclerosis	• Align trials to predominant major organ involvement and target predamage stages of disease
	• Evaluation of immune reset therapy in appropriate patients (ie, CAR-T)
	• Targeting very early/predamage stages of disease
	• Optimised sequencing of immune- vs fibrosis-directed therapies
	• Defining and addressing *D2T-SSc*
	• Need for improved outcome measures and companion diagnostics
	• Development of strategies for high-burden manifestations (calcinosis, Gastrointestinal, Raynaud's, and sexual dysfunction)
Osteoarthritis	• Better defining disease phenotypes (eg, pain phenotypes and inflammatory disease), and the need to target these phenotypes with appropriate therapies
	• Evaluation of novel intra-articular and gene therapies
	• Targeted interventions for phenotype-specific subgroups
	• Evaluation of anti-inflammatory approaches (Methotrexate, IL-1 inhibition, and colchicine)
	• Integration of metabolic interventions (GLP-1 agonists, metformin, and weight loss strategies)
	• Identification of structure-modifying therapies with long-term benefit

CAR, chimeric antigen receptor; ERAP1, endoplasmic reticulum aminopeptidase 1; PsA, psoriatic arthritis; RA, rheumatoid arthritis; TCR, T-cell receptor.

from Gilead Sciences. She serves as an Associate Editor of *Annals of the Rheumatic Diseases* but was not involved in the handling or review of this manuscript. AK has received grants and/or consulting honoraria from Amgen, Eli Lilly, Galapagos, Gilead, Janssen, Novartis, UCB, and Pfizer. XB has received grants and/or consulting honoraria from Alphasigma, Amgen, BMS, Celltrion, Cesas, Eli Lilly, Galapagos, Janssen, Moonlake, Novartis, Pfizer, Roche, Sandoz, Springer, Stada, Takeda, Pfizer, and UCB. MKC is on the scientific advisory boards of AbelZeta, Aboleris, and AMPEL BioSolutions; has received consulting honoraria from BMS, GSK, Lilly, Novartis, Palleon, and Takeda; and has received a research grant from Gilead Sciences. MB has received grants and/or consulting honoraria (all paid to host institution) from AbbVie, Boehringer-Ingelheim, Galapagos, Gilead, and Pfizer Ltd. SS has received grants and/or consulting honoraria from Amgen, AbbVie, AstraZeneca, Eli Lilly, GSK, Johnson & Johnson (Janssen), Novartis, Pfizer, Syncona, Teijin Pharma, and UCB. NB has received grants and/or consulting honoraria from Astra Zeneca, GSK, VSL Vifor, AlfaSigma, and Lilly. PC has received grants and/or consulting from Eli Lilly, Formation Bio, Galapagos, Genascence, GSK, Grunenthal, Kolon TissueGene, Levicept, Moebius, Novartis, Pacira, Stryker & Takeda, AbbVie, Janssen, Kolon TissueGene, Moebius, and Novartis. MK has received grants and/or consulting honoraria (all paid to institution) from UCB, Pfizer, Novartis, CHDR, GSK, and Peptinov and royalties (all paid to institution) from Springer Verlag and Wolters-Kluwer. OD has received honoraria and/or research funds from 4P-pharma, Abbvie, Acepodia, Aera, AnaMar, Anabeon, Argenx, AzstraZeneca, Boehringer Ingelheim, Bristol Meyer Squibb, Calluna, Cantargia AB, CSL Behring, EMD Serono, Galderma, Galapagos, Goassamer, Hemetron, Innovaderm, Janssen, Lilly, MSD Merck, Nkarta, Novartis, Oorja Bio, Orion, Pilan, Prometheus, Quell, Redxpharma, Scleroderma Research Foundation, Sumitomo, Topadu, UCB, and Umlau bio RL has received grants and/or consulting honoraria from AbbVie, Alfasigma, Galapagos, Janssen, Novartis, and UCB and is director of Joint Imaging BV. DEO has no competing interests to disclose. KW has received grants and/or consulting honoraria from Merck, Gilead, AnaptysBio, and Pfizer. DA has received grants and/or consulting honoraria from AbbVie, Amgen, Galapagos, Lilly, Janssen, Merck, Novartis, Pfizer, Sandoz, and Sanofi. IBM has received grants and/or consulting honoraria from AbbVie, Amgen, Absci, BMS, Causeway Therapeutics, Cabaletta, Dextera, Eli Lilly, Janssen, Novartis, Pfizer, Sanofi, UCB, Compugen, AstraZeneca, Moonlake, Montai, Pioneering Medicines, Takeda, and Recludix and serves as a NHS Greater Glasgow and Clyde board member, Versus Arthritis Trustee Status. HT has no competing interests to disclose; VR has received grants and/or consulting honoraria from AbbVie, Amgen, Boehringer-Ingelheim, BMS, Janssen-Cilag, GSK, Hexal, Neutrolis, Novartis, and Pfizer. EMG serves as an associate editor at the *New England Journal of Medicine* and receives royalties from Elsevier. FCB has no competing interests to disclose. JSS has received research grants and/or consulting honoraria from AbbVie, Amgen, AstraZeneca, Ananda, Bristol-Myers Squibb, Chugai, Immunovant, Janssen, Lilly, Merck Sharp & Dohme, Novartis-Sandoz, Pfizer, R-Pharma, Roche, Samsung, and UCB and serves as the editor of *Annals of Rheumatic Diseases* but was not involved in the handling or review of this manuscript.

Acknowledgements

The authors would like to thank Danielle Gerken and Dawn Esser from Oregon Health and Sciences University for assistance with manuscript submission

Contributors

All authors contributed to the study design, data collection, discussion, and critical revision of the manuscript.

Funding

The Advances in Targeted Therapies meeting was supported by: Abbvie, AnaptysBio, Chugai, Eli Lilly, Alfasigma, GSK, Janssen, Mitsubishi Tanabe, Novartis, Sunpharma, Union Chimique Belge, BMS, Pfizer, and Amgen.

Patient consent for publication

Not applicable.

Ethical approval

Not applicable.

Provenance and peer review

Not applicable.

Data availability statement

Not applicable

Orcid

Kevin L. Winthrop: http://orcid.org/0000-0002-3892-6947
Philip Mease: http://orcid.org/0000-0002-3478-5665
Maya Buch: http://orcid.org/0000-0002-8962-5642
Stefan Siebert: http://orcid.org/0000-0002-1802-7311
Margreet Kloppenburg: http://orcid.org/0000-0002-9294-2307
Oliver Distler: http://orcid.org/0000-0002-0546-8310
Robert Landewe: http://orcid.org/0000-0002-0577-6620
Dana E. Orange: http://orcid.org/0000-0003-2108-0030
Daniel Aletaha: http://orcid.org/0000-0003-2108-0030

REFERENCES

[1] Winthrop KL, Mease P, Kerschbaumer A, Voll RE, Breedveld FC, Smolen JS, et al. Unmet need in rheumatology: reports from the Advances in Targeted Therapies meeting, 2023. Ann Rheum Dis 2024 Mar 12;83(4):409–16. doi: 10.1136/ard-2023-224916.
[2] Nagy G, Roodenrijs NMT, Welsing PMJ, Kedves M, Hamar A, van der Goes MC, et al. EULAR definition of difficult-to-treat rheumatoid arthritis. Ann Rheum Dis 2021;80(1):31–5. doi: 10.1136/annrheumdis-2020-217344.
[3] Nagy G, Roodenrijs NMT, Welsing PMJ, Kedves M, Hamar A, van der Goes MC, et al. EULAR points to consider for the management of difficult-to-treat rheumatoid arthritis. Ann Rheum Dis 2022 Jan;81(1):20–33. doi: 10.1136/annrheumdis-2021-220973.
[4] Giollo A, Zen M, Larosa M, Astorri D, Salvato M, Calligaro A, et al. Early characterization of difficult-to-treat rheumatoid arthritis by suboptimal initial management: a multicentre cohort study. Rheumatology (Oxford) 2023 Jun 1;62(6):2083–9. doi: 10.1093/rheumatology/keac563.
[5] Bécède M, Alasti F, Gessl I, Haupt L, Kerschbaumer A, Landesmann U, et al. Risk profiling for a refractory course of rheumatoid arthritis. Semin Arthritis Rheum 2019 Oct;49(2):211–7. doi: 10.1016/j.semarthrit.2019.02.004.
[6] Burgers LE, Raza K, van der Helm-van Mil AH. Window of opportunity in rheumatoid arthritis - definitions and supporting evidence: from old to new perspectives. RMD Open 2019;5(1):e000870. doi: 10.1136/rmdopen-2018-000870.
[7] MacDonald L, Elmesmari A, Somma D, Frew J, Di Mario C, Madhu R, et al. Synovial tissue myeloid dendritic cell subsets exhibit distinct tissue-niche localization and function in health and rheumatoid arthritis. Immunity 2024 Dec 10;57(12) 2843-2862.e12. doi: 10.1016/j.immuni.2024.11.004.
[8] Zhang F, Jonsson AH, Nathan A, Millard N, Curtis M, Xiao Q, et al. Deconstruction of rheumatoid arthritis synovium defines inflammatory subtypes. Nature 2023;623(7987):616–24. doi: 10.1038/s41586-023-06708-y.
[9] Mantel I, Fein MR, Donlin LT. Emerging synovial cell states in rheumatoid arthritis as potential therapeutic targets. Curr Opin Rheumatol 2023 Jul 1;35(4):249–54. doi: 10.1097/bor.0000000000000940.
[10] Vo T, Prakrithi P, Jones K, Yoon S, Lam PY, Kao YC, et al. Assessing spatial sequencing and imaging approaches to capture the molecular and pathological heterogeneity of archived cancer tissues. J Pathol 2025 Mar;265(3):274–88. doi: 10.1002/path.6383.
[11] Alivernini S, Cañete JD, Bacardit J, Kurowska-Stolarska M. Using explainable artificial intelligence to predict and forestall flare in rheumatoid arthritis. Nat Med 2024 Apr;30(4):925–6. doi: 10.1038/s41591-024-02818-w.
[12] Schwenck J, Sonanini D, Cotton JM, Rammensee HG, la Fougère C, Zender L, et al. Advances in PET imaging of cancer. Nat Rev Cancer 2023 Jul;23(7):474–90. doi: 10.1038/s41568-023-00576-4.
[13] Chen YM, Hsiao TH, Lin CH, Fann YC. Unlocking precision medicine: clinical applications of integrating health records, genetics, and immunology through artificial intelligence. J Biomed Sci 2025 Feb 7;32(1):16. doi: 10.1186/s12929-024-01110-w.
[14] RA-MAP Consortium. Novel methodology to discern predictors of remission and patterns of disease activity over time using rheumatoid arthritis clinical trials data. RMD Open 2018;4(2):e000721. doi: 10.1136/rmdopen-2018-000721.
[15] Komatsu N, Takayanagi H. Mechanisms of joint destruction in rheumatoid arthritis — immune cell–fibroblast–bone interactions. Nat Rev Rheumatol 2022;18(7):415–29. doi: 10.1038/s41584-022-00793-5.
[16] Zhang F, Wei K, Slowikowski K, Fonseka CY, Rao DA, Kelly S, et al. Defining inflammatory cell states in rheumatoid arthritis joint synovial tissues by integrating single-cell transcriptomics and mass cytometry. Nat Immunol 2019 Jul;20(7):928–42.
[17] Nygaard G, Firestein GS. Restoring synovial homeostasis in rheumatoid arthritis by targeting fibroblast-like synoviocytes. Nat Rev Rheumatol 2020 Jun;16(6):316–33. doi: 10.1038/s41584-020-0413-5.
[18] Qian H, Deng C, Chen S, Zhang X, He Y, Lan J, et al. Targeting pathogenic fibroblast-like synoviocyte subsets in rheumatoid arthritis. Arthritis Res Ther 2024;26(1):103. doi: 10.1186/s13075-024-03343-4.
[19] Snowden JA, Kapoor S, Wilson AG. Stem cell transplantation in rheumatoid arthritis. Autoimmunity 2008;41(8):625–31. doi: 10.1080/08916930802198550.
[20] Mackensen A, Müller F, Mougiakakos D, Böltz S, Wilhelm A, Aigner M, et al. Anti-CD19 CAR T cell therapy for refractory systemic lupus erythematosus. Nat Med 2022 Oct;28(10):2124–32. doi: 10.1038/s41591-022-02017-5.
[21] Haghikia A, Hegelmaier T, Wolleschak D, Böttcher M, Pappa V, Motte J, et al. Clinical efficacy and autoantibody seroconversion with CD19-CAR T cell therapy in a patient with rheumatoid arthritis and coexisting myasthenia gravis. Ann Rheum Dis 2024 Oct 21;83(11):1597–8. doi: 10.1136/ard-2024-226017.
[22] Ribeiro AL, Singla S, Chandran V, Chronis N, Liao W, Lindsay C, et al. Deciphering difficult-to-treat psoriatic arthritis (D2T-PsA): a GRAPPA perspective from an international survey of healthcare professionals. Rheumatol Adv Pract 2024;8(3):rkae074. doi: 10.1093/rap/rkae074.
[23] Proft F, Lucas Ribeiro A, Singla S, Chandran V, Liao W, Lindsay C, et al. OP0175 Establishing definitions for difficult-to-treat psoriatic arthritis (D2T-PsA) and complex-to-manage psoriatic arthritis (C2M-PsA): insights from the group for research and assessment of psoriasis and psoriatic arthritis (GRAPPA) initiative. Ann Rheum Dis 2025;84:143–5. doi: 10.1016/j.ard.2025.05.188.
[24] Marzo-Ortega H, Harrison SR, Fragoulis G, Michelena X, Macia-Villa C, Aydin S, et al. POS1269 Eular points to consider for the definitions of difficult-to-manage and treatment-refractory psoriatic arthritis. Ann Rheum Dis 2025;84:1319–20. doi: 10.1016/j.ard.2025.06.619.
[25] Marzo-Ortega H, Harrison SR, Nagy G, Machado PM, McGonagle DG, Aydin SZ, et al. Time to address the challenge of difficult to treat psoriatic arthritis: results from an international survey. Ann Rheum Dis 2024;83(3):403–4. doi: 10.1136/ard-2023-225087.
[26] Proft F, Ribeiro AL, Singla S, Chandran V, Liao W, Lindsay C, et al. Consensus definitions of complex-to-manage and treatment-refractory psoriatic arthritis: a GRAPPA initiative. Nat Rev Rheumatol 2026 Feb;22(2):132–44. doi: 10.1038/s41584-025-01329-3.

[27] Ribeiro AL, Proft F. Navigating the complexities of difficult-to-treat axial spondyloarthritis. Joint Bone Spine 2024;91(5):105770. doi: 10.1016/j.jbspin.2024.105770.
[28] Poddubnyy D, Navarro-Compán V, Torgutalp M, Arends S, Aydin SZ, Battista S, et al. The Assessment of SpondyloArthritis International Society (ASAS) Consensus-Based Expert Definition of Difficult-to-Manage, including Treatment-Refractory, Axial Spondyloarthritis. Ann Rheum Dis 2025;84(4):538–46. doi: 10.1016/j.ard.2025.01.035.
[29] Gossec L, Kerschbaumer A, Ferreira RJO, Aletaha D, Baraliakos X, Bertheussen H, et al. EULAR recommendations for the management of psoriatic arthritis with pharmacological therapies: 2023 update. Ann Rheum Dis 2024 May 15;83(6):706–19. doi: 10.1136/ard-2024-225531.
[30] Philippoteaux C, Delepine T, Cailliau E, Philippe P, Taisne N, Pascart T, et al. Characteristics of difficult-to-treat axial spondyloarthritis: results of a real-world multicentric study. Joint Bone Spine 2024;91(2):105670. doi: 10.1016/j.jbspin.2023.105670.
[31] Philippoteaux C, Marty-Ane A, Cailliau E, Labreuche J, Philippe P, Cortet B, et al. Characteristics of difficult-to-treat psoriatic arthritis: a comparative analysis. Semin Arthritis Rheum 2023;63:152275. doi: 10.1016/j.semarthrit.2023.152275.
[32] Nielung LM, Di Giuseppe D, Lund Hetland M, Askling J, Nordström D, Aarrestad Provan S, et al. OP0177—Exploring definitions and prevalence of difficult-to-treat psoriatic arthritis in 13,872 patients from five nordic registries. Ann Rheum Dis 2025;84:146–7. doi: 10.1016/j.ard.2025.05.190.
[33] Porta S, Otero-Losada M, Kölliker Frers RA, Cosentino V, Kerzberg E, Capani F. Adipokines, cardiovascular risk, and therapeutic management in obesity and psoriatic arthritis. Front Immunol 2020;11:590749. doi: 10.3389/fimmu.2020.590749.
[34] Smolen JS, Schöls M, Braun J, Dougados M, FitzGerald O, Gladman DD, et al. Treating axial spondyloarthritis and peripheral spondyloarthritis, especially psoriatic arthritis, to target: 2017 update of recommendations by an international task force. Ann Rheum Dis 2018 Jan;77(1):3–17. doi: 10.1136/annrheumdis-2017-211734.
[35] Husted JA, Tom BD, Farewell VT, Schentag CT, Gladman DD. A longitudinal study of the effect of disease activity and clinical damage on physical function over the course of psoriatic arthritis: does the effect change over time? Arthritis Rheum 2007 Mar;56(3):840–9. doi: 10.1002/art.22443.
[36] Kerschbaumer A, Baker D, Smolen JS, Aletaha D. The effects of structural damage on functional disability in psoriatic arthritis. Ann Rheum Dis 2017 Dec;76(12) 2038-45. doi: 10.1136/annrheumdis-2017-211433.
[37] Kerschbaumer A, Steiner M, Khalili S, Shehab A, Jordanov A, Wildner B, et al. Global recruiting patterns affect placebo response rates in clinical trials of psoriatic arthritis and plaque psoriasis. Arthritis Rheumatol 2026 Jan;78(1):141–51. doi: 10.1002/art.43302.
[38] Mease P, Reed G, Ogdie A, Pappas DA, Kremer JM. Prevalence of fibromyalgia and widespread pain in psoriatic arthritis: association with disease severity assessment in a large US Registry. Arthritis Care Res (Hoboken) 2024 Sep;76(9):1313–21. doi: 10.1002/acr.25358.
[39] Orbai AM, de Wit M, Mease PJ, Callis Duffin K, Elmamoun M, Tillett W, et al. Updating the Psoriatic Arthritis (PsA) Core Domain Set: a Report from the PsA Workshop at OMERACT 2016. J Rheumatol 2017 Oct;44(10):1522–8. doi: 10.3899/jrheum.160904.
[40] Baraliakos X, Gossec L, Pournara E, Jeka S, Mera-Varela A, D'Angelo S, et al. Secukinumab in patients with psoriatic arthritis and axial manifestations: results from the double-blind, randomised, phase 3 MAXIMISE trial. Ann Rheum Dis 2021;80(5):582–90. doi: 10.1136/annrheumdis-2020-218808.
[41] Gladman DD, Mease PJ, Bird P, Soriano ER, Chakravarty SD, Shawi M, et al. Efficacy and safety of guselkumab in biologic-naïve patients with active axial psoriatic arthritis: study protocol for STAR, a phase 4, randomized, double-blinded, placebo-controlled trial. Trials 2022 Sep 5;23(1):743. doi: 10.1186/s13063-022-06589-y.
[42] Eder L, Mylvaganam S, Pardo J, Petkovic J, Strand V, Mease P, et al. Sex-related differences in patient characteristics, and efficacy and safety of advanced therapies in randomised clinical trials in psoriatic arthritis: a systematic literature review and meta-analysis. Lancet Rheumatol 2023;5(12):e716–27. doi: 10.1016/S2665-9913(23)00264-3.
[43] Mease PJ. Navigating the complexity of pain in psoriatic arthritis and axial spondyloarthritis. Curr Opin Rheumatol 2024 Jul 1;36(4):282–8. doi: 10.1097/bor.0000000000001023.
[44] Martins A, Oliveira D, Nicolau R, Rocha TM, Bernardo A, Costa L, et al. What is the association of depression with clinical response to therapy in patients with psoriatic arthritis treated with biologic disease-modifying antirheumatic drugs? Clin Rheumatol 2024 Jan;43(1):251–8. doi: 10.1007/s10067-023-06806-2.
[45] Poddubnyy D, Baraliakos X, Van den Bosch F, Braun J, Coates LC, Chandran V, et al. Axial Involvement in Psoriatic Arthritis cohort (AXIS): the protocol of a joint project of the Assessment of SpondyloArthritis international Society (ASAS) and the Group for Research and Assessment of Psoriasis and Psoriatic Arthritis (GRAPPA). Ther Adv Musculoskelet Dis 2021;13:1759720x211057975. doi: 10.1177/1759720x211057975.
[46] Torgutalp M, Azevedo V, Baraliakos X, Van den Bosch F, Braun J, Cauli A, et al. Characteristics of Patients with Psoriatic Arthritis Presenting with Axial Involvement: results of a Prospective International Multicenter Study (AXIS). presented at: ACR Convergence 2024; published as part of Arthritis & Rheumatology Abstracts (ACR Meeting Abstracts); 2024 2024; San Diego, CA. https://acrabstracts.org/abstract/characteristics-of-patients-with-psoriatic-arthritis-presenting-with-axial-involvement-results-of-a-prospective-international-multicenter-study-axis/
[47] Feld J, Chandran V, Haroon N, Inman R, Gladman D. Axial disease in psoriatic arthritis and ankylosing spondylitis: a critical comparison. Nat Rev Rheumatol 2018 Jun;14(6):363–71. doi: 10.1038/s41584-018-0006-8.
[48] Scher JU, Ogdie A, Merola JF, Ritchlin C. Preventing psoriatic arthritis: focusing on patients with psoriasis at increased risk of transition. Nat Rev Rheumatol 2019 Mar;15(3):153–66. doi: 10.1038/s41584-019-0175-0.
[49] Meer E, Merola JF, Fitzsimmons R, Love TJ, Wang S, Shin D, et al. Does biologic therapy impact the development of PsA among patients with psoriasis? Ann Rheum Dis 2022;81(1):80–6. doi: 10.1136/annrheumdis-2021-220761.
[50] Haberman RH, MacFarlane KA, Catron S, Samuels J, Blank RB, Toprover M, et al. Efficacy of guselkumab, a selective IL-23 inhibitor, in Preventing Arthritis in a Multicentre Psoriasis At-Risk cohort (PAMPA): protocol of a randomised, double-blind, placebo controlled multicentre trial. BMJ Open 2022 Dec 23;12(12):e063650. doi: 10.1136/bmjopen-2022-063650.
[51] Creagh AP, Hamy V, Yuan H, Mertes G, Tomlinson R, Chen WH, et al. Digital health technologies and machine learning augment patient reported outcomes to remotely characterise rheumatoid arthritis. NPJ Digit Med 2024 Feb 12;7(1):33. doi: 10.1038/s41746-024-01013-y.
[52] Miloslavsky EM, Marston B. The challenge of addressing the rheumatology workforce shortage. J Rheumatol 2022 Jun;49(6):555–7. doi: 10.3899/jrheum.220300.
[53] Miloslavsky EM, Bolster MB. Addressing the rheumatology workforce shortage: a multifaceted approach. Semin Arthritis Rheum 2020 Aug;50(4):791–6. doi: 10.1016/j.semarthrit.2020.05.009.
[54] Britanova OV, Lupyr KR, Staroverov DB, Shagina IA, Aleksandrov AA, Ustyugov YY, et al. Targeted depletion of TRBV9+ T cells as immunotherapy in a patient with ankylosing spondylitis. Nat Med 2023;29(11):2731–6. doi: 10.1038/s41591-023-02613-z.
[55] Nasonov EL, Mazurov VI, Lila AM, Dubinina TV, Gaidukova IZ, Lapshina SA, et al. The efficacy and safety of BCD-180, an Anti-TRBV9+ T cell monoclonal antibody, in patients with active radiographic axial spondyloarthritis: 36-week results from the randomized, double-blind, placebo-controlled phase 2 clinical study ELEFTA. Dokl Biochem Biophys 2025 Jun;522(1):387–403. doi: 10.1134/s1607672925700140.
[56] Yang X, Garner LI, Zvyagin IV, Paley MA, Komech EA, Jude KM, et al. Autoimmunity-associated T cell receptors recognize HLA-B*27-bound peptides. Nature 2022 Dec;612(7941):771–7. doi: 10.1038/s41586-022-05501-7.
[57] Penkava F, Sansom S, Bowness P. Pathogenic T-cell clones in axial spondyloarthritis: what is the evidence? Rheumatology (Oxford) 2024 Dec 1;63(Suppl 2):ii4–6. doi: 10.1093/rheumatology/keae522.
[58] Costello ME, Elewaut D, Kenna TJ, Brown MA. Microbes, the gut and ankylosing spondylitis. Arthritis Res Ther 2013;15(3):214. doi: 10.1186/ar4228.
[59] Asquith M, Elewaut D, Lin P, Rosenbaum JT. The role of the gut and microbes in the pathogenesis of spondyloarthritis. Best Pract Res Clin Rheumatol 2014 Oct;28(5):687–702. doi: 10.1016/j.berh.2014.10.018.
[60] Gill T, Stauffer P, Asquith M, Laderas T, Martin TM, Davin S, et al. Axial spondyloarthritis patients have altered mucosal IgA response to oral and fecal microbiota. Front Immunol 2022;13:965634. doi: 10.3389/fimmu.2022.965634.
[61] Reeves E, Elliott T, James E, Edwards CJ. ERAP1 in the pathogenesis of ankylosing spondylitis. Immunol Res 2014 Dec;60(2-3):257–69. doi: 10.1007/s12026-014-8576-2.
[62] López de Castro JA. How ERAP1 and ERAP2 Shape the Peptidomes of Disease-Associated MHC-I Proteins. Front Immunol 2018;9:2463. doi: 10.3389/fimmu.2018.02463.
[63] Haroon N, Inman RD. ERAP1 and the return of the UPR in ankylosing spondylitis. Nat Rev Rheumatol 2023;19(3):134–5. doi: 10.1038/s41584-023-00910-y.
[64] Roberts AR, Appleton LH, Cortes A, Vecellio M, Lau J, Watts L, et al. ERAP1 association with ankylosing spondylitis is attributable to common genotypes rather than rare haplotype combinations. Proc Natl Acad Sci U S A 2017 Jan 17;114(3):558–61. doi: 10.1073/pnas.1618856114.
[65] Fanouriakis A, Kostopoulou M, Andersen J, Aringer M, Arnaud L, Bae SC, et al. EULAR recommendations for the management of systemic lupus erythematosus: 2023 update. Ann Rheum Dis 2024;83(1):15–29. doi: 10.1136/ard-2023-224762.
[66] Sammaritano LR, Askanase A, Bermas BL, Dall'Era M, Duarte-García A, Hiraki LT, et al. 2024 American College of Rheumatology (ACR) guideline for the

screening, treatment, and management of lupus nephritis. Arthritis Rheumatol 2025 Sep;77(9):1115–35. doi: 10.1002/art.43212.
[67] Bachali P, Daamen A, Korish S, Hu Y, Schafer P, Grammer A, et al. Responsiveness of systemic lupus erythematosus subjects to iberdomide based on molecular endotypes. Ann Rheum Dis 2025;84(6):1001–10. doi: 10.1016/j.ard.2025.01.044.
[68] Depascale R, Da Mutten R, Lindblom J, Cetrez N, Palazzo L, Iaccarino L, et al. Unsupervised machine learning identifies distinct SLE patient endotypes with differential response to belimumab. Rheumatology (Oxford) 2025;64(8):4650–8. doi: 10.1093/rheumatology/keaf215.
[69] Furie RA, Rovin BH, Garg JP, Santiago MB, Aroca-Martínez G, Zuta Santillán AE, et al. Efficacy and safety of obinutuzumab in active lupus nephritis. N Engl J Med 2025 Apr 17;392(15):1471–83. doi: 10.1056/NEJMoa2410965.
[70] Akthar M, Nair N, Carter LM, Vital EM, Sutton E, McHugh N, et al. Deconvolution of whole blood transcriptomics identifies changes in immune cell composition in patients with systemic lupus erythematosus (SLE) treated with mycophenolate mofetil. Arthritis Res Ther 2023 Jun 30;25(1):111. doi: 10.1186/s13075-023-03089-5.
[71] Ugarte-Gil MF, Gamboa-Cárdenas RV, Reátegui-Sokolova C, Pimentel-Quiroz VR, Elera-Fitzcarrald C, Pastor-Asurza C, et al. The Lupus Foundation of America-Rapid Evaluation of Activity in Lupus Clinician-Reported Outcome Predicts Damage in Patients With Systemic Lupus Erythematosus. Data from the almenara lupus cohort. J Clin Rheumatol 2024 Aug 1;30(5) e129-32. doi: 10.1097/rhu.0000000000002102.
[72] Xie L, Lopes Almeida Gomes L, Stone CJ, Faden DF, Werth VP. An update on clinical trials for cutaneous lupus erythematosus. J Dermatol 2024 Jul;51(7):885–94. doi: 10.1111/1346-8138.17161.
[73] Buie J, Bloch L, Morand EF, van Vollenhoven RF, Werth VP, Touma Z, et al. Meeting report: the ALPHA project: a stakeholder meeting on lupus clinical trial outcome measures and the patient perspective. Lupus Sci Med 2023 Feb;10(1):e000901. doi: 10.1136/lupus-2023-000901.
[74] Dimelow R, Liefaard L, Green Y, Tomlinson R. Extrapolation of the efficacy and pharmacokinetics of belimumab to support its use in children with lupus nephritis. Clin Pharmacokinet 2024 Sep;63(9):1313–26. doi: 10.1007/s40262-024-01422-y.
[75] Schreiber K, Graversgaard C, Hunt BJ, Wason JMS, Costedoat-Chalumeau N, Aguilera S, et al. Challenges of designing and conducting cohort studies and clinical trials in populations of pregnant people. Lancet Rheumatol 2024 Aug;6(8):e560–72. doi: 10.1016/s2665-9913(24)00118-8.
[76] Distler O, Highland KB, Gahlemann M, Azuma A, Fischer A, Mayes MD, et al. Nintedanib for systemic sclerosis-associated interstitial lung disease. N Engl J Med 2019 Jun 27;380(26):2518–28. doi: 10.1056/NEJMoa1903076.
[77] Volkmann ER, Tashkin DP. Enrichment strategies for systemic sclerosis-interstitial lung disease trials. Am J Respir Crit Care Med 2024 May 1;209(9):1067–8. doi: 10.1164/rccm.202401-0246ED.
[78] Hoa S, Berger C, Lahmek N, Larché M, Osman M, Choi M, et al. Characterization of incident interstitial lung disease in late systemic sclerosis. Arthritis Rheumatol 2025 Apr;77(4):450–7. doi: 10.1002/art.43051.
[79] Hoffmann-Vold AM, Allanore Y, Alves M, Brunborg C, Airó P, Ananieva LP, et al. Progressive interstitial lung disease in patients with systemic sclerosis-associated interstitial lung disease in the EUSTAR database. Ann Rheum Dis 2021 Feb;80(2):219–27. doi: 10.1136/annrheumdis-2020-217455.
[80] Hoffmann-Vold AM, Distler O. Further progression in patients with systemic sclerosis-associated interstitial lung disease – authors' reply. Lancet Rheumatol. 2025 Aug 12;7(10):e670–1. doi: 10.1016/S2665-9913(25)00217-6.
[81] Conrad N, Verbeke G, Molenberghs G, Goetschalckx L, Callender T, Cambridge G, et al. Autoimmune diseases and cardiovascular risk: a population-based study on 19 autoimmune diseases and 12 cardiovascular diseases in 22 million individuals in the UK. Lancet 2022 Sep 3;400(10354):733–43. doi: 10.1016/S0140-6736(22)01349-6.
[82] Mobasheri A, Loeser R. Clinical phenotypes, molecular endotypes and theratypes in OA therapeutic development. Nat Rev Rheumatol 2024 Sep;20(9):525–6. doi: 10.1038/s41584-024-01126-4.
[83] Angelini F, Widera P, Mobasheri A, Blair J, Struglics A, Uebelhoer M, et al. Osteoarthritis endotype discovery via clustering of biochemical marker data. Ann Rheum Dis 2022 May;81(5):666–75. doi: 10.1136/annrheumdis-2021-221763.
[84] Conaghan P, Guermazi A, Katz N, Bihlet A, Rom D, Perkins M, et al. LEVI-04, a novel neurotrophin-3 inhibitor, substantially improves pain and function without deleterious effects on joint structure in people with knee osteoarthritis: a randomized controlled phase ii trial. presented at: ACR Convergence 2024; 2024; https://acrabstracts.org/abstract/levi-04-a-novel-neurotrophin-3-inhibitor-substantially-improves-pain-and-function-without-deleterious-effects-on-joint-structure-in-people-with-knee-osteoarthritis-a-randomized-controlled-phase-ii/ American College of Rheumatology
[85] Wang Y, Jones G, Keen HI, Hill CL, Wluka AE, Kasza J, et al. Methotrexate to treat hand osteoarthritis with synovitis (METHODS): an Australian, multisite, parallel-group, double-blind, randomised, placebo-controlled trial. Lancet 2023 Nov 11;402(10414):1764–72. doi: 10.1016/s0140-6736(23)01572-6.
[86] Kingsbury SR, Tharmanathan P, Keding A, Watt FE, Scott DL, Roddy E, et al. Pain reduction with oral methotrexate in knee osteoarthritis: a randomized, placebo-controlled clinical trial. Ann Intern Med 2024 Sep;177(9):114556. doi: 10.7326/m24-0303.
[87] Fleischmann RM, Bliddal H, Blanco FJ, Schnitzer TJ, Peterfy C, Chen S, et al. A phase II trial of lutikizumab, an anti-interleukin-1α/β dual variable domain immunoglobulin, in knee osteoarthritis patients with synovitis. Arthritis Rheumatol 2019 Jul;71(7):1056–69. doi: 10.1002/art.40840.
[88] Schieker M, Conaghan PG, Mindeholm L, Praestgaard J, Solomon DH, Scotti C, et al. Effects of interleukin-1β inhibition on incident hip and knee replacement: exploratory analyses from a randomized, double-blind, placebo-controlled trial. Ann Intern Med 2020 Oct 6;173(7):509–15. doi: 10.7326/m20-0527.
[89] Heijman MWJ, Fiolet ATL, Mosterd A, Tijssen JGP, van den Bemt BJF, Schut A, et al. Association of low-dose colchicine with incidence of knee and hip replacements: exploratory analyses from a randomized, controlled, double-blind trial. Ann Intern Med 2023 Jun;176(6):737–42. doi: 10.7326/m23-0289.
[90] Cohen S, Conaghan P, Hochberg M, Kivitz A, Joy N, Jackson D, et al. Sustained clinical effects after a single intra-articular injection of PCRX-201 for moderate-to-severe osteoarthritis of the knee. presented at: ACR Convergence 2024; November 17, 2024; https://acrabstracts.org/abstract/sustained-clinical-effects-after-a-single-intra-articular-injection-of-pcrx-201-for-moderate-to-severe-osteoarthritis-of-the-knee/
[91] Donatello Study Group. DONATELLO: -a phase 1b randomized controlled trial evaluating safety and pharmacodynamics of a novel IL-1Ra gene therapy (GNSC-001) injection for knee OA: 6-month interim results abstract. Aging Clinical and Experimental Research 2025;37(Suppl):678.
[92] Bliddal H, Bays H, Czernichow S, Uddén Hemmingsson J, Hjelmesæth J, Hoffmann Morville T, et al. Once-weekly semaglutide in persons with obesity and knee osteoarthritis. N Engl J Med 2024 Oct 31;391(17):1573–83. doi: 10.1056/NEJMoa2403664.
[93] Pan F, Wang Y, Lim YZ, Urquhart DM, Estee MM, Wluka AE, et al. Metformin for knee osteoarthritis in patients with overweight or obesity: a randomized clinical trial. JAMA 2025 May 27;333(20):1804–12. doi: 10.1001/jama.2025.3471.

Ann Rheum Dis 85 (2026) 1694–1703

Contents lists available at ScienceDirect

Annals of the Rheumatic Diseases

journal homepage: https://www.sciencedirect.com/journal/annals-of-the-rheumatic-diseases

Rheumatoid arthritis

Uncovering the heterogeneity of care trajectories leading up to a rheumatoid arthritis diagnosis: a Swedish 10-year study

Maxime Raffray *, Helga Westerlind, Bénédicte Delcoigne, Thomas Frisell, Johan Askling

Division of Clinical Epidemiology, Department of Medicine Solna, Karolinska Institutet, Stockholm, Sweden

ARTICLE INFO

Article history:
Received 31 October 2025
Received in revised form 11 May 2026
Accepted 2 June 2026

ABSTRACT

Objectives: This study aimed to identify types of care trajectories leading to rheumatoid arthritis (RA) diagnosis, and to identify if, and when, such trajectories deviate from those in the general population.

Methods: We included patients with a first-ever RA diagnosis between 2016 and 2020 in the Swedish nationwide multiregister system and matched general population controls. We performed group-based multitrajectory modelling on 9 healthcare components over the 10 years preceding the index date, grouping patients based on their pattern of healthcare use. We described these groups, or 'types of trajectories', and compared these to those of the matched population controls.

Results: Based on 6824 patients with seropositive RA, we describe 5 trajectories: (i) Healthy (60%), low healthcare use across all care components; (ii) High sick leave (18%), no musculoskeletal (MSK) or infection-related inpatient care but high sick leave; (iii) Chronic pain (10%), high use of analgesics with frequent MSK-related inpatient care; (iv) High infection (9%), frequent infection-related inpatient use; and (v) High burden (3%), with an overall high use of healthcare. Deviations from the 'expected' trajectories in the general population emerged as early as 10 (types 1, 3, 5), 3 (type 4), and 2 years (type 2) before the index date.

Conclusions: Individuals with new-onset RA can be grouped into clusters, each with its own signature in terms of pre-RA healthcare resource utilisation and deviation from the expected years before the RA diagnosis. Our results open for identification of individuals at elevated risk, for potential preventive action, and may highlight aetiopathologically important events.

INTRODUCTION

Rheumatoid arthritis (RA) is a chronic inflammatory joint disease where early diagnosis and institution of effective antirheumatic therapy are recognised to be of critical importance for its long-term outcome [1–4]. Despite efforts to shorten the time to RA diagnosis, substantive delays between RA symptom onset and RA diagnosis are well documented, with both patient- and provider-level factors at play. For instance, in the recent pragmatic 4-arm NORD-STAR (Nordic Rheumatic Diseases Strategy Trials and Registries) clinical trial of newly diagnosed RA, patients were randomised to their study treatment within 48 hours of their RA diagnosis. At that time point, however, the average duration of RA symptoms amounted to 6 months [5].

Previous studies have shown a rapid increase in ambulatory care utilisation and a decrease in work ability during the year before the diagnosis of RA [6–8]. Although these observations pertain to the period of RA symptom onset imminent to

*Correspondence to Dr. Maxime Raffray, Division of Clinical Epidemiology, Department of Medicine Solna, Karolinska Institutet, Solna, Sweden.
E-mail address: maxime.raffray@ki.se (M. Raffray).
Handling editor Josef S. Smolen.

https://doi.org/10.1016/j.ard.2026.06.004

0003-4967/© 2026 The Author(s). Published by Elsevier B.V. on behalf of European Alliance of Associations for Rheumatology (EULAR). This is an open access article under the CC BY license (http://creativecommons.org/licenses/by/4.0/)

WHAT IS ALREADY KNOWN ON THIS TOPIC

- Individuals who later develop rheumatoid arthritis (RA) show increased healthcare use, work disability, and sick leave in the months preceding RA diagnosis.
- Most previous studies have focused on the short period immediately before the RA diagnosis, providing limited understanding of longer-term healthcare trajectories up until the RA diagnosis.

WHAT DOES THIS STUDY ADD

- Using nationwide, longitudinal Swedish register data, this study identified 5 distinct types of prediagnosis care trajectories among individuals later diagnosed with seropositive RA.
- Each trajectory showed its own pattern of deviation from matched population controls, emerging as early as 10, 3, or 2 years before the RA diagnosis, depending on the trajectory type.

HOW MIGHT THIS AFFECT RESEARCH, PRACTICE OR POLICY

- The identification of distinct, trajectory-specific windows of deviation provides opportunities for earlier detection and preventive action in subgroups of individuals at higher risk of developing RA.
- These findings inform risk stratification models, interdisciplinary care pathways, and future research into the mechanisms linking prediagnostic health events to RA onset.

diagnosis, considerably less is known about healthcare trajectories during a longer time span before the clinical RA diagnosis. Yet it is well established that serological markers of RA (antibodies to citrullinated peptides) may appear years before the onset of clinical symptoms and diagnosis [4,9].

Together, these observations raise the question of what the healthcare trajectories among individuals later diagnosed with RA look like. Specifically, (i) how do the care trajectories among individuals later diagnosed with RA differ from those in the general population? (ii) Are there different 'typical' care trajectories among individuals later diagnosed with RA? (c) Can time points or windows be identified during which trajectories in individuals or groups of individuals later diagnosed with RA start to deviate from those in the general population?

In this study, our objectives were (i) to identify and describe types of pre-RA diagnosis care trajectories, and (ii) to investigate if and when any such trajectories start to deviate from those in the general population.

METHODS

We performed a cohort study based on prospectively recorded longitudinal data from Swedish clinical and other registers linked together.

Data sources

The register linkage used in this study has been described in detail elsewhere [10]; we provide an overview in Supplementary Table S1. In brief, we used an extraction from the Swedish national registers, including all individuals with a chronic inflammatory disease diagnosis, along with a general population sample. Using unique personal identifiers, we linked together information on diagnoses and procedures recorded in inpatient and outpatient speciality care (National Patient Register [NPR], no primary care) with all filled prescriptions at pharmacies (Prescribed Drug Register [PDR], primary and speciality care), causes of death, and demographics (census and taxation registers).

Setting, study population, and definition of index date

In Sweden, RA is diagnosed and managed by rheumatologists, typically at hospital-based outpatient clinics. More than 95% of all care for RA is managed via public care providers. We identified all individuals with a first-ever primary or contributory diagnosis code (International Classification of Diseases 10th revision [ICD10]) in speciality care (any speciality) for RA between January 1, 2016 and December 12, 2020. For inclusion, we required at least 1 second visit listing RA within 180 days, or at least 2 visits within 365 days of the first RA diagnosis.

We studied healthcare utilisation during the 10 years leading up to the index date, which we defined as the earliest of (i) the first visit listing an RA diagnosis in speciality care, (ii) the first visit listing any inflammatory arthritis diagnosis (ICD10: M12, M13, M07, M08, M09, M45, M46) in speciality care, or (iii) the first dispensation of an RA disease-modifying antirheumatic drug (DMARD). The rationale behind this definition was that the first-ever RA diagnosis may not be the actual starting point at which RA is first recognised and/or actively treated. For instance, many individuals diagnosed with RA receive an initial diagnosis of 'polyarthritis' during workup. Defining index date as the first occurrence of an RA diagnosis would thus introduce an artificial delay, with a mix-up of healthcare resource utilisation before and clinical intervention against the incident RA. For sensitivity analyses, we defined a secondary definition of index date as the first visit listing RA, disregarding any previous inflammatory arthritis diagnosis or DMARD use. We treated seropositive and seronegative RA separately, based on diagnosis codes, with seropositive RA defined as M05*, M060L, or M068L, and seronegative RA defined as M06*. The approach ICD-code–based approach to define a diagnosis of RA has been previously positively validated in the Swedish context, with 91% of cases correctly diagnosed with RA when comparing with chart review [11]. Preliminary data in our population validating ICD codes vs serology indicate good positive predictive values of a clinical diagnosis of 'seropositive RA', ranging from 94% to 98% depending on the definition of RA seropositivity from stored sera [12]. In addition, in a recent US study, the use of ICD-10 was described as a reasonable proxy to identify seropositive and seronegative RA with high sensitivity and positive predictive values [13]. For each unique individual with RA, we matched 5 control subjects from the Swedish general population, on sex, age, and region of residence at the year of the RA case's index date.

Data collection

From the Swedish Population Register and the Longitudinal database for insurance and labour market studies (LISA), we extracted information on country of birth, marital status, and the highest educational level achieved by the index date. From the NPR and the PDR, we extracted data on the history of comorbidities up until the index date; see Supplementary Table S2 for a complete list [14]. To compose care trajectories, we extracted healthcare and sick leave use during the 10 years leading up to the index date. Healthcare use was extracted from the NPR and PDR, and sick leave from the LISA database. Based on these data, we defined 9 care components covering aspects of possible symptoms or symptomatic treatment heralding RA. This

included (i) inpatient care: musculoskeletal (MSK)-related diagnoses or hospitalisations, infection-related diagnoses or hospitalisations, and all other hospitalisations; (ii) outpatient care: visits in any medical speciality, fillings of nonsteroidal anti-inflammatory drugs (NSAIDs), analgesics other than NSAIDS, glucocorticoids, and antibiotics; and (iii) days on sick leave. Detailed information on diagnosis and drug codes is available in Supplementary Table S3. In the sensitivity analysis, for the secondary definition of the index date, we included a tenth component: fillings of DMARDs. We then summed the counts of each care component in 6-month periods throughout the 10 years up until the index date (thus, a total of 20 six-month bins).

Statistical analysis

We performed a group-based multitrajectory (GBMT) analysis to identify distinct care trajectories leading up to the RA diagnosis. GBMT analysis identifies latent groups of individuals who follow similar trajectories across multiple indicators of an outcome [15]. In our study, the outcome was RA diagnosis, and the indicators were the 9 care components described above. The number of trajectory groups is a parameter specified a priori by the researchers. Using a stepwise approach, we evaluated models with 1 to 7 groups. We used the GBMT package for R (version 4.3.2; R Core Team, 2023) [16] to fit regression models with a 2-degree polynomial function of time. First, the models estimated a set of average trajectories, 1 per group, which described the evolution of the care components over the 10-year period preceding the index date. Then, each individual was assigned a probability of belonging to each group, based on how well their data fitted each group's estimated trajectories. Individuals were assigned to the group for which this probability was the highest. We repeated the modelling in a stepwise approach, changing the number of groups from 1 to 7. We chose the number of groups that allowed a balance between representing the complexity of the data (goodness of fit measures) and clinical interpretability. At each step, we visually inspected the shapes of the trajectories and described each group to determine the most optimal, clinically relevant number of groups to settle on. The complete set of trajectories from 1 to 7 groups provided by the models is available in Supplementary Figures S1 and S2, along with the goodness of fit of the models (Supplementary Table S4) and the checklist for reporting on latent trajectory studies (Guidelines for Reporting on Latent Trajectory Studies Checklist, Supplementary Table S5). To assess the validity of the solution, we performed a series of analyses, including random starts and bootstrap sampling (Extended methods supplement, page 9). We will refer to the groups of individuals we identified as 'types of trajectories' throughout the article. We next compared the characteristics and healthcare use of RA cases between each of the trajectories observed by plotting the average healthcare use during a 6-month period per 100 patients (visits, fills, or days) during the 10 years before RA diagnosis. To assess deviations from the general population over time, we plotted this average healthcare use for each type of trajectory alongside the average healthcare use of the population controls matched to the individuals assigned to each trajectory. The above analyses were performed separately for seropositive and seronegative RA. After applying the GBMT analysis to the RA population, we performed the clustering and description on the general population controls to check if we could find qualitatively and quantitatively the same groups and thus assess to what extent our results were specific to the RA population.

Patient and public Involvement

We gratefully acknowledge the contribution of Kerstin Vikman, patient research partner, for her feedback regarding the interpretation of the results (Swedish Rheumatology Association, Reumatikerförbundet R-1013521).

RESULTS

We included 6824 individuals with seropositive RA and 4189 individuals with seronegative RA (Fig 1). For 79% of individuals with seropositive RA, the index date was defined by the first-ever RA diagnosis. For 15%, the index date was based on a preceding diagnosis of inflammatory arthritis (median time 89 days before the first listing of RA, IQR [29-217] days), and for 6%, a dispensation of a DMARD (median time 134 days before the first listing of RA, IQR [83-308] days). At the time of the index date, individuals with seropositive RA were younger (61 vs 65 years) and more often female (71% vs 62%) than those with seronegative RA (Table 1).

The types of trajectories identified

For seropositive RA, we identified 5 types of pre-RA diagnosis trajectories (Fig 2, Table 2). Type 1, referred to as the 'healthy' type, comprised 60.2% of all seropositive RA (n = 4108) and was characterised by an absence of MSK- and infection-related inpatient care and low healthcare use across all care components, including sick leave. Median age was 60 years, and 69% were women (Table 2). History of comorbidities in this trajectory was less frequent than in the other trajectories, and also vs their matched population controls. Similarly to type 1, type 2, or the 'high sick leave' type (n = 1251, 18.3% of all seropositive RA), was characterised by an absence of MSK- and infection-related inpatient use. However, the sick leave throughout the 10 years was among the highest of all RA cases. Median age was 56 years, and the proportion of women was higher compared with the other groups, 79.6% (Table 2). Type 3, or the 'chronic pain' type (n = 687, 10.1%), was characterised by high and constant use of analgesics and NSAIDs with frequent inpatient use for MSK diagnoses and outpatient visits. Median age was 67 years, and the socioeconomic profile was that of a lower educational level than in types 1 and 2. Type 4, or the 'high infection' type (n = 592, 8.7%), was characterised by frequent infection-related inpatient use throughout the 10 years. Median age was 72 years. Type 5, or the 'high-burden' type (n = 186, 2.7%), was characterised by frequent use of healthcare in general. Compared with type 4, type 5 had a higher long-term analgesic use and outpatient care use. Median age was 67 years.

Deviations from the matched controls' average trajectories

In addition to the differences between each type of trajectory preceding RA diagnosis, we observed deviations between each of the 5 trajectories, and that of the population controls individually matched to each RA case in each trajectory (Fig 3). For seropositive RA, and for type 1, 'the healthy' type, the average healthcare use was only higher than the matched controls in the year before the index date. Throughout the

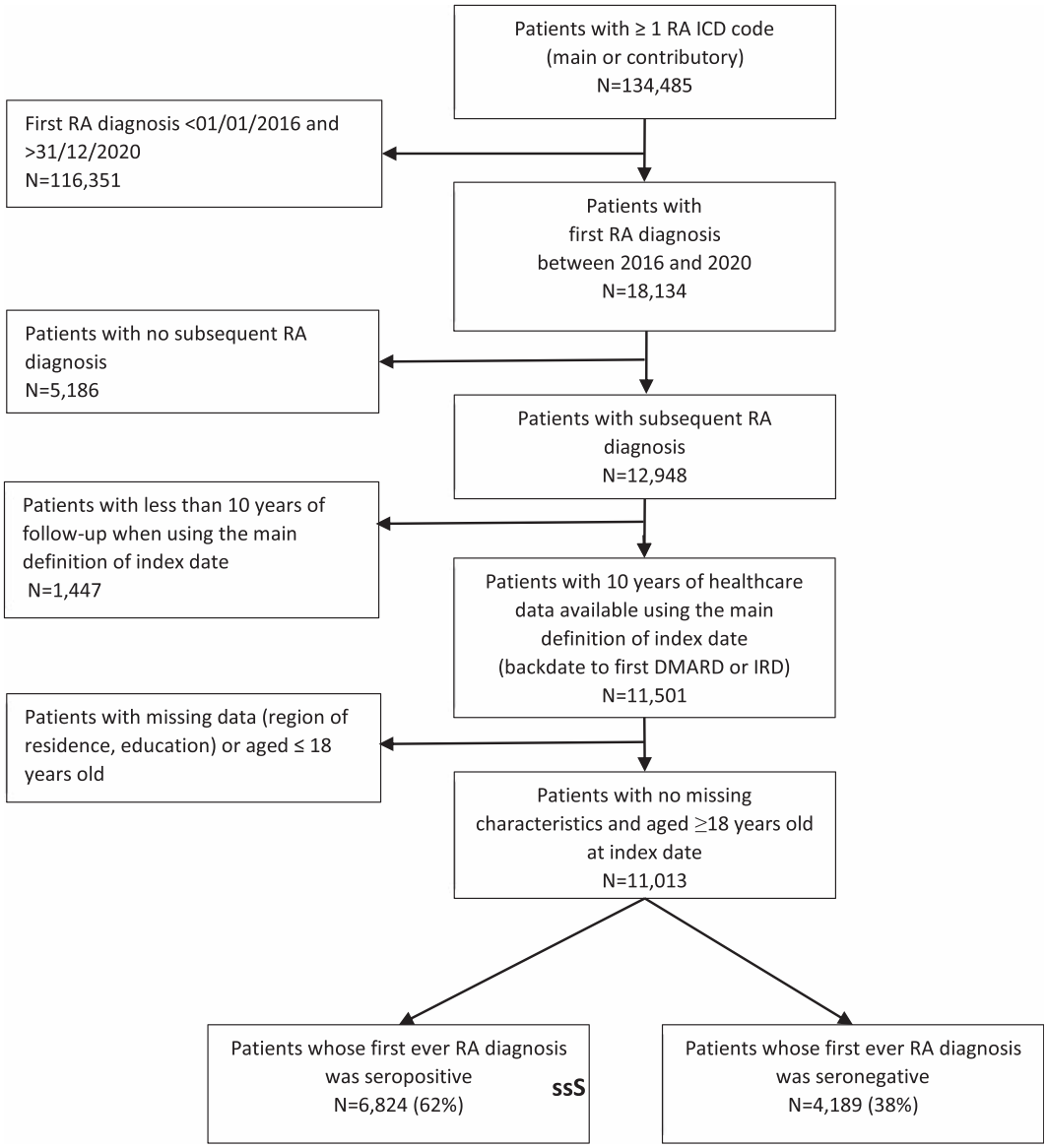

Figure 1. Flowchart. DMARD, disease-modifying antirheumatic drug; IRD, Inflammatory Rheumatic Diseases; ICD, International Classification of Diseases, 10th revision; RA, rheumatoid arthritis.

10 years, their average sick leave burden was lower compared with their matched controls. For type 2, the 'high sick leave' type, the mean healthcare use across most components was on par with that of their matched controls up until 2 years before the index date. The exception was the mean sick leave use, which was already higher from the beginning of the observation period (ie, 10 years before the index date) and with a constant increase during the last 5 years until the index date. For type 3, the 'chronic pain' type, we observed a higher MSK-related use of inpatient care, and higher use of analgesics and NSAIDs, already from the start of the observation period. Among the RA cases in this trajectory, 80% had at least 1 filling of a prescription for analgesics between the years 10 and 6 before RA diagnosis vs 41% of their matched general population controls (Supplementary Table S6). For type 4, the 'high infection' type, outpatient visits sharply increased 3 years before the index date. Inpatient use for infections was more frequent among RA cases compared with controls throughout the 10 years, with a sharp increase in the last 2 years. For type 5, the 'higher-burden' type, most of the care use was higher than the matched control population, starting already 10 years before the RA diagnosis. Compared with their matched controls, the use of glucocorticoids increased starting from the fifth year before RA diagnosis.

The seronegative RA group

The seronegative group had similar mean healthcare use compared with seropositive RA throughout the 10-year observation period, aside from a higher mean inpatient use listing MSK diagnoses (Supplementary Fig S3).

Among those with seronegative RA, we identified 4 distinct pre-RA trajectories (Supplementary Tables S7 and S8, Supplementary Figs S4 and S5), all of which were qualitatively similar to those of seropositive RA. When assigning 5 groups in the seronegative RA group, a trajectory corresponding to seropositive RA type 4, 'high infection' type (8.7% of seropositive RA cases), was found in only 1% of the seronegative RA population. In the 4 trajectory type configurations, the first type (n = 2345, 56%, median age 67) was similar to seropositive RA type 1, 'the healthy' type (60.2%, median age 60); the second type (n = 1054, 25.2%, median age 66) was similar to seropositive RA type 3 'chronic pain' type (10.1%, median age 67); the third type (n = 617, 14.7%, median age 58) was similar to

Table 1
Characteristics of the study population at the index date

Characteristic	Seropositive RA N = 6824	Population controls to seropositive RA N = 33,096	Seronegative RA N = 4189	Population controls to seronegative RA N = 20,297	Overall N = 64,406
Age in years (median, Q1-Q3)	61 (49, 72)	61 (49, 72)	65 (53, 74)	65 (53, 74)	63 (50, 73)
Women, n (%)	4870 (71.4)	23,655 (71.5)	2578 (61.5)	12,494 (61.6)	43,597 (67.7)
Region of birth, n (%)					
Sweden	5602 (82.1)	27,087 (81.8)	3529 (84.2)	16,828 (82.9)	53,046 (82.4)
Europe, other than Sweden	655 (9.6)	3303 (10.0)	384 (9.2)	1940 (9.6)	6282 (9.8)
Outside Europe	567 (8.3)	2,706 (8.2)	276 (6.6)	1529 (7.5)	5,078 (7.9)
Married, n (%)	3275 (48.0)	16,534 (50.0)	2242 (53.5)	10,247 (50.5)	32,298 (50.1)
Highest education level, n (%)					
≤High school	3630 (53.2)	15,709 (47.5)	2235 (53.4)	10,012 (49.3)	31,586 (49.0)
>High school	3194 (46.8)	17,387 (52.5)	1954 (46.6)	10,285 (50.7)	32,820 (51.0)
Annual disposable income in thousands € (median, Q1-Q3)	18,964 (13,528, 26,682)	20,164 (13,779, 28,586)	19,135 (13,830, 27,522)	19,395 (13,705, 28,520)	19,694 (13,731, 28,277)
History of comorbidities,[a] n (%)					
Cardiovascular	435 (6.4)	2048 (6.2)	368 (8.8)	1507 (7.4)	4358 (6.8)
Noncardiac vascular	1452 (21.3)	6897 (20.8)	1067 (25.5)	4798 (23.6)	14,214 (22.1)
Respiratory	255 (3.7)	622 (1.9)	130 (3.1)	418 (2.1)	1425 (2.2)
Gastrointestinal	376 (5.5)	1791 (5.4)	301 (7.2)	1154 (5.7)	3622 (5.6)
Psychiatric	1198 (17.6)	5833 (17.6)	752 (18.0)	3406 (16.8)	11,189 (17.4)
Renal	41 (0.6)	241 (0.7)	31 (0.7)	180 (0.9)	493 (0.8)
Infectious	396 (5.8)	1357 (4.1)	227 (5.4)	1001 (4.9)	2981 (4.6)
Endocrine	1417 (20.8)	5370 (16.2)	933 (22.3)	3394 (16.7)	11,114 (17.3)
Cancer	480 (7.0)	2761 (8.3)	363 (8.7)	1939 (9.6)	5543 (8.6)
Neurological	455 (6.7)	1312 (4.0)	330 (7.9)	841 (4.1)	2938 (4.6)

RA, rheumatoid arthritis.
[a] Within 5 years before the index date.

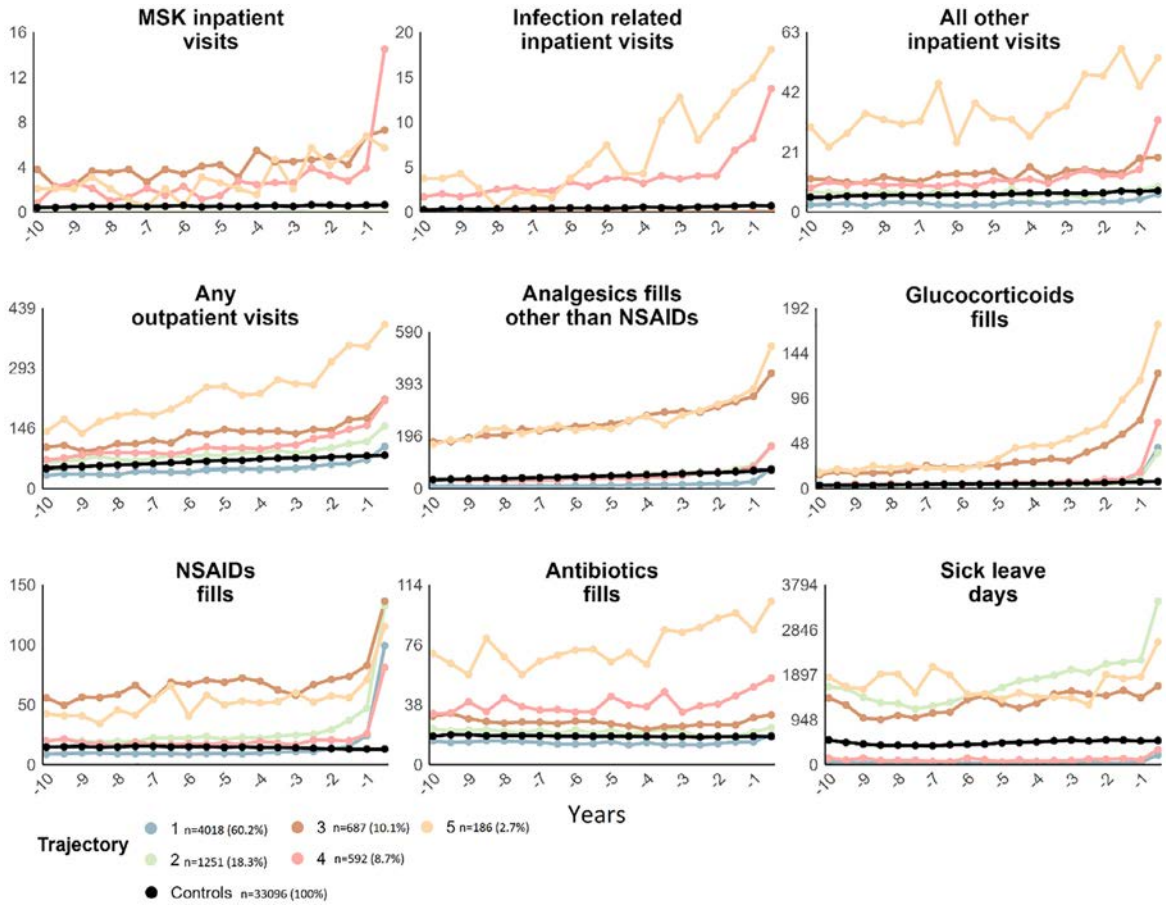

Figure 2. Types of care trajectories leading up to seropositive RA diagnosis (n = 6824). The 5 types of trajectories are displayed as the coloured curves. The trajectory of the general population sample matched to the entire seropositive group (controls) is displayed as the black curve. For each care component, the y-axis represents the mean healthcare use during a 6-mo period per 100 patients (visits, fills, or days). The x-axis denotes the years before the index date; the latter is defined as the first visit listing an RA diagnosis, an inflammatory arthritis diagnosis, or the first dispensation of a DMARD. DMARD, disease-modifying antirheumatic drug; MSK, musculoskeletal; NSAID, nonsteroidal anti-inflammatory drug; RA, rheumatoid arthritis.

Table 2

Characteristics of individuals with seropositive RA, stratified by the type of trajectory (n = 5), and of the general population sample matched to each individual with RA

	Type 1 Healthy (n = 4108, 60.2%)		Type 2 High sick leave (n = 1251, 18.3%)		Type 3 Chronic pain (n = 687, 10.1%)		Type 4 High infection (n = 592, 8.7%)		Type 5 Higher burden (n = 186, 2.7%)	
Characteristic	Cases	Controls	Cases	Controls	Cases	Controls	Cases	Controls	Cases	Controls
Age in years (median, Q1-Q3)	60 (46, 72)	60 (47, 72)	56 (47, 63)	56 (47, 63)	67 (58, 74)	67 (58, 74)	72 (62, 78)	72 (62, 78)	67 (57, 73)	67 (57, 73)
Women	2879 (70.1)	13982 (70.1)	996 (79.6)	4889 (79.7)	484 (70.5)	2364 (70.7)	376 (63.5)	1809 (63.8)	135 (72.6)	665 (73.0)
Region of birth, n (%)										
Sweden	3313 (80.6)	16,302 (81.8)	1051 (84.0)	4869 (79.4)	589 (85.7)	2789 (83.4)	496 (83.8)	2416 (85.2)	153 (82.3)	768 (84.3)
Europe, other than Sweden	394 (9.6)	1961 (9.8)	109 (8.7)	616 (10.0)	60 (8.7)	353 (10.5)	66 (11.1)	294 (10.4)	26 (14.0)	87 (9.5)
Outside Europe	401 (9.8)	1672 (8.4)	91 (7.3)	651 (10.6)	38 (5.5)	204 (6.1)	30 (5.1)	127 (4.5)	7 (3.8)	56 (6.1)
Married, n (%)	2053 (50.0)	9845 (49.4)	550 (44.0)	3117 (50.8)	325 (47.3)	1751 (52.3)	272 (45.9)	1375 (48.5)	75 (40.3)	486 (53.3)
Highest education level, n (%)										
≤High School	2053 (50.0)	9240 (46.4)	634 (50.7)	2624 (42.8)	445 (64.8)	1819 (54.4)	370 (62.5)	1569 (55.3)	128 (68.8)	490 (53.8)
>High School	2055 (50.0)	10695 (53.6)	617 (49.3)	3512 (57.2)	242 (35.2)	1527 (45.6)	222 (37.5)	1268 (44.7)	58 (31.2)	421 (46.2)
Annual disposable income in thousands € (median, Q1-Q3)	19,593 (13,357, 27,973)	20,173 (13,708, 28,472)	20,842 (15,349, 26,578)	23,016 (15,366, 30,412)	16,631 (13,155, 22,931)	18,253 (13,610, 27,815)	16,073 (12,893, 23,131)	16,519 (12,989, 25,119)	14,744 (12,026, 19,849)	18,364 (13,602, 27,725)
History of comorbidities[a], n (%)										
Cardiovascular	176 (4.3)	1212 (6.1)	71 (5.7)	219 (3.6)	72 (10.5)	266 (7.9)	84 (14.2)	286 (10.1)	32 (17.2)	73 (8.0)
Noncardiac vascular	724 (17.6)	4048 (20.3)	224 (17.9)	877 (14.3)	234 (34.1)	883 (26.4)	202 (34.1)	859 (30.3)	68 (36.6)	243 (26.7)
Respiratory	97 (2.4)	364 (1.8)	29 (2.3)	93 (1.5)	50 (7.3)	75 (2.2)	50 (8.4)	74 (2.6)	29 (15.6)	16 (1.8)
Gastrointestinal	166 (4.0)	1053 (5.3)	77 (6.2)	309 (5.0)	53 (7.7)	213 (6.4)	53 (9.0)	169 (6.0)	27 (14.5)	52 (5.7)
Psychiatric	432 (10.5)	3417 (17.1)	360 (28.8)	1133 (18.5)	221 (32.2)	621 (18.6)	112 (18.9)	523 (18.4)	73 (39.2)	155 (17.0)
Renal	15 (0.4)	153 (0.8)	6 (0.5)	29 (0.5)	7 (1.0)	30 (0.9)	6 (1.0)	24 (0.8)	7 (3.8)	5 (0.5)
Infectious	3 (0.1)	770 (3.9)	0 (0.0)	190 (3.1)	0 (0.0)	164 (4.9)	276 (46.6)	191 (6.7)	117 (62.9)	44 (4.8)
Endocrine	740 (18.0)	3140 (15.8)	267 (21.3)	844 (13.8)	188 (27.4)	661 (19.8)	149 (25.2)	592 (20.9)	73 (39.2)	145 (15.9)
Cancer	209 (5.1)	1616 (8.1)	84 (6.7)	388 (6.3)	67 (9.8)	331 (9.9)	72 (12.2)	342 (12.1)	48 (25.8)	98 (10.8)
Neurological	172 (4.2)	743 (3.7)	135 (10.8)	241 (3.9)	74 (10.8)	149 (4.5)	49 (8.3)	131 (4.6)	25 (13.4)	50 (5.5)

RA, rheumatoid arthritis.

[a] Within 5 years of the index date.

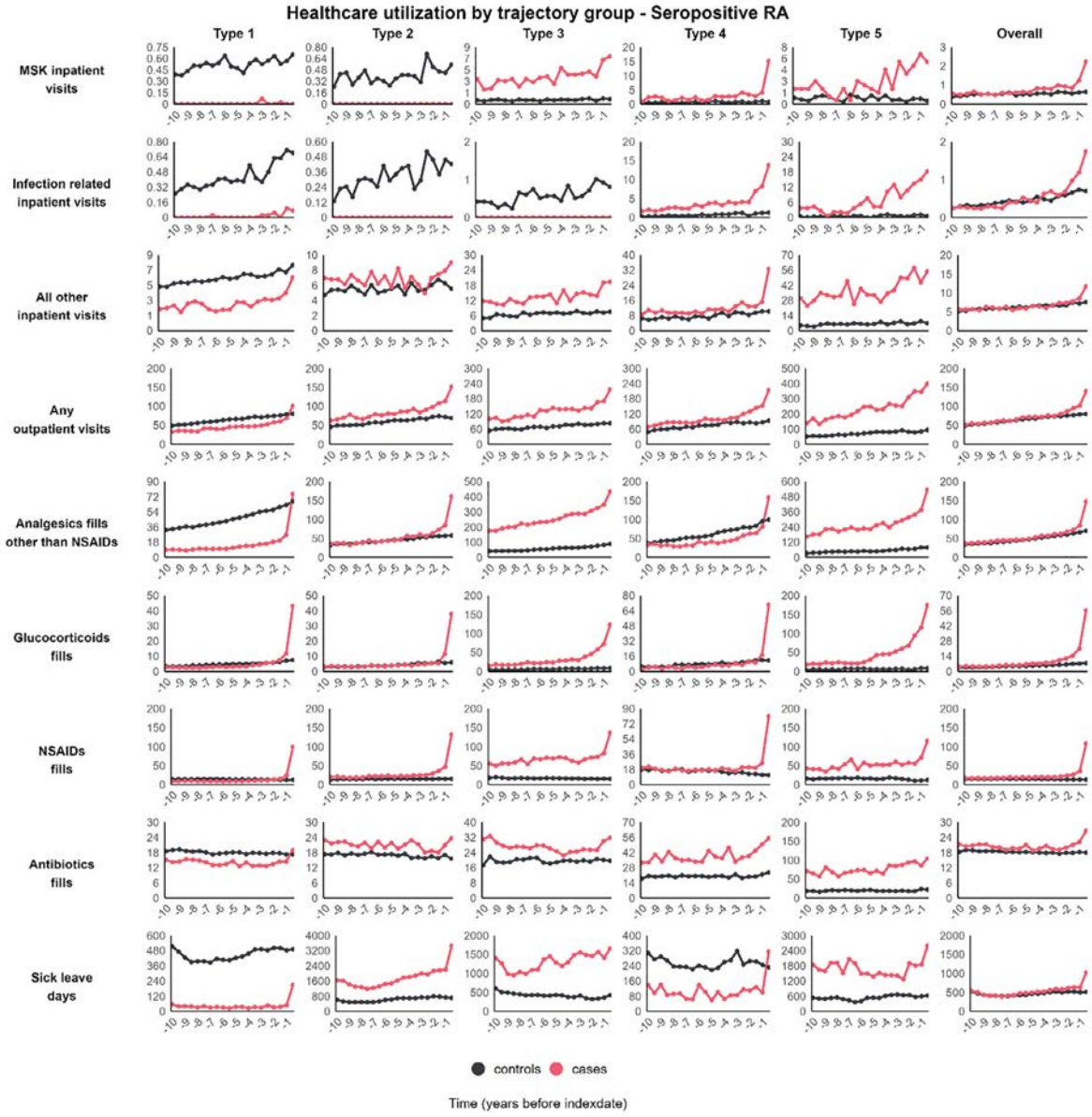

Figure 3. Healthcare use 10 years before the index date for RA cases whose first diagnosis was seropositive (red) and their matched general population control (black), stratified by type of trajectory. The y-axis represents the mean healthcare use per 100 patients per 6-mo period (either visits, dispensations, or days). The x-axis denotes the 10 years leading up to the index date, RA diagnosis. Note that the purpose of the figure is to compare deviations from controls within each type and thus be aware of the changing y-scale between types of trajectory. MSK, musculoskeletal; NSAID, nonsteroidal anti-inflammatory drug; RA, rheumatoid arthritis.

seropositive RA type 2, 'high sick leave' type (18.3%, median age 56); and the fourth type (n = 173, 4.1%, median age 72) was similar to seropositive RA type 5, the 'higher-burden' type (2.7%, median age 67).

Sensitivity analyses

In sensitivity analyses in which the index date was defined without attention to previous DMARD use (Supplementary Tables S9-S12 and Supplementary Figs S6-S11), most trajectory types previously described remained, and most of their characteristics were consistent with those of the primary analysis.

When performing the same GBMT analysis among the general population controls, we found qualitatively and quantitatively similar 'healthy', 'high sick leave', and 'higher-burden' types (Supplementary Fig S12 and Supplementary Table S13). However, although the 'chronic pain' and 'high infection' types found within RA cases shared similarities with 2 types found within the general population regarding some care components, we observed differences in others, particularly regarding the use of analgesics and glucocorticoids.

DISCUSSION

In this nationwide register-based study, we uncovered 5 distinct types of care trajectories leading up to RA diagnosis: 'the healthy' type (type 1), the 'high sick leave' type (type 2), the 'chronic pain' type (type 3), the 'high infection' type (type 4), and the 'high-burden' type (type 5), each with its own deviation from the general population's healthcare utilisation, in some instances years before the RA diagnosis.

Previous studies have found that individuals who go on to develop RA already experience rising healthcare use, sick leave, and work disability in the months before diagnosis. They consult

primary care and specialists more often, undergo more imaging, and accrue higher medical costs [6–8,17]. To some extent, such findings are inherent by design (as RA is not diagnosed without a workup). Here, we expand on those studies by demonstrating the heterogeneity of patient journeys up until RA beyond the established overall increase of care near the time of diagnosis, and how they deviate, all in their own manner, from the average healthcare use in matched general population subjects. Those deviations can be interpreted as windows of opportunity for earlier identification of individuals at elevated risk of future RA.

Importantly, our findings suggest that for a large group of individuals newly diagnosed with RA, the prospect of earlier clinical identification seems limited. Indeed, over half of the RA population fell in the 'healthy' type (type 1, 60%), sharing low-profile, quiet trajectories in terms of healthcare utilisation throughout the 10 years up until the last year before RA diagnosis. In contrast, fewer individuals shared the 'high sick leave' type of trajectory (type 2, 18%), with observed deviations in analgesics dispensation (including NSAIDs) as early as 2 years before RA diagnosis. In addition, their average number of sick leave days was triple that of the general population during and before that period (21 days vs 8 days per individual in a 6-month window). This suggests that—for such individuals—there is indeed an opening for earlier identification and intervention. For the 'high infection' type (type 4, 8.7%), we found an average number of inpatient stays for infections and antibiotics dispensations that were higher than those in the general population throughout the 10-year period. Starting 3 years before RA diagnosis, the overall healthcare use increased sharply, including outpatient visits. Notably, the RA cases within this type were older and presented with a more frequent history of comorbidity than both the matched general population and other RA cases. These findings suggest that improving the management of comorbidities might reduce the risk of progression to RA. The potential role of recurrent infections in the development of RA within this subgroup warrants further investigation. The increased infection rates observed before diagnosis could be consistent with both a causal effect of infections on disease onset and an increased susceptibility to infections, possibly caused by inflammatory or immune-mediated disease processes during the pre-RA phase. The 'chronic pain' type (type 3, 10%) showed a long history of MSK inpatient stays and dispensations of analgesics, including averages notably higher than those of other types and the matched general population. This deviation was observed already from the start of the observation period, 10 years before RA diagnosis. We argue that these patients could be individuals who experience difficulties in reaching a definitive diagnosis in the form of RA and/or co-occurring MSK complaints unrelated to RA, thus suggesting a wide time window for RA identification.

Age and sex are common factors associated with healthcare use. We performed the trajectory analysis solely on longitudinal healthcare data, not conditioning on age and sex. When examining the characteristics of and differences between the types of trajectories, we observed variations in age and sex (defined as biological sex, male/female, as recorded in medical records), but also socioeconomic status, eg, type 2 contains more women than the other types (80% vs 71% overall). However, this was not an absolute 1:1 relationship, ie, not all women were grouped into one type of trajectory. This indicates that although there is an influence of those 'conventional' characteristics, we still capture a heterogeneity of trajectories that arises specifically from a pattern of healthcare use over time. Performing the analysis in a stratified approach, ie, among subgroups of the population, would address age and sex influence. However, this poses the challenging questions of (i) when to end the choice of which factors to stratify on and (ii) the utility of the resulting output. By contrast, and for our second objective of identifying deviations between each trajectory type and the general population, we did account for the influence of age and sex by matching the RA cases and their population controls on those factors before the trajectory analysis. We observed variations in average socioeconomic status across the different trajectory types, which may partly explain the shape and intensity of some healthcare utilisation patterns. The most evident example concerns the 'high burden' trajectory, for which the interplay between lower education level, lower income, and a higher burden of comorbidities is well documented and may contribute to more frequent healthcare use [18,19]. In addition, the 'chronic pain' trajectory, marked by sustained pain medication use several years before RA diagnosis, may reflect diagnostic delay or diagnostic wandering, with prolonged symptomatic management of nonspecific MSK complaints rather than early recognition of inflammatory disease. The lower socioeconomic status observed in this group may contribute to a higher prevalence of mechanically driven MSK pain related to physically demanding occupations. The higher proportion of women in the 'sick leave' trajectory type (80% vs 71% overall) might reflect the fact that women have substantially higher rates of sick leave than men, across all ages, and even more pronounced for women with higher socioeconomic status [20].

The question of whether the observed trajectories are specific to RA is important. We performed the same GBMT analysis among the general population controls. Although we found the same 'healthy' and 'high sick leave' types in the general population, we did not find the 'chronic pain' and 'high infection' types (Supplementary Fig S12), indicating that our study does give us insights about the heterogeneity, specifically in the population with RA. Those 2 types represent an interesting point of departure in the search for risk factors for RA. Still, the fact that we identified similar types, including the 'healthy' type encompassing 60% of the population, suggests that there might be patterns of care use specific to later RA development that we could not pick up because they were not as strong as others occurring in the general population at large. In addition, because individuals who develop RA, or any other chronic disease, are also part of the general population, they are bound to share many of the features of care trajectories in the general population. Further, the choice of care components could influence the observed strength of the patterns by either adding (ie, primary care level data, see limitations) or removing (ie, overall outpatient and inpatient visits, sick leave) some components.

Because the method used to identify types of trajectory was an unsupervised data-driven approach, the possibility of identifying spurious patterns should be considered and discussed [21,22]. We acted to minimise such a possibility. First, we reported the process following the reporting guidelines for this method (Supplementary Table S5). Second, regarding the question of how many groups, ie, types of trajectories, to settle on and on which basis, we argue that there is no 'true' nor 'correct' number of groups. Therefore, as Nagin et al [15] developed, the choice of how many groups to settle on cannot be left solely on 'mechanical application of fit statistics and model diagnostics', and we argue for qualitative considerations. For example, a 4-group model might yield better Bayesian Information Criterion or Akaike Information Criterion metrics than a 5-group model. However, the 5-group model might include a new group that has a substantive interest, eg, the identification of a potentially

actionable time window for improvement, and thus should be described. Finally, we performed the trajectory analysis separately among patients with seropositive and seronegative RA, and also among the general population, and found similarities. This could reflect a true observation that both seropositive and seronegative RA share the same types of healthcare use trajectories, which in turn only partially differ from those in the general population, or that our approach did not allow the observation of other true differences (eg, differences in other healthcare use components), or that misclassification between the 2 RA groups occurs. The main difference was the presence of a 'high infection' trajectory type among the seropositive RA population, but not in the seronegative RA population. This may reflect a specific capture of airway infections and, thus, smokers, a risk factor for seropositive RA but not seronegative RA [23].

In our study, the use of a nationwide multiregister linkage allowed the inclusion of RA cases bordering on exhaustiveness in Sweden. We considered multiple components of care use as signals of disease progression (inpatient and outpatient visits, drug dispensations, and sick leaves) with a long observation period (10 years). Furthermore, to avoid confusion in measuring healthcare use during the diagnostic (workup) phase, we defined the index date as the date of the first recorded inflammatory arthritis diagnosis. Some limitations should be considered. In the absence of data on other types of inflammatory or noninflammatory rheumatic conditions other than RA, we cannot tell to what extent the patterns we observed are unique to RA or shared with other conditions. Future studies should seek to replicate these findings in other rheumatic and MSK disease populations and potentially in other healthcare systems to improve the precision of identifying groups at risk of RA. Incorporating primary care data would also contribute to this objective. Indeed, we did not have access to primary care visits, ie, visits to general practitioners or nonphysician care (eg, physiotherapists). However, the medication components we studied included both primary and speciality care, reducing that potential blind spot. The addition of this data could refine our typology by identifying new patterns and thus new windows of opportunity. This is particularly relevant for the 'healthy' type representing 60% of the patients with RA, where early symptoms not recorded in speciality care could be identified. Finally, we cannot exclude misclassification of seronegative vs seropositive RA using the ICD-10 diagnosis code. However, preliminary data validating ICD codes vs serology in our data are reassuring, with positive predictive values of a clinical diagnosis of 'seropositive RA' ranging from 94% to 98% depending on the definition of RA seropositivity from stored sera [12].

To conclude, individuals with new-onset RA can be grouped into clusters, each with its own signature in terms of healthcare resource utilisation and deviation from the expected years before the RA diagnosis. Our results open for identification of individuals at elevated risk, for preventive action, and may highlight aetiopathologically important events.

Competing interests

JA: PI for agreements between Karolinska Institutet and AbbVie, BMS, Eli Lilly, Pfizer, Roche, Samsung Bioepis, and Sanofi for safety monitoring of antirheumatic therapies (ARTIS). BD is partly employed by the ARTIS Swedish national safety monitoring system, for which grants from AbbVie, BMS, Eli Lilly, Pfizer, Roche, Samsung Bioepis, and Sanofi have been received.

CRediT authorship contribution statement

Maxime Raffray: Writing – review & editing, Writing – original draft, Visualization, Methodology, Investigation, Formal analysis, Conceptualization. **Helga Westerlind:** Writing – review & editing, Supervision, Methodology, Data curation, Conceptualization. **Bénédicte Delcoigne:** Writing – review & editing, Methodology. **Thomas Frisell:** Writing – review & editing, Methodology, Data curation, Conceptualization. **Johan Askling:** Writing – review & editing, Supervision, Methodology, Funding acquisition, Conceptualization.

Acknowledgements

We thank Kerstin Vikman, patient research partner, for her valuable comments and contributions throughout the conduct of the study (Swedish Rheumatology Association, Reumatikerförbundet R-1013521).

Funding

This study was funded by a HORIZON EU Grant Agreement No 101080711 (SPIDeRR). MR received financial support from Karolinska Institutet Research Foundation Grants 2024-2025 (2024-02392) and Karolinska Institutet Foundation Grants for Rheumatology Research 2024 (2024-03867); Ulla and Gustaf af Uggla Foundation (2025-02580); Konung Gustaf V:s 80-årsfond (SGI-2024-1077). TF's contribution was supported by the Swedish Research Council (2024-02744) and HORIZON EU Grant Agreement No 101137154 (WISDOM). HW received support for the project from Reumatikerförbundet, Stiftelsen Professor Nanna Svartz Fond, Stiftelsen Konung Gustaf V:s 80-årsfond, and Karolinska Institutet foundations.

Patient consent for publication

Not applicable.

Ethics approval

This study was approved by the Regional Ethics Committee, Stockholm, Sweden (Dnr 2015/1844-31/2).

Provenance and peer review

Not commissioned; externally peer-reviewed.

Data availability statement

For reasons related to the legal framework governing the raw data used for this study, individual-level data cannot be freely shared. For requests for study data please contact the corresponding author.

Supplementary materials

Supplementary material associated with this article can be found in the online version at doi:10.1016/j.ard.2026.06.004.

Orcid

Maxime Raffray: http://orcid.org/0000-0002-1482-6298

REFERENCES

[1] Aletaha D, Smolen JS. Diagnosis and management of rheumatoid arthritis: a review. JAMA 2018;320(13):1360–72.

[2] Symmons DPM. Epidemiology of rheumatoid arthritis: determinants of onset, persistence and outcome. Best Pract Res Clin Rheumatol. 2002;16 (5):707–22.

[3] Gwinnutt JM, Symmons DPM, MacGregor AJ, Chipping JR, Marshall T, Lunt M, et al. Twenty-year outcome and association between early treatment and mortality and disability in an inception cohort of patients with rheumatoid arthritis: results from the Norfolk Arthritis Register. Arthritis Rheumatol. 2017;69(8):1566–75.

[4] Kastbom A, Turcinov S, Malmström V. Windows for intervention in the prearthritis phase of rheumatoid arthritis? A narrative review of key triggering events and potential preventive strategies. RMD Open [Internet] 2025 Jul 10;11:3. [cited 2025 Jul 15]. Available from: https://rmdopen.bmj.com/content/11/3/e005778.

[5] Lend K, van Vollenhoven RF, Lampa J, Lund Hetland M, Haavardsholm EA, Nordström D, et al. Sex differences in remission rates over 24 weeks among three different biological treatments compared to conventional therapy in patients with early rheumatoid arthritis (NORD-STAR): a post-hoc analysis of a randomised controlled trial. Lancet Rheumatol. 2022 Oct;4(10):e688–98.

[6] Lai NS, Tsai TY, Li CY, Koo M, Yu CL, Lu MC. Increased frequency and costs of ambulatory medical care utilization prior to the diagnosis of rheumatoid arthritis: a national population-based study. Arthritis Care Res. 2014 Mar;66 (3):371–8.

[7] Neovius M, Simard JF, Klareskog L, Askling J, ARTIS Study Group. Sick leave and disability pension before and after initiation of antirheumatic therapies in clinical practice. Ann Rheum Dis. 2011 Aug;70(8):1407–14.

[8] Björk M, Thyberg I, Rikner K, Balogh I, Gerdle B. Sick leave before and after diagnosis of rheumatoid arthritis —a report from the Swedish TIRA Project. J Rheumatol. 2009 Jun;36(6):1170–9.

[9] O'Neil LJ, Alpízar-Rodríguez D, Deane KD. Rheumatoid arthritis: the continuum of disease and strategies for prediction, early intervention, and prevention. J Rheumatol. 2024 Apr;51(4):337–49.

[10] Frisell T, Bower H, Morin M, Baecklund E, Di Giuseppe D, Delcoigne B, et al. Safety of biological and targeted synthetic disease-modifying antirheumatic drugs for rheumatoid arthritis as used in clinical practice: results from the ARTIS programme. Ann Rheum Dis. 2023 May;82(5):601–10.

[11] Waldenlind K, Eriksson JK, Grewin B, Askling J. Validation of the rheumatoid arthritis diagnosis in the Swedish National Patient Register: a cohort study from Stockholm County. BMC Musculoskelet Disord. 2014 Dec;15:432.

[12] Raffray M, Laalou Y, Rönnelid J, Grönwall C, Di Giuseppe D, Westerlind H, et al. POS0530 How well does rheumatoid arthritis serostatus assigned in routine clinical practice match actual RA serology. Ann Rheum Dis. 2025 Jun;84:740–1.

[13] Curtis JR, Xie F, Zhou H, Salchert D, Yun H. Use of ICD-10 diagnosis codes to identify seropositive and seronegative rheumatoid arthritis when lab results are not available. Arthritis Res Ther. 2020;22(1):242.

[14] Tidblad L, Westerlind H, Delcoigne B, Askling J, Saevarsdottir S. Comorbidities at diagnosis of rheumatoid arthritis: a population-based case-control study. Rheumatol (Oxf Engl). 2021 Aug;60(8):3760–9.

[15] Nagin DS, Jones BL, Passos VL, Tremblay RE. Group-based multi-trajectory modeling. Stat Methods Med Res 2018 Jul;27(7):2015–23.

[16] Magrini A. Assessment of agricultural sustainability in European Union countries: a group-based multivariate trajectory approach. AStA Adv Stat Anal. 2022 Dec;106(4):673–703.

[17] de Thurah A, Jensen H, Maribo T, Jensen MB, Sandbæk A, Hauge EM, et al. Use of primary health care and radiological imaging preceding a diagnosis of rheumatoid arthritis: a nationwide cohort study in Denmark. Rheumatol Oxf Engl. 2023 Feb;62(2):555–64.

[18] Frølich A, Ghith N, Schiøtz M, Jacobsen R, Stockmarr A. Multimorbidity, healthcare utilization and socioeconomic status: A register-based study in Denmark. PLOS One. 2019;14(8):e0214183.

[19] Manfredi L, Sodano B, Raganato C, Buscema F, Milani L, Catalano A, et al. A longitudinal analysis of the association between socioeconomic position and multimorbidity in the European Prospective Investigation into Cancer and Nutrition Study. Aging Dis. 2024 Dec;16(6):3625–37.

[20] Magnusson C, Shahbazian R, Kjellsson S. Does higher education make women sicker? A study of the gender gap in sickness absence within educational groups. PLOS ONE. 2024 Jun;19(6):e0303852.

[21] Mésidor M, Rousseau MC, O'Loughlin J, Sylvestre MP. Does group-based trajectory modeling estimate spurious trajectories? BMC Med Res Methodol. 2022 Jul;22(1):194.

[22] Steinz N, Maarseveen TD, van den Akker EB, Cope AP, Isaacs JD, Winkler AR, et al. Time-independent disease state identification defines distinct trajectories determined by localised vs systemic inflammation in patients with early rheumatoid arthritis. Ann Rheum Dis [Internet] 2025 May 9 [cited 2025 May 13]. Available from: https://www.sciencedirect.com/science/article/pii/S0003496725009008.

[23] Kronzer VL, Westerlind H, Alfredsson L, Crowson CS, Nyberg F, Tornling G, et al. Respiratory diseases as risk factors for seropositive and seronegative rheumatoid arthritis and in relation to smoking. Arthritis Rheumatol. 2021 Jan;73(1):61–8.

Ann Rheum Dis 85 (2026) 1704–1715

Contents lists available at ScienceDirect

Annals of the Rheumatic Diseases

journal homepage: https://www.sciencedirect.com/journal/annals-of-the-rheumatic-diseases

Rheumatoid arthritis

Low-dose blinatumomab in multidrug-resistant rheumatoid arthritis—a case series

Laura Bucci[1,2], Melanie Hagen[1,2], Sebastian Böltz[1,2], Carlo Tur[1,2,3], Danae-Mona Nöthling[1,2], Tobias Dashi[1,2], Janina Auth[1,2], Tobias Rothe[1,2], Andreas Wirsching[1,2], Jochen Wacker[1,2], Futoshi Iwata[1,2], Andrea Zoli[1,2,3], Anna-Maria Liphardt[1,2], Stefano Alivernini[3], Luis Munoz[1,2], Verena Schönau[1,2], Jürgen Rech[1,2], Armin Atzinger[4], Maria-Antonietta D'Agostino[3], Aline Bozec[1,2], Markus Eckstein[5], Maria Gabriella Raimondo[1,2], Georg Schett[1,2,3,6,†], Ricardo Grieshaber-Bouyer[1,2,†,*]

[1] *Department of Internal Medicine 3 – Rheumatology and Immunology, Friedrich-Alexander-Universität Erlangen-Nürnberg and Universitätsklinikum Erlangen, Erlangen, Germany*
[2] *Deutsches Zentrum Immuntherapie, Friedrich-Alexander-Universität Erlangen-Nürnberg and Universitätsklinikum Erlangen, Erlangen, Germany*
[3] *Department of Rheumatology, Fondazione Policlinico Universitario A. Gemelli, IRCSS, Catholic University of Sacred Heart, Roma, Italy*
[4] *Department of Nuclear Medicine, Friedrich-Alexander-Universität Erlangen-Nürnberg and Universitätsklinikum Erlangen, Erlangen, Germany*
[5] *Department of Pathology, Friedrich-Alexander-Universität Erlangen-Nürnberg and Universitätsklinikum Erlangen, Erlangen, Germany*
[6] *Department of Medicine, Karolinska Institutet, Stockholm, Sweden*

ARTICLE INFO

Article history:
Received 19 December 2025
Received in revised form 16 July 2026
Accepted 19 July 2026

ABSTRACT

Objectives: T-cell engagers (TCEs) are well-established treatments in haematology; strategies in autoimmune diseases are evolving. As an alternative to high-dose protocols optimising depletion, lower-dose protocols might optimise safety.

Methods: We assessed safety and efficacy of low-dose blinatumomab in a named patient use case series of 15 patients (median age 55) with multidrug-resistant rheumatoid arthritis (MDR-RA) (28-joint disease activity score C-reactive protein 5.0; clinical disease activity index [CDAI] 28). We monitored safety (cytokine release syndrome [CRS]; immune effector cell-related neurotoxicity syndrome [ICANS]), clinical scores, and tissue inflammation via ultrasound and fibroblast activation protein inhibitor (FAPI)-positron emission tomography/computed tomography (PET/CT). B-cell depletion was quantified in blood, synovium, and lymph nodes.

Results: CRS (grade 1) occurred in 3 of 15 patients. No ICANS occurred. One patient developed hypogammaglobulinaemia. One fatal cardiovascular event occurred after 1 year; it was adjudicated as unrelated by treating investigators but not independently reviewed. By week 12, disease activity decreased; 9 of 15 patients achieved CDAI low disease activity, and 3 of 15 patients achieved CDAI remission. Synovial B cells were depleted (4 of 5 biopsies) but not in lymph nodes. FAPI PET/CT showed reduced tracer uptake in the involved joints after blinatumomab.

*Correspondence to Dr Ricardo Grieshaber-Bouyer, Department of Internal Medicine 3 – Rheumatology and Immunology, Friedrich-Alexander-Universität Erlangen-Nürnberg and Universitätsklinikum Erlangen, Erlangen, Germany.

E-mail address: ricardo.grieshaber@fau.de (R. Grieshaber-Bouyer).

Handling editor Josef Smolen.

† Georg Schett and Ricardo Grieshaber-Bouyer contributed equally.

https://doi.org/10.1016/j.ard.2026.07.011

0003-4967/© 2026 The Authors. Published by Elsevier B.V. on behalf of European Alliance of Associations for Rheumatology (EULAR). This is an open access article under the CC BY license (http://creativecommons.org/licenses/by/4.0/)

Although 14 of 15 patients flared, disease activity remained lower, and responsiveness lasting >3 months to previously failed drugs (Janus kinase inhibitors, abatacept, tumour necrosis factor inhibitors) was observed in 7 of 15 patients.

Conclusions: Short-term control of RA disease activity, depleted synovial B cells, and reduced fibroblast activation on FAPI-PET were observed 3 months after blinatumomab. Flares after blinatumomab responded to previously ineffective disease-modifying antirheumatic drugs in some patients. Low-dose TCE therapy may offer an accessible path to disease control in MDR-RA, although causal inference and generalisability require validation in controlled trials.

WHAT IS ALREADY KNOWN ON THIS TOPIC

- Deep B-cell depletion via T-cell engagers (TCEs) is a rapidly expanding treatment concept in autoimmune diseases. The CD3xCD19 TCE blinatumomab has shown promise in patients with multidrug-resistant rheumatoid arthritis (MDR-RA), but different dosing strategies and expected benefits are poorly understood.

WHAT THIS STUDY ADDS

- In this case series of low-dose blinatumomab therapy in patients with refractory rheumatoid arthritis, we observed short-term clinical remission, depletion of synovial B cells, and reduction of synovial fibroblast activation in fibroblast activation protein inhibitor-positron emission tomography. Moreover, after experiencing a flare, a subset of patients with rheumatoid arthritis responded to disease-modifying antirheumatic drugs (the same agent or a different agent within the same class), which they previously failed on.

HOW THIS STUDY MIGHT AFFECT RESEARCH, PRACTICE OR POLICY

- Low-dose TCE protocols might represent a clinically valuable and easily accessible treatment strategy in MDR-RA. This finding may expand the range of possible applications for T-cell redirecting therapies in autoimmune diseases, warranting further controlled studies.

INTRODUCTION

B-cell depletion is an established treatment for autoimmune diseases, and the B-cell-depleting chimeric anti-CD20 monoclonal antibody rituximab is an approved treatment for rheumatoid arthritis (RA) [1,2]. Recently, deep B-cell depletion through chimeric antigen receptor T cells and T-cell engagers (TCEs) has been introduced into autoimmune diseases, holding promise to better control diseases like RA [3–6].

Blinatumomab, the first approved TCE, consists of 2 linked single-chain variable fragments targeting CD3 on T cells and CD19 on B cells [7]. Its lower molecular weight (54 kDa) compared with immunoglobulins (Ig, 150 kDa) and its short half-life (1-2 hours) necessitate continuous infusion but allow for rapid reversibility of T-cell engagement. Approved for acute lymphoblastic B-cell leukaemia (ALL) [8,9], blinatumomab demonstrated the ability to eradicate minimal residual disease [10,11], a strong predictor of disease relapse, by eliminating malignant cells below the detection threshold of traditional diagnostics.

We and others have reported on the first successful treatments of RA, systemic sclerosis, and myasthenia gravis with blinatumomab, showing the feasibility of treating autoimmune diseases with a CD19-targeting TCE [5,12,13]. However, the knowledge on blinatumomab-based treatment of autoimmune diseases remains very limited. Furthermore, the impact of different dosing strategies of TCE on tissue cell depletion and the ability to reach immune reset are currently not well understood. Although higher doses of TCE in haematology maximise depletion, they carry significant risks of neurotoxicity and cytokine release syndrome (CRS). Recently, therapeutic concepts beyond full 'immune reset' have gained interest, recognising that different degrees of immune intervention and different degrees of B-cell depletion may serve distinct clinical objectives [14]. Establishing whether a safer, low-dose TCE regimen can sufficiently modify the disease course, even without full 'immune reset', is a critical unmet need.

In this study, we present data on safety and clinical efficacy of blinatumomab in a cohort of 15 patients with active multidrug-resistant RA (MDR-RA), including long-term data on the 6 patients (#1-6) previously described [5], as well as safety and efficacy data on an additional 9 patients (#7-15).

METHODS

Patients

Patients with MDR-RA were recruited at the Department of Internal Medicine 3 (Rheumatology and Immunology) of the Friedrich-Alexander University Erlangen-Nürnberg. Eligibility criteria included: (i) diagnosis of RA according to the 2010 American College of Rheumatology (ACR)/European Alliance of Associations for Rheumatology (EULAR) criteria [15]; (ii) evidence for B-cell involvement based on positivity of rheumatoid factor (RF), anticitrullinated protein antibodies, antimodified peptide antibodies, antinuclear antibodies (ANA), or presence of B cells in the synovial membrane; (iii) active disease with a 28-joint disease activity score C-reactive protein (DAS28-CRP) over 3.2 units; and (iv) treatment resistance to methotrexate and at least 3 different targeted synthetic (ts) or biologic (b) disease-modifying antirheumatic drugs (DMARDs).

Blinatumomab was used via a compassionate use program in accordance with the German Medicinal Products Act (AMG), §21/2, and the Compassionate Use Regulation (AMHV), §2, that allows experimental treatment if (i) patients are afflicted by severe life-threatening disease, (ii) have failed on previous treatments, and (iii) a scientific rationale exists for the potential efficacy of the respective treatment in the disease. Use of patient data and biomaterial in this study is covered by license 334_18 B of the Institutional Review Board of the University Clinic of Erlangen. All procedures were performed in accordance with the Good Clinical Practice guidelines of the International Council for Harmonization. Self-reported gender (identity) and biological sex were identical in all patients. All participants provided written informed consent in accordance with the principles

of the Declaration of Helsinki. No commercial sponsor was involved.

Treatment

Before treatment initiation, the daily glucocorticoid dose was tapered to ≤10 mg. Methotrexate was continued in patients #1 (7.5 mg weekly), #2 (15 mg weekly), #3 (10 mg weekly), #5 (20 mg weekly), #9 (15 mg weekly), and #13 (20 mg weekly). All other DMARDs were discontinued at least 3 weeks before starting blinatumomab. In patients receiving rituximab as the last treatment (#5, #7, #10, #12, #14, #15), the last rituximab infusion was given more than 3 months before blinatumomab.

Blinatumomab was administered in an inpatient setting with continuous monitoring of vital signs. The incidence of side effects potentially related to the therapy, such as CRS, immune effector cell-related neurotoxicity syndrome (ICANS), myelotoxicity, cardiotoxicity, and infections, was monitored during the therapy and for 12 months of follow-up. Patients received at least 2 cycles of blinatumomab. Premedication was performed with 16 mg dexamethasone before initiating blinatumomab. Per cycle, 36 μg to 38.5 μg blinatumomab were administered via continuous infusion over 96 hours (9 μg/d). The second cycle was initiated after a 1-week treatment-free interval. The blinatumomab dose was increased to 28 μg/d in 5 patients in cycle 2 (#10, #12, #13, #14, #15) and in 1 patient in cycle 3 (#9). Four patients received a third cycle of blinatumomab (#1, #4, #9, #12). The cumulative dose of blinatumomab throughout all treatment cycles ranged from 77 μg to 189 μg. Hence, compared with the approved doses in haematology (up to 784 μg per treatment cycle), this was a low-dose protocol, with a significantly shorter infusion duration of only 96 hours and breaks between cycles compared with the 28-day continuous infusion [9].

Clinical and laboratory evaluation

Clinical disease activity was assessed by tender and swollen joint counts and patient global disease activity via a visual analogue scale (VAS). C-reactive protein (CRP) was measured as an acute phase reactant, and DAS28-CRP, clinical disease activity index (CDAI), and simplified disease activity index (SDAI) were used as a composite outcome measure. Flow cytometry was performed to assess peripheral CD19+ B cells, CD4+ T cells, and CD8+ T cells at baseline and at 5 to 7 months and 9 to 12 months of follow-up. Absolute cell counts were measured using BD Trucount tubes (BD Biosciences) according to the manufacturer's instructions. To define different B-cell subpopulations, peripheral blood mononuclear cells (PBMCs) were isolated by density-gradient centrifugation and stained with the following antibody panel: CD19 (clone HIB19; dilution: 1:400), CD20 (2H7; 1:1000), CD21 (Bu32;1:200), CD24 (ML5, 1:200), CD27 (M-T271;1:100; all Biolegend), and CD38 (HIT2; 1:200; BD Biosciences). In addition, CD3 was stained (SK7; 1:400; Biolegend) and viability was assessed by Fixable Viability Stain 780 (Thermo Fisher). PBMCs were acquired on a Cytek Northern Lights spectral analyser, and analyses were performed using FlowJo v10 software (Tree Star). Serum immunoglobulins and inflammatory cytokine levels (tumour necrosis factor [TNF], interleukin [IL]-10, IL-2R, IL-6, and IL-8) were obtained at baseline and periodically monitored during therapy. Serum levels of RF-IgM were assessed by nephelometry (Optilite Assay; The Binding Site), anticyclic citrullinated peptide 2 antibodies (CCP2), and anti–mutated citrullinated vimentin antibodies (aMCV) by enzyme-linked immunosorbent assay (Orgentec).

Fibroblast activation protein inhibitor PET/CT

Fibroblast activation protein inhibitor (FAPI) positron emission tomography/computed tomography (PET/CT) was performed to evaluate synovial fibroblast activation in the joints [16]. 68Gallium-labelled FAPI-04 tracer uptake was detected by the Biograph Vision 600 system (Siemens Healthineers). Whole-body PET imaging (skull to toes) with an additional hand scan was performed, with a 3-minute acquisition per bed position (axial field-of-view of 26.3 cm). PET data were corrected for random and scattered coincidences, as well as for decay. Attenuation correction was performed using the CT component. Image reconstruction and corrections were carried out using the manufacturer's PET/CT software. The PET/CT images were analysed using Syngo via Siemens Molecular Imaging. Three specialists (2 nuclear medicine physicians and 1 radiologist, blinded to clinical and ultrasound data) performed a visual assessment of the scans. The datasets were reviewed by interpreting coronal, sagittal, and transverse slices. For the purpose of this exploratory analysis, we focused on 6 anatomical regions (shoulders, elbows, hands, knees, ankles, and feet). Each region was assigned a semiquantitative score based on the standardised uptake value (SUV)-max using a 3-point scale (0-2): 0 = absent or minimal uptake (SUV ≤2); 1 = mild uptake (SUV >2 and ≤7); 2 = moderate uptake (SUV >7). This scoring system is not standardised and primarily intended to assess the overall SUV trends.

Musculoskeletal ultrasound

Musculoskeletal ultrasound (MSUS) was used to detect the presence and the severity of active synovitis. Ultrasound was performed by 2 experienced rheumatologists (LB, MH, not blinded to clinical data but blinded to FAPI-PET/CT images) using the MyLab25 (Esaote Biomedica) with a 4 to 13 MHz linear transducer and graded according to the EULAR-Outcome Measures in Rheumatology (OMERACT) standardised scoring [17]. Images were acquired in B mode and Power Doppler (PD) mode. Ultrasound evaluation was conducted at the individual joint level, targeting the most clinically affected joint among eighteen joint regions, as defined by the presence of swelling and/or tenderness on clinical examination. We hereby acknowledge that focusing on the most clinically affected joints may have introduced a selection bias. PD signal was evaluated by the EULAR-OMERACT standardised scoring system, ranging from no signal (grade 0) to a PD signal affecting more than 50% of the synovium (grade 3).

Synovial biopsy

Sequential minimally invasive ultrasound-guided synovial biopsy (N = 2 wrist; N = 2 knee; and N = 1 proximal interphalangeal joint) was performed in 5 patients using a standardised protocol [18]. The procedure was performed under sterile conditions at baseline and after therapy. Biopsies were performed at the following time points: patient #1 (242 days after treatment initiation, patient #4 (100 days), patient #6 (59 days), patient #9 (114 days), and patient #12 (29 days). Written consent was obtained from all patients before the procedure. Wrist and knee synovial biopsies were performed under

ultrasound guidance after local infiltration of 2% mepivacaine. For wrist biopsy, the needle (Precisa 1410-HS, Hospital Service Spa) was advanced between the fourth and fifth extensor compartments into areas of synovial hypertrophy. For the knee biopsy, synovial hypertrophy was targeted in the suprapatellar recess.

Synovial samples were fixed in 10% formalin, embedded in paraffin, sectioned at 2 µm, deparaffinised and further processed on a VENTANA BenchMark ULTRA autostainer. Antigen retrieval was carried out with CC1 reagent (Ventana). The samples were stained for CD15 (neutrophils), CD19 and CD20 (B cells), CD68 (macrophages), CD138 (plasma cells), and CD31 (vascular endothelial cells). Panel and protocols are listed in Supplementary Table S3. Stained slides were digitised using a Hamamatsu S210 slide scanner (Hamamatsu) at 400× magnification and imported into the open-source QuPath (v.0.4.3) digital slide analysis environment. The area of interest for cell quantification per mm^2 tissue area was defined as the synovial lining and the surrounding stroma, and annotated by a board-certified pathologist. CD19, CD20, and CD138 cell populations were quantified and validated by a pathologist and target cell counts per mm^2 of region of interest were reported.

Lymph node biopsy

Sequential, minimally invasive ultrasound-guided lymph-node biopsy was performed in 4 patients as previously described [18,19]. Biopsies were performed at the following time points: patient #8 (97 days after treatment initiation), patient #12 (29 days), patient #13 (32 days), and patient #14 (35 days). Biopsies were performed under ultrasound guidance (20 MHz linear probe, Esaote MyLabX90/X80) using a sterile technique. Local anaesthesia (10 ml of 2% mepivacaine) was administered, followed by a 0.5 cm skin incision to reduce skin resistance. A 16-G semiautomated biopsy needle (Precisa 1610-HS) was used for tissue retrieval. In brief, tissues were cut, deparaffinised, and further processed on a VENTANA BenchMark ULTRA autostainer. Antigen retrieval was carried out with CC1 reagent (Ventana). All lymph node-biopsy samples were stained for CD19, CD20, CD138, CD23 (follicular dendritic cells [FDCs]), PD-1 (follicular T helper cells [TFH]), Ki67 (MIB1 antigen, proliferation fraction of germinal centre B cells), CD3 (T cells), and CD68 (macrophages). Panel and protocols are listed in Supplementary Table S3. Stained slides were digitised using a Hamamatsu S210 slide scanner (Hamamatsu) at 400× magnification and imported into the open-source QuPath (v0.4.3) digital slide analysis environment. CD3, CD19, CD20, CD68, and CD138 cell populations were automatically quantified with the positive cell detection platform; the results were visually validated, and target cell counts were reported as number of positive cells per mm^2 region of interest (ROI). To assess the architecture of the B-cell maturation compartment (follicular area) of the lymph node, a semi-quantitative score integrating general distribution and presence of B cells, architecture of the FDC network, the proliferation rate of germinal centre B cells, and the presence of TFH cells was used, which has been extensively described previously [19,20].

Statistical analysis

Based on the exploratory nature of this study, analyses are descriptive. Data are presented as medians or geometric means (95% CI) (RF, anti-CCP, and aMCV). All analyses and graphs were performed using Prism software (version 10, GraphPad Software). All baseline and follow-up values were source verified by 2 rheumatologists.

RESULTS

Among the 38 patients with MDR-RA considered by specialised rheumatologists between April 2023 and November 2024, 15 patients were selected for blinatumomab therapy. The remaining 23 patients either did not fulfil strict severity (N = 11) or resistance criteria (N = 8) or refused informed consent (N = 4). Patient characteristics are listed in Table 1. Patient selection is summarised in the flow diagram shown in Supplementary Figure S1. The median age at application was 55 years (range: 27-64), 60% were female, and baseline disease activity was high, with a median DAS28-CRP of 5.03 (range: 3.46-7.88), CDAI of 28 (range: 15-64), and SDAI of 27 (range: 16.1-66). Median disease duration was 13 years (range: 3-33). Historically, small joints of the hands and feet were the first affected joints in our cohort of patients. In all patients, RA was refractory to methotrexate and at least 3 b/tsDMARDs. Overall, 66.7% (10 of 15) of patients were refractory to rituximab.

Safety of blinatumomab

The cumulative blinatumomab dose and adverse events are summarised in Table 2. We observed 3 cases of low-grade CRS (all grade 1), with resolution upon metamizole in 1 patient and resolution after a single dose of tocilizumab (8 mg/kg) in 2 patients (#9, #14). Although in oncology, tocilizumab is usually given in grade ≥2 CRS, in autoimmune disease, tocilizumab is often given for grade 1 CRS and, in our centre, is the standard of care if fever recurs after the initial administration of metamizole. CRS was not clearly linked to the blinatumomab dose, as 2 events developed on day 1 at first infusion and 1 event occurred during dose increase at cycle 3 (patient #9). No cases of ICANS were observed. Of note, 1 patient (#9) with pre-existing coronary artery disease and a heavy smoking history (40 pack years) developed a fatal cardiovascular event after 1 year. This event was categorised as not related to treatment by the treating investigators but was not independently reviewed.

Five mild infections occurred in 4 of 15 (26.6%) patients, whereas severe infections were not observed. Patient #2 developed herpes labialis 3 weeks after the first blinatumomab cycle and a SARS-CoV-2 infection at week 12. Patient #4 developed a urinary tract infection during the first cycle, which was treated with systemic antibiotics. Patient #10 developed dysuria, which resolved without antibiotic therapy. Patient #14 experienced a periodontitis at the end of the first cycle, which was treated with antibiotics.

T-cell engagement and B-cell depletion

T-cell engagement led to a transient decrease in circulating CD3+ cells, without changes in the CD4/CD8 ratio (Fig 1A,B). T-cell engagement was accompanied by a transient increase in acute phase proteins and proinflammatory cytokines during the first infusion of blinatumomab (Supplementary Fig 2A–C).

In 3 patients (#5, #7, and #10), B cells were already depleted due to previous treatment with rituximab 3 to 4 months before blinatumomab (Fig 1C). In the other patients, blinatumomab induced fast and rather short B-cell aplasia in the peripheral blood (Fig 1D). Two patients achieved B-cell depletion after the first, 5 patients after the second, and 2 patients after the third blinatumomab infusion. Three patients (#2, #4,

Table 1
Baseline characteristics of patients treated with blinatumomab

Patient #	1	2	3	4	5	6	7	8	9[a]	10	11	12	13	14	15
Follow-up (mo)	26	24	24	24	23	22	22	19	8[b]	14	14	9	9	9	6
Demographic characteristics															
Age (y)	55	48	51	31	60	55	45	46	62	55	27	57	57	62	64
Sex	M	F	F	F	M	M	F	F	M	F	M	F	F	M	F
Disease-specific characteristics															
Disease duration (y)	6	4	27	6	18	3	10	16	12	33	21	25	13	21	11
Disease activity score 28 CRP (units)	5.70	5.54	5.52	4.62	4.05	4.13	4.27	4.75	5.03	3.46	3.89	7.09	7.3	5.51	7.88
CDAI	44	36	30	23	24	26	28	19	20	16	15	64	62	40	58
Tender joint count (N)	27	11	3	9	7	9	4	6	3	2	2	32	39	6	28
Swollen joint count (N)	10	12	19	4	2	7	1	3	5	1	2	35	16	4	18
Global disease activity (VAS, mm)	81	72	47	62	51	61	75	70	70	70	60	80	90	70	100
Global pain (VAS, mm)	62	60	41	56	58	61	80	67	65	80	52	78	85	60	90
ACPA (U/L)	0.8	155	2	301	163	64	64	153	0.89	1.8	0.96	104	154	1027	322
Rheumatoid factor (U/L)	<5	417	165	18	222	64	26	40	13	82	<5	635	86	381	391
aMCV (U/mL)	2	730	26	690	750	17	60.8	174	1	4.8	5.8	55.7	590	2872	600
ANA	-	1:320	-	1:320	-	-	-	-	-	1:320	1:1000	1:320	1:100	-	1:100
CRP (mg/L)	3.6	13.2	23.7	4.5	3.2	0.5	5.4	13	63	5.4	11.4	20	35.9	5.2	18
Previous immunomodulatory treatments															
Methotrexate	+	+	+	+	+	+	+	+	+	+	+	+	+	+	+
Leflunomide	+	+	+	+	+	+	+	-	+	-	+	+	-	-	+
Etanercept	-	-	+	-	+	-	+	+	-	-	+	+	+	+	+
Adalimumab	+	+	+	+	+	+	+	+	+	+	+	+	+	+	+
Golimumab	-	-	+	-	-	-	+	-	+	-	-	-	-	-	-
Infliximab	+	-	+	-	+	-	+	-	+	-	-	+	+	-	-
Tocilizumab	+	-	+	+	+	+	+	-	+	+	-	+	+	+	+
Sarilumab	-	-	-	-	-	-	-	-	-	-	+	+	-	-	+
Upadacitinib	+	+	+	+	+	+	+	-	-	+	-	+	+	+	+
Baricitinib	+	-	+	+	+	+	+	-	-	+	+	+	-	+	+
Filgotinib	+	-	-	+	-	+	+	-	-	-	-	-	-	-	+
Tofacitinib	-	-	+	-	-	-	+	-	+	-	-	-	-	-	+
Abatacept	+	+	+	-	-	-	+	+	+	-	-	+	-	-	-
Rituximab	+	-	+	-	+	-	+	-	+	+	-	+	+	+	+
Last immunomodulatory treatment															
Methotrexate	+	+	+	-	+	-	-	-	-	+	-	-	+	-	-
Filgotinib	+	-	-	+	-	+	-	-	-	-	-	-	-	-	-
Adalimumab	-	+	+	-	-	+	-	-	-	-	-	-	-	-	-
Certolizumab	-	-	-	-	-	-	-	-	+	-	-	-	-	-	-
Abatacept	-	-	-	-	-	-	-	+	-	-	-	-	-	-	-
Sarilumab	-	-	-	-	-	-	-	-	-	-	+	-	-	-	-
Infliximab	-	-	-	-	-	-	-	-	-	-	-	-	+	-	-
Rituximab	-	-	-	-	+	-	+	-	-	+	-	+	-	+	+

ACPA, anticitrullinated protein antibodies; aMCV, antimutated citrullinated vimentin antibodies; ANA, antinuclear antibodies; CDAI, clinical disease activity index; CRP, C-reactive protein; F, female; M, male; VAS, visual analogue scale.
[a] Patient #9 died 12 months after blinatumomab, outside our scheduled follow-up. The information was confirmed through external medical records.
[b] Clinical follow-up for assessment of rheumatoid arthritis outcomes was available for 8 months.

and #11) did not achieve full B-cell depletion in the peripheral blood. The median time to B-cell recovery was 21 days (range: 7-51) (N = 9; 3 predepleted and 3 nondepleted patients excluded) (Fig 1E). Flow cytometric analysis revealed a transient expansion of $CD20^{+}CD27^{-}$ naïve B cells at 5 to 7 months, associated with a concomitant reduction in preswitched and switched memory B cells (Fig 1F–K). By 9 to 12 months, B-cell subsets approximated baseline distribution, whereas plasmablasts remained relatively stable over time (Fig 1K).

Effects on Igs, light chains, and disease-associated autoantibodies

Serum immunoglobulins remained stable. No significant decrease in IgG, IgA, and IgM levels was observed (Fig 1L,

Table 2
Adverse events in patients treated with blinatumomab

Patient #	1	2	3	4	5	6	7	8	9	10	11	12	13	14	15
Cumulative dose (μg)	115.5	77	77	115.5	77	77	77	77	189	150.5	77	189	150.5	150.5	150.2
Cycles received	3	2	2	3	2	2	2	2	3	2	2	3	2	2	2
CRS grade 1	0	0	0	0	0	0	0	0	1	0	0	0	1	1	0
CRS grade 2	0	0	0	0	0	0	0	0	0	0	0	0	0	0	0
CRS grade 3-4	0	0	0	0	0	0	0	0	0	0	0	0	0	0	0
ICANS	0	0	0	0	0	0	0	0	0	0	0	0	0	0	0
Hypogammaglobulinaemia	0	0	0	0	0	1	0	0	0	0	0	0	0	0	0
Infections	0	HSV, Cov	0	UTI	0	0	0	0	0	Dysuria	0	0	0	Perio-dontitis	0
Fatal events									1						

Cov, SARS-CoV-2 infection; CRS, cytokine release syndrome; HSV, Herpes simplex virus; ICANS, immune effector cell-related neurotoxicity syndrome; UTI, urinary tract infection.

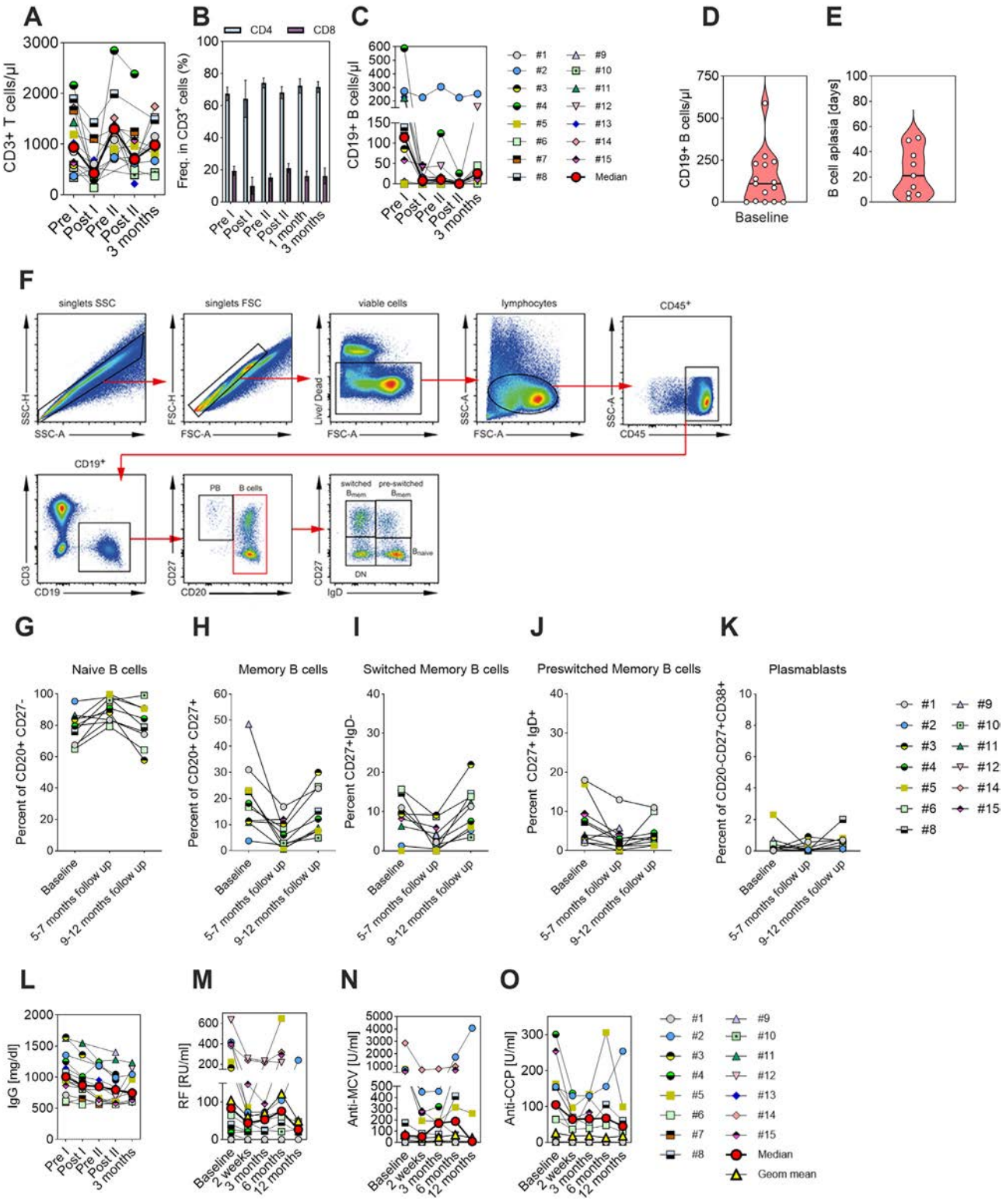

Figure 1. Serologic effects of blinatumomab. (A) Effects of blinatumomab on CD3+ cells in the peripheral blood and (B) CD4+/CD8+ cell ratio. (C) Effects of blinatumomab on CD19+ B cells in the peripheral blood. (D) Quantification of CD19+ B cells in peripheral blood at baseline (N = 15). (E) Duration of B-cell aplasia after blinatumomab (y: days, N = 9 evaluable patients). Peripheral B cells of patients #5, #7, and #10 were already depleted at baseline. Patients #2, #4, and #11 did not achieve full B-cell depletion in the peripheral blood. (F) Gating strategy used for B-cell phenotyping. (G) Quantification of naïve B cells, (H) memory B cells, (I) switched memory B cells, (J) preswitched memory B cells, and (K) plasmablasts. (L) Quantification of immunoglobulin G (IgG) in serum of patients treated with blinatumomab. Patient #7 was lost in follow-up and is therefore excluded. Patient #13 started teclistamab at month 3 and is therefore also excluded. (M-O) Effects of blinatumomab on rheumatoid factor (RF), antimutated citrullinated vimentin antibodies (aMCV), and anticyclic citrullinated peptide antibodies (aCCP) are presented as individual values with median and geometric mean. Patients #1, #9, and #11 were negative for RF, aCCP, and aMCV; patient #1 and #9 had B-cell infiltration in the synovial tissue; patient #1 was positive for antiacetylated vimentin autoantibodies, and #11 had positive ANA and antinative vimentin antibodies. ANA, antinuclear antibodies; DN, double-negative; FSC, forward scatter; PB, plasmablast; SSC, side scatter.

Supplementary Fig S3A,B). Only 1 patient (#6) developed mild hypogammaglobulinaemia at week 3 (IgG: 449.4 mg/dL) but did not require Ig substitution and reverted to normal levels by week 6 (IgG: 663.4 mg/dL). Kappa and lambda light chain levels also remained stable (Supplementary Fig S3C,D). IgG kinetics were analysed according to the infection status (Supplementary Fig S3E–G).

A decrease in autoantibody levels was observed after blinatumomab (Fig 1M–O). By month 3, RF levels decreased by an average of 62.1%, aMCV by 54%, and anti-CCP2 by 45%. Autoantibody levels increased again between 3 and 6 months after the treatment, which coincided with an increase in clinical disease activity.

Short-term clinical responses

Clinical efficacy was assessed through the number of tender and swollen joints, patient global assessment by VAS, DAS28-CRP, CDAI, and SDAI (Fig 2A–E; Supplementary Fig S4). Rapid clinical response was observed in all 15 patients. By week 12, the median number of tender joints had decreased from 7 to 2 (range: 2-39 to 0-23) (Fig 2A), swollen joints from 5 to 1 (range: 1-35 to 0-12) (Fig 2B) and VAS improved from 70 to 35 (range: 40-100 to 0-90) (Fig 2C). Consequently, DAS28-CRP decreased from 5.03 to 2.4 (range: 3.46-7.88 to 1.85-7.5) (Fig 2D) and CDAI from 28 to 8 (range: 15-64 to 2-49) (Fig 2E). By CDAI, 3 of 15 patients reached remission (≤2.8), 9 of 15 reached low disease activity or better (≤10), and only patient #15 remained in high disease activity due to a high number of tender and swollen joints. Using established CDAI response thresholds, 91% (10 of 11) of patients with high baseline CDAI disease activity and 75% (3 of 4) of those with moderate baseline CDAI disease activity achieved a clinically meaningful response. Based on ACR response criteria, all 15 patients achieved at least an ACR20 response, with 73% (11 of 15) reaching at least ACR50, 53% (8 of 15) reaching at least ACR70. With respect to DAS28-CRP, 33% (5 of 15) of the patients attained DAS28-CRP remission by month 3.

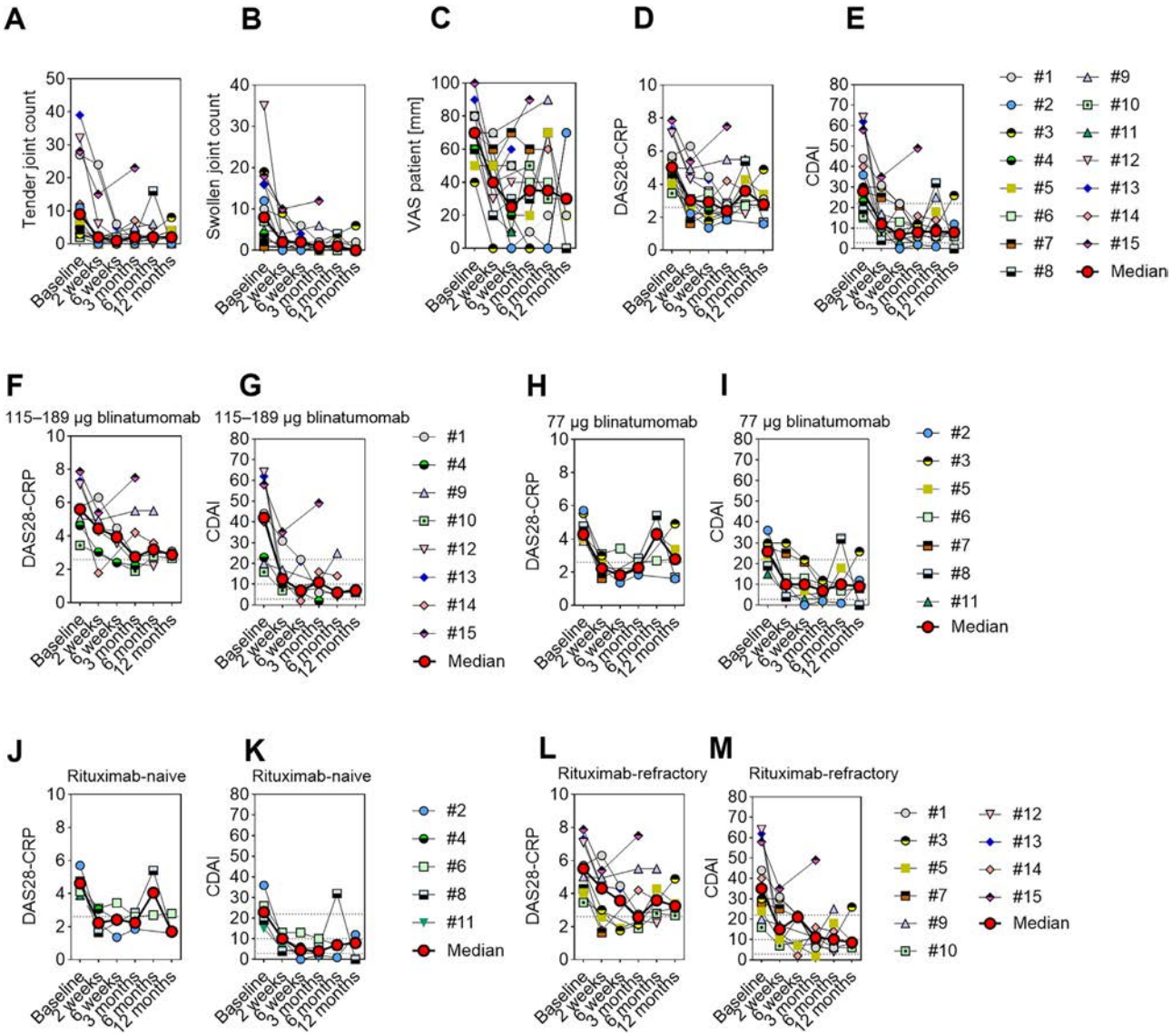

Figure 2. Clinical efficacy and durability of blinatumomab. Number of (A) tender joints and (B) swollen joints. (C) Patient visual analogue scale (VAS) (0-100), (D) DAS28-CRP, and (E) CDAI. (F) DAS28-CRP and (G) CDAI in patients treated with either high-dose 2-cycle or 3-cycle regimens (cumulative dose range 115-189 µg) (N = 8). (H) DAS28-CRP and (I) CDAI in patients treated with 2 cycles of blinatumomab (cumulative dose 77 µg) (N = 7). (J) DAS28-CRP and (K) CDAI in rituximab-naïve patients (N = 5). (L) DAS28-CRP and (M) CDAI in patients with prior rituximab failure (N = 10). Dotted lines in DAS28-CRP indicate 2.6 as a cut-off for remission; in CDAI indicate 2.8, 10, and 22, as cut-off for remission, LDA, MDA, respectively. >22 indicates high disease activity. CDAI, clinical disease activity index; DAS28-CRP, 28-joint disease activity score C-reactive protein; LDA, low disease activity; MDA, moderate disease activity.

Subgroup analyses (not randomised) revealed trends to better clinical responses in patients who had higher exposure to blinatumomab (Fig 2F,G; Supplementary Fig S5A) compared with those receiving lower doses (Fig 2H,I; Supplementary Fig S5B). Both rituximab-naïve and rituximab-refractory patients responded to blinatumomab, consistent with the known incomplete tissue depletion of rituximab. Nevertheless, there was a trend to faster response in patients with RA who were rituximab-naïve (Fig 2J,K; Supplementary Fig S5C) compared with rituximab-exposed (Fig 2L,M; Supplementary Fig S5D). Of note, the single use of tocilizumab for CRS in 2 patients did not have a meaningful effect on responses and could not explain the cohort-wide responses (Supplementary Fig S5E–J).

Long-term clinical response

Following these initial clinical responses, most patients (14 of 15) subsequently developed disease flares of RA, whereas 1 patient (#11) remained in drug-free remission at 9-month follow-up. VAS, DAS28-CRP, and CDAI tended to increase in the cohort after an average of 5 months (range: 1-18). Hence, different b/tsDMARDs were reintroduced at the discretion of the treating physician (Fig 3A). Because of the highly therapy-refractory nature of the cohort, many patients received b/tsDMARDs, which they had previously failed to, and, in some cases, glucocorticoids (Supplementary Tables S1 and S2). Some of these patients were treated again with the same DMARD they had previously failed (#1, #3, #9, #10, #12, and #15), whereas others switched to a different drug within the same pharmacological class (#2, #6, and #14).

Secondary loss of response was the most frequent reason for failure of these drugs before the initiation of blinatumomab (Supplementary Fig S6), although some patients had experienced primary failure. The concept of pharmacological resensitisation is primarily related to secondary failure, which should be considered when interpreting these findings.

Abatacept (in combination with methotrexate or leflunomide) was initiated in 5 patients (#1, #3, #4, #5, and #6), Janus kinase (JAK) inhibitors (as monotherapy or in combination with csDMARDs) were used in 5 patients (#2, #6 after abatacept, #8, #10, and #14), TNF-inhibitors were used in 3 patients (#9: infliximab, #12: etanercept, #15: adalimumab), and 2 patients received the B cell maturation antigen (BCMA) TCE teclistamab (#3 at month 6 after relapsing on Abatacept at month 5, and #13).

Notably, clinical efficacy of the reintroduced b/tsDMARDS was even seen in patients who had failed on the same class of drug before the introduction of blinatumomab. At month 3, disease activity had improved in patients receiving abatacept (Fig 3B), JAK inhibitors (Fig 3C), and to a lesser extent, TNF inhibitors (Fig 3D), despite the fact that 2 of 5 patients receiving abatacept, 4 of 5 patients receiving JAK inhibitors, and all patients receiving TNF inhibitors had previously failed the respective mechanism of action. Overall, 9 of 15 patients were retreated either with a b/tsDMARD they had previously received (6 of 15) or with a different drug (3 of 15) within the same class, and a clinical response lasting more than 3 months was achieved in 7 of 15 patients. The contribution of within-class switching to the observed clinical responses cannot be excluded.

Effects of blinatumomab on tissue

Five patients (#1, #4, #6, #9, #12) received minimally invasive ultrasound-guided fine needle synovial biopsy before and a median of 100 days (range: 29-242) after blinatumomab therapy. In 4 of 5 patients (#1, #6, #9, #12), CD20+ B cells had decreased to zero at follow-up biopsy (Fig 4A,B). Conversely, B cells were reduced but not fully depleted in the inguinal lymph node biopsy, which was performed at baseline and a median of 34 days (range: 29-97) after blinatumomab therapy in 4 patients (#8, #12, #13, #14) (Fig 4C,D) [19]. Paired CD19/CD20 quantification in synovial tissue and lymph node is shown in Supplementary Figure S7.

No significant changes were observed in plasma cell, T cell, and macrophage numbers in the lymph nodes (Fig 4E–G). One of 4 biopsied patients showed a posttreatment increase in lymph-node CD138$^+$ plasma cells, in line with the known resistance of long-lived plasma cells to CD19-directed depletion.

We also evaluated synovial inflammation and fibroblast activation by ultrasound and FAPI PET/CT. Synovitis was assessed by ultrasound and graded according to the EULAR-OMERACT definition of synovitis [17]. A clear reduction of synovitis was observed (Fig 3E,F). Synovial fibroblast activation was assessed by FAPI PET/CT in 5 patients and showed overall reduced tracer uptake after treatment (Fig 3G–L). The only exception was patient #1, who showed increased FAPI uptake 3 months after treatment, at a time when the patient had experienced flares (Fig 3H). Lower posttreatment FAPI scores, in particular of the hands, were associated with a longer duration of initial clinical response before additional therapy was required (Fig 3M).

DISCUSSION

In this case series of 15 patients with MDR-RA, we analysed the safety, pharmacodynamic effects, and clinical efficacy of low-dose TCE therapy with blinatumomab. Patients with RA failing on multiple DMARDs constitute a major therapeutic challenge and require the development of new therapeutic concepts. Although T-cell redirecting therapies have advanced the treatment of B-cell malignancies, their application in autoimmunity is still emerging.

Adverse events were limited to grade 1 CRS and mild infections. In a patient with advanced coronary artery disease based on multiple cardiovascular risk factors, including heavy smoking, a fatal cardiovascular event occurred 1 year after blinatumomab exposure. This event in a patient with extensive preexisting coronary disease was adjudicated as unlikely related to the treatment by the treating physicians; however, no independent adjudication or autopsy was performed. Although in oncology, the majority of cardiovascular adverse events upon TCE treatment occurred within the first weeks to months after treatment initiation, delayed events have also been reported [21,22]. Hence, the long-term monitoring of cardiovascular events is warranted in high-risk patients exposed to T-cell redirecting therapies. In contrast to haematology, no neurotoxicity was observed, underscoring the generally more favourable safety profile of TCEs in autoimmune diseases compared with their application in haematology and oncology [23].

Notably, B-cell aplasia in the peripheral blood was short-lived after blinatumomab, and the levels of free kappa and lambda chains, as well as immunoglobulins, remained stable. Accordingly, no immunoglobulin supplementation was required. Disease-related autoantibodies (RF, anti-CCP, and aMCV) were markedly reduced after blinatumomab, but increased in conjunction with disease flares.

Our long-term analysis, with a median follow-up time of 19 months, revealed a 2-fold pattern of response to blinatumomab. In the short term, we observed a robust clinical improvement in

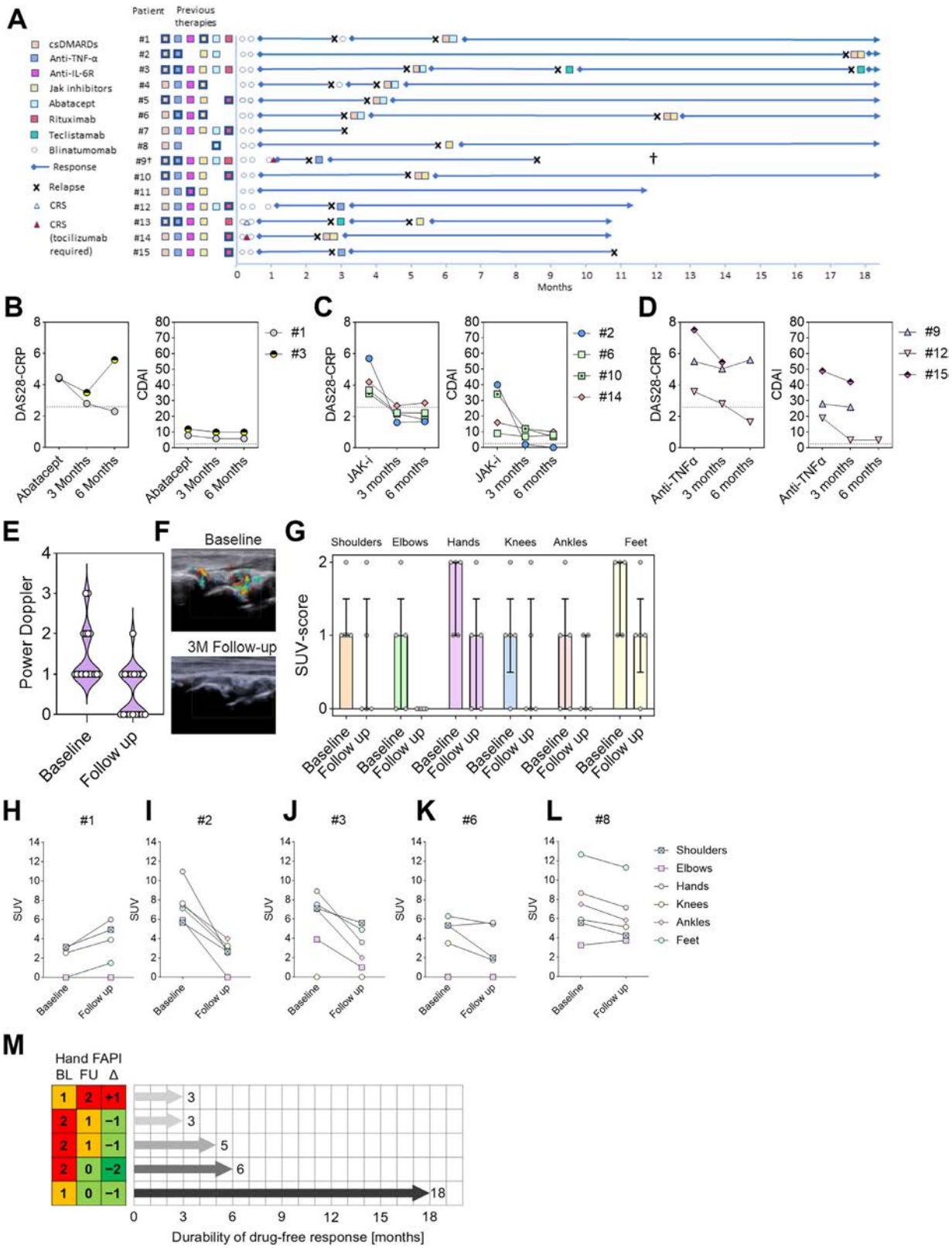

Figure 3. Clinical efficacy and durability of blinatumomab. (A) Clinical course after blinatumomab and the reintroduction of previous therapies after a disease flare. Bold boxes indicate the last therapy received before blinatumomab. † indicates the fatal event. (B-D) DAS28-CRP and CDAI in patients treated again with 3 different therapies after disease flares after blinatumomab. (E) Power Doppler activity in MSUS before and after blinatumomab (N = 18 joints, N = 14 individual patients). (F) Representative wrist ultrasound before and at 3-month follow-up after blinatumomab (#10). (G) Semi-quantitative score (3-point scale [0-2]) based on SUV-max in FAPI PET in different anatomical regions (shoulders, elbows, hands, knees, ankles, and feet) at baseline and 3-month follow-up. (H-L) Individual patient SUV-trajectories. (M) FAPI PET/CT activity of the hands at baseline (BL) and follow-up (FU), as well as the Δ, and the link to the durability of response. CDAI, clinical disease activity index; CRS, cytokine release syndrome; csDMARD; DAS28-CRP, 28-joint disease activity score C-reactive protein; FAPI, fibroblast activation protein inhibitor; JAK-i, janus kinase inhibitor; MSUS, musculoskeletal ultrasound; PET/CT, positron emission tomography/computed tomography; SUV, standardised uptake value; TNF-α, tumour necrosis factor α.

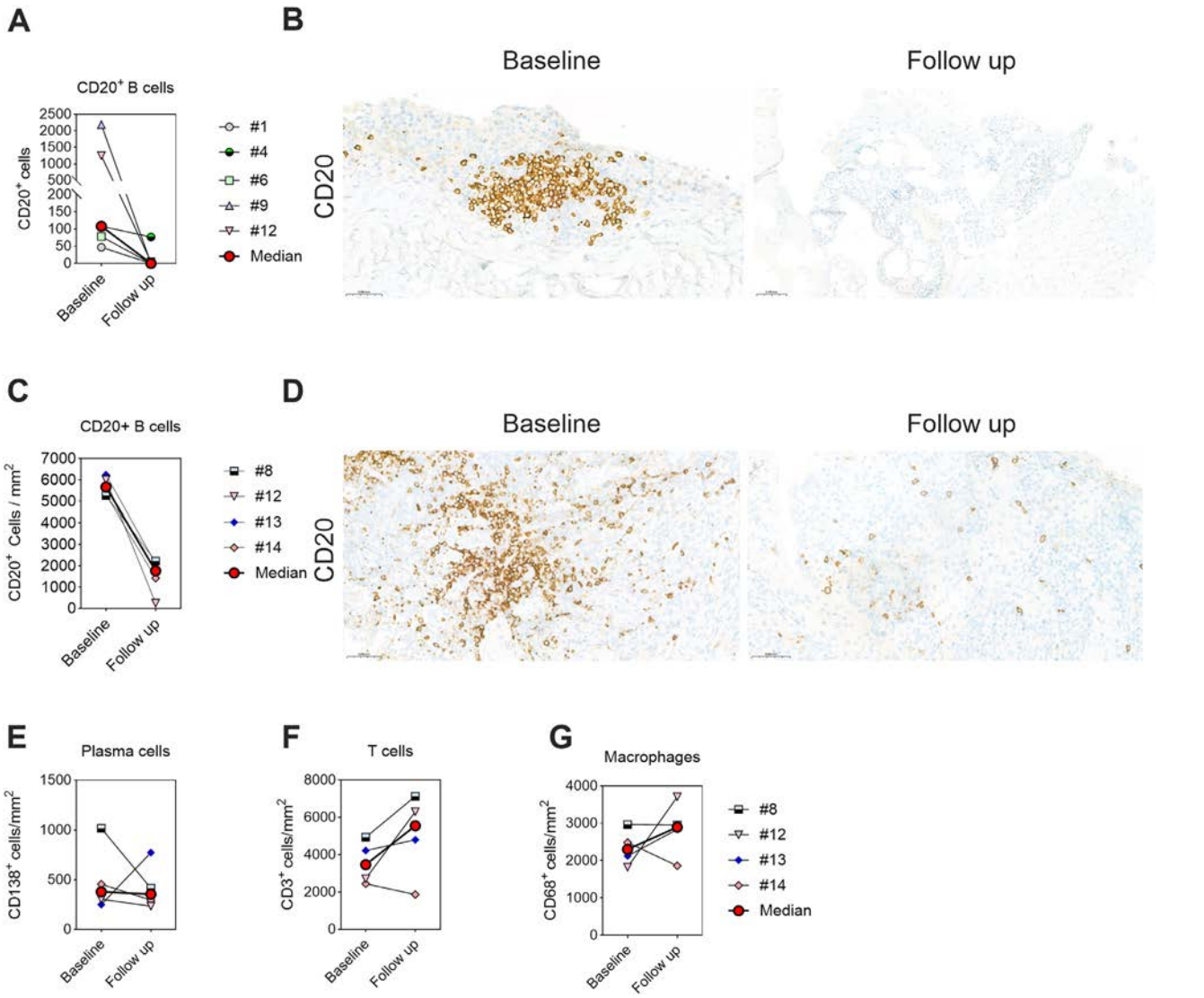

Figure 4. Tissue-specific effects of blinatumomab. (A) Quantification of B cells in the synovial tissue at baseline and 12 weeks after blinatumomab (N = 5). A segmented y-axis was used to facilitate the visualisation of both high and low cell counts. (B) Representative immunohistochemistry images of synovial tissue of knee joint biopsy before and at follow-up (median of 100 days [range: 29-242]). (C) Quantification of B cells in the lymph node of patients treated with blinatumomab at baseline (≈5500 cells/mm²) and at follow-up (≈1800 cells/mm²) (median of 33.5 days [range: 29-97]) vs (D) representative immunohistochemistry images of inguinal lymph node biopsy at baseline and at follow-up. (E-G) Quantification of (E) plasma cells, (F) T cells, and (G) macrophages in the lymph node at baseline and at follow-up.

patients with MDR-RA, with 73% of patients achieving an ACR50 response. This finding underscores a clinical benefit of low doses of TCE, considering the highly refractory nature of the treated patients. It is important to mention that the doses of blinatumomab were very low (at the microgram level), which is very different from conventional B-cell depleting agents and anticytokine antibodies used in RA. Furthermore, blinatumomab was not used as a continuous treatment but stopped in between each of the 2 to 3 cycles, which might have contributed to incomplete B-cell depletion in the lymph node, albeit depletion in the synovium was already remarkable.

After an average of 5 months, patients developed disease flares and required the reintroduction of b/tsDMARDs. Although patients did not remain in drug-free remission, we observed that RA became easier to manage with established drugs after exposure to blinatumomab. Notably, patients often responded to DMARDs to which they had previously become refractory. Thus, even though disease activity eventually returned, post-blinatumomab flares appeared to represent a deescalated phenotype, which, unlike the MDR baseline state, was in several cases again responsive to standard interventions with abatacept, JAK inhibitors, and, to some extent, TNF inhibitors. Further data are required to formally test this concept, and these findings should also be interpreted in light of the inclusion of both same-agent rechallenge and within-class switching. One can, however, hypothesise that this phenomenon results from a reduction of synovial stromal cell activation as suggested by the reduction in FAPI-PET. In this model, synovial B-cell depletion, even in the absence of full depletion in the lymph node, may contribute to the disruption of the local B-cell–fibroblast interactions. A larger cohort of patients and sampling would be needed to further explore this hypothesis. Importantly, the proposed B-cell –fibroblast mechanism should be considered as a hypothesis for the later tissue-level and serological findings, rather than as an explanation for the early clinical response, which preceded all tissue-based assessments and may also have been partly influenced by concomitant glucocorticoid treatment. Furthermore, T-cell exhaustion induced by TCEs could add to the improved effects of cytokine inhibitors [24]. An alternative explanation is that a drug holiday (the period off the failed agent during

blinatumomab therapy) may allow pharmacokinetic resensitisation and thereby contribute to the reversal of secondary loss of response.

The lack of long-lasting, drug-free remission could be linked to insufficient B-cell depletion in the secondary lymphatic organs or to RA-intrinsic mechanisms such as a fixed fibroblast activation in the joints that continues to attract immune cells. Of note, the doses and length of blinatumomab treatment used in this study were substantially lower than those in B-ALL [9]. Consequently, blinatumomab may have been underdosed for achieving deep B-cell depletion in tissue niches to maximise clinical benefit. Residual B-cell infiltration in the lymph nodes after blinatumomab may support this concept. Although full peripheral B-cell depletion was achieved in the majority of patients, 3 patients did not obtain full peripheral B-cell depletion. Higher TCE doses, in conjunction with a subcutaneous formulation to extend half-life, may improve B-cell depletion in the tissues and allow better responses. Indeed, patients who received higher cumulative doses of blinatumomab tended to have superior clinical responses. Of note, dose and prior-rituximab subgroups remain descriptive, as they were not randomised, and assignments reflected physician discretion and might have been subject to responder-selection bias. In addition to dosing, alterations in the T-cell functional state, which may occur in some patients with RA, may influence the killing of B cells via TCEs, as appropriate T-cell function is needed for the cytotoxic effects of TCEs.

In general, TCE designs that extend the half-life (either via an Fc domain or addition of a human serum albumin-binding domain) or modulate the binding affinity to target cells, effector cells, and Fc-receptor binding may allow increased efficacy of TCE treatment in autoimmune diseases at a reasonable safety profile. Disease-intrinsic mechanisms, however, also have to be considered, such as the activated synovial fibroblast compartment in RA, a substantial myeloid cell contribution to synovitis, and the persistence of certain pathogenic T-cell subsets, such as resident memory T cells, that could drive disease flares and activity independent of the 'depth' of B-cell depletion [25].

This study is limited by the exploratory nature as an uncontrolled case series. Of note, early clinical improvement observed within the first 2 weeks may in part reflect the anti-inflammatory effects of glucocorticoids, as patients received 16 mg dexamethasone as premedication per infusion cycle. Nevertheless, the sustained clinical benefit over months, the responsiveness to previously failed therapies, and the tissue-level changes (B-cell depletion in synovium, reduced FAPI uptake) are unlikely to be explained by dexamethasone exposure alone. Biopsy timing heterogeneity (lymph node 29-97 days; joints 29-242 days, including 1 biopsy after 3 cycles at day 242) constitutes another limitation, as it might sample active B-cell repopulation rather than residual posttreatment tissue burden, and precludes definitive comparisons between depletion efficacy in synovium and lymph nodes. The qualitative depletion differences between tissues, while an intriguing hypothesis, should be interpreted in this light. Notably, the dynamics of lymphocyte infiltration, retention, residence, and egress may differ between the lymph node and the synovium.

Ultimately, although immune reset remains the aspirational goal for curative autoimmunity treatments, low-dose protocols could represent a pragmatic and immediately valuable clinical advancement. Future strategies must now balance dose escalation to achieve deep tissue depletion against the safety profile, but our findings suggest that total eradication of the pathogenic B-cell clone is not the only path to achieve long-term clinical responses.

Competing interests

MAD'A reports consulting or advisory relationships with Amgen, AbbVie, UCB, Pfizer, Johnson & Johnson, Galapagos, Novartis, Bristol-Myers Squibb Company, Biogen, MSD, and Eli Lilly; funding grants from Amgen, AbbVie, UCB, Pfizer, Johnson & Johnson, Galapagos; and speaking and lecture fees from Amgen, AbbVie, UCB, Johnson & Johnson, Galapagos, Novartis, Bristol-Myers Squibb Company, Biogen, MSD, Eli Lilly, and Galapagos. GS reports speaking and lecture fees from Bristol-Myers Squibb Company, Cabaletta, Janssen, Kyverna Therapeutics, Miltenyi, and Novartis. RG-B reports funding grants from AbbVie, Alfasigma, AstraZeneca, Bristol-Myers Squibb Company, Candid Therapeutics, Cullinan Therapeutics, Epana Bio, Gilead, Kite, Johnson & Johnson, Kyverna Therapeutics, Eli Lilly, Novartis, Pfizer, Sanofi, Xencor, and UCB; and speaking and lecture fees from AbbVie, Alfasigma, AstraZeneca, Bristol-Myers Squibb Company, Candid Therapeutics, Cullinan Therapeutics, Epana Bio, Kite, Johnson & Johnson, Kyverna Therapeutics, Eli Lilly, Novartis, Pfizer, Sanofi, Xencor, and UCB. All other authors declare that they have no known competing financial interests or personal relationships that could have appeared to influence the work reported in this paper.

Contributors

LB, GS, and RG-B conceived the study, recruited patients, analysed data, and wrote the manuscript. MH, SB, CT, D-MN, AW, JA, JW, SA, LM, JR, AB, MAD'A, and MGR recruited patients. TR and ME analysed data. All authors approved the final manuscript. The present work was performed in (partial) fulfilment of the requirements for obtaining the degree of 'PhD' for LB.

Funding

The work was supported by the Deutsche Forschungsgemeinschaft (DFG) through the Leibniz Award 2023 (to GS), the Research Group FOR2886 PANDORA, the Collaborative Research Centers (CRC) 1483 (EmpkinS) and 1755 (CASCAID), the Transregio 369 (DIONE), the Clinician Scientist Program NOTICE (493624887 to LB and MGR), GR 5979/2-1 (RG-B). Further funding was obtained from the Lupus Research Alliance (GS), the Else Kröner-Fresenius-Stiftung (2022_EKEA.72; RGB), the Interdisciplinary Centre for Clinical Research (IZKF) Erlangen (grant N10, to RGB; P049 and J106 to MGR), the Boehringer Ingelheim Foundation (R.G.B.), the Lupus Research Alliance (to RGB), the European Union (MDR-RA projectfunded by the Horizon Europe research and innovation programme) and the Staedtler Foundation. The work was also supported by donations from the Bendel family and the Bleyl family.

Patient and public involvement

Patients and/or the public were not involved in the design, or conduct, or reporting, or dissemination plans of this research.

Patient consent for publication

Consent was obtained directly from the patients.

Ethics approval

All procedures were performed in accordance with the Good Clinical Practice guidelines of the International Council for

Harmonization and covered by license 334_18B of the Institutional Review Board (IRB). Self-reported and biological sexes were identical in all patients. All participants gave written informed consent in compliance with the Declaration of Helsinki principles. No commercial sponsor was involved.

Provenance and peer review

Not commissioned; externally peer reviewed.

Data availability statement

Not applicable.

Supplementary materials

Supplementary material associated with this article can be found in the online version at doi:10.1016/j.ard.2026.07.011.

Orcid

Ricardo Grieshaber-Bouyer: http://orcid.org/0000-0002-2873-5135

REFERENCES

[1] Schett G, Nagy G, Kronke G, Mielenz D. B-cell depletion in autoimmune diseases. Ann Rheum Dis 2024;83(11):1409–20. doi: 10.1136/ard-2024-225727.

[2] Edwards JC, Szczepanski L, Szechinski J, Filipowicz-Sosnowska A, Emery P, Close DR, et al. Efficacy of B-cell-targeted therapy with rituximab in patients with rheumatoid arthritis. N Engl J Med. 2004;350(25):2572–81. doi: 10.1056/NEJMoa032534.

[3] Mackensen A, Muller F, Mougiakakos D, Böltz S, Wilhelm A, Aigner M, et al. Anti-CD19 CAR T cell therapy for refractory systemic lupus erythematosus. Nat Med. 2022;28(10):2124–32. doi: 10.1038/s41591-022-02017-5.

[4] Muller F, Taubmann J, Bucci L, Wilhelm A, Bergmann C, Völkl S, et al. CD19 CAR T-cell therapy in autoimmune disease - a case series with follow-up. N Engl J Med. 2024;390(8):687–700. doi: 10.1056/NEJMoa2308917.

[5] Bucci L, Hagen M, Rothe T, Raimondo MG, Fagni F, Tur C, et al. Bispecific T cell engager therapy for refractory rheumatoid arthritis. Nat Med. 2024;30(6):1593–601. doi: 10.1038/s41591-024-02964-1.

[6] Bucci L, Boltz S, Hagen M, Tur C, Nöthling DM, Rothe T, et al. BCMA T-cell engager therapy in patients with refractory autoimmune disease. N Engl J Med. 2025;393(15):1544–7. doi: 10.1056/NEJMc2506740.

[7] Löffler A, Kufer P, Lutterbüse R, Zettl F, Daniel PT, Schwenkenbecher JM, et al. A recombinant bispecific single-chain antibody, CD19 × CD3, induces rapid and high lymphoma-directed cytotoxicity by unstimulated T lymphocytes. Blood. 2000;95(6):2098–103.

[8] Topp MS, Gokbuget N, Stein AS, Zugmaier G, O'Brien S, Bargou RC, et al. Safety and activity of blinatumomab for adult patients with relapsed or refractory B-precursor acute lymphoblastic leukaemia: a multicentre, single-arm, phase 2 study. Lancet Oncol. 2015;16(1):57–66. doi: 10.1016/S1470-2045(14)71170-2.

[9] Kantarjian H, Stein A, Gokbuget N, Fielding AK, Schuh AC, Ribera JM, et al. Blinatumomab versus chemotherapy for advanced acute lymphoblastic leukemia. N Engl J Med. 2017;376(9):836–47. doi: 10.1056/NEJMoa1609783.

[10] Litzow MR, Sun Z, Mattison RJ, Paietta EM, Roberts KG, Zhang Y, et al. Blinatumomab for MRD-negative acute lymphoblastic leukemia in adults. N Engl J Med. 2024;391(4):320–33. doi: 10.1056/NEJMoa2312948.

[11] Borowitz MJ, Wood BL, Devidas M, Loh ML, Raetz EA, Salzer WL, et al. Prognostic significance of minimal residual disease in high risk B-ALL: a report from Children's Oncology Group study AALL0232. Blood. 2015;126(8):964–71. doi: 10.1182/blood-2015-03-633685.

[12] Ruck T, Huntemann N, Ozturk M, Schreiber S, Lichtenberg S, Masanneck L, et al. CD19xCD3 T cell engager blinatumomab effective in refractory generalized myasthenic syndromes. Mol Ther. 2025;33(9):4135–42. doi: 10.1016/j.ymthe.2025.06.042.

[13] Subklewe M, Magno G, Gebhardt C, Bücklein V, Szelinski F, Arévalo HJR, et al. Application of blinatumomab, a bispecific anti-CD3/CD19 T-cell engager, in treating severe systemic sclerosis: a case study. Eur J Cancer. 2024;204:114071. doi: 10.1016/j.ejca.2024.114071.

[14] Isaacs JD. Immune reset and immune retune: approaching cure? Nat Rev Rheumatol. 2026;22(4):215–7. doi: 10.1038/s41584-026-01357-7.

[15] Aletaha D, Neogi T, Silman AJ, Funovits J, Felson DT, Bingham 3rd CO, et al. 2010 rheumatoid arthritis classification criteria: an American College of Rheumatology/European League Against Rheumatism collaborative initiative. Ann Rheum Dis. 2010;69(9):1580–8. doi: 10.1136/ard.2010.138461.

[16] Kuwert T, Schmidkonz C, Prante O, Schett G, Ramming A. FAPI PET Opens a new window to understanding immune-mediated inflammatory diseases. J Nucl Med 2022;63(8):1136–7. doi: 10.2967/jnumed.122.263922.

[17] D'Agostino MA, Terslev L, Aegerter P, Backhaus M, Balint P, Bruyn GA, et al. Scoring ultrasound synovitis in rheumatoid arthritis: a EULAR-OMERACT ultrasound taskforce-Part 1: definition and development of a standardised, consensus-based scoring system. RMD Open. 2017;3(1):e000428. doi: 10.1136/rmdopen-2016-000428.

[18] Moller I, Largo R, Bong DA, Filer A, Najm A, Alivernini S, et al. EULAR standardised training model for ultrasound-guided, minimally invasive synovial tissue biopsy procedures in large and small joints. RMD Open. 2025;11(1):e005065. doi: 10.1136/rmdopen-2024-005065.

[19] Tur C, Eckstein M, Velden J, Rauber S, Bergmann C, Auth J, et al. CD19-CAR T-cell therapy induces deep tissue depletion of B cells. Ann Rheum Dis 2025;84(1):106–14. doi: 10.1136/ard-2024-226142.

[20] Tur C, Eckstein M, Bucci L, Auth J, Bergmann C, Rauber S, et al. Effects of different B-cell-depleting strategies on the lymphatic tissue. Ann Rheum Dis. 2025;84(12):2065–74. doi: 10.1016/j.ard.2025.06.2120.

[21] Baik AH, Oluwole OO, Johnson DB, Shah N, Salem JE, Tsai KK, et al. Mechanisms of cardiovascular toxicities associated with immunotherapies. Circ Res. 2021;128(11):1780–801. doi: 10.1161/CIRCRESAHA.120.315894.

[22] Sayed A, Munir M, Ghazi SM, Ferdousi M, Krishan S, Shaaban A, et al. Cardiovascular toxicities associated with bispecific T-cell engager therapy. J Immunother Cancer. 2024;12(2):e008518. doi: 10.1136/jitc-2023-008518.

[23] Stein AS, Schiller G, Benjamin R, Jia C, Zhang A, Zhu M, et al. Neurologic adverse events in patients with relapsed/refractory acute lymphoblastic leukemia treated with blinatumomab: management and mitigating factors. Ann Hematol. 2019;98(1):159–67. doi: 10.1007/s00277-018-3497-0.

[24] Philipp N, Kazerani M, Nicholls A, Vick B, Wulf J, Straub T, et al. T-cell exhaustion induced by continuous bispecific molecule exposure is ameliorated by treatment-free intervals. Blood. 2022;140(10):1104–18. doi: 10.1182/blood.2022015956.

[25] Croft AP, Campos J, Jansen K, Turner JD, Marshall J, Attar M, et al. Distinct fibroblast subsets drive inflammation and damage in arthritis. Nature. 2019;570(7760):246–51. doi: 10.1038/s41586-019-1263-7.

Ann Rheum Dis 85 (2026) 1716–1728

Contents lists available at ScienceDirect

Annals of the Rheumatic Diseases

journal homepage: https://www.sciencedirect.com/journal/annals-of-the-rheumatic-diseases

Rheumatoid arthritis

Time-resolved immune dynamics in rheumatoid arthritis under methotrexate therapy

Teresa Preglej[1], Anela Tosevska[1], Marie Brinkmann[1], Philipp Schatzlmaier[2,3], Franziska Schmidt[4], Jakov Korzhenevich[4], Elisabeth Simader[1], Daniela Sieghart[1], Philipp Hofer[5], Thomas Krausgruber[6,7], Lina Dobnikar[6], Christoph Bock[6,7], Thomas Karonitsch[1], Renate Kain[5], Hannes Stockinger[2], Josef S. Smolen[1], Wilfried Ellmeier[8], Leonid Padyukov[9,10], Marta Rizzi[4,11,12,13], Daniel Aletaha[1], Lisa Göschl[1,*], Michael Bonelli[1,**]

[1] *Department of Internal Medicine 3, Division of Rheumatology, Medical University of Vienna, Vienna, Austria*
[2] *Center for Pathophysiology, Infectiology and Immunology, Institute for Hygiene and Applied Immunology, Medical University of Vienna, Vienna, Austria*
[3] *Department of Biological Sciences and Pathobiology, Physiology & Pathophysiology, University of Veterinary Medicine Vienna, Vienna, Austria*
[4] *Division of Clinical and Experimental Immunology, Center for Pathophysiology, Infectiology and Immunology, Institute of Immunology, Medical University of Vienna, Vienna, Austria*
[5] *Department of Pathology, Medical University of Vienna, Vienna, Austria*
[6] *CeMM Research Center for Molecular Medicine of the Austrian Academy of Sciences, Vienna, Austria*
[7] *Center for Medical Data Science, Institute of Artificial Intelligence, Medical University of Vienna, Vienna, Austria*
[8] *Division of Immunobiology, Center for Pathophysiology, Infectiology and Immunology, Institute of Immunology, Medical University of Vienna, Vienna, Austria*
[9] *Division of Rheumatology, Department of Medicine Solna, Karolinska Institutet and Karolinska University Hospital, Stockholm, Sweden*
[10] *Center for Molecular Medicine, Karolinska Institutet, Stockholm, Sweden*
[11] *Department of Rheumatology and Clinical Immunology, University Medical Center Freiburg, Faculty of Medicine, University of Freiburg, Freiburg, Germany*
[12] *Center for Chronic Immunodeficiency, University Medical Center Freiburg, Faculty of Medicine, University of Freiburg, Freiburg, Germany*
[13] *CIBSS – Centre for Integrative Biological Signalling Studies, University of Freiburg, Freiburg, Germany*

ARTICLE INFO

Article history:
Received 1 October 2025
Received in revised form 2 March 2026
Accepted 11 May 2026

ABSTRACT

Objectives: Methotrexate (MTX) is the first-line treatment for rheumatoid arthritis (RA), yet its immunological mechanisms remain incompletely understood. This study aimed to define the time-resolved cellular and molecular changes induced by MTX.

Methods: In a prospective longitudinal study, newly diagnosed patients with RA initiating MTX were systematically profiled over time. We applied an integrated single-cell multiomics approach combining high-parameter immunophenotyping and single-cell RNA sequencing of PBMCs (peripheral blood mononuclear cells) obtained from 6 patients at baseline and at

*Correspondence to Dr. Lisa Göschl, Department of Internal Medicine 3, Division of Rheumatology, Medical University of Vienna, Vienna, Austria.
**Correspondence to Dr. Michael Bonelli, Department of Internal Medicine 3, Division of Rheumatology, Medical University of Vienna, Vienna, Austria.
E-mail addresses: lisa.goeschl@meduniwien.ac.at (L. Göschl), michael.bonelli@meduniwien.ac.at (M. Bonelli).
Handling editor Rik Lories.
Teresa Preglej and Anela Tosevska contributed equally.

https://doi.org/10.1016/j.ard.2026.05.018

0003-4967/© 2026 The Author(s). Published by Elsevier B.V. on behalf of European Alliance of Associations for Rheumatology (EULAR). This is an open access article under the CC BY license (http://creativecommons.org/licenses/by/4.0/)

sequential time points during therapy. Functional *in vitro* assays were conducted to evaluate direct effects of MTX. Key findings were validated in an independent cohort of 22 patients with RA, stratified by clinical response, and integrated with external transcriptomic datasets.

Results: MTX-induced rapid immune remodelling that was detectable as early as 3 weeks after treatment initiation and preceded clinical improvement. The earliest and most pronounced alterations occurred in T follicular helper (Tfh) cells and plasmablasts, which declined selectively in clinical responders but remained largely unchanged in nonresponders across independent cohorts and external datasets, underscoring their potential as early biomarkers of treatment response. Functional plasmablast differentiation assays further linked MTX treatment to impaired development. Transcriptomic network analyses identified novel regulatory hubs associated with MTX exposure, including *LMNA, SCO2, GVQW3*, and members of the *GIMAP* family. To promote data accessibility, we developed an interactive single-cell browser for community-driven exploration.

Conclusions: Together, these findings reveal an unexpectedly rapid and coordinated immune reconfiguration after MTX initiation and position early alterations in Tfh cells and plasmablasts as biomarkers of treatment response.

WHAT IS ALREADY KNOWN ON THIS TOPIC

- Methotrexate (MTX) is the first-line treatment for rheumatoid arthritis (RA), with well-established clinical efficacy.
- The molecular and cellular mechanisms underlying the efficacy of MTX are largely unknown.
- A longitudinal cellular and molecular profile of patients with RA who respond to MTX therapy is missing.

WHAT THIS STUDY ADDS

- Time-resolved high-dimensional profiling reveals MTX-driven immunomodulatory effects as early as 3 weeks after treatment initiation.
- Rapid shifts in naïve and memory lymphocyte populations, particularly T follicular helper cells and plasmablasts, together with molecular changes in key immune pathways, have been identified.
- Complementary *in vitro* assays demonstrate that MTX directly modulates plasmablast development.
- Stratified cellular and transcriptomic analyses distinguish responders from nonresponders, highlighting potential early markers of treatment efficacy.

HOW THIS STUDY MIGHT AFFECT RESEARCH, PRACTICE OR POLICY

- Early immune and molecular signatures could be used to predict treatment response to MTX.
- The provided cell browser tool is a powerful resource to validate target genes involved in the mode of action of MTX.

INTRODUCTION

Rheumatoid arthritis (RA) represents a systemic autoimmune disease primarily affecting the joints, leading to cartilage degradation, joint erosion, and, if left untreated, irreversible destruction of the joints and functional disability [1,2]. Although the precise aetiology of RA remains elusive, the disease is marked by an aberrant immune cell activity that disrupts the delicate immunological balance. A complex interplay of diverse immune cell types contributes to the initiation and progression of RA. Key players include B cells, T cells, and myeloid cells, which infiltrate the synovium and circulate in peripheral blood, perpetuating inflammatory and destructive processes [3].

Disease-modifying antirheumatic drugs (DMARDs) have revolutionised RA management, enabling targeted control of inflammation, deceleration of disease progression, and improved physical function [4]. Furthermore, DMARDs have been shown to mitigate structural damage, alleviate symptoms, and improve the quality of life in patients with RA [1,2]. Among available DMARDs, methotrexate (MTX) remains the first-line therapy due to its proven efficacy, safety, and tolerability [1,2]. Its efficacy is hypothesised to be rooted in a multifaceted interplay of anti-inflammatory effects targeting various pathogenic cell types. Proposed mechanisms include inhibition of cellular proliferation, enhancement of anti-inflammatory adenosine signalling, and modulation of critical inflammatory signalling circuits such as the JAK/STAT and NF-κB pathways [1,5,6]. In addition, MTX contributes to the restoration of $CD4^+$ T-cell homeostasis. [7–10].

Despite its overall efficacy, it has to be considered that 30% to 60% of patients fail to achieve an adequate therapeutic response to MTX [11–15]. This challenge is compounded by MTX's slow onset of action, which delays the routine assessment of treatment efficacy. As a result, nonresponders may remain exposed to ineffective therapy for up to 3 months. Therefore, identifying cellular response indicators as biomarkers is essential for the early prediction of treatment response.

To capture both immune cell population dynamics and transcriptional changes after MTX treatment, we performed single-cell RNA sequencing (scRNA-seq) and multicolour immunophenotyping of PBMCs from treatment-naïve patients with RA, sampled at baseline (BL), and at 3, 6, and 12 weeks after treatment initiation. This longitudinal, time-resolved analysis revealed early MTX-induced changes in both cellular composition and gene expression. Complementary *in vitro* assays indicated a direct modulatory effect of MTX on plasmablast development, supporting the observed *in vivo* immune remodelling. Through stratified analysis by treatment response in an independent cohort of MTX responders and nonresponders, we highlighted potential biomarkers predictive of therapeutic outcome. In addition, our interactive cell browser platform enables the exploration of gene expression and gene set dynamics in the scRNA-seq data, facilitating further validation of MTX-induced molecular effects.

METHODS

Study design

Six patients with RA (diagnosed according to American College of Rheumatology/European Alliance of Associations for Rheumatology criteria [16]) and 6 age-, sex-, body mass index-,

Table
Characteristics of patients with RA

Patient characteristics at week 0	Patient no. 1	2	3	4	5	6	Mean ± SD
Sex (m/f)	f	f	f	f	m	m	
Age (y)	64	62	57	53	39	60	55.83 ± 9.11
Body mass index	25.89	32.22	24.8	26.03	30.35	26.42	27.62 ± 2.95
Rheumatoid factor (IU/mL)	pos	pos	pos	pos	pos	pos	
ACPA (U/mL)	pos	pos	pos	pos	pos	pos	
Smoking status							
Current smoker		X	x	x	x	x	
Ex-smoker	for 5 years						
Pack years	10	2	37	10	40	30	21.5 ± 16.12
CDAI	29.5	3.2	20.6	10.8	6.3	26.3	16.12 ± 10.90
DAS 28	5.016	3.53	4.748	2.98	3.263	4.725	4.044 ± 0.88
Swollen joints (n)	9	1	4	1	1	7	3.83 ± 3.49
Tender joints (n)	12	2	9	4	2	8	6.17 ± 4.12
CRP (mg/dL)	0.69	2.3	1.04	0.21	1.1	0.57	0.99 ± 0.72
Patient characteristics after week 12							
CDAI	14.5	5.3	5.3	4	2.2	13.7	7 ± 5.24
DAS 28	3.817	3.138	2.528	2.068	1.68	3.73	2.83 ± 0.88
Swollen joints (n)	1	0	2	0	0	4	1.17 ± 1.6
Tender joints (n)	7	2	0	1	0	3	1.83 ± 2.64
CRP (mg/dL)	0.25	1.61	0.96	0.08	0.63	0.88	0.74 ± 0.55
Patient characteristics after week 12							
Remission	no (LDA: yes)	yes	yes	yes	yes	yes	
Sustained remission	no	yes	yes	yes	yes	yes	

ACPA, anti-citrullinated protein antibody; CDAI, clinical disease activity index; CRP, C-reactive protein; DAS28, disease activity score in 28 joints; LDA, low disease activity; pos, positive.

and smoking-matched healthy control (HC) were enrolled from the outpatient clinic at Medical University of Vienna. All participants provided informed consent, and ethical approval was obtained (EK: 1075/2021; 2071/2020; 1526/2025). At BL, all participants were glucocorticoid-naïve and had only used over-the-counter NSAIDs (nonsteroidal anti-inflammatory drugs). Patients with RA initiated MTX treatment at 15 mg/wk, which was increased to 25 mg/wk at week 3, and were monitored over 12 weeks with blood samples collected at BL, weeks 3, 6, and 12. Disease activity was assessed by clinical disease activity index (CDAI) and DAS28 at BL and at week 12. Further details and participant characteristics are provided in the Table and the online Supplementary Methods; the second patient cohort is described in the Supplementary Methods.

Sample processing for flow sorting and immunophenotyping

Details on PBMC isolation, freezing, thawing, and processing are provided in the online supplementary methods. In brief, samples from 1 HC and 1 patient with RA (all time points) were processed in parallel. After thawing, PBMCs were stained for viability. Viable PBMCs were sorted and assessed for purity. Unsorted L/D-stained PBMCs were used for surface staining with a 37-antibody panel for immunophenotyping.

scRNA-seq, deconvolution, and downstream analyses

Full details and parameters are provided in the online Supplementary Methods.

PBMC immunophenotyping and analysis

PBMCs were stained for immunophenotyping as described previously [18,19]. Flow cytometry data were imported into FlowJo (BD Biosciences). Detailed parameters and gating strategies are provided in Supplementary Figure S1 and the online Supplementary Methods.

Downstream data analysis and statistics in R

Data analysis was performed in RStudio (Posit, PBC). Hierarchical clustering and statistical tests (paired/unpaired t-tests with BH [Benjamini-Hochberg] correction) were conducted using standard R packages. Significance was defined as follows: $^{\#}P < .1$, $^{*}P < .05$, $^{**}P < .01$, $^{***}P < .001$, and $^{****}P < .0001$. Detailed analysis steps and parameters are available in the online Supplementary Methods.

RESULTS

MTX therapy induces longitudinal PBMC subset perturbations

To investigate cellular and transcriptional alterations in the immune landscape of patients with RA in response to MTX treatment, newly diagnosed and treatment-naïve patients were enrolled in a prospective observational study. PBMCs were collected at BL (before therapy initiation), as well as 3, 6, and 12 weeks after MTX treatment initiation (Fig 1A). None of the patients received glucocorticoids at the start of treatment. The included patients showed a clear therapeutic response to MTX, defined by at least a 50% reduction in the CDAI, together with decreases in DAS28 and C-reactive protein (CRP) levels. Patients' demographic details and clinical/laboratory data are summarised in the Table. PBMCs were analysed by spectral flow cytometry (Supplementary Fig S1) for immunophenotyping and by complementary scRNA-seq (Supplementary Fig S2B-D). Temporal changes were analysed and compared with sex- and age-matched HCs. Dimensionality reduction of immunophenotyping data revealed clear clustering of the RA and HC cohorts, underscoring the homogeneity within each study group (Supplementary fig S2A).

To capture longitudinal effects of MTX, we expressed immune cell frequencies at weeks 3, 6, and 12 as changes relative to RA BL. BL differences between patients with RA and HCs served as a reference point to interpret whether MTX-associated

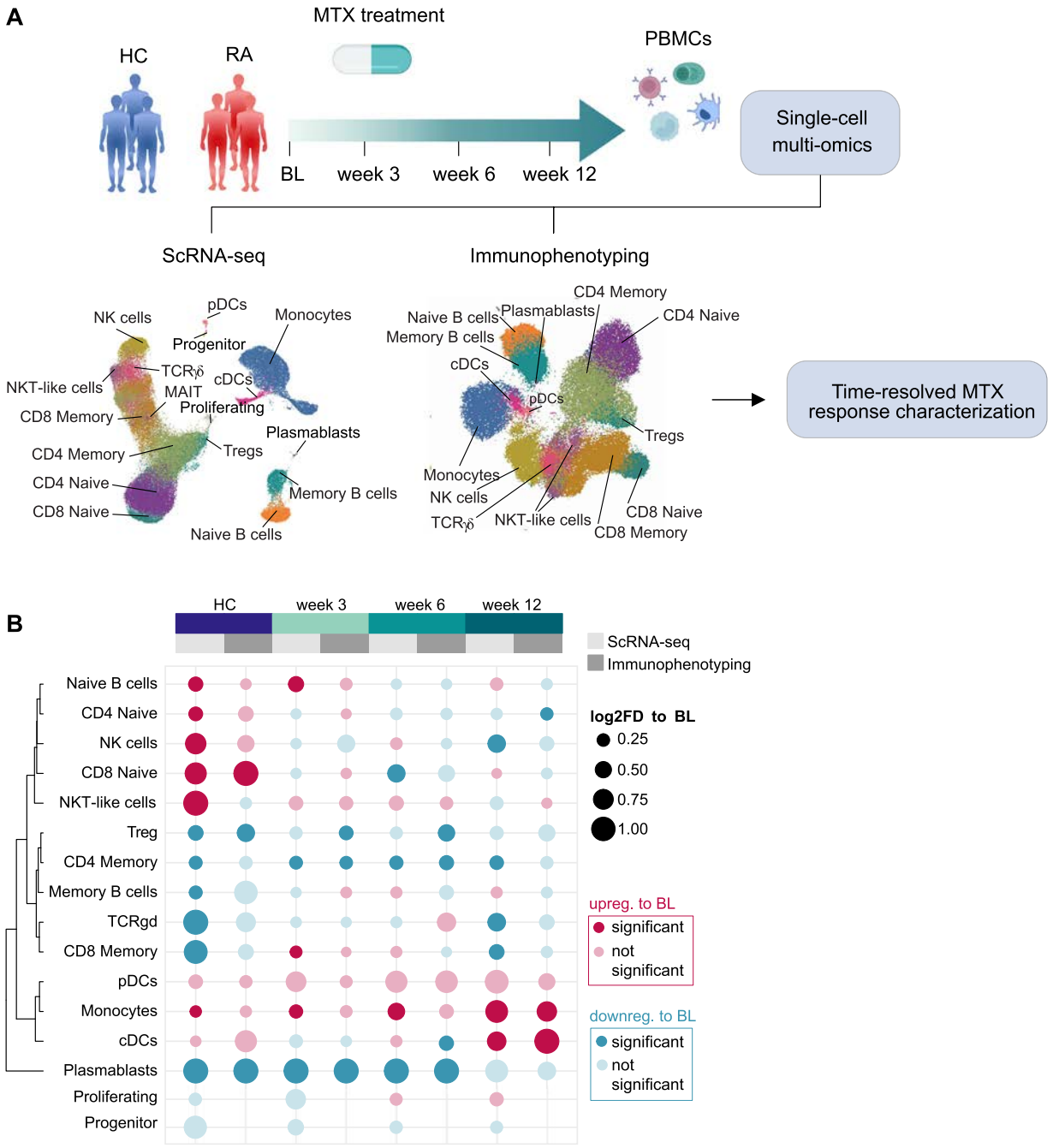

Figure 1. Multimodal analysis of PBMC subset perturbation during MTX therapy in patients with RA. (A) Schematic representation of the study design and sampling time points. PBMCs were isolated from 6 treatment-naïve patients at baseline and at 3, 6, and 12 wk after initiation of MTX therapy, as well as from 6 age- and sex-matched healthy controls. The cells were subjected to immunophenotyping (n = 6) and single-cell RNA sequencing (scRNA-seq) (n = 5). Uniform Manifold Approximation and Projection plots are shown, representing the global cell types. (B) Cell-type abundance comparison across the 2 methodologies and cell types. HC and each time point in MTX-treated patients with RA (3, 6, and 12 wk after treatment initiation) were compared with those of RA BL. Dot size reflects the magnitude of MTX-induced perturbations in cell types, represented as changes relative to RA BL and capped at an absolute value of 1, whereas dot colour indicates significance (*P* values calculated using a permutation test and BH-corrected; significance was defined as $P < .05$). BL, baseline; cDC, conventional dendritic cells; HC, healthy controls; MTX, methotrexate; NKT-like cells, natural killer T cell; pDC, plasmacytoid dendritic cells; RA, rheumatoid arthritis; TCR$\gamma\delta$, T-cell receptor gamma delta T cell; Treg, regulatory T cell.

changes reflect a shift towards the healthy phenotype (Fig 1B). ScRNA-seq and immunophenotyping were comparable in detecting PBMC subpopulations, as the cellular abundances of different cell types showed a strong concordance between the 2 methods. Longitudinal changes in cell-type abundances were categorised based on hierarchical clustering. Naïve B cells, naïve CD4+ T cells, naïve CD8+ T cells, natural killer (NK) cells, and NK T-cell (NKT)–like cells were grouped into a 'naïve' cluster, whereas memory cells (CD4+ memory T cells, CD8+ memory T cells, memory B cells), as well as regulatory T cells (Tregs) and T-cell receptor gamma delta (TCR$\gamma\delta$) T cells, formed a 'memory' cluster. A third 'myeloid' cluster contained dendritic cells (DCs) and monocytes; the fourth cluster comprised plasmablasts. Cells within the naïve cluster, particularly naïve B cells and NKT-like cells, were reduced in RA but increased post MTX to resemble HC levels, whereas memory subsets, elevated in RA, declined after treatment and remained low. Myeloid cluster cells (plasmacytoid DCs [pDCs], conventional DC [cDCs], monocytes) were

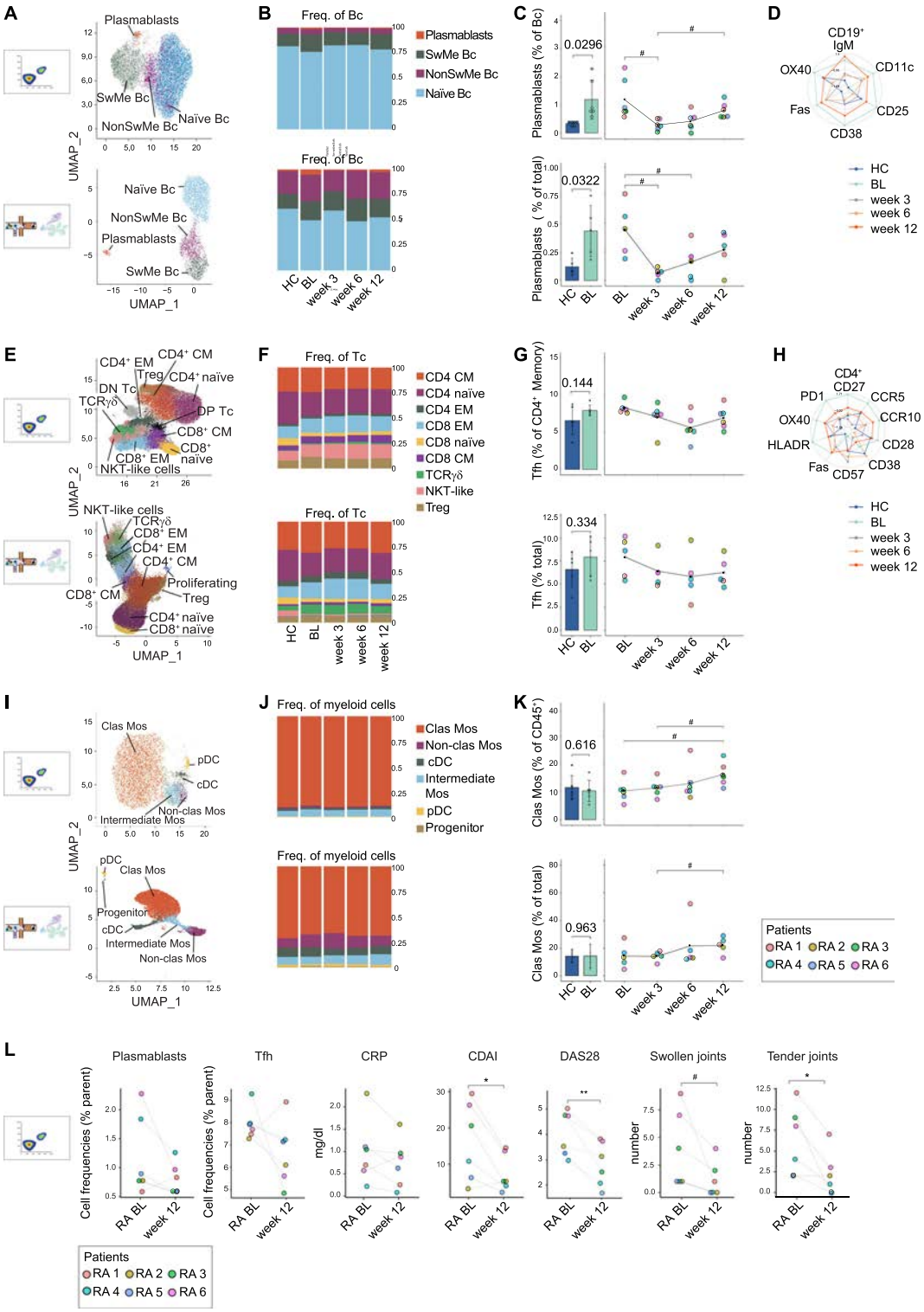

Figure 2. Dynamic modulation of immune cell subsets and activation markers during MTX therapy in patients with RA. (A,E,I) Uniform Manifold Approximation and Projection (UMAP) of (A) B-cell subsets, (E) T cell subsets, and (I) myeloid cell populations from concatenated samples of HCs and patients with RA at baseline (BL) and during therapy. UMAPs were generated from immunophenotyping (upper panels) and scRNA-seq (lower panels) data. (B,F,J) Peripheral blood mononuclear cells (PBMC) subsets were defined according to the gating strategy shown in Supplementary Figure S1. Frequencies of (B) B-cell subpopulations (% of $CD19^+$ cells), (F) T cell subpopulations (% of $CD3^+$ cells), and (J) myeloid subpopulations (% of $CD45^+$ cells) (upper panels), and as a percentage of total cells (lower panels). (C,G,K) Bar charts and dot plots depict changes in (C) plasmablasts (% of $CD19^+$ cells), (G) Tfh cells (% of $CD4^+$ memory T cells), and (K) classical monocytes (% of $CD45^+$ cells) (upper panels), and as a percentage of total cells (lower panels). Data were generated using immunophenotyping (upper panels) (n = 6) and scRNA-seq (lower panels) (n = 5). (D,H) Radar plots display longitudinal changes in activation markers for (D) B cells and (H) $CD4^+$ T cells, generated by immunophenotyping. (L) Dot plots depict changes in plasmablasts (% of $CD19^+$ cells), Tfh cells (% of $CD4^+$ memory T cells) defined by immunophenotyping, as well as changes in CRP (mg/dL), CDAI, Disease activity score in 28 joints (DAS28), swollen joints, and tender joints (number of joints). For paired comparisons during the MTX treatment time course in patients with RA, paired t-tests with Benjamini–Hochberg adjustment were applied, using a 90% CI. Significance thresholds were defined as follows: #$P < .1$, *$P < .05$, **$P < .01$, ***$P < .001$, ****$P < .0001$. Only significant values are shown, unless otherwise indicated. Comparisons between HCs and patients with RA were conducted using unpaired t-tests, with the same significance criteria. CDAI, clinical disease activity index; cDC, conventional

slightly higher in HC and tended to increase in patients with RA post MTX. Plasmablasts exhibited the strongest RA-associated increase but dropped to HC levels by week 3, as reflected by the most substantial $\log_2$ fold-decrease among all evaluated subsets. These data highlight MTX's time-dependent, cell-type–specific effects on PBMC subpopulations, ultimately restoring cell subset distributions in patients with RA.

Lymphocyte and myeloid modulation by MTX in RA

Observing shifts in all major immune cell populations well before week 12, a clinically critical time point for evaluating therapeutic response, we performed a more detailed subclustering of B cell, T cell, and monocyte subtypes to identify MTX-responsive populations.

Distinct B-cell subsets, including naïve, nonswitched memory (NonSwMe), switched memory (SwMe), and plasmablasts (Fig 2A), were defined by immunophenotyping and scRNA-seq. Compared with HC, patients with RA displayed reduced frequencies of naïve B cells, whereas SwMe B cells and plasmablasts were elevated (Fig 2B). MTX treatment was associated with a significant reduction in plasmablast proportions as early as 3 weeks after initiation, followed by a slight rebound at week 12 (Fig 2C). This partial recovery may be related to the upregulation of survival-associated factors in plasmablasts (Supplementary fig S3B). Further subsetting revealed multiple naïve and NonSwMe B-cell substates (Supplementary fig S3A,E), none of which were substantially altered by MTX. Immunophenotyping of activation markers confirmed heightened B-cell activation in untreated RA, which progressively declined after MTX, reaching levels comparable with HCs by week 3 (Fig 2D). Overall, MTX treatment was associated with a partial normalisation of B-cell subset distribution and activation status in patients with RA. The most pronounced changes were observed in plasmablasts as early as 3 weeks after treatment initiation.

Using immunophenotyping and scRNA-seq, we identified and quantified distinct $CD3^+$ T-cell subsets, including naïve, central memory (CM), and effector memory $CD4^+$ and $CD8^+$ T cells, as well as Tregs, double-positive and double-negative T cells, TCR$\gamma\delta$, and NKT-like cells (Fig 2E). At BL, patients with RA displayed reduced frequencies of naïve $CD4^+$ and naïve $CD8^+$ T cells, alongside elevated CM $CD4^+$ and CM $CD8^+$ T cells, Tregs, and NKT-like cells (Fig 2F). MTX treatment partially normalised these distributions, increasing naïve and reducing memory T cells towards levels observed in HC (Figs 2B and 2F), with a particularly pronounced reduction in T follicular helper (Tfh) cells within the first 6 weeks of therapy (Fig 2G). Subclustering by scRNA-seq confirmed BL differences between HC and RA, although only a limited number of subsets, including $CD8^+$ effector cells, MAIT cells (mucosal-associated invariant T cells), and memory Tregs, showed significant treatment-related changes (Supplementary fig S3C,E). Analysis of T-cell activation markers further demonstrated increased expression on $CD4^+$ T cells in RA, which declined significantly by week 3, approaching HC levels (Fig 2H). Taken together, MTX treatment partially restored T-cell subsets and reduced activation in patients with RA, with Tfh cells showing the strongest effects already at week 3.

A detailed analysis of the myeloid compartment using immunophenotyping and scRNA-seq confirmed known subsets, including classical, intermediate, and nonclassical monocytes, cDCs, pDCs, and $CD34^+$ haematopoietic progenitors [20] (Fig 2I). Classical monocytes and cDCs were largely unaffected in patients with RA compared with HCs but showed a tendency to increase over time (Fig 2J,K). Further scRNA-seq subclustering of classical monocytes also revealed MTX-induced changes in the IL1B subset at weeks 3 and 6, and in the interferon (IFN) subset at 12 weeks (Supplementary Fig S3D,E).

Given that plasmablasts and Tfh cells showed the most pronounced responses to MTX, we investigated whether these changes were mirrored by clinical measures of disease activity. In line with a decline in clinical disease activity parameters, such as CRP, CDAI, DAS28, and counts of swollen and tender joints, we observed a reduction in plasmablasts and Tfh cells (Fig 2L).

In brief, MTX treatment modulated circulating immune cell populations, progressively normalising lymphocyte subsets. These effects included a rapid reduction in immune cell activation markers and shifts in cellular proportions observed as early as 3 weeks after treatment initiation. These data suggest, for the first time, MTX induces early cellular perturbations that precede the clinical response.

In vitro modelling recapitulates MTX-mediated effects

To functionally interrogate our *ex vivo* observations, we next sought to model MTX-mediated immune modulation *in vitro*. PBMCs from treatment-naïve patients with RA were activated for 24 hours in the presence or absence of MTX, followed by immunophenotyping (Fig 3A). Consistent with our *ex vivo* findings, MTX exposure was associated with increased frequencies of naïve B cells and naïve $CD4^+$ T cells, accompanied by reduced proportions of Tfh cells and plasmablasts (Fig 3B). These findings may suggest a preferential sensitivity of activated and differentiating lymphocyte subsets to MTX, leading to a relative enrichment of naïve populations.

Given the pronounced effect observed in the plasmablast compartment, we next examined this population in greater detail using a plasmablast differentiation assay. B cells were isolated from PBMCs and stimulated with cytosine–phosphate–guanine oligodeoxynucleotides in the presence or absence of MTX. Immunophenotypic analyses were performed after 3 and 6 days of culture (Fig 3C). MTX-treated cultures exhibited reduced total $CD19^+$ B-cell numbers and decreased frequencies of antibody-secreting cells (ASCs) at day 6 (Fig 3D,E). Notably, $CD19^+$ cell counts remained relatively stable between day 3 and day 6 in the presence of MTX, suggesting that the observed reduction in ASC may not primarily reflect impaired survival but rather altered proliferative dynamics. As proliferation is closely linked to plasmablast differentiation [21], these findings suggest that MTX may primarily limit the proliferative expansion required for ASC development. In contrast, other B-cell subsets were only modestly affected (Fig 3F), indicating a preferential impact on the plasmablast/ASC compartment. Together, these data support a selective sensitivity of plasmablast development to MTX.

dendritic cells; Clas Mos, classical monocytes; CM, central memory; CRP, C-reactive protein; DN, double negative; EM, effector memory; HC, healthy controls; Mos, monocytes; MTX, methotrexate; NKT-like cells, natural killer T cells; Non-clas Mos, nonclassical monocytes; NonSwMe Bc, nonswitched memory B cells; pDC, plasmacytoid dendritic cells; RA, rheumatoid arthritis; ScRNA-seq, single-cell RNA sequencing; SwMe Bc, switched memory B cells; TCR$\gamma\delta$, T-cell receptor gamma delta T cell; Tfh, T follicular helper; Treg, regulatory T cell.

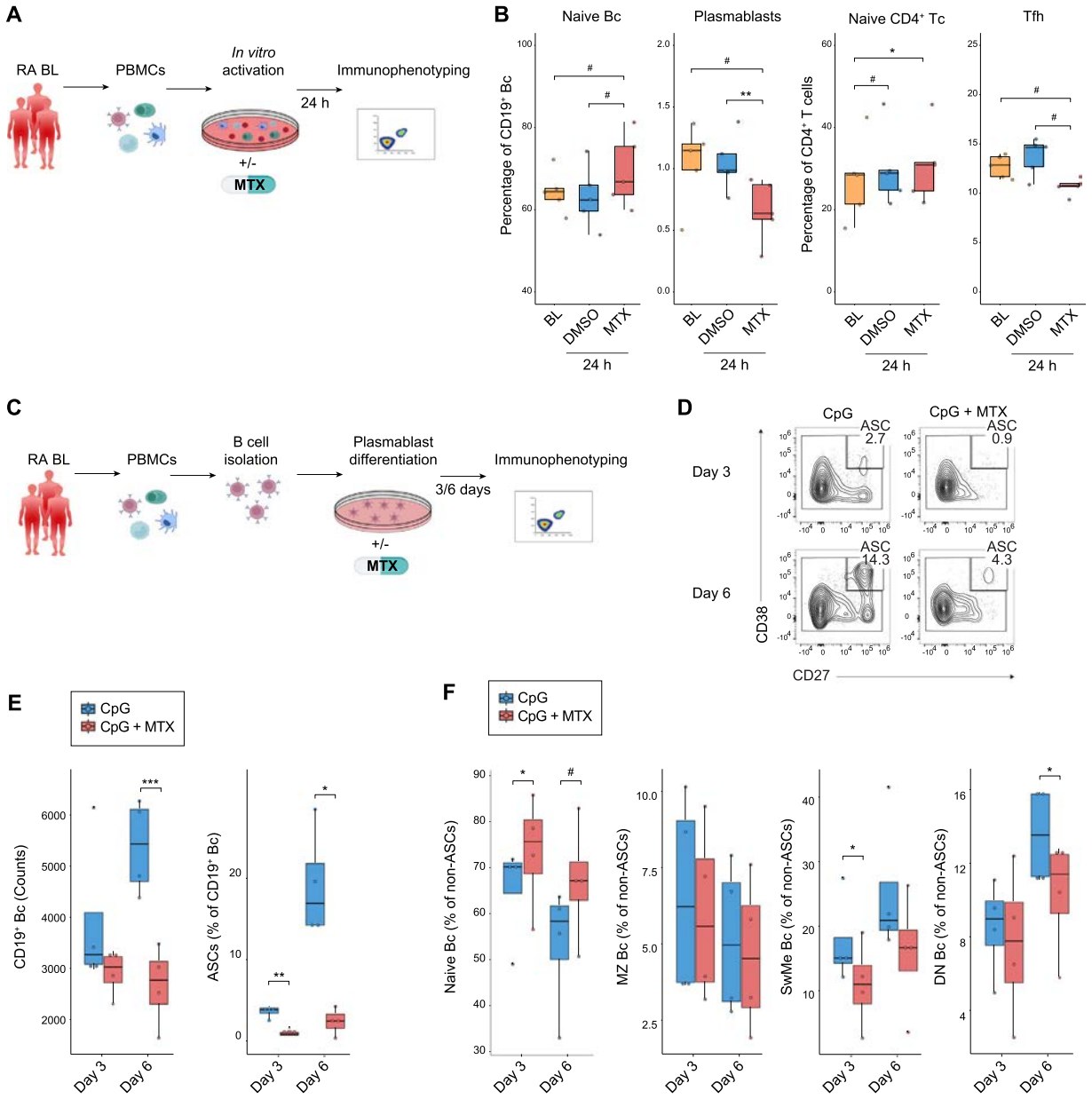

Figure 3. *In vitro* validation of MTX effects on peripheral blood mononuclear cells (PBMC) subsets. (A) Workflow of the *in vitro* assay. PBMCs from treatment-naïve patients with RA (n = 5) were activated with phytohaemagglutinin (PHA) for 24 hours in the presence of DMSO (dimethyl sulfoxide) or 100 nM MTX, followed by immunophenotyping of major PBMC compartments. (B) Boxplots showing percentages of naïve B cells and plasmablasts (% of CD19⁺ B cells), and naïve CD4⁺ T cells and Tfh cells (% of CD4⁺ T cells). (C) Schematic overview of the plasmablast differentiation assay. CD19⁺ B cells were isolated from PBMCs of treatment-naïve patients with RA (n = 3) and 1 healthy control and stimulated with CpG in the presence or absence of 100 nM MTX for 6 days. Immunophenotyping was performed on day 3 and day 6. (D) Representative fluorescence-activated cell sorting (FACS) plots showing CD27 and CD38 expression on CD19⁺ B cells, distinguishing plasmablasts/antibody-secreting cells (ASCs) from non-ASC populations. Numbers indicate the percentage of cells within the respective quadrant. (E,F) Boxplots displaying (E) total CD19⁺ B-cell counts and the proportion of ASCs (% of CD19⁺ B cells), and (F) the distribution of indicated B-cell subsets (Naïve [IgD⁺ CD27⁻], MZ [IgD⁺ CD27⁺], SwMe [IgD⁻ CD27⁺], DN [IgD⁻ CD27⁻]) within the non-ASC compartment. A paired t-test with Benjamini–Hochberg correction was employed to compare conditions. Significance thresholds were defined as follows: #$P < .1$, *$P < .05$, **$P < .01$, ***$P < .001$, ****$P < .0001$. Only significant values are shown, unless otherwise indicated. ASC, antibody-secreting cells; Bc, B cells; BL, baseline; CpG, Cytosine–phosphate–guanine oligodeoxynucleotide; DN, double negative; MTX, methotrexate; MZ, marginal zone; RA, rheumatoid arthritis; SwMe, switched memory; Tc, T cells; Tfh, T follicular helper.

Early MTX-induced immune remodelling reveals response-associated cellular signatures

To validate and extend our observations of early MTX-associated immune modulation in relation to treatment response, we recruited an independent cohort of patients with RA and performed longitudinal immunophenotyping during MTX therapy. Patients were stratified by clinical outcomes to assess response-specific immune trajectories. HCs and longitudinal time points were compared with RA BL separately for responders and non-responders to delineate response-specific immune trajectories. Overall, MTX rapidly remodelled the circulating immune landscape, with patients with RA shifting towards an HC-like phenotype as early as week 3, which persisted throughout follow-up (Fig 4A). Specific populations showed response-related dynamics: plasmablasts and Tfh cells declined mainly in responders, with early reductions by week 3, whereas nonresponders exhibited minimal or delayed changes (Fig 4A,B). T peripheral helper

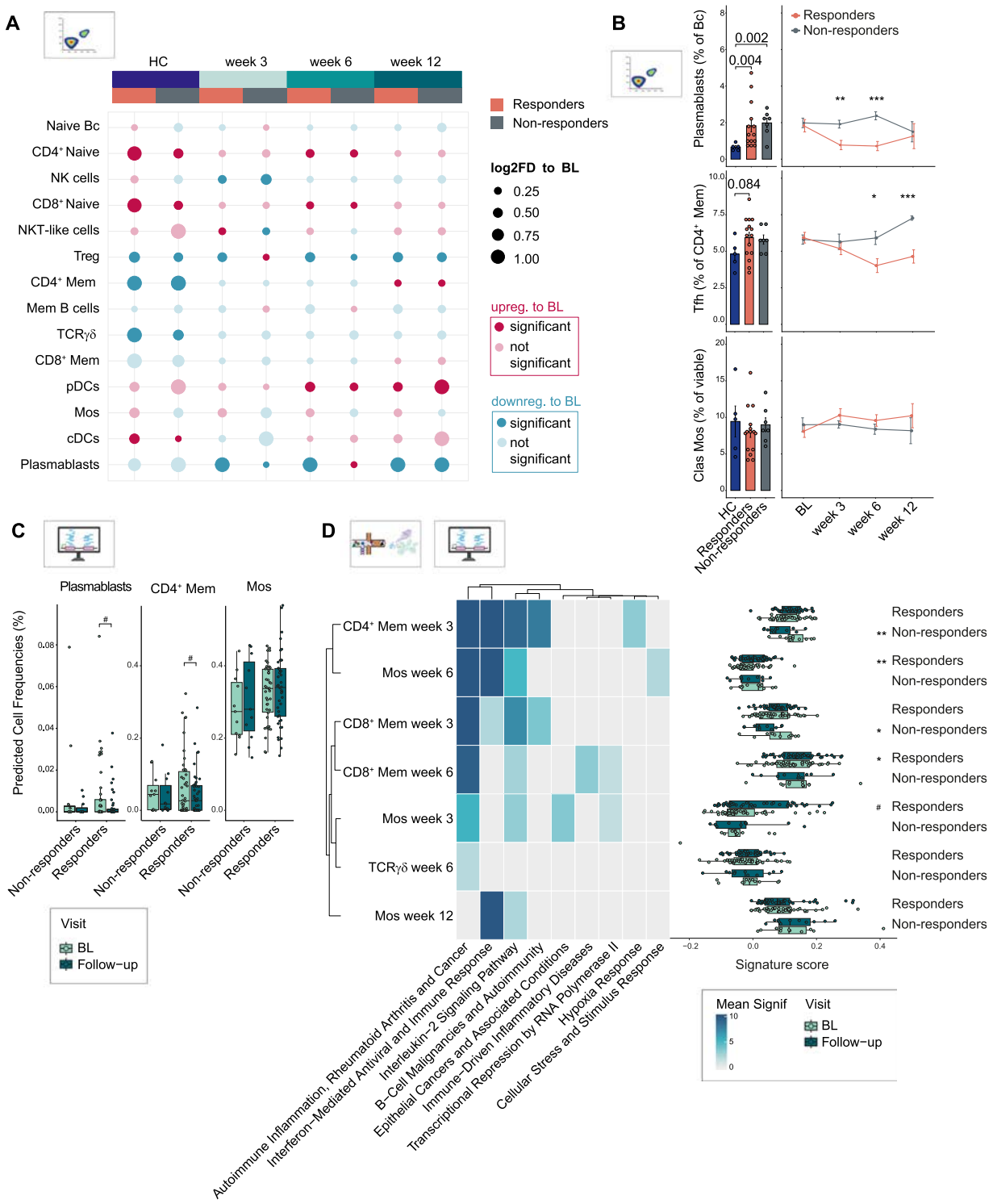

Figure 4. Validation of MTX-induced immune perturbations in independent cohorts. (A,B) Immunophenotyping was performed on HCs and patients with RA (n = 22), including clinical responders and nonresponders, at BL and 3, 6, and 12 wk after MTX treatment initiation. (A) Cell-type abundance comparison across cell types. Dot size depicts MTX-induced perturbations in cell types, represented as changes relative to MTX responders and nonresponders, respectively, at BL. Dot size reflects the magnitude of perturbations (capped at an absolute value of 1), whereas dot colour indicates significance for upregulation or downregulation (*P* values calculated using a permutation test and BH-corrected; significance was defined as $P < .05$). (B) Bar charts and line plots depict changes in cell frequencies of plasmablasts (% of $CD19^+$ cells), Tfh cells (% of $CD4^+$ memory T cells), and classical monocytes (% of viable cells) in HCs (n = 5), MTX responders (n = 15), and MTX nonresponders (n = 7). Lines indicate mean ± SE. Comparisons were conducted using unpaired t-tests. (C) Cell-type deconvolution analysis from a bulk RNA sequencing dataset [17]. Box plots show the predicted percentages of plasmablasts, $CD4^+$ memory T cells, and monocytes in MTX responders (n = 42) and nonresponders (n = 11) at baseline and 12 wk after MTX initiation. A paired t-test was employed to compare abundances. (D) Summarised enrichment results for cell type- and time point–specific gene signatures. Colour represents the negative log10 of the averaged adjusted *P* value per cluster (left panel). Corresponding box plots show the calculated gene signature scores in MTX responders and nonresponders at baseline and 12 wk after MTX initiation (right panel). A paired t-test was employed to compare the signature scores. Significance thresholds were defined as follows: $\#P < .1$, $*P < .05$, $**P < 0.01$, $***P < .001$, $****P < .0001$. Only significant values are shown, unless otherwise indicated. Bc, B cells; BL, baseline; cDC, conventional dendritic cells; HC, healthy controls; Mem, memory; Mos, monocytes; MTX, methotrexate; NK, cells, natural killer; NKT-like cells, natural killer T cell; pDC, plasmacytoid dendritic cells; RA, rheumatoid arthritis; TCR$\gamma\delta$, T-cell receptor gamma delta T cell; Tfh, T follicular helper cells; Treg, regulatory T cells.

cells (Tph) were slightly elevated at BL in responders, but their MTX-induced decrease was not clearly associated with treatment outcome (Supplementary fig S4A,B). To further validate the proposed link to treatment response, we integrated our findings into published bulk RNA-seq data from PBMCs of patients with RA undergoing 12 weeks of MTX treatment [17], allowing stratified analysis of responder and nonresponder patients. Patients showing a response to MTX after 12 weeks displayed a significant reduction in plasmablasts and CD4$^+$ memory T cells compared with nonresponders (Fig 4C). These data suggest that plasmablasts and Tfh cells/CD4$^+$ memory T cells contribute to the mechanism of action of MTX and may serve as potential markers for treatment response.

We next investigated whether cell-type–specific MTX treatment signatures identified in our scRNA-seq data could also be detected in patients with RA who responded to MTX treatment [17]. To this end, we performed an enrichment analysis of cell- and time point–specific MTX-response gene signatures from our scRNA-seq study within the bulk RNA-seq dataset (Fig 4D). Although only a few MTX-response signatures showed statistically significant changes, the overall tendency suggested higher enrichment in MTX responders and lower enrichment in nonresponders at follow-up compared with BL. In addition, we performed pathway enrichment analysis, which showed that these MTX-response signatures are associated with *Autoimmune inflammation, Rheumatoid Arthritis, and Cancer*, indicating that MTX preferentially targets RA-specific transcriptional programmes (Fig 4D).

In summary, our data confirm that MTX alters immune subset distributions, most notably Tfh cells and plasmablasts, which appear to be specifically targeted in patients responding to therapy.

MTX targets multiple pathways and gene hubs over time

Having established a link between early immunological changes and treatment response, we next examined how MTX shapes the molecular landscape. To specifically capture the transcriptional programmes perturbed by MTX treatment over time, we performed enrichment analysis across immune cell subsets in our scRNA-seq data. We observed significant enrichment in terms reflecting apoptosis, as well as canonical inflammatory drivers, including interferon- and TNF-α–associated pathways (Fig 5A, Supplementary fig S5A), supporting that MTX mediates its effects through modulation of central immune-activating pathways. Among all subsets, monocytes and CD4$^+$ memory T cells were among the most transcriptionally perturbed populations. This broad immunomodulatory effect was accompanied by cell-type–specific changes in monocytes, where MTX primarily affected cytokine and innate immune programmes, and in naïve and memory CD4$^+$ T cells, where it influenced interleukin-4 signalling and differentiation processes (Fig 5A). To further assess the relevance of these findings at the site of inflammation, we interrogated publicly available synovial scRNA-seq data from the Accelerating Medicines Partnership Rheumatoid Arthritis phase II cohort [22]. Strikingly, transcriptional features of CD4$^+$ memory T-cell subsets and monocytes identified in peripheral blood were also evident within the synovial tissue (Supplementary Fig S6A,C), indicating that these cell populations represent disease-relevant targets of MTX-mediated modulation (Supplementary Fig S6B,D).

Given that monocytes and CD4$^+$ memory T cells exhibited particularly marked transcriptional changes, we next applied gene expression and co-expression network analyses to delineate the regulatory mechanisms driving MTX-induced effects in these subsets. In monocytes, MTX reshaped gene coregulatory networks, gradually shifting the disturbed RA profile towards 1 resembling HCs (Fig 5B). Several regulatory hub genes were central to this transition, including *EGR1, JAK2, CXCL8, IGSF6*, and *FCN1* (Fig 5B), all of which have established roles in RA pathogenesis. In addition, we identified hubs such as *LMNA, ATP2B1-AS1, SCO2*, and *GVQW3*, which represent unexplored or emerging candidates with potential relevance to RA. Hub genes exhibited dynamic changes in expression over time (Fig 5C). Additional network analysis revealed that MTX influences immune-related regulators such as TNFAIP3 and NFKBIZ (Supplementary Fig S7A). These changes highlight shifts in monocyte regulatory programmes during MTX treatment.

In CD4$^+$ memory T cells, MTX treatment also restored gene regulatory networks towards the HC profile at week 6 (Fig 5D). Multiple key regulatory hub genes were identified as drivers of this transition, including *SOCS1, DUSP2, DUSP1, DUSP5*, and *MNDA*, all of which have established immunomodulatory functions and roles in RA pathogenesis, as well as members of the *GIMAP* family (*GIMAP1, GIMAP4*, and *GIMAP7*), which represent novel candidate genes not previously implicated in RA (Fig 5D,E; Supplementary Fig S7B). These changes highlight shifts in regulatory programmes of monocytes and CD4$^+$ T cells during MTX treatment.

To facilitate further exploration of our data, we provide an interactive cell browser app enabling visualisation of gene expression patterns, differential expression results, and custom signature analyses across cell types and treatment stages. Collectively, our findings reveal that MTX treatment partially normalises transcriptional perturbations in circulating immune cells of patients with RA, providing new insights into its immunomodulatory effects.

DISCUSSION

MTX remains a cornerstone of RA treatment due to its efficacy, safety, and cost-effectiveness. Although its mode of action is not fully understood, this study employed multiomics (scRNA-seq and immunophenotyping) to investigate the longitudinal treatment effects in circulating immune cells. Results suggest that MTX modulates early immune cell dynamics, particularly those of plasmablasts, T cells, and monocytes, progressively realigning RA immune profiles with those observed in HC.

Many studies have compared PBMC abundances in RA and HC [18,23–30], but reports on MTX-induced cellular changes remain limited and conflicting [7,17,25,31,32]. These discrepancies may arise from varying immune cell definitions, study designs, treatment durations, and different profiling techniques. Most studies assessed changes at later time points (>12 weeks), tendentially missing the opportunity to identify early biomarkers predictive of clinical response [7,17,25,31,32]. MTX is known to restore the profile of different cellular compartments [7,17,25,31,32]. A consistent observation is its effect on plasmablasts, which are elevated in RA and typically decrease after 12 weeks [18,25,32,33]. In our study, we provide novel evidence that plasmablast levels decline as early as 3 weeks after treatment initiation. This reduction occurs significantly earlier than previously reported and is primarily observed in clinical responders, whereas nonresponders show delayed or minimal changes. These findings suggest that MTX induces cellular alterations well before clinical improvement becomes apparent. This

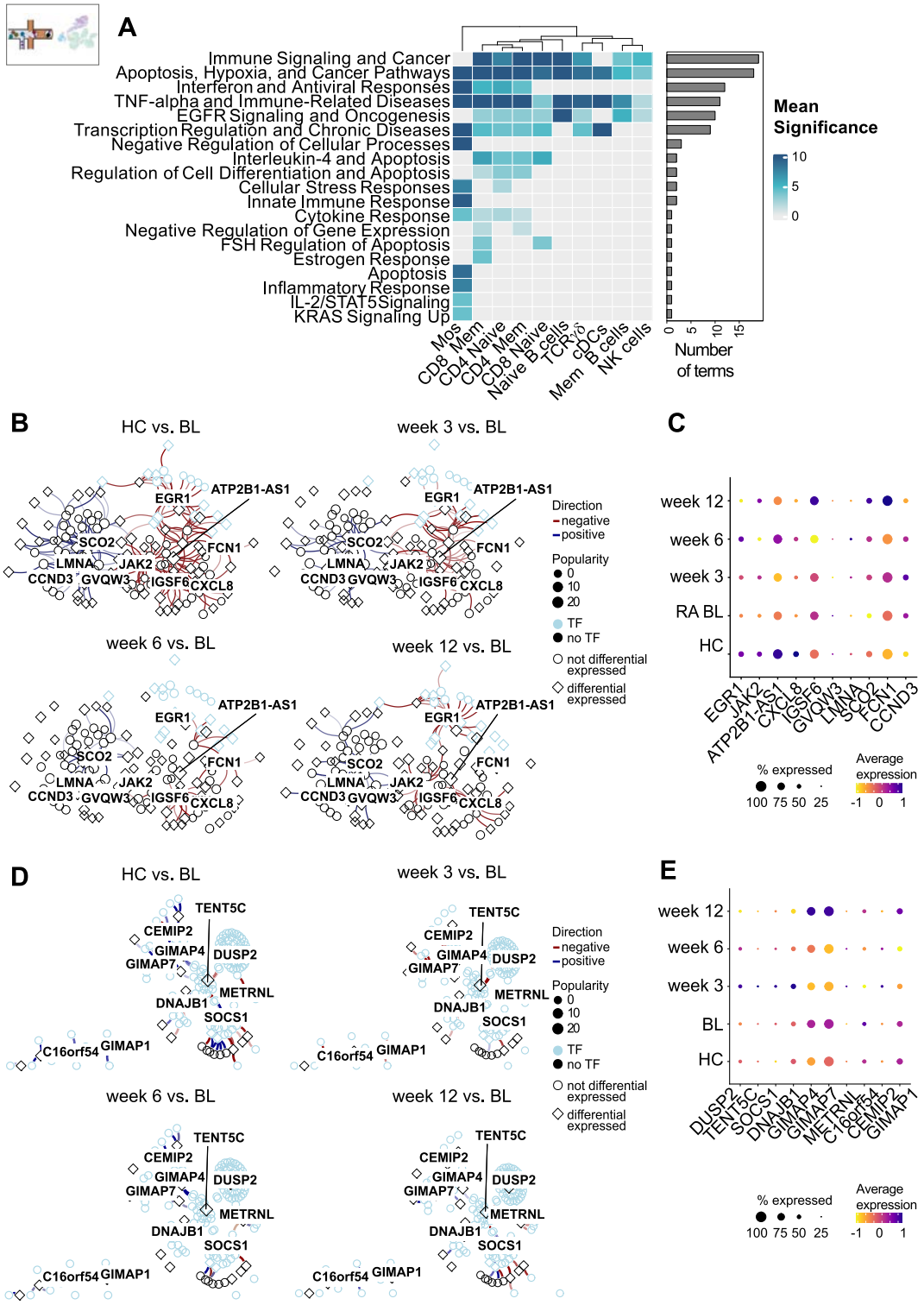

Figure 5. Pathway and gene regulation perturbation by MTX in peripheral blood mononuclear cells (PBMC) subsets. (A) Summary of pathway enrichment results derived from genes identified by longitudinal differential expression analysis over time (baseline, week 3, week 6, week 12) within each immune cell subset. Genes were considered differentially expressed if they reached an absolute log2 fold change of 0.1 and an adjusted *P* value below .05. Colour represents the negative log10 of the averaged adjusted *P* value per cluster. (B,D) Simplified coregulatory network in (B) monocytes and (D) $CD4^+$ memory T cells. Networks were constructed between either HC and RA BL or weeks 3, 6, and 12 of MTX treatment and RA BL. The intensity of the colour represents the magnitude of the difference. Light blue nodes represent TF, and diamond-shaped nodes represent genes affected by MTX treatment in the corresponding cell type. (C) Hub genes corresponding to (B). (E) Hub genes corresponding to (D) (n = 5). BL, baseline; cDC, conventional dendritic cells; HC, healthy controls; Mem, memory; Mos, monocytes; MTX, methotrexate; NK, natural killer; RA, rheumatoid arthritis; TCR$\gamma\delta$, T-cell receptor gamma delta T cell; TF, transcription factor; Treg, regulatory T cell.

is supported by findings that active MTX metabolites appear in PBMCs within 1 week. [34]. MTX also reduced effector T cells, particularly Tfh cells, which declined by week 3, predominantly in clinical responders. These cells are well known to play a central role in RA pathogenesis by supporting B-cell activation and plasmablast formation [35–38]. Tph cells were likewise elevated in patients with RA, consistent with previous reports [39]; however, within our cohorts, MTX-induced modulation of this

subset was not distinctly linked to clinical response. By week 12, plasmablasts and Tfh cells had partially rebounded but remained near HC levels. Notably, our *in vitro* experiments recapitulated the preferential sensitivity of plasmablast differentiation to MTX, supporting a direct effect on this compartment. In summary, the reduction in plasmablasts and Tfh was specific to clinical responders, highlighting these cells as potential early biomarkers of treatment outcome.

Only a few studies have examined transcriptomic changes in PBMCs after MTX treatment, typically using bulk samples and sampling at or beyond 12 weeks. Previous studies proposed several MTX mechanisms, including downregulation of folate pathway genes, reduced proliferation, suppression of FOXP3, and type I interferon–related signatures linked to nonresponse, yet none established a definitive mode of action, likely due to late sampling or bulk-level approaches [17,40–43]. A recent scRNA-seq study reported widespread metabolic changes and shifts towards naïve T-cell subsets with reduced Tfh cells but unchanged plasmablasts; however, analyses were limited to a late time point and combination therapy [32]. In contrast, our MTX monotherapy cohort reveals early and robust transcriptional perturbations detectable by week 3, and integration with external datasets shows divergent trajectories between responders and nonresponders, indicating molecular changes that precede clinical outcomes. Further analysis uncovered key MTX-related transcriptional changes across immune subsets, particularly in $CD4^+$ T cells and monocytes. Consistent with prior work, MTX modulated cytokine signalling, splicing, cell cycle, and apoptosis pathways in $CD4^+$ T cells [44], likely restoring immune homeostasis and reducing lymphocyte-driven joint inflammation. In contrast, monocytes showed enrichment in autoimmune, antigen processing, TNF-α (tumor necrosis factor-alpha), and IFN-γ response pathways, supporting distinct roles of monocytes and T cells in RA and highlighting MTX's cell-type –specific immunomodulatory effects [44,45].

Gene regulatory network analyses in monocytes and $CD4^+$ memory T cells underscored the ability of MTX to restore a healthy-like transcriptional profile. Identified hub genes, including those previously implicated in RA pathogenesis (eg, *EGR1, JAK2, CXCL8, FCN1, SOCS1, IGSF6*), exhibited restored expression patterns under MTX therapy, reflecting known immunoregulatory mechanisms [23,46–51]. These results are consistent with prior studies indicating that MTX mitigates pathogenic immune signalling by modulating key transcription factors (eg, *TNFAIP3, NFKBIZ*) and immune-related pathways [52,53]. Several previously uncharacterised genes, including *ATP2B1-AS1, SCO2, LMNA, GVQW3*, and members of the *GIMAP* family, were identified as novel candidates potentially contributing to RA pathogenesis and represent promising targets for further mechanistic and therapeutic investigation.

We acknowledge the limitation of our small sample size, which reflects the challenge of obtaining high-quality, treatment-naïve patient samples with longitudinal follow-up and well-defined treatment outcomes. Despite this, our study identified early cellular and transcriptional changes that were validated in independent cohorts and integrated with external datasets. As our analyses were based on PBMCs, they may not capture MTX's full effects on tissue-resident or stromal cells at the site of inflammation. However, RA-associated signatures observed in blood were conserved in synovial populations [22]. Prospective studies are now needed to functionally validate candidate genes that could serve as biomarkers. Overall, our dataset provides novel insight into MTX-induced immune modulation and serves as a valuable resource for biomarker discovery. To facilitate exploration and validation, we provide an interactive cell browser highlighting MTX-induced molecular effects and candidate markers.

In conclusion, this study shows for the first time that MTX induces early cell-type–specific immunomodulatory effects in RA even before clinical response. Using a longitudinal multiomics approach, we demonstrate that MTX rapidly shifts immune cell distributions and gene expression towards a more physiological state. Our identified signatures could serve as markers to monitor and predict therapeutic response.

Competing interests

MaB and TP received funding from Lilly. MiB received grants from AlphaSigma. DA received grants and consulting fees from AbbVie, Amgen, Lilly, Merck, Novartis, Pfizer, Roche, and Sandoz. ES received funding from Pfizer, Bristol-Myers Squibb, Boehringer-Ingelheim, AstraZeneca, Lilly, and AbbVie. JSS received grants from AbbVie, AstraZeneca, Eli Lilly and Company, Novartis, Galapagos, and Roche, consulting fees or honoraria from AbbVie, Amgen, Ananda, Astro, BMS, Celltrion, Chugai, Eli Lilly and Company, Gilead, Immunovant, MSD, Novartis, Pfizer, Roche, R-Pharma, Samsung, Sanofi, and UCB. The other authors declare that they have no competing interests.

Acknowledgements

We thank all the patients who participated. We thank Martina Durechova, Daffodil Dioso, and Michael Zauner for their support, and Andreas Spittler, Brigitte Meyer, Carl-Walter Steiner, Birgit Niederreiter, and Karolina von Dalwigk for their technical assistance. We thank Sylvia Taxer for her support and Birgit Reiter for helpful discussions on MTX metabolites. We thank Andreea-Maria Iuhaniak for her support with the interactive visualisation of scRNA-seq data. This study was supported by the MedUni Vienna Biobank KIP. We thank Anna-Marina Mrak for her support with data management and submission to Array Express.

Contributors

TP, DA, LG, and MiB contributed to conceptualisation. TP, AT, MaB, PS, ES, DS, LP, FS, and JK contributed to data curation. TP, AT, MaB, and LD contributed to formal analysis. CB, WE, DA, and MiB contributed to funding acquisition. TP, AT, MaB, and LG contributed to investigation. TP, AT, MaB, PS, TKr, FS, and JK contributed to methodology. TP, AT, LG, and MiB contributed to project administration. ES, DS, PH, TKr, LD, CB, RK, HS, LP, and MR contributed to resources. AT, MaB, and LD contributed to software. CB, TKa, RK, HS, JSS, WE, DA, MiB, and MR contributed to supervision. TP, AT, MaB, PS, LG, and MiB contributed to validation. TP, AT, and MaB contributed to visualisation. TP, AT, MaB, LG, and MiB contributed to writing – original draft. All authors contributed to writing – review and editing.

Funding

This work has been supported by the following grants: F70 - HDACs as Regulators of T-Cell–Mediated Immunity in Health and Disease (10.55776/F70). The European Union (Horizon Europe) under grant agreement no. 101095052 (SQUEEZE).

Patient consent for publication

Not applicable.

Ethics approval

All participants provided informed consent, and ethical approval was obtained (EK: 1075/2021; 2071/2020; 1526/2025).

Provenance and peer review

Not commissioned; externally peer reviewed.

Data availability statement

Raw and processed scRNA-seq data have been deposited on ArrayExpress under the accession number E-MTAB-17153. All other data are available from the autors upon reasonable request. A cell browser website is available at https://github.com/bonellilab/shinyMTX to visualise our data and results.

Declaration of generative AI and AI-assisted technologies in the writing process

During the preparation of this work, the authors used ChatGPT (version GPT-4, https://openai.com/) to improve the grammar, sentence structure, and overall clarity of the manuscript. After using this tool/service, the authors reviewed and edited the content as needed and take full responsibility for the content of the published article.

Supplementary materials

Supplementary material associated with this article can be found in the online version at doi:10.1016/j.ard.2026.05.018.

REFERENCES

[1] Aletaha D, Smolen JS. Diagnosis and management of rheumatoid arthritis: a review. JAMA. 2018;320(13):1360–72.

[2] Smolen JS, Aletaha D, McInnes IB. Rheumatoid arthritis. Lancet 2016;388(10055):2023–38.

[3] Jang S, Kwon EJ, Lee JJ. Rheumatoid arthritis: pathogenic roles of diverse immune cells. Int J Mol Sci. 2022;23(2):905.

[4] Kerschbaumer A, Sepriano A, Bergstra SA, Smolen JS, van der Heijde D, Caporali R, et al. Efficacy of synthetic and biological DMARDs: a systematic literature review informing the 2022 update of the EULAR recommendations for the management of rheumatoid arthritis. Ann Rheum Dis. 2023;82(1):95–106.

[5] Brown PM, Pratt AG, Isaacs JD. Mechanism of action of methotrexate in rheumatoid arthritis, and the search for biomarkers. Nat Rev Rheumatol. 2016;12(12):731–42.

[6] Chan ES, Cronstein BN. Methotrexate—how does it really work? Nat Rev Rheumatol 2010;6(3):175–8.

[7] Lina C, Conghua W, Nan L, Ping Z. Combined treatment of etanercept and MTX reverses Th1/Th2, Th17/Treg imbalance in patients with rheumatoid arthritis. J Clin Immunol. 2011;31(4):596–605.

[8] Luo P, Wang P, Xu J, Hou W, Xu P, Xu K, et al. Immunomodulatory role of T helper cells in rheumatoid arthritis: a comprehensive research review. Bone Joint Res. 2022;11(7):426–38.

[9] Szalay B, Vasarhelyi B, Cseh A, Tulassay T, Deak M, Kovacs L, et al. The impact of conventional DMARD and biological therapies on CD4+ cell subsets in rheumatoid arthritis: a follow-up study. Clin Rheumatol. 2014;33(2):175–85.

[10] Xinqiang S, Fei L, Nan L, Yuan L, Fang Y, Hong X, et al. Therapeutic efficacy of experimental rheumatoid arthritis with low-dose methotrexate by increasing partially CD4+CD25+ Treg cells and inducing Th1 to Th2 shift in both cells and cytokines. Biomed Pharmacother. 2010;64(7):463–71.

[11] Duong SQ, Crowson CS, Athreya A, Atkinson EJ, Davis 3rd JM, Warrington KJ, et al. Clinical predictors of response to methotrexate in patients with rheumatoid arthritis: a machine learning approach using clinical trial data. Arthritis Res Ther. 2022;24(1):162.

[12] Duquesne J, Bouget V, Cournede PH, Fautrel B, Guillemin F, de Jong PHP, et al. Machine learning identifies a profile of inadequate responder to methotrexate in rheumatoid arthritis. Rheumatology (Oxford). 2023;62(7):2402–9.

[13] Teitsma XM, Jacobs JWG, Welsing PMJ, de Jong PHP, Hazes JMW, Weel A, et al. Inadequate response to treat-to-target methotrexate therapy in patients with new-onset rheumatoid arthritis: development and validation of clinical predictors. Ann Rheum Dis. 2018;77(9):1261–7.

[14] van Vollenhoven RF, Ernestam S, Geborek P, Petersson IF, Coster L, Waltbrand E, et al. Addition of infliximab compared with addition of sulfasalazine and hydroxychloroquine to methotrexate in patients with early rheumatoid arthritis (Swefot trial): 1-year results of a randomised trial. Lancet. 2009;374(9688):459–66.

[15] Wolfe F, Michaud K, Stephenson B, Doyle J. Toward a definition and method of assessment of treatment failure and treatment effectiveness: the case of leflunomide versus methotrexate. J Rheumatol. 2003;30(8):1725–32.

[16] Aletaha D, Neogi T, Silman AJ, Funovits J, Felson DT, Bingham 3rd CO, et al. 2010 Rheumatoid arthritis classification criteria: an American College of Rheumatology/European League Against Rheumatism collaborative initiative. Arthritis Rheum. 2010;62(9):2569–81.

[17] Brynedal B, Yoosuf N, Ulfarsdottir TB, Ziemek D, Maciejewski M, Folkersen L, et al. Molecular signature of methotrexate response among rheumatoid arthritis patients. Front Med (Lausanne). 2023;10:1146353.

[18] Preglej T, Brinkmann M, Steiner G, Aletaha D, Goschl L, Bonelli M. Advanced immunophenotyping: a powerful tool for immune profiling, drug screening, and a personalized treatment approach. Front Immunol. 2023;14:1096096.

[19] Park LM, Lannigan J, Jaimes MC. OMIP-069: forty-color full Spectrum flow cytometry panel for deep Immunophenotyping of major cell subsets in human peripheral blood. Cytometry A. 2020;97(10):1044–51.

[20] Monaco G, Lee B, Xu W, Mustafah S, Hwang YY, Carre C, et al. RNA-Seq signatures normalized by mRNA abundance allow absolute deconvolution of human immune cell types. Cell Rep. 2019;26(6):1627–1640.e7.

[21] Hodgkin PD, Lee JH, Lyons AB. B cell differentiation and isotype switching is related to division cycle number. J Exp Med. 1996;184(1):277–81.

[22] Zhang F, Jonsson AH, Nathan A, Millard N, Curtis M, Xiao Q, et al. Deconstruction of rheumatoid arthritis synovium defines inflammatory subtypes. Nature. 2023;623(7987):616–24.

[23] Binvignat M, Miao BY, Wibrand C, Yang MM, Rychkov D, Flynn E, et al. Single-cell RNA-Seq analysis reveals cell subsets and gene signatures associated with rheumatoid arthritis disease activity. JCI Insight. 2024;9(16):e178499.

[24] Fonseka CY, Rao DA, Teslovich NC, Korsunsky I, Hannes SK, Slowikowski K, et al. Mixed-effects association of single cells identifies an expanded effector CD4(+) T cell subset in rheumatoid arthritis. Sci Transl Med. 2018;10(463):eaaq0305.

[25] Hedman AK, Winter E, Yoosuf N, Benita Y, Berg L, Brynedal B, et al. Peripheral blood cellular dynamics of rheumatoid arthritis treatment informs about efficacy of response to disease modifying drugs. Sci Rep. 2023;13(1):10058.

[26] Mahmood Z, Schmalzing M, Dorner T, Tony HP, Muhammad K. Therapeutic cytokine inhibition modulates activation and homing receptors of peripheral memory B cell subsets in rheumatoid arthritis patients. Front Immunol. 2020;11:572475.

[27] Nakajima S, Tsuchiya H, Fujio K. Unraveling immune cell heterogeneity in autoimmune arthritis: insights from single-cell RNA sequencing. Immunol Med. 2024;47(4):217–29.

[28] Song X, Zhang Y, Zhao L, Fan J, Peng T, Ma Y, et al. Analyzation of the peripheral blood mononuclear cells Atlas and cell communication of rheumatoid arthritis patients based on single-cell RNA-Seq. J Immunol Res. 2023;2023:6300633.

[29] Takeshita M, Suzuki K, Kondo Y, Morita R, Okuzono Y, Koga K, et al. Multidimensional analysis identified rheumatoid arthritis-driving pathway in human T cell. Ann Rheum Dis. 2019;78(10):1346–56.

[30] Wu X, Liu Y, Jin S, Wang M, Jiao Y, Yang B, et al. Single-cell sequencing of immune cells from anticitrullinated peptide antibody positive and negative rheumatoid arthritis. Nat Commun. 2021;12(1):4977.

[31] Herman S, Zurgil N, Langevitz P, Ehrenfeld M, Deutsch M. Methotrexate selectively modulates TH1/TH2 balance in active rheumatoid arthritis patients. Clin Exp Rheumatol. 2008;26(2):317–23.

[32] Yang Z, Liang Q, Liang H, Chen W, Li C, Xiao Y, et al. Single-cell RNA transcriptomic and plasma Lipidomic reveal the potential mechanisms of a methotrexate-based therapy against rheumatoid arthritis. Phytomedicine. 2023;115:154816.

[33] Glaesener S, Quach TD, Onken N, Weller-Heinemann F, Dressler F, Huppertz HI, et al. Distinct effects of methotrexate and etanercept on the B cell

compartment in patients with juvenile idiopathic arthritis. Arthritis Rheumatol. 2014;66(9):2590–600.
[34] Daraghmeh DN, Moghaddami M, Bobrovskaya L, Proudman SM, Wiese MD. Quantitation of methotrexate polyglutamates in human whole blood, erythrocytes and leukocytes collected via venepuncture and volumetric absorptive micro-sampling: a green LC-MS/MS-based method. Anal Bioanal Chem. 2022;414(20):6029–46.
[35] King C, Tangye SG, Mackay CR. T follicular helper (TFH) cells in normal and dysregulated immune responses. Annu Rev Immunol. 2008;26:741–66.
[36] Wang J, Shan Y, Jiang Z, Feng J, Li C, Ma L, et al. High frequencies of activated B cells and T follicular helper cells are correlated with disease activity in patients with new-onset rheumatoid arthritis. Clin Exp Immunol. 2013;174(2):212–20.
[37] Zhang Y, Li Y, Lv TT, Yin ZJ, Wang XB. Elevated circulating Th17 and follicular helper CD4(+) T cells in patients with rheumatoid arthritis. APMIS. 2015;123(8):659–66.
[38] Lu J, Wu J, Xia X, Peng H, Wang S. Follicular helper T cells: potential therapeutic targets in rheumatoid arthritis. Cell Mol Life Sci. 2021;78(12):5095–106.
[39] Rao DA, Gurish MF, Marshall JL, Slowikowski K, Fonseka CY, Liu Y, et al. Pathologically expanded peripheral T helper cell subset drives B cells in rheumatoid arthritis. Nature. 2017;542(7639):110–4.
[40] Blits M, Jansen G, Assaraf YG, van de Wiel MA, Lems WF, Nurmohamed MT, et al. Methotrexate normalizes up-regulated folate pathway genes in rheumatoid arthritis. Arthritis Rheum. 2013;65(11):2791–802.
[41] Palmowski A, Strehl C, Pfeiffenberger M, Haupl T, Schad M, Kallarackal J, et al. Identification of gene expression biomarkers to predict clinical response to methotrexate in patients with rheumatoid arthritis. Clin Rheumatol. 2024;43(1):511–9.
[42] Plant D, Maciejewski M, Smith S, Nair N, Maximising Therapeutic Utility in Rheumatoid Arthritis Consortium tRSG, Hyrich K, et al. Profiling of gene expression biomarkers as a classifier of methotrexate nonresponse in patients with rheumatoid arthritis. Arthritis Rheumatol. 2019;71(5):678–84.
[43] Tasaki S, Suzuki K, Kassai Y, Takeshita M, Murota A, Kondo Y, et al. Multi-omics monitoring of drug response in rheumatoid arthritis in pursuit of molecular remission. Nat Commun. 2018;9(1):2755.
[44] Cronstein BN, Aune TM. Methotrexate and its mechanisms of action in inflammatory arthritis. Nat Rev Rheumatol. 2020;16(3):145–54.
[45] Firestein GS, McInnes IB. Immunopathogenesis of rheumatoid arthritis. Immunity 2017;46(2):183–96.
[46] Cambier S, Gouwy M, Proost P. The chemokines CXCL8 and CXCL12: molecular and functional properties, role in disease and efforts towards pharmacological intervention. Cell Mol Immunol. 2023;20(3):217–51.
[47] Trizzino M, Zucco A, Deliard S, Wang F, Barbieri E, Veglia F, et al. EGR1 is a gatekeeper of inflammatory enhancers in human macrophages. Sci Adv. 2021;7(3):eaaz8836.
[48] Tanaka Y, Luo Y, O'Shea JJ, Nakayamada S. Janus kinase-targeting therapies in rheumatology: a mechanisms-based approach. Nat Rev Rheumatol. 2022;18(3):133–45.
[49] Isomaki P, Alanara T, Isohanni P, Lagerstedt A, Korpela M, Moilanen T, et al. The expression of SOCS is altered in rheumatoid arthritis. Rheumatology (Oxford). 2007;46(10):1538–46.
[50] van Beers JJ, Schwarte CM, Stammen-Vogelzangs J, Oosterink E, Bozic B, Pruijn GJ. The rheumatoid arthritis synovial fluid citrullinome reveals novel citrullinated epitopes in apolipoprotein E, myeloid nuclear differentiation antigen, and beta-actin. Arthritis Rheum. 2013;65(1):69–80.
[51] Moon SJ, Lim MA, Park JS, Byun JK, Kim SM, Park MK, et al. Dual-specificity phosphatase 5 attenuates autoimmune arthritis in mice via reciprocal regulation of the Th17/Treg cell balance and inhibition of osteoclastogenesis. Arthritis Rheumatol. 2014;66(11):3083–95.
[52] Wu Y, He X, Huang N, Yu J, Shao B. A20: a master regulator of arthritis. Arthritis Res Ther. 2020;22(1):220.
[53] Slowikowski K, Nguyen HN, Noss EH, Simmons DP, Mizoguchi F, Watts GFM, et al. CUX1 and IkappaBzeta (NFKBIZ) mediate the synergistic inflammatory response to TNF and IL-17A in stromal fibroblasts. Proc Natl Acad Sci U S A. 2020;117(10):5532–41.

Ann Rheum Dis 85 (2026) 1729–1742

Contents lists available at ScienceDirect

Annals of the Rheumatic Diseases

journal homepage: https://www.sciencedirect.com/journal/annals-of-the-rheumatic-diseases

Psoriatic arthritis

Efficacy and safety of deucravacitinib, an oral, selective tyrosine kinase 2 inhibitor, in patients with active psoriatic arthritis: 52-week results from the randomised, double-blind, placebo-controlled phase 3 POETYK PsA-1 trial

Désirée van der Heijde[1], Philip J. Mease[2,*], Carle Paul[3], Frank Behrens[4], Laure Gossec[5], Yuko Kaneko[6], Lihi Eder[7], Laura C. Coates[8], Andrew E. Pink[9], Weiguo Wan[10], Enrique R. Soriano[11], Piotr Leszczyński[12], Jose U. Scher[13], Atul Deodhar[14], Chahin Pachai[15], Janice Li[15], Xue Fan[15], Sahar Rabbat[15], Caroline Sardinas[15], Eleni Vritzali[16], John Vaile[15], Joseph F. Merola[17]

[1] *Department of Rheumatology, Leiden University Medical Center, Leiden, the Netherlands*
[2] *Department of Rheumatology, Providence Swedish Medical Center and University of Washington, Seattle, WA, USA*
[3] *Department of Dermatology, Institut National de la Santé et de la Recherche Médicale Infinity, Centre Hospitalier Universitaire, Toulouse University, Toulouse, France*
[4] *Department of Translational, Rheumatology, Immunology, and Inflammation Medicine, University Hospital and Fraunhofer Institute for Translational Medicine and Pharmacology, Fraunhofer Cluster of Excellence Immune-Mediated Diseases, Goethe University, Frankfurt am Main, Germany*
[5] *Sorbonne Université, Institut National de la Santé et de la Recherche Médicale, Institut Pierre Louis d'Epidémiologie et de Santé Publique, Team Pepites, and Assistance Publique-Hôpitaux de Paris, Pitié-Salpêtrière Hospital, Rheumatology Department, Paris, France*
[6] *Division of Rheumatology, Department of Internal Medicine, Keio University School of Medicine, Tokyo, Japan*
[7] *Department of Medicine, Women's College Hospital, University of Toronto, Toronto, ON, Canada*
[8] *Nuffield Department of Orthopaedics, Rheumatology and Musculoskeletal Sciences, and Kennedy Institute of Rheumatology, University of Oxford, Headington, Oxford, UK*
[9] *St John's Institute of Dermatology, Guy's and St Thomas' National Health Service Foundation Trust and King's College London, London, UK*
[10] *Division of Rheumatology, Huashan Hospital, Fudan University, Shanghai, China*
[11] *Rheumatology Unit, Internal Medicine Service, Department of Medicine, and University Institute, Hospital Italiano de Buenos Aires, Buenos Aires, Argentina*
[12] *Department of Internal Medicine and Metabolic Disorders, Poznań University of Medical Sciences, Poznań, Poland*
[13] *Department of Medicine, Division of Rheumatology, New York University Grossman School of Medicine and New York University Psoriatic Arthritis Center, New York University Langone Health, New York, NY, USA*
[14] *Division of Arthritis and Rheumatic Diseases, Oregon Health & Science University, Portland, OR, USA*
[15] *Bristol Myers Squibb, Princeton, NJ, USA*
[16] *Bristol Myers Squibb, Boudry, Switzerland*
[17] *Department of Dermatology and Department of Medicine, Division of Rheumatology, and Peter O'Donnell Jr School of Public Health, The University of Texas Southwestern Medical Center, Dallas, TX, USA*

*Correspondence to Dr. Philip J. Mease, Rheumatology Research, Providence Swedish Medical Center, Seattle, WA, USA.
E-mail address: pmease@philipmease.com (P.J. Mease).
Handling editor Josef Smolen.

https://doi.org/10.1016/j.ard.2026.05.029

0003-4967/© 2026 Published by Elsevier B.V. on behalf of European Alliance of Associations for Rheumatology (EULAR).

ARTICLE INFO

Article history:
Received 23 December 2025
Received in revised form 12 March 2026
Accepted 22 May 2026

ABSTRACT

Objectives: The randomised, double-blind, placebo-controlled, phase 3 Program fOr Evaluation of TYK2 inhibitor Psoriatic Arthritis-1 (POETYK PsA-1) trial evaluated the efficacy, safety, and tolerability of deucravacitinib, an oral, selective tyrosine kinase 2 inhibitor, in patients with PsA naïve to biologic disease-modifying antirheumatic drugs.

Methods: Adults with active PsA, high-sensitivity C-reactive protein concentration ≥ 3 mg/L, and ≥ 1 PsA-related hand and/or foot erosion detectable via radiograph were randomised 1:1 to oral deucravacitinib 6 mg once daily or placebo through week (W) 16. At W16, patients continued receiving deucravacitinib or switched from placebo to deucravacitinib through W52. The primary endpoint was American College of Rheumatology 20% improvement in response (ACR20) at W16. Nonresponder imputation was used for missing data. Efficacy and safety were evaluated through W52. Post hoc rank analysis of covariance was used to evaluate structural damage with no missing data imputation.

Results: In 670 patients, a significantly greater proportion of those receiving deucravacitinib vs placebo achieved ACR20 at W16 (54.2% vs 34.1%, $P < .001$). Responses with deucravacitinib were increased at W52. Patients who switched from placebo to deucravacitinib achieved improvements similar to those in patients who received continuous deucravacitinib. Inhibition of structural damage was observed at W16 and W52. At W16, incidences of serious adverse events (AEs) (deucravacitinib, 1.8%; placebo, 2.4%) and discontinuations due to AEs (2.4%; 1.8%) were low and remained low through W52, without imbalances in cardiovascular events, malignancies, or opportunistic infections. No new safety signals were detected; no deaths occurred.

Conclusions: Deucravacitinib demonstrated superiority vs placebo for clinical responses, patient-reported outcomes, and structural damage inhibition in patients with PsA, with favourable tolerability and safety.

WHAT IS ALREADY KNOWN ON THIS TOPIC

- There remains an unmet need for oral treatments that are tolerable, safe, and effective for multiple domains of psoriatic arthritis (PsA; eg, musculoskeletal, skin) as well as structural damage, quality of life, pain, and function.
- Tyrosine kinase 2 (TYK2) modulates the downstream effects of certain immune-mediating cytokines (eg, interleukin [IL]-23, IL-12, and type I interferons) PsA pathophysiology.
- The unique mechanism of binding of deucravacitinib drives its selectivity for TYK2 over Janus kinases 1/2/3; deucravacitinib is the first in a new class of oral TYK2 inhibitors under investigation for the treatment of active PsA.

WHAT THIS STUDY ADDS

- The Program fOr Evaluation of TYK2 inhibitor Psoriatic Arthritis-1 (POETYK PsA-1) study showed that deucravacitinib had superior efficacy vs placebo across multiple endpoints at week (W) 16, including overall disease activity measures, joint and skin clinical responses, and quality of life in adults with active PsA who were naïve to biologic disease-modifying antirheumatic drugs; clinical responses continued to increase after W16 and were maintained through W52.
- Post hoc analyses demonstrated an inhibition of progression of structural damage at W16; this inhibition was sustained at W52. Patients who switched from placebo to deucravacitinib also experienced a reduction in radiographic progression after switching to active treatment at W16.
- Deucravacitinib was well tolerated, with ~80% of patients completing study treatment through W52; safety was consistent with the established profile, and no new safety signals were identified.

HOW THIS STUDY MIGHT AFFECT RESEARCH, PRACTICE OR POLICY

- POETYK PsA-1 is 1 of the 2 phase 3 trials that confirm that deucravacitinib, a selective TYK2 inhibitor, is effective in multiple domains of PsA and improved patient-reported pain, fatigue, and health-related quality of life and has a favourable safety profile.
- The inhibition of TYK2 with deucravacitinib may play a role in the inhibition of progression of structural damage.
- Deucravacitinib was shown to be safe and efficacious through W52 in POETYK PsA-1.

INTRODUCTION

Psoriatic arthritis (PsA) is characterised by musculoskeletal and dermatologic manifestations and irreversible structural damage to joints, which impact quality of life [1,2]. Although several therapies are available for PsA, patients often have an inadequate clinical response [3,4]. Available treatments also vary in terms of safety and tolerance [3–8].

Deucravacitinib is a first-in-class, oral, selective tyrosine kinase 2 (TYK2) inhibitor [9] approved in multiple countries for use in moderate to severe plaque psoriasis (PsO) and active PsA [10,11], with > 5 years of long-term data [12]. Deucravacitinib has a unique mechanism of action, inhibiting TYK2 by binding to the regulatory domain rather than the catalytic domain, where Janus kinase (JAK) 1/2/3 inhibitors bind [13,14]. This mechanism of action drives the selectivity of deucravacitinib for TYK2 over JAK1/2/3 [13,14]. Inhibition of TYK2 by deucravacitinib prevents downstream effects of several cytokines (eg, interleukin [IL]-23, IL-12, and type I interferons) that are implicated in the pathophysiology of several immune-mediated diseases, including PsA [13,14]. In a phase 2 trial of deucravacitinib in active PsA (NCT03881059), the primary and all key secondary efficacy endpoints were met, with an acceptable safety profile [9].

To evaluate the efficacy and safety of deucravacitinib in patients with active PsA naïve to treatment with biologic disease-modifying antirheumatic drugs, the 52-week, randomised, double-blind, placebo-controlled phase 3 Program fOr

Evaluation of TYK2 inhibitor Psoriatic Arthritis-1 (POETYK PsA-1; NCT04908202) trial was initiated.

METHODS

Trial design and treatment

POETYK PsA-1 was a multicentre, randomised, double-blind, placebo-controlled, phase 3 study (Supplementary Fig S1) conducted at 186 study sites across 21 countries in North America, South America, Europe, Australia, and Asia. After a 4-week screening period, interactive response technology was used to centrally randomise patients 1:1 to receive deucravacitinib 6 mg once daily or placebo during the placebo-controlled period (week [W] 0-16). Deucravacitinib and placebo-matched tablets were packaged in bottles and appeared identical. Randomisation was stratified by high-sensitivity C-reactive protein (hsCRP) levels (< 10 vs ≥ 10 mg/L) and conventional synthetic disease-modifying antirheumatic drug (csDMARD) use at baseline (yes/no) to ensure balance of clinically relevant baseline factors that could influence American College of Rheumatology (ACR) response criteria. Patients initially randomised to placebo were reallocated to receive deucravacitinib 6 mg once daily through the 36-week active period (W16-52). Patients initially randomised to deucravacitinib continued that treatment through the active period. The sponsor was unblinded at the W16 database lock. The investigative site staff, cardiovascular and infection adjudication committees, and patients and their families remained blinded until the end of the study. Patients who completed all protocol-required visits could enrol in an optional 104-week open-label extension period (W52-156).

The study was conducted in accordance with the Declaration of Helsinki, the International Council for Harmonisation of Technical Requirements for Pharmaceuticals for Human Use Guidelines for Good Clinical Practice, and local regulations. The study protocol, consent form, and any other written information given to patients was approved by an institutional review board or independent ethics committee at each study site. All patients provided written informed consent before the first study assessment. Investigators and study sites are listed in Supplementary Materials S1. The study protocol and statistical analysis plan are available at https://clinicaltrials.gov/study/NCT04908202.

Patients

Eligible patients were aged ≥ 18 years with a diagnosis of PsA ≥ 3 months at screening; met Classification Criteria for Psoriatic Arthritis; had an active or documented history of PsO; and had active disease including ≥ 3 swollen joints, ≥ 3 tender joints, hsCRP concentration ≥ 3 mg/L, and ≥ 1 PsA-related hand and/or foot erosion detectable with radiography by central readers (ie, enriched for radiographic progression). Patients were permitted concurrent use of 1 csDMARD and/or oral glucocorticoid (stable doses for ≥ 28 days), and/or 1 nonsteroidal anti-inflammatory drug (stable doses for ≥ 14 days prior to day 1). Patients with nonplaque-PsO at screening or day 1, other autoimmune conditions, an active or documented history of an inflammatory joint disease other than PsA, active fibromyalgia, or prior receipt of an approved or investigational biologic therapy for the treatment of PsA or psoriasis were not eligible. Additional criteria are provided in Supplementary Materials S2. Supplementary Table S1 compares the study designs and outcomes of POETYK PsA-1 and PsA-2 (NCT04908189; another phase 3 trial evaluating deucravacitinib in PsA).

Assessments

Efficacy assessments

The primary endpoint was ACR 20% improvement in response (ACR20) at W16, defined as ≥ 20% improvement from baseline tender (68) and swollen (66) joint counts and ≥ 20% improvement in 3 of the 5 following measures: Patient Global Assessment of Disease Activity, Patient Global Assessment of Pain, Health Assessment Questionnaire Disability Index (HAQ-DI), Physician Global Assessment of disease activity, and hsCRP level.

The study had 9 multiplicity-controlled key secondary endpoints, including change from baseline (CfB) in HAQ-DI; 75% improvement in the Psoriasis Area and Severity Index (PASI75; in patients with ≥ 3% body surface area [BSA] and static Physician Global Assessment [sPGA] score ≥ 2 at baseline); CfB in 36-Item Short Form Survey physical component summary (SF-36 PCS); achievement of minimal disease activity (MDA); enthesitis resolution (in patients with enthesitis at baseline per the Leeds Enthesitis Index [LEI]; pooled analysis with POETYK PsA-2); CfB in radiographic progression by PsA-modified Sharp–van der Heijde (mSvdH) total score; CfB in Functional Assessment of Chronic Illness Therapy–Fatigue (FACIT-Fatigue); dactylitis resolution (per tender dactylitis count in patients with dactylitis at baseline; pooled analysis with POETYK PsA-2); and CfB in Disease Activity Score 28 with CRP (DAS28-CRP). Additional prespecified, non–multiplicity-controlled analyses were completed for ACR50, ACR70, clinically meaningful improvement in HAQ-DI (HAQ-DI response), pooled Spondyloarthritis Research Consortium of Canada (SPARCC) enthesitis resolution, 50% improvement in Bath Ankylosing Spondylitis Disease Activity Index (BASDAI50), proportion of patients with nonprogression of structural damage (defined as a CfB in mSvdH total score ≤ 0 or ≤ 0.5), pain visual analogue scale (VAS), the SF-36 PCS bodily pain subscale, the pain/discomfort dimension of the EuroQol 5 Dimensions 5 Levels (EQ-5D-5L) questionnaire, and Disease Activity Index for PsA (DAPSA) low disease activity or remission. Endpoints are defined in Supplementary Table S2. ACR20 response by demographics (eg, biological sex, as defined by sex at birth) and baseline clinical characteristic subgroup was analysed.

Radiographic assessment

Radiographic assessments were completed centrally by 2 independent primary readers in 2 reading rounds. The first round included baseline and W16 radiographs; the second round included baseline, W16, and W52 radiographs. If a significant discrepancy occurred, adjudication was performed by a third independent reviewer blinded to results from the first 2 reviewers. Readers were blinded to clinical data, treatment, and chronological order of the radiographs. The average of the 2 scores provided by the primary readers was calculated for the total score and for defining the proportion of nonprogressors. Available radiographic assessments from round 1 were used for W16 analyses and those from round 2 were used for W52 analyses.

Safety

Serious adverse events (SAEs) and all AEs related to SARS-CoV-2 infection were monitored after consent was obtained. AEs of special interest (AESIs) included certain skin-related AEs (eg, acne, folliculitis), select infections (influenza, herpes infections, opportunistic infections, tuberculosis, and COVID-19),

creatine kinase elevations, malignancies, major adverse cardiac events (MACE), and venous thromboembolism (VTE). AEs, treatment-related AEs, SAEs, AEs leading to treatment discontinuation, AESIs, and clinical laboratory parameters were monitored through W52 or ≤ 30 days after the last treatment dose. Safety data were coded using the Medical Dictionary for Regulatory Activities v27.1 and v28.0 and analysed descriptively in the overall safety population (all randomised patients who received ≥ 1 dose of study treatment).

Statistical analysis

SAS v9.4 (SAS Institute Inc) was used for statistical analyses. A sample size of 650 patients randomised 1:1 provided > 99% power to detect a 20% treatment difference between deucravacitinib and placebo at W16 for ACR20 (assuming a 55% response with deucravacitinib and 35% with placebo, 2-sided $\alpha = 0.05$, χ^2 test). This sample size provided sufficient power for all key secondary endpoints; enthesitis (> 99%) and dactylitis (98%) power estimates were based on a planned pooled analysis with POETYK PsA-2. To control for type I error rate at 5% (2-sided), a hierarchical testing strategy was implemented [15]. Following achievement of statistical significance of the primary endpoint, a fixed-sequence testing method was used for key secondary endpoints. Statistical testing proceeded only if the endpoint met statistical significance of $P < .05$ (ie, the null hypothesis was rejected at a 2-sided $\alpha = 0.05$). When an endpoint failed to reach statistical significance, the hierarchy was broken, and subsequent $P < .05$ were considered only nominally significant. Additional endpoints were not multiplicity adjusted; P values were regarded as nominal.

The endpoint of the main estimand was the difference in the proportion of patients in the deucravacitinib and placebo arms who achieved ACR20 at W16 and completed 16 weeks of treatment. Any study treatment discontinuation before W16 was considered an intercurrent event (ICE), and a composite variable strategy was applied; thus, a patient was considered a nonresponder for binary variables, and the CfB value at W16 was set to zero to imply no improvement or worsening relative to baseline for continuous variables. Rescue medication–related ICEs reflect observed data collected under the treatment policy strategy irrespective of rescue medication use; no additional action was required in the data handling for that ICE (ie, no data were imputed). After ICEs were handled, nonresponder imputation (binary measures) or a control-based multiple imputation approach (continuous measures) was used to handle missing data. Multiple imputation assumed that patients with missing data followed the distribution of observed placebo outcomes. A regression model using the Full Conditional Specification method was used, with missing outcomes at W16 imputed by baseline value, treatment group, stratification factors, and outcome from prior visits. No interaction terms or nonlinear effects were included in the model. A total of 200 imputed datasets were generated for each continuous endpoint.

A Cochran–Mantel–Haenszel (CMH) test was used to test binary endpoints using the same randomisation strata to align the analysis with the randomisation scheme. Risk differences (95% CI) were calculated.

Continuous data were analysed using analysis of covariance (ANCOVA), with treatment, randomisation stratification variables, and baseline score for the endpoint as independent variables and CfB as the dependent variable.

W16 ACR20 subgroup analyses were performed using logistic regression models with treatment group and subgroup factor included as covariates, together with a treatment-by-subgroup interaction term. The reported P value refers to the interaction between treatment and the subgroup factor. The 95% CI was calculated for each treatment arm and subgroup.

The protocol-defined radiographic analysis included randomised patients with W16 scans that occurred between days 100 and 127 or before the first dose date in the active treatment period, whichever occurred earlier. Data were analysed using parametric ANCOVA with CfB as the dependent variable and treatment, randomisation stratification variables, and baseline value as the independent variables. Missing data, including those with radiographic assessments performed outside the analysis window, were imputed with control-based multiple imputation.

Due to the nonnormal distribution of radiographic data, post hoc analyses using a nonparametric rank ANCOVA model were completed to assess CfB in mSvdH total score. The rank of CfB was the dependent variable; treatment, randomisation stratification variables, and baseline value were the independent variables. The post hoc P value was calculated using the rank ANCOVA model to evaluate the between-group difference. Given the strict windowing rules that excluded ~20% of available radiographic assessments and the need to evaluate all available radiographic assessments in the final analysis, 2 populations were analysed post hoc: the protocol-defined population (W16 scans within days 100-127 or before the first dose date in the active treatment period) and the full population comprising all randomised patients with radiographic assessments at baseline and W16 nominal visits. No missing data imputation was applied to the post hoc analyses.

The proportion of patients with nonprogression (ie, CfB in mSvdH total score ≤ 0 or ≤ 0.5) was assessed at W16 in both populations using a CMH test stratified by screening hsCRP level and csDMARD use at baseline.

Safety was analysed in the overall safety population. AEs were treatment emergent and included AEs with an onset date on or after the first dose date and ≤ 30 days after the last dose date. Data were summarised descriptively for each arm for the placebo-controlled and cumulative periods, including the number and proportion of patients with ≥ 1 event, number of patient-years (PYs), and exposure-adjusted incidence rates per 100 PYs to account for the treatment switch from placebo to deucravacitinib at W16.

Patient and public involvement

Neither patients nor the public were involved in the design, conduct, reporting, or dissemination plans of POETYK PsA-1.

RESULTS

Patients

The study was initiated in July 2021. The last W52 visit occurred in May 2025. Among 1840 screened patients, 670 were randomised, and 81.8% completed 52 weeks of treatment (Fig 1). In all patients, mean (SD) disease duration since diagnosis was 7.7 (8.0) years; 38.5% of patients had an hsCRP level ≥ 10 mg/L, and 69.9% were receiving csDMARDs at baseline, the majority being methotrexate (58.5%), followed by leflunomide (7.1%) and sulfasalazine (4.8%). More patients were classified as having enthesitis per SPARCC (63.7%) vs LEI (51.5%) criteria, mean baseline SPARCC enthesitis scores were higher than baseline LEI scores, and 35.8% of patients had a dactylitis count > 1

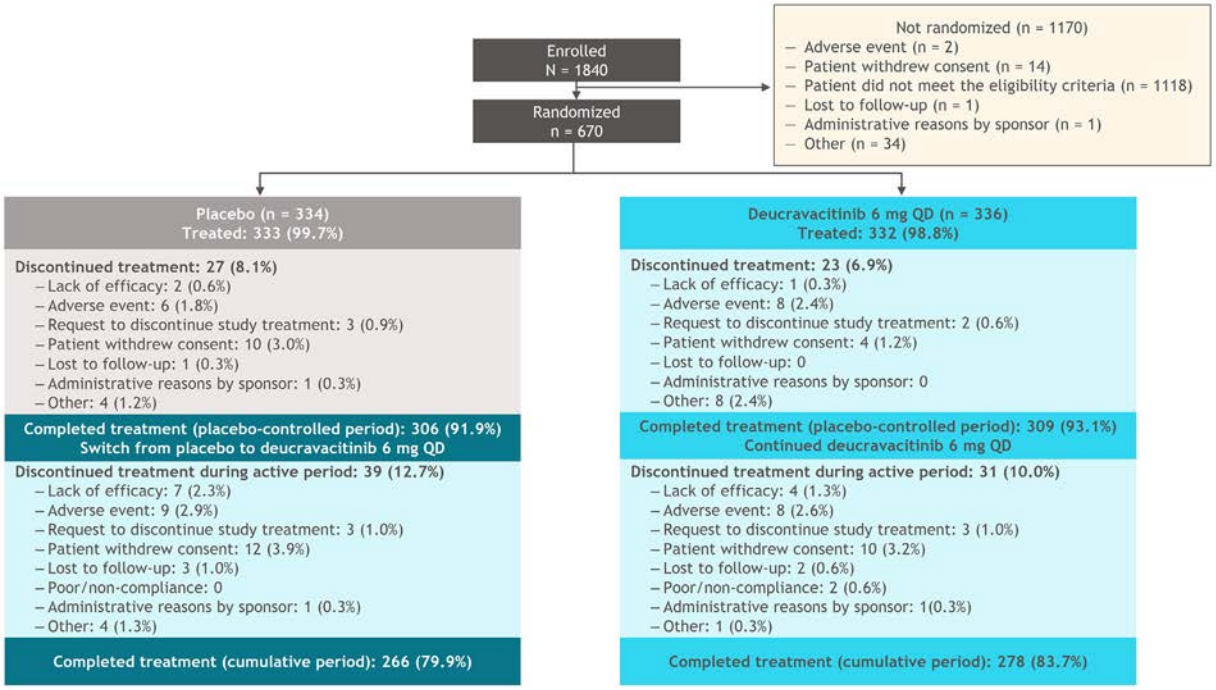

Figure 1. POETYK PsA-1 CONSORT (Consolidated Standards of Reporting Trials) diagram. Percentages are based on the total number of treated patients with ≥ 1 visit during the placebo-controlled and active treatment periods. A data entry error identified after database lock resulted in 1 patient incorrectly being classified as ongoing in the active period. This patient successfully completed the active period. POETYK PsA-1, Program fOr Evaluation of TYK2 inhibitor Psoriatic Arthritis-1; QD, once daily.

at baseline. The predominant forms of PsA were polyarthritis (78.1%), oligoarthritis (10.3%), and predominant distal interphalangeal joint involvement (8.4%); 15.5% of the population had both axial involvement of PsA and peripheral arthritis. There were 332 patients with ≥ 3% BSA and an sPGA score ≥ 2 at baseline evaluable for PASI. Demographics, baseline clinical characteristics, and concomitant medication use were similar between groups (Table 1).

Efficacy

Primary and secondary endpoints

Significantly more patients treated with deucravacitinib vs placebo achieved ACR20 at W16 (54.2% vs 34.1%, $P < .001$) (Table 2). ACR20 response rates increased with deucravacitinib at W24 and W52 (Fig 2). ACR50 (24.7% vs 13.5%) and ACR70 (11.6% vs 5.4%) response rates with deucravacitinib vs placebo followed a similar pattern at W16, with further increases with deucravacitinib at W24 and W52 (Fig 2). A previously published longitudinal analysis of ACR20/50/70 responses showed that separation between arms began at W4, and responses continued to increase through W24 and were maintained through W52 [16].

Table 2 summarises secondary efficacy endpoints for deucravacitinib vs placebo at W16. PASI75 (51.9% vs 7.1%, $P < .001$) and MDA (19.0% vs 10.2%, $P = .001$) were achieved in significantly more patients treated with deucravacitinib vs placebo. Pooled POETYK PsA-1 and PsA-2 W16 enthesitis and dactylitis data were previously reported [17]. Briefly, more patients receiving deucravacitinib achieved LEI enthesitis resolution vs placebo; however, statistical significance was not reached ($P = .18$). Per SPARCC, significantly more patients receiving deucravacitinib achieved enthesitis resolution vs placebo (nominal $P = .002$). More dactylitis resolution was observed with deucravacitinib vs placebo (nominal $P = .01$).

Patients receiving deucravacitinib had a greater CfB in disease activity per DAS28-CRP vs placebo (−1.33 vs −0.83, nominal $P < .001$) and a greater rate of DAPSA low disease activity or remission (34.8% vs 21.6%, nominal $P = .001$). More patients receiving deucravacitinib vs placebo reported improvements in patient-reported outcomes (PROs), including HAQ-DI (−0.39 vs −0.22, $P < .001$), SF-36 PCS (6.06 vs 3.71, $P < .001$), and FACIT-Fatigue (4.6 vs 2.0, nominal $P < .001$), and achieved an HAQ-DI response (51.3% vs 38.8%, nominal $P = .001$). BASDAI50 was not different between groups. For pain-related PROs, patients receiving deucravacitinib had a greater CfB vs placebo in the SF-36 bodily pain subscale (16.8 vs 9.5, nominal $P < .001$), EQ-5D-5L pain/discomfort dimension (−0.6 vs −0.3, nominal $P < .001$), and in the ACR20/50/70 component Patient Global Assessment of Pain (VAS) scores (−23.1 vs −13.3, nominal $P < .001$).

Clinical efficacy measures and PROs improved beyond W16 with deucravacitinib. Responses were sustained at W52 and were comparable in patients who received continuous deucravacitinib and those who switched from placebo to deucravacitinib at W16 (Table 3).

ACR20 at W16 subgroup analyses

More patients receiving deucravacitinib vs placebo achieved ACR20 at W16 in both male (56.4% vs 37.8%) and female (51.8% vs 30.6%) subgroups; the treatment-by-sex interaction was not significant ($P = .67$). ACR20 in subgroups based on study randomisation factors (hsCRP level and csDMARD use) showed superiority with deucravacitinib vs placebo (Supplementary Table S3). Similar effects were seen in additional baseline subgroups (Supplementary Table S3).

ACR components through W16

For each ACR component (Patient Global Assessment of Pain [VAS], tender joint count, swollen joint count, HAQ-DI, Patient Global Assessment of Disease Activity, Physician Global

Table 1
Demographics, baseline clinical characteristics, and concomitant medication use

Characteristic	Placebo (n = 334)	Deucravacitinib 6 mg once daily (n = 336)	Total (N = 670)
Age, mean (SD), y	52.3 (12.3)	51.7 (12.5)	52.0 (12.41)
BMI, mean (SD), kg/m^2	29.6 (5.6)	30.3 (6.4)	29.9 (6.0)
Female, n (%)	170 (50.9)	164 (48.8)	334 (49.9)
Race, n (%)			
American Indian or Alaska Native	19 (5.7)	17 (5.1)	36 (5.4)
Asian	14 (4.2)	25 (7.4)	39 (5.8)
Black or African American	1 (0.3)	4 (1.2)	5 (0.7)
White	279 (83.5)	263 (78.3)	542 (80.9)
Other	21 (6.3)	27 (8.0)	48 (7.2)
PsA subtype, n (%)			
Polyarthritis	261 (78.1)	262 (78.0)	523 (78.1)
Oligoarthritis[a]	33 (9.9)	36 (10.7)	69 (10.3)
Predominant distal interphalangeal joint involvement	27 (8.1)	29 (8.6)	56 (8.4)
Predominant axial involvement	5 (1.5)	1 (0.3)	6 (0.9)
Arthritis mutilans	8 (2.4)	5 (1.5)	13 (1.9)
Not reported	0	3 (0.9)	3 (0.4)
PsA phenotype, n (%)			
Peripheral arthritis	285 (85.3)	278 (82.7)	563 (84.0)
Peripheral arthritis plus axial involvement	49 (14.7)	55 (16.4)	104 (15.5)
Not reported	0	3 (0.9)	3 (0.4)
csDMARD use, n (%)[b]	231 (69.2)	237 (70.5)	468 (69.9)
Methotrexate use, n (%)	191 (57.2)	198 (58.9)	389 (58.5)
Glucocorticoid use, n/N (%)[c]	58/333 (17.4)	56/332 (16.9)	114/665 (17.1)
Duration of disease since diagnosis, mean (SD), y	8.0 (7.6)	7.3 (8.3)	7.7 (8.0)
hsCRP, mean (SD), mg/L	14.2 (19.4)	12.9 (16.1)	13.5 (17.8)
hsCRP ≥10 mg/L, n (%)	134 (40.1)	124 (36.9)	258 (38.5)
DAS28-CRP score, mean (SD)	5.0 (0.9)	5.0 (0.9)	5.0 (0.9)
HAQ-DI score, mean (SD)	1.3 (0.6)	1.4 (0.6)	1.4 (0.6)
PASI score >1, n (%)	261 (78.1)	262 (78.0)	523 (78.1)
PASI score, mean (SD)[d]	9.7 (7.8)	8.9 (6.2)	9.3 (7.0)
BSA >3%, n (%)	193 (57.8)	178 (53.0)	371 (55.4)
Tender joint count (68), mean (SD)	19.0 (13.7)	19.0 (12.8)	19.0 (13.3)
Swollen joint count (66), mean (SD)	10.3 (7.5)	10.7 (6.9)	10.5 (7.2)
Enthesitis: LEI, mean (SD); n (%)[e]	2.3 (1.4); 167 (50.0)	2.6 (1.5); 178 (53.0)	2.4 (1.5); 345 (51.5)
Enthesitis: SPARCC, mean (SD); n (%)[f]	4.2 (3.4); 211 (63.2)	5.1 (3.7); 216 (64.3)	4.7 (3.6); 427 (63.7)
Tender dactylitis count ≥1, n (%)	108 (32.3)	132 (39.3)	240 (35.8)
FACIT-Fatigue score, mean (SD)	29.4 (10.8)	28.9 (11.1)	29.2 (10.9)
SF-36 PCS score, mean (SD)	35.2 (7.9)	34.8 (7.7)	35.0 (7.8)
mSvdH score, mean (SD)	29.1 (50.7)	20.2 (36.8)	24.7 (44.5)

BMI, body mass index; BSA, body surface area; csDMARD, conventional synthetic disease-modifying antirheumatic drug; DAS28-CRP, Disease Activity Score 28 with C-reactive protein; FACIT-Fatigue, Functional Assessment of Chronic Illness Therapy–Fatigue; HAQ-DI, Health Assessment Questionnaire Disability Index; hsCRP, high-sensitivity C-reactive protein; LEI, Leeds Enthesitis Index; mSvdH, PsA-modified Sharp–van der Heijde; PASI, Psoriasis Area and Severity Index; PsA, psoriatic arthritis; SF-36 PCS, 36-Item Short Form Survey physical component summary; SPARCC, Spondyloarthritis Research Consortium of Canada.

[a] Oligoarthritis was defined as involvement of ≤ 4 joints.

[b] As recorded on the case report form; methotrexate use was evaluated in the treated population (N = 665).

[c] Values reported for glucocorticoid use are based on concomitant medication use on day 1 in the treated population.

[d] Of 332 patients evaluated for PASI with ≥ 3% BSA and static Physician Global Assessment score ≥ 2 at baseline (placebo, n = 170; deucravacitinib, n = 162).

[e] Of 345 evaluable patients with an enthesitis (LEI) score ≥ 1 at baseline.

[f] Of 427 evaluable patients with an enthesitis (SPARCC) score ≥ 1 at baseline.

Assessment, and hsCRP level), patients receiving deucravacitinib had numerically greater CfB vs placebo at W16 (Supplementary Fig S2).

Radiographic damage assessments

At W16, using the protocol-defined parametric ANCOVA, there was no difference in radiographic progression between deucravacitinib and placebo (P = .76) (Table 2). Due to the protocol-defined analysis visit windowing rule, ~20% of radiographic assessments were excluded. When analysed using nonparametric ANCOVA to account for nonnormal data distribution, deucravacitinib demonstrated significant inhibition of radiographic progression vs placebo in both the protocol-defined (rank ANCOVA, P = .019) and full (rank ANCOVA, P = .009) populations at W16.

In patients with available scans at baseline, W16, and W52, inhibition of radiographic progression was observed at W16 and was maintained through W52 (Fig 3A). Deucravacitinib was associated with lower mean CfB in mSvdH score vs placebo over the placebo-controlled period (W0-16), suggesting reduced radiographic progression. This effect was maintained through W52, with a numerically lower CfB in structural damage progression in patients receiving continuous deucravacitinib and those who switched from placebo at W16. (Fig 3A). Significantly more patients receiving deucravacitinib vs placebo showed no radiographic progression at W16 in the protocol-defined (82.0% vs 72.9%, P = .017) and full (82.0% vs 71.5%, P = .003) populations (Fig 3B); similar results were observed when nonprogression was defined as a CfB in mSvdH total score ≤ 0.5, in both the protocol-defined (86.5% vs 81.7%, P = .16) and full (86.6%

Table 2
Primary and secondary endpoints at W16[a]

Parameter	Placebo (n = 334)	Deucravacitinib 6 mg once daily (n = 336)	Δ[b] (95% CI)	*P* value
Primary endpoint				
ACR20, %	34.1	54.2	20.0 (12.7 to 27.4)	< .001
Ranked secondary endpoints				
HAQ-DI, adjusted mean CfB (SE)	−0.22 (0.03)	−0.39 (0.03)	−0.17 (−0.2 to −0.1)	< .001
PASI75, %[c]	7.1	51.9	44.1 (35.4 to 52.7)	< .001
SF-36 PCS, adjusted mean CfB (SE)	3.71 (0.41)	6.06 (0.41)	2.34 (1.3 to 3.4)	< .001
Minimal disease activity, %	10.2	19.0	8.9 (3.6 to 14.2)	.001
Enthesitis (LEI) resolution, %[d]	45.1	50.3	5.3(−2.4 to 12.9)	.18
mSvdH, adjusted mean CfB (SE)	0.64 (0.32)	0.78 (0.35)	0.14 (−0.8 to 1.0)	.76
FACIT-Fatigue, adjusted mean CfB (SE)	2.0 (0.48)	4.6 (0.48)	2.6 (1.4 to 3.9)	*< .001*[h]
Dactylitis resolution, %[d]	44.1	57.6	12.8 (3.2 to 22.4)	*.01*[h]
DAS28-CRP, adjusted mean CfB (SE)	−0.83 (0.06)	−1.33 (0.06)	−0.51 (−0.7 to −0.3)	*< .001*[h]
Nonranked secondary endpoints				
Enthesitis (SPARCC) resolution, %[d]	36.1	47.1	10.8 (4.1 to 17.6)	*.002*[h]
HAQ-DI clinically meaningful improvement, n/N (%)[e]	307/334 (38.8)	314/336 (51.3)	12.8 (5.1 to 20.5)	*.001*[h]
DAPSA low disease activity or remission, %[f]	21.6	34.8	13.2 (6.6 to 19.9)	*.001*[h]
BASDAI50, n/N (%)[g]	49/334 (14.3)	55/336 (25.5)	10.6 (−4.9 to 26.2)	.19

ACR20, American College of Rheumatology 20% improvement in response; BASDAI50, 50% improvement in Bath Ankylosing Spondylitis Disease Activity Index; CfB, change from baseline; DAPSA, Disease Activity Index for Psoriatic Arthritis; DAS28-CRP, Disease Activity Score 28 with C-reactive protein; FACIT-Fatigue, Functional Assessment of Chronic Illness Therapy–Fatigue; HAQ-DI, Health Assessment Questionnaire Disability Index; LEI, Leeds Enthesitis Index; mSvdH, PsA-modified Sharp–van der Heijde; PASI75, 75% improvement in the Psoriasis Area and Severity Index; PsA, psoriatic arthritis; SF-36 PCS, 36-Item Short Form Survey physical component summary; SPARCC, Spondyloarthritis Research Consortium of Canada; W, week.

[a] Treatment discontinuation prior to W16 was considered treatment failure (composite variable strategy). For binary variables, the composite outcome was set to zero. For continuous variables, the W16 value was set to zero to imply neither improvement nor worsening relative to baseline. All rescue medication–related intercurrent events were treated with a treatment policy–estimand strategy. After intercurrent events were handled, nonresponder imputation was used to handle missing binary data and control-based pattern imputation was used to handle missing data for continuous endpoints. Binary endpoints were analysed with a Cochran–Mantel–Haenszel test stratified by screening high-sensitivity C-reactive protein level (< 10 vs ≥ 10 mg/L) and conventional synthetic disease-modifying antirheumatic drug use at baseline (yes vs no) to compare the response rates with deucravacitinib vs placebo. Response rate (%) is the proportion of responders to total number of patients in the randomised population and in the patient subset for the endpoint, when applicable. Continuous endpoints were analysed using analysis of covariance with treatment, randomisation stratification variables, and baseline value as independent variables and CfB as the dependent variable. The adjusted mean CfB (least squares means) with SE and 95% CI per treatment group and the difference between deucravacitinib and placebo in adjusted mean CfB with SE and 95% CI were provided from each analysis model.

[b] Δ is the response rate risk difference for binary endpoints or adjusted CfB mean treatment difference for continuous endpoints. The 95% CI was calculated using the Clopper–Pearson exact method for binary endpoints and the Wald method for continuous endpoints.

[c] Analysed in randomised patients with ≥ 3% body surface area and static Physician Global Assessment score ≥ 2 at baseline (placebo, n = 170; deucravacitinib, n = 162).

[d] Pooled analysis from POETYK PsA-1 and POETYK PsA-2 in patients with enthesitis by LEI (placebo, n = 317; deucravacitinib, n = 318) or SPARCC (placebo, n = 407; deucravacitinib, n = 393) at baseline or patients with a tender dactylitis count ≥ 1 (placebo, n = 188; deucravacitinib, n = 210) at baseline.

[e] Analysed in all randomised patients with a baseline HAQ-DI score ≥ 0.35. Clinically meaningful improvement was defined as ≥ 0.35 improvement from baseline HAQ-DI score.

[f] DAPSA disease remission is defined as a score ≤ 4. DAPSA low disease activity is defined as a score > 4 and ≤ 14.

[g] BASDAI50 was assessed in patients with spondylitis in addition to peripheral involvement at baseline.

[h] Italics indicate that the *P* value is nominally significant.

vs 79.7%, *P* = .028) populations. Cumulative probability plots for CfB in mSvdH total score with deucravacitinib vs placebo at W16 are shown in Figure 3C.

Safety

Placebo-controlled period (W0-16)

AEs occurred in 60.2% with deucravacitinib and 48.0% with placebo during the placebo-controlled period (Table 4). Of the most common AEs (≥ 5% in any arm), upper respiratory tract infection was more frequent with deucravacitinib vs placebo. No inflammatory bowel disease (IBD) or IBD flares were reported. The frequency of SAEs was low and comparable between deucravacitinib (1.8%) and placebo (2.4%) (Table 4; Supplementary Table S4). Few AEs leading to discontinuation were observed with deucravacitinib (2.4%) and placebo (1.8%) (Table 4; Supplementary Table S5). The most frequent AESIs by system organ class with deucravacitinib were skin events (30 [9.0%], 18 of which were acneiform) and infections (COVID-19, 9 [2.7%]; herpes simplex, 5 [1.5%]; influenza events, 4 [1.2%]; herpes zoster, 1 [0.3%]), consistent with the known deucravacitinib safety profile (Supplementary Table S6). No new safety signals related to MACE, VTE, malignancies, or opportunistic infections occurred during the placebo-controlled period, and no deaths were reported (Table 4).

Cumulative period (W0-52)

The exposure-adjusted incidence rate of AEs with deucravacitinib was 196.0 per 100 PYs with placebo–deucravacitinib and 218.7 per 100 PYs with deucravacitinib–deucravacitinib. Of the most common AEs (≥ 5% in any arm), upper respiratory tract infection, nasopharyngitis, hypertension, COVID-19, and urinary tract infection were more frequent with deucravacitinib –deucravacitinib. Cumulative period SAE incidence rates were 9.0 per 100 PYs with placebo–deucravacitinib and 8.9 per 100 PYs with deucravacitinib–deucravacitinib (Table 4; Supplementary Table S4). Incidence rates of AEs leading to discontinuation in the cumulative period were 5.2 per 100 PYs with placebo

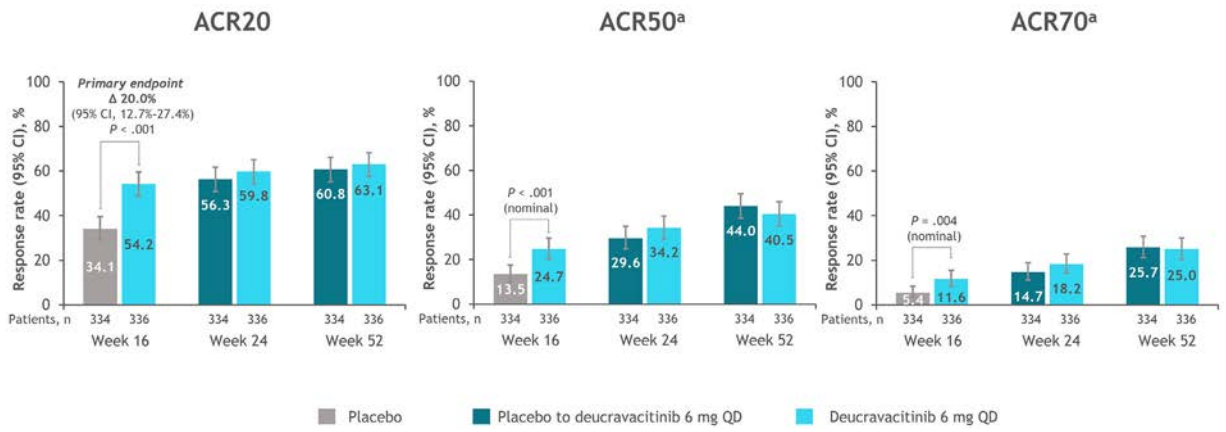

Figure 2. ACR20/50/70 responses at W16, W24, and W52. All randomised patients were assessed. A composite variable strategy was used for treatment discontinuation up to W16 (the composite outcome was set to zero). A treatment policy strategy was applied for the use of rescue medication up to W16. Nonresponder imputation was used for missing data. [a]Additional secondary endpoint at W16 and exploratory endpoint at W24 and W52. *P* values are nominal at W24 and W52. ACR20/50/70, American College of Rheumatology 20%/50%/70% improvement in response; QD, once daily; W, week.

Table 3
Exploratory efficacy endpoints at W52[a]

Parameter	Placebo → deucravacitinib 6 mg once daily (n = 334)	Deucravacitinib → deucravacitinib 6 mg once daily (n = 336)
Clinical efficacy		
ACR20, %	60.8	63.1
ACR50, %	44.0	40.5
ACR70, %	25.7	25.0
PASI75, n/N (%)[b]	88/170 (51.8)	107/162 (66.0)
PASI90, n/N (%)[b]	63/170 (37.1)	73/162 (45.1)
PASI100, n/N (%)[b]	48/170 (28.2)	50/162 (30.9)
Minimal disease activity, %	34.4	33.9
DAS28-CRP, adjusted mean CfB (SE)	−2.05 (0.07)	−2.11 (0.07)
Extra-articular musculoskeletal manifestations[c]		
Dactylitis resolution, n/N (%)	119/188 (63.3)	149/210 (71.0)
Enthesitis (LEI) resolution, n/N (%)	190/317 (59.9)	187/318 (58.8)
Enthesitis (SPARCC) resolution, n/N (%)	230/407 (56.5)	213/393 (54.2)
Patient-reported outcomes		
SF-36 PCS, adjusted mean CfB (SE)	8.32 (0.48)	8.57 (0.47)
FACIT-Fatigue, adjusted mean CfB (SE)	6.3 (0.53)	6.4 (0.53)
HAQ-DI, adjusted mean CfB (SE)	−0.49 (0.03)	−0.51 (0.03)
HAQ-DI clinically meaningful improvement, n/N (%)[d]	156/307 (50.8)	173/314 (55.1)

ACR20/50/70, American College of Rheumatology 20%/50%/70% improvement in response; CfB, change from baseline; DAS28-CRP, Disease Activity Score 28 with C-reactive protein; FACIT-Fatigue, Functional Assessment of Chronic Illness Therapy–Fatigue; HAQ-DI, Health Assessment Questionnaire Disability Index; LEI, Leeds Enthesitis Index; PASI75/90/100, 75%/90%/100% improvement in the Psoriasis Area and Severity Index; PsA, psoriatic arthritis; SF-36 PCS, 36-Item Short Form Survey physical component summary; SPARCC, Spondyloarthritis Research Consortium of Canada; W, week.

[a] All randomised patients were assessed unless otherwise noted. The estimand strategy was not implemented for W52 analyses. Nonresponder imputation was used to handle missing data for binary variables, and control-based pattern multiple imputation was used to handle missing data for continuous variables unless otherwise noted.

[b] Analysed in all randomised patients with ≥ 3% body surface area and a static Physician Global Assessment score ≥ 2 at baseline; n/N denotes the number of responders over the total number of patients assessed.

[c] POETYK PsA-1 and PsA-2 pooled analysis in patients with enthesitis by LEI or SPARCC at baseline or patients with a tender dactylitis count ≥ 1 at baseline.

[d] Analysed in all randomised patients with a baseline HAQ-DI score ≥ 0.35. Clinically meaningful improvement was defined as ≥ 0.35 improvement from baseline HAQ-DI score.

−deucravacitinib and 6.0 per 100 PYs with deucravacitinib −deucravacitinib (Table 4; Supplementary Table S5). Exposure-adjusted incidence rates of skin and infection AESIs did not increase in the cumulative period compared with the placebo-controlled period. The most frequently reported AESIs by system organ class in the cumulative period were skin events (deucravacitinib−deucravacitinib, 41 [12.3%], 15.0 per 100 PYs; placebo −deucravacitinib, 34 [11.1%], 19.0 per 100 PYs), which is consistent with the known profile of deucravacitinib. Rash was the most frequently reported skin AESI in the deucravacitinib−deucravacitinib group (14 [2.2%]); all rash events were mild to moderate in severity, and no serious skin events occurred. One skin event in the deucravacitinib−deucravacitinib group (urticaria) and 3 skin events in the placebo−deucravacitinib group (urticaria, allergic dermatitis, and rash) led to treatment discontinuation. No new safety signals related to MACE, VTE, malignancies, or opportunistic infections occurred (Table 4). No deaths occurred.

Laboratory parameters

No meaningful changes were observed in mean CfB in alanine aminotransferase, aspartate aminotransferase, creatine kinase, and triglyceride levels through W52 (Fig 4; Supplementary Table S7). Laboratory parameters generally remained within the normal range. No cases of drug-induced liver injury or rhabdomyolysis events were reported through W52.

A. Sustained inhibition of progression of structural damage (as observed, post hoc analysis)[a]

Mean CfB (SD) in mSvDH score	Placebo→ deucravacitinib 6 mg QD (n = 266)	Deucravacitinib→ deucravacitinib 6 mg QD (n = 273)
BL to week 16 *Placebo-controlled period*	.57 (1.71)	.40 (1.71)
BL to week 52 *Cumulative treatment period*	.90 (2.97)	.71 (2.51)

Patients who were initially randomized to receive placebo crossed over to deucravacitinib 6 mg QD at week 16.

B. Proportion of nonprogressors at week 16 (mSvdH total score change from baseline of ≤ 0 at week 16)[b]

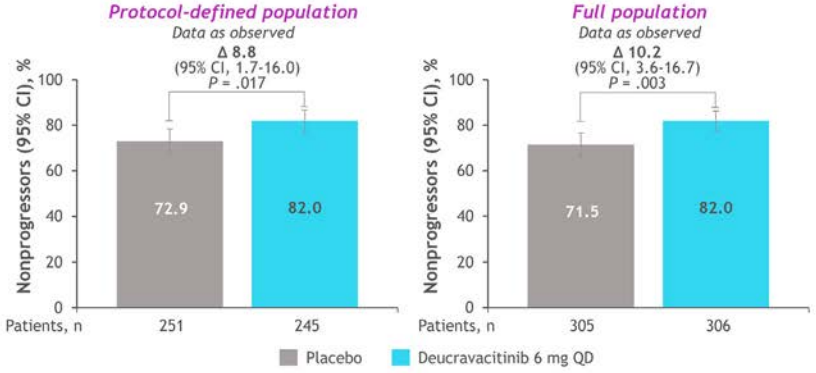

C. Cumulative probability plots at week 16

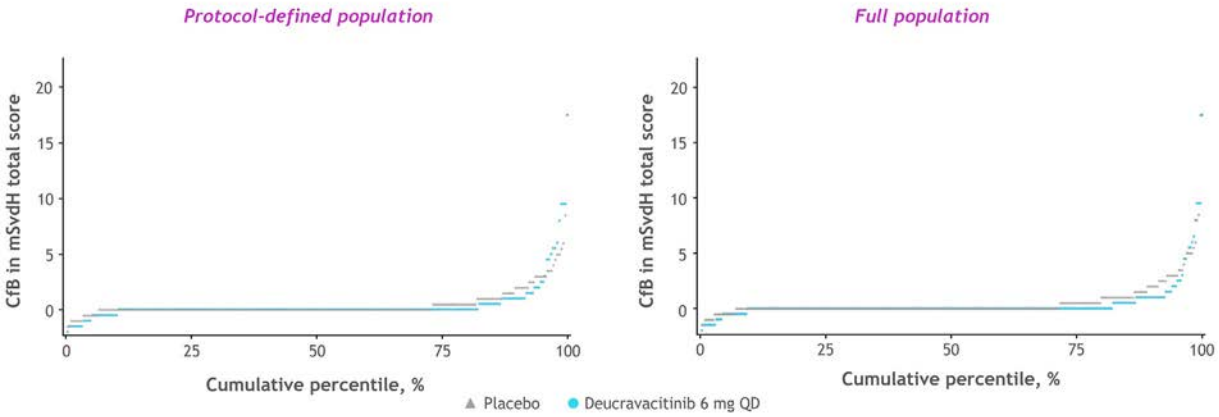

Figure 3. Inhibition of radiographic progression. (A) CfB in mSvdH total score in the placebo-controlled period (W0-16) and the cumulative treatment period (W0-52). (B) Radiographic nonprogressors at W16. A composite variable strategy was used for treatment discontinuation up to W16. A treatment policy strategy was used for rescue medication up to W16. The 95% CI for response rate was calculated using the Clopper–Pearson exact method. Risk difference was obtained from stratified contingency tables. *P* value was calculated using a Cochran–Mantel–Haenszel test stratified by screening high-sensitivity C-reactive protein levels and conventional synthetic disease-modifying antirheumatic drug use at baseline. (C) Cumulative probability plots of CfB in mSvdH total score. [a]The population was based on randomised patients with available, observed mSvdH total score, which was collected at screening, W16, and W52 visits. Descriptive statistics were based on purely observed data for the total number of patients with nonmissing BL, W16, and W52 values. Missing data were not imputed (data as observed). [b]Nonprogression was defined as a CfB in mSvdH total score of ≤ 0. The protocol-defined population included randomised patients with available, observed mSvdH data that were collected during the analysis window at BL and W16, which was from days 100 to 127 and before the first dose in the active treatment period. The full population included randomised patients with nonmissing BL and W16 mSvdH total score data based on purely observed data. BL, baseline; CfB, change from baseline; mSvdH, PsA-modified Sharp–van der Heijde; QD, once daily; W, week.

DISCUSSION

The POETYK PsA-1 trial, 1 of 2 global, double-blind, placebo-controlled, phase 3 studies, achieved its primary endpoint of ACR20, demonstrating superior clinical efficacy of deucravacitinib vs placebo at W16.

Key secondary endpoints at W16 were met across multiple PsA domains, including skin, musculoskeletal, and overall disease activity measures. Although the pooled analysis of enthesitis resolution per LEI was not statistically significant, enthesitis resolution per SPARCC showed a nominally significant difference between deucravacitinib and placebo groups. A recent meta-analysis reported that, although LEI is the most commonly used enthesitis scoring tool, it may underestimate total enthesitis sites because only 6 peripheral entheses are evaluated vs 16 sites with SPARCC [18], corroborating current findings. Indeed, a lack of enthesitis resolution per LEI has been observed in the FUTURE-2 phase 3 trial, which did not show a

Table 4
Overall safety summary

Placebo-controlled period (W0-16)		
Patients with an AE	Placebo (n = 333)	Deucravacitinib 6 mg once daily (n = 332)
	n (%)	n (%)
Any AEs	160 (48.0)	200 (60.2)
Treatment-related AEs	39 (11.7)	64 (19.3)
Serious AEs	8 (2.4)	6 (1.8)
AEs leading to discontinuation	6 (1.8)	8 (2.4)
Deaths	0	0
Most frequent AEs (≥ 5%) in any arm by preferred term		
Upper respiratory tract infection	10 (3.0)	17 (5.1)

Cumulative treatment period (W0-52)				
	Placebo → deucravacitinib 6 mg once daily (n = 306)		Deucravacitinib → deucravacitinib 6 mg once daily (n = 332)	
	n (%)	IR/ 100 PYs	n (%)	IR/ 100 PYs
Any AEs	206 (67.3)	196.0	262 (78.9)	218.7
Treatment-related AEs	54 (17.6)	31.2	92 (27.7)	38.0
Serious AEs	17 (5.6)	9.0	26 (7.8)	8.9
AEs leading to discontinuation	10 (3.3)	5.2	18 (5.4)	6.0
Deaths	0	0	0	0
Most frequent AEs (≥ 5%) in any arm by preferred term				
Upper respiratory tract infection	33 (10.8)	18.0	46 (13.9)	16.6
Nasopharyngitis	26 (8.5)	14.2	30 (9.0)	10.6
Hypertension	14 (4.6)	7.4	26 (7.8)	9.1
COVID-19	9 (2.9)	4.7	24 (7.2)	8.4
Urinary tract infection	7 (2.3)	3.7	19 (5.7)	6.5
AEs of interest (adjudicated)				
Major adverse cardiac events				
Myocardial infarction	1 (0.3)	1.0	0	0
Stroke haemorrhagic	0	0	1 (0.3)	0.6
Stroke ischaemic	1 (0.3)	0.6	0	0
Venous thromboembolism				
Deep vein thrombosis	1 (0.3)	0.6	0	0
Malignancies				
Prostate cancer	0	0	2 (0.6)	0.7
Glioblastoma	0	0	1 (0.3)	0.3
Endometrial cancer	1 (0.3)	0.5	0	0

AEs are defined as treatment-emergent AEs with an onset date on or after the first dose date of study treatment up to 30 days after the last dose date of treatment in the study. For cumulative-period data, only treatment-emergent events with deucravacitinib were tallied (placebo–deucravacitinib, W16-52; deucravacitinib–deucravacitinib, W0-52). Incidence rate per 100 PYs of exposure (IR/100 PYs): event count × 100/PYs of exposure. MedDRA v27.1 was used to define preferred terms in the placebo-controlled period and v28.0 was used to define preferred terms in the cumulative period. The following AEs were considered AEs of interest: dermatologic AEs, select infections (ie, influenza, opportunistic infections, herpes infections, tuberculosis, and COVID-19), malignancies, and cardiovascular events.
AE, adverse event; IR, incidence rate; MedDRA, Medical Dictionary for Regulatory Activities; PY, patient-year; W, week.

significant difference in LEI between secukinumab and placebo [19]. Of note, SPARCC may not be the optimal indicator of enthesitis in all situations; when ultrasound is used to differentiate inflammatory and noninflammatory PsA phenotypes, higher SPARCC score may be related to pain and fibromyalgia but not a persistent inflammatory phenotype [20]. As such, a better understanding of the presence and resolution of enthesitis with deucravacitinib is needed. Clinical efficacy continued to improve numerically beyond W16 with deucravacitinib, and responses were maintained through W52, including over one-third of patients achieving MDA at W52. Greater improvements in PROs, including pain, fatigue, physical functioning, and overall quality of life, were reported for patients receiving deucravacitinib vs placebo at W16. PROs continued to improve beyond W16 and were maintained with deucravacitinib through W52. This time-dependent improvement is consistent with the sustained pharmacologic inhibition of TYK2 and downstream inflammatory pathways, which may be an important consideration in evaluating clinical efficacy in real-world settings. The efficacy profile observed in POETYK PsA-1 is consistent with results from phase 3 trials of deucravacitinib in moderate to severe PsO, where deucravacitinib demonstrated sustained PASI and sPGA responses [21–24].

ACR20/50/70 responses continued to increase with deucravacitinib through W24 and started to plateau at approximately 28 weeks for ACR20, 36 weeks for ACR50, and 40 weeks for ACR70, suggesting that achievement of maximal response with deucravacitinib occurs beyond W16 and is maintained through W52. ACR20/50/70 achievement in this trial is consistent with that observed with zasocitinib, another oral TYK2 inhibitor, in a phase 2 trial at W12 [25]. ACR20 responses with deucravacitinib were also consistent across subgroups, including response by sex. Similar to the JAK inhibitors tofacitinib and upadacitinib, the TYK2 inhibitor deucravacitinib appears to have a less disparate ACR20 response by sex compared with those observed with IL-17 or

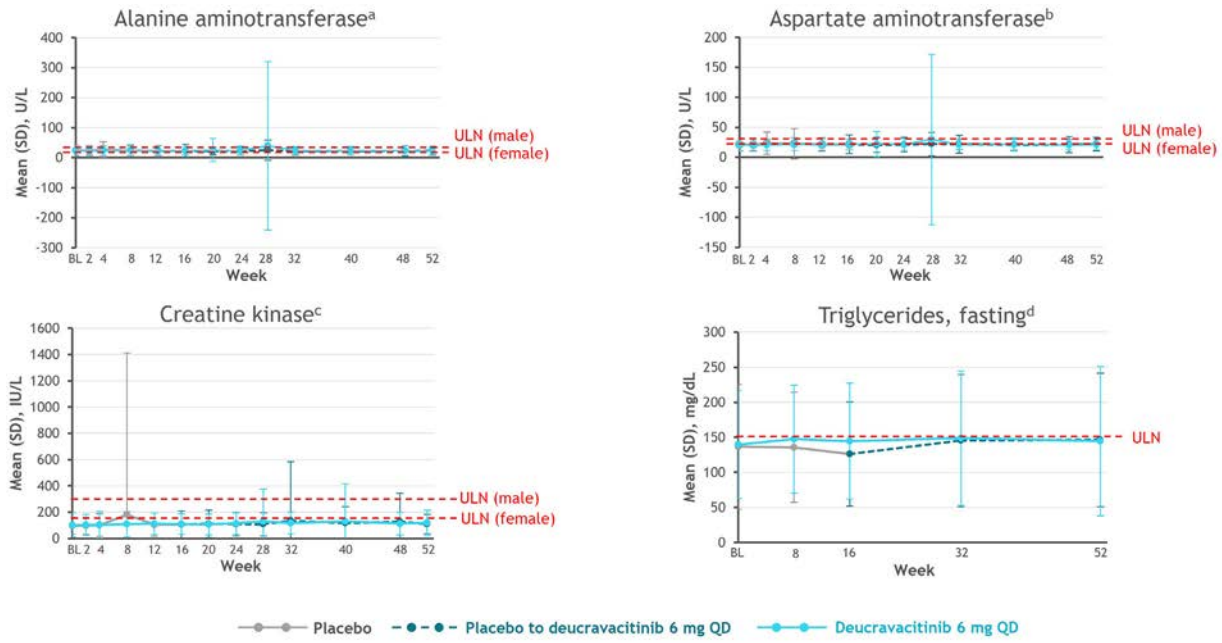

Figure 4. Laboratory parameters through W52 in the treated population. CfB in alanine aminotransferase, aspartate aminotransferase, creatine kinase, and triglyceride levels through W52 are shown. All patients who were randomised and received ≥ 1 dose of study treatment was included. [a]ULN is defined as 33 U/L for females and 41 U/L for males. [b]ULN is defined as 31 U/L for females and 37 U/L for males. [c]ULN is defined as 192 IU/L for females and 308 IU/L for males. [d]ULN is defined as 150 mg/dL. BL, baseline; CfB, change from baseline; QD, once daily; ULN, upper limit of normal; W, week.

IL-23 inhibitors, with which higher response rates are reported in male vs female patients [26].

Radiographic data in this study were nonnormally distributed, and the protocol-defined windowing rules resulted in exclusion of ~20% of cases. To address these factors, the analysis approach was revised post hoc to use a nonparametric ANCOVA with no missing data imputation and to define more inclusive patient populations without windowing rules. In these post hoc radiographic analyses, deucravacitinib was associated with inhibition of structural damage progression at W16. This effect was sustained with continuous deucravacitinib at W52. For patients initially receiving placebo, radiographic progression from W16 to W52 was attenuated after switching to deucravacitinib, similar to the reduced progression observed in patients who received deucravacitinib continuously over 52 weeks [16]. More radiographic nonprogressors were observed at W16 with deucravacitinib vs placebo. The magnitude of difference in nonprogressors observed in this study is consistent with radiographic assessments in other phase 3 studies of PsA, including guselkumab in the APEX trial [27] and secukinumab in the FUTURE 5 trial [28]. As the number of treatment options for structural damage in PsA and related diseases continues to grow [27–31], results suggest that TYK2 signalling inhibition may be a strategy to manage structural damage progression with PsA.

Deucravacitinib was well tolerated through the cumulative period with no new safety signals identified, similar to that observed in POETYK PsA-2 through W52 [32]. The safety profile was consistent with the 5-year safety data from the phase 3 PsO trials [12] and a phase 2 study in systemic lupus erythematosus [33]. Incidences of SAEs and AEs leading to discontinuation were low and comparable between deucravacitinib and placebo at W16; these events were low with deucravacitinib through W52, suggesting no increased safety risk with longer deucravacitinib exposure. The most commonly observed AESIs were skin events (eg, acne and rash) and infections, consistent with the known deucravacitinib safety profile. No serious skin events occurred. Although more patients in the deucravacitinib group experienced AEs during the 52-week period, most were mild to moderate and resolved without intervention. Unlike JAK inhibitors, deucravacitinib selectively inhibits TYK2 [13,14], which may result in a differentiated safety profile. Analyses from the postauthorisation ORAL Surveillance study of JAK inhibitors in other rheumatic diseases have raised concerns regarding potential cardiovascular and malignancy risks [6,8]. Deucravacitinib showed no increase in adjudicated MACE, VTE, or malignancies in this trial, in line with the low incidence of these events observed in the pivotal upadacitinib [34,35] and tofacitinib [36,37] trials in PsA. Long-term safety of deucravacitinib in PsA will be evaluated in the open-label extension.

Limitations of this study included that study site was not considered as a random effect in the statistical model. However, given the large number of sites and the small number of patients at many sites, and that the primary objective of the trial was the overall population-average treatment effect across the intended target population, the analysis approach was aligned to the estimand rather than a site random-effects model. Additionally, the 16-week placebo-controlled period may have limited the ability to observe radiographic progression in the placebo group with a less sensitive imaging method such as radiography. Of note, the study population was enriched for radiographic progression (ie, inclusion criteria required the presence of ≥ 1 hand or foot erosion at baseline and high hsCRP level [≥ 3 mg/L]) to enable measurement of the impact of deucravacitinib on radiographic progression. Hierarchical testing, including the radiographic progression endpoint, was implemented to control for type I error. Other limitations included the predefined statistical methodology (ie, ANCOVA) for evaluating radiographic progression (CfB in mSvdH), as radiographic data were characterised by a nonnormal distribution pattern. Further, the strict windowing rule excluded almost 20% of available radiographic assessments. To account for these shortcomings, a post hoc analysis was conducted using rank ANCOVA, which is a method suitable for

nonnormally distributed data, to assess all available radiographs around W16, irrespective of the windowing rule.

Conclusions

In the POETYK PsA-1 trial, deucravacitinib demonstrated superiority over placebo in multiple key domains of PsA and PROs. Durable improvements were noted in joints, skin, enthesitis, dactylitis, and overall disease activity outcomes, as well as PROs related to pain, fatigue, physical function, and overall quality of life. Deucravacitinib demonstrated inhibition of radiographic progression at W16 in the post hoc analyses, an effect that was sustained at W52. Taken together, deucravacitinib was shown to be safe and efficacious in POETYK PsA-1.

Competing interests

DvdH: Consulting fees: AbbVie, Alfasigma, argenx, Bristol Myers Squibb, Eli Lilly, Greywolf Therapeutics, Janssen, Novartis, Pfizer, Takeda, and UCB Pharma; Associate Editor: *Annals of the Rheumatic Diseases*; Editorial board member: *Journal of Rheumatology*; Director of Imaging Rheumatology bv. Given their role as Associate Editor of *Annals of the Rheumatic Diseases*, Désirée van der Heijde had no involvement in the peer review of this article and has no access to information regarding its peer review. Full responsibility for the editorial process for this article was delegated to another journal editor. PJM: Research grants: AbbVie, ACELYRIN, Amgen, Bristol Myers Squibb, Eli Lilly, Johnson & Johnson, Novartis, Pfizer, and UCB; Consulting and/or speaker fees: AbbVie, ACELYRIN, Amgen, Bristol Myers Squibb, Century, Cullinan, Eli Lilly, Johnson & Johnson, MoonLake Pharma, Novartis, Pfizer, Spyre, Sun Pharma, Takeda, and UCB. CPaul: Grants and consultant: AbbVie, Almirall, Amgen, Boehringer Ingelheim, Bristol Myers Squibb, Celgene, Eli Lilly, Janssen, LEO Pharma, Merck, Mylan, Novartis, Pfizer, and UCB. FB: None declared. LG: Grants/research support: AbbVie, Lilly, Novartis, and UCB; Consulting fees: AbbVie, Alfasigma, Bristol Myers Squibb, Celltrion, Johnson & Johnson, MoonLake, Novartis, Oruka, Pfizer, Takeda, and UCB; Honoraria for lectures: AbbVie, Alfasigma, Amgen, Bristol Myers Squibb, Celltrion, Johnson & Johnson, Lilly, MoonLake, Novartis, Pfizer, Stada, and UCB; Support for attending meetings and/or travel: AbbVie, Biogen, and Lilly; Medical writing support: AbbVie, Amgen, Bristol Myers Squibb, Celltrion, Johnson & Johnson, Pfizer, and UCB; Membership on an entity's Board of Directors or advisory committees: European Alliance of Associations for Rheumatology elected board member. YK: Consultant: Bristol Myers Squibb; Lecture honorarium: Bristol Myers Squibb. LE: Research and educational grants: AbbVie, Novartis, UCB, Pfizer, Fresenius Kabi, Eli Lilly, Novo Nordisk, Amgen, and Janssen; Advisory boards: AbbVie, Novartis, UCB, Pfizer, Eli Lilly, and Janssen. LCC: Grants/research support: AbbVie, Amgen, Janssen, and UCB; Consultancy: AbbVie, Amgen, Bristol Myers Squibb, Eli Lilly, Enlivex, Janssen, MoonLake Pharma, Novartis, Pfizer, Takeda, and UCB; Speaker: AbbVie, Amgen, Eli Lilly, Janssen, Novartis, Pfizer, and UCB. AEP: None declared. WW: None declared. ERS: Consultancy: AbbVie, Janssen, Novartis, and Roche; Grant/research support: AbbVie, Johnson & Johnson, Novartis, Pfizer, Roche, and UCB; Speaker fees: AbbVie, Amgen, Bristol Myers Squibb, Eli Lilly, Janssen, Novartis, Pfizer, Roche, and UCB. PL: Research support: Bristol Myers Squibb; Speaker fees: Novartis, AbbVie, AstraZeneca, Bristol Myers Squibb, Pfizer, and UCB. JUS: Consultancy: Bristol Myers Squibb, UCB, Johnson & Johnson, Novartis, and Pfizer; Research: Pfizer and Johnson & Johnson. AD: Consulting and/or advisory boards: Bristol Myers Squibb, Eli Lilly, Johnson & Johnson, Novartis, Pfizer, and UCB; Research grants: Bristol Myers Squibb, Eli Lilly, Johnson & Johnson, MoonLake Pharma, Novartis, Pfizer, and UCB. CPachai, JL, XF, SR, CS, EV, and JV: Employees and shareholders: Bristol Myers Squibb. JFM: Consultant and/or investigator: Amgen, AstraZeneca, Biogen, Boehringer Ingelheim, Bristol Myers Squibb, AbbVie, Dermavant, Eli Lilly, MoonLake, Novartis, Janssen, Oruka, UCB, Sanofi, Regeneron, Sun Pharma, Galderma, Biogen, and Pfizer.

Acknowledgements

We thank the patients and families who made this study possible and the clinical study teams that participated. All authors contributed to and approved the manuscript in its current form; professional medical writing and editorial assistance was provided by Stephanie V Koebele, PhD, of Nucleus Global, funded by Bristol Myers Squibb. Portions of this research were previously presented at The European Alliance of Associations for Rheumatology (EULAR) 2025 Congress in Barcelona, Spain (van der Heijde D et al. Oral presentation LB0001. Ann Rheum Dis. 2025;84:313-314) and the American College of Rheumatology (ACR) Convergence 2025 in Chicago, IL, USA (van der Heijde D et al. Oral presentation LB20. Arthritis Rheumatol. 2025;77[suppl 9]).

Contributors

DvdH: Conceptualisation, validation, writing – original draft, writing – review and editing. PJM: Conceptualisation, investigation, validation, writing – original draft, writing – review and editing. CPaul: Investigation, validation, writing – original draft, writing – review and editing. FB: Investigation, validation, writing – original draft, writing – review and editing. LG: Investigation, validation, writing – original draft, writing – review and editing. YK: Investigation, validation, writing – original draft, writing – review and editing. LE: Investigation, validation, writing – original draft, writing – review and editing. LCC: Investigation, validation, writing – original draft, writing – review and editing. AEP: Investigation, validation, writing – original draft, writing – review and editing. WW: Investigation, validation, writing – original draft, writing – review and editing. ERS: Investigation, validation, writing – original draft, writing – review and editing. PL: Investigation, validation, writing – original draft, writing – review and editing. JUS: Investigation, validation, writing – original draft, writing – review and editing. AD: Conceptualisation, investigation, validation, writing – original draft, writing – review and editing. CPachai: Data curation, formal analysis, methodology, validation, writing – original draft, writing – review and editing. JL: Data curation, formal analysis, methodology, validation, writing – original draft, writing – review and editing. XF: Data curation, formal analysis, methodology, validation, writing – original draft, writing – review and editing. SR: Data curation, formal analysis, methodology, validation, writing – original draft, writing – review and editing. CS: Methodology, supervision, validation, writing – original draft, writing – review and editing. EV: Conceptualisation, methodology, supervision, validation, writing – original draft, writing – review and editing. JV: Supervision, validation, writing – original draft, writing – review and editing. JFM: Conceptualisation, methodology, supervision, validation, writing – original draft, writing – review and editing.

Funding

The study was supported by Bristol Myers Squibb.

Patient consent for publication

All participants provided written informed consent prior to participation in the study.

Ethics approval

The study was conducted in accordance with the Declaration of Helsinki, the International Council for Harmonisation of Technical Requirements for Pharmaceuticals for Human Use Guidelines for Good Clinical Practice, and local regulations. The study protocol, consent form, and any other written information given to patients was approved by an institutional review board or independent ethics committee at each study site.

Provenance and peer review

Not commissioned; externally peer reviewed.

Data availability statement

The Bristol Myers Squibb policy on data sharing may be found at https://www.bms.com/researchers-and-partners/independent-research/data-sharing-request-process.html.

Supplementary materials

Supplementary material associated with this article can be found in the online version at doi:10.1016/j.ard.2026.05.029.

Orcid

Désirée van der Heijde: http://orcid.org/0000-0002-5781-158X

Philip J. Mease: http://orcid.org/0000-0002-6620-0457

REFERENCES

[1] Ritchlin CT, Colbert RA, Gladman DD. Psoriatic arthritis. N Engl J Med. 2017;376(10):957–70.
[2] Stober C. Pathogenesis of psoriatic arthritis. Best Pract Res Clin Rheumatol. 2021;35(2):101694.
[3] Coates LC, Helliwell PS. Psoriatic arthritis: state of the art review. Clin Med (Lond). 2017;17(1):65–70.
[4] Lopez-Medina C, Kalyoncu U, Gossec L. Unmet needs in psoriatic arthritis, a narrative review. Arch Rheumatol. 2024;39(2):159–71.
[5] Buch MH, Bhatt DL, Charles-Schoeman C, Giles JT, Mikuls T, Koch GG, et al. Risk of extended major adverse cardiovascular event endpoints with tofacitinib versus TNF inhibitors in patients with rheumatoid arthritis: a post hoc analysis of a phase 3b/4 randomised safety study. RMD Open. 2024;10(2):e003912.
[6] Charles-Schoeman C, Buch MH, Dougados M, Bhatt DL, Giles JT, Ytterberg SR, et al. Risk of major adverse cardiovascular events with tofacitinib versus tumour necrosis factor inhibitors in patients with rheumatoid arthritis with or without a history of atherosclerotic cardiovascular disease: a post hoc analysis from ORAL Surveillance. Ann Rheum Dis. 2023;82(1):119–29.
[7] Gossec L, Kerschbaumer A, Ferreira RJO, Aletaha D, Baraliakos X, Bertheussen H, et al. EULAR recommendations for the management of psoriatic arthritis with pharmacological therapies: 2023 update. Ann Rheum Dis. 2024;83(6):706–19.
[8] Ytterberg SR, Bhatt DL, Mikuls TR, Koch GG, Fleischmann R, Rivas JL, et al. Cardiovascular and cancer risk with tofacitinib in rheumatoid arthritis. N Engl J Med. 2022;386(4):316–26.
[9] Mease PJ, Deodhar AA, van der Heijde D, Behrens F, Kivitz AJ, Neal J, et al. Efficacy and safety of selective TYK2 inhibitor, deucravacitinib, in a phase II trial in psoriatic arthritis. Ann Rheum Dis. 2022;81(6):815–22.
[10] SOTYKTU (deucravacitinib) package insert [Internet]. Princeton, NJ: Bristol-Myers Squibb Company; March 2026. [cited 2026 June 12]. Available from: https://www.accessdata.fda.gov/drugsatfda_docs/label/2026/214958s002lbl.pdf.
[11] SOTYKTU (deucravacitinib) summary of product characteristics [Internet]. Dublin, Ireland: Bristol-Myers Squibb Pharma EEIG; June 2026. [cited 2026 June 12]. Available from: https://www.ema.europa.eu/en/documents/product-information/sotyktu-epar-product-information_en.pdf.
[12] Armstrong AW, Warren RB, Strober B, Blauvelt A, Tada Y, Passeron T, et al. Deucravacitinib in moderate to severe plaque psoriasis: 5-year, long-term safety and efficacy results from the phase 3 POETYK PSO-1, PSO-2, and LTE trials. J of Skin. 2025;9(2):s532.
[13] Burke JR, Cheng L, Gillooly KM, Strnad J, Zupa-Fernandez A, Catlett IM, et al. Autoimmune pathways in mice and humans are blocked by pharmacological stabilization of the TYK2 pseudokinase domain. Sci Transl Med. 2019;11(502):eaaw1736.
[14] Wrobleski ST, Moslin R, Lin S, Zhang Y, Spergel S, Kempson J, et al. Highly selective inhibition of tyrosine kinase 2 (TYK2) for the treatment of autoimmune diseases: discovery of the allosteric inhibitor BMS-986165. J Med Chem. 2019;62(20):8973–95.
[15] Dmitrienko A, Tamhane AC. Gatekeeping procedures with clinical trial applications. Pharm Stat 2007;6(3):171–80.
[16] van der Heijde D, Mease PJ, Paul C, Behrens F, Gossec L, Kaneko Y, et al. Efficacy and safety of deucravacitinib up to week 52: a multicenter, randomized, double-blind, placebo-controlled, phase 3 study in patients with active psoriatic arthritis who are naive to biologic disease-modifying antirheumatic drugs [abstract]. Arthritis Rheumatol. 2025;77(suppl 9):LB20.
[17] Mease PJ, Chandran V, Armstrong AW, Blanco R, Ogdie A, Siegel EL, et al. Deucravacitinib in active psoriatic arthritis: efficacy and safety up to 52 weeks from the randomized, double-blind, phase 3 POETYK PsA-2 trial. Arthritis Rheumatol. 2026. Epub ahead of print. doi: 10.1002/art.70280.
[18] Pignon C, Bibas N, Lopez-Medina C, Fautrel B, Gossec L. Clinical enthesitis in patient with psoriatic arthritis, a systematic literature review with metaanalysis. Joint Bone Spine. 2025;92(2):105807.
[19] McInnes IB, Mease PJ, Kirkham B, Kavanaugh A, Ritchlin CT, Rahman P, et al. Secukinumab, a human anti-interleukin-17A monoclonal antibody, in patients with psoriatic arthritis (FUTURE 2): a randomised, double-blind, placebo-controlled, phase 3 trial. Lancet. 2015;386(9999):1137–46.
[20] Zabotti A, Cabas N, Di Nicola C, Perrotta FM, Guiotto A, Franzolini N, et al. Using ultrasound to define inflammatory and non-inflammatory phenotypes in difficult-to-treat psoriatic arthritis. RMD Open. 2025;11(3):e005785.
[21] Armstrong AW, Augustin M, Beaumont JL, Pham TP, Hudgens S, Gordon KB, et al. Deucravacitinib improves patient-reported outcomes in patients with moderate to severe psoriasis: results from the phase 3 randomized POETYK PSO-1 and PSO-2 trials. Dermatol Ther (Heidelb). 2024;14(8):2235–48.
[22] Armstrong AW, Gooderham M, Warren RB, Papp KA, Strober B, Thaç D, et al. Deucravacitinib versus placebo and apremilast in moderate to severe plaque psoriasis: efficacy and safety results from the 52-week, randomized, double-blinded, placebo-controlled phase 3 POETYK PSO-1 trial. J Am Acad Dermatol. 2023;88(1):29–39.
[23] Armstrong AW, Lebwohl M, Warren RB, Sofen H, Morita A, Paul C, et al. Deucravacitinib in plaque psoriasis: four-year safety and efficacy results from the phase 3 POETYK PSO-1, PSO-2 and long-term extension trials. J Eur Acad Dermatol Venereol. 2025;39(7):1336–51.
[24] Strober B, Thaçi D, Sofen H, Kircik L, Gordon KB, Foley P, et al. Deucravacitinib versus placebo and apremilast in moderate to severe plaque psoriasis: efficacy and safety results from the 52-week, randomized, double-blinded, phase 3 program for evaluation of TYK2 inhibitor psoriasis second trial. J Am Acad Dermatol. 2023;88(1):40–51.
[25] Kivitz A, Baraliakos X, Muensterman ET, Kavanaugh A, van der Heijde D, Klimiuk PA, et al. Highly selective tyrosine kinase 2 inhibition with zasocitinib (TAK-279) improves outcomes in patients with active psoriatic arthritis: a randomised phase 2b study. Ann Rheum Dis. 2025;84(10):1660–74.
[26] Eder L, Mylvaganam S, Pardo Pardo J, Petkovic J, Strand V, Mease P, et al. Sex-related differences in patient characteristics, and efficacy and safety of advanced therapies in randomised clinical trials in psoriatic arthritis: a systematic literature review and meta-analysis. Lancet Rheumatol. 2023;5(12):e716–27.
[27] Mease PJ, Ritchlin CT, Coates LC, Kollmeier AP, Zhou B, Jiang Y, et al. Inhibition of structural damage progression with the selective interleukin-23 inhibitor guselkumab in participants with active PsA: results through week 24 of the phase 3b, randomised, double-blind, placebo-controlled APEX study. Ann Rheum Dis. 2025;84(12):1983–94.
[28] Mease P, van der Heijde D, Landewé R, Mpofu S, Rahman P, Tahir H, et al. Secukinumab improves active psoriatic arthritis symptoms and inhibits

radiographic progression: primary results from the randomised, double-blind, phase III FUTURE 5 study. Ann Rheum Dis. 2018;77(6):890–7.
[29] Coates LC, Mease PJ, Gladman DD, Navarra S, Bao W, Gaillez C. Secukinumab improves physical function and quality of life and inhibits structural damage in patients with PsA with sustained remission or low disease activity: results from the 2-year phase 3 FUTURE 5 study. RMD Open. 2023;9(2):e002939.
[30] van der Heijde D, Kartman CE, Xie L, Beattie S, Schlichting D, Mo D, et al. Radiographic progression of structural joint damage over 5 years of baricitinib treatment in patients with rheumatoid arthritis: results from RA-BEYOND. J Rheumatol 2022;49(2):133–41.
[31] Gratacós-Masmitja J, Beltrán Catalán E, Álvarez Vega JL, Urruticoechea-Arana A, Fito C, Maceiras F, et al. Real-world apremilast use in biologic-naïve psoriatic arthritis patients. Data from Spanish clinical practice. Reumatol Clin (Engl Ed). 2024;20(1):24–31.
[32] Mease PJ, Chandran V, Armstrong AW, Blanco R, Ogdie A, Siegel E, et al. OP0095 Efficacy and safety of deucravacitinib up to week 52 from POETYK PsA-2: a multicenter, randomized, double-blind, placebo-controlled, phase 3 study in patients with psoriatic arthritis. Ann Rheum Dis. 2025;84(suppl 1):84–5.
[33] Morand E, Pike M, Merrill JT, van Vollenhoven R, Werth VP, Hobar C, et al. Deucravacitinib, a tyrosine kinase 2 inhibitor, in systemic lupus erythematosus: a phase II, randomized, double-blind, placebo-controlled trial. Arthritis Rheumatol. 2023;75(2):242–52.
[34] McInnes IB, Anderson JK, Magrey M, Merola JF, Liu Y, Kishimoto M, et al. Trial of upadacitinib and adalimumab for psoriatic arthritis. N Engl J Med. 2021;384(13):1227–39.
[35] Mease PJ, Lertratanakul A, Anderson JK, Papp K, Van den Bosch F, Tsuji S, et al. Upadacitinib for psoriatic arthritis refractory to biologics: SELECT-PsA 2. Ann Rheum Dis. 2021;80(3):312–20.
[36] Gladman D, Rigby W, Azevedo VF, Behrens F, Blanco R, Kaszuba A, et al. Tofacitinib for psoriatic arthritis in patients with an inadequate response to TNF inhibitors. N Engl J Med. 2017;377(16):1525–36.
[37] Mease P, Hall S, FitzGerald O, van der Heijde D, Merola JF, Avila-Zapata F, et al. Tofacitinib or adalimumab versus placebo for psoriatic arthritis. N Engl J Med. 2017;377(16):1537–50.

Ann Rheum Dis 85 (2026) 1743–1750

Contents lists available at ScienceDirect

Annals of the Rheumatic Diseases

journal homepage: https://www.sciencedirect.com/journal/annals-of-the-rheumatic-diseases

Axial spondyloarthritis

Comparison of the established ASAS definition and preliminary proposed data-driven cut-offs for inflammatory and structural MRI lesions in the sacroiliac joints for eligibility of patients with nonradiographic axial spondyloarthritis in clinical trials

Xenofon Baraliakos[1,*], Victoria Navarro-Compán[2], Sofia Ramiro[3,4], Hagen Russ[5], Marcus Ngantcha[5], Khai J. Ng[5], Mohamed Sheesh[5], Rebecca J. Bolce[5], Pedro M. Machado[6,7,8], Denis Poddubnyy[9,10]

[1] *Rheumazentrum Ruhrgebiet Herne, Ruhr University Bochum, Herne, Germany*
[2] *Rheumatology Department, La Paz University Hospital, IdiPaz, Madrid, Spain*
[3] *Rheumatology, Leiden University Medical Center, Leiden, The Netherlands*
[4] *Rheumatology, Zuyderland Medical Center, Heerlen, The Netherlands*
[5] *Eli Lilly and Company, Indianapolis, IN, USA*
[6] *Department of Neuromuscular Diseases, University College London, London, UK*
[7] *NIHR University College London Hospitals Biomedical Research Centre, University College London Hospitals (UCLH) NHS Foundation Trust, London, UK*
[8] *Department of Rheumatology, Northwick Park Hospital, London North West University Healthcare NHS Trust, London, UK*
[9] *Division of Rheumatology, University of Toronto and Schroeder Arthritis Institute, University Health Network, Toronto, ON, Canada*
[10] *Gastroenterology, Infectious Diseases and Rheumatology (including Nutrition Medicine), Charité Universitaetsmedizin Berlin, Berlin, Germany*

ARTICLE INFO

Article history:
Received 20 December 2025
Received in revised form 30 May 2026
Accepted 1 June 2026

ABSTRACT

Objectives: The purpose of this paper is to evaluate patient characteristics and treatment outcomes in patients with nonradiographic axial spondyloarthritis (nr-axSpA) eligible for a clinical trial based on the 2009 established Assessment of SpondyloArthritis International Society (ASAS) magnetic resonance imaging (MRI)-sacroiliac joint (SIJ) definition for sacroiliitis (established definition [ED]) in comparison to the 2021 preliminary proposed data-driven definitions (proposed definitions [PD]) for inflammatory and structural lesions on MRI-SIJ.

Methods: COAST-X is a phase 3, multicentre, randomised, double-blind, placebo-controlled nr-axSpA study on ixekizumab (IXE) or placebo up to 52 weeks. In this post hoc analysis, baseline MRI-SIJ scans of IXE and placebo arms were independently categorised using the ED (bone marrow oedema [BME]) and PD (PD-BME; PD-erosion/fat lesions [FAT]/deep FAT; PD Total) cut-

*Corresponding author: Dr. Xenofon Baraliakos, Rheumazentrum Ruhrgebiet Herne, Ruhr University Bochum, Herne, Germany.
E-mail address: baraliakos@me.com (X. Baraliakos).

Part of this manuscript was presented as an abstract and poster at the International Congress on Spondyloarthritides (ICS) 2024 and as an abstract at the American College of Rheumatology (ACR) 2024.

Handling editor Josef Smolen.

https://doi.org/10.1016/j.ard.2026.06.001

0003-4967/© 2026 The Author(s). Published by Elsevier B.V. on behalf of European Alliance of Associations for Rheumatology (EULAR). This is an open access article under the CC BY license (http://creativecommons.org/licenses/by/4.0/)

offs for MRI-SIJ lesions into groups fulfilling ED, PD, ED but not PD, and vice versa. Patient demographics, baseline characteristics, and clinical outcomes at week 16, including ASAS40 and Bath Ankylosing Spondylitis Disease Activity Index 50% improvement (BASDAI50) response, mean BASDAI change from baseline, Axial Spondyloarthritis Disease Activity Score (ASDAS) clinically important improvement, and attainment of different ASDAS disease states, were reported descriptively for each definition.

Results: Patient demographics and baseline disease characteristics were balanced between all ED or PD MRI-SIJ+ cut-off subgroups. Within each treatment arm, the respective clinical outcomes showed similar results across all ED or PD MRI-SIJ+ cut-off subgroups, whereas outcomes in subgroups fulfilling ED but not PD and vice versa were slightly lower compared with ED or PD MRI-SIJ+ cut-off subgroups.

Conclusions: Patients fulfilling ED or PD of a positive MRI-SIJ showed similar baseline characteristics and clinical outcomes at week 16. In this analysis, PD did not outperform ED in the identification of patients for a clinical trial in nr-axSpA.

INTRODUCTION

Axial spondyloarthritis (axSpA) is a chronic inflammatory disease that affects the axial skeleton [1]. Depending upon the presence or absence of radiographic evidence of structural changes in the sacroiliac joints (SIJs), axSpA is classified into radiographic axSpA (r-axSpA) and nonradiographic axSpA (nr-axSpA) [2]. According to the Assessment of SpondyloArthritis international Society (ASAS), r-axSpA is characterised by definite radiographic structural damage in the SIJ, fulfilling the modified New York criteria [3], which may be observed years after symptom onset [1], whereas patients who exhibit symptoms indicative of axSpA but have not yet shown definite radiographic evidence of sacroiliitis are designated as nr-axSpA [4].

WHAT IS ALREADY KNOWN ON THIS TOPIC

- The presence of bone marrow oedema/osteitis is a key feature in the Assessment of SpondyloArthritis international Society (ASAS) classification criteria for axial spondyloarthritis (axSpA). The 2009 established ASAS definition of a magnetic resonance imaging (MRI)-positive sacroiliac joint (SIJ) for classification to axSpA (established definition [ED]) includes qualitative and quantitative components.
- In 2021, the ASAS MRI working group preliminarily proposed data-driven definitions (proposed definitions [PD]) for active/inflammatory and structural MRI lesions in the SIJ in axSpA.

WHAT THIS STUDY ADDS

- In this post hoc analysis, we compared the baseline characteristics and treatment outcomes of patients with nonradiographic axSpA who were eligible for the COAST-X study of ixekizumab based on the ED with the PD.
- Baseline characteristics and clinical outcomes at week 16 were similar, independent of which definition (ED or PD) and which lesion type (inflammatory or structural) were applied.
- The results of our analysis indicate that the PD did not outperform the ED in the correct identification of patients for a clinical trial in nonradiographic axSpA.

HOW THIS STUDY MIGHT AFFECT RESEARCH, PRACTICE, OR POLICY

- These findings may serve as an important basis for decisions on defining positive MRI-SIJ criteria for axSpA that may attempt to take not only the inflammatory but also the structural lesions into account.

According to the ASAS 2009 axSpA classification criteria, a patient can be classified as having axSpA by the presence of sacroiliitis confirmed by either radiography or by magnetic resonance imaging (MRI) along with at least 1 spondyloarthritis (SpA) feature (imaging arm) or by the presence of human leukocyte antigen B27 (HLA-B27) plus at least 2 SpA features (clinical arm) after satisfying the entry criteria of having chronic back pain for at least 3 months and being under 45 years old at the age of onset [4,5].

The clear presence of bone marrow oedema (BME)/osteitis is considered essential for defining active/inflammatory sacroiliitis on MRI and is one of the key features in the ASAS classification criteria for axSpA [4]. The definition of an MRI-positive (MRI+) SIJ for classification to axSpA includes a qualitative component (BME highly suggestive of axSpA) and a quantitative component (1 BME lesion on at least 2 consecutive MRI slices or more than 1 BME lesion on a single slice). In 2016, the 2009 ASAS definition of active sacroiliitis in an MRI used for fulfilment of the ASAS classification criteria was reviewed by the ASAS MRI working group. The group concluded that the definition of a positive MRI for active sacroiliitis should continue to primarily rely on the clear presence of BME on MRI and the importance of MRI findings should always be determined in the clinical context [6].

However, concerns remained about insufficient specificity of the quantitative component of the 2009 ASAS MRI-SIJ definition for active sacroiliitis as it was reported that false-positive BME lesions meeting the ASAS definition may be observed in 20% to 40% of healthy individuals as well as those with nonspecific back pain disorders [7–9].

In 2021, the ASAS MRI working group preliminarily proposed data-driven definitions for inflammatory and structural MRI lesions in the SIJs and assessed their predictive utility for a rheumatologist's clinical diagnosis of axSpA for application in disease classification and clinical research [10].

Although it was suggested that applying these more stringent quantitative MRI-SIJ lesion cut-offs could contribute to higher specificity for axSpA classification without substantial decrease in sensitivity, their validation in other cohorts and their implications for clinical outcomes have yet not been performed [10]. Such validation is especially important in populations with patients in the nonradiographic stage of axSpA, where misclassification due to false positively evaluated BME could lead to unnecessary study inclusion, overtreatment of patients, and dilution of clinical outcomes.

Therefore, in this post hoc analysis, we compared the baseline characteristics and treatment outcomes of patients with nr-

axSpA who were eligible for a clinical trial based on the 2009 established ASAS MRI-SIJ definition for active sacroiliitis with the 2021 preliminary proposed cut-offs for inflammatory and structural MRI-SIJ lesions using data from the COAST-X study of ixekizumab (IXE), a high-affinity monoclonal antibody selectively targeting interleukin-17A that has demonstrated efficacy in treating both r-axSpA and nr-axSpA [11–13].

METHODS

Study design

COAST-X (NCT02757352) was a 52-week, multicentre, randomised, parallel-group, double-blind, placebo (PBO)-controlled, phase 3 study in adult patients (aged ≥18 years) with active nr-axSpA and objective signs of inflammation evidenced by sacroiliitis on MRI using the established ASAS MRI-SIJ definition and/or elevated C-reactive protein (CRP >5 mg/L), total back pain score of ≥4 (0-10 scale), a Bath Ankylosing Spondylitis Disease Activity Index (BASDAI) score of ≥4, and an inadequate response or intolerance to 2 or more nonsteroidal anti-inflammatory drugs. Patients were randomly assigned (1:1:1) to receive subcutaneous 80 mg IXE every 2 weeks or every 4 weeks or PBO [11].

MRI scans of the SIJ were performed at the screening visit (as baseline), week 16, and week 52. The SIJ MRI was performed using an oblique coronal and oblique axial plane in the short tau inversion recovery and T1-weighted sequences [14] with a field strength of 1.5 or 3 Tesla. The MRI scans were available in digital format.

This post hoc analysis includes baseline MRI-SIJ scans from the per-protocol set 16 (PPS-16) population (ie, patients who completed the COAST-X study without any protocol deviation during weeks 0-16) and uses complete cases of Spondyloarthritis Research Consortium of Canada (SPARCC) MRI-SIJ structural scores to categorise patients as MRI+. The PPS-16 population was selected to ensure that the patients included were the most compliant.

The established ASAS MRI-SIJ definition for active sacroiliitis, here referred to as 'established definition (ED)', was defined as BME highly suggestive of axSpA and either ≥2 BME lesions on a single slice or 1 BME lesion on ≥2 consecutive MRI slices (Table 1, ED-BME). According to the 2021 preliminary proposed data-driven cut-offs for active/inflammatory and structural MRI-SIJ lesions, here referred to as 'preliminary proposed definitions (PD)', cut-offs that best reflect a positive MRI for definite inflammatory lesions typical of axSpA were defined as the presence of BME in either ≥4 SIJ quadrants at any location or at the same location on ≥3 consecutive slices (Table 1, PD-BME). As the optimal cut-offs for a positive MRI of definite structural lesions typical of axSpA, any one of ≥3 SIJ quadrants with erosion (ERO) at any location or at the same location on ≥2 consecutive slices or ≥5 SIJ quadrants with fat lesions (FAT) at any location or at the same location on ≥3 consecutive slices or the presence of a deep (ie, >1-cm depth) FAT at any location were determined (Table 1, PD-ERO/FAT/deep FAT) [10]. The PD Total group (PD Total) comprises patients with an MRI-SIJ fulfilling the cut-offs for any inflammatory (PD-BME) or structural (PD-ERO or FAT or deep FAT) lesions.

We compared baseline characteristics and clinical outcomes at week 16 for ED-BME and each of the 3 groups included in the definition for the PD, such as the definition of BME (PD-BME), the definition of structural lesions, such as erosions (PD-ERO), (PD-FAT), deep FAT, and total score (PD Total) between the IXE (every 2 weeks and every 4 weeks combined) group and the PBO group. We also assessed the baseline characteristics and clinical outcomes at week 16 for patients categorised as ED-BME MRI+ but PD MRI− and vice versa, both for inflammatory and/or structural SIJ lesions.

Clinical outcomes included ASAS ≥40% improvement (ASAS40 response), Bath Ankylosing Spondylitis Disease Activity Index 50% improvement (BASDAI50 response), mean BASDAI change from baseline, Axial Spondyloarthritis Disease Activity Score (ASDAS) clinically important improvement (CII; improvement ≥1.1), and ASDAS disease states.

Statistical analysis

For the descriptive post hoc analysis reported here, the IXE (every 2 weeks and every 4 weeks combined) group and PBO group were evaluated separately. We report continuous variables as averages along with their standard deviations to accurately reflect variability in the measurements. Categorical variables are presented as counts accompanied by their respective percentages for a clear representation of distribution. To assess clinical outcome improvements at week 16, we measured changes from baseline. For categorical clinical assessments, missing data were imputed using the nonresponder imputation; for continuous outcomes, missing data were imputed using the modified baseline observation carried forward, ie, for patients who discontinued study drug due to an adverse event, the baseline observation was carried forward and for patients who discontinued study drug for any other reason, the last nonmissing observation was used.

Table 1

2009 established ASAS definition of a positive MRI-SIJ lesion (ED) and 2021 preliminary proposed data-driven definitions of a positive MRI-SIJ lesion (PD)

Established ASAS definition of a positive MRI-SIJ lesion (ED)	Preliminary proposed data-driven definitions of a positive MRI-SIJ lesion (PD)
Active (inflammatory) lesion highly suggestive of axSpA: BME is present in either of the following: • ≥2 SIJ quadrants at any location or • at the same location on ≥2 consecutive slices	Cut-offs for definite active (inflammatory) lesions typical of axSpA were BME in either of the following: • ≥4 SIJ quadrants at any location or • at the same location on ≥3 consecutive slices Cut-offs for definite structural lesions were any 1 of the following: • ≥3 SIJ quadrants with erosion (ERO) at any location or • erosion (ERO) at the same location on ≥2 consecutive slices or • ≥5 SIJ quadrants with fat lesions (FAT) at any location or • fat lesions (FAT) at the same location on ≥3 consecutive slices or • presence of a deep (ie, >1-cm depth) fat lesion (deep FAT) at any location

ASAS, Assessment of SpondyloArthritis international Society; axSpA, axial spondyloarthritis; BME, bone marrow oedema; ED, established ASAS positive MRI definition; ERO, erosion; FAT, fat lesions; MRI, magnetic resonance imaging; PD, preliminary proposed data-driven definition for positive MRI; SIJ, sacroiliac joint.

Patient and public involvement

Patients and/or the public were not involved in the conduct, reporting, or dissemination plans of this research.

RESULTS

Patient distribution, demographics, and disease characteristics at baseline

Of 303 patients enrolled on COAST-X, 269 patients were in the PPS-16 population, and baseline MRI data were available for 263, of whom 173 of 263 (65.8%) were in the combined IXE arm and 90 of 263 (34.2%) were in the PBO arm. In particular, 102 of 173 (59.0%) patients with IXE and 63 of 90 (70.0%) patients with PBO were classified as MRI+ according to the ED-BME. In comparison, 89 of 173 (51.4%) patients with IXE and 49 of 90 (54.4%) patients with PBO were MRI+ applying the PD-BME definition. In addition, 44 of 173 (25.4%) patients with IXE and 23 of 90 (25.6%) patients with PBO were classified as MRI+ using the cut-offs for structural lesions according to the preliminary PD (PD-ERO or FAT or deep FAT). A total of 133 of 173 (76.9%) patients with IXE and 72 of 90 (80.0%) patients with PBO were classified as MRI+ using the cut-offs that define a positive MRI according to the PD Total definition. The distribution of patients categorised as ED-BME MRI+ but PD MRI- and vice versa, both for inflammatory and/or structural SIJ lesions, was also evaluated (Tables 2 and 3).

Patient demographics and baseline disease characteristics were generally balanced between all MRI+ subgroups, except for the proportion of female patients, HLA-B27-positive patients, and patients with ASDAS very high disease activity, which were higher in the PD-ERO/FAT/deep FAT MRI+ and ED-BME MRI-/PD-ERO/FAT MRI+ subgroups, whereas the CRP levels were lower in the ED-BME MRI+/PD MRI- subgroups compared with the other subgroups (Tables 2 and 3).

Clinical outcomes

At week 16, patients treated with IXE had substantially higher ASAS40 and BASDAI50 response rates, larger mean BASDAI change from baseline, and higher proportions of patients who achieved ASDAS CII as well as ASDAS inactive disease and low disease activity compared with PBO in each subgroup when applying the ED-BME definition and the PD for inflammatory and/or structural MRI-SIJ lesions. Within each treatment arm (IXE and PBO, respectively), the respective clinical outcomes showed similar results across the ED and PD MRI-SIJ+ cut-off subgroups, whereas clinical outcomes in patients categorised as ED-BME MRI+ but PD MRI− for inflammatory (PD-BME MRI−) and/or structural (PD-ERO/FAT MRI−, PD Total MRI−) SIJ lesions and vice versa were slightly lower compared with the ED and PD MRI-SIJ+ cut-off subgroups. However, this is based on low patient numbers (Table 4 and Fig 1).

DISCUSSION

To our knowledge, this is the first analysis to compare the 2021 preliminary proposed data-driven definitions for the combination of inflammatory and structural MRI-SIJ lesions with the 2009 established ASAS definition for a positive MRI-SIJ and their effect on clinical outcomes.

Although the established ASAS MRI definition is based on the presence of BME lesions only, identification of these positive

Table 2

Demographics and baseline disease characteristics of patients in the ixekizumab arm categorised by applying the established ASAS MRI-SIJ definition for active sacroiliitis (ED) and the 2021 preliminary proposed cut-offs for inflammatory and structural MRI-SIJ lesions (PD)

Total, N = 173	ED-BME MRI+	PD-BME MRI+	PD-ERO or FAT or deep FAT MRI+	PD Total MRI+	ED-BME MRI +/PD-BME MRI-	ED-BME MRI-/PD-BME MRI+	ED-BME MRI +/PD-ERO/FAT MRI-	ED-BME MRI-/PD-ERO/FAT MRI+	ED-BME MRI+/PD Total MRI-	ED-BME MRI-/PD Total MRI+
n (%)	102 (59.0)	89 (51.4)	44 (25.4)	133 (76.9)	13 (7.5)	0	19 (11.0)	37 (21.4)	6 (3.5)	37 (21.4)
Age, y, mean (SD)	40.8 (13.2)	40.3 (13.2)	39.9 (13.7)	40.2 (13.3)	44.1 (12.7)		48.6 (13.0)	40.0 (14.4)	49.3 (14.5)	40.0 (14.4)
Female, n (%)	36 (35.3)	30 (33.7)	27 (61.4)	57 (42.9)	6 (46.2)		5 (26.3)	25 (67.6)	4 (66.7)	25 (67.6)
Symptom duration, y, mean (SD)	11.2 (9.7)	11.4 (10.0)	10.8 (10.2)	11.2 (10.0)	9.3 (7.1)		14.6 (11.4)	11.6 (10.9)	12.4 (8.9)	11.6 (10.9)
CRP, mg/L, mean (SD)	11.9 (19.3)	12.8 (20.4)	11.3 (13.1)	12.3 (18.3)	6.2 (6.7)		5.5 (7.1)	11.7 (13.9)	3.3 (2.0)	11.7 (13.9)
HLA-B27 positive, n (%)	67 (66.3)	59 (67.0)	34 (77.3)	93 (70.5)	8 (61.5)		8 (42.1)	28 (75.7)	2 (33.3)	28 (75.7)
BASDAI, mean (SD)	7.1 (1.3)	7.1 (1.4)	7.1 (1.3)	7.1 (1.3)	7.2 (1.2)		7.2 (1.1)	7.0 (1.3)	7.2 (1.3)	7.0 (1.3)
ASDAS, mean (SD)	3.8 (0.8)	3.8 (0.8)	3.9 (0.8)	3.8 (0.8)	3.7 (0.5)		3.5 (0.5)	3.9 (0.8)	3.5 (0.4)	3.9 (0.8)
ASDAS disease state, n (%)										
ID or LDA	0	0	0	0	0		0	0	0	0
HDA	41 (40.2)	36 (40.5)	15 (34.1)	51 (38.4)	5 (38.5)		9 (47.4)	13 (35.1)	3 (50.0)	13 (35.1)
vHDA	61 (59.8)	53 (59.6)	29 (65.9)	82 (61.7)	8 (61.5)		10 (52.6)	24 (64.9)	3 (50.0)	24 (64.9)

ASAS, Assessment of SpondyloArthritis International Society; ASDAS, Axial Spondyloarthritis Disease Activity Score; BASDAI, Bath Ankylosing Spondylitis Disease Activity Index; BME, bone marrow oedema; CRP, C-reactive protein; ED, established ASAS positive MRI definition; ERO, erosion; FAT, fat lesion or deep fat lesion; HDA, high disease activity; HLA-B27, human leukocyte antigen B27; ID, inactive disease; LDA, low disease activity; MRI, magnetic resonance imaging; n, number of patients in the specified category; N, number of patients in the analysis population; PD, preliminary proposed data-driven definition for positive MRI; SIJ, sacroiliac joint; vHDA, very high disease activity.

Table 3

Demographics and baseline disease characteristics of patients in the placebo arm categorised by applying the established ASAS MRI-SIJ definition for active sacroiliitis (ED) and the 2021 preliminary proposed cut-offs for inflammatory and structural MRI-SIJ lesions (PD)

Total, N = 90	ED-BME MRI+	PD-BME MRI+	PD-ERO or FAT or deep FAT MRI+	PD Total MRI+	ED-BME MRI +/PD-BME MRI-	ED-BME MRI-/PD-BME MRI+	ED-BME MRI +/PD-ERO/FAT MRI-	ED-BME MRI-/PD-ERO/FAT MRI+	ED-BME MRI+/PD Total MRI-	ED-BME MRI-/PD Total MRI+
n (%)	63 (70.0)	49 (54.4)	23 (25.6)	72 (80.0)	14 (15.6)	0	12 (13.3)	15 (16.7)	6 (6.7)	15 (16.7)
Age, y, mean (SD)	39.7 (13.2)	38.2 (13.3)	40.9 (10.1)	39.1 (12.4)	45.1 (11.7)		40.1 (14.1)	40.1 (8.9)	48.7 (10.2)	40.1 (8.9)
Female, n (%)	36 (57.1)	28 (57.1)	15 (65.2)	43 (59.7)	8 (57.1)		7 (58.3)	10 (66.7)	3 (50.0)	10 (66.7)
Symptom duration, y, mean (SD)	9.3 (7.6)	8.7 (7.6)	10.6 (7.4)	9.3 (7.6)	11.6 (7.4)		9.0 (7.6)	11.2 (7.6)	14.2 (7.3)	11.2 (7.6)
CRP, mg/L, mean (SD)	16.6 (29.8)	17.7 (31.4)	11.8 (19.0)	15.8 (28.0)	12.6 (24.0)		8.8 (15.0)	9.6 (10.1)	8.1 (14.0)	9.6 (10.1)
HLA-B27 positive, n (%)	39 (61.9)	31 (63.3)	19 (82.6)	50 (69.4)	8 (57.1)		6 (50.0)	14 (93.3)	3 (50.0)	14 (93.3)
BASDAI, mean (SD)	7.1 (1.6)	7.1 (1.6)	7.4 (1.4)	7.2 (1.5)	7.1 (1.6)		7.4 (1.7)	7.6 (1.2)	7.2 (1.7)	7.6 (1.2)
ASDAS, mean (SD)	3.8 (1.0)	3.8 (1.0)	3.9 (0.8)	3.8 (1.0)	3.7 (0.9)		3.7 (0.9)	4.0 (0.6)	3.7 (0.9)	4.0 (0.6)
ASDAS disease state, n (%)										
ID or LDA	0	0	0	0	0		0	0	0	0
HDA	28 (44.4)	21 (42.9)	8 (34.8)	29 (40.3)	7 (50.0)		7 (58.3)	4 (26.7)	3 (50.0)	4 (26.7)
vHDA	35 (55.6)	28 (57.1)	15 (65.2)	43 (59.7)	7 (50.0)		5 (41.7)	11 (73.3)	3 (50.0)	11 (73.3)

ASAS, Assessment of SpondyloArthritis international Society; ASDAS, Axial Spondyloarthritis Disease Activity Score; BASDAI, Bath Ankylosing Spondylitis Disease Activity Index; BME, bone marrow oedema; CRP, C-reactive protein; ED, established ASAS positive MRI definition; ERO, erosion; FAT, fat lesion or deep fat lesion; HDA, high disease activity; HLA-B27, human leukocyte antigen B27; ID, inactive disease; LDA, low disease activity; MRI, magnetic resonance imaging; n, number of patients in the specified category; N, number of patients in the analysis population; PD, preliminary proposed data-driven definition for positive MRI; SIJ, sacroiliac joint; vHDA, very high disease activity.

Table 4

Clinical outcomes at week 16 of patients in the IXE and PBO arms categorised by applying the established ASAS MRI-SIJ definition for active sacroiliitis (ED) and the 2021 preliminary proposed cut-offs for inflammatory and structural MRI-SIJ lesions (PD)

	BASDAI50 response n (%)		BASDAI CfB mean (SD)		ASDAS CII n (%)		ASDAS disease state, n (%)							
							ID		LDA		HDA		vHDA	
	IXE	PBO	IXE	PBO	IXE	PBO	IXE	PBO	IXE	PBO	IXE	PBO	IXE	PBO
ED-BME MRI+ (n = 102 IXE, n = 63 PBO)	35 (34.3)	8 (12.7)	−2.5 (2.3)	−1.4 (1.6)	51 (50.0)	16 (25.4)	16 (15.7)	3 (4.8)	17 (16.7)	6 (9.5)	53 (52.0)	29 (46.0)	16 (15.7)	25 (39.7)
PD-BME MRI+(n = 89 IXE, n = 49 PBO)	33 (37.1)	5 (10.2)	−2.6 (2.3)	−1.4 (1.6)	45 (50.6)	12 (24.5)	15 (16.9)	3 (6.1)	14 (15.7)	4 (8.2)	46 (51.7)	22 (45.0)	14 (15.7)	20 (40.8)
PD-ERO or FAT or deep FAT MRI+ (n = 44 IXE, n = 23 PBO)	12 (27.3)	2 (8.7)	−2.1 (2.2)	−1.3 (1.6)	23 (52.3)	4 (17.4)	3 (6.8)	0	11 (25.0)	3 (13.0)	21 (47.7)	9 (39.1)	9 (20.5)	11 (47.8)
PD Total MRI+ (n = 133 IXE, n = 72 PBO)	45 (33.8)	7 (9.7)	−2.5 (2.2)	−1.4 (1.6)	68 (51.1)	16 (22.2)	18 (13.5)	3 (4.2)	25 (18.8)	7 (9.7)	67 (50.4)	31 (43.1)	23 (17.3)	31 (43.1)
ED-BME MRI+/PD-BME MRI-(n = 13 IXE, n = 14 PBO)	2 (15.4)	3 (21.4)	−2.0 (2.7)	−1.2 (2.3)	6 (46.2)	4 (28.6)	1 (7.7)	0	3 (23.1)	2 (14.3)	7 (53.9)	7 (50.0)	2 (15.4)	5 (35.7)
ED-BME MRI-/PD-BME MRI+ (n = 0 IXE, n = 0 PBO)	0	0	0	0	0	0	0	0	0	0	0	0	0	0
ED-BME MRI+/PD-ERO/FAT MRI- (n = 19 IXE, n = 12 PBO)	4 (21.1)	1 (8.3)	−1.9 (2.3)	−1.4 (2.1)	7 (36.8)	3 (25.0)	3 (15.8)	0	3 (15.8)	0	11 (57.9)	7 (58.3)	2 (10.5)	5 (41.7)
ED-BME MRI-/PD-ERO/FAT MRI+ (n = 37 IXE, n = 15 PBO)	11 (29.7)	0	−2.2 (2.2)	−1.4 (1.4)	19 (51.4)	2 (13.3)	3 (8.1)	0	9 (24.3)	1 (6.7)	17 (46.0)	6 (40.0)	8 (21.6)	8 (53.3)
ED-BME MRI+/PD Total MRI- (n = 6 IXE, n = 6 PBO)	1 (16.7)	1 (16.7)	−2.1 (3.4)	−1.1 (2.9)	2 (33.3)	2 (33.3)	1 (16.7)	0	1 (16.7)	0	3 (50.0)	4 (66.7)	1 (16.7)	2 (33.3)
ED-BME MRI-/PD Total MRI+ (n = 37 IXE, n = 15 PBO)	11 (29.7)	0	−2.2 (2.2)	−1.4 (1.4)	19 (51.4)	2 (13.3)	3 (8.1)	0	9 (24.3)	1 (6.7)	17 (46.0)	6 (40.0)	8 (21.6)	8 (53.3)

ASAS, Assessment of SpondyloArthritis international Society; ASDAS, Axial Spondyloarthritis Disease Activity Score; BASDAI50, Bath Ankylosing Spondylitis Disease Activity Index 50% improvement; BME, bone marrow oedema; CfB, change from baseline; CII, clinically important improvement (ie, ASDAS improvement ≥1.1); ED, established ASAS positive MRI definition; ERO, erosion; FAT, fat lesion or deep fat lesion; HDA, high disease activity; ID, inactive disease; IXE, ixekizumab; LDA, low disease activity; MRI, magnetic resonance imaging; n, number of patients in the analysis population; PBO, placebo; PD, preliminary proposed data-driven definition for positive MRI; SIJ, sacroiliac joint; vHDA, very high disease activity.

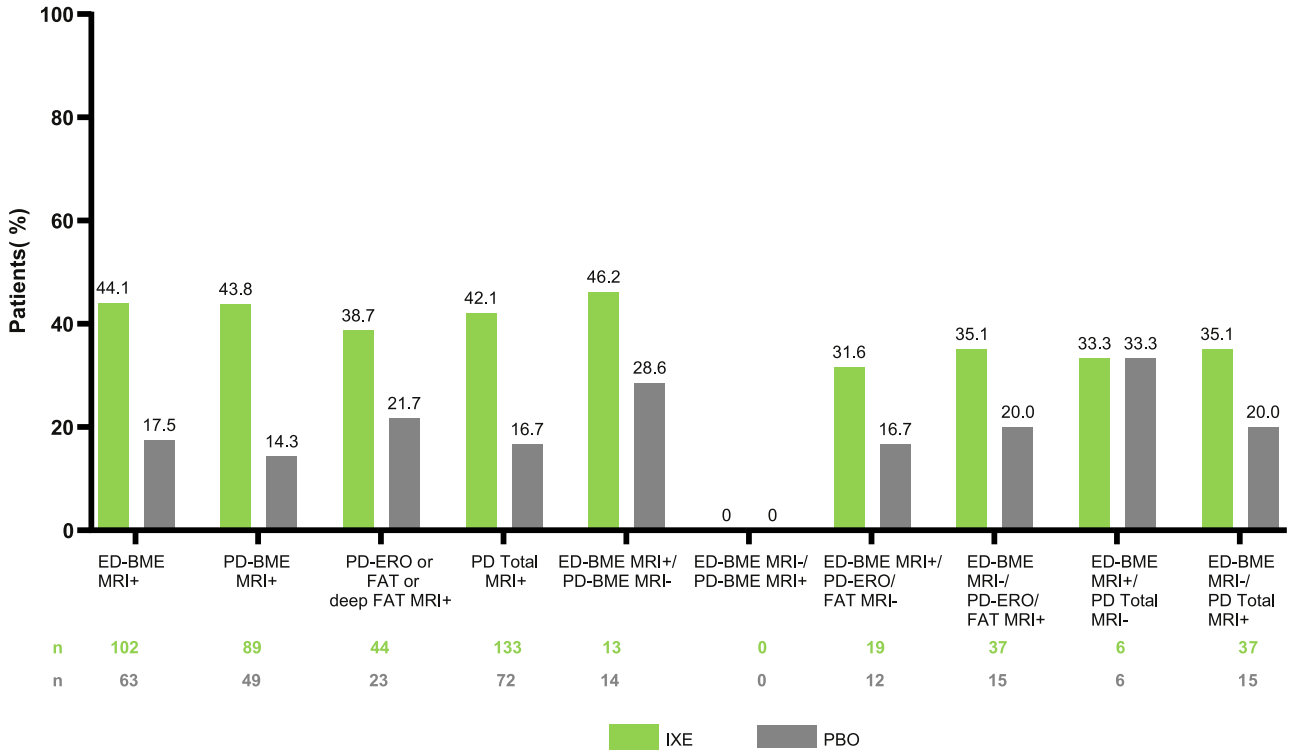

Figure 1. ASAS40 response rates at week 16 in the IXE and PBO arms categorised by applying the established ASAS MRI-SIJ definition for active sacroiliitis (ED) and the 2021 preliminary proposed cut-offs for inflammatory and structural MRI-SIJ lesions (PD). ASAS, Assessment of SpondyloArthritis international Society; ASAS40, ASAS ≥40% improvement; BME, bone marrow oedema; ED, established ASAS positive MRI definition; ERO, erosion; FAT, fat lesion or deep fat lesion; IXE, ixekizumab; MRI, magnetic resonance imaging; n, number of patients in the analysis population; PBO, placebo; PD, preliminary proposed data-driven definition for positive MRI; SIJ, sacroiliac joint.

lesions for 'inflammation' is also made in a qualitative way, thus incorporating (concomitant) structural changes in the interpretation of BME as being axSpA-suggestive or not. In comparison, the preliminary data-driven definitions include not only the qualitative approach for selection of BME lesions but also the detection of structural lesions without considering the presence of BME. Based on the application in the COAST-X population and taking advantage of the possibility of a direct comparison of both definitions, we revealed that both captured patients with largely similar baseline characteristics, with no advantage of 1 definition over the other. Interestingly, these data are in accordance with recently presented information from an independent cohort, reporting higher sensitivity of the ED and higher specificity of the PD (total), as compared to axSpA diagnosis [15].

Within the IXE and PBO groups, respectively, the clinical outcomes analysed at week 16 were similar, independent of which definition (ED or PD) and which lesion type (inflammatory or structural) were used.

Regarding the clinical outcomes in patients categorised by the ED and PD cut-offs for MRI-SIJ positive inflammatory lesions alone, our findings are in accordance with a post hoc analysis of part A of the phase 3 open-label C-OPTIMISE (NCT02505542) study in patients with nr-axSpA and r-axSpA treated with certolizumab pegol that showed similar outcomes, including ASAS40 response and ASDAS disease states as well as mean BASDAI and ASDAS change from baseline to week 48 for both definitions in both r-axSpA and nr-axSpA [16]. Similarly, our analysis identified that most clinical outcomes for the subgroup that is MRI+ according to the ED but MRI− for inflammatory lesions according to the PD were slightly lower than the totality of MRI+ patients, which was also observed in the C-OPTIMISE study. This supports the conclusion that the more stringent cut-offs for MRI-SIJ positive inflammatory lesions from the PD are associated with a slightly higher specificity in patient selection compared with the ED MRI-SIJ definition for active sacroiliitis. However, this was seen in only a small proportion of patients. In addition to the above-mentioned study, our findings revealed that the inclusion of structural changes in the entire PD has only a small gain in the correct identification of patients for a clinical trial in nr-axSpA.

The strengths of this study include the analysis of both inflammatory and structural MRI-SIJ lesions according to the entire preliminary proposed data-driven definitions and their effect on patient selection and treatment outcomes in future clinical studies in nr-axSpA. Furthermore, this analysis was conducted on patients with nr-axSpA only and therefore focuses on the subgroup of patients who are more susceptible to misclassification, which may be leading to less accurate information on treatment outcomes.

As a post hoc analysis, this study was subject to inherent constraints. Other limitations include the low number of patients in some of the MRI-SIJ cut-off subgroups and the short follow-up period of 16 weeks for the interpretation of clinical outcomes based on the different MRI-SIJ definitions. However, we aimed to test the definitions with respect to outcomes in clinical studies, and especially the primary outcomes, which are usually measured after 12 to 16 weeks. Finally, patients in COAST-X were recruited using the ED, which might represent a potential selection bias when excluding patients who might have fulfilled the part of the PD that included the chronic lesions. Nevertheless, we believe that this group of patients is extremely small, since the study included patients in the nonradiographic stage of the disease.

In conclusion, the results of this post hoc analysis indicate that neither the presence of structural lesions alone nor the combination of inflammatory and structural lesions leads to different clinical outcomes compared with the selection of patients based on inflammatory lesions only. The preliminary proposed data-driven definitions for positive MRI-SIJ did not outperform the established ASAS positive MRI-SIJ definition in the correct identification of patients for a clinical trial in nr-axSpA. This information may serve as an important basis for decisions on any revision of positive MRI-SIJ criteria for axSpA that may attempt to take into account not only the inflammatory lesions but also the structural lesions.

Funding

This article was based on the original study COAST-X (NCT02757352). This study and COAST-X were funded by Eli Lilly and Company.

Patient consent for publication

Not applicable.

Ethics approval

Not applicable.

Provenance and peer review

Not commissioned; externally peer reviewed.

Data availability statement

Eli Lilly and Company provides access to all individual participant data collected during the trial, after anonymisation, with the exception of pharmacokinetic or genetic data. Data are available on request. No expiration date for data requests is currently set once data are made available. Access is provided after a proposal has been approved by an independent review committee identified for this purpose and after receipt of a signed data-sharing agreement. Data and documents, including the study protocol, statistical analysis plan, clinical study report, blank or annotated case report forms, will be provided in a secure data-sharing environment. Requests should be submitted online. For details on submitting a request, see the instructions provided at www.vivli.org.

Competing interests

XB received speaking fees from Alfasigma, Amgen, BMS, Cesas, Celltrion, Galapagos, Janssen, Eli Lilly and Company, Moonlake, Novartis, Pfizer, Roche, Sandoz, Springer, Stada, Takeda, UCB, and Zuellig; consulting fees from AbbVie, Alfasigma, Amgen, BMS, Cesas, Celltrion, Galapagos, Janssen, Eli Lilly and Company, Moonlake, Novartis, Pfizer, Roche, Sandoz, Springer, Stada, Takeda, UCB, and Zuellig; and research support from AbbVie, Celltrion, Janssen, and Moonlake; ASAS past president, European Alliance of Associations for Rheumatology (EULAR) president. VN-C received speaking fees from AbbVie, Alfasigma, Fresenius Kabi, Janssen, Eli Lilly and Company, Novartis, Pfizer, and UCB; consulting fees from AbbVie, Alfasigma, Galapagos, Eli Lilly and Company, Novartis, Pfizer, and UCB; and research support from Novartis and ASAS; and is a member of the executive committee and president of ASAS. SR received research grants from AbbVie, Alfasigma, Eli Lilly and Company, MSD, Novartis, Pfizer, and UCB; consultancy fees from AbbVie, Alfasigma, Eli Lilly and Company, Johnson & Johnson, MSD, Novartis, Takeda, and UCB; and is a member of the executive committee of ASAS and of the EULAR Quality of Care Committee. HR, MN, KJN, and MS are employees and shareholders of Eli Lilly and Company. RJB is a shareholder of Eli Lilly and Company and at the time of the study and was an employee of Eli Lilly and Company. PMM received speaking fees from AbbVie, BMS, Celgene, Eli Lilly and Company, Galapagos/Alfasigma, Janssen, MSD, Novartis, Orphazyme, Pfizer, Roche, and UCB; and consulting fees from AbbVie, BMS, Celgene, Eli Lilly and Company, Galapagos/Alfasigma, Greywolf, Janssen, MSD, Novartis, Orphazyme, Pfizer, Roche, and UCB. DP received research support from AbbVie, Bristol Myers Squibb, Eli Lilly and Company, Johnson & Johnson, Novartis, Pfizer, and UCB; consulting fees from AbbVie, Eli Lilly and Company, GlaxoSmithKline, Greywolf Therapeutics, Johnson & Johnson, Merck, Moonlake, Novartis, Pfizer, and UCB; speaker fees from AbbVie, Canon, Celltrion, Eli Lilly and Company, Globemed, Johnson & Johnson, Medscape, Novartis, Peervoice, Pfizer, and UCB; serves as a member of executive committee of ASAS; and a member of steering committee of Group for Research and Assessment of Psoriasis and Psoriatic Arthritis (GRAPPA).

CRediT authorship contribution statement

Xenofon Baraliakos: Writing – review & editing, Supervision, Project administration, Methodology, Investigation, Formal analysis, Data curation, Conceptualization. **Victoria Navarro-Compán:** Writing – review & editing, Methodology, Formal analysis, Conceptualization. **Sofia Ramiro:** Writing – review & editing, Methodology, Formal analysis, Conceptualization. **Hagen Russ:** Writing – review & editing, Writing – original draft, Visualization, Supervision, Project administration, Methodology, Investigation, Formal analysis, Data curation, Conceptualization. **Marcus Ngantcha:** Writing – review & editing, Validation, Methodology, Formal analysis, Data curation. **Khai J. Ng:** Writing – review & editing, Formal analysis. **Mohamed Sheesh:** Writing – review & editing, Formal analysis. **Rebecca J. Bolce:** Writing – review & editing, Methodology, Conceptualization. **Pedro M. Machado:** Writing – review & editing, Formal analysis. **Denis Poddubnyy:** Writing – review & editing, Methodology, Formal analysis, Conceptualization.

Acknowledgements

We would like to thank the investigators of COAST-X for their contributions and the patients who participated in the COAST-X study. We also thank Rishabh Bahl (Eli Lilly and Company), Mizan Md Alam (Eli Lilly and Company), and Gohar Dallakyan (Eli Lilly and Company) for statistical support, and Athulya Krishna (Eli Lilly and Company) for writing support based on the authors' input and direction.

Orcid

Xenofon Baraliakos: http://orcid.org/0000-0002-9475-9362

REFERENCES

[1] Michelena X, López-Medina C, Marzo-Ortega H. Non-radiographic versus radiographic axSpA: what's in a name? Rheumatol (Oxf Engl) 2020;59(Supplement_4):iv18–24.

[2] Dougados M, Sepriano A, Molto A, van Lunteren M, Ramiro S, de Hooge M, et al. Sacroiliac radiographic progression in recent onset axial spondyloarthritis: the 5-year data of the DESIR cohort. Ann Rheum Dis. 2017;76 (11):1823–8.

[3] Van Der Linden S, Valkenburg HA, Cats A. Evaluation of diagnostic criteria for ankylosing spondylitis. A proposal for modification of the New York criteria. Arthritis Rheum. 1984;27(4):361–8.

[4] Rudwaleit M, Van Der Heijde D, Landewé R, Listing J, Akkoc N, Brandt J, et al. The development of Assessment of SpondyloArthritis international Society classification criteria for axial spondyloarthritis (part II): validation and final selection. Ann Rheum Dis. 2009;68(6):777–83.

[5] Robinson PC, Sengupta R, Siebert S. Non-radiographic axial spondyloarthritis (nr-axSpA): advances in classification, imaging and therapy. Rheumatol Ther. 2019;6(2):165–77.

[6] Lambert RGW, Bakker PAC, van der Heijde D, Weber U, Rudwaleit M, Hermann K-G, et al. Defining active sacroiliitis on MRI for classification of axial spondyloarthritis: update by the ASAS MRI working group. Ann Rheum Dis. 2016;75(11):1958–63.

[7] de Winter J, de Hooge M, van de Sande M, de Jong H, van Hoeven L, de Koning A, et al. Magnetic resonance imaging of the sacroiliac joints indicating sacroiliitis according to the Assessment of SpondyloArthritis international Society definition in healthy individuals, runners, and women with postpartum back pain. Arthritis Rheumatol. 2018;70(7):1042–8.

[8] Weber U, Jurik AG, Zejden A, Larsen E, Jørgensen SH, Rufibach K, et al. Frequency and anatomic distribution of magnetic resonance imaging features in the sacroiliac joints of young athletes: exploring "background noise" toward a data-driven definition of sacroiliitis in early spondyloarthritis. Arthritis Rheumatol. 2018;70(5):736–45.

[9] Baraliakos X, Richter A, Feldmann D, Ott A, Buelow R, Schmidt CO, Braun J. Frequency of MRI changes suggestive of axial spondyloarthritis in the axial skeleton in a large population-based cohort of individuals aged< 45 years. Ann Rheum Dis. 2020;79(2):186–92.

[10] Maksymowych WP, Lambert RG, Baraliakos X, Weber U, Machado PM, Pedersen SJ, et al. Data-driven definitions for active and structural MRI lesions in the sacroiliac joint in spondyloarthritis and their predictive utility. Rheumatology (Oxford). 2021;60(10):4778–89.

[11] Deodhar A, van der Heijde D, Gensler LS, Kim T-H, Maksymowych WP, Østergaard M, et al. Ixekizumab for patients with non-radiographic axial spondyloarthritis (COAST-X): a randomised, placebo-controlled trial. Lancet. 2020;395(10217):53–64.

[12] van der Heijde D, Wei JC-C, Dougados M, Mease P, Deodhar A, Maksymowych WP, et al. Ixekizumab, an interleukin-17A antagonist in the treatment of ankylosing spondylitis or radiographic axial spondyloarthritis in patients previously untreated with biological disease-modifying anti-rheumatic drugs (COAST-V): 16 week results of a phase 3 randomised, double-blind, active-controlled and placebo-controlled trial. Lancet. 2018;392(10163):2441–51.

[13] Deodhar A, Poddubnyy D, Pacheco-Tena C, Salvarani C, Lespessailles E, Rahman P, et al. Efficacy and safety of ixekizumab in the treatment of radiographic axial spondyloarthritis: sixteen-week results from a phase III randomized, double-blind, placebo-controlled trial in patients with prior inadequate response to or intolerance of tumor necrosis factor inhibitors. Arthritis Rheumatol. 2019;71(4):599–611.

[14] Sieper J, Rudwaleit M, Baraliakos X, Brandt J, Braun J, Burgos-Vargas R, et al. The Assessment of SpondyloArthritis international Society (ASAS) handbook: a guide to assess spondyloarthritis. Ann Rheum Dis. 2009;68(Supplement 2):ii1–ii44.

[15] De Bruin LJE, Marques M, Van Lunteren M, De Hooge M, Exarchou S, Fagerli KM, et al. POS0503 predictive validity of data-driven definitions for active and structural lesions in the SI joints typical for axial SPA: a 2-year follow-up in the spondyloarthritis caught early cohort. Ann Rheum Dis. 2024;83:903–4.

[16] Baraliakos X, Machado PM, Bauer L, Hoepken B, Kim M, Kumke T, et al. Comparison of established and preliminarily proposed ASAS MRI working group cutoffs for inflammatory MRI lesions in the sacroiliac joints in radiographic and non-radiographic axial spondyloarthritis. RMD Open. 2024;10(3):e003886.

Ann Rheum Dis 85 (2026) 1751–1760

Contents lists available at ScienceDirect

Annals of the Rheumatic Diseases

journal homepage: https://www.sciencedirect.com/journal/annals-of-the-rheumatic-diseases

Systemic lupus erythematosus

Symmetrical dimethylarginine as the central antigenic determinant of anti-Smith autoantibodies in systemic lupus erythematosus

Lars C. van Vliet[1], Annemarie L. Dorjée[1], Martijn van der Heide[1], Annette Grummels[2], Esther van Andel[2], Gerda M. Steup-Beekman[1], Thomas W.J. Huizinga[1], René E.M. Toes[1], Jolien Suurmond[1,*]

[1] *Department of Rheumatology, Leiden University Medical Center, Leiden, The Netherlands*
[2] *Department of Clinical Chemistry and Laboratory Medicine, Leiden University Medical Center, Leiden, The Netherlands*

ARTICLE INFO

Article history:
Received 22 December 2025
Received in revised form 24 April 2026
Accepted 12 June 2026

Handling editor Josef S Smolen

ABSTRACT

Objectives: Systemic lupus erythematosus (SLE) is a chronic autoimmune disease causing multi-organ damage. The most specific autoantibody response in SLE, present in 20% to 30% of patients, targets the Smith (Sm)-protein complex and has been shown to recognise a linear Sm-derived B cell epitope containing a posttranslational modification (PTM) of arginine termed symmetrical dimethyl arginine (sDMA). As autoantibodies to other PTM-modified proteins are often promiscuous, we aimed to determine the specificity and cross-reactivity of anti-Sm antibodies.

Methods: Specificity and promiscuity/cross-reactivity of anti-Sm immunoglobulin G (IgG) were measured using enzyme-linked immunosorbent assay in patients with SLE and healthy donors using peptides containing either sDMA or unmodified arginine. Inhibition and cross-reactivity were determined using competitive enzyme-linked immunosorbent assay and affinity purification. Recognition of endogenous Epstein-Barr nuclear antigen 1 (EBNA1) by anti-Sm IgG was performed using a Western blot of lysates of Epstein-Barr virus-bearing lymphoblastoid cell lines.

Results: The sDMA residue is recognised by patients with anti-Sm+ SLE regardless of the peptide amino acid sequence, with a modest impact of amino acids flanking sDMA on recognition. Most notably, IgGs targeting sDMA comprise the overall majority (~90%) of the anti-Sm antibody repertoire and are highly cross-reactive between $SmD3_{108\text{-}122}$ and several sDMA-containing viral-derived epitopes, including full-length (EBNA1).

Conclusion: Our data implicate that the majority of anti-Sm IgGs target the sDMA residue irrespective of its Sm-context, thus representing a prototypic anti-PTM response. These antibodies are highly promiscuous, recognising several sDMA-modified targets, including naturally occurring viral sDMA-expressing epitopes. These findings suggest a new mechanism by which molecular mimicry of sDMA-modified viral proteins could contribute to a breach of tolerance in patients with anti-Sm+ SLE.

*Correspondence to Dr. Jolien Suurmond, Department of Rheumatology, Leiden University Medical Center, Albinusdreef 2, LUMC - Postzone C1-R 2333 ZA, Leiden, The Netherlands.

E-mail address: j.suurmond@lumc.nl (J. Suurmond).

Handling editor Josef S. Smolen

https://doi.org/10.1016/j.ard.2026.06.012

0003-4967/© 2026 The Author(s). Published by Elsevier B.V. on behalf of European Alliance of Associations for Rheumatology (EULAR). This is an open access article under the CC BY license (http://creativecommons.org/licenses/by/4.0/)

WHAT IS ALREADY KNOWN ON THIS TOPIC

- Symmetrical dimethylarginine (sDMA) residues are present on arginine-glycine-glycine/arginine-glycine repeat regions within the SmD1, SmD3, and SmB/B′ subunits of the Sm protein complex *in vivo*.
- The introduction of sDMA is essential for the recognition of minimal antigenic epitopes spanning amino acids Nos. 95 to 119 on the SmD1 and Nos. 108 to 122 on the SmD3 subunits by a specific subset of anti-Sm autoantibodies.

WHAT THIS STUDY ADDS

- We show that autoantibodies targeting sDMA residues are common in patients with anti-Sm+ SLE s and represent the majority of the anti-Sm autoantibody repertoire.
- We demonstrated that anti-sDMA autoantibodies are highly cross-reactive and can also bind to sDMA residues on other targets, including several virus-derived epitopes, thus representing a prototypic antimodified protein antibody (AMPA) response directed against posttranslationally modified proteins through symmetrical dimethylation of arginine.

HOW THIS STUDY MIGHT AFFECT RESEARCH, PRACTICE, OR POLICY

- The high cross-reactivity of Sm antibodies to various sDMA-containing epitopes, combined with a dominant antigenic specificity, provides mechanistic insight into the potential link between viral infection and tolerance breach in patients with anti-Sm+ SLE.

INTRODUCTION

Systemic lupus erythematosus (SLE) is a chronic systemic autoimmune disease characterised by immune cell dysfunction, leading to widespread inflammation and tissue damage [1]. Autoreactive B cells are central to SLE pathophysiology, a concept further emphasised by the recent successes of anti-CD19 chimeric antigen receptor T cell therapy in achieving clinical remission [2]. Among the antibodies produced by these self-reactive B cells are antinuclear antibodies (ANAs), a heterogeneous group of autoantibodies that recognise different chromatin components (eg, double-stranded DNA [dsDNA] and histones) or RNA-associated proteins (eg, Smith [Sm] and Ro60). Although ANAs can be present in various autoimmune diseases, anti-dsDNA and anti-Sm antibodies are most specific to SLE and have therefore been included among the 2019 European League Against Rheumatism (EULAR)/American College of Rheumatology (ACR) criteria for classification of this disease [1,3].

The Sm protein complex is composed of 8 subunits with molecular weights varying between 9 and 29.5 kDa. It is part of the spliceosome complex, involved in the processing of nuclear premessenger RNA [4]. Using peptide screens, several antigenic epitopes have been characterised on the Sm protein complex, most prominently within the C-terminal domains of SmB/B', SmD1, and SmD3 [5–8]. Intriguingly, these regions are rich in arginine (Arg)-glycine-glycine/Arg-glycine repeats, which mediate RNA binding, and contain Arg that can undergo posttranslational modification (PTM) to form symmetrical dimethylArg (sDMA) residues *in vivo* [9,10]. These modifications appear to have immunological relevance, as subsequent research showed strong recognition of $SmD1_{95\text{-}119}$ and $SmD3_{108\text{-}122}$ peptides, each containing sDMA residues [11,12]. Antibody reactivity to $SmD3_{108\text{-}122}$ correlated with reactivity to components of the Sm protein complex (SmB/B' and SmD), supporting its relevance as a target epitope. Importantly, both studies demonstrated that the introduction of an sDMA residue was essential for recognition by anti-Sm autoantibodies. Nonetheless, the context of surrounding amino acids (AAs) to which anti-Sm autoantibodies bind remains uncertain, as their recognition has thus far been evaluated only in the context of the Sm protein complex.

By comparison, autoantibodies to PTMs, particularly citrullinated, carbamylated, and acetylated epitopes, form a major component of the autoimmune response in rheumatoid arthritis (RA) and are strongly associated with disease development [13]. These PTM-directed autoantibodies, also referred to as antimodified protein antibodies, are often described as 'promiscuous', reflecting their ability to cross-react with multiple citrullinated epitopes [14]. Whether anti-Sm autoantibodies in SLE share this feature and recognise sDMA residues across different epitopes has not been established. To address this gap, we sought to clarify the specificity and cross-reactivity of anti-Sm, focusing on the role of sDMA residues. In the current study, we showed that antibodies targeting sDMA are common in patients with anti-Sm+ SLE and represent the vast majority of the anti-Sm autoantibody repertoire. We further demonstrated that anti-sDMA immunoglobulin G (IgGs) are highly cross-reactive and can also bind to sDMA on multiple other targets, including several virus-derived epitopes, thus representing a prototypical anti-PTM response.

METHODS

Patients and healthy subjects

For the primary cohort, serum was obtained from 24 patients (12 anti-SmD+ and 12 anti-SmD−) with a clinical diagnosis of SLE, and all but 1 fulfilled the 2019 EULAR/ACR classification criteria for SLE, from the Rheumatology outpatient clinic at the Leiden University Medical Centre (LUMC), the Netherlands [3]. The second cohort comprised 40 additional patients with SLE (20 anti-SmD+ and 20 anti-SmD−), all meeting the 2019 EULAR/ACR classification criteria for SLE, obtained from the neuropsychiatric (NP-) SLE biobank at the LUMC [3,15]. It is important to note that only approximately one-third of the patients with SLE in this cohort were diagnosed with NP-SLE. Information regarding patient characteristics can be found in Supplementary Tables S1 and S2. No information on ethnicity was available in the primary cohort. Anti-Sm(D) positivity was established through routine clinical diagnostics by the Clinical Chemistry and Laboratory Medicine department at the LUMC. Most samples were analysed using fluorescence enzyme immunoassay using the EliA SmD^p assay (Thermo Scientific), while 3 older samples from the secondary cohort were analysed using enzyme-linked immunosorbent assay (ELISA) using native purified Sm (Inova Diagnostics). Positive results were subsequently confirmed using an in-house anti-Sm protein ELISA as described below. Clinical and routine laboratory data were collected within 1 week of serum collection for both cohorts. None of the patients with SLE in the primary cohort had been treated with belimumab or rituximab in the 12 months preceding serum collection. ANA staining was performed on HEp-2000 cells using a standardised indirect immunofluorescence assay using 10 μg/mL isolated antibody or diluted serum (1:80), further detailed in the Supplementary Methods.

The study with the primary cohort was approved by the Leiden, Den Haag, and Delft medical ethics committee, while the study with the secondary cohort was approved by the LUMC Biobank committee. Serum from 32 healthy donors (HDs) was obtained from the LUMC Voluntary Donor Service, with approval from the LUMC Biobank committee. All subjects have given written informed consent.

Peptide synthesis and integrity identification

Biotinylated peptides were synthesised by the Peptide and Tetramer Facility, Immunology, at the LUMC, as previously described [16] (detailed sequences in Supplementary Table S3). Briefly, peptides were synthesised using standard solid-phase 9-fluorenylmethoxycarbonyl chemistry on an automated peptide synthesiser. After chain assembly, peptides were cleaved from the resin with trifluoroacetic acid, purified using reverse-phase high-performance liquid chromatography, and lyophilised. Peptide cyclisation was performed via thioether bond formation in a 20 mM Tris-HCl buffer (pH ~8.0). Lyophilised peptides were added slowly to 10 mL of buffer and incubated at room temperature (RT) for 3 hours, and cyclisation was monitored using analytical reverse-phase ultraperformance liquid chromatography. The mixture was acidified with 90% acetic acid and purified on a Biotage Selekt system using a Sfär C18 Duo 100 Å, 30 µm, 6 g column (Biotage, FSUD-0401-0006). The integrity of the synthesised peptides after purification was assessed using ultraperformance liquid chromatography using an Acquity system (Waters), and the exact masses were determined using mass spectrometry on a Microflex instrument (Bruker) and compared with the calculated values.

Among the peptides synthesised, several sequences were derived from viral proteins. For both Epstein-Barr virus (EBV)-derived peptides, the Arg selected for modification is located within an Arg-glycine repeat region in which sDMA modifications have been reported [17–18]. However, as the exact modified residues have not been definitively identified, 1 Arg within this repeat was selected for modification. For the other viral peptides, the exact positions of the modified Arg residues have been described and were synthesised accordingly [19,20].

ELISAs

Standard capacity 384-well streptavidin microplates (Microcoat, 604500) were coated with 1 μg/mL of the respective peptide in phosphate-buffered saline (PBS; pH~7.6) with 0.1% bovine serum albumin (BSA) for 1 hour at 37°C. Plates were washed and incubated with sera (diluted 1:200) in PBS + BSA + Tween 80 (PBS/1% BSA/50 mM Tris/0.05% Tween-20, pH~8.0), for 1 hour at 37°C. All washing steps were performed by washing 4x with 0.05% Tween-20 (Sigma-Aldrich, P1379) in PBS. After incubation, the plates were washed and incubated with 1 μg/mL anti-IgG horse-radish peroxidase (Bethyl; A80-104P).

IgGs against specific nuclear antigens were determined using the protocol described above, with some adjustments. Clear flat-bottom 384-well microplates (Corning, 3640) were coated overnight at 4°C with either 0.8 µg/mL native purified bovine Sm complex (Diarect, A175), 1 µg/mL salmon sperm dsDNA (Invitrogen, 15632011), 0.5 µg/mL native purified bovine histones (Diarect, A311), 0.5 µg/mL recombinant U1-snRNP 68/70 kDa (Diarect, A130), or 0.5 µg/mL recombinant Ro60/SS-A (Diarect, A174). The purified Sm extract used in this study primarily contains proteins corresponding to the expected size of the components of the Sm protein complex (SmE/F/G: ~10 kDa, SmD1/D2/D3: ~16 to 18 kDa, and SmB/B': ~29 kDa) (Supplementary Fig S1). Prior to serum incubation, plates were blocked with PBT (PBS/1% BSA/50 mM Tris, pH~8.0) for 1 hour. All procedures were conducted at RT. In-house ELISAs for specific ANAs were previously developed and validated [21].

All ELISAs were developed using 2,2′-azino-bis(3-ethylbenzothiazoline-6-sulfonic acid) (ABTS; Sigma-Aldrich, A1888) and H_2O_2 (Merck, 1072100250) and measured on an iMark Microplate Absorbance Reader (BioRad). Samples were assessed with technical duplicates. Further methodological details are provided in the Supplementary Methods.

Statistical analysis

Statistical tests were performed in GraphPad Prism version 10.1.0. Paired comparisons were calculated using the Wilcoxon signed-rank test, and comparisons across multiple groups using a Friedman test were corrected for multiple testing using the Bonferroni-Dunn method. P values < .05 were considered statistically significant.

Patient and public involvement

Patient feedback was obtained on the study design. Patients and/or the public were not involved in the conduct, reporting, or dissemination plans of this research.

RESULTS

sDMA is an essential constituent of the antigen recognised by anti-Sm antibodies, irrespective of the flanking regions

To validate the requirement of an sDMA residue for recognition of the $SmD3_{108\text{-}122}$ epitope by patients with anti-Sm+ SLE [12], we assessed IgG reactivity against the complete Sm protein complex as well as $SmD3_{108\text{-}122}$ variants containing either sDMA, asymmetrical dimethyl Arg, or unmodified Arg (Fig 1A). We tested sera from patients with anti-Sm+ SLE, anti-Sm− SLE, and HDs. Consistent with previous studies, the $SmD3_{108\text{-}122}$ epitope was recognised exclusively by patients with anti-Sm+ SLE and only when containing sDMA (Fig 1B) [11,12]. One sDMA residue per peptide was sufficient for antibody binding, as increasing the number of sDMA residues did not significantly enhance $SmD3_{108\text{-}122}$ recognition by these patients (Supplementary Fig S2). A scrambled peptide of the same AA composition was also included (sequence in Supplementary Table S3) and, surprisingly, was still specifically recognised by anti-Sm+ SLE sera (Fig 1C). These observations are intriguing as they point to anti-Sm autoantibodies directly targeting the PTM, similar to autoantibodies in RA directly recognising citrulline (another PTM of Arg) in a variety of peptides [22,23]. Consequently, we continued to investigate whether anti-Sm antibodies represent a bona fide anti-PTM response by generating a cyclic sDMA-containing peptide (CP-sDMA) modelled after the cyclic citrullinated peptide 4 used in RA (substituting citrulline with sDMA) [24]. This peptide allows assessment of sDMA reactivity entirely independent of the context of the Sm protein complex. We tested sera from patients with anti-Sm+ SLE, anti-Sm− SLE, and HDs and observed that the CP-sDMA was recognised exclusively by patients with anti-Sm+ SLE (Fig 1D). These results suggest that patients with anti-Sm+ SLE contain IgG antibodies targeting sDMA in different contexts. To validate our findings, we assessed $SmD3_{108\text{-}122}$ and CP-sDMA and reactivity in an independent second cohort (Fig 1E, F). Again, the

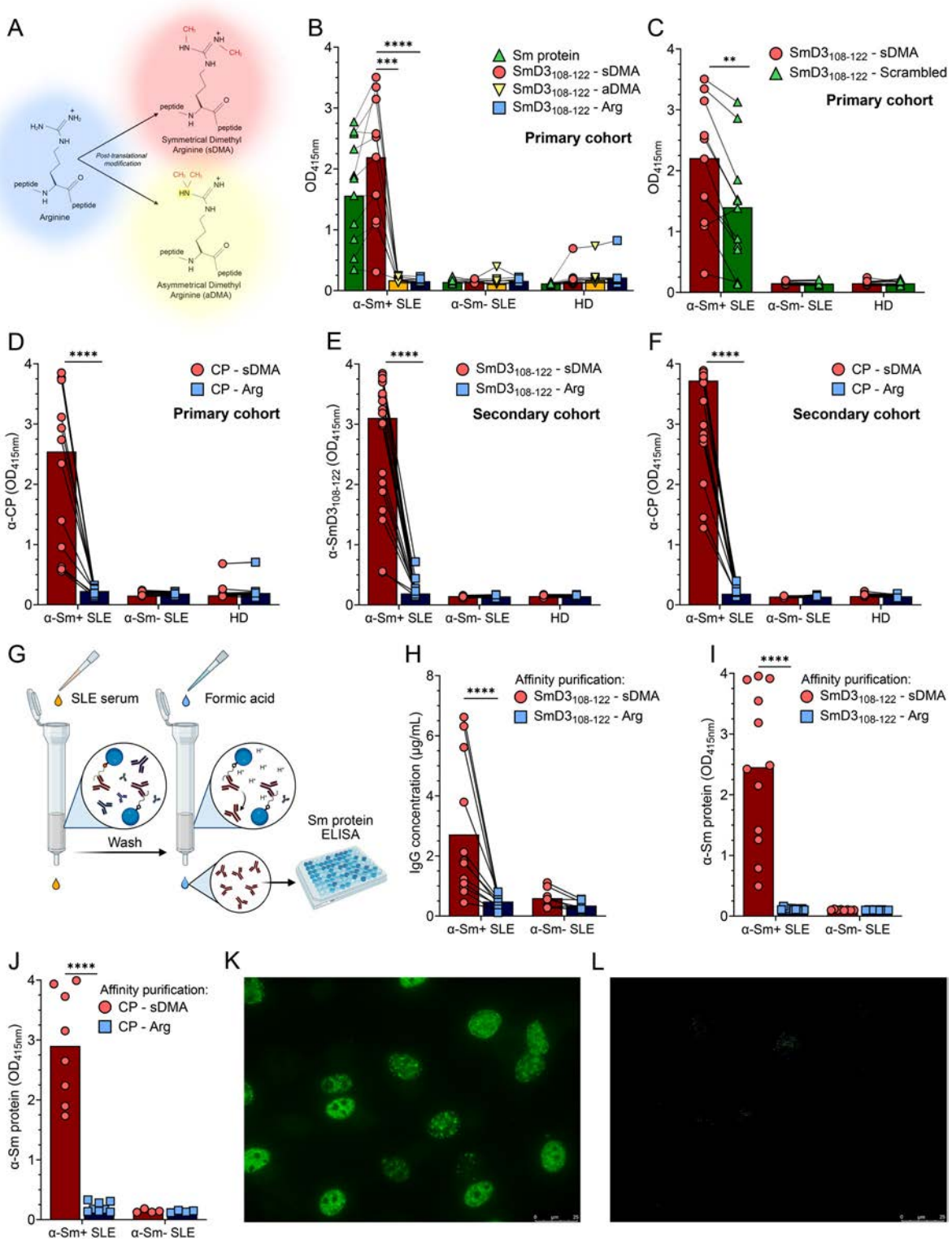

Figure 1. Characterisation of anti-SmD3$_{108-122}$ and other sDMA-containing peptides in patients with anti-Sm+ SLE. (A) Schematic overview of Arg and its posttranslational modification to form sDMA and aDMA. Sera from patients with anti-Sm+ (n = 12), anti-Sm− (n = 12) SLE, as well as HDs (n = 12), were analysed using enzyme-linked immunosorbent assay (ELISA) for immunoglobulin G (IgG) reactivity against (B) the Sm protein complex and SmD3$_{108-122}$ peptide variants containing either sDMA, aDMA, or unmodified Arg; (C) SmD3$_{108-122}$ variant with a scrambled sequence; and (D) a cyclic peptide modified either with sDMA or an unmodified Arg. (E) Reactivity to SmD3$_{108-122}$ and (F) a cyclic peptide, each tested in sDMA-modified or unmodified (Arg) form, was assessed in an independent secondary cohort of anti-Sm+ (n = 20) and anti-Sm− (n = 20) patients with SLE and HDs (n = 20). (G) Schematic overview of antibody affinity purification, where SmD3$_{108-122}$ binding antibodies were isolated from sera of patients with anti-Sm+ (n = 12) and anti-Sm− (n = 8) SLE using either sDMA or Arg control variants. (H) IgG concentration after affinity purification and (I) antibody binding to the Sm protein complex after affinity purification were measured using ELISA. (J) Antibodies binding the cyclic peptide, either the sDMA or Arg variant, were similarly purified and tested for binding to the Sm protein complex using ELISA. (K) HEp-2000 cells were stained with isolated anti-sDMA antibodies derived from a patient with anti-Sm+ SLE at a concentration of 10 µg/mL. (L) HEp-2000 staining with the purified fraction from a patient with anti-Sm− SLE was included as a negative control. All bar graphs show the median with lines connecting data points from individual samples. One representative experiment of 3 is shown. Data were analysed using simple linear regression or a Friedman test; $^{**}P \leq .01$, $^{***}P \leq .001$, $^{****}P \leq .0001$. aDMA, asymmetrical dimethyl arginine; Arg, arginine; CP, cyclic peptide; HD, healthy donor; OD415nm, optical density at 415 nm; sDMA, symmetrical dimethyl arginine; SLE, systemic lupus erythematosus; Sm, Smith.

CP-sDMA was recognised exclusively by patients with anti-Sm+ SLE and to a similar extent as $SmD3_{108-122}$, confirming that anti-PTM antibodies targeting sDMA are present in all patients with anti-Sm+ SLE from 2 cohorts.

Next, to evaluate whether IgGs targeting sDMA-containing peptides recognise the full-length Sm protein complex, we isolated antibodies by affinity purification with $SmD3_{108-122}$ (sDMA or Arg) (Fig 1H). Significantly higher amounts of IgGs were isolated from patients with anti-Sm+ SLE using the sDMA-modified $SmD3_{108-122}$ peptide compared with the unmodified control (Fig 1H). Only the anti-sDMA antibodies from patients with anti-Sm+ SLE exhibited binding to the full-length Sm protein complex (Fig 1I). Similarly, only affinity-purified anti-sDMA IgGs from patients with anti-Sm+ SLE, obtained using the CP-sDMA peptide, exhibited binding to the Sm protein complex (Fig 1J). Reactivity of these CP-sDMA-isolated antibodies to the Sm protein complex was confirmed by Western blot. The isolated antibodies displayed strong staining of the ~14/15 kDa band, similar to binding by the anti-sDMA monoclonal antibody (SYM11) and the corresponding diluted serum sample, with no reactivity to other components of the Sm protein extract (Supplementary Fig 3). On HEp-2000 cells, sDMA-affinity-purified IgG from 3 patients with anti-Sm+ SLE produced a positive ANA staining (Fig 1J, Supplementary Fig S4), whereas the purified fraction from patients with anti-Sm- SLE showed no staining (Fig 1K). Isolated antibodies from 2 patients exhibited a pleomorphic speckled nucleoplasmic staining pattern (PCNA-like; AC-13), while the result for one patient was less clear, possibly due to lower signal intensity.

Overall, our findings indicate that IgG from patients with anti-Sm+ SLE sera recognise the $SmD3_{108-122}$ epitope through its sDMA residue and these anti-sDMA IgGs are capable of targeting the full-length Sm protein complex. Importantly, sDMA recognition can occur in the context of sequences independent from Sm.

sDMA forms the predominant target of the anti-Sm response in patients with SLE

We noticed a strong correlation between the levels of IgG reactive to $SmD3_{108-122}$ and the complete Sm protein complex (Fig 2A). Therefore, we sought to determine to what extent IgGs targeting sDMA-containing epitopes contribute to the overall anti-Sm IgG response in patients with SLE. To assess this, we conducted an inhibition assay, incubating anti-Sm+ SLE serum with various concentrations of $SmD3_{108-122}$ (sDMA or Arg). In order to confirm that anti-sDMA IgGs were effectively blocked, we first tested the blocked serum for recognition of the cognate $SmD3_{108-122}$-sDMA peptide using ELISA. Blocking with $SmD3_{108-122}$-sDMA effectively inhibited recognition in a dose-dependent manner in most samples, whereas blocking with $SmD3_{108-122}$-Arg had no effect on recognition (Supplementary Fig S5). At the highest concentration of blocking peptide, nearly all sDMA-specific IgGs were successfully blocked. Next, we tested the serum for recognition of the complete Sm protein complex (Fig 2B). Blocking anti-$SmD3_{108-122}$-sDMA IgG resulted in a significant reduction in Sm protein complex recognition (Fig 2C), with an average inhibition of ~90% (Fig 2E). No effect in Sm complex recognition was observed when anti-Sm+ sera were blocked with the Arg control peptide (Fig 2D) or in patients with anti-Sm− SLE and HDs (Supplementary Fig S6). Furthermore, to confirm that this inhibition of Sm complex recognition depends exclusively on the sDMA residue, we performed a similar inhibition assay using the CP-sDMA (or Arg control) (Fig 2F), resulting once more in an average inhibition of ~90% (Fig 2G-I). Importantly, blocking sDMA did not affect the recognition of other nuclear antigens (dsDNA, histone, RNP70, and Ro60/SS-A), confirming the specificity of sDMA antibodies for the anti-Sm response (Supplementary Fig S7). For comparison, anti-Sm+ SLE sera were also incubated with the cross-reactive PPPGMRPP peptide, previously described as an early target in the anti-Sm response [5]. Notably, the PPPGMRPP peptide was not differently recognised by anti-Sm+ SLE sera compared with anti-Sm− SLE or HDs (Fig 2J), and inhibition with this peptide had no effect on Sm protein complex recognition (Fig 2K). Taken together, our findings show that the sDMA residue is an essential constituent of the antigens targeted by the majority of the anti-Sm repertoire.

Anti-Sm IgG is cross-reactive to viral sDMA-containing epitopes

In addition to the Sm protein complex, emerging evidence suggests that several viral proteins carry sDMA residues as well [25–27]. To determine whether anti-sDMA IgG from patients with anti-Sm+ SLE can recognise viral sDMA-containing epitopes, we synthesised peptides of several viral proteins, each containing sDMA at a specified position or unmodified Arg as a control. We assessed peptides derived from EBV nuclear antigen 1 (EBNA1) [17], EBNA2 [18,28], hepatitis C virus (HCV) non-structural protein 3 [19], and infectious bursal disease virus (IBDV) RNA polymerase viral protein 1 [20]. All sDMA-containing viral peptides were specifically recognised by patients with anti-Sm+ SLE (Fig 3A-D). Similar to the $SmD3_{108-122}$ epitope, recognition was dependent on the presence of sDMA. We also occasionally observed recognition of viral peptides in patients with anti-Sm− SLE and HDs, but this reactivity was not sDMA-dependent, as the unmodified control was recognised equally well. Binding to the viral protein $1_{420-439}$-sDMA peptide was modest compared with the other peptides (Fig 3D).

To assess whether anti-sDMA IgGs are cross-reactive between $SmD3_{108-122}$ and viral sDMA-containing peptides, we performed a similar inhibition assay as described previously by preincubating anti-Sm+ SLE serum with various concentrations of $SmD3_{108-122}$ (sDMA or Arg) before assessing binding to viral peptides using ELISA (Fig 3E). This resulted in an average inhibition ranging from 65% to 95%, indicating that anti-sDMA IgGs are highly cross-reactive to sDMA-containing peptides of various origins (Fig 3F, Supplementary Fig S8A-H). Conversely, we tested whether sDMA-containing viral peptides could similarly inhibit Sm protein complex recognition. Anti-Sm+ SLE sera were preincubated with the respective viral peptides (sDMA or Arg), which resulted in approximately 80% to 90% inhibition, indicating strong cross-reactivity between viral sDMA-containing epitopes and the Sm protein complex (Fig 3G, Supplementary Fig S8I-P).

Next, we sought to determine whether anti-sDMA IgG could also recognise sDMA residues within endogenous viral proteins. To this end, we selected EBNA1 as a model antigen. To confirm the presence of sDMA on endogenous EBNA1, we performed Western blotting on lysates from EBV− and EBV+ B cell lines using anti-sDMA (SYM11) and anti-EBNA1 (1H4) monoclonal antibodies (Fig 3H, Supplementary Fig S9A, B). The alignment of both signals at the same molecular weight supports the presence of sDMA on EBNA1. Next, blots were stained with polyclonal anti-sDMA IgG affinity-purified from multiple patients with SLE (Fig 1H, I). In addition to the presumable SmD band at approximately 15 kDa, IgG binding was observed at the same molecular weight as the anti-EBNA1 band in the EBV+ lysate (Fig 3I, Supplementary Fig S9C, D), suggesting that patient-

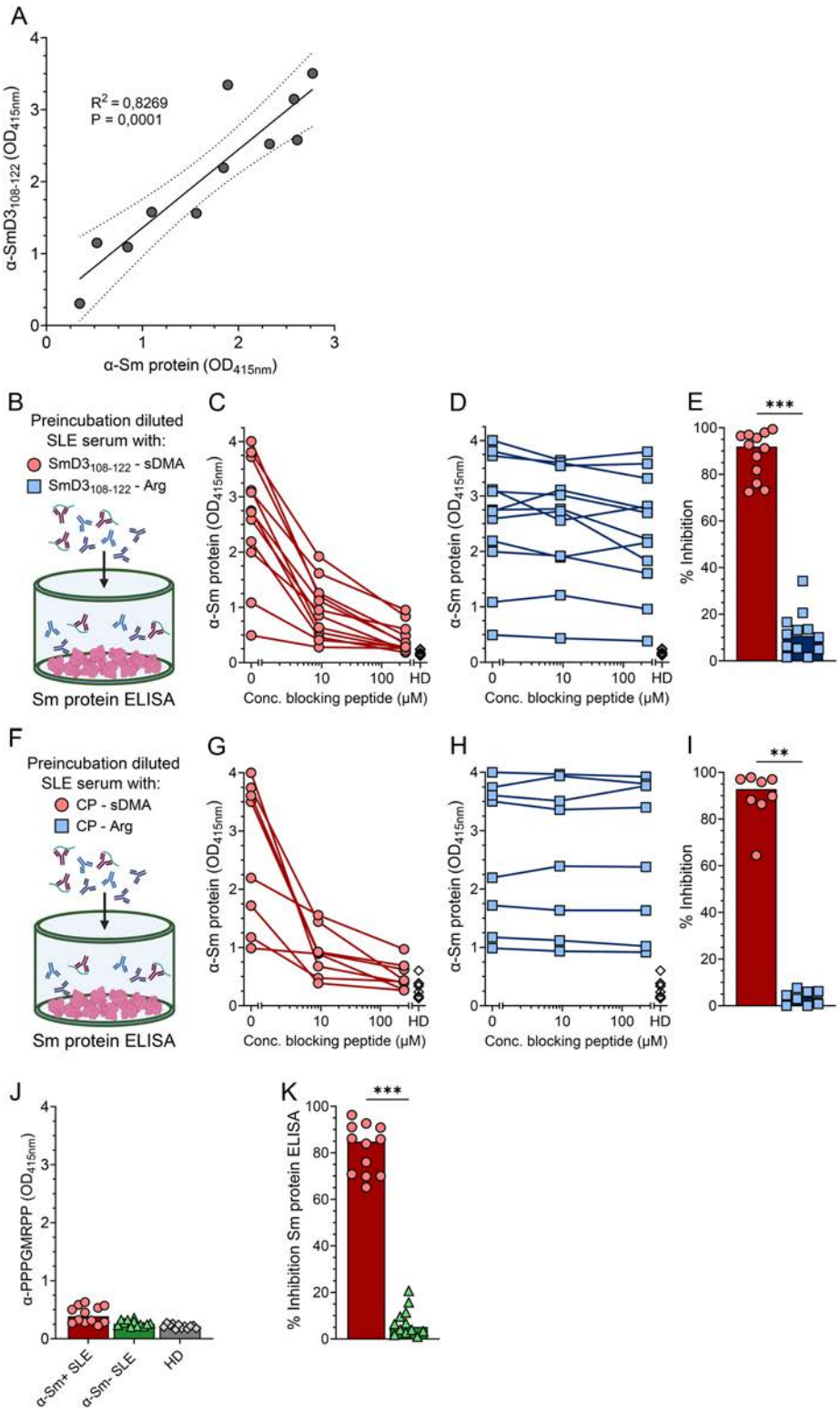

Figure 2. sDMA forms the predominant target of the anti-Sm response in patients with SLE. (A) Correlation of anti-$SmD3_{108-122}$-sDMA OD_{415} with anti-Sm OD_{415} in patients with anti-Sm+ SLE (n = 12) (data from Fig 1A). (B, F) Schematic overview of the inhibition assay, where sera from patients with anti-Sm+ SLE were incubated with increasing concentrations of blocking (C-E) $SmD3_{108-122}$ peptide (n = 12) or (G-I) cyclic peptide (n = 8) (sDMA [red circles] or Arg control [blue squares]) and subsequently measured on the Sm protein complex using ELISA. (J) ELISA showing PPPGMRPP peptide binding by sera from patients with anti-Sm+ (n = 12), anti-Sm- (n = 12) SLE, and HDs (n = 12). (K) Inhibition assay where sera of patients with anti-Sm+ SLE (n = 6) were incubated with increasing concentrations of PPPGMRPP or $SmD3_{108-122}$-sDMA and subsequently measured on Sm using ELISA. (E, I, J) Bar graphs show percent inhibition at 250 μM relative to the unblocked condition. All bar graphs show the median, and line graphs connect individual measurements from the same patient sample. One representative experiment of 3 independent repetitions is shown. Data were analysed using simple linear regression or a Wilcoxon signed-rank test; *$P \leq .05$, * $P \leq .01$, ** $P \leq .001$. Arg, arginine; ELISA, enzyme-linked immunosorbent assay; OD_{415nm}, optical density at 415 nm; sDMA, symmetrical dimethylarginine; SLE, systemic lupus erythematosus; Sm, Smith.

derived anti-sDMA IgGs can bind endogenous EBNA1. Overall, our results indicate that IgGs targeting sDMA are highly cross-reactive to other sDMA-containing epitopes, including several viral-derived proteins.

DISCUSSION

This study sought to deepen the understanding of the fine specificity and cross-reactivity of the anti-Sm autoantibody response in SLE. Several antigenic targets have been identified on the Sm protein complex, with $SmD3_{108-122}$ being recognised as a highly specific epitope that is also currently used in certain clinical diagnostic assays [11,12]. Building on previous studies, our findings now demonstrate that the sDMA residue is a primary target, largely independent of the AA sequence in which it is embedded. This conclusion is supported by the sustained recognition of scrambled $SmD3_{108-122}$ and numerous other sDMA-containing peptides outside the structural context of the Sm antigen by sera from patients with anti-Sm+ SLE, including several viral-derived epitopes. Thus, the anti-Sm response represents a prototypic anti-PTM response, resembling the anticitrullinated protein antibodies response and other antimodified protein antibody responses described in RA [23]. Reactivity to $SmD3_{108-122}$ was maintained even when not all Args were converted to sDMA

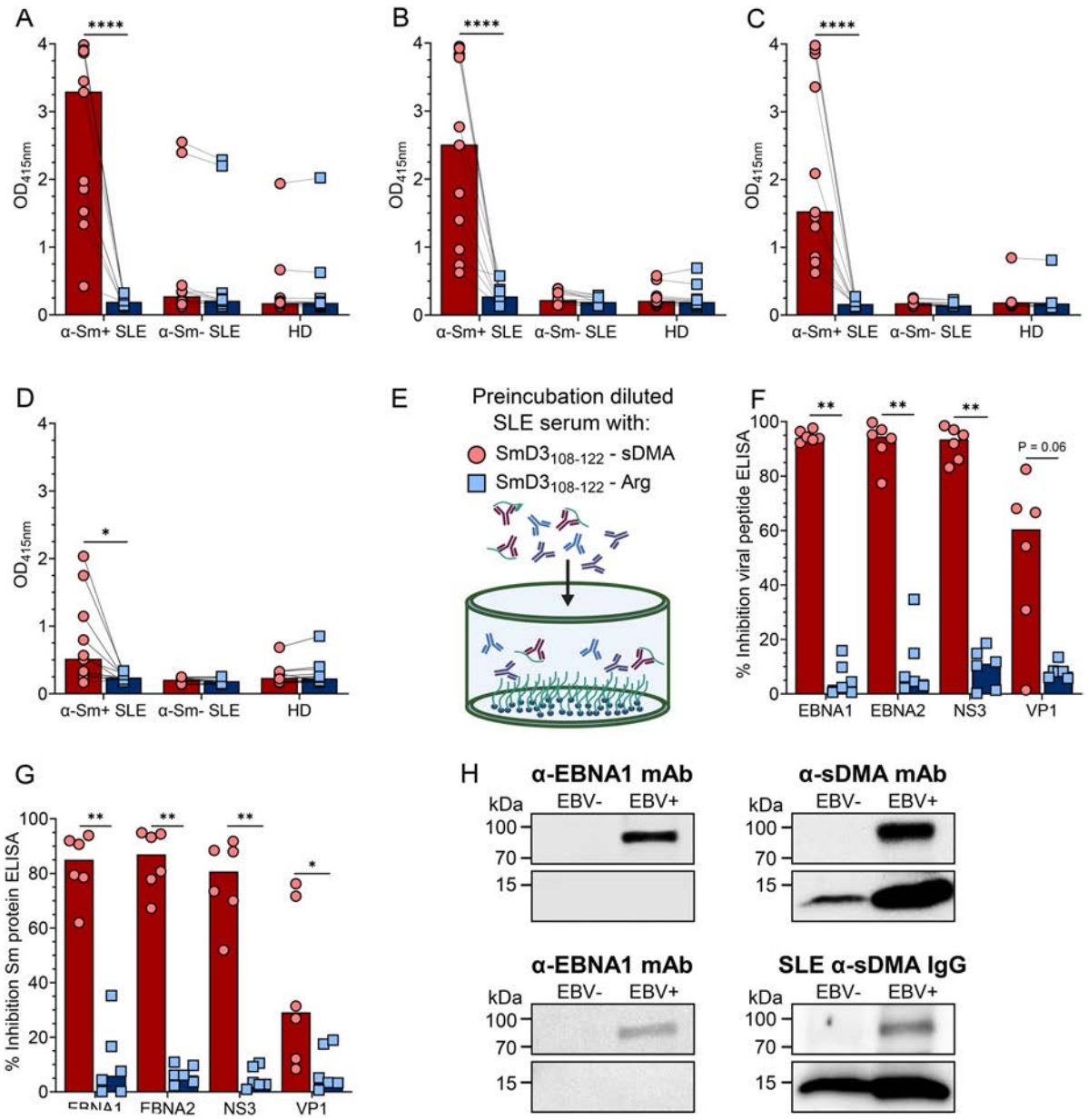

Figure 3. Anti-sDMA immunoglobulin G (IgG) antibodies from patients with SLE are cross-reactive to multiple viral sDMA-containing epitopes. Sera from patients with anti-Sm+ (n = 12) and anti-Sm− (n = 12) SLE, as well as HDs (n = 12), were analysed using ELISA for IgG reactivity against viral sDMA-containing epitopes or corresponding Arg controls: EBV-derived (A) $EBNA1_{34\text{-}52}$ or (B) $EBNA2_{335\text{-}360}$, (C) HCV-derived $NS3_{1486\text{-}1494}$, and (D) IBDV-derived $VP1_{420\text{-}439}$. (E) Schematic overview of an inhibition assay, where sera of patients with anti-Sm+ SLE (n = 6) was incubated with increasing concentrations of blocking $SmD3_{108\text{-}122}$ peptide (sDMA or arginine control) and (F) subsequently measured on the respective sDMA-containing viral peptide using ELISA. (G) Inhibition assay where sera of patients with anti-Sm+ SLE (n = 6) were incubated with respective viral peptides (sDMA or Arg control) and subsequently measured on the Sm protein using ELISA. (H) Lysates from EBV− IMM and EBV+ JY B cell lines were subjected to Western blot analysis to detect EBNA1 and other sDMA-modified proteins and (H) subsequently tested for recognition by sDMA-specific IgG antibodies purified from pooled anti-Sm+ SLE sera. (F, G) Bar graphs show percent inhibition at 250 μM relative to the unblocked condition. All bar graphs represent the median, with lines connecting paired samples. One representative experiment of 3 is shown. Data were analysed using a Wilcoxon signed-rank test; $^{*}P \leq .05$, $^{**}P \leq .01$, $^{****}P \leq .0001$. Arg, arginine; EBNA1, Epstein-Barr nuclear antigen 1; EBNA2, Epstein-Barr nuclear antigen 2; EBV, Epstein-Barr virus; HCV, hepatitis C virus; HD, healthy donor; IBDV, infectious bursal disease virus; IMM, BCL-6/Bcl-xL transduced immortalised; NS3, nonstructural protein 3; OD_{415nm}, optical density at 415 nm; sDMA, symmetrical dimethylarginine; SLE, systemic lupus erythematosus; Sm, Smith; VP1, viral protein 1.

[12], and increasing the number of sDMA residues did not enhance recognition, indicating that a single sDMA residue is sufficient for anti-Sm binding.

The fine specificity of the anti-Sm response has been studied before by performing overlapping peptide screens using sera collected before and after SLE diagnosis. The PPPGMRPP motif of SmB/B' was identified as a primary target of the early anti-Sm response and was suggested to be an initiating factor, though several other peptides were also recognised [5,8,29]. Although a potential initiating role cannot be ruled out, we did not observe a significant contribution of antibodies targeting PPPGMRPP to the anti-Sm antibody repertoire in established patients with SLE from both cohorts. Importantly, peptide screens are inherently limited by the absence of PTMs in the peptides being used, thereby failing to capture the full spectrum of the antibody response against endogenous proteins. It is important to note that older studies already suggested that only native purified Sm proteins, or Sm proteins produced in

baculovirus-infected insect cells, and not bacterially expressed Sm, were recognised by anti-Sm+ SLE serum [11]. These observations can now be explained by our findings, as sDMA is the major determinant of Sm complex recognition, and symmetrical dimethylation by bacteria has not been observed to date [30]. In addition, sole recognition of sDMA residues also elucidates why anti-Sm antibodies were shown to recognise cross-reactive epitopes on both the B′/B and D subunits of the Sm complex, despite their limited AA sequence homology [31].

Here, we demonstrated for the first time that the majority (>90%) of anti-Sm IgGs specifically target sDMA residues, highlighting a central role of this PTM in the development of the SLE-specific B cell response to Sm. Additional human proteins, such as RNP70 and histones, have been suggested to carry sDMA [27,32], which may explain the strong association between anti-RNP70 and anti-Sm antibody responses in patients with SLE [33,34]. Still, blocking anti-sDMA IgGs did not significantly affect the recognition of other nuclear antigens, including recombinant RNP70 and native purified histones, in patients with anti-Sm+ SLE. Furthermore, purified anti-sDMA antibodies and monoclonals had restricted recognition of proteins from cell lysates on Western blot. Therefore, the presence and recognition of sDMA residues on other (self-)proteins may be limited, potentially due to low abundance or interfering flanking AAs. Intriguingly, a proteomic study showed that anti-Sm+ sera from patients with SLE could recognise other Arg-methylated proteins as well, with methylation-dependent immunoreactivity reduced when methylation was inhibited [35], indicating that anti-Sm autoreactivity extends beyond recognition of the Sm protein complex. Why the sDMA-containing peptides play such a significant role in the recognition of Sm remains to be determined, but similarities between viral antigens and Sm-derived epitopes may offer a plausible explanation.

Numerous viruses have been linked to SLE pathogenesis, with a particular focus on EBV [36]. Molecular mimicry between viral and self-antigens could provide a trigger in the initiation of autoimmunity, and our results suggest strong mimicry between various sDMA-containing viral proteins and Sm. While some studies focused on a motif within EBV EBNA-1 (AA Nos. 398-404), which showed mimicry to the PPPGMRPP motif of SmB/B' [8,29,37], we could not confirm reactivity to this peptide, nor did blocking with this peptide significantly reduce binding to the complete Sm protein complex. Our findings of sDMA recognition as a determining factor in cross-reactivity between Sm and viral proteins provide new insight into the potential triggers of anti-Sm autoimmunity. Although further studies are required to substantiate this possibility, many viral proteins, including those from common viruses (EBNA-1/EBNA-2 from EBV and PB2 from Influenza A), have been reported to contain sDMA [25,26,28], and thus, different viruses may have the capacity to trigger a cross-reactive response targeting sDMA. Expression of the entire EBNA-1 protein in mice through an expression vector induced IgGs that bound to the native Sm protein complex [38]. Since EBNA-1 expressed in mouse cells could acquire sDMA residues, our results may explain the cross-reactivity that was induced. We hypothesised that the cross-reactive anti-Sm response in patients with SLE could arise from B cells that recognise sDMA-containing epitopes but receive T cell help specific for a viral antigen. When cross-reactivity is present within the B cell compartment, these B cells can receive help from foreign-reactive nonautoreactive T cells when they internalise and present peptides from the cross-reactive viral protein, thereby leading to a break in B cell tolerance. Exposure to the viral antigen would be essential for this initial tolerance breach, as sDMA-reactive B cells would otherwise not receive CD4+ T cell help. Notably, anti-Sm positivity in SLE is strongly associated with particular combinations of human leukocyte antigen class II haplotypes [39], underscoring the central role of CD4+ T cells in shaping these pathogenic B cell responses. Interestingly, antibodies against the sDMA-containing $SmD3_{108\text{-}122}$ peptide were not detected during acute or chronic viral infection in otherwise healthy individuals, including cytomegalovirus, HCV, or EBV [12]. This suggests that viral infection alone is not sufficient to trigger an anti-sDMA response and that other factors in patients with SLE likely contribute to loss of tolerance against sDMA-containing self-antigens [36]. Recent work has demonstrated that patients with SLE have higher numbers of EBV-infected B cells and that these cells are more activated [40]. Whether this is the cause or consequence of SLE remains to be determined. While seropositivity for EBV early antigen has been linked to anti-Sm and other ANA specificities [41,42], its specificity is limited by the near-universal EBV exposure in SLE [43,44], including Sm-negative disease. Still, increased exposure to EBV-derived proteins containing sDMA may contribute to loss of tolerance and may thereby provide a potential bridge between EBV infection and the emergence of Sm autoreactivity in SLE.

Despite the evidence provided in this study, several limitations need to be considered. In this study, we primarily relied on synthetic peptides and included only 1 model viral protein antigen: EBNA1. Although we demonstrated cross-reactivity to various viruses at the peptide level, evidence at the viral protein level remains indirect. It therefore remains speculative at this stage whether anti-sDMA IgG autoantibodies are truly cross-reactive to viral proteins *in vivo* and whether such cross-reactivity contributes to the initiation of the anti-Sm response in SLE.

In conclusion, our findings highlighted the central role of sDMA residues in the development of anti-Sm autoantibodies in SLE, thereby representing a prototypic anti-PTM response. Furthermore, the high cross-reactivity of Sm antibodies to various sDMA-containing epitopes revealed a novel mechanistic perspective on the potential link between viral infection and tolerance breach in patients with anti-Sm+ SLE.

Competing interests

All authors declare they have no competing interests.

CRediT authorship contribution statement

Lars C. van Vliet: Writing – review & editing, Writing – original draft, Visualization, Validation, Methodology, Investigation, Formal analysis, Data curation, Conceptualization. **Annemarie L. Dorjée:** Methodology, Investigation, Formal analysis, Data curation. **Martijn van der Heide:** Writing – review & editing, Investigation. **Annette Grummels:** Investigation. **Esther van Andel:** Investigation. **Gerda M. Steup-Beekman:** Writing – review & editing, Resources. **Thomas W.J. Huizinga:** Writing – review & editing, Resources. **René E.M. Toes:** Writing – review & editing, Supervision, Conceptualization. **Jolien Suurmond:** Writing – review & editing, Supervision, Project administration, Methodology, Funding acquisition, Conceptualization.

Acknowledgements

Some figure components were generated using BioRender (see licensed resources at https://BioRender.com/fecyzs6, https://BioRender.com/694mb1q, https://BioRender.com/

e8wwcm5). We gratefully acknowledge J.W. Drijfhout for his helpful contributions and discussions, and K. van Schie for her assistance with microscopy imaging.

Funding

This work was supported by the Dutch Arthritis Society [grant number 22-1-402].

Patient consent for publication

All participants provided written infromed consent.

Ethics approval

The study was conducted in concordance with the Declaration of Helsinki and was approved by the Leiden Den Haag Delft medical ethics committee and the LUMC biobank committee.

Provenance and peer review

Not commissioned; externally peer reviewed.

Supplementary materials

Supplementary material associated with this article can be found in the online version at doi:10.1016/j.ard.2026.06.012.

REFERENCES

[1] Suurmond J, Diamond B. Autoantibodies in systemic autoimmune diseases: specificity and pathogenicity. J Clin Invest 2015;125(6):2194–202. doi: 10.1172/JCI78084.
[2] Müller F, Taubmann J, Bucci L, Wilhelm A, Bergmann C. Völkl Set al. CD19 CAR T-cell therapy in autoimmune disease - a case series with follow-up. N Engl J Med 2024;390(8):687–700. doi: 10.1056/NEJMoa2308917.
[3] Aringer M, Costenbader K, Daikh D, Brinks R, Mosca M, Ramsey-Goldman R, et al. 2019 European League Against Rheumatism/American College of Rheumatology classification criteria for systemic lupus erythematosus. Ann Rheum Dis 2019;78(9):1151–9. doi: 10.1136/annrheumdis-2018-214819.
[4] Thandapani P, O'Connor TR, Bailey TL, Richard S. Defining the RGG/RG motif. Mol Cell 2013;50(5):613–23. doi: 10.1016/j.molcel.2013.05.021.
[5] Arbuckle MR, Reichlin M, Harley JB, James JA. Shared early autoantibody recognition events in the development of anti-Sm B/B' in human lupus. Scand J Immunol 1999;50(5):447–55. doi: 10.1046/j.1365-3083.1999.00640.x.
[6] Riemekasten G, Marell J, Trebeljahr G, Klein R, Hausdorf G, Häupl T, et al. A novel epitope on the C-terminus of SmD1 is recognized by the majority of sera from patients with systemic lupus erythematosus. J Clin Invest 1998;102(4):754–63. doi: 10.1172/JCI2749.
[7] McClain MT, Ramsland PA, Kaufman KM, James JA. Anti-sm autoantibodies in systemic lupus target highly basic surface structures of complexed spliceosomal autoantigens. J Immunol 2002;168(4):2054–62. doi: 10.4049/jimmunol.168.4.2054.
[8] James JA, Harley JB. Linear epitope mapping of an Sm B/B' polypeptide. J Immunol 1992;148(7):2074–9.
[9] Brahms H, Meheus L, de Brabandere V, Fischer U, Lührmann R. Symmetrical dimethylation of arginine residues in spliceosomal Sm protein B/B' and the Sm-like protein LSm4, and their interaction with the SMN protein. RNA 2001;7(11):1531–42. doi: 10.1017/s135583820101442x.
[10] Friesen WJ, Massenet S, Paushkin S, Wyce A, Dreyfuss G. SMN, the product of the spinal muscular atrophy gene, binds preferentially to dimethylarginine-containing protein targets. Mol Cell 2001;7(5):1111–7. doi: 10.1016/s1097-2765(01)00244-1.
[11] Brahms H, Raymackers J, Union A, de Keyser F, Meheus L, Lührmann R. The C-terminal RG dipeptide repeats of the spliceosomal Sm proteins D1 and D3 contain symmetrical dimethylarginines, which form a major B-cell epitope for anti-Sm autoantibodies. J Biol Chem 2000;275(22):17122–9. doi: 10.1074/jbc.M000300200.
[12] Mahler M, Fritzler MJ, Blüthner M. Identification of a SmD3 epitope with a single symmetrical dimethylation of an arginine residue as a specific target of a subpopulation of anti-Sm antibodies. Arthritis Res Ther 2005;7(1):R19–29. doi: 10.1186/ar1455.
[13] Sokolova MV, Schett G, Steffen U. Autoantibodies in rheumatoid arthritis: historical background and novel findings. Clin Rev Allergy Immunol 2022;63(2):138–51. doi: 10.1007/s12016-021-08890-1.
[14] Biersteker R, Athanasiadou A, Van Der Meulen S, Van Wesemael TJ, Slot LM, Kissel T, et al. Insights into the detection of AMPA cross-reactivity: comparing cyclic peptide- to protein-based assays. Arthritis Res Ther 2025;27(1):138. doi: 10.1186/s13075-025-03591-y.
[15] Magro-Checa C, Zirkzee E, Beaart-van de Voorde L, Middelkoop H, van der Wee N, Huisman M, et al. Value of multidisciplinary reassessment in attribution of neuropsychiatric events to systemic lupus erythematosus: prospective data from the Leiden NPSLE cohort. Rheumatology (Oxford) 2017;56(10):1676–83. doi: 10.1093/rheumatology/kex019.
[16] Nell MJ, Tjabringa GS, Wafelman AR, Verrijk R, Hiemstra PS, Drijfhout JW, et al. Development of novel LL-37 derived antimicrobial peptides with LPS and LTA neutralizing and antimicrobial activities for therapeutic application. Peptides 2006;27(4):649–60. doi: 10.1016/j.peptides.2005.09.016.
[17] Shire K, Kapoor P, Jiang K, Hing MNT, Sivachandran N, Nguyen T, Frappier L. Regulation of the EBNA1 Epstein-Barr virus protein by serine phosphorylation and arginine methylation. J Virol 2006;80(11):5261–72. doi: 10.1128/JVI.02682-05.
[18] Ayoubian H, Fröhlich T, Pogodski D, Flatley A, Kremmer E, Schepers A, et al. Antibodies against the mono-methylated arginine-glycine repeat (MMA-RG) of the Epstein-Barr virus nuclear antigen 2 (EBNA2) identify potential cellular proteins targeted in viral transformation. J Gen Virol 2017;98(8):2128–42. doi: 10.1099/jgv.0.000870.
[19] Rho J, Choi S, Seong YR, Choi J, Im D-S. The arginine-1493 residue in QRRGRTGR1493G motif IV of the hepatitis C virus NS3 helicase domain is essential for NS3 protein methylation by the protein arginine methyltransferase 1. J Virol 2001;75(17):8031–44. doi: 10.1128/jvi.75.17.8031-8044.2001.
[20] Hu X, Chen Z, Wu X, Fu Q, Chen Z, Huang Y, Wu H. PRMT5 facilitates infectious bursal disease virus replication through arginine methylation of VP1. J Virol 2023;97(3):e0163722 Erratum in: J Virol. 2026:100(3):e0200225.. doi: 10.1128/jvi.01637-2210.1128/jvi.02002-25.
[21] van Dooren HJ, Atisha-Fregoso Y, Dorjée AL, Huizinga TWJ, Mackay M, Aranow C, et al. Interferon signatures fuel B cell hyperactivity and plasmablast expansion in systemic lupus erythematosus. J Autoimmun 2025;154:103438. doi: 10.1016/j.jaut.2025.103438.
[22] Ioan-Facsinay A, el-Bannoudi H, Scherer HU, van der Woude D, Ménard HA, Lora M, et al. Anti-cyclic citrullinated peptide antibodies are a collection of anti-citrullinated protein antibodies and contain overlapping and non-overlapping reactivities. Ann Rheum Dis 2011;70(1):188–93. doi: 10.1136/ard.2010.131102.
[23] Steiner G, Toes REM. Autoantibodies in rheumatoid arthritis - rheumatoid factor, anticitrullinated protein antibodies and beyond. Curr Opin Rheumatol 2024;36(3):217–24. doi: 10.1097/BOR.0000000000001006.
[24] Kissel T, Reijm S, Slot LM, Cavallari M, Wortel C, Vergroesen R, et al. Antibodies and B cells recognising citrullinated proteins display a broad cross-reactivity towards other post-translational modifications. Ann Rheum Dis 2020;79(4):472–80. doi: 10.1136/annrheumdis-2019-216499.
[25] Zheng K, Chen S, Ren Z, Wang Y. Protein arginine methylation in viral infection and antiviral immunity. Int J Biol Sci 2023;19(16):5292–318. doi: 10.7150/ijbs.89498.
[26] Sun H, Tu S, Luo D, Dai C, Jin M, Chen H, Zou J, Zhou H. Protein arginine methyltransferase 5 mediates arginine symmetric dimethylation of influenza A virus PB2 and supports viral replication. J Med Virol 2023;95(10):e29171. doi: 10.1002/jmv.29171.
[27] Boisvert FM, Côté J, Boulanger MC, Richard S. A proteomic analysis of arginine-methylated protein complexes. Mol Cell Proteomics 2003;2(12):1319–30. doi: 10.1074/mcp.M300088-MCP200.
[28] Gross H, Hennard C, Masouris I, Cassel C, Barth S, Stober-Grässer U, et al. Binding of the heterogeneous ribonucleoprotein K (hnRNP K) to the Epstein-Barr virus nuclear antigen 2 (EBNA2) enhances viral LMP2A expression. PLoS One 2012;7(8):e42106. doi: 10.1371/journal.pone.0042106.
[29] James J, Gross T, Scofield R, Harley J. Immunoglobulin epitope spreading and autoimmune disease after peptide immunization: Sm B/B'-derived PPPGMRPP and PPPGIRGP induce spliceosome autoimmunity. J Exp Med 1995;181(2):453–61. doi: 10.1084/jem.181.2.453.
[30] Lassak J, Koller F, Krafczyk R, Volkwein W. Exceptionally versatile - arginine in bacterial post-translational protein modifications. Biol Chem 2019;400(11):1397–427. doi: 10.1515/hsz-2019-0182.
[31] Hirakata M, Craft J, Hardin J. Autoantigenic epitopes of the B and D polypeptides of the U1 snRNP. Analysis of domains recognized by the Y12 monoclonal anti-Sm antibody and by patient sera. J Immunol 1993;150(8 Pt 1):3592–601.

[32] Migliori V, Müller J, Phalke S, Low D, Bezzi M, Mok WC, et al. Symmetric dimethylation of H3R2 is a newly identified histone mark that supports euchromatin maintenance. Nat Struct Mol Biol 2012;19(2):136–44. doi: 10.1038/nsmb.2209.

[33] Pisetsky DS, Lipsky PE. New insights into the role of antinuclear antibodies in systemic lupus erythematosus. Nat Rev Rheumatol 2020;16(10):565–79. doi: 10.1038/s41584-020-0480-7.

[34] Ching KH, Burbelo PD, Tipton C, Wei C, Petri M, Sanz I, et al. Two major autoantibody clusters in systemic lupus erythematosus. PLoS One 2012;7(2): e32001. doi: 10.1371/journal.pone.0032001.

[35] Chang HH, Hu HH, Lee YJ, Wei HM, MC Fan-June, Hsu TC, et al. Proteomic analyses and identification of arginine methylated proteins differentially recognized by autosera from anti-Sm positive SLE patients. J Biomed Sci 2013;20(1):27. doi: 10.1186/1423-0127-20-27.

[36] Quaglia M, Merlotti G, De Andrea M, Borgogna C, Cantaluppi V. Viral infections and systemic lupus erythematosus: new players in an old story. Viruses 2021;13(2):277. doi: 10.3390/v13020277.

[37] Poole BD, Gross T, Maier S, Harley JB, James JA. Lupus-like autoantibody development in rabbits and mice after immunization with EBNA-1 fragments. J Autoimmun 2008;31(4):362–71. doi: 10.1016/j.jaut.2008.08.007.

[38] Sundar K, Jacques S, Gottlieb P, Villars R, Benito ME, Taylor DK, et al. Expression of the Epstein-Barr virus nuclear antigen-1 (EBNA-1) in the mouse can elicit the production of anti-dsDNA and anti-Sm antibodies. J Autoimmun 2004;23(2):127–40. doi: 10.1016/j.jaut.2004.06.001.

[39] Graham RR, Ortmann W, Rodine P, Espe K, Langefeld C, Lange E, et al. Specific combinations of HLA-DR2 and DR3 class II haplotypes contribute graded risk for disease susceptibility and autoantibodies in human SLE. Eur J Hum Genet 2007;15(8):823–30. doi: 10.1038/sj.ejhg.5201827.

[40] Younis S, Moutusy SI, Rasouli S, Jahanbani S, Pandit M, Wu X, et al. Epstein-Barr virus reprograms autoreactive B cells as antigen-presenting cells in systemic lupus erythematosus. Sci Transl Med 2025;17(824):eady0210. doi: 10.1126/scitranslmed.ady0210.

[41] Esen BA, Yılmaz G, Uzun S, Özdamar M, Aksözek A, Kamalı S, et al. Serologic response to Epstein-Barr virus antigens in patients with systemic lupus erythematosus: a controlled study. Rheumatol Int 2012;32(1):79–83. doi: 10.1007/s00296-010-1573-4.

[42] Vista ES, Weisman MH, Ishimori ML, Chen H, Bourn RL, Bruner BF, et al. Strong viral associations with SLE among Filipinos. Lupus Sci Med 2017;4 (1):e000214. doi: 10.1136/lupus-2017-000214.

[43] McClain MT, Heinlen LD, Dennis GJ, Roebuck J, Harley JB, James JA. Early events in lupus humoral autoimmunity suggest initiation through molecular mimicry. Nat Med 2005;11(1):85–9. doi: 10.1038/nm1167.

[44] Yadav P, Tran H, Ebegbe R, Gottlieb P, Wei H, Lewis RH, et al. Antibodies elicited in response to EBNA-1 may cross-react with dsDNA. PLoS One 2011;6 (1):e14488. doi: 10.1371/journal.pone.0014488.

Ann Rheum Dis 85 (2026) 1761–1773

Contents lists available at ScienceDirect

Annals of the Rheumatic Diseases

journal homepage: https://www.sciencedirect.com/journal/annals-of-the-rheumatic-diseases

Systemic lupus erythematosus

CNS immune remodelling in SLE associated with anti-CD19 CAR-T therapy

Jinjian Sun[1,2,3,4], Xiaoru Hu[1,2,3], Weina Li[1,2], Zuge Tian[5], Shouli Xiao[1,2], Wanhan Li[1,2], Cuiwei Xie[6], Peng Xia[6], Zhen Xia[6], Xiang Chen[7,*], Hui Luo[1,2,3,*], Hongjun Zhao[1,2,3,*], Yuzi Tian[1,2,3,*]

[1] *Department of Rheumatology, Xiangya Hospital, Central South University, Changsha, Hunan, China*
[2] *Provincial Clinical Research Center for Rheumatic and Immunologic Diseases, Xiangya Hospital, Central South University, Changsha, Hunan, China*
[3] *National Clinical Research Center for Geriatric Disease, Xiangya Hospital, Central South University, Changsha, Hunan, China*
[4] *Department of General &Vascular Surgery, Xiangya Hospital, Central South University, Changsha, Hunan, China*
[5] *Department of Bioinformatics, Hunan Agricultural University, Changsha, Hunan, China*
[6] *JW Therapeutics (Shanghai) Co Ltd, Shanghai, China*
[7] *Department of Dermatology, Xiangya Hospital, Central South University, Changsha, Hunan, China*

ARTICLE INFO

Article history:
Received 23 October 2025
Received in revised form 26 June 2026
Accepted 26 June 2026

ABSTRACT

Objectives: Autologous anti-CD19 chimeric antigen receptor T-cell (CAR-T) therapy shows promise for refractory systemic lupus erythematosus (SLE), but its impact on central nervous system (CNS) immune remodelling and the cellular features associated with CAR-T–associated neurotoxicity remains unclear.

Methods: We performed integrated single-cell RNA/T-cell receptor (TCR) sequencing and Olink proteomics on cerebrospinal fluid (CSF) from patients with SLE treated longitudinally with CAR-T therapy (baseline n = 2, D9 n = 4, D60 n = 5), plus independent baseline single-cell RNA sequencing (n = 2) and Olink samples (n = 3).

Results: Single-cell profiling of 47,222 CSF cells showed dynamic CNS immune composition following CAR-T therapy, with notable changes in T cells. CAR-T cells were detected in the CNS and displayed predominantly proliferative and cytotoxic states at D9, whereas memory- and exhaustion-associated states predominated at D60. Endogenous $CD8^+$ T cells exhibited diverse effector subsets at day 9, including granzyme B $(GZMB)^+$, natural killer–like, type I interferon (IFN)–responsive, and human leukocyte antigen $(HLA)^+$ granzyme H $(GZMH)^+$ populations, followed by predominance of memory and proliferating subsets at day 60. $CD4^+$ T cells at day 9 were enriched for type I IFN signalling. Ligand–receptor analysis showed extensive interactions between myeloid populations and lymphocytes. TCR analysis showed changes in clonal diversity and dynamics following treatment.

Conclusions: These findings suggest an association between CAR-T therapy and CNS immune remodelling in SLE, and provide cellular and molecular observations that may inform future studies of CNS immunity.

*Correspondence to Drs Yuzi Tian, Hongjun Zhao, Hui Luo, and Xiang Chen.
E-mail addresses: chenxiangck@csu.edu.cn (X. Chen), Luohui@csu.edu.cn (H. Luo), hongjunzhao2015@sina.com (H. Zhao), yuzit@csu.edu.cn (Y. Tian).
Handling editor Josef Smolen

https://doi.org/10.1016/j.ard.2026.06.030

0003-4967/© 2026 European Alliance of Associations for Rheumatology (EULAR). Published by Elsevier B.V. All rights are reserved, including those for text and data mining, AI training, and similar technologies.

WHAT IS ALREADY KNOWN ON THIS TOPIC

- Autologous anti-CD19 chimeric antigen receptor T-cell (CAR-T) therapy is effective in refractory systemic lupus erythematosus (SLE), associated with rapidly depleting B cells and improving clinical outcomes.
- CAR-T therapy can cause neurotoxicity (NT), but central nervous system (CNS) immune changes related to NT remain poorly understood.

WHAT THIS STUDY ADDS

- Infused CAR-T cells were detected in the CNS and show dynamic transcriptional states, ranging from proliferative and cytotoxic to memory and exhausted-associated states.
- Endogenous CNS immune cells, particularly $CD8^+$ and $CD4^+$ T cells, exhibited functional changes following CAR-T therapy.
- In 1 patient with CAR-T–related NT, the CNS immune profile showed enrichment of effector CAR-T cells, natural killer–like $CD8^+$ T cells, and elevated inflammatory mediators.

HOW THIS STUDY MIGHT AFFECT RESEARCH, PRACTICE OR POLICY

- Provides insight into the cellular and molecular dynamics of CNS immunity following CAR-T therapy in SLE.
- Describes immune features potentially associated with immune effector cell–associated neurotoxicity syndrome in SLE, which may inform monitoring and potential interventions.

INTRODUCTION

Systemic lupus erythematosus (SLE) is a chronic, multisystem autoimmune disease, characterised by widespread immune dysregulation, production of pathogenic autoantibodies, and progressive multiorgan damage [1]. B cells are central players in SLE pathogenesis, and therapeutic strategies have therefore focused on B cell–directed interventions. Although monoclonal antibodies such as anti-CD20 showed efficacy in subsets of patients, responses are often incomplete, and relapses remain common, reflecting insufficient or transient depletion of autoreactive B cells [2,3].

Chimeric antigen receptor (CAR) T-cell therapy targeting CD19 has revolutionised the treatment of B cell malignancies, achieving durable remissions even in refractory disease [4]. Recently, pioneering clinical studies have extended this approach to autoimmunity, where CD19 CAR-T cells have shown the capacity to rapidly eliminate pathogenic B cells in both circulation and deep tissues, thereby inducing sustained, drug-free remission in refractory SLE [5–10]. These findings suggest that CAR-T therapy may achieve a durable reset of immune tolerance—an outcome that prior B cell–directed interventions could not accomplish.

Beyond its therapeutic promise, CAR-T therapy is known to induce profound shifts in systemic immunity [11]. This raises a critical but underexplored question: how do such systemic perturbations extend to the central nervous system (CNS)—an immune-privileged site with unique homeostatic constraints and frequent involvement in lupus pathogenesis [12,13]? In SLE, neuropsychiatric syndromes and subclinical immune alterations in cerebrospinal fluid (CSF) are well recognised and closely linked to B cell–mediated pathology [14], yet the CNS immune landscape during CAR-T therapy remains largely undefined. Key gaps include whether CAR-T cells traffic into the CNS in patients with SLE, how they integrate with or remodel resident immune populations, and to what extent these dynamics contribute not only to therapeutic benefit but also to immune effector cell–associated neurotoxicity syndrome (ICANS), a major safety concern in CAR-T recipients.

METHODS

Please refer to the Supplementary Methods section.

RESULTS

Clinical improvement and single-cell profiling of CNS immune dynamics in patients with SLE treated with anti-CD19 CAR-T cells

Five patients with refractory SLE without neuropsychiatric involvement received autologous anti-CD19 CAR-T cell therapy, with baseline characteristics summarised in Supplementary Table S1. CAR-T cells became detectable in peripheral blood as early as day 4 postinfusion, peaked around day 8, and declined to near-baseline levels by approximately day 22. Efficient B cell depletion was achieved, with peripheral B cells reduced to minimal levels by day 1 and beginning to recover around day 60 to 90 (Supplementary Fig S1A,B).

Four of the 5 patients reached or temporarily reached SLE responder index-4 (SRI-4) within 60 days, and all 5 reached SRI-4 by day 180, with 2 patients attaining lupus low disease activity state (LLDAS) during the 180-day follow-up (Supplementary Fig S1C), indicating an overall favourable clinical response. Consistently, disease activity scores, including the Systemic Lupus Erythematosus Disease Activity Index 2000 (SLEDAI-2K), Physician Global Assessment (PGA), and British Isles Lupus Assessment Group (BILAG), decreased substantially in all patients, although occasional flares were observed (Supplementary Fig S1D). This clinical improvement was accompanied by amelioration of autoimmune serological markers, with broad reductions in anti-dsDNA, antinuclear, and antihistone antibody (Supplementary Fig S1E). In parallel, hypocomplementaemia resolved, with serum C3 and C4 levels returning to the normal range within 2 months and remaining stable through month 6 (Supplementary Fig S1F).

To explore CNS immune states in response to anti-CD19 CAR-T therapy in patients with SLE, single-cell RNA sequencing was performed on CSF samples collected at baseline before lymphodepletion and CAR-T infusion (D0: P4-P5) to represent patient-specific pretreatment states, at the peak of CAR-T cell expansion (D9: P2-P5), and at an early posttreatment timepoint corresponding to clinical improvement (D60: P1-P5) (Fig 1A). Because baseline CSF was not obtained from P1 to P3, 2 additional independent patients with refractory SLE and comparable clinical characteristics (C1-C2) were included to provide additional baseline reference; an additional control (C3) was included for Olink only (Supplementary Table S1; specific sample details in Supplementary Methods). In total, 47,222 CSF cells were profiled, including 1610 cells at D0, 33,712 cells at D9, and 11,900 cells at D60. CSF-derived cells were categorised into 10 major immune clusters: neutrophils, $CD8^+$ T cells, $CD4^+$ T cells, natural killer (NK) cells, $CD4^+CD8^+$ T cells, plasmacytoid dendritic cells, CNS-associated macrophages, type 2 conventional dendritic cells (cDC2), monocytes, and a type 1 conventional dendritic cell (cDC1) cluster (Fig 1B and Supplementary Fig S2A). Among these, T cells accounted for the majority of infiltrating immune cells, whereas monocytes, CNS-associated macrophages, and cDC2 represented the predominant myeloid populations (Fig 1C).

At baseline, CNS-associated macrophages were the most abundant population (26.6% [IQR, 16.7%-31.5%]), followed by $CD4^+$ T cells (19.1% [IQR, 15.4%-24.6%]) and

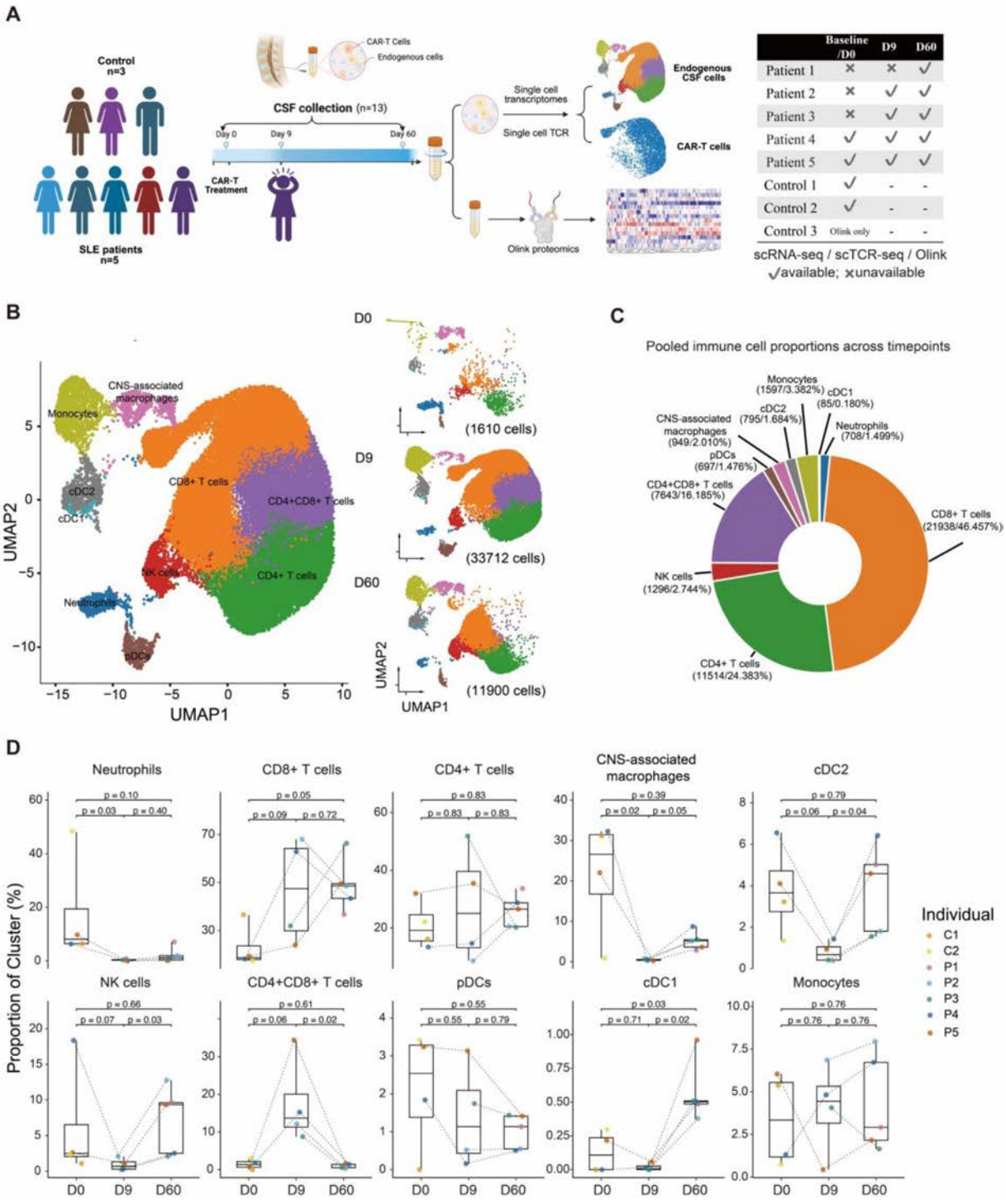

Figure 1. Single-cell transcriptomics of CSF captures temporal changes in immune cell composition in patients with SLE treated with CAR-T therapy. (A) Schematic overview of the study design and sample inclusion table. (B) UMAP plots illustrating CSF immune cell clusters across all samples (left) and stratified by timepoint (D0, D9, D60, right). (C) Donut plots showing immune cell proportions (pooled across all timepoints) for CSF clusters. (D) Boxplots quantifying changes in CSF immune cell frequencies across timepoints. Boxplots represent the median (centre line), IQR (box bounds), and whiskers extending to the minimum and maximum values. Statistical significance indicated in the figure was determined using post hoc Dunn's test with Benjamini–Hochberg correction applied within each cell subset (unpaired; paired test limited by small n and incomplete sampling). Raw *P* values and globally adjusted *P* values are provided in Supplementary Figure S2E for transparency. CAR-T therapy, chimeric antigen receptor T-cell therapy; cDC, conventional dendritic cell; CNS, central nervous system; CSF, cerebrospinal fluid; pDC, plasmacytoid dendritic cell; scRNA-seq, single-cell RNA sequencing; scTCR-seq, single-cell T-cell receptor sequencing; SLE, systemic lupus erythematosus; TCR, T-cell receptor, NK cells, natural killer cells; UMAP, uniform manifold approximation and projection.

CD8⁺ T cells (18.7% [IQR, 18.0%-23.6%]). By day 9, CSF immune cell composition differed from baseline, with T cells accounting for nearly 93% of total CSF immune cells. Among these, CD8⁺ T cells represented 47.4% (IQR, 29.9%-64.2%) of total CSF immune cells, with a nonsignificant trend towards higher frequencies compared with D0 (P = .09). Neutrophils and CNS-associated macrophages showed significantly lower relative proportions at day 9,

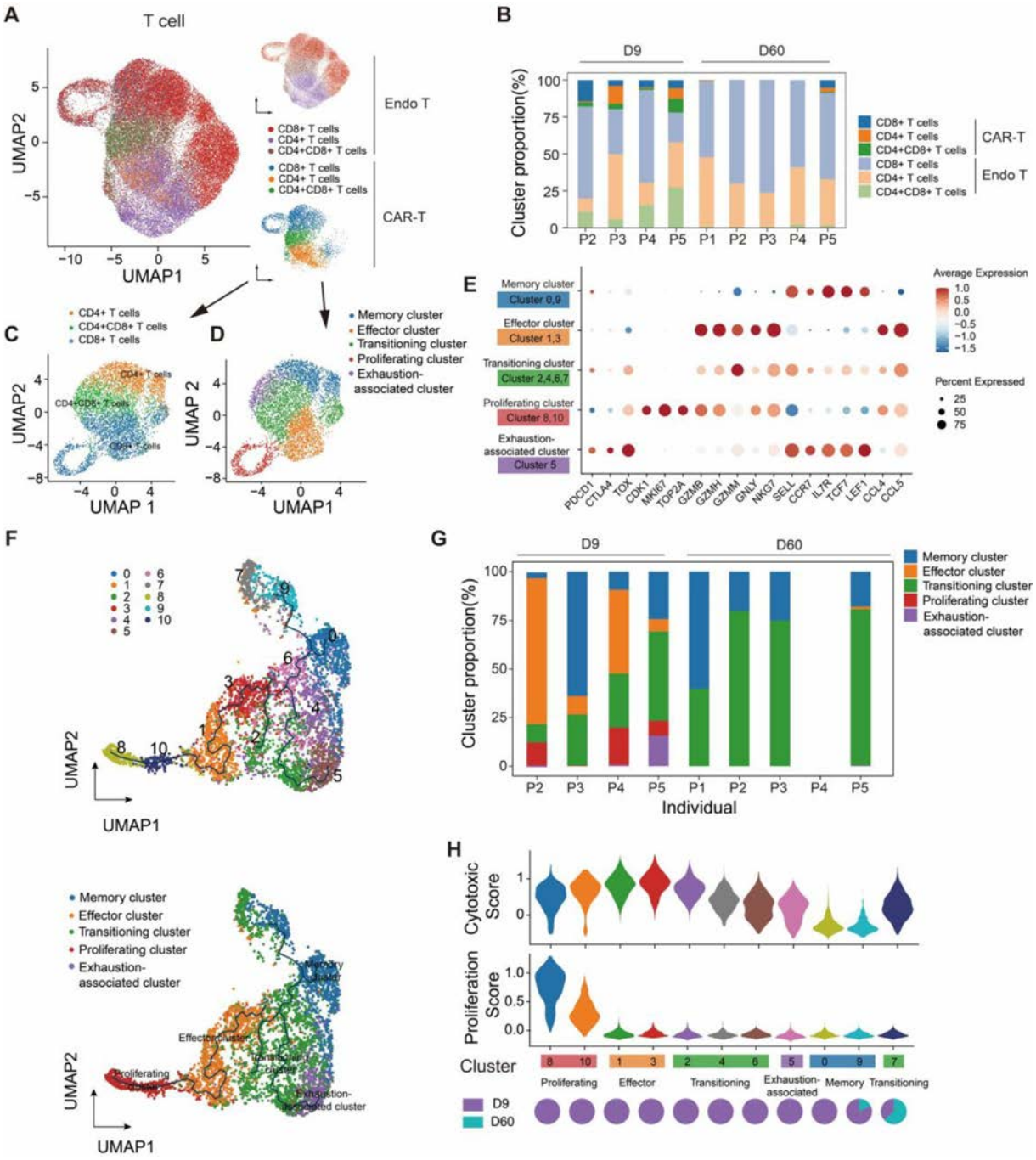

Figure 2. Transcriptional states of CAR-T cells in CSF of patients with SLE after CAR-T treatment. (A) UMAP visualisation of T-cell subsets in CSF, including both endogenous T and CAR-T cells. The top-right and the bottom-right UMAP panels depict the subset composition of endogenous T cells (endo T) and CAR-T cells, respectively. (B) Proportional distribution of T-cell clusters for endogenous T and CAR-T cells across timepoints. (C) UMAP visualisation of CAR-T cells, coloured by $CD4^+$, $CD8^+$, and $CD4^+CD8^+$ subsets. (D) UMAP visualisation of CAR-T functional states defined by gene signatures. (E) Dot plot showing expression of representative functional markers across CAR-T clusters. (F) The transcriptional state map of CAR-T cells inferred by Monocle3. Upper: distribution of unsupervised CAR-T clusters across the transcriptional continuum. Lower: distribution of functional clusters along the continuum of transcriptional states. (G) Proportions of CAR-T clusters across patients at different timepoints. (H) Violin plots showing cytotoxicity and proliferation score across CAR-T clusters. Pie chart below depicts the proportion of cells from D9 and D60 in each cluster. CAR-T therapy, chimeric antigen receptor T-cell therapy; CSF, cerebrospinal fluid; SLE, systemic lupus erythematosus; UMAP, uniform manifold approximation and projection.

whereas $CD4^+$ T cells and monocytes did not exhibit notable changes. By day 60, $CD8^+$ T (48.6% [IQR, 43.4%-49.5%]) and $CD4^+$ T cells (26.5% [IQR, 20.5%-28.7%]) continued to present major components of the CSF immune populations, with no significant changes from day 9. In contrast, several other populations, including cDC2, NK cells, and cDC1, showed significant increases relative to day 9 (Fig 1D and Supplementary Fig S2B-D).

Heterogeneous transcriptional states of CAR-T cells in the CSF following CAR-T therapy

To delineate the nature of CAR-T cells in the CNS after infusion, we isolated all T cells from CSF samples and distinguished infused CAR-T cells from endogenous T cells by mapping sequencing reads to the unique CAR transgene (Fig 2A). At day 9, the majority of T cells detected in CSF were endogenous

(84%), whereas ~16% were identified as CAR-T cells. By day 60, only a small fraction of CAR-T cells (3%) remained detectable in the CSF (Fig 2B). This observation may reflect the low frequency of CAR-T cells in the CSF at later timepoints, though reduced detectability due to transgene downregulation in memory CAR-T cells cannot be excluded.

Uniform manifold approximation and projections (UMAP) showed that CAR-T cells largely overlapped with endogenous T cells, with similar CD4+/CD8+/CD4+CD8+ distributions (Fig 2B,C, Supplementary Fig S3A,B). Subclustering analysis restricted to CAR-T cells identified 11 subclusters (0-10) (Supplementary Fig S3C-E), which were grouped into 5 functional states based on transcriptional signatures: (1) exhaustion-associated cluster (cluster 5): enriched for exhaustion markers (*PDCD1*, *CTLA4*, and *TOX*) and coexpressing memory-associated genes (*SELL*, *CCR7*, *IL7R*, *TCF7*, and *LEF1*); (2) proliferating clusters (clusters 8, 10): expressing cell cycle genes (CDK1, MKI67, and TOP2A); (3) effector clusters (clusters 1, 3): high levels of cytotoxic effectors (*GZMB*, *GZMH*, *GZMM*, *GNLY*, *NKG7*); (4) transitioning clusters (clusters 2, 4, 6, 7): hybrid populations coexpressing cytotoxic, exhaustion, and/or memory markers; (5) memory clusters (clusters 0, 9): enriched for memory markers (Fig 2D,E).

To further delineate the transcriptional organisation of CAR-T cells in CSF, we used Monocle3 to construct a transcriptional state map (Fig 2F). The analysis showed an ordered arrangement of transcriptional states, beginning with proliferating clusters (clusters 8 and 10), followed by cytotoxic effector clusters (clusters 1 and 3), and then separating into 3 state branches: (1) a transitional pathway (cluster 2) coexpressing cytotoxic and exhaustion markers; (2) an exhaustion trajectory, passing through the transitioning cluster and culminating in a exhaustion-associated cluster (cluster 5); and (3) a memory differentiation pathway (clusters 0 and 9). Notably, T-cell receptor (TCR) tracking revealed no shared clonotypes between D9 and D60 CAR-T cells in the CSF, although clonotype overlap was observed within D9 across different clusters (eg, proliferative and memory states) (Supplementary Fig S3F). These observations indicate that CAR-T cells in the CSF adopt distinct transcriptional states organised by transcriptional similarity, potentially reflecting population-level dynamics rather than direct clonal lineage progression.

CAR-T cell states in the CSF varied among patients. At D9, patients 2 and 4 were dominated by effector clusters, patient 5 showed enrichment of transitioning clusters, and patient 3 was characterised by a large proportion of memory clusters (Fig 2G). Clinically, patients 2 and 4 achieved relatively rapid and sustained responses, as shown by SRI-4 and LLDAS, compared with patients 3 and 5 (Supplementary Fig S3G). This interpatient variation suggests that CNS-infiltrating CAR-T cells exhibit a shared transcriptional state organisation with variable distributions across patients. We cautiously interpret that high effector-dominant CAR-T cells may be associated with strong early immune activation, and the relative balance between effector and memory states could potentially influence the therapeutic efficacy. However, these observations are exploratory and require validation.

By D60, only a small fraction of CAR-T cells were detected in the CSF, predominantly comprising a transitioning population coexpressing effector and memory programmes alongside a memory cluster (Fig 2G).

Proliferation and cytotoxicity are key hallmarks of CAR-T functionality. Module scoring showed that proliferative capacity declined steadily, whereas cytotoxicity peaked at the effector stage before declining along either exhaustion- or memory-associated states. Consistent with this transcriptional state map, proliferative, effector, and transitional/exhausted populations were enriched at D9, coinciding with peak expansion, whereas D60 samples were dominated by memory-associated CAR-T cells (Fig 2H).

Aside from their intrinsic developmental dynamics, CAR-T cells within the CSF also displayed extensive cellular crosstalk with the surrounding immune landscape. Cell−cell communication analysis revealed that CAR-T cells engaged in broad ligand−receptor interactions with multiple CNS endogenous immune populations, including $CD8^+$ T cells (Supplementary Fig S4A,B).

Characterisation of $CD8^+$ T-cell subsets in the CNS following CAR-T therapy

T cells were the predominant population in the CSF after CAR-T therapy, and unsupervised clustering of endogenous $CD8^+$ T cells identified 6 distinct subsets (Fig 3A and Supplementary Fig S5A). At baseline and at D60, central memory $CD8^+$ T cells ($CD8^+$ TCM)—defined by high expression of *IL7R*, *TCF7*, *KLF3*, and *CXCR4*—were the predominant subset (Fig 3B), accounting for 85.1% (IQR, 76.0%-90.2%) of $CD8^+$ T cells at D0 and accounting for 98.1% (IQR, 97.1%-99.0%) by D60. At D0, another major subset comprised proliferating $CD8^+$ T cells (11.3% [IQR, 4.3%-23.5%]), characterised by elevated *MKI67*, *CDK1*, and *TOP2A* expression, consistent with active cell cycling and heightened immune activation during the pretreatment disease state (Fig 3B,C, Supplementary Fig S5A-C). Notably, the relatively low number of $CD8^+$ T cells at these 2 timepoints may also have limited the identification of additional subsets.

The 4 effector $CD8^+$ T-cell subsets were mainly enriched at D9. Among them, a type I interferon (IFN)−responsive $CD8^+$ T-cell subset exhibited interferon-stimulated signatures (*IFI44L*, *RSAD2*, *ISG15*, and *IFI44*) with moderate *TOX* and *LAG3* expression, potentially reflecting type I IFN pathway activity implicated in SLE pathogenesis. A second NK-like $CD8^+$ T-cell subset expressed NK-associated receptors (*KLRD1*, *KLRC1*, and *KLRC2*) together with cytotoxic mediators (*GZMK*, *GNLY*, and *PRF1*), consistent with the possibility that $CD8^+$ T cells acquired innate-like properties along a continuum bridging adaptive and innate immunity. Both subsets showed an increase at D9 compared with D0 ($P = .05$), followed by a decrease at D60 ($P = .02$ and .05, respectively). A third granzyme B (GZMB)$^+$ effector subset, expressing high levels of cytotoxic genes (*GZMB*, *PRF1*, and *GNLY*) along with inhibitory markers such as LAG3, likely representing terminally differentiated cytotoxic T cells, showed a similar trend that did not reach statistical significance ($P = .17$). A fourth human leukocyte antigen $(HLA)^+$ granzyme H $(GZMH)^+$ effector population, coexpressing PDCD1 and major histocompatibility complex (MHC) class II molecules (*HLA-DPA1*, *HLA-DRB5*, and *HLA-DQA1*), also showed nonsignificant increase at D9 vs D0 ($P = 0.07$), but with no significant difference between D9 and D60 (Fig 3B,C, Supplementary Fig S5B,C).

Pathway enrichment analysis further supported these functional annotations: $GZMB^+$ cells were enriched for cytotoxicity and apoptosis pathways; NK-like $CD8^+$ cells for NK-mediated cytotoxicity; type I IFN−responsive $CD8^+$ T cells for interferon and antiviral response pathways; and HLA^+ $GZMH^+$ cells for antigen processing (Supplementary Fig S5D).

Notably, CSF $CD8^+$ T cells composition varied across patients, with patients 2 and 4 showing the high proportions, mainly composed of cytotoxic/effector subsets, whereas patients 3 and 5 exhibited relatively low proportions, predominantly central memory or type I IFN−responsive subsets. These patterns were

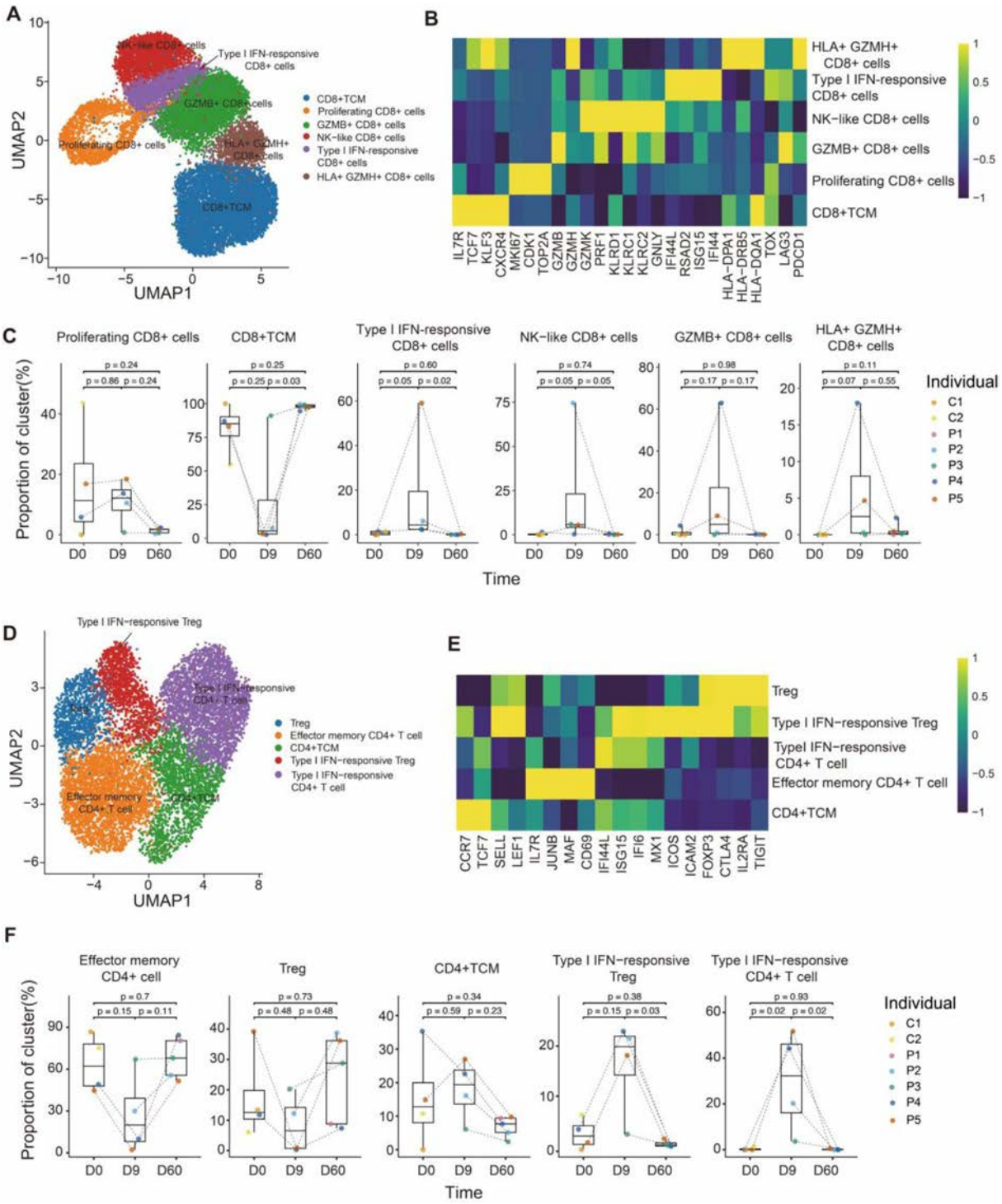

Figure 3. Diversity and functional states of endogenous CD8⁺ and CD4⁺ T cells after CAR-T treatment. (A) UMAP projection of 6 endogenous CD8⁺ T-cell subclusters in CSF. (B) Heatmap showing the average expression of representative marker genes across CD8⁺ T-cell subclusters. (C) Boxplots showing the proportion of each CD8 + T-cell subcluster across different timepoints. (D) UMAP projection of 5 endogenous CD4⁺ T-cell subclusters in CSF. (E) Heatmap of representative marker gene expression for each CD4⁺ T-cell subcluster. (F) Boxplots showing the proportion of each CD4⁺ T-cell subcluster across timepoints. Boxplots represent the median (centre line), IQR (box bounds), and whiskers extending to the minimum and maximum values. Statistical significance indicated in the figure was determined using post hoc Dunn's test with Benjamini–Hochberg correction applied within each cell subset (unpaired; paired test limited by small n and incomplete sampling). Raw *P* values and globally adjusted *P* values are provided in Supplementary Figures S5C and S6C for transparency. CAR-T therapy, chimeric antigen receptor T-cell therapy; CSF, cerebrospinal fluid; IFN, interferon; NK, natural killer; GZMB, granzyme B; GZMH, granzyme H; HLA, human leukocyte antigen; TCM, central memory T cells; UMAP, uniform manifold approximation and projection.

observed alongside heterogeneity observed in CAR-T cell states and clinical responses. Future studies may investigate whether the magnitude and functional polarisation of endogenous CD8⁺ T-cell responses are associated with CNS immune modulation or therapeutic efficacy (Supplementary Fig S5E,F).

Type I IFN–associated CD4⁺ T cells in CNS following CAR-T therapy

CD4⁺ T cells were classified into 5 subsets by gene and pathway signatures. At baseline, the compartment comprised

predominantly effector memory CD4+ T cells (62.1% [IQR, 47.9%-78.0%]) (CD4+ TEM; *IL7R*, *JUNB*, *MAF*, and *CD69*), regulatory T cells (12.5% [IQR, 10.3%-19.8%]) (Treg; *FOXP3*, *CTLA4*, *IL2RA*, and *TIGIT*), and central memory T cells (12.8% [IQR, 8.1%-20.0%]) (CD4+ TCM; *CCR7*, *TCF7*, and *SELL*) (Fig 3D−F and Supplementary Fig S6A−C).

Two type I IFN−associated CD4+ subsets were mainly enriched at D9. One subset (type I IFN−responsive Treg) (20.0% [IQR, 14.4%-21.9%]) exhibited a Treg-like phenotype but simultaneously expressed IFN-stimulated genes (*IFI44L*, *ISG15*, *IFI6*, and *MX1*) together with activation/adhesion markers (*ICOS*, *ICAM2*, *SELL*, and *LEF1*). This subset showed an upwards trend from D0 to D9 that did not reach statistical significance ($P = .15$), followed by a significant decrease from D9 to D60. Pathway analysis revealed nuclear factor kappa-light-chain-enhancer of activated B cells (NF-κB) activation and inflammatory responsiveness, suggesting a reprogrammed regulatory population potentially capable of modulating CNS immune tone in a type I IFN−mediated manner. A second subset displayed a more restricted transcriptional programme, defined primarily by type I IFN signatures (type I IFN−responsive CD4+ T) (32.3% [IQR, 16.1%-46.1%]), which showed a significant increase at D9 compared with D0 and a significant decrease at D60. Pathway analysis exhibited genes consistent with acute IFN signalling (Fig 3E, F and Supplementary Fig S6A-E).

Single-cell TCR sequencing of endogenous T cells following CAR-T therapy

To examine endogenous T-cell dynamics after CAR-T infusion, we performed paired TCR sequencing across 3 timepoints (Fig 4A and Supplementary Fig S7A,B). T cells sharing an identical TCR sequence with at least 1 other cell was defined as clonal, and clone sizes were categorised as small (2-5 cells), medium (6-20), large (21-100), or hyperexpanded (101-500) [15]. Hyperexpanded, large, and medium clonotypes were more frequent within the CD8+ compartment (Fig 4B). At day 9, the absolute number of clonotypes showed a significant increase compared with day 0, with a nonsignificant decreasing trend at day 60 ($P = .168$) (Fig 4C,D). However, because cell numbers varied substantially across timepoints, absolute clonotype counts are depth sensitive and are therefore presented as descriptive measures only. To address this limitation, we applied rarefaction analysis. Rarefied diversity metrics ($q = 0$, $q = 1$, $q = 2$) were significantly higher at day 9 compared with both day 0 and day 60 (Fig 4E-G and Supplementary Fig S7C), indicating temporal differences in TCR diversity across treatment timepoints. To investigate dynamics at the peak phase, we examined the top 5 expanded clones at D9. In 2 patients (P4 and P5), 1 dominant clone was already detectable at baseline, whereas the remaining clones were not detected at baseline. Importantly, most top D9 clones persisted through D60 in 4 patients, potentially suggesting that expanded clones include both resident CSF-derived T cells and newly recruited clones, some of which may transition into long-lived memory, whereas others are eliminated (Fig 4H). To assess cross-patient clonotype similarity at D60, we used Dandelion to compare CDR3 sequences of T-cell receptor alpha (TRA) and T-cell receptor beta (TRB) chains. We identified a limited number of shared clonotypes—2 between P2 and P3 and 1 between P2 and P1—suggesting modest convergent TCR repertoire remodelling, which may reflect a common autoantigen-associated response (Supplementary Fig S7D,E).

Given the predominance of CD8+ clonal clones, we next analysed the TCR repertoire by subset. At D0, small clonal clusters were mainly detected in TCM and proliferating CD8+ subsets. By D9, although 4 effector CD8+ populations were transcriptionally defined, clonal amplification was largely restricted to the HLA+ GZMH+ subset. By D60, clonal proliferation was concentrated within the TCM compartment, spanning from small clones to hyperexpanded ones. This pattern is consistent with the possibility of durable CNS-resident memory establishment following CAR-T−mediated immune remodelling (Fig 4I,J).

Functional features of CSF myeloid subsets and their interactions with T cells after CAR-T therapy

Although myeloid cells constitute a minor CSF population, their antigen presentation and cytokine activity are involved in T-cell−mediated immunity. Among the top 3 subsets—monocytes, CNS-associated macrophages, and cDC2s—each plays a distinct role in CNS immunity. CNS-associated macrophages, phenotypically resembling CNS-resident microglia, were uniquely enriched in the CSF and implicated in local antigen presentation and immune regulation [16,17]. By contrast, cDC2s involved in CD4+ T-cell priming and adaptive immune responses [18].

To investigate the functional states of CSF myeloid subsets across timepoints, we performed pathway enrichment analyses. In pseudobulk analysis, at day 9 relative to day 60, monocytes, CNS-associated macrophages, and cDC2s were enriched for pathways related to cytokine signalling, antiviral responses, innate immunity, and metabolic reprogramming. Potentially given the limited myeloid cell numbers, baseline heterogeneity, and small cohort size, relatively few genes showed notable differences (gene list provided in Supplemental Source Data Table), and no clear pathway enrichment was observed between D0 and D9 (Fig 5A,B).

Ligand−receptor interaction analysis at day 9 showed interactions between myeloid cells and lymphocytes. Monocytes exhibited a high number of outgoing interactions, but their average interaction weights were lower than those of T cells, although notable interactions with CD8+ T cells remained (Fig 5C,D and Supplementary Fig S8A-D). Analysis of specific ligand−receptor pairs highlighted several examples, such as MHC class I− and II−dependent signalling with CD8+ and CD4+ T cells, which is consistent with a role in local antigen presentation and T-cell activation in the CNS during the early phase after CAR-T therapy (Supplementary Fig S9A-C), and CXCL16−CXCR6 interactions with CD8+ cells, which may be relevant to T-cell trafficking, positioning, and retention in the CNS following CAR-T therapy (Fig 5E,F and Supplementary Fig S9D). However, the CellChat data are descriptive and do not imply causal interactions. Further functional studies are needed to confirm these interactions.

Exploratory analysis of immune features in a patient with neurotoxicity following CAR-T therapy

Among the 5 enrolled patients, 1 individual (P2) developed neurotoxicity (NT) following CAR-T infusion. On day 7, the patient presented with acute neurological symptoms, including confusion, disorientation, language impairment, and muscle spasms, consistent with CAR-T−associated NT [19] (ICANS grade 2, Immune Effector Cell Encephalopathy (ICE) score 4). The patient was treated promptly with tocilizumab, phenobarbital sodium, and levetiracetam, and neurological symptoms resolved by day 10 (Fig 6A).

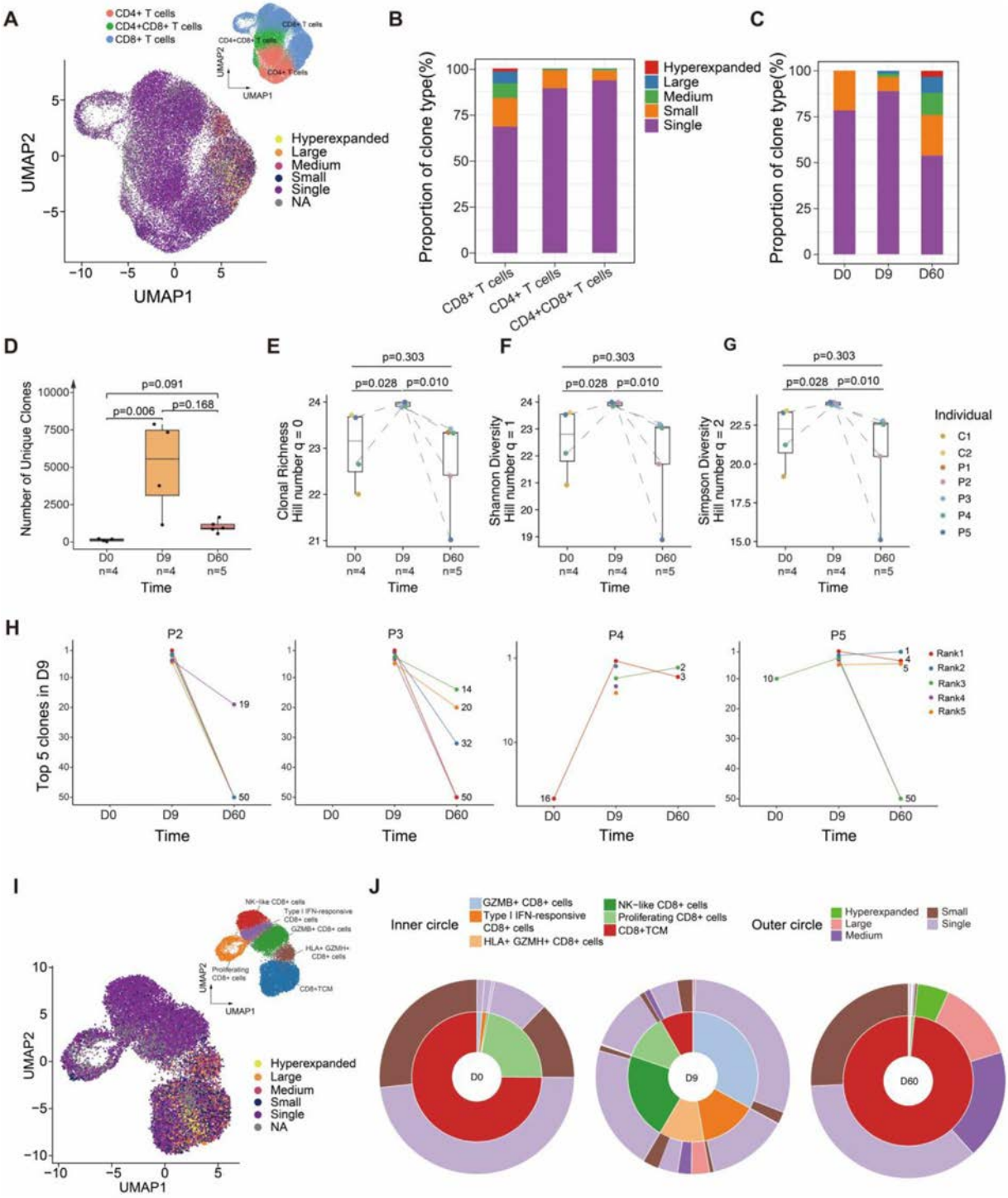

Figure 4. TCR analysis of endogenous T cells after CAR-T treatment. (A) UMAP projection of endogenous T-cell clonality based on paired TCR sequencing. (B) Barplot depicting the proportion of clone sizes within each T-cell cluster. (C) Barplot showing the proportion of clone sizes across timepoints. (D) Boxplot showing the number of unique clones in endogenous T cells across timepoints. (E-G) Hill numbers (q = 0 for clonal richness, q = 1 for Shannon diversity, q = 2 for Simpson diversity) were calculated per patient at a standardised subsampling depth. Individual patient values are shown in panels. (H) Rank dynamics of the top 5 clones at D9 across the full repertoire. Clone ranks are shown at each timepoint. P2 and P3 were analysed at D9 and D60 only; P4 and P5 include all 3 timepoints. (I) UMAP projection of endogenous $CD8^+$ T-cell clonality based on TCR sequencing. (J) Multilevel donut chart depicting the composition of $CD8^+$ T-cell subclusters (inner ring) and the distribution of TCR clone sizes within each subcluster (outer ring) across timepoints. Boxplots depict the median (centre line), IQR (box bounds), and whiskers extending to the minimum and maximum values for (D-G). Statistical significance was determined using post hoc Dunn's test with Benjamini–Hochberg correction for panels (D-G) (unpaired; paired test limited by small n and incomplete sampling). CAR-T therapy, chimeric antigen receptor T-cell therapy; IFN, interferon; NK, natural killer. NA : not applicable.

To illustrate the potential immune features associated with NT in this single case, we conducted an exploratory observation comparing the immune profile in the CNS of this patient with that of the other patients. Analysis of CSF samples at day 9, coinciding with NT onset, showed a high proportion of effector CAR-T cells in this patient (Fig 6B). Functional scoring showed elevated cytotoxic signatures in CAR-T cells from this sample (Supplementary Fig S10A), and differential gene expression

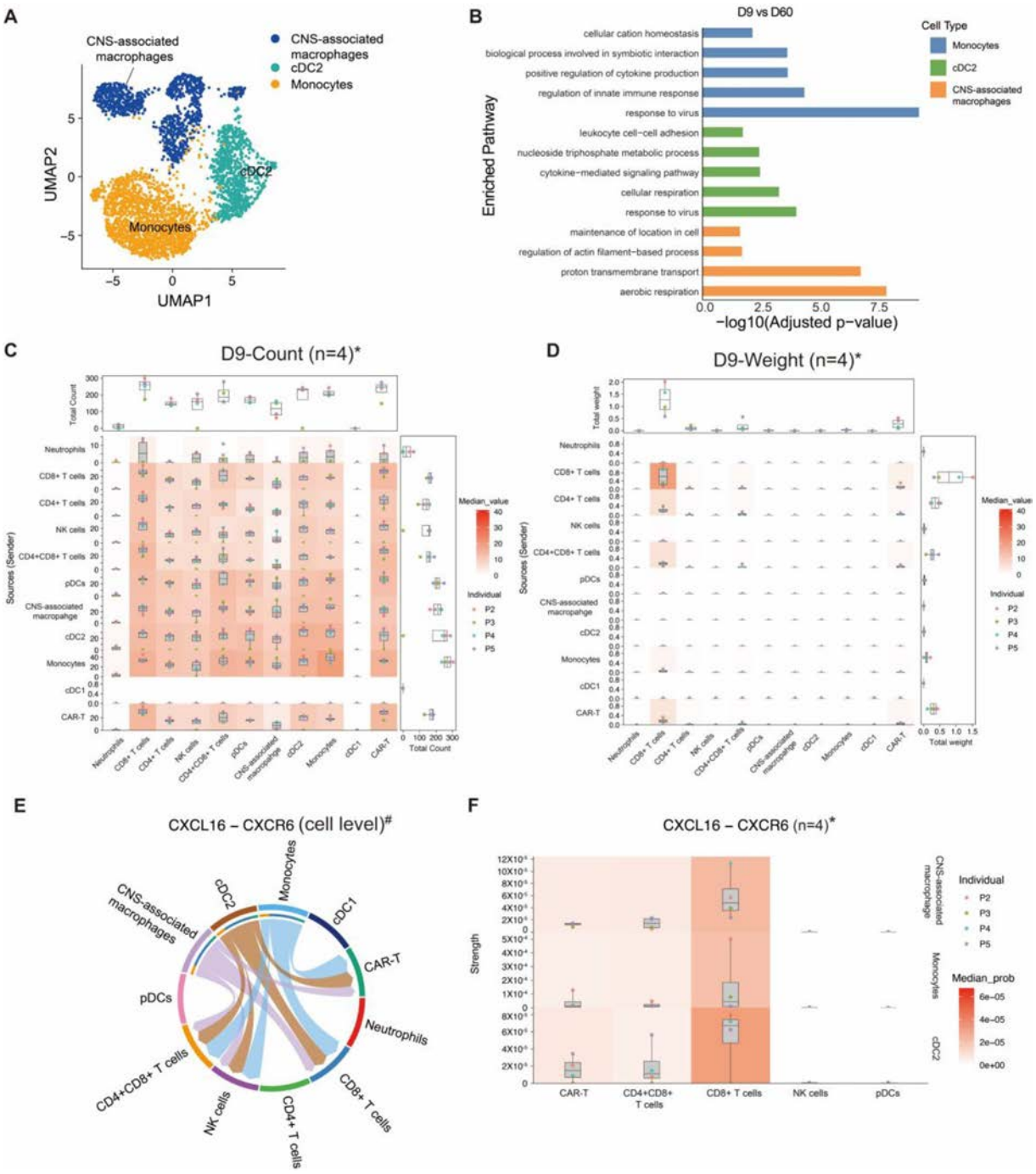

Figure 5. Functional profiling and intercellular communication of CSF myeloid populations after CAR-T therapy. (A) UMAP visualisation of CSF myeloid populations, including monocytes, cDC2, and CNS-associated macrophages. (B) Representative signalling pathways enriched in each myeloid subset, identified by Gene Ontology analysis of DESeq2-based pseudobulk DEGs between D9 and D60. (C-D) Aggregate cell−cell interaction counts (C) and strength (weight) (D) inferred by CellChat across all patients at D9. The heatmap shows the median interaction counts and strength between sender (rows) and receiver (columns) cell types, with boxplots summarising total outgoing and incoming interaction counts and weight per cell type. Points represent individual patients, n = 4. (E) Chord diagram illustrating CXCL16−CXCR6−mediated interactions among CSF cell types at the cell level. Arrow direction indicates the receiving (target) cell population. (F) Heatmap showing median interaction strength of CXCL16−CXCR6 interaction across patients. n = 4. Rows indicate signalling cells, and columns indicate target cells. *(C−D, F): No patient-level inferential statistical tests were applied; the figures are presented as descriptive visualisations only. #Pooled cells from all patients. Descriptive visualisation only; no patient-level statistical inference. CAR-T therapy, chimeric antigen receptor T-cell therapy; cDC2, type 2 conventional dendritic cells; CNS, central nervous system; CSF, cerebrospinal fluid; NK, natural killer; pDC, plasmacytoid dendritic cell; CXCL16, C-X-C motif chemokine ligand 16; CXCR6, C-X-C motif chemokine receptor 6; DEG, differentially expressed genes; NK, natural killer cells; UMAP, uniform manifold approximation and projection.

analysis identified upregulated pathways related to cytokine production, leukocyte-mediated immunity, and lymphocyte-mediated immunity (Supplementary Fig S10B). Consistent with this, effector CAR-T cells displayed relatively high ICANS-associated module scores (Supplementary Fig S10C). The gene set was curated from previously reported serum studies [20] and CSF-related gene programmes [21−26] for exploratory purposes.

Concomitantly, the CSF immune compartment in this sample showed a prominent presence of endogenous CD8⁺ T cells (Fig 6C). Among CD8⁺ subsets, NK-like effector CD8⁺ cells

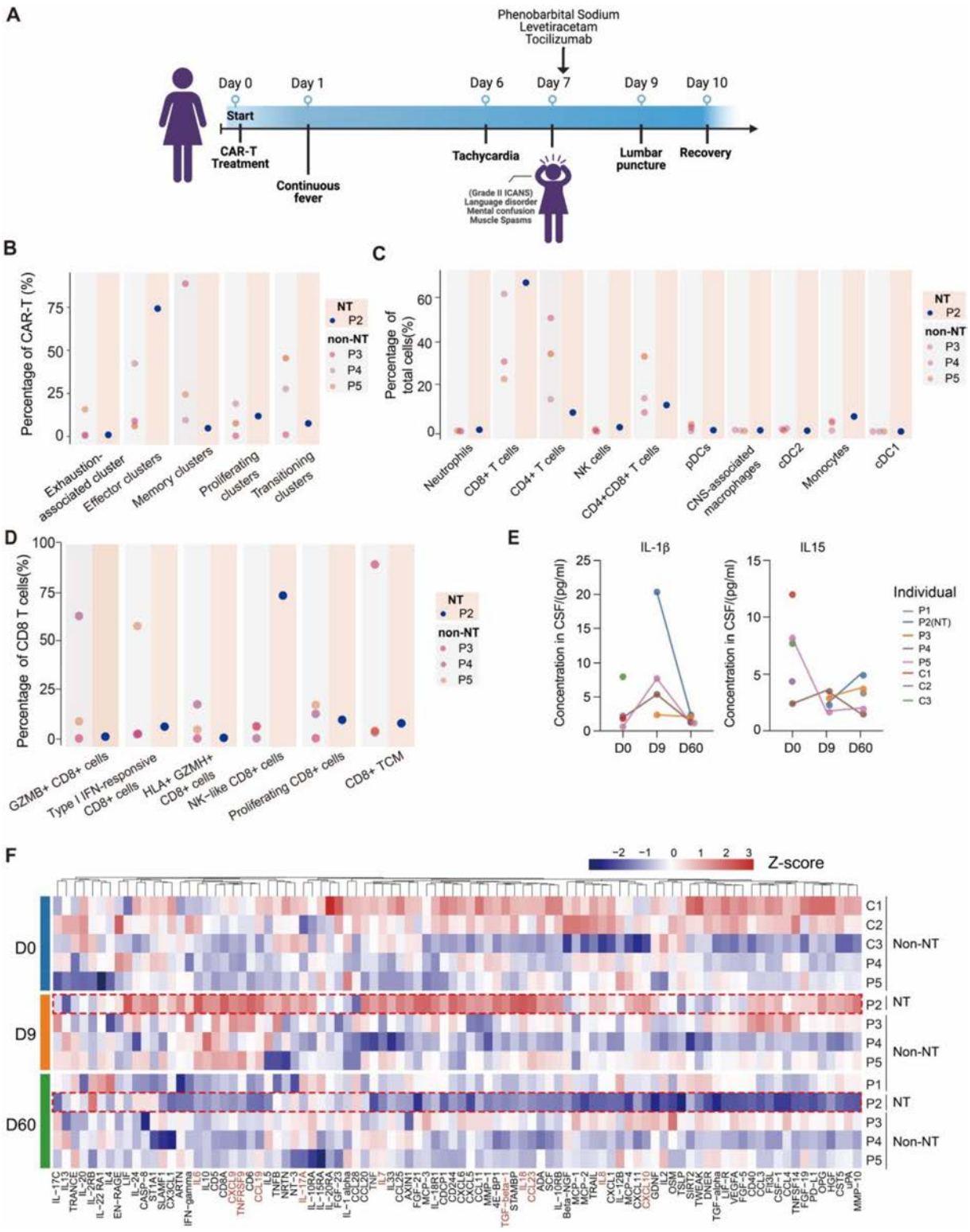

Figure 6. CSF immune features observed in the patient with neurotoxicity following CAR-T therapy. (A) Clinical symptom trajectory of the patient with NT (P2) following CAR-T infusion. (B) Dotplots showing proportions of CAR-T functional clusters in patients with NT (n = 1) and without NT (n = 3). (C-D) Dotplots showing proportions of all CSF cell clusters (C) and CD8$^+$ T subclusters (D) in patients with NT (n = 1) and without NT (n = 3). (E) ELISA measurements of IL-1β and IL-15 protein levels in CSF. (F) Heatmap of inflammatory protein profiles measured by Olink across all patients at D0, D9, and D60, with the patient with NT highlighted in red. Proteins marked in red are representative inflammatory proteins elevated at day 9 in the patient with NT. CAR-T therapy, chimeric antigen receptor T-cell therapy; cDC2, type 2 conventional dendritic cells; CSF, cerebrospinal fluid; ELISA, enzyme-linked immunoassay; ICANS, immune effector cell–associated neurotoxicity syndrome; IFN, interferon; NK, natural killer; NT, neurotoxicity; pDC, plasmacytoid dendritic cell.

represented a substantial fraction and exhibited high ICANS-associated signature scores (Fig 6D and Supplementary Fig S10D). Ligand–receptor analysis revealed that this NK-like population received a high number of incoming signals among all CSF immune subsets (Supplementary Fig S11A), including HLA-dependent antigen presentation from both innate and adaptive immune

cells and chemokine inputs from innate immune cells (Supplementary Fig S11B,C), potentially pointing to a highly activated endogenous CD8$^+$ effector niche in this patient with ICANS.

Given prior evidence implicating blood–brain barrier (BBB) disruption, inflammation, and endothelial injury in NT [27], we examined key genes related to these pathways at single-cell resolution. Although most canonical genes were expressed at relatively low levels, IL1B in cDC2s and IL-15 in monocytes were selectively elevated in the patient with NT at day 9 compared with cases without NT (Supplementary Fig S12). Consistent with this, CSF IL-1β protein levels increased at day 9 and declined by day 60, with high levels observed in patient 2, who developed ICANS. In contrast, despite increased IL-15 transcripts in CSF monocytes, IL-15 protein levels in CSF did not show a consistent temporal pattern or enrichment in the patient with NT (Fig 6E). This may reflect the fact that IL-15 primarily acts via surface presentation through IL-15Rα rather than as a secreted cytokine [28].

To assess broader inflammatory activity, we profiled 96 inflammatory proteins by Olink in CSF samples. The patient with NT exhibited overall higher levels of inflammatory mediators at day 9 (Fig 6F). When all patients were analysed longitudinally, several cytokines and chemokines showed a trend of upregulation at day 9 compared with baseline or day 60, including CCL19, CCL23, CCL3, CXCL9, IFN-γ, IL-1α, IL-10, IL-18, IL-6, MCP-1, and TNFRSF9, alongside T-cell–associated molecules such as CD5, CD6, and CD8A (Fig 6F). Notably, several previously reported proteins potentially linked to ICANS, such as IL-6 and IL-18, showed elevation in P2. Given the single-patient nature of the NT analysis, these observations remain exploratory and warrant validation in larger cohorts.

DISCUSSION

This study provides a longitudinal, multiomics dissection of the CNS immune landscape in patients with refractory SLE undergoing autologous anti-CD19 CAR-T therapy. These findings provide insights into underexplored dimensions of CAR-T biology in autoimmunity, particularly within the CNS, a site of both therapeutic opportunity and vulnerability.

CAR-T sequence tracking enabled precise resolution of CAR-T persistence, phenotypic evolution, and interplay with the endogenous immune compartment in the CNS microenvironment. A subset of infused CAR-T cells was detected in the CSF, potentially reflecting the migratory potential of activated T cells and/or passive entry across a disrupted BBB in SLE [29]. Notably, the detection of CAR-T cells in the CSF at day 60 despite their absence in peripheral blood suggests potential tissue-specific retention or tropism within the CNS microenvironment, a phenomenon also reported in tumour settings where CAR-T persistence differs between tissues and circulation [30]. Within the CNS, CAR-T cells exhibited a proliferative–cytotoxic–dysfunctional/memory transcriptional state organisation, highlighting the CNS as an active niche that may influence CAR-T functional states. Notably, this transcriptional organisation mirrors patterns observed in the peripheral blood of patients with lymphoma [31,32], suggesting a conserved transcriptional pattern across disease settings and tissue compartments. Beyond intrinsic transcriptional states, CAR-T cells engaged in extensive crosstalk with resident immune populations, underscoring local circuits that may sustain or restrain CNS immune dynamics.

An observation was a nonsignificant trend towards an increase of distinct cytotoxic CD8$^+$ effector T-cell subsets within the CSF, including GZMB$^+$ and HLA$^+$GZMH$^+$ populations, which recapitulate cytotoxic programmes previously implicated in peripheral SLE [33,34]. This suggests that CAR-T therapy transiently amplifies disease-relevant effector pathways in the CNS, potentially promoting clearance of autoreactive cells while also imposing a local proinflammatory milieu. Concurrently, during the acute peak phase following CAR-T infusion, we observed an increase in ISG-stimulated T cells, encompassing CD8$^+$ effectors and 2 distinct CD4$^+$ subsets. SLE is a type I IFN–mediated disease. Meanwhile, it is important to note that emerging data suggest CAR-T therapy itself can transiently induce IFN-associated programmes, even in the absence of autoimmune disease [35]. However, recent studies of anti-B-cell maturation antigen (BCMA) CAR-T therapy in neuromyelitis optica spectrum disorder did not observe a dominant IFN signature in CSF T cells, indicating that IFN activation in the CNS is not a universal consequence of CAR-T therapy [36]. Therefore, we propose that the IFN-responsive phenotype observed in our study likely reflects the interaction between CAR-T–induced immune perturbations and a preexisting IFN-biased disease milieu, rather than being a direct or disease-independent effect of CAR-T therapy. Notably, Wilhelm et al [37] reported that CD19 CAR-T therapy suppresses the type I IFN signature in PBMCs from patients with SLE—a discrepancy that may reflect compartment-specific responses or differences in patient populations and sampling timepoints.

The case of 1 patient who developed grade 2 ICANS provides a descriptive view of the neuroimmune consequences of CAR-T therapy in autoimmunity. Although traditional models of ICANS have emphasised endothelial activation and systemic cytokine storm [23,38], our multiomics analysis shows a more layered process in which CAR-T–intrinsic states and endogenous immune dynamics converge. Notably, effector CAR-T cells and cytotoxic/effector CD8$^+$ T cells were present at relatively high proportions in the CSF of the patient with ICANS, suggesting that local infiltration of these cells may contribute to tissue damage and neuroinflammation. Interestingly, patients 2 and 4, who showed relatively high proportions of effector CAR-T cells and cytotoxic endogenous CD8$^+$ T cells, also achieved relatively rapid and sustained clinical responses, potentially suggesting that an appropriate balance of these effector populations may optimise therapeutic efficacy while modulating NT risk. Of note, this patient had both a high CSF CAR-T burden and the most pronounced BBB disruption, as reflected by the albumin quotient. Given the inherent confounding in this single case, it is unclear whether the high CAR-T burden reflects ICANS-associated immune activation—potentially facilitated by BBB disruption promoting immune cell entry into the CNS—or is a consequence of nonspecific CAR-T-cell infiltration into the CNS due to the degree of BBB compromise. Complementary proteomic profiling of CSF further reinforced this multilayered model, revealing an elevation trend of chemokines and proinflammatory cytokines within the CNS compartment. Notably, we observed that IL-6 and IL-1β were elevated at day 9 in the patient with ICANS and declined as ICANS resolved—a pattern consistent with the literature on IL-6/IL-1 blockade in ICANS [39–41]. However, this single-patient observation is hypothesis-generating and warrants validation in larger cohorts. At the same time, it should be noted that Olink measurements may underestimate functional signalling for certain molecule-specific regulators—particularly transpresentation or membrane-restricted mediators such as IL-15 or IL-2. Nevertheless, most soluble cytokines and chemokines remain informative indicators of CNS immune activity.

Our study has several limitations. First, the small sample size limits generalisability and precludes definitive causal inference

and reduces statistical power, and incomplete paired sampling further precludes formal paired comparisons. Therefore, the unpaired Dunn's test was applied as an exploratory approach, and the statistical results should be interpreted with caution. Interpatient heterogeneity may be further complicated by the pooling of pretreatment and independent control samples, as well as by differences in baseline disease activity, CAR-T infusion characteristics, or other individual factors. Second, the absence of healthy controls or comparison groups receiving alternative B cell–depleting therapies limits our ability to distinguish CAR-T–specific effects from those related to general B cell depletion. In addition, factors such as repeated lumbar puncture effects and disease fluctuation cannot be excluded as contributors to the observed changes. Third, the lymphodepletion regimen we used, cyclophosphamide/fludarabine, can also cause NT; however, such events typically occur later (often 20-60 days posttreatment) and are characterised by global T-cell reduction [42,43] rather than the selective enrichment of effector T-cell states observed here. Nevertheless, immune effects related to the lymphodepletion process cannot be fully excluded. Additional limitations include the lack of functional validation, unknown antigen specificities of expanded clones, and reliance on a single NT case. Alternative explanations for some immune signatures—such as immune complex–driven IFN responses, bystander clonal expansion, or secondary myeloid activation—also remain possible.

In summary, our study provides the integrative view of CNS immune remodelling during CAR-T therapy in refractory SLE, showing how CAR-T persistence, T-cell reprogramming, and myeloid–lymphoid crosstalk is collectively associated with neuroimmune dynamics. These observations highlight the CNS as an active immunological niche where the balance of these processes may be relevant to both efficacy and safety.

Competing interests

CX, PX, and ZX are employed by JW Therapeutics (Shanghai) Co Ltd, Shanghai, China. All other authors declare that they have no known competing financial interests or personal relationships that could have appeared to influence the work reported in this paper.

CRediT authorship contribution statement

Jinjian Sun: Writing – original draft, Visualization, Methodology, Funding acquisition, Formal analysis, Data curation. **Xiaoru Hu:** Resources, Data curation. **Weina Li:** Data curation. **Zuge Tian:** Formal analysis, Data curation. **Shouli Xiao:** Resources. **Wanhan Li:** Resources. **Cuiwei Xie:** Resources. **Peng Xia:** Resources. **Zhen Xia:** Resources. **Xiang Chen:** Supervision, Resources, Project administration, Investigation, Conceptualization. **Hui Luo:** Writing – review & editing, Supervision, Resources, Project administration, Investigation, Conceptualization. **Hongjun Zhao:** Writing – review & editing, Validation, Supervision, Resources, Project administration, Investigation, Conceptualization. **Yuzi Tian:** Writing – review & editing, Validation, Supervision, Resources, Project administration, Methodology, Investigation, Funding acquisition, Data curation, Conceptualization.

Funding

This study was supported by the National Natural Science Foundation of China (Grant Nos. 82572076, 82203931, and 82200536), the Excellent Youth Project of Hunan Provincial Natural Science Foundation (Grant No. 2024JJ4094), and the Scientific Research Program of FuRong Laboratory (Grant Nos. 2025PT5010 and 2025PT5004). JW Therapeutics (Shanghai) Co., Ltd. provided the investigational drug (relma-cel) and financial support for the clinical trial, including patient compensation and examination costs. All other work described in this study was conducted independently and is not related to the company.

Patient consent for publication

Not required.

Ethics approval

The study protocol was approved by the Ethics Committee of Xiangya Hospital, Central South University. All participants provided written informed consent before enrollment.

Provenance and peer review

Not commissioned; externally peer reviewed.

Data availability statement

Single-cell RNA sequencing and TCR sequencing data generated in this study are available from the corresponding authors upon reasonable request. All other relevant data are included within the manuscript and its supplementary materials.

Supplementary materials

Supplementary material associated with this article can be found, in the online version, at doi:10.1016/j.ard.2026.06.030.

Orcid

Yuzi Tian: http://orcid.org/0000-0001-5267-2456

REFERENCES

[1] Hoi A, Igel T, Mok CC, Arnaud L. Systemic lupus erythematosus. Lancet 2024 May;403(10441):2326–38. doi: 10.1016/s0140-6736(24)00398-2.
[2] Morawski PA, Bolland S. Expanding the B cell-centric view of systemic lupus erythematosus. Trends Immunol. 2017 May;38(5):373–82. doi: 10.1016/j.it.2017.02.001.
[3] Stockfelt M, Teng YKO, Vital EM. Opportunities and limitations of B cell depletion approaches in SLE. Nat Rev Rheumatol. 2025 Feb;21(2):111–26. doi: 10.1038/s41584-024-01210-9.
[4] Rampotas A, Roddie C. The present and future of CAR T-cell therapy for adult B-cell ALL. Blood. 2025 Apr;145(14):1485–97. doi: 10.1182/blood.2023022922.
[5] Wang D, Wang X, Tan B, Wen X, Ye S, Wu Y, et al. Allogeneic CD19-targeted CAR-T therapy in refractory systemic lupus erythematosus achieved durable remission. Med. 2025 Oct;6(10):100749. doi: 10.1016/j.medj.2025.100749.
[6] Müller F, Taubmann J, Bucci L, Wilhelm A, Bergmann C, Völkl S, et al. CD19 CAR T-cell therapy in autoimmune disease - a case series with follow-up. N Engl J Med. 2024 Feb;390(8):687–700. doi: 10.1056/NEJMoa2308917.
[7] Wang W, He S, Zhang W, Zhang H, DeStefano VM, Wada M, et al. BCMA-CD19 compound CAR T cells for systemic lupus erythematosus: a phase 1 open-label clinical trial. Ann Rheum Dis. 2024 Sep;83(10):1304–14. doi: 10.1136/ard-2024-225785.
[8] Krickau T, Naumann-Bartsch N, Aigner M, Kharboutli S, Kretschmann S, Spoerl S, et al. CAR T-cell therapy rescues adolescent with rapidly progressive lupus nephritis from haemodialysis. Lancet. 2024 Apr;403(10437):1627–30. doi: 10.1016/s0140-6736(24)00424-0.
[9] Shu J, Xie W, Mei C, Ren A, Ke S, Ma M, et al. Safety and clinical efficacy of Relmacabtagene autoleucel (relma-cel) for systemic lupus erythematosus: a

phase 1 open-label clinical trial. EClinicalMedicine. 2025 Apr;83:103229. doi: 10.1016/j.eclinm.2025.103229.
[10] Tur C, Eckstein M, Velden J, Rauber S, Bergmann C, Auth J, et al. CD19-CAR T-cell therapy induces deep tissue depletion of B cells. Ann Rheum Dis. 2025 Jan;84(1):106–14 (2025). doi: 10.1136/ard-2024-226142.
[11] Huang S, Wang X, Wang Y, Wang Y, Fang C, Wang Y, et al. Deciphering and advancing CAR T-cell therapy with single-cell sequencing technologies. Mol Cancer. 2023 May;22(1):80. doi: 10.1186/s12943-023-01783-1.
[12] Legge AC, Hanly JG. Recent advances in the diagnosis and management of neuropsychiatric lupus. Nat Rev Rheumatol 2024 Nov;20(11):712–28. doi: 10.1038/s41584-024-01163-z.
[13] Carrión-Barberà I, Salman-Monte TC, Vílchez-Oya F, Monfort J. Neuropsychiatric involvement in systemic lupus erythematosus: a review. Autoimmun Rev. 2021 Apr;20(4):102780. doi: 10.1016/j.autrev.2021.102780.
[14] Nikolopoulos D, Sentis G, Kitsios I, Garantziotis P, Kapsala N, Pieta A, et al. Enhanced B cell and complement cascade gene signatures in patients with neuropsychiatric systemic lupus erythematosus. Ann Rheum Dis. 2025 Aug;84(8):1342–53. doi: 10.1016/j.ard.2025.04.006.
[15] Llaó-Cid L, Wong J, Fernandez Botana I, Paul Y, Wierz M, Pilger LM, et al. Integrative multi-omics reveals a regulatory and exhausted T-cell landscape in CLL and identifies galectin-9 as an immunotherapy target. Nat Commun. 2025 Aug;16(1):7271. doi: 10.1038/s41467-025-61822-x.
[16] Cantoni C, Smirnov RA, Firulyova M, Andhey PS, Bradstreet TR, Esaulova E, et al. A single-cell compendium of human cerebrospinal fluid identifies disease-associated immune cell populations. J Clin Invest. 2025 Jan;135(1): e177793. doi: 10.1172/jci177793.
[17] Ostkamp P, Deffner M, Schulte-Mecklenbeck A, Wünsch C, Lu IN, Wu GF, et al. A single-cell analysis framework allows for characterization of CSF leukocytes and their tissue of origin in multiple sclerosis. Sci Transl Med. 2022 Nov;14(673):eadc9778. doi: 10.1126/scitranslmed.adc9778.
[18] Macri C, Pang ES, Patton T, O'Keeffe M. Dendritic cell subsets. Semin Cell Dev Biol 2018 Dec;84:11–21. doi: 10.1016/j.semcdb.2017.12.009.
[19] Lee DW, Santomasso BD, Locke FL, Ghobadi A, Turtle CJ, Brudno JN, et al. ASTCT consensus grading for cytokine release syndrome and neurologic toxicity associated with immune effector cells. Biol Blood Marrow Transplant. 2019 Apr;25(4):625–38. doi: 10.1016/j.bbmt.2018.12.758.
[20] Gust J, Ponce R, Liles WC, Garden GA, Turtle CJ. Cytokines in CAR T cell-associated neurotoxicity. Front Immunol. 2020 Dec;11:577027. doi: 10.3389/fimmu.2020.577027.
[21] Gust J, Finney OC, Li D, Brakke HM, Hicks RM, Futrell RB, et al. Glial injury in neurotoxicity after pediatric CD19-directed chimeric antigen receptor T cell therapy. Ann Neurol. 2019 Jul;86(1):42–54. doi: 10.1002/ana.25502.
[22] Gust J, Hay KA, Hanafi LA, Li D, Myerson D, Gonzalez-Cuyar LF, et al. Endothelial activation and blood-brain barrier disruption in neurotoxicity after adoptive immunotherapy with CD19 CAR-T cells. Cancer Discov. 2017 Dec;7 (12):1404–19. doi: 10.1158/2159-8290.Cd-17-0698.
[23] Santomasso BD, Park JH, Salloum D, Riviere I, Flynn J, Mead E, et al. Clinical and biological correlates of neurotoxicity associated with CAR T-cell therapy in patients with B-cell acute lymphoblastic leukemia. Cancer Discov. 2018 Aug;8(8):958–71. doi: 10.1158/2159-8290.Cd-17-1319.
[24] Lu IN, Müller-Miny L, Krekeler C, Cheung PFY, Antonopoulou G, Jeibmann A, et al. The CXCL16/CXCR6 axis is linked to immune effector cell-associated neurotoxicity in chimeric antigen receptor (CAR) T cell therapy. Genome Med. 2025 Jun;17(1):71. doi: 10.1186/s13073-025-01498-6.
[25] Gust J, Rawlings-Rhea SD, Wilson AL, Tulberg NM, Sherman AL, Seidel KD, et al. GFAP and NfL increase during neurotoxicity from high baseline levels in pediatric CD19-CAR T-cell patients. Blood Adv. 2023 Mar;7(6):1001–10. doi: 10.1182/bloodadvances.2022008119.
[26] Gomez-Llobell M, Serra Smith C, Gómez-Costas D, Gómez-Centurión I, García Domínguez JM, Escudero-Vilaplana V, et al. ICANS risk model in CD19 CAR-T therapy: insights from serum and CSF cytokine profiling. Bone Marrow Transplant. 2025 Oct;60(10):1351–60. doi: 10.1038/s41409-025-02679-y.
[27] Brudno JN, Kochenderfer JN. Current understanding and management of CAR T cell-associated toxicities. Nat Rev Clin Oncol 2024 Jul;21(7):501–21. doi: 10.1038/s41571-024-00903-0.
[28] Olsen SK, Ota N, Kishishita S, Kukimoto-Niino M, Murayama K, Uchiyama H, et al. Crystal structure of the interleukin-15.interleukin-15 receptor alpha complex: insights into trans and cis presentation. J Biol Chem. 2007 Dec;282 (51):37191–204. doi: 10.1074/jbc.M706150200.
[29] Salomonsson T, Rumetshofer T, Jönsen A, Bengtsson AA, Zervides KA, Nilsson P, et al. Abnormal cerebral hemodynamics and blood-brain barrier permeability detected with perfusion MRI in systemic lupus erythematosus patients. Neuroimage Clin. 2023;38:103390. doi: 10.1016/j.nicl.2023.103390.
[30] Wang Z, Li N, Feng K, Chen M, Zhang Y, Liu Y, et al. Phase I study of CAR-T cells with PD-1 and TCR disruption in mesothelin-positive solid tumors. Cell Mol Immunol. 2021 Sep;18(9):2188–98. doi: 10.1038/s41423-021-00749-x.
[31] Wilson TL, Kim H, Chou CH, Langfitt D, Mettelman RC, Minervina AA, et al. Common trajectories of highly effective CD19-specific CAR T cells identified by endogenous T-cell receptor lineages. Cancer Discov. 2022 Sep;12 (9):2098–119. doi: 10.1158/2159-8290.Cd-21-1508.
[32] Li X, Guo X, Zhu Y, Wei G, Zhang Y, Li X, et al. Single-cell transcriptomic analysis reveals BCMA CAR-T cell dynamics in a patient with refractory primary plasma cell leukemia. Mol Ther. 2021 Feb;29(2):645–57. doi: 10.1016/j.ymthe.2020.11.028.
[33] Perez RK, Gordon MG, Subramaniam M, Kim MC, Hartoularos GC, Targ S, et al. Single-cell RNA-seq reveals cell type-specific molecular and genetic associations to lupus. Science. 2022 Apr;376(6589):eabf1970. doi: 10.1126/science.abf1970.
[34] Chen PM, Tsokos GC. The role of CD8+ T-cell systemic lupus erythematosus pathogenesis: an update. Curr Opin Rheumatol. 2021 Nov;33(6):586–91. doi: 10.1097/bor.0000000000000815.
[35] Louie RHY, Cai C, Samir J, Singh M, Deveson IW, Ferguson JM, et al. CAR^+ and CAR^- T cells share a differentiation trajectory into an NK-like subset after CD19 CAR T cell infusion in patients with B cell malignancies. Nat Commun. 2023 Nov;14(1):7767. doi: 10.1038/s41467-023-43656-7.
[36] Qin C, Zhang M, Mou DP, Zhou LQ, Dong MH, Huang L, et al. Single-cell analysis of anti-BCMA CAR T cell therapy in patients with central nervous system autoimmunity. Sci Immunol. 2024 May;9(95):eadj9730. doi: 10.1126/sciimmunol.adj9730.
[37] Wilhelm A, Chambers D, Müller F, Bozec A, Grieshaber-Bouyer R, Winkler T, et al. Selective CAR T cell-mediated B cell depletion suppresses IFN signature in SLE. JCI Insight. 2024 May;9(12):e179433. doi: 10.1172/jci.insight.179433.
[38] Morris EC, Neelapu SS, Giavridis T, Sadelain M. Cytokine release syndrome and associated neurotoxicity in cancer immunotherapy. Nat Rev Immunol. 2022 Feb;22(2):85–96. doi: 10.1038/s41577-021-00547-6.
[39] Gazeau N, Liang EC, Wu QV, Voutsinas JM, Barba P, Iacoboni G, et al. Anakinra for refractory cytokine release syndrome or immune effector cell-associated neurotoxicity syndrome after chimeric antigen receptor T cell therapy. Transplant Cell Ther. 2023 Jul;29(7):430–7. doi: 10.1016/j.jtct.2023.04.001.
[40] Wehrli M, Gallagher K, Chen YB, Leick MB, McAfee SL, El-Jawahri AR, et al. Single-center experience using anakinra for steroid-refractory immune effector cell-associated neurotoxicity syndrome (ICANS). J Immunother Cancer. 2022 Jan;10(1):e003847. doi: 10.1136/jitc-2021-003847.
[41] Ludwig H, Terpos E, van de Donk N, Mateos MV, Moreau P, Dimopoulos MA, et al. Prevention and management of adverse events during treatment with bispecific antibodies and CAR T cells in multiple myeloma: a consensus report of the European Myeloma Network. Lancet Oncol. 2023 Jun;24(6): e255–69. doi: 10.1016/s1470-2045(23)00159-6.
[42] Graham CE, Velasco R, Alarcon Tomas A, Stewart OP, Dachy G, Del Bufalo F, et al. Non-ICANS neurological complications after CAR T-cell therapies: recommendations from the EBMT Practice Harmonisation and Guidelines Committee. Lancet Oncol. 2025 Apr;26(4):e203–13. doi: 10.1016/S1470-2045(24)00715-0.
[43] Lowe KL, Mackall CL, Norry E, Amado R, Jakobsen BK, Binder G. Fludarabine and neurotoxicity in engineered T-cell therapy. Gene Ther. 2018 Jun;25 (3):176–91. doi: 10.1038/s41434-018-0019-6.

Ann Rheum Dis 85 (2026) 1774–1783

Contents lists available at ScienceDirect

Annals of the Rheumatic Diseases

journal homepage: https://www.sciencedirect.com/journal/annals-of-the-rheumatic-diseases

Sjögren's Disease

Functional insights into autoantibodies targeting muscarinic acetylcholine receptors in Sjögren's disease

Fiona Engelke[1,*], Harald Heidecke[2], Kai Schulze-Forster[2], Heike Bähre[3], Yasmin Liß[3], Tina Hagedorn[3], Thomas Dörner[4], Diana Ernst[1], Jan Gras[5], Luca Quartuccio[6], Jacob Ritter[4], Benjamin Seeliger[5,7], Detlef Neumann[3], Torsten Witte[1]

[1] *Department of Rheumatology and Clinical Immunology, Hannover Medical School, Hannover, Germany*
[2] *CellTrend GmbH, Luckenwalde, Germany*
[3] *Institute of Pharmacology, Hannover Medical School, Hannover, Germany*
[4] *Rheumatology and Clinical Immunology, Charité – Universitätsmedizin Berlin, Berlin, Germany*
[5] *Department of Respiratory Medicine, Hannover Medical School, Hannover, Germany*
[6] *Rheumatology Division, Department of Medicine, Azienda Sanitaria Universitaria del Friuli Centrale, University of Udine, Udine, Italy*
[7] *German Center for Lung Research (DZL), Biomedical Research in End-Stage and Obstructive Lung Disease Hannover (BREATH), Hannover, Germany*

ARTICLE INFO

Article history:
Received 18 August 2025
Received in revised form 17 June 2026
Accepted 17 June 2026

ABSTRACT

Objectives: G protein-coupled receptors (GPCRs) participate in various pathophysiological processes in Sjögren's disease (SjD); in particular, autoantibodies against muscarinic acetylcholine receptor 3 (M_3R) inhibit the secretion of saliva and tears by exocrine glands. We aimed to identify autoantibodies targeting other muscarinic receptors in SjD and assess their potential functional relevance to signalling pathways.

Methods: Autoantibodies against all muscarinic acetylcholine receptor subtypes were investigated in the serum of patients with SjD (n = 347) using enzyme-linked immunosorbent assays (ELISAs). Healthy controls (HCs; n = 50), patients with non-Sjögren's sicca syndrome (NSS; n = 44), and patients with other autoimmune diseases (AIDs; n = 67) served as controls. To analyse the functional role of muscarinic receptor autoantibodies against muscarinic acetylcholine receptors 1 to 3 and 5 (M_1R, M_2R, M_3R, and M_5R, respectively), purified immunoglobulin (Ig) G fractions from patients with SjD (n = 10) and HCs (n = 10) were examined in Chinese hamster ovary (CHO) cells transfected with the specific receptor using calcium mobilisation and cyclic adenosine monophosphate (cAMP) accumulation assays.

Results: IgG autoantibodies against M_1R to M_5R were significantly increased in patients with SjD compared with HCs ($p \leq .05$) and detected in up to 30% of patients. A combination of anti-M_2R, anti-M_3R, and anti-M_5R identified up to 31% of Ro/SSA-negative SjD cases, with 96% and 75% specificity for SjD vs HCs and SjD vs NSS, respectively. Functionally, purified IgG from SjD serum reduced calcium flux by up to 30% in M_1R-, M_3R-, and M_5R-expressing CHO cells, whereas its effects on cAMP accumulation in M_2R-transfected cells were absent.

*Correspondence to Dr Fiona Engelke, Department of Rheumatology and Clinical Immunology, Hannover Medical School, Carl-Neuberg-Str. 1, 30625 Hannover, Germany.

E-mail address: engelke.fiona@mh-hannover.de (F. Engelke).

Detlef Neumann and Torsten Witte contributed equally to this work.

Handling editor Josef S Smolen

https://doi.org/10.1016/j.ard.2026.06.016

0003-4967/© 2026 The Author(s). Published by Elsevier B.V. on behalf of European Alliance of Associations for Rheumatology (EULAR). This is an open access article under the CC BY license (http://creativecommons.org/licenses/by/4.0/)

Conclusions: The association between autoantibodies targeting M_1R to M_5R in patients with SjD and their functional quantification provides strong evidence that autoantibodies against all muscarinic receptor isotypes may have pathogenic relevance in SjD.

INTRODUCTION

Sjögren's disease (SjD) is a chronic inflammatory autoimmune disorder characterised by lymphocytic infiltration of the lacrimal and salivary glands, resulting in their dysfunction.

What is already known about this topic

- Muscarinic acetylcholine receptors 1 to 5 (M_1R-M_5R) are G protein-coupled receptors found on human labial cells.
- Autoantibodies targeting M_3R suppress intracellular calcium flux and lead to reduced tear and salivary flow in patients with Sjögren's disease (SjD).

What this study adds

- Enzyme-linked immunosorbent assays detected autoantibodies against M_1R to M_5R in patients with SjD.
- Purified immunoglobulin (Ig) G from patients with SjD significantly inhibited calcium flux via $G\alpha_q$-coupled muscarinic acetylcholine receptors.

How this study might affect research, practice or policy

- Detection of muscarinic autoantibodies, combined with functional analysis, enhances understanding of the pathogenesis of SjD and provides a basis for new therapeutic strategies aimed at inhibiting the activity of these functional autoantibodies in order to reduce their suppressive effect and potentially alleviate symptoms in patients with SjD.

As a result, patients with SjD complain about ocular and oral dryness. Furthermore, 40% of patients with SjD develop extraglandular manifestations, including lung involvement, and they also have an increased risk of developing B-cell non-Hodgkin lymphoma [1]. The exact pathophysiological mechanism of SjD is poorly understood. Histopathological findings of the salivary glands of patients with SjD indicate that exocrine glands may retain their structural integrity despite pronounced secretory dysfunction. In addition, acinar tissue may regain its function *in vitro* [2]. Therefore, impaired glandular secretion in SjD cannot be solely a consequence of tissue destruction; other factors must interfere with the secretory process.

Autoantibodies against muscarinic acetylcholine receptor 3 (M_3R) were discovered decades ago [3]. In SjD, autoantibodies targeting the second extracellular loop of M_3R exert an antagonistic effect on human salivary gland cells, suppressing the increase in intracellular calcium. Consequently, tear and salivary flow are reduced in patients with SjD [4–6]. Antibodies against M_3R are not found in all patients with SjD and reduce gland control via muscarinic nerves only partially; therefore, they cannot be the sole cause of glandular hypofunction.

M_3R belongs to the G protein-coupled receptor (GPCR) family, a group of 7-transmembrane receptors that form the largest class of integral membrane proteins in humans [7,8]. The muscarinic acetylcholine receptor subclass consists of 5 members (muscarinic acetylcholine receptors 1-5 [M_1R-M_5R]). Subtypes of muscarinic receptors are found on human labial cells from both healthy and SjD individuals. However, M_2R has been reported at very low levels in both groups [9,10].

The present study aimed to investigate autoantibodies against M_1R to M_5R and to analyse their functional activity in SjD.

METHODS

Study subjects

Serum samples from a total of 347 patients with primary SjD were recruited from the Department of Rheumatology and Immunology at the Hannover Medical School, Germany (n = 171), the Department of Respiratory Medicine at Hannover Medical School, Germany (n = 46), the Department of Medicine/Rheumatology and Clinical Immunology at Charité in Berlin, Germany (n = 72), and the Department of Medicine/Rheumatology Clinic at the University of Udine, Italy (n = 58). Additional serum samples from patients with rheumatoid arthritis (RA; n = 33), systemic lupus erythematosus (SLE; n = 34), non-Sjögren's sicca syndrome (NSS; n = 44) who did not fulfil the 2016 American College of Rheumatology/European Alliance of Associations for Rheumatology (ACR/EULAR) classification criteria for SjD, and healthy controls (HCs; n = 48-50) were obtained from the Department of Rheumatology and Immunology at the Hannover Medical School. None of the controls with other autoimmune diseases was diagnosed with secondary SjD; only individuals confirmed to be negative for Ro/SSA antibodies and without sicca symptoms (as verified by Saxon and Schirmer tests) were included. All study participants fulfilled the ACR/EULAR classification criteria for their respective diseases [11–13]. Serum samples were aliquoted and stored at −80°C until use.

The clinical and demographic characteristics of the 289 patients with SjD from Hannover and Berlin, and the controls (RA, SLE, NSS, and HCs), are shown in Table 1. The characteristics of the SjD samples from Udine were not registered.

Quantification of autoantibodies against muscarinic acetylcholine receptors by enzyme-linked immunosorbent assay

Human immunoglobulin (Ig) G autoantibodies against M_1R to M_5R were detected in serum samples using enzyme-linked immunosorbent assays (ELISAs; CellTrend GmbH) according to the manufacturer's instructions. Briefly, GPCR-coated polystyrene plates were incubated with a 1:100 serum dilution for 2 hours at 4°C, followed by incubation with horseradish peroxidase (HRP)-labelled goat anti-human IgG for 1 hour. The autoantibody concentration was quantified in arbitrary units (U) per millilitre using a 5-point standard curve, ranging from 2.5 to 40 U/mL.

Quantification of autoantibodies against muscarinic acetylcholine receptors by Western blot

Recombinantly expressed and purified M_1R to M_5R proteins were provided by CellTrend GmbH. These were separated by sodium dodecyl sulfate–polyacrylamide gel electrophoresis (SDS-PAGE) and transferred onto nitrocellulose membranes along with a molecular weight marker (YesBlot Western Marker

Table 1
Characteristics of Sjögren's disease patients and healthy controls in autoantibody quantification and functional analysis, as well as control groups, including non-Sjögren's sicca syndrome, rheumatoid arthritis, and systemic lupus erythematosus, in autoantibody screening.

	Autoantibody quantification						Functional analysis	
	HC n = 50	SjD n = 289		Other AIDs n = 67		NSS n = 44	HC n = 10	SjD n = 10
		Hannover n = 217	Berlin n = 72	RA n = 33	SLE n = 34			
Female, (%)	63.6	77.3	94.3	66.7	76.5	90	70.0	90.0
Age (y) at visit	46.8	61	47	57.8	47.3	54.7	39	64
Age (y) at onset		56	NA					48
Laboratory values, (%)								
ANA ≥ 1:160		77.2	NA	48.5	100.0	52.3		100.0
Rheumatoid factor-positive		31.8	64.2	72.7	2.9	4.5		80.0
Presence of Ro/SSA antibodies		61.6	80.6	0.0	35.3	0.0		60.0
Presence of La/SSB antibodies		21.4	45.8	0.0	5.9	0.0		10.0
Oral and ocular tests, (%)								
Saxon test pathological		49.3	100.0			54.5		20.0
Schirmer test pathological		68.5	33.3			65.9		60.0
Salivary gland biopsy, (%)								
Biopsy performed		42.3	11.4			45.5		80.0
Chisholm-Mason grade ≥3		58.8	62.5			0.0		87.5
ESSDAI, (%)								
Constitutional symptoms		9.7	50.0					10.0
Lymphadenopathy		2.7	1.4					0.0
Glandular involvement		5.3	51.4					0.0
Articular involvement		26.9	31.4					40.0
Cutaneous involvement		3.4	8.6					0.0
Pulmonary involvement		57.2	4.3					10.0
Renal involvement		4.0	0.0					10.0
Muscular involvement		3.4	2.9					10.0
Peripheral nervous system involvement		11.1	5.7					50.0
Central nervous system involvement		2.9	0.0					0.0
Haematological involvement		30.2	42.9					50.0
Biological involvement		15.7	21.4					10.0

AID, autoimmune disease; ANA, antinuclear antibody; ESSDAI, EULAR Sjögren's Syndrome Disease Activity Index; HC, healthy control; NA, not available; NSS, non-Sjögren's sicca syndrome; RA, rheumatoid arthritis; SjD, Sjögren's disease; SLE, systemic lupus erythematosus.

I, SMOBio Technology). Membranes were blocked (ROTI Block, Carl ROTH) and incubated overnight at 4°C with 1:50 dilutions (in ROTI Block) of purified IgG isolated from either HC sera or SjD patient sera (see 'Purification of IgG from patient serum'). Following the washing steps, bound antibodies were detected using HRP-conjugated anti-human IgG (Jackson ImmunoResearch, 1:2000 dilution in ROTI Block) and Westar ECL substrate (Cyanagen). Signal acquisition of chemiluminescent immunoreactive bands was performed using exposure times of 5 and 15 seconds on a Chemostar Plus imager (Intas).

Cell culture of Chinese hamster ovary cells

Chinese hamster ovary (CHO) cells were stably transfected with human muscarinic acetylcholine receptors obtained from the European Collection of Authenticated Cell Cultures (ECACC; CHO-CHRM1, CHO-CHRM2, T02J-7/10 [CHO-CHRM3], and CHO-CHRM5). Cells were cultivated in Ham's F12 medium (Bio&Sell) supplemented with 10% fetal bovine serum (FBS; Bio&Sell), 1% glutamine (Bio&Sell), and 0.5 mg/mL G418 (Gibco).

Cell-surface expression of the muscarinic acetylcholine receptors was verified by a commercial supplier (InSCREENeX GmbH), as described by Schucht et al. [14]. Unpublished data from InSCREENeX GmbH showed that nontransfected CHO cells did not endogenously express muscarinic acetylcholine receptors. In CHO cells transfected with M_4R, receptor expression could not be verified; therefore, no further functional analyses were performed.

Purification of IgG from patient serum

IgG was isolated from patient sera using immobilised Pierce Protein A Agarose (Thermo Fisher Scientific) according to the manufacturer's instructions. The purified IgG was buffered with phosphate-buffered saline (PBS; Bio&Sell) and diluted to a final concentration of 3 g/L.

Calcium mobilisation assay

Intracellular calcium flux was assessed by incubating $G\alpha_q$-coupled muscarinic acetylcholine receptor-transfected cells with Calbryte 520 AM (4 µM; AAT Bioquest) in calcium-free Hanks' balanced salt solution (HBSS) buffer (Sigma-Aldrich) containing 20 mM HEPES (Carl ROTH) for 1 hour at 37°C. After staining, cells were washed, resuspended in HBSS buffer containing purified human IgG, and incubated for 15 minutes at 37°C. The muscarinic receptor agonist carbachol (Merck Millipore) was added at a cell line-specific concentration corresponding to the half-maximal effective concentration (EC50). The EC_{50} values were determined from prior dose-response experiments (CHO-M_1R: 7 nM; CHO-M_3R: 2 nM; CHO-M_5R: 10 nM). Changes in intracellular calcium concentrations were determined using a Synergy HTX reader (BioTek) at 520 nm and calculated from baseline, minimum, and maximum fluorescence intensity signals obtained after the subsequent addition of ethylene glycol tetraacetic acid (EGTA; 600 mM; Sigma-Aldrich) and 30% Triton X-100 (Sigma-Aldrich). All conditions were tested in technical triplicate and validated in 3 independent experiments.

Table 2
Prevalence of muscarinic autoantibodies in Sjögen's disease patients at the study centres Hannover, Berlin, and Udine.

				% Positive patients						
				SjD (n = 347)						
Antigen	*P* value[a]	*P* value[b]	HC n = 50	All	Ro/SSA-negative	H n = 217	B n = 72	U n = 58	NSS n = 44	AID n = 67
IgG_M_1R	$3.52.10^{-05}$	$1.60.10^{-03}$	3.8	10.4	6.7	6.5	22.2	10.3	2.3	11.9
IgG_M_2R	$2.98.10^{-05}$	$1.00.10^{-04}$	3.8	29.7	23.3	21.7	52.8	31.0	15.9	14.9
IgG_M_3R	$3.24.10^{-02}$	$1.00.10^{-04}$	3.8	13.8	12.2	14.7	15.3	8.6	9.1	6.0
IgG_M_4R	$3.22.10^{-04}$	$1.00.10^{-04}$	3.8	16.4	8.8	12.9	26.4	17.2	15.9	11.9
IgG_M_5R	$2.03.10^{-02}$	$1.00.10^{-03}$	1.9	16.7	7.8	12.4	16.7	32.8	0.0	13.4

HCs and patients with NSS, as well as patients with AIDs, including those with rheumatoid arthritis (RA; n = 33) and systemic lupus (SLE; n = 34), served as controls. Patients with a positive status are reported as a percentage and defined using the receiver operating characteristic (ROC) curve, with the optimal likelihood ratio serving as the cutoff.
AID, autoimmune disease; B, Berlin; H, Hannover; HC, healthy control; IgG, immunoglobulin G; M_1R to M_5R, muscarinic acetylcholine receptors 1 to 5; NSS, non-Sjögren's sicca syndrome; U, Udine.
[a] Comparison of *P* values for patients with SjD vs HCs using the Mann-Whitney U test.
[b] Comparison of *P* values for patients with SjD vs HCs using Fisher's exact test.

Cyclic adenosine monophosphate accumulation assay

Cells with Gα_i-coupled muscarinic acetylcholine receptors were preincubated with purified human IgG for 15 minutes at 37°C and then stimulated with a mixture of carbachol and 5 μM forskolin (Sigma-Aldrich) for 10 minutes at room temperature (RT). Forskolin was used to increase intracellular cyclic adenosine monophosphate (cAMP) levels, thereby providing a measurable signal for inhibition. Meanwhile, carbachol acted as an agonist at muscarinic receptors, counteracting the effects of forskolin-induced cAMP accumulation. The half-maximal inhibitory concentration (IC_{50}) value of carbachol in the presence of 5 μM forskolin was quantified in initial dose-response experiments (CHO-M_2R: 5 nM). The concentration of forskolin was selected based on previous studies in CHO cells [15]. This setup allowed assessment of whether IgG interferes with the inhibitory effect of carbachol on forskolin-stimulated cAMP signalling. Following stimulation, the cells were lysed in acetonitrile (Th. Geyer GmbH & Co. KG), methanol (Avantor Performance Materials), and water (2:2:1), supplemented with 25 ng/mL tenofovir (internal standard [IS]; National Institutes of Health). Intracellular cAMP concentrations were analysed by high-performance liquid chromatography-tandem mass spectrometry (HPLC-MS/MS; Shimadzu Nexera, Shimadzu Scientific Instruments; Sciex QTRAP 5500 System). All conditions were tested in technical triplicate and validated in 3 independent experiments.

Data analysis

The antigen profiles of patients with SjD and HCs were compared using the Mann-Whitney U test, and *p* values of <.05 were considered statistically significant. In addition, the data were binarised using the receiver operating characteristic (ROC) curve based on the optimal likelihood ratio for SjD classification, and further statistically tested with Fisher's exact test. The antigen profile results were visualised using heatmaps and violin plots.

For a comparative analysis of mobilised calcium across measurements, the calcium concentrations observed in the calcium mobilisation assay were normalised to the maximum signal from carbachol-only stimulation. The percentage of calcium in carbachol-activated CHO cells, in the presence of purified IgG from HCs and patients with SjD, was plotted as a scatter plot. Statistical analysis was performed using the Mann-Whitney U test. ROC analysis was used to determine inhibitory reactivity by comparing patients with SjD with HCs. Correlation analyses were performed using Pearson's correlation coefficient to examine the relationship between the calcium assay and ELISA concentrations. The results were visualised as scatter plots with linear regression lines and 95% CIs.

Regarding the data analysis of the cAMP accumulation assay, the observed cAMP concentrations were normalised to the maximum cAMP concentration induced by forskolin, expressed as a percentage, and plotted as a scatter plot. A Kruskal-Wallis test was conducted to compare cAMP concentrations between HCs and patients with SjD.

RESULTS

Autoantibodies against muscarinic receptors in SjD

Autoantibodies against M_1R to M_5R were measured in patients with SjD (n = 347), HCs (n = 48-50), NSS (n = 44), and patients with other autoimmune diseases (AIDs; n = 67) using ELISA.

The concentrations of muscarinic autoantibodies were significantly higher in patients with SjD than that in HCs (Mann-Whitney U test; Table 2). The prevalence of autoantibodies in the study groups was determined using antigen-specific cutoffs defined by the ROC curve and the optimal likelihood ratio. Autoantibodies against M_1R to M_5R were found in 10% to ~30% of patients with SjD (Figs 1 and 2A-E, Table 2, and Supplementary Fig S2).

Using principal component analysis, comparative studies of autoantibody reactivity in patients with SjD across the study centres revealed similarities in global distribution (Supplementary Fig S3). Minor differences were found in anti-M_2R autoantibodies across the study centres. The Berlin cohort had approximately twice as many autoantibodies as the Hannover cohort (Table 2). Furthermore, the autoantibody profiles of patients with SjD and controls (HCs, NSS, and AIDs) showed distinct yet overlapping patterns.

Notably, autoantibodies against muscarinic receptors were more prevalent in patients with SjD than in HCs. Specifically, anti-M_1R, anti-M_2R, anti-M_3R, and anti-M_5R were more frequent in patients with SjD than in patients with NSS, with distinct overlap observed across groups, including shared anti-M_4R reactivity, while anti-M_1R and anti-M_5R were largely absent in patients with NSS (Table 2 and Supplementary Fig S2).

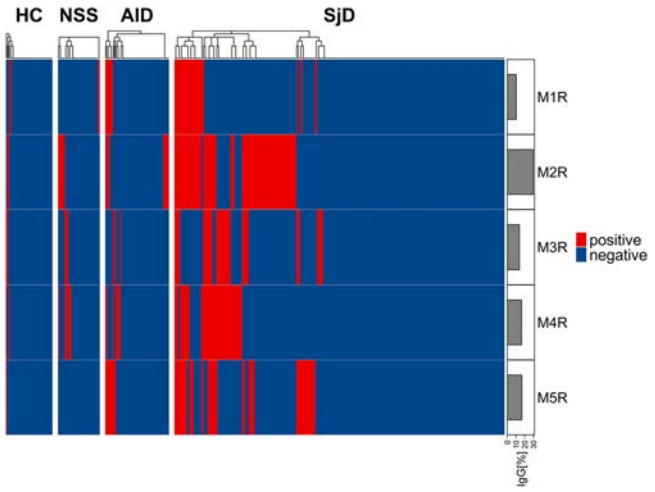

Figure 1. Unsupervised hierarchical cluster analysis of autoantibody reactivity of the muscarinic acetylcholine receptors 1 to 5 (M_1R-M_5R) as antigen targets in Sjögren's disease (SjD; n = 347) compared with patients with healthy individuals (HC, n≤50), non-Sjögren's sicca syndrome (NSS, n = 44) and other autoimmune disease patients (AID, n = 67). Each column represents an individual patient, and each row corresponds to a specific muscarinic autoantibody. The colour code indicates whether individuals are positive (red) or negative (blue) for the specific autoantibody. The bar chart on the right shows the overall prevalence of each muscarinic autoantibody among all patients with SjD, expressed as the percentage of patients with detectable immunoglobulin (Ig) G against that antigen.

Given the diagnostic challenges in identifying Ro/SSA-negative patients with SjD, we investigated the presence of muscarinic autoantibodies in this subgroup (n = 90). These autoantibodies were found in up to 23% of patients in this subcohort, with anti-M_2R demonstrating the highest IgG reactivity (Table 2). Combining all muscarinic autoantibodies enabled the detection of 33% of patients with SjD who were negative for Ro/SSA, with specificities of 92% and 64% are for SjD vs HCs and SjD vs NSS, respectively. The specificity improved when the detection panel consisted only of anti-M_2R, anti-M_3R, and anti-M_5R, enabling the detection of 31% of patients with SjD, with specificities of 96% and 75% are for SjD vs HCs and SjD vs NSS, respectively.

Furthermore, associations between the presence of antibodies against M_1R to M_5R and antinuclear antibodies (ANA), hypergammaglobulinemia, rheumatoid factor and complement depletion, markers of glandular involvement (pathological saliva and tear production and salivary gland biopsy results), and clinical manifestations (selected European Alliance of Associations for Rheumatology Sjögren's Syndrome Disease Activity Index (ESSDAI) domains, disease activity, duration, and onset) were investigated using Fisher's exact test; the 289 patients with SjD from Hannover and Berlin were included in the analysis (Supplementary Table S1). Notably, a positive rheumatoid factor result was associated with the presence of anti-M_2R, anti-M_4R, and anti-M_5R antibodies. Higher IgG concentrations showed a significant positive correlation with anti-M_2R, whereas the haematological domain was positively associated with anti-M_5R. However, none of these associations remained statistically significant after accounting for multiple testing using the Benjamini-Hochberg procedure. Furthermore, the presence of inhibitory autoantibodies was not associated with clinical manifestations, including dryness, as assessed by the Saxon and Schirmer tests.

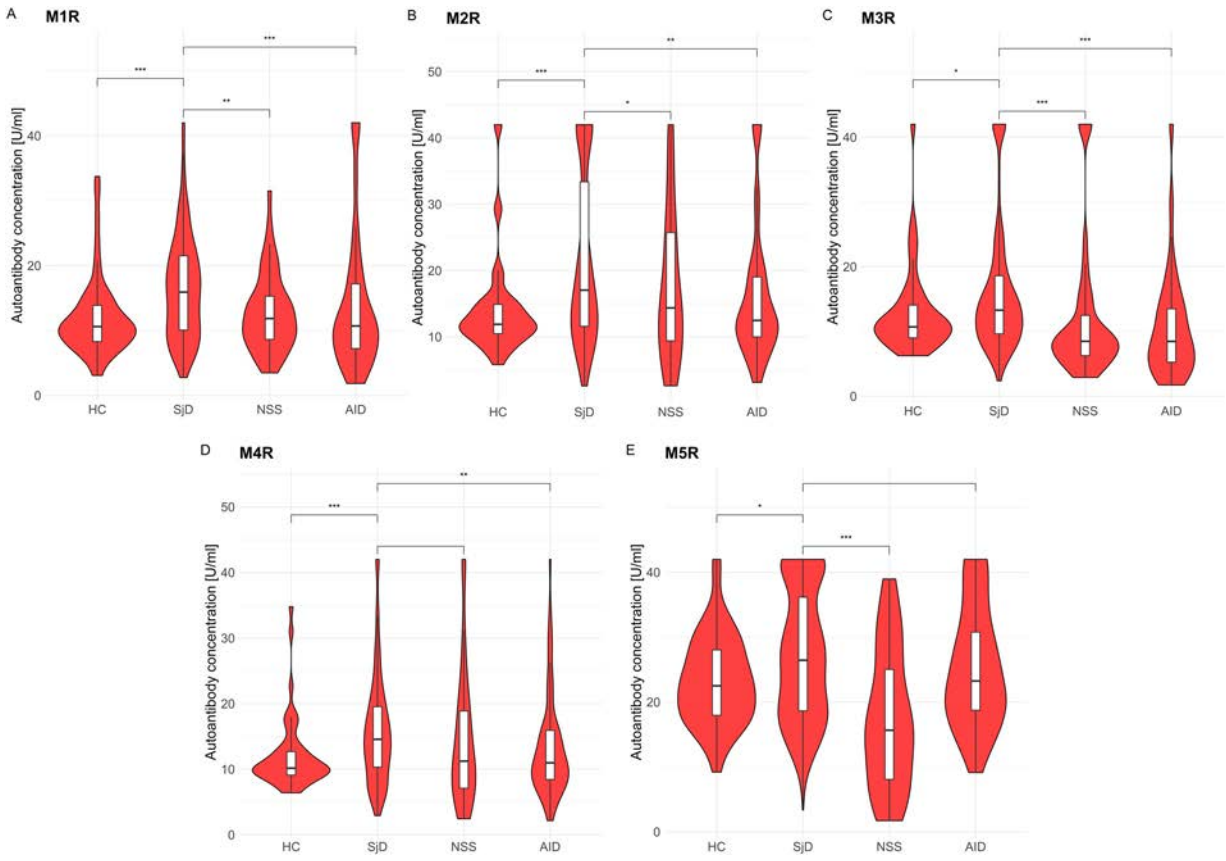

Figure 2. A-E, Violin plots of autoantibody concentration (in U/mL) of muscarinic autoantibodies (muscarinic acetylcholine receptors 1-5 [M_1R-M_5R]) are shown for the individual sample groups (patients with Sjögren's disease [SjD], n = 347; healthy controls [HCs], n ≤ 50; patients with non-Sjögren's sicca syndrome [NSS], n = 44; and patients with other autoimmune disease patients [AIDs], n = 67). Statistical analysis was performed by the Mann-Whitney U test. *$p \leq .05$; **$p \leq .01$; ***$p \leq .001$.

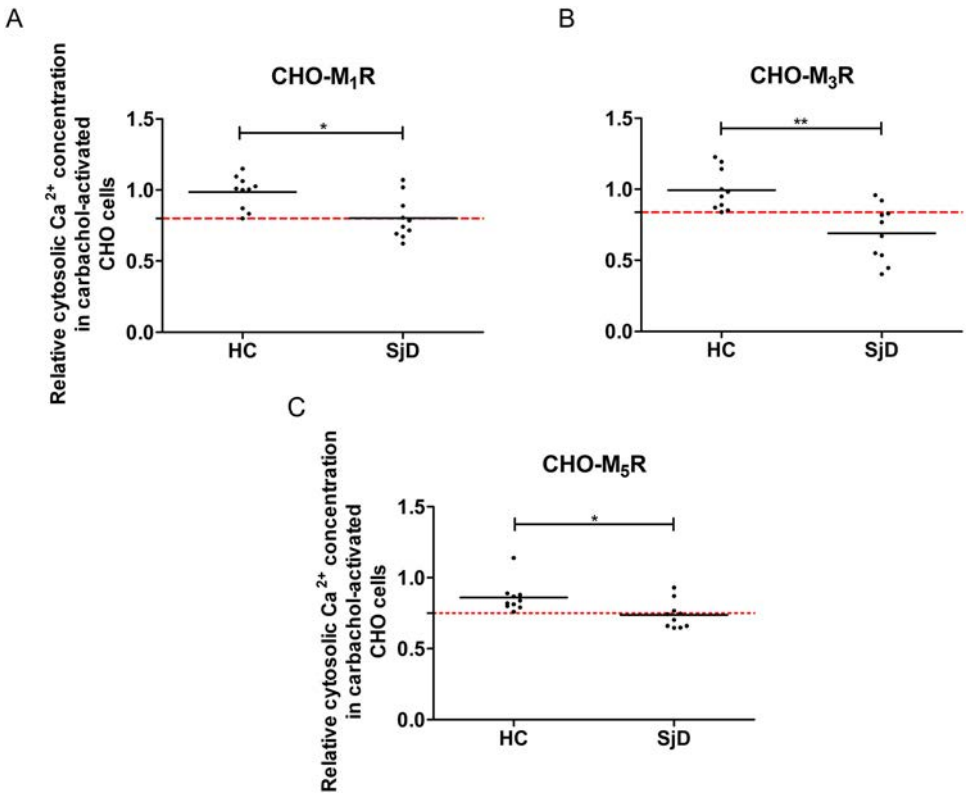

Figure 3. Relative cytosolic calcium concentrations in carbachol-activated Chinese hamster ovary (CHO) cells preincubated with purified human immunoglobulin (Ig) G from Sjögren's disease (SjD; n = 10) patients and healthy controls (HCs; n = 10). Normalisation was performed to the individual maximal calcium concentration in CHO cells (A: CHO-M_1R; B: CHO-M_3R; C: CHO-M_5R) induced by carbachol without preincubation. The mean of 3 replicate experiments per patient or control is represented by a data point. Red dotted lines indicate the inhibitory cutoff. Statistical analysis was performed by the Mann-Whitney U test. *$p \leq .05$; **$p \leq .01$ compared with HCs.

The specificity of the ELISA was confirmed by inhibition and cross-inhibition assays performed with well-characterised antibody-positive and antibody-negative sera, thereby enabling discrimination between specific and nonspecific signal contributions. Preincubating SjD sera on separate ELISA plates coated with identical muscarinic receptor antigens resulted in lower optical densities for the receptor-specific antibodies (anti-M_1R to anti-M_5R) in question (Supplementary Fig S1). Additionally, supplementing the sera with a 10-fold higher concentration of soluble M_3R antigen almost completely inhibited binding to M_3R-coated ELISA plates. This decrease in signal intensity indicates that antigen-specific Igs present in the sera were competitively absorbed during the preincubation step. Cross-inhibition was ruled out, as preincubation with any of the other 4 muscarinic receptor subtypes did not significantly reduce the optical densities.

Despite the demonstrated specificity of the ELISA, a second independent method was established to further verify the presence of muscarinic receptor autoantibodies in SjD sera. To this end, purified recombinant muscarinic receptor proteins were subjected to Western blot analysis and probed with purified IgG fractions from either patients with SjD or HCs. Immunoreactive bands at ~70 kDa were readily detectable in lanes where M_3R and M_4R proteins were loaded. In contrast, in lanes loaded with M_1R, M_2R, and M_5R, only very faint bands appeared at 70 kDa, whereas stronger immunoreactivity was observed at ~15 kDa. However, consistent with the ELISA findings, IgG from patients with SjD, on average, exhibited stronger M_3R- and M_4R-immunoreactive bands compared with IgG from HCs (Supplementary Fig S4), indicating increased antibody reactivity against muscarinic receptor proteins in patients' samples. Thus, Western blot analysis independently confirmed the presence of muscarinic receptor autoantibodies in SjD patient sera, probably at a higher titre and/or reactivity than in HC samples.

Impact of purified serum IgG on CHO cells transfected with $G\alpha_q$-coupled muscarinic acetylcholine receptors

To address the functional relevance of autoantibodies against $G\alpha_q$-coupled M_1R, M_3R, and M_5R in SjD, calcium mobilisation was quantified by measuring cytosolic calcium concentration in CHO cells in the presence of purified IgG from patients with SjD (n = 10) or HCs (n = 10; Table 1). SjD sera were selected based on their positivity in the ELISA. A detailed overview of these results can be found in Supplementary Table S2. Notably, none of the 10 patients tested positive for all muscarinic receptor autoantibodies. Rather, each patient tested positive for only a subset of the antibodies tested.

No intrinsic activity was observed when cells were stimulated with purified IgG alone. Preincubation with purified IgG (final concentration 1.5 g/L) from patients with SjD or HCs, followed by stimulation with carbachol at an EC_{50} concentration, showed that IgG from patients with SjD significantly inhibited calcium flux through all $G\alpha_q$-coupled muscarinic acetylcholine receptors, in contrast to IgG from HCs (Fig 3). Depending on the receptor, calcium flux was inhibited by up to 30% (M_1R: 20%; M_3R: 30%; M_5R: 10%) relative to the mean calcium flux in HC samples. Calcium concentrations ≤75% to 84% were determined as inhibitory with a specificity of 100% using ROC analysis (M_1R: ≤80%; M_3R: ≤84%; M_5R: ≤75%). Accordingly, 60% to 80% of patients with SjD had inhibitory antimuscarinic autoantibodies (M_1R: 60%; M_3R: 80%; M_5R: 70%).

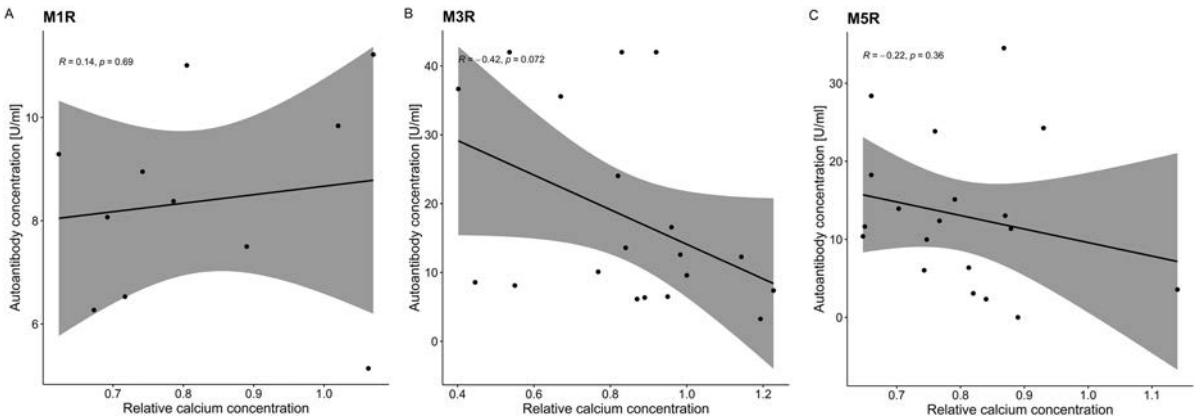

Figure 4. Correlation-based comparison of the muscarinic autoantibody concentration derived from enzyme-linked immunosorbent assay (ELISA) and the relative calcium concentration determined by the calcium mobilisation assay. (A) CHO-M_1R, (B) CHO-M_3R, and (C) CHO-M_5R. M_1R, M_3R, and M_5R, muscarinic acetylcholine receptors 1, 3, and 5, respectively.

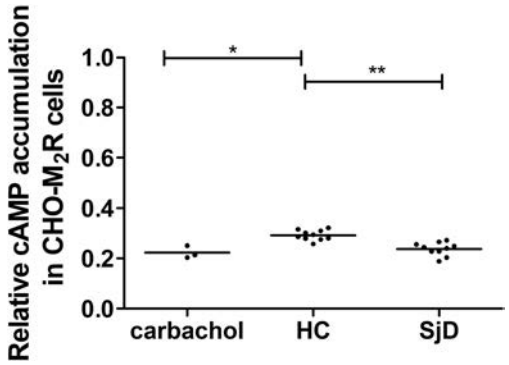

Figure 5. Relative cyclic adenosine monophosphate (cAMP) accumulation in CHO-M_2R cells preincubated with purified immunoglobulin (Ig) G from patients with Sjögren's disease (SjD; n = 10) or healthy controls (HCs; n = 10). To test the effects of IgG, the cells were subsequently stimulated with a mixture of forskolin and carbachol, with forskolin increasing intracellular cAMP levels and carbachol at its half-maximal inhibitory concentration (IC_{50}) confirming M_2R-mediated inhibition. Data were normalised to the maximum forskolin-induced cAMP response. The mean of 3 replicate experiments per patient or control is represented by a data point. Statistical analysis was performed by the Kruskal-Wallis test. *$p \leq .05$; **$p \leq .01$.

Furthermore, the correlation between the autoantibody concentration determined by ELISA and the inhibitory activity of autoantibodies in the calcium mobilisation assay was assessed (Fig 4). A nonsignificant negative association between the 2 assays was observed for M_3R and M_5R, suggesting that increased inhibitory activity in the calcium mobilisation assay was related to a higher autoantibody concentration in the ELISA. In contrast, a nonsignificant positive correlation was observed between the 2 M_1R assays, indicating that a greater inhibitory effect was associated with a lower autoantibody concentration.

Impact of purified serum IgG on CHO cells transfected with Gα_i-coupled M_2R

The functional relevance of autoantibodies against Gα_i-coupled M_2R in SjD was examined using a cAMP accumulation assay. No intrinsic activity of purified IgG alone was observed in CHO-M_2R. To evaluate the impact of IgG fractions on M_2R signalling, forskolin was used to increase intracellular cAMP levels. Carbachol acts as an agonist at muscarinic receptors and inhibits forskolin-induced cAMP accumulation. It was used at its IC_{50} concentration as a positive control to verify receptor-mediated inhibition, thereby providing a functional readout to assess whether IgG interferes with inhibitory signalling. In this system, IgG from HCs partially restored cAMP levels above the minimum induced by carbachol, indicating agonistic or synergistic activity (Fig 5). By contrast, IgG from patients with SjD did not modify cAMP accumulation, which remained at the level suppressed by carbachol.

DISCUSSION

In this study, we systematically investigated autoantibodies targeting all muscarinic acetylcholine receptor subtypes in a large cohort of patients with SjD and in individuals with sicca symptoms. To our knowledge, this is the first study to comprehensively analyse the presence of autoantibodies against multiple muscarinic receptors in patients with SjD, whereas previous reports have focused primarily on M_3R and M_5R [5,16,17]. Additionally, we conducted functional analyses to evaluate the effect of these autoantibodies on receptor activity. While previous studies have primarily focused on M_3R, our work extends these findings by providing the first functional data on M_1R and M_5R.

In the muscarinic autoantibody reactivity study, autoantibodies against M_1R to M_5R were significantly more common in patients with SjD than in HCs. This observation extends previous studies reporting the presence of autoantibodies against M_3R and M_5R in patients with SjD. In addition, anti-M_3R were also found in patients with other AIDs, including systemic sclerosis (SSc) and SLE [18,19]. Since autoantibodies against M_1R to M_5R were also found in the Ro/SSA-negative SjD patient group, they could be used to improve the identification of these patients, which currently relies on invasive salivary gland biopsy. Combining 3 of the 5 muscarinic autoantibodies (anti-M_2R, anti-M_3R, and anti-M_5R) enabled the detection of approximately one-third of Ro/SSA-negative patients with SjD. Furthermore, this study revealed that autoantibodies against M_2R, M_3R, and M_4R were also more common among individuals with sicca symptoms who did not meet the classification criteria for SjD than in HCs. SjD was excluded in these patients because they had no Ro/SSA autoantibodies, and the salivary gland biopsy did not meet the Chisholm-Mason grade 3 or higher criteria. In our cohort, 33/35 biopsies from Ro/SSA-positive patients with SjD revealed a Chisholm-Mason grade of at least 3, indicating a biopsy sensitivity of 94.3% at our institution. However, a

proportion of NSS individuals may have SjD that is not detected on salivary gland biopsy. There may, however, be an additional subset of NSS individuals in whom autoantibodies against muscarinic acetylcholine receptors may contribute to the pathogenesis of reduced glandular function.

In our functional analysis, purified IgG from patients with SjD was found to significantly inhibit calcium flux in CHO-M_3R cells, resulting in a reduction of approximately 30% in calcium signalling. Similar inhibitory effects were observed in CHO-M_1R and CHO-M_5R cells, demonstrating for the first time that autoantibodies against these receptor subtypes can impair Gα_q-coupled receptor signalling. These results corroborate previous studies indicating reduced calcium responses in CHO-M_3R cells and human submandibular gland (HSG) cells when exposed to SjD IgG and support the notion that autoantibodies can interfere with agonist binding to salivary gland membranes [4,20,21]. To the best of our knowledge, this is the first study to show that autoantibodies have an antagonistic effect on M_1R and M_5R, thereby inhibiting their activity and subsequent signalling. As both M_1R and M_5R have been identified in salivary gland tissue, these findings suggest a possible mechanistic link to glandular hypofunction in SjD. Beyond the classical focus on M_3R, which has been extensively studied in the context of impaired calcium-dependent secretion, our data suggest that other muscarinic receptor subtypes may contribute to pathogenesis. Antagonistic autoantibodies against M_1R and M_5R could reduce intracellular signalling via Gα_q-coupled pathways, leading to diminished secretory responses. Furthermore, we assume that glandular hypofunction in SjD is unlikely to result from a single receptor-antibody interaction but rather from a broader imbalance in muscarinic receptor signalling. Antagonistic autoantibodies that target multiple receptor subtypes can simultaneously impair distinct calcium-dependent pathways, leading to reductions in secretory function that are either additive or synergistic. This multifaceted disruption of receptor signalling could explain why clinical manifestations vary among patients, as different combinations or concentrations of autoantibodies may affect glandular activity in distinct ways.

In contrast, no functional role for autoantibodies targeting Gα_i-coupled M_2R in modulating cAMP signalling was observed. While IgG fractions from HCs occasionally showed minor effects on cAMP accumulation, these were likely attributable to background reactivity or nonspecific IgG interactions rather than to disease-related autoantibodies. This is consistent with previous reports showing that M_2R is only minimally expressed in labial salivary gland tissue and is not predominantly localised to secretory epithelial cells, suggesting that this receptor subtype is unlikely to play a physiologically meaningful role in glandular dysfunction. Transfection of M_4R did not result in cell-surface expression; therefore, functional analysis was not possible.

Studies on anti-M_3R autoantibodies have produced conflicting results, with some researchers failing to detect antibodies [22]. These discrepancies may be due to differences in the detection techniques used. Notably, ELISA using intact GPCR proteins, as employed in our initial experiments, is likely to have limited sensitivity to these antibodies, highlighting the challenges in this area of research [23]. Consistent with this, we also observed discrepancies between our ELISA results and those of the functional assays, supporting the view that ELISA is poorly correlated with functional assay positivity. Importantly, this underscores the need to analyse both ELISA-positive and ELISA-negative SjD sera in functional assays to obtain a more reliable assessment of antibody activity.

However, to confirm receptor-binding specificity in ELISA, inhibition and cross-inhibition assays were performed. Preincubating SjD sera with identical muscarinic receptor antigens on separate plates markedly reduced the corresponding optical density values, indicating specific antibody-antigen interactions. Interestingly, preincubation of the sera with a 10-fold excess of soluble M_3R antigen almost completely inhibited subsequent binding to M_3R-coated ELISA plates. By contrast, preincubation with heterologous muscarinic receptor subtypes did not affect the optical density, indicating that the autoantibodies recognised only their respective receptor subtypes and showed no cross-reactivity between different muscarinic receptors.

Despite the demonstrated specificity of the ELISA, as evidenced by inhibition and cross-inhibition experiments, we validated the presence of muscarinic receptor autoantibodies using a second, independent detection method. This was particularly important due to inconsistent findings in anti-M_3R autoantibody detection and the challenges of using ELISA to analyse membrane-bound GPCRs.

To address this, we established a modified Western blot approach. Recombinant muscarinic receptor proteins were separated by SDS-PAGE, transferred onto nitrocellulose membranes, and probed with purified serum IgG fractions serving as primary antibodies. Consistent with the ELISA findings, immunoreactive bands were observed, providing independent evidence of autoantibody reactivity against muscarinic receptor proteins in SjD sera. Moreover, the Western blot approach also confirmed increased reactivity against M_3R and M_4R in SjD patient-derived sera compared with HCs. However, this Western blot system has not yet been fully established and should therefore be interpreted with caution. For M_1R, M_2R, and M_5R, major bands were detected at lower molecular weights than expected, a finding that was also evident in Ponceau S and Coomassie staining of the recombinant protein preparations (data not shown). These low-molecular-weight species may represent degradation products or partial recombinant proteins; however, no detailed information regarding the composition of the protein preparations was available from the manufacturer. Nevertheless, the Western blot approach supports the conclusion that muscarinic receptor autoantibodies are present in SjD sera.

Correlation analysis of oral and ocular dryness, as assessed by the Saxon and Schirmer test, revealed no association with the presence of muscarinic autoantibodies, not even with anti-M_3R. This may be partially explained by the heterogeneity of our cohort. We included both patients with a recent diagnosis of SjD, in whom glands are probably still largely intact and functional autoantibodies are likely relevant, and patients with a long disease duration, in whom glands are likely mostly destroyed and functional autoantibodies will no longer affect glandular secretion. Furthermore, not all muscarinic autoantibodies detected by ELISA may be functionally relevant, since antibodies against the complete proteins, rather than only the acetylcholine-binding domain, are measured. Finally, additional autoantibodies against other water channels involved in glandular secretion, such as aquaporin-5, have been described in SjD and may also be functionally relevant [24].

It will be interesting to see in ongoing studies whether B-cell-directed drugs, such as Ianalumab, or IgG-reducing drugs such as nipocalimab or efgartigimod, improve salivary and lachrymal gland function in patients with SjD with M_1R, M_3R, or M_5R, or with antibodies against water channels, to a greater extent than in patients without these autoantibodies.

This study was strengthened by a 2-step selection and quantification of autoantibodies targeting the muscarinic acetylcholine

receptor, thereby enhancing the reliability of the findings. Furthermore, validation was carried out on a large SjD cohort recruited from 3 different study centres, as well as on disease controls, including individuals with other AIDs and sicca symptoms. Furthermore, CHO cells, as a model system, are well established in *in vitro* studies and allow standardisation through defined cell numbers and uniform environmental conditions, compared with smooth muscle from the bladder or colon as a model system for demonstrating functional antibodies [25]. In addition, unpublished data from InSCREENeX GmbH showed that no endogenous muscarinic acetylcholine receptors were present in the nontransfected CHO-K1 cells. Accordingly, the observed calcium and cAMP signals were entirely generated by the specific transfected receptor.

With regard to the autoantibody quantification, the limitations of this study include that the autoantibody concentration may be affected by drugs such as immunosuppressants, which induce B lymphocyte depletion and thus may alter autoantibody concentrations. Approximately 5% of patients in our study had received rituximab therapy, which may have contributed to reduced antibody levels. In addition, all study participants were recruited from university hospitals, where disease activity and manifestations were more severe than in medical practice, which may introduce a bias into autoantibody reactivity or correlation analyses. Future studies should examine the consistency of autoantibodies over time and include patients from medical practice. In addition, we observed that autoantibody levels can differ between patient groups. These differences could be influenced by preanalytical factors, such as sample collection, processing, and storage conditions. This underscores the importance of including local control groups when interpreting autoantibody measurements to account for potential procedural variability and ensure reliable comparisons across studies. Regarding the functional analysis of muscarinic autoantibodies, this study lacks an age-matched control group, which is an important consideration for future research. Furthermore, it should be noted that functional experiments conducted on CHO cells may not accurately reflect signalling dynamics, eg, in primary human salivary gland cells. Differences in receptor density, expression patterns, and coupling efficiency can affect the magnitude of calcium or cAMP responses and other downstream signalling events. In addition, *in vitro* systems cannot fully replicate the complex *in vivo* environment, in which additional regulatory factors, cell-to-cell interactions, and tissue architecture influence muscarinic receptor function. Therefore, while these experiments provide valuable mechanistic insight, the observed effects may differ under physiological conditions.

A further limitation of the current study is that receptor subtype expression was not systematically assessed at the RNA or signalling levels in minor salivary gland tissue. Importantly, previous studies investigating muscarinic receptor expression in minor salivary glands were limited by small cohort sizes, inconsistent findings, and methodological challenges, particularly regarding the specificity and validation of antibodies against individual muscarinic receptor subtypes. Future studies using transcriptomic or spatial RNA-based approaches may therefore provide a more comprehensive and reliable characterisation of receptor expression patterns and downstream signalling pathways in salivary gland tissue from patients with SjD.

However, a deeper understanding of the functional properties of autoantibodies is crucial for developing and optimising therapeutic approaches for patients with SjD. For instance, pilocarpine, an M_3R agonist, is used to stimulate saliva and tear secretion for symptomatic relief. The efficacy of pilocarpine may be limited in patients with functionally blocking M_3R antibodies, as the receptor is blocked by these antibodies. Without functional characterisation of autoantibodies, resistance to therapy would remain unrecognised. Therefore, analysing antibody function is essential for understanding the disease, planning individualised therapies, and developing targeted treatment strategies.

In conclusion, autoantibodies against muscarinic receptors (M_1R-M_5R) are present in patients with SjD and may be implicated in the pathogenesis of the disease. These findings, along with further functional analysis, could lead to new therapeutic strategies aimed at targeting functional muscarinic autoantibodies and reducing their inhibitory activity, thereby improving symptom outcomes in SjD.

Competing interests

TW reports a relationship with Amgen, Novartis AG, Johnson & Johnson, that includes: speaking and lecture fees and also reports a relationship with Takeda that includes: funding grants. BS reports a relationship with Boehringer Ingelheim GmbH, GlaxoSmithKline Inc, and AstraZeneca that includes: speaking and lecture fees. All other authors declare they have no competing interests.

CRediT authorship contribution statement

Fiona Engelke: Writing – review & editing, Writing – original draft, Visualization, Resources, Project administration, Methodology, Investigation, Formal analysis, Data curation, Conceptualization. **Harald Heidecke:** Writing – review & editing, Resources. **Kai Schulze-Forster:** Writing – review & editing, Resources. **Heike Bähre:** Writing – review & editing, Supervision. **Yasmin Liß:** Writing – review & editing, Methodology. **Tina Hagedorn:** Methodology, Writing – review & editing. **Thomas Dörner:** Writing – review & editing, Resources. **Diana Ernst:** Writing – review & editing, Resources. **Jan Gras:** Writing – review & editing, Resources. **Luca Quartuccio:** Writing – review & editing, Resources. **Jacob Ritter:** Writing – review & editing, Resources. **Benjamin Seeliger:** Writing – review & editing, Resources. **Detlef Neumann:** Writing – review & editing, Supervision. **Torsten Witte:** Writing – review & editing, Supervision, Funding acquisition.

Acknowledgements

We are grateful to all members of the outpatient clinics for their support in patient recruitment. We are deeply grateful to the late Prof Salvatore De Vita (University of Udine, Udine, Italy) for facilitating access to the SjD cohort. We would like to thank Katja Kniesch for performing an additional ELISA to confirm the specificity of the assay.

Parts of this work were previously presented at the European Congress of Rheumatology (June 2024, Vienna, Austria) and the 14th International Congress on Autoimmunity (May 2024, Ljubljana, Slovenia).

Funding

Funded by the Deutsche Forschungsgemeinschaft (DFG, German Research Foundation) and Germany's Excellence Strategy - EXC 2155 (project number 390874280).

Patient consent for publication

Written informed consent from study participants was received for the use of their blood material for research purposes.

Ethics approval

This study adhered to the tenets of the Declaration of Helsinki and was approved by the local ethics committee (Vote Hannover Medical School ethical committee number 5582, 29.03.2010; Vote Charité Universitätsmedizin Berlin ethical committee numbers EA1/002/16 and EA1/089/08; Vote University of Udine CEUR-2017-Os-027-ASUIUD, 19.04.2017).

Provenance and peer review

Not commissioned; externally peer reviewed.

Data availability statement

Data are available on reasonable request.

Supplementary materials

Supplementary material associated with this article can be found in the online version at doi:10.1016/j.ard.2026.06.016.

REFERENCES

[1] Mariette X, Criswell LA. Primary Sjögren's syndrome. N Engl J Med. 2018;378(10):931–9. doi: 10.1056/NEJMcp1702514.

[2] Dawson LJ, Field EA, Harmer AR, Smith PM. Acetylcholine-evoked calcium mobilization and ion channel activation in human labial gland acinar cells from patients with primary Sjögren's syndrome. Clin Exp Immunol. 2001;124(3):480–5. doi: 10.1046/j.1365-2249.2001.01526.x.

[3] Bacman S, Sterin-Borda L, Camusso JJ, Arana R, Hubscher O, Borda E. Circulating antibodies against rat parotid gland M3 muscarinic receptors in primary Sjögren's syndrome. Clin Exp Immunol. 1996;104(3):454–9. doi: 10.1046/j.1365-2249.1996.42748.x.

[4] Preuss B, Tunaru S, Henes J, Offermanns S, Klein R. A novel luminescence-based method for the detection of functionally active antibodies to muscarinic acetylcholine receptors of the M3 type (mAchR3) in patients' sera. Clin Exp Immunol. 2014;177(1):179–89. doi: 10.1111/cei.12324.

[5] Tsuboi H, Matsumoto I, Wakamatsu E, Nakamura Y, Iizuka M, Hayashi T, et al. New epitopes and function of anti-M3 muscarinic acetylcholine receptor antibodies in patients with Sjögren's syndrome. Clin Exp Immunol. 2010;162(1):53–61. doi: 10.1111/j.1365-2249.2010.04188.x.

[6] Watson EL, Abel PW, DiJulio D, Zeng W, Makoid M, Jacobson KL, et al. Identification of muscarinic receptor subtypes in mouse parotid gland. Am J Physiol. 1996;271(3 Pt 1):C905–13. doi: 10.1152/ajpcell.1996.271.3.C905.

[7] Flock T, Hauser AS, Lund N, Gloriam DE, Balaji S, Babu MM. Selectivity determinants of GPCR-G-protein binding. Nature. 2017;545(7654):317–22. doi: 10.1038/nature22070.

[8] Venkatakrishnan AJ, Deupi X, Lebon G, Tate CG, Schertler GF, Babu MM. Molecular signatures of G-protein-coupled receptors. Nature. 2013;494(7436):185–94. doi: 10.1038/nature11896.

[9] Ryberg AT, Warfvinge G, Axelsson L, Soukup O, Götrick B, Tobin G. Expression of muscarinic receptor subtypes in salivary glands of rats, sheep and man. Arch Oral Biol. 2008;53(1):66–74. doi: 10.1016/j.archoralbio.2007.07.012.

[10] Ueda H, Mitoh Y, Fujita M, Kobashi M, Yamashiro T, Sugimoto T, et al. Muscarinic receptor immunoreactivity in the superior salivatory nucleus neurons innervating the salivary glands of the rat. Neurosci Lett. 2011;499(1):42–6. doi: 10.1016/j.neulet.2011.05.029.

[11] Kay J, Upchurch KS. ACR/EULAR 2010 rheumatoid arthritis classification criteria. Rheumatology (Oxford) 2012;51(Suppl 6):vi5–9. doi: 10.1093/rheumatology/kes279.

[12] Aringer M, Costenbader K, Daikh D, Brinks R, Mosca M, Ramsey-Goldman R, et al. 2019 European League Against Rheumatism/American College of Rheumatology classification criteria for systemic lupus erythematosus. Arthritis Rheumatol. 2019;71(9):1400–12. doi: 10.1002/art.40930.

[13] Shiboski CH, Shiboski SC, Seror R, Criswell LA, Labetoulle M, Lietman TM, et al. 2016 American College of Rheumatology/European League Against Rheumatism classification criteria for primary Sjögren's syndrome: a consensus and data-driven methodology involving three international patient cohorts. Arthritis Rheumatol. 2017;69(1):35–45. doi: 10.1002/art.39859.

[14] Schucht R, Lydford S, Andzinski L, Zauers J, Cooper J, Hauser H, et al. Rapid establishment of G-protein-coupled receptor-expressing cell lines by site-specific integration. J Biomol Screen. 2011;16(3):323–31. doi: 10.1177/1087057110396371.

[15] Yoon C, Kim D, Lim JH, Lee GM. Forskolin increases cAMP levels and enhances recombinant antibody production in CHO cell cultures. Biotechnol J. 2020;15:2000264. doi: 10.1002/biot.202000264.

[16] Kovács L, Marczinovits I, György A, Tóth GK, Dorgai L, Pál J, et al. Clinical associations of autoantibodies to human muscarinic acetylcholine receptor 3 (213-228) in primary Sjogren's syndrome. Rheumatology (Oxford). 2005;44(8):1021–5. doi: 10.1093/rheumatology/keh672.

[17] Longobardi S, Lopez-Davis C, Khatri B, Georgescu C, Pritchett-Frazee C, Lawrence C, et al. Autoantibodies identify primary Sjögren's syndrome in patients lacking serum IgG specific for Ro/SS-A and La/SS-B. Ann Rheum Dis. 2023;82(9):1181–90. doi: 10.1136/ard-2022-223105.

[18] Reina S, Pisoni C, Eimon A, Carrizo C, Arana R, Borda E. Anti-M3 muscarinic acetylcholine receptor antibodies in systemic lupus erythematosus. Pharmacol Pharm. 2015;6:25–33. doi: 10.4236/pp.2015.61004.

[19] Kawaguchi Y, Nakamura Y, Matsumoto I, Nishimagi E, Satoh T, Kuwana M, et al. Muscarinic-3 acetylcholine receptor autoantibody in patients with systemic sclerosis: contribution to severe gastrointestinal tract dysmotility. Ann Rheum Dis. 2009;68(5):710–4. doi: 10.1136/ard.2008.096545.

[20] Li J, Ha YM, Kü NY, Choi SY, Lee SJ, Oh SB, et al. Inhibitory effects of autoantibodies on the muscarinic receptors in Sjögren's syndrome. Lab Invest. 2004;84(11):1430–8. doi: 10.1038/labinvest.3700173.

[21] Robinson CP, Brayer J, Yamachika S, Esch TR, Peck AB, Stewart CA, et al. Transfer of human serum IgG to nonobese diabetic Igmu null mice reveals a role for autoantibodies in the loss of secretory function of exocrine tissues in Sjögren's syndrome. Proc Natl Acad Sci U S A. 1998;95(13):7538–43. doi: 10.1073/pnas.95.13.7538.

[22] Dawson LJ, Allison HE, Stanbury J, Fitzgerald D, Smith PM. Putative anti-muscarinic antibodies cannot be detected in patients with primary Sjogren's syndrome using conventional immunological approaches. Rheumatology (Oxford). 2004;43(12):1488–95. doi: 10.1093/rheumatology/keh389.

[23] Roescher N, Kingman A, Shirota Y, Chiorini JA, Illei GG. Peptide-based ELISAs are not sensitive and specific enough to detect muscarinic receptor type 3 autoantibodies in serum from patients with Sjogren's syndrome. Ann Rheum Dis. 2011;70(1):235–6. doi: 10.1136/ard.2010.129049.

[24] Wang X, Wu H, Zhong B, Zhang L, Wang Y. Autoantibody against aquaporin-5 may be a new diagnostic biomarker for primary Sjögren's syndrome. Clin Rheumatol. 2024;43(12):3781–7. doi: 10.1007/s10067-024-07190-1.

[25] Waterman SA, Gordon TP, Rischmueller M. Inhibitory effects of muscarinic receptor autoantibodies on parasympathetic neurotransmission in Sjögren's syndrome. Arthritis Rheum. 2000;43(7):1647–54. doi: 10.1002/1529-0131(200007)43:7<1647::AID-ANR31>3.0.CO;2-P.

Ann Rheum Dis 85 (2026) 1784–1799

Contents lists available at ScienceDirect

Annals of the Rheumatic Diseases

journal homepage: https://www.sciencedirect.com/journal/annals-of-the-rheumatic-diseases

Sjögren's Disease

Mitochondrial-impaired ductal epithelium fuels TLS formation in Sjögren's disease

Yuan Zong[1,a], Yi Yang[1,a], Jiawen Zhao[1,a], Shiyi Wen[2,a], Lei Li[3], Na Xiong[2], Tong Wu[1], Xiaoyu Zhao[1], Yiming Gao[1], Ning Li[1,*], Guojun Shi[2,**], Liting Jiang[1,***]

[1] *Department of Stomatology, Ruijin Hospital, Shanghai Jiao Tong University School of Medicine; College of Stomatology, Shanghai Jiao Tong University, Shanghai, China*

[2] *Department of Endocrinology & Metabolism, Guangdong Provincial Key Laboratory of Diabetology, The Third Affiliated Hospital of Sun Yat-sen University, Guangzhou, China*

[3] *Department of Pathology, Ruijin Hospital, Shanghai Jiao Tong University School of Medicine, Shanghai, China*

ARTICLE INFO

Article history:
Received 31 July 2025
Received in revised form 17 April 2026
Accepted 11 May 2026

ABSTRACT

Objectives: Progressive inflammatory cell infiltration within salivary glands is a defining feature of advanced Sjögren's disease (SjD) and is frequently accompanied by tertiary lymphoid structure (TLS) formation. However, the initial events driving this pathogenic trait in SjD progression are not fully understood.

Methods: We collected 848 labial salivary gland (LSG) biopsies (668 SjD, 180 non-SjD) and profiled bulk transcriptomics, single cell RNA-sequencing (scRNA-seq), spatial transcriptomics, transmission electron microscopy (TEM), and histology. *In vivo* functional validation was performed in NOD/ShiLtj mice with spontaneous SjD via nicotinamide mononucleotide administration to restore mitochondrial function.

Results: Mitochondrial function was impaired in LSG tissues from SjD patients, with functional validation in NOD/ShiLtj mice showing attenuated ductal injury and reduced immune cell infiltration. scRNA-seq analyses revealed that each LSG cellular subset harbours a distinct mitochondrial transcriptional profile, which we identified here as a molecular fingerprint for individual cellular subsets. TEM established an ultrastructural atlas of human minor salivary glands, showing that striated duct (SD) cells are most enriched with mitochondria among all epithelial subtypes. In SjD LSGs, particularly those with TLSs, profound mitochondrial dysfunction and impaired oxidative phosphorylation were observed. A previously unrecognized proinflammatory SD subset, SD-C1 (marked by matrix metalloproteinase 7), was markedly expanded in SjD-TLS+ tissues and exhibited severe mitochondrial impairment. SD-C1 cells showed enhanced crosstalk with T cells, B cells, and macrophages via immune signalling pathways and were spatially colocalized with immune cell aggregates in periductal regions where TLSs formed.

Conclusions: Mitochondrial injury in SD epithelial cells emerges as a trigger of TLS formation and progressive autoimmunity in SjD. Therapies that preserve mitochondrial integrity and functionality in ductal cells may mitigate salivary gland degeneration during SjD progression.

*Correspondence to Dr Ning Li. **Correspondence to Dr Guojun Shi. ***Correspondence to Dr Liting Jiang.

E-mail addresses: ln11448@rjh.com.cn (N. Li), shigj6@mail.sysu.edu.cn (G. Shi), jlt11392@rjh.com.cn (L. Jiang).

Handling editor Josef S Smolen

[a] Yuan Zong, Yi Yang, Jiawen Zhao, and Shiyi Wen contributed equally to this work and share first authorship.

https://doi.org/10.1016/j.ard.2026.05.014

0003-4967/© 2026 The Author(s). Published by Elsevier B.V. on behalf of European Alliance of Associations for Rheumatology (EULAR). This is an open access article under the CC BY-NC-ND license (http://creativecommons.org/licenses/by-nc-nd/4.0/)

WHAT IS ALREADY KNOWN ON THIS TOPIC

- Organ-specific lymphocytic infiltration is central to the pathogenesis and diagnosis of Sjögren's disease (SjD). The infiltrates accumulate preferentially around salivary duct epithelia, a distribution pattern that is challenging to interpret.
- Persistent activation of these infiltrating lymphocytes can drive their organization into ectopic lymphoid structures, establishing a self-perpetuating circuit between immune and epithelial cells.
- Mitochondrial injury and dysfunction have been documented in both salivary gland epithelial cells and lymphocytes from patients with SjD.
- Previous studies of labial salivary glands suggest the mitochondria-related phenotypic changes and disturbed organelle homeostasis in disease pathobiology.

WHAT THIS STUDY ADDS

- Single-cell RNA sequencing combined with spatial transcriptomics identified and localized striated duct (SD) epithelial cells that harbour extensive mitochondrial dysfunction and play potential roles in immune cell recruitment.
- Mitochondrial gene expression profiles serve as cell type-specific signatures, which distinguish epithelial subsets within the salivary gland.
- Systematic transmission electron microscopy analysis revealed the first ultrastructural atlas of mitochondrial morphology across major cell clusters in salivary gland.
- Comparative mapping of immune microenvironment was performed in salivary glands from SjD patients and controls. It revealed that a high MMP7-expressing SD subcluster in salivary glands with mitochondrial dysfunction correlates with lymphocyte recruitment and tertiary lymphoid structure formation, delineating a proinflammatory niche that might induce SjD initiation and progression.

HOW THIS STUDY MIGHT AFFECT RESEARCH, PRACTICE OR POLICY

- This study demonstrates that mitochondrial dysfunction in specific SD cell subclusters may play a pivotal role in SjD by promoting immune infiltration, which represents a potential target for preventing SjD onset and progression.
- This study introduces a stratification strategy that may enable more refined risk assessment and precision medicine for SjD patients based on pathology.

INTRODUCTION

Sjögren's disease (SjD) is a common autoimmune disorder primarily causing ocular and oral dryness [1,2]. Reduced salivary flow leads to dry mouth, swallowing difficulties, taste alterations, and oral discomfort, all of which significantly increase the risk of dental caries [3]. Current management of SjD mainly involves immunosuppressors; targeted therapies are still lacking [4,5] due to the limited knowledge on the identified molecular drivers of SjD pathogenesis. Persistent inflammatory response is recognized as a central pathogenic mechanism in autoimmune diseases like SjD [6]. Unlike the self-limiting inflammation caused by acute insults, autoimmune-mediated chronic inflammation persists due to microenvironmental reprogramming that sustains activation of immune response and disruption of cellular homeostasis [7,8]. Recent studies have revealed the involvement of various immune cells and inflammatory cytokines in the development of SjD [9].

Salivary gland epithelial cells (SGECs) may serve as antigen-presenting cells that orchestrate both innate and acquired immune responses and are acknowledged as central regulators of localized autoimmune responses in SjD by secreting diverse proinflammatory molecules that mediate local lymphocyte activation [10,11]. Conversely, infiltrating immune cells and the proinflammatory microenvironment further activate immune response or regulate survival of epithelial cells [12]. This reciprocal activation between somatic and immune cells sustains chronic autoimmune reactivity in their respective tissues [10]. In biopsy samples of labial salivary glands (LSGs), lymphocyte clusters are frequently observed around the ductal epithelium [10], and with persistent stimulation from chronic inflammation, specialized lymphoid aggregates known as tertiary lymphoid structures (TLSs) form. The appearance of TLSs increases the risk of B-cell lymphoma, which commonly arises in the salivary gland [13]. TLSs might serve as observable biomarkers for risk stratification of patients as well as B-cell targeted therapy [14]. Although damage of epithelial cells is regarded as a critical step in the formation of TLSs [15], the timing-dependent molecular events necessary for TLS development, as well as their role in the pathogenesis of SjD, remain to be investigated.

Among the numerous cellular and molecular events that maintain the homeostasis of SGECs, the role of the unique metabolic profile of SGECs has recently emerged. Under steady-state conditions, SGECs require a considerable amount of energy to maintain the function of ion pumps for nutrient transport and cellular homeostasis [16]. As the central organelle for cellular energy and metabolite production, mitochondria are integral to apoptosis, maintenance of cellular homeostasis, and regulation of immune responses [17,18]. The structural integrity of mitochondrial membranes and cristae determines electron transport chain efficiency and respiratory capacity, and structural perturbations are closely associated with bioenergetic dysfunction [19,20]. Increasing evidence has demonstrated mitochondrial bioenergetic impairment and ultrastructural abnormalities in SGECs of SjD patients [21]. A recent study in a SjD disease model reported the combined cellular events of dysregulated Ca^{2+} signalling, secretory defects, and abnormal mitochondrial morphology and function [22]. Our previous studies also demonstrated the coexistence of mitochondrial dysfunction and immune microenvironmental remodelling in SjD salivary glands [23–25]. It is important to note that mitochondrial metabolism may be differentially regulated across SGEC subtypes. For example, the striated ducts (SDs) and intercalated ducts (IDs), which serve as the primary site for ion reabsorption, require the persistent function of Na^+/K^+-ATPase [26]. Although these reports suggest that mitochondrial dysfunction in epithelial cells plays a critical role in triggering the regulatory networks underlying microenvironment remodelling in SjD [1,17,27], whether and how mitochondrial alterations in specific epithelial cell types drive TLS formation remains to be illustrated.

Here, TLS-positive SjD salivary glands exhibited reduced oxidative phosphorylation (OXPHOS) complex protein levels and diminished cytochrome c oxidase (COX), succinate dehydrogenase (SDH), and nicotinamide adenine dinucleotide (NADH) histochemical activity, indicative of impaired mitochondrial respiratory function. Through ultrastructural analysis, a comprehensive mitochondrial atlas of key cell clusters was established in salivary gland tissue from SjD patients and revealed that SD epithelial cells were enriched in mitochondria exhibiting extensive structural abnormalities. Guided by single-cell RNA sequencing (scRNA-seq) and spatial transcriptomic (ST) analysis, a pathogenic ductal subpopulation was identified with elevated inflammatory cytokine expression, which orchestrated TLS-related remodelling of the immune microenvironment. These findings indicate that mitochondrial dysfunction in

specific ductal cell populations may trigger signalling cascades that promote the periductal lymphoid infiltration, potentially culminating in TLS formation.

This study suggests a potentially pathogenic crosstalk between epithelial and immune cells in SjD progression, providing not only new insights on pathogenic mechanisms, but also therapeutic strategies against SjD.

METHODS

Methods are detailed in the Supplementary Materials.

RESULTS

Mitochondrial dysfunction in LSG features in SjD cases with TLS

To investigate the pathogenesis of SjD and define the cellular drivers of lymphocytic infiltration, we established a multimodal profiling cohort of 848 LSG samples from 848 patients, among which 668 patients were classified as SjD and 180 patients were classified as non-SjD, accordingly [28] (Fig 1A). To dissect the molecular and cellular basis of the disease, we performed bulk RNA sequencing (bulk RNA-seq) on a subset of 178 samples (117 SjD, 61 non-SjD). To resolve these bulk transcriptomic signals into cell type-specific programs and identify distinct molecular endotypes, we conducted scRNA-seq on 10 samples (7 SjD, 3 non-SjD). The resulting single cell atlas was further integrated with ST data from 11 samples (7 SjD, 4 non-SjD). Complementary histologic and ultrastructural analyses were performed on selected cases (36 samples) for validation in single-cell analyses. Transcriptomic analysis revealed that pathways associated with apoptosis and inflammatory response were upregulated in patients with SjD versus non-SjD, which is in accordance with the histopathology of lymphocyte aggregation in SjD (Fig 1B and Supplementary Table S3). Furthermore, the mRNA level of AQP5, which is a water channel protein that plays a critical role in saliva secretion [29], was significantly downregulated in the SjD group. The apoptosis pathway was also significantly upregulated in patients with SjD (Fig 1C and Supplementary Table S3). Gene set enrichment analysis (GSEA) based on bulk RNA-seq indicated that the SjD group was associated with a mitochondrial damage-associated molecular pattern (DAMP) and activation of the innate immune response (Fig 1D and Supplementary Table S3). These data suggest that mitochondrial dysfunction may play an important role in SjD pathogenesis.

TLSs, which are formed at sites of chronic inflammation in nonlymphoid organs and are characterized by B cell follicles surrounded by T cell-enriched zones [13], have been shown to be associated with increased disease severity in autoimmune diseases [15,30]. Previous studies have reported that TLS formation in SjD is associated with increased disease severity, specific pathological features, and increased risk of secondary B-cell lymphoma [31–34]. To investigate the association between TLSs and SjD progression, patients were grouped into 2 cohorts based on histologic identification of TLSs, those with (SjD-TLS +) and without (SjD-TLS-) TLSs. Histopathological assessment of LSGs from SjD-TLS+ patients demonstrated prominent TLS formation characterised by organized B-cell follicles (marked by CD20) encircled by T cells (marked by CD3) and a central follicular dendritic cell (FDC) (marked by CD21), which was notably absent in SjD-TLS- patients. Besides, SjD-TLS+ samples had elevated protein levels of MHC-I, MHC-II and BCL-2, exhibiting enhanced antigen-presenting capacity and severe mitochondrial impairment (Fig 1E). We further investigated the potential correlation among clinical characteristics of patients (SjD-related serological markers), glandular function, mitochondrial function, and the pathways highlighted in Figure 1D. The Mantel test showed that the expression levels of either glandular function- or mitochondrial function-related genes were negatively correlated with clinical markers (Fig 1F and Supplementary Table S3). Western blot analysis with antibodies against representative subunits of the mitochondrial OXPHOS complexes, NDUFA9 (complex I), SDHB (complex II), UQCRC2 (complex III), MTCO1 (complex IV), and ATP5A (complex V), confirmed a decline of the expression levels of these OXPHOS complex proteins in SjD-TLS+ tissues (Fig 1G). In line with previous reports [21], LSGs from the SjD-TLS+ group exhibited impaired mitochondrial function accompanied by increased apoptosis (Fig 1H and Supplementary Fig S1). Expression levels of mitochondrial enzymes were further assessed by Alcian blue–periodic acid–Schiff, modified Gomori trichrome, NADH, SDH, as well as COX staining on frozen tissue sections [35] (Fig 1I). Healthy salivary glands exhibited normal levels of COX mitochondrial enzymes in ductal compartments, which were markedly diminished in SjD-TLS+ tissues. These findings reveal that mitochondrial impairment in ductal epithelial cells coexists with local immune activation and TLS formation, and that this co-occurring phenomenon correlates with more active clinical features in SjD patients.

To further investigate the contribution of mitochondrial dysfunction to SjD pathogenesis, nicotinamide mononucleotide (NMN) was administered to nonobese diabetic (NOD/ShiLtJ) mice, a well-established SjD model, to verify the effect of enhanced mitochondrial function on glandular functional restoration (Fig 1J). NMN, a biosynthetic precursor of NAD^+, an essential coenzyme in mitochondrial energy metabolism [36], has been shown to improve mitochondrial function in various disease models [37–39]. OXPHOS-related gene sets were scored using single-sample gene set enrichment (ssGSEA) analysis [40]. The ssGSEA heatmap revealed significant upregulation of core OXPHOS pathways in NMN-treated samples compared with controls (Fig 1K), indicating NMN-mediated restoration of mitochondrial functionality. After administration of NMN, focal aggregation of lymphocytes was alleviated, and the swollen mitochondrial morphology was significantly restored in salivary gland tissues of NOD mice (Fig 1L-N). Spearman correlation analysis in human samples further revealed that mitochondrial function positively correlated with acinar and ductal markers but negatively with fibroblast-associated genes (Fig 1O). Overall, we confirmed the correlation between mitochondrial impairment and glandular dysfunction in SjD, indicating that amelioration of mitochondrial impairment could serve as a therapeutic target for SjD.

Signatures of mitochondrial gene expression profiles distinguish LSG cellular subsets

To elucidate a possible role of cell-type dependent mitochondrial disfunction in the pathogenesis of SjD patients, scRNA-seq analysis was conducted on human LSG samples (Fig 2A). A total of 123,876 cells from 10 individuals (SjD, $n = 7$; non-SjD, $n = 3$) were sequenced, and 84,005 cells were retained for downstream analysis. Unsupervised clustering delineated 21 transcriptionally distinct subpopulations comprising 6 acinar subtypes, 3 ductal subtypes, 6 immune cell subtypes, and 4 stromal subtypes (Fig 2B-C and Supplementary Table S4). Within the LSG subpopulations, a distinct MT (mitochondria gene)-high subset was identified. These MT-high cells not only showed

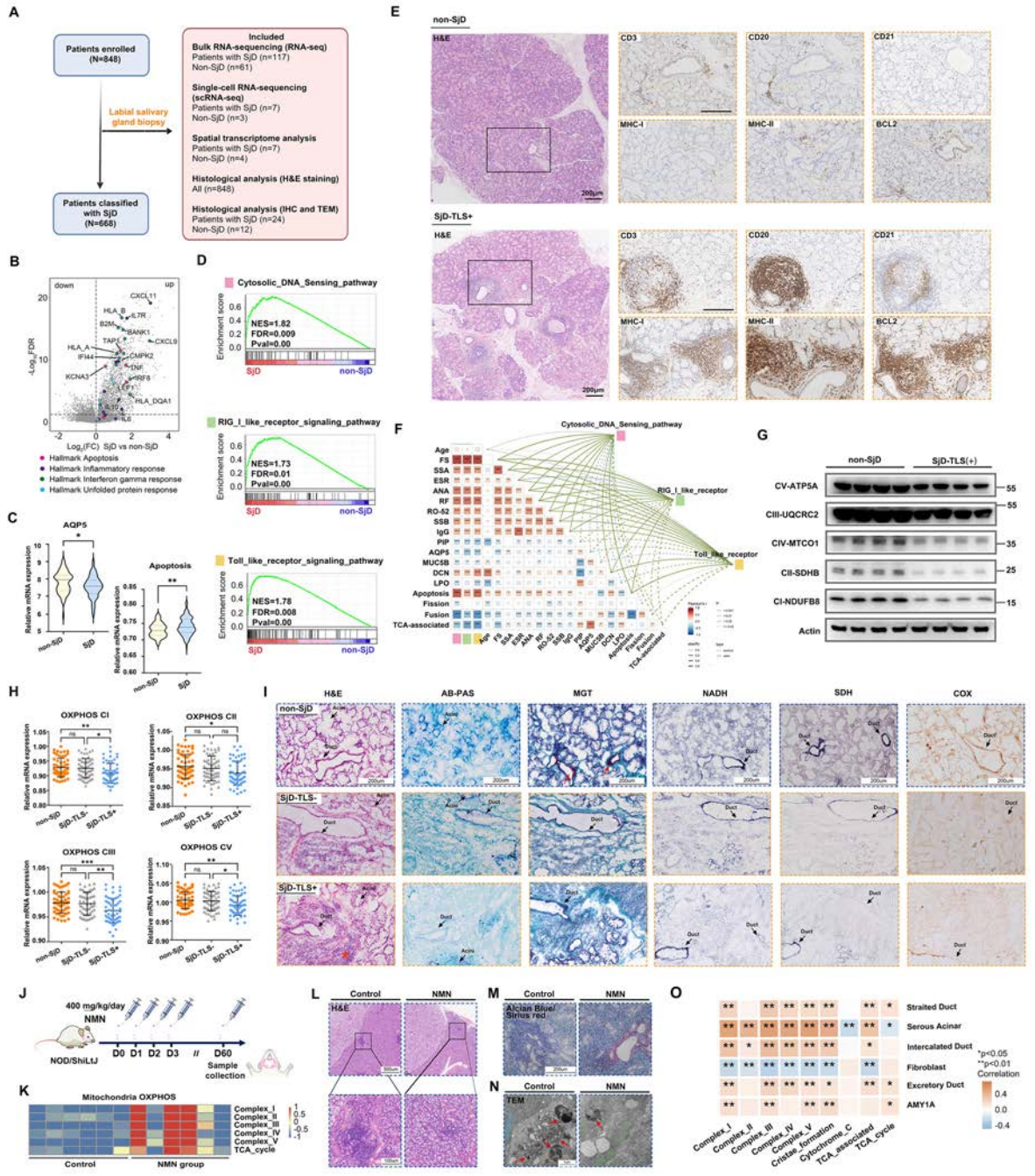

Figure 1. Transcriptional and histological profiling reveals mitochondrial signatures in SjD labial salivary glands (LSGs). A, Study overview. Bulk RNA-seq: SjD (n = 117), non-SjD (n = 61); scRNA-seq: SjD (n = 7), non-SjD (n = 3); spatial transcriptomics: SjD (n = 7), non-SjD (n = 4). H&E staining was performed on all participants (n = 848); IHC and TEM on selected SjD (n = 24) and non-SjD (n = 12) samples. B, Volcano plot showing upregulated DEGs enriched in Hallmark pathways in SjD vs non-SjD. Dotted lines denote FDR = 0.05 and fold-change threshold. C, mRNA expression of AQP5 and ssGSEA score for apoptosis in non-SjD and SjD groups (*P < .05; **P < .01). D, GSEA plots comparing pathway enrichment between SjD and non-SjD; NES, FDR, and P values are indicated. E, Representative H&E and IHC images showing CD3, CD20, CD21, major histocompatibility complex (MHC)-I, MHC-II, and BCL2 in non-SjD and SjD-TLS + tissues. Scale bars, 200 μm. F, Correlation among the selected pathways, namely, cytosolic DNA sensing, RIG-I-like receptor, and Toll-like receptor signalling pathways, the clinical characteristics of patients, mRNA expression of genes related to glandular function, and ssGSEA scores for mitochondrial function. Statistical analysis was performed using the Mantel test, with green lines indicating $P < 0.001$, blue lines $.001 \leq P < .01$, and red lines $.01 \leq P < .05$. The edge width corresponds to the R-value (Mantel test). The solid lines indicate a positive correlation, and the dotted lines indicate a negative correlation. The relationship between variables was examined by estimating Pearson correlation coefficients. G, Western blot analysis of mitochondrial oxidative phosphorylation (OXPHOS) complex proteins in non-SjD and SjD-TLS + groups. H, ssGSEA scores for OXPHOS Complex I, II, III, and IV across non-SjD, SjD-TLS−, and SjD-TLS + groups (*P < .05; **P < .01; ***P < .001). I, Representative LSG fresh frozen tissue sections stained with H&E, Alcian blue-periodic acid-Schiff (AB-PAS), modified Gomori trichrome (MGT), nicotinamide adenine dinucleotide (NADH), succinate dehydrogenase (SDH), and cytochrome c oxidase (COX). Black arrows: acini and ducts; red arrows: MGT-positive ducts; red asterisks: lymphocyte infiltrates. Scale bars, 200 μm. J, Schematic diagram describing experimental strategies in SjD model mice. NOD/ShiLtJ, nonobese diabetic mice; NMN, nicotinamide mononucleotide. K, Heatmap of mitochondria OXPHOS-related ssGSEA scores across mice samples from the control and NMN groups. L, Representative H&E images of mice glandular tissues from the control and NMN groups. Low-magnification scale bar, 500 μm; high-magnification scale bar, 100 μm. M, Representative Alcian blue/Sirius red staining images of mice glandular tissues from the control and NMN groups. Scale bar, 200 μm. N, Representative TEM images of mice glandular tissues from the control and NMN groups.

elevated expression of mitochondrial DNA (mtDNA)-encoded genes but also exhibited negligible expression of OXPHOS-related genes, which may represent dying or necrotic cells (Supplementary Fig S2). Canonical marker-driven principal component analysis (PCA) demonstrated that adjacent clusters, such as acinar and ID populations, might share a common developmental origin [16] (Fig 2D). mRNA expression profiles of the 13 protein-coding mitochondrial genes encoded by mtDNA were analysed across clusters [41], revealing that MT-high cells expressed these genes at markedly elevated levels (Fig 2E). Intriguingly, PCA based on mitochondrial gene expression demonstrated discriminatory power comparable to that of canonical markers across cell clusters (Fig 2F). These findings suggest that mitochondrial gene expression profiles could serve as "fingerprints" capable of reliably distinguishing epithelial and immune cell subtypes, thereby proposing mitochondrial transcripts as potential markers of cellular identity. Among epithelial subtypes, SD cells showed increased mitochondrial gene expression, consistent with their mitochondria-rich phenotype. However, SD cells from SjD patients showed marked downregulation of genes involved in mitochondrial function compared with cells from non-SjD controls. We further validated these results by integrating and reprocessing the public GSE272409 dataset with the same analytical workflow (Fig 2G, Supplementary Table S4, and Supplementary Fig S11 and S12).

To investigate the localization of the subpopulations identified via scRNA-seq, the marker genes were mapped onto the ST matrix, thereby validating the identified cell types and delineating their spatial organization (Fig 2H). Within the region of interest from SjD-TLS+ tissues, ST analysis revealed a marked enrichment of B cell-dominated immune infiltrates surrounding SDs, as well as a substantial accumulation of T cells and myeloid populations. To verify the consistency of multimodal data, we performed integrative deconvolution analyses using our scRNA-seq cell atlas as the reference: Bisque was applied to deconvolute bulk RNA-seq data [42], and cell2location was used to resolve spatial cellular composition from ST data. All 3 deconvolution approaches consistently revealed disease-associated cellular shifts in LSGs (Fig 2I and Supplementary Table S4). Acinar cells were reduced in SjD, consistent with glandular atrophy, as reported previously [43]. Notably, scRNA-seq revealed a specific expansion of SD cells in SjD (3% in non-SjD controls vs 7% in SjD). This observation, together with our expression heatmaps, confirmed that the reduced mitochondrial protein levels observed by western blotting are not explained by changes in epithelial cell abundance, thus eliminating compositional bias as a confounding factor (Fig 1G). In parallel, T and B cell infiltration was markedly increased in SjD, reflecting robust chronic inflammation and immune recruitment.

Overall, these findings delineate a unique cell type-specific landscape of mitochondrial gene expression across major cell populations in human LSGs. Mitochondrial dysfunction signatures were selectively and prominently enriched in SD cells, representing a key disease-associated feature of SjD. Meanwhile, the spatial clustering pattern further supports that damaged SD cells contribute to mediating local immune responses in the LSG microenvironment.

Quantitative mitochondrial characteristics distinguish glandular and stromal cell subsets in SjD-TLS+ group

Consistent with our prior histologic staining results for mitochondrial oxidative respiratory chain enzyme activities on frozen tissue sections (Fig 1I), staining for COXIV (often used as a mitochondrial resident protein marker) revealed reduced COXIV protein levels in paraffin-embedded SjD-TLS+ LSG tissue sections compared with SjD-TLS− tissue, consistent with the above data on scRNA-seq and disruption of ductal epithelial integrity. Prominent lymphocytic infiltration was observed surrounding disrupted ducts, and COXIV expression was notably reduced in these regions in SjD-TLS+ LSG tissues (Fig 3A). Furthermore, ultrastructural mitochondrial architectures were systematically mapped across distinct epithelial cell subtypes in salivary gland as well as other stromal cells using TEM. Distinct mitochondrial morphologies were identified in LSGs and classified into 3 types: Type I (normal), Type II (abnormal, mild), and Type III (abnormal, severe) (Fig 3B). In non-SjD samples, ductal epithelial cells exhibited mitochondria with well-organized cristae and closely associated endoplasmic reticulum (ER) structures. Desmosomal junctions linking adjacent cells were also evident (Fig 3C, non-SjD). Given that ID cells function as bipotent secretory progenitors, and SD cells are dedicated to active ion transport via Na^+/K^+-ATPase [26], both cell types demand an intensive energy supply. Consistently, TEM revealed abundant mitochondria in both duct cell types, with SD cells having the most mitochondria among the salivary gland epithelial subtypes (Fig 3F). In SjD-TLS+ patients, mitochondria within intercalated and SD cells displayed pronounced swelling, reduced cristae density, and disrupted ultrastructure, which are hallmarks of Type III morphology, indicating marked mitochondrial morphologic abnormality. Necrotic cells were observed adjacent to severely compromised ducts (Fig 3C, SjD). Ultrastructural analysis of seromucous acinar cells revealed abundant rough ER and elongated, rod-shaped mitochondria adjacent to homogeneous secretory vesicles within the apical cytoplasm (Fig 3D). In contrast, mucous acinar cells exhibited fewer rough ER structures, fewer mitochondria, and larger secretory granules. In SjD-TLS+ acinar cells, both ER and mitochondria appeared swollen, and mitochondrial cristae were disrupted compared with non-SjD cells. Similar mitochondrial abnormalities were observed in other epithelial cells and fibroblasts from SjD-TLS+ samples (Fig 3E), and mitochondrial autophagosomes were also detected in vascular endothelial cells. Quantitative assessment confirmed a significant increase of abnormal mitochondria in LSGs from SjD patients compared with non-SjD controls, which is consistent with the mitochondrial ultrastructural changes previously observed in the SGECs of SjD patients [17]. We then conducted a detailed quantitative analysis of the proportion of abnormal mitochondria. Notably, the proportion of abnormal mitochondria in SD cells from SjD samples approached almost 100% (Fig 3G), underscoring the extensive morphologic alterations associated with TLS formation. Complementing our scRNA-seq profiles, these findings demonstrated pronounced accumulation of abnormal mitochondria in SD cells in the SjD-TLS+ group.

Green, blue, and orange pseudocolour indicates normal mitochondria, swollen mitochondria, and severely swollen mitochondria with disrupted cristae. Red asterisks: lysosomes. Scale bar, 1 μm. O, Spearman correlation between the mitochondrial function and glandular function in human LSGs. Colours reflect the strength of the correlations (*$P < .05$; **$P < .01$). AQP5, aquaporin 5; DEG, differentially expressed gene; FDR, false discovery rate; H&E, haematoxylin and eosin; IHC, immunohistochemistry; NES, normalized enrichment score; ssGSEA, single-sample gene set enrichment analysis; SjD, Sjögren's disease; TCA, tricarboxylic acid; TEM, transmission electron microscopy; TLS, tertiary lymphoid structure.

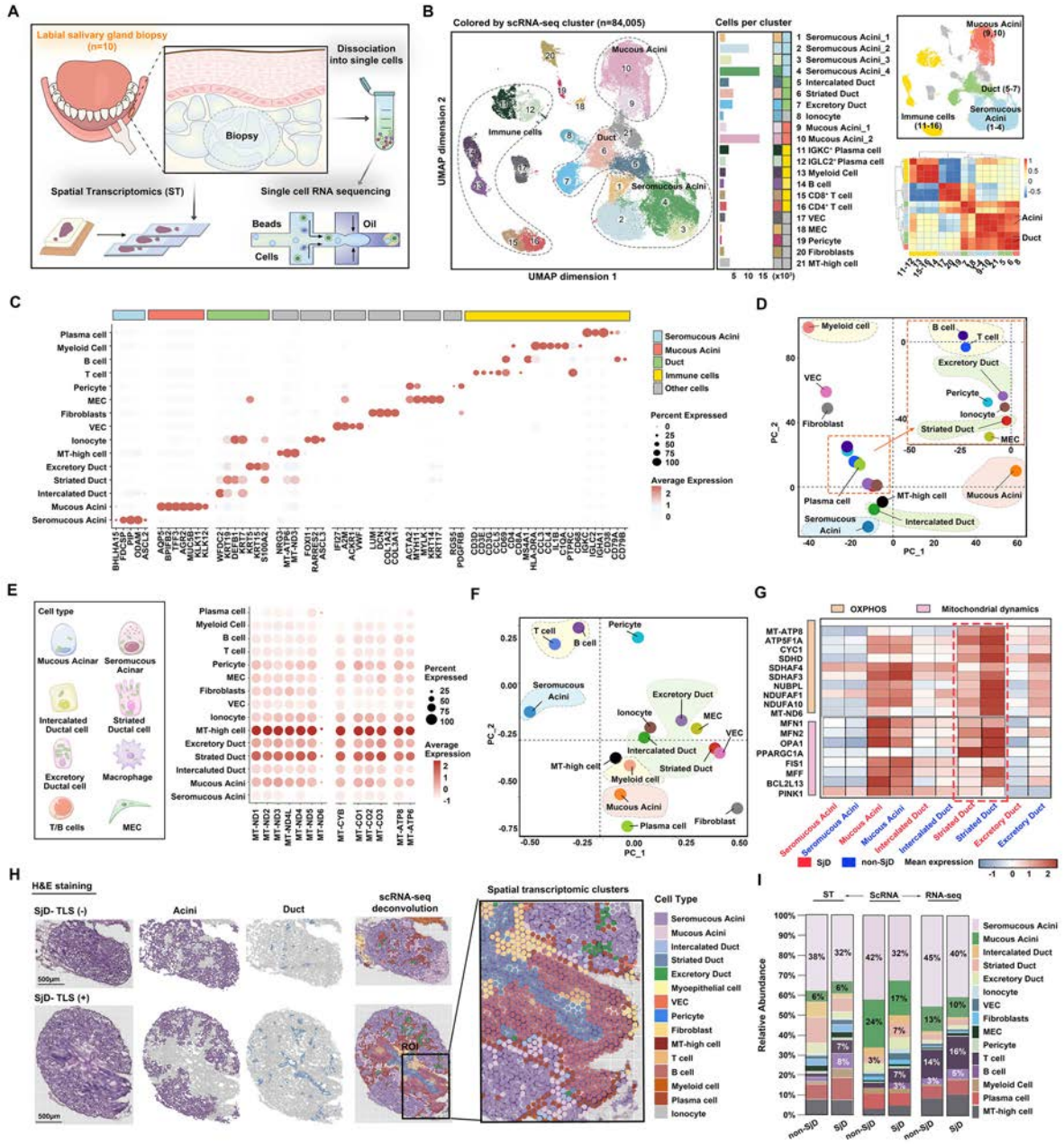

Figure 2. Single-cell atlas of labial salivary glands (LSGs) in SjD and non-SjD. A, Overview of LSG biopsy processing for scRNA-seq. B, UMAP plot of 10 LSG samples (SjD and non-SjD) identifying 21 cell clusters. Bar graph shows cell abundance per cluster; right panels show cluster annotations and correlation heatmap. C, Dot plot of marker genes for cell type identification. Dot size: percentage of expressing cells; colour: expression level. D, PCA of gene expression profiles, with each point representing a cluster. Background colours indicate cell classification. E, Left: schematic of mitochondrial content across cell types. Right: dot plot of mitochondrial gene expression. F, PCA based on mitochondrial gene expression. G, Heatmap of representative OXPHOS and mitochondrial dynamics genes across acini and duct cell types. H, Left: H&E staining (first column) and spatial mapping of cell clusters (derived from scRNA-seq signatures) in SjD-TLS− and SjD-TLS + tissues. Scale bar, 500 μm. Right: Zoom-in of the region of interest (ROI) from a representative SjD-TLS + spatial profile. Colours denote distinct cell clusters. I, Proportions of major cell populations in SjD vs non-SjD LSGs based on RNA-seq, scRNA-seq and spatial transcriptomics (ST) data. H&E, haematoxylin and eosin; LSG, labial salivary gland; MEC, myoepithelial cell; MT-high, high mitochondrial gene expression; OXPHOS, oxidative phosphorylation; PCA, principal component analysis; scRNA-seq, single-cell RNA sequencing; SjD, Sjögren's disease; TLS, tertiary lymphoid structure; UMAP, Uniform Manifold Approximation and Projection; VEC, vascular endothelial cell.

Mitochondrial abnormalities within SD cells correlate with local immune cell accumulation

scRNA-seq and TEM results revealed both functional impairment and structural abnormalities of mitochondria in duct cells from SjD-TLS + LSGs. As intercellular communications among duct and immune cells are critical for formation of lymphoepithelial lesions [12], differential intercellular communication patterns were compared between SjD-TLS + and non-SjD samples through scRNA-seq analysis (Fig 4A and Supplementary Figs S3 and S4). Compared with non-SjD controls, SD cells in SjD-TLS + LSGs showed enhanced crosstalk with T cells, B cells, and MT-high cells (Fig 4B), suggesting that these duct cell immune interactions may contribute to inflammatory cascades and apoptotic signalling in SjD. TEM revealed that in SjD-TLS + LSGs, stromal infiltration of immune cells—including mast cells, plasma cells, and lymphocytes—was evident in regions where SD cells displayed structural abnormalities, namely increased

lysosomes, rarefied cytoplasm, and mitochondrial swelling; together, they formed a complex cellular interaction network (Fig 4C). Lymphocyte accumulation was observed within and around blood vessels adjacent to these abnormal duct cells

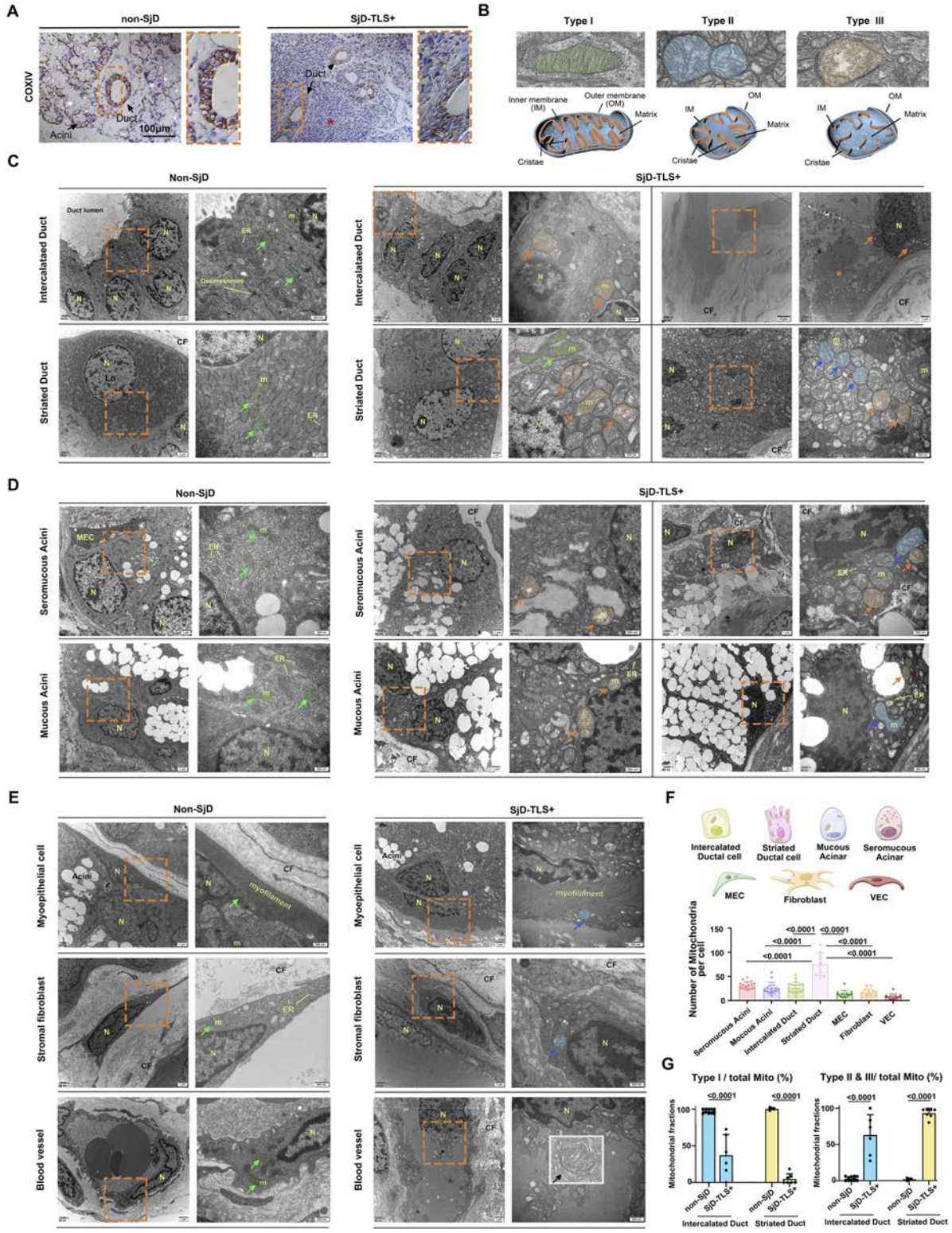

Figure 3. Mitochondrial damage and altered morphology in salivary gland cells from SjD-TLS+ patients. A, Immunohistochemical staining of COX IV in minor salivary gland sections from non-SjD and SjD-TLS+; red asterisks indicate lymphocyte infiltration. B, TEM images of 3 mitochondrial morphologies: Type I (normal), Type II (swollen), and Type III (severely swollen with disrupted cristae). Colour-coded overlays (green, blue, orange) and schematic diagrams shown below. C-E, Representative transmission electron microscopy images of ducts (C), acini (D), and other epithelial cells (E) from non-SjD and SjD-TLS+ LSGs. Green, blue, and orange arrows respectively indicate Type I-III mitochondria; asterisks: necrotic epithelial cells; black arrows: mitochondria within lysosomes. F, Quantification of mitochondrial number across 7 cell types with schematic of mitochondrial content trends: Seromucous acini, $n = 18$; mucous acini, $n = 16$; intercalated duct, $n = 16$; striated duct, $n = 11$; MEC, $n = 14$; fibroblast, $n = 14$; VEC: $n = 16$. MEC, myoepithelial cells; VEC, vascular endothelial cells. G, Proportion of Type I vs Type II & III mitochondria in duct cells, based on cristae and membrane morphology: intercalated duct, $n = 11$ for non-SjD, $n = 6$ for SjD-TLS+; striated duct, $n = 3$ for non-SjD, $n = 7$ for SjD-TLS+. CF, collagen fibers; COX IV, cytochrome c oxidase subunit 4; ER, endoplasmic reticulum; LSG, labial salivary gland; m, mitochondrion; N, nucleus; SjD, Sjögren's disease; TLS, tertiary lymphoid structure.

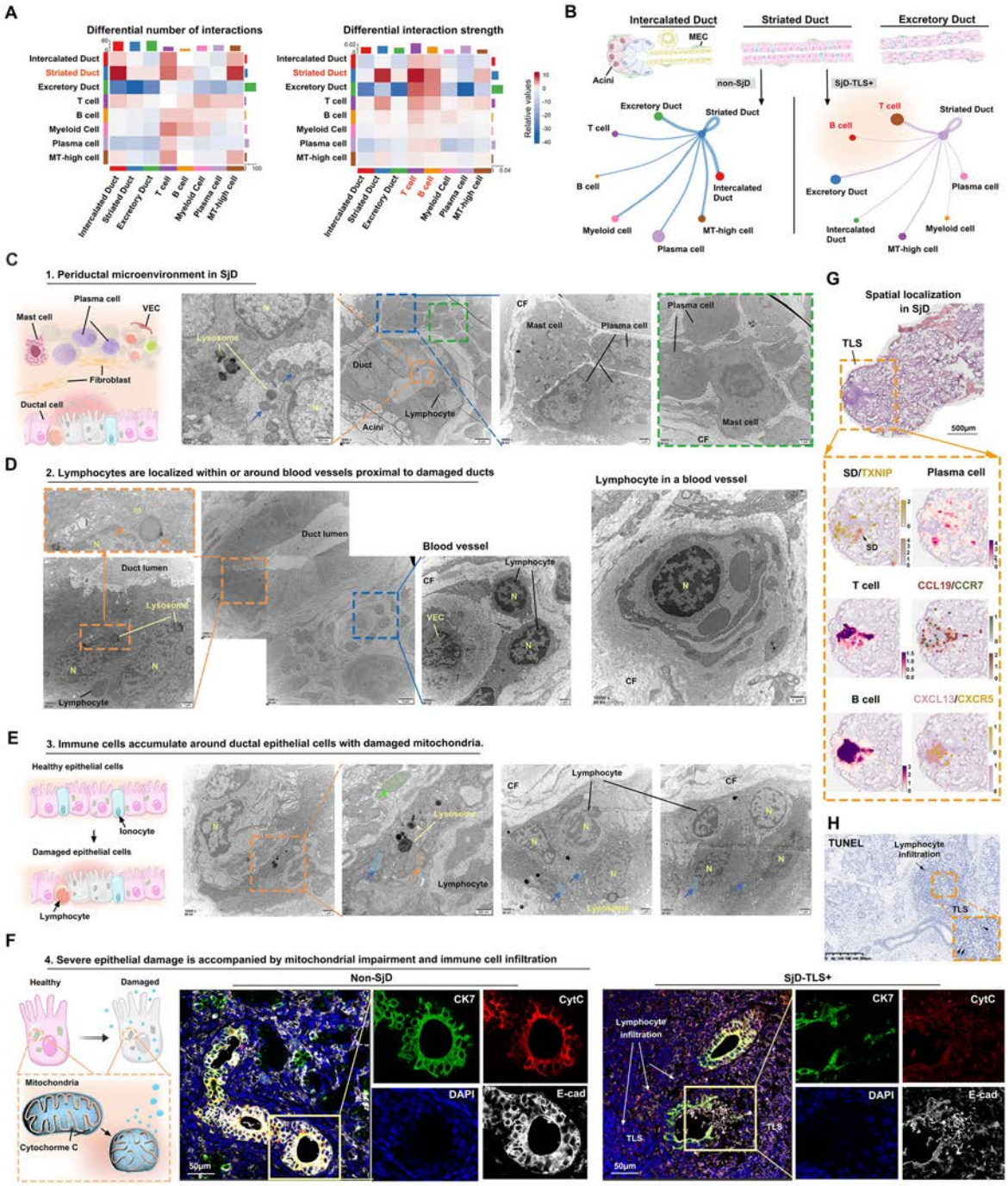

Figure 4. Epithelial-immune cell interactions in the LSG microenvironment. A, Heatmap of differential interaction strength and number between ductal and immune cell subsets in SjD vs non-SjD. Colour indicates communication probability. B, Top: schematic of glandular epithelial cell types. Bottom: CellChat-predicted ligand-receptor interactions for striated duct cells in non-SjD (left) and SjD-TLS + (right). Arrows indicate ligand-to-receptor direction; line width denotes interaction number; dot size reflects population size. C, Left: schematic of cellular components in the SjD periductal niche. Right: representative TEM images of the same region. D, TEM images showing lymphocytes in damaged regions and blood vessels of SjD LSGs. E, Left: schematic of healthy vs damaged duct epithelium. Right: TEM images showing lymphocyte infiltration near damaged ducts in SjD; colour-coded arrows indicate mitochondrial types (green: Type I; blue: Type II; orange: Type III). F, Left: schematic of mitochondrial morphology and cytochrome c distribution in healthy vs damaged duct cells. Right: immunofluorescence of CytC (red), CK7 (green), E-cadherin (white), and DAPI (blue) in non-SjD and SjD-TLS + tissues. G, Spatial distribution of the gene expression intensity of TXNIP, CCL19, CCR7, CXCL13, and CXCR5, and cell abundance of striated duct (SD), T, B, and plasma cells within the region of ROI with TLS. H, Representative image of TUNEL staining in the SjD-TLS + group. Scale bar, 300 μm. CF, collagen fibres; DAPI, 4′,6-diamidino-2-phenylindole; m, mitochondrion; LSG, labial salivary gland; MEC, myoepithelial cell; MT-high, high mitochondrial gene expression; N, nucleus; SjD, Sjögren's disease; TEM, transmission electron microscopy; TLS, tertiary lymphoid structure; TUNEL, terminal deoxynucleotidyl transferase dUTP nick end labelling; VEC, vascular endothelial cell.

(Fig 4D). Furthermore, lymphocyte invasion into the ductal structure became apparent with greater numbers of swollen mitochondria and more severe ductal damage (Fig 4E), indicating an association between mitochondrial injury in duct cells and the spatial distribution and infiltration of lymphocytes.

Multiplex immunofluorescence staining confirmed these observations: in non-SjD controls, morphologically normal SD

cells with a continuous epithelial structure showed intact distribution of cytokeratin 7 (CK7, an epithelial marker), cytochrome c (a mitochondrial marker), and E-cadherin (a key transmembrane mediator of epithelial adhesion) [44]. In contrast, SjD-TLS+ tissues exhibited discontinuous expression of CK7 and E-cadherin in ductal structures (Fig 4F), suggesting impaired integrity of the ductal epithelial barrier. Concurrently, reduced cytochrome c staining intensity in SjD-TLS+ ductal cells was consistent with abnormal mitochondrial function. Collectively, these findings indicate that SD epithelial injury in SjD-TLS+ is associated with mitochondrial damage and surrounding immune cell infiltration.

We further used ST analysis to characterize the spatial organization of the periductal microenvironment (Fig 4G). Chemokines including CCL19/CCR7 and CXCL13/CXCR5 are critical for B cell recruitment during TLS neogenesis [45]. ST analysis revealed marked colocalization of SD cells with CCL19/CCR7 and CXCL13/CXCR5 expressing cells in SjD-TLS+ tissues, with immune cells accumulating specifically around SD cells. These spatial patterns raise the possibility that SD cells (or cells in their vicinity) secrete CCL19 and other chemokines, potentially facilitating local immune cell recruitment and subsequent TLS formation. Terminal deoxynucleotidyl transferase dUTP nick end labelling (TUNEL) staining showed that TUNEL-positive signals were sparsely distributed within TLS and adjacent to the ductal epithelium (Fig 4H), indicating that apoptotic cells were primarily confined to areas of lymphocytic infiltration and that the overall proportion of apoptotic/necrotic cells was low—consistent with the chronic pathological features of SjD. These findings suggest that mitochondrial abnormalities are not merely a consequence of widespread terminal apoptosis in this setting; however, whether they represent an early event or occur in parallel to cell death remains to be determined. Further studies are required to evaluate the potential of targeting mitochondrial function as a therapeutic strategy in SjD.

Identification of a distinct cluster of duct cells in LSGs with SjD

To characterize ductal epithelial cell heterogeneity in SjD, we performed unsupervised subclustering analysis of high-resolution scRNA-seq data. Ductal cells were stratified into 3 transcriptionally distinct lineages using canonical lineage markers [16,46,47]: 3 excretory duct (ED) subsets, 4 SD subsets, and 2 ID subsets (Fig 5A, Supplementary Fig S5, and Supplementary Table S5). Matrix metalloproteinase 7 (MMP7), an enzyme involved in extracellular matrix remodelling and inflammatory progression [48], was highly enriched in a previously unrecognized SD subset, designated SD-C1-MMP7.

Compared with non-SjD, SjD LSGs exhibited altered ductal subset composition: the proportion of SD cells was increased, driven primarily by an expansion of SD-C1 cells (from 15.4% to 24%), whereas the relative frequency of ID cells was decreased (Fig 5B). Transcriptional profiling confirmed substantial heterogeneity among ductal subsets [26] (Fig 5C). Differentiation status of ductal cell subsets was inferred using CytoTRACE2. ID cells, which connect to acinar structures [16], displayed terminally differentiated features with high expression of glandular genes. ED cells retained progenitor-like features with expression of stem cell-associated genes. Notably, SD-C1 cells displayed an intermediate differentiation state, with enriched gene signatures related to senescence, inflammation, and antigen presentation.

Kyoto Encyclopedia of Genes and Genomes (KEGG) pathway analysis demonstrated enrichment of genes related to apoptosis, RIG-I-like receptor, cytosolic DNA sensing, and Toll-like receptor signalling pathways in SD-C1 (Fig 5D, Supplementary Fig S7, and Supplementary Table S5). Genes encoding mitochondrial complex components were significantly downregulated in SjD-derived SD-C1 cells (Fig 5E and Supplementary Fig S6), consistent with a link between SD-C1 and mitochondrial damage-associated inflammation. We next constructed cellular trajectories of SGECs across non-SjD (n = 3), SjD-TLS− (n = 4), and SjD-TLS+ (n = 3) groups. Pseudotemporal lineage tracing revealed aberrant epithelial differentiation in SjD pathogenesis (Supplementary Fig S9A). Integration of CytoTRACE2 and Monocle3 analyses delineated the canonical ductal maturation trajectory in non-SjD: from ED to SD to ID lineages, where each duct subset retained self-renewal potential, consistent with previous reports [46] (Fig 5F and Supplementary Fig S9B). However, SjD-TLS+ group displayed notable remodelling of this trajectory: Uniform Manifold Approximation and Projection (UMAP) projections showed sparse SD-C1 distribution in non-SjD controls, whereas SjD-TLS+ featured marked SD-C1 expansion. Accumulation of SD-C1 correlated with impaired lineage commitment towards ID and acinar fates (Supplementary Fig S8B). Reduction in self-renewal capacity was observed across ductal subsets in SjD-TLS+ group (Fig 5F). These data suggest an association between SjD-TLS+ pathogenesis, SD-C1 expansion, elevated tissue inflammation, and compromised ductal epithelial differentiation potential and lineage commitment.

Cell-cell communication analysis was performed to compare interactions of key ductal subsets with epithelial and immune populations between non-SjD (n = 3) and SjD-TLS+ (n = 3) (Fig 5F-H). SD-C1 exhibited markedly enhanced crosstalk with multiple cell clusters, particularly with T cells and B cells. Genes related to T and B cell activation, including CD22, CD45, ALCAM, CD6, TIGIT, CD86, and CD70, were among the most significantly enriched pathways in SjD-TLS+, aligning with CellChat results (Fig 5I). Subsequent analysis of ligand-receptor pairs indicated that crosstalk between SD-C1 cells and T cells, B cells in SjD-TLS+ was mainly mediated by the macrophage migration inhibitory factor (MIF) pathway (Fig 5J). MIF has been shown to promote autoimmune pathogenesis through antagonizing glucocorticoid-mediated immunosuppression [49]. In line with this, elevated MIF levels have been reported in the serum and urine from SjD patients [50]. Spatial localization analysis of the primary functional MIF receptors CD74 and CXCR4 revealed their spatial colocalization with adjacent T cells and B cells in SjD-TLS+ tissues (Fig 5K). This spatial distribution supports a role for the MIF−CD74/CXCR4 axis in mediating crosstalk in SD-C1−lymphocyte crosstalk within the SjD-TLS+ microenvironment.

Together, these findings identified a distinct ductal cell subset (SD-C1) that was markedly increased in SjD. This subset is characterized by elevated inflammatory signalling and transcriptional signatures suggestive of mitochondrial dysfunction. Located at the terminus of the ductal pseudotime trajectory and exhibiting enhanced crosstalk with T and B lymphocytes, SD-C1 is associated with glandular dysfunction and may contribute to immune cell recruitment during SjD pathogenesis.

A single-cell landscape of immune cell infiltration in SjD TLS LSGs

The SjD microenvironment demonstrates bidirectional crosstalk between SGECs and innate or adaptive immune cells [12], while exhibiting structured immune infiltrates including TLS, with periductal spatial organization [10]. Clustering analysis identified 6 $CD4^+$ T cell subsets, 4 $CD8^+$ T cell subsets, and 1

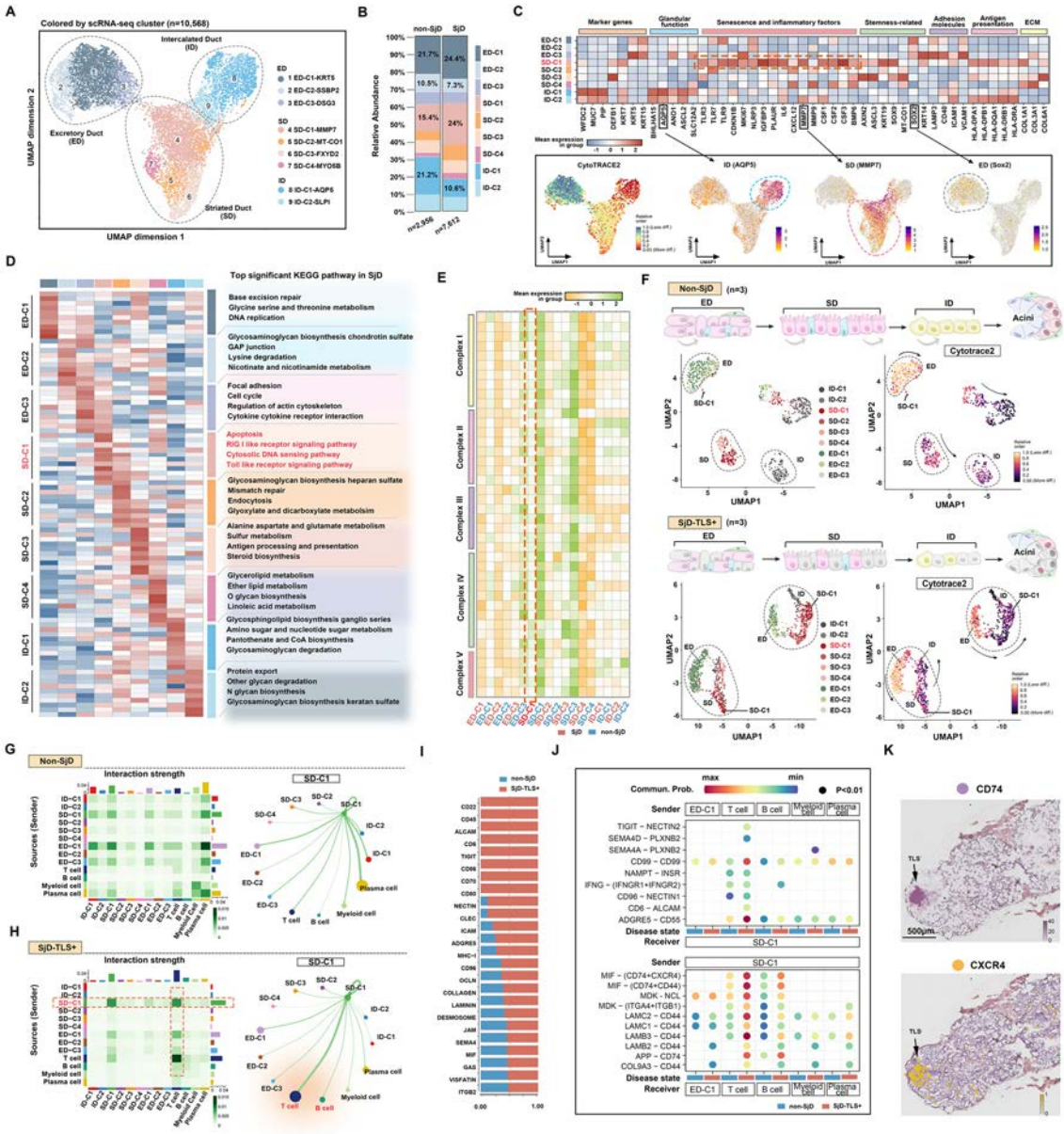

Figure 5. Identification and characterization of ductal cell subsets in human salivary glands. A, UMAP plot showing 9 duct cell clusters: 3 excretory duct (ED), 4 striated duct (SD), and 2 intercalated duct (ID) subsets. B, Bar plot of duct subtype composition in non-SjD (n = 3) vs SjD (n = 10). C, Top: heatmap of marker and functional gene expression across ductal subsets. Bottom: CytoTRACE score distributions and UMAP feature plots of selected genes. D, Heatmap of top 10 enriched KEGG pathways per duct subset; 4 representative pathways per cluster are shown on the right. E, Heatmap of OXPHOS-related gene expression across ductal subsets in non-SjD and SjD. F, CytoTRACE UMAP boxplots showing cell type classification and differentiation status in non-SjD (top, n = 3) and SjD-TLS+ (bottom, n = 3) with schematic of ED, SD, ID, and acini architecture. Arrows indicate self-replication potential. G, Left: heatmap of interaction strength between duct and immune cell subsets in non-SjD (n = 3). Middle/right: CellChat-predicted interactions for ED-C1 and SD-C1. H, Same analyses as (G) for SjD-TLS+ (n = 3) group. I, Differential signalling pathway activity ranked by total information flow in non-SjD (blue) and SjD-TLS+ (red). J, Bubble plot showing ligand–receptor pairs in SD-C1 interactions with ED-C1, T, B, myeloid, and plasma cells. Top: SD-C1 as sender; bottom: as receiver. Dot size and colour reflect interaction probability and significance; empty spaces indicate no interaction. K, Spatial distribution of the gene expression intensity of CD74 and CXCR4 within the region of interest with TLS. ECM, extracellular matrix; KEGG, Kyoto Encyclopedia and Genes and Genomes; OXPHOS, oxidative phosphorylation; scRNA-seq, single-cell RNA sequencing; SjD, Sjögren's disease; TEM, transmission electron microscopy; TLS, tertiary lymphoid structure; UMAP, Uniform Manifold Approximation and Projection.

natural killer cell subset (Fig 6A). Notably, a previously uncharacterized T cell population—termed interferon (IFN)-induced T cells—was uniquely enriched in LSGs from SjD-TLS+ tissue. The nomenclature of this subset was based on the upregulated expression of IFN-stimulated genes. Among all the T cell subsets, $CD4^+$ effector memory T cells exhibited the most pronounced expansion during SjD progression, consistent with chronic inflammation in LSGs with SjD-TLS+ (Fig 6B, C). To demonstrate the developmental trajectory of T cell lineages, pseudotemporal ordering was constructed, defining $CD4^+$ naïve T cells as the origin point (Fig 6D). IFN-induced T cells were positioned terminally along differentiation trajectories, suggesting that they represent a distinct, terminally differentiated T cell subset (Fig 6E). Comparative gene expression analysis of T cell clusters from non-SjD and SjD LSGs highlighted differential expression of genes associated with TLSs, Toll-like receptors (TLRs), proinflammatory cytokines, and adhesion molecules (Fig 6F). IFN-induced T cells displayed elevated expression of

TLRs, establishing a potential mechanistic link to SjD progression [12]. Additionally, these cells exhibited enhanced expression of inflammatory mediators and adhesion molecules compared with other T cell subsets, a transcriptional signature commonly associated with proinflammatory functions and immune cell recruitment.

B cells were clustered into 5 distinct subpopulations (Fig 6G). Among them, plasma-like B cells exhibited the most substantial expansion in SjD-TLS+ samples, consistent with prior observations of increased circulating antibodies in SjD patients [51] (Fig 6G-I). Myeloid cells in LSGs were primarily comprised of M1 and M2 macrophage subsets (Fig 6J). In agreement with intercellular communication analysis, significant interactions between the SD-C1 ductal subset and macrophages were identified through MHC class I and II signalling pathways (Fig 6K).

Heatmap analysis of gene expression revealed that the M1-2 subset of M1 macrophages exhibited the enriched expression levels of genes associated with TLS formation and TLR activation, implicating its role in SjD progression and ectopic lymphoid neogenesis (Fig 6L). The presence of mature TLSs containing germinal centre (GC) structures in LSGs was confirmed via immunohistochemistry (IHC) (Fig 6M). TLSs exhibited a B cell-dominant architecture, with coordinated infiltration of $CD4^+$ and $CD8^+$ T cells, $CD20^+$ B cells, and interstitial distribution of $CD68^+$ macrophages. GC formation was evidenced by the presence of $CD21^+$ follicular dendritic cell networks, while elevated protein levels of CXCL13, a known marker of TLSs, further validated the presence of organized lymphoid structures.

Collectively, these findings reveal dynamic remodelling of immune cell subpopulations within LSGs during SjD progression, marked by the emergence of a novel IFN-responsive T cell subset and macrophages functioning in mediating innate or adaptive immunity.

Spatiotemporal characteristics of TLS formation in SjD LSGs

Our findings suggest that duct cells in salivary glands exhibit location-dependent mitochondrial injury and proinflammatory signalling, promoting immune cell infiltration in periductal regions. ST analysis of SjD TLS regions revealed differences in the relative abundance of epithelial, immune, and stromal cell subsets, with immune cells predominating compared with non-TLS regions (Fig 7A). Interaction strength analysis indicated enhanced intercellular communication between SD-C1 cells and T cells and B cells and myeloid cells in TLS regions (Fig 7B). Ligand–receptor analysis further revealed that SD-C1 cells may signal to T cells and myeloid cells via MHC-II molecules (HLA DR/HLA DQ) on $CD4^+$ T cells (Fig 7C). Spatial distribution analysis showed that $CD4^+$ T colocalized with MHC II^+ (HLA DRB1 and HLA DRA) cells and $CD8^+$ cells with MHC I^+ (HLA B and HLA A) cells in periductal TLS regions, with SD-C1 cells positioned at the core of immune cell aggregates (Fig 7D).

Immunofluorescence staining confirmed the reduced levels of cytochrome c and COXIV proteins in damaged SGECs, surrounded by infiltrated T and B lymphocytes in SjD-TLS+ samples (Fig 7E). In contrast, non-SjD LSGs exhibited sparse lymphocyte distribution devoid of organized periductal lymphoid aggregates. Based on these observations, we present a 3-stage model of bidirectional epithelial–immune crosstalk that drives the pathological progression of TLS in SjD. In the preinjury stage (stage 0), the glandular and ductal architecture remains intact, with only sparse infiltration of lymphocytes. In the ductal injury stage (stage 1), ductal epithelial cells develop mitochondrial dysfunction and release DAMPs, which initiate the recruitment of immune cells to the injured ductal regions. In the progressive disease stage (stage 2), recruited lymphocytes are persistently activated by damage-related signals and secrete a large panel of cytokines, chemokines, adhesion molecules, and survival signals. These mediators shape a self-sustaining TLS immune microenvironment through a bidirectional epithelial–immune positive feedback loop, which further recruits innate and adaptive immune cells and thereby perpetuates ductal epithelial injury and functional impairment (Fig 7F). As reactive oxygen species (ROS) may contribute to initiation or amplification of immune cell recruitment [52], fluorescent staining of ROS signals was performed and revealed increased ROS generation in periductal regions of TLS associated with increased lymphocyte infiltration, whereas duct cells lacking adjacent lymphocytes showed no increased ROS signal. Representative images of stage 1 revealed limited immune cell aggregation around damaged ducts in the absence of fully developed TLS (Fig 7G). To investigate the spatial colocalization between SD-C1 and immune cells, we applied cell2location to calculate a predefined proximity score across SjD-TLS− and SjD-TLS+ samples [53], which was defined as the sum of T-cell or B-cell abundances within a 25 μm radius of each spot containing SD-C1 cells. Results indicated that both T and B cells were more densely distributed within the defined spatial radius of SD-C1 cells in the SjD-TLS+ group (Fig 7H). Furthermore, the spatial proximity of SD C1 cells to myeloid cells, plasma cells, vascular endothelial cells, and fibroblasts was also significantly increased within TLS regions (Supplementary Fig S10), reflecting the enhanced spatial colocalization between epithelial and immune cells.

Spatial cell segmentation analysis further revealed that SD-C1 cells were surrounded by B cell aggregates within TLS regions, whereas T cells, myeloid cells, and plasma cells were predominantly localized to the periphery of the B cell enriched zones. This architecture recapitulates the canonical spatial organization of mature TLSs in the second stage of disease progression (Fig 7I). To validate these findings, we visualized key markers associated with immune and inflammatory signalling. We observed marked enrichment of TLS-associated immune cells defined by CD4, CD8, CD20, and CD21 in SD-C1 enriched regions, where SD-C1 cells spatially colocalized with the inflammatory mediator MMP7, consistent with our previous scRNA-seq data. Compared with non-TLS regions, TLR4, a pattern recognition receptor that involved in DAMP sensing [54], was preferentially clustered around SD-C1 cells in TLS regions, suggesting that TLR4 may serve as a potential target for inflammatory regulation in this niche. Spatial visualization of the proapoptotic molecule BAX showed a distribution pattern highly concordant with TLR4, indicating the involvement of epithelial apoptotic signalling in the TLS inflammatory niche. Furthermore, the spatial distribution of CXCL13, a canonical TLS marker, confirmed TLS formation adjacent to SD-C1 cells (Fig 7J). Collectively, these data support a model in which signalling pathways driven by SD injury are closely associated with immune cell recruitment and TLS formation during the progression of SjD.

DISCUSSION

This study reveals that mitochondrial dysfunction in SD epithelial cells emerges as a key player in the immunopathogenesis of SjD, closely linked to local immune activation and TLS formation. By integrating scRNA-seq, spatial mapping, ultrastructural

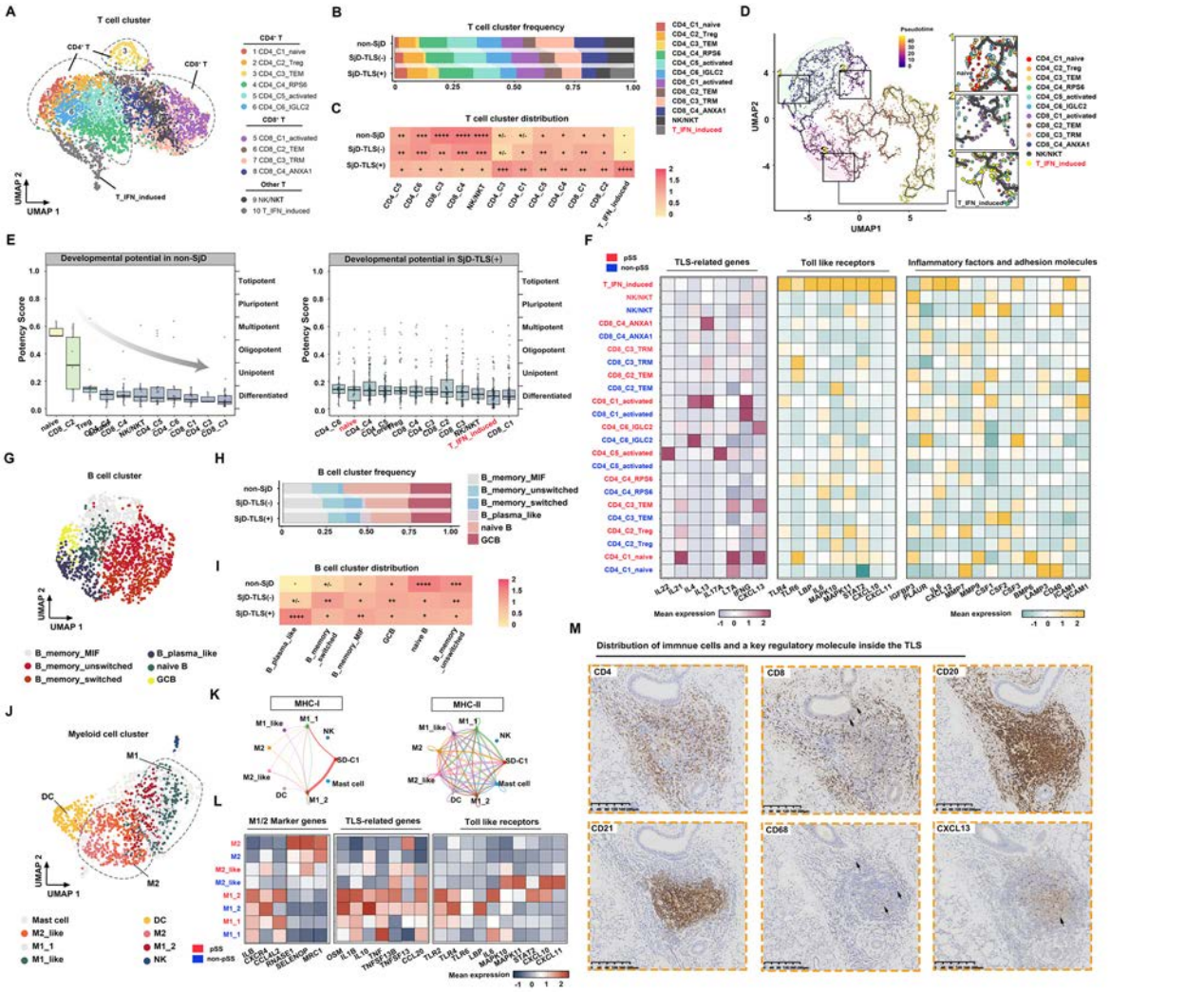

Figure 6. Identification and characterization of immune cell subsets in human LSGs. A, UMAP of T cell subsets. Treg, regulatory T; TEM, effector memory T; TRM, tissue-resident memory T cells. (B, Bar plot showing T cell subcluster composition in non-SjD, SjD-TLS−, and SjD-TLS + groups. C, Heatmap of T cell subcluster distribution across groups based on scRNA-seq. Ro/e, observed-to-expected ratio: + + + +, Ro/e > 1.4; + + +, 1.4≥Ro/e > 1.2; + +, 1.2≥Ro/e > 1.0; +, 1.0≥Ro/e > 0.5; +/−, 0.5≥Ro/e > 0.05; −, 0.05≥Ro/e > 0. D, Monocle 3 pseudotime trajectory of T cells. Left: coloured by pseudotime (purple to yellow); right: coloured by subpopulation. E, Boxplots of CytoTRACE scores for T cell subsets in non-SjD and SjD-TLS +. F, Heatmaps of TLS-, TLR-, cytokine-, and adhesion-related gene expression in T cell subsets. (G) UMAP of B cell subsets; GCB, germinal center B cells. (H, Bar plot showing B cell subcluster composition across groups. I, Heatmap of B cell subcluster distribution across tissues. J, UMAP of myeloid cell subsets; DC, dendritic cells. K, Circle plots of SD-C1 interactions with myeloid subsets via MHC-I (left) and MHC-II (right) signalling. L, Heatmaps of gene expression in macrophage subsets: M1/M2 markers, TLS- and TLR-related genes. M, Immunohistochemical staining of CD4, CD8, CD20, CD21, CD68, and CXCL13 in LSG tissues from SjD-TLS + samples. Scale bars, 200 μm. LSG, labial salivary gland; scRNA-seq, single-cell RNA sequencing; SjD, Sjögren's disease; TEM, transmission electron microscopy; TLR, Toll-like receptor; TLS, tertiary lymphoid structure; UMAP, Uniform Manifold Approximation and Projection.

imaging, and IHC staining, we uncovered robust associations among epithelial mitochondria damage, immune cell recruitment, and TLS formation in SjD pathogenesis. We identified MMP7^{+} SDs as a spatially and transcriptionally distinct ductal cell subset that is closely associated with immune cell infiltration and TLS formation, highlighting a potentially pathological role for epithelial cells in SjD-related immune dysregulation.

Our ultrastructural atlas reveals subtype-specific mitochondrial heterogeneity in SGECs, with SD cells exhibiting a high abundance of mitochondria under physiological conditions—an observation that aligns directly with their roles in energy-consuming ion transport [26]. The severe mitochondrial abnormality morphologically observed in SD cells from TLS-positive SjD patients provides a structural basis for the featured salivary hypofunction. It should be noted that abnormal mitochondrial morphology observed by TEM does not directly indicate functional impairment, as such ultrastructural alterations could also reflect the physiological mitochondrial dynamics [55]. However, scRNA-seq data showed that the mitochondrial fusion gene MFN2 was reduced in SD cells, while the expression of mitophagy markers (PINK1) was elevated, suggesting that the observed morphologic changes are probably associated with mitochondrial dysfunction. Our multimodal approach integrates structural pathology with transcriptional profiling, establishing a framework that redefines autoimmune epithelitis as a mitochondrial-epithelial-immune triad [10]. Therapeutic strategies targeting mitochondrial quality control or metabolic support in SD cells may interrupt this self-amplifying positive feedback loop and block disease progression, offering promising interventions that extend beyond conventional immunosuppression for SjD.

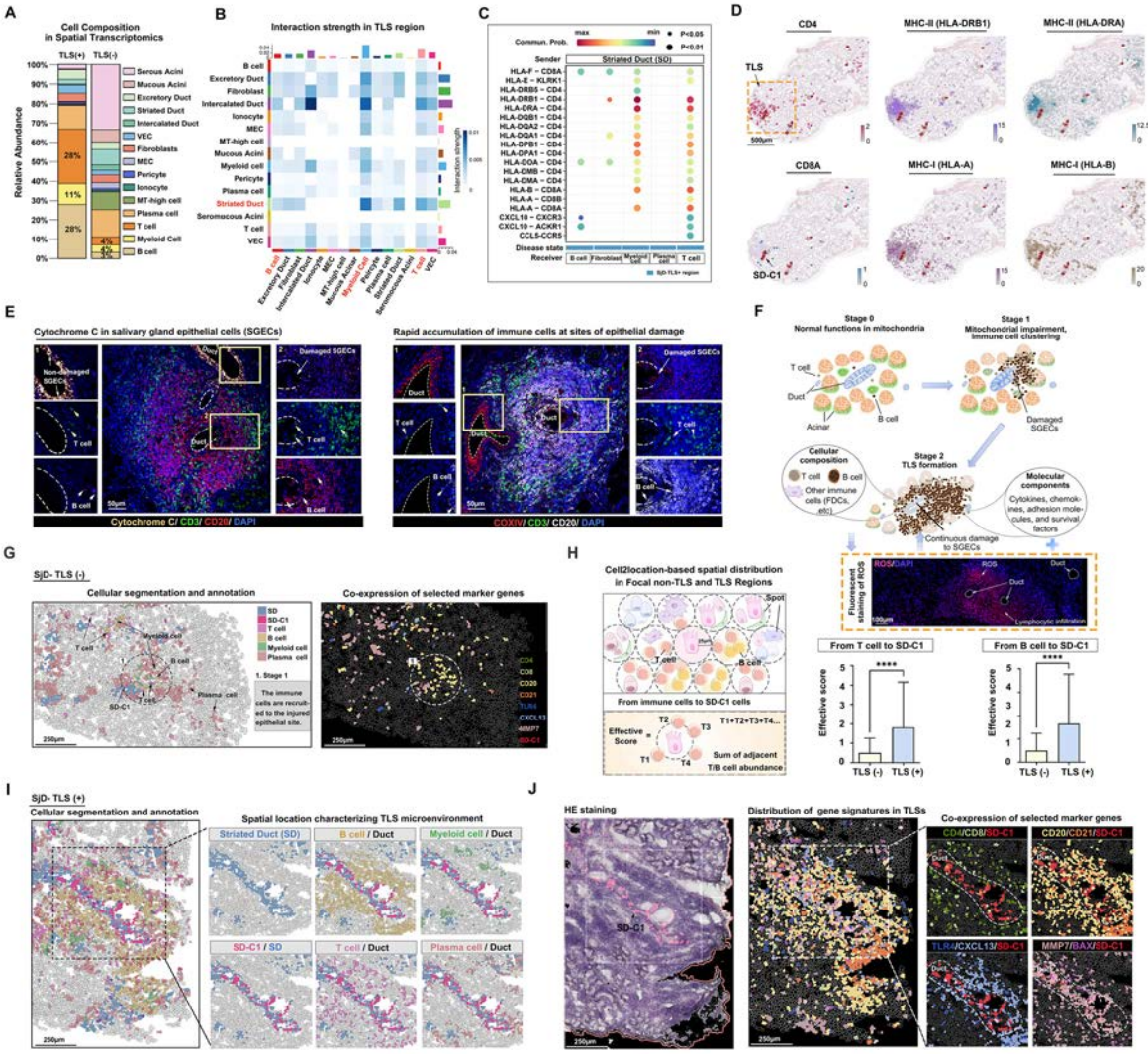

Figure 7. Spatially resolved analysis of human LSGs in SjD. A, Proportions of major cell populations in TLS(+) vs TLS(−) regions based on spatial transcriptomics data. B, Heatmap of differential interaction strength between cell subsets in TLS(+) vs TLS(−) regions based on spatial transcriptomics data. Colour indicates interaction strength. C, Bubble plot illustrating ligand−receptor interactions from SD cells to fibroblasts, T cells, B cells, myeloid cells, and plasma cells. Dot size and colour reflect interaction probability and significance; empty spaces indicate no interaction. D, Spatial distribution of the gene expression intensity of CD4, HLA-DRB1, HLA-DRA, CD8A, HLA-A and HLA-B within the region of interest with TLS. E, IF images of SjD LSGs showing Cytochrome c (yellow), CD3 (green), CD20 (red), and DAPI (blue) (left); and COXIV (red), CD3 (green), CD20 (white), and DAPI (blue) (right). Scale bars, 50 μm. F, Above: Schematic of immune cell recruitment and TLS formation during SjD progression. FDCs, follicular dendritic cells; SGECs, salivary gland epithelial cells. Below: IF images of SjD-TLS+ LSGs showing reactive oxygen species (ROS) distribution. Scale bars, 100 μm. G, Left: Colocalization of cell clusters in SjD-TLS− tissue based on scRNA-seq signatures. Right: Spatial expression of selected genes and their co-localization with SD-C1 in SjD-TLS−. Scale bar, 250 μm. H, Left: Illustration of the distance analysis involving SD-C1 and surrounding B or T cells. The Gray dotted circle represents the radius of 25 μm. Effective score = the sum of T-cell or B-cell abundances within the 25 μm radius of each spot containing SD-C1 cells. Right: Comparison of the effective scores from SD-C1 cells to T or B cells between TLS(+) and TLS(−) regions. I, Co-localization of cell clusters in SjD-TLS + tissue based on scRNA-seq signatures. Scale bar, 250 μm. J, Spatial expression of selected genes and their colocalization with SD-C1 in SjD-TLS + tissue, and the corresponding haematoxylin and eosin staining image of the region. Scale bar, 250 μm. DAPI, 4′,6-diamidino-2-phenylindole; HLA, human leukocyte antigen; IF, immunofluorescence; LSG, labial salivary gland; MEC, myoepithelial cell; MT-high, high mitochondrial gene expression; scRNA-seq, single cell RNA-sequencing; SD, striated duct; SjD, Sjögren's disease; TLS, tertiary lymphoid structure; VEC, vascular endothelial cell.

Each mitochondrion harbours multiple copies of mtDNA, which encodes essential components of the OXPHOS system [41]. Our scRNA-seq and bioinformatic analyses reveal that distinct cell populations can be distinguished based on mtDNA-encoded gene signatures. We further demonstrated that mitochondrial gene expression profiles were sufficient to distinguish major SGEC subsets, aligning with classifications based on canonical lineage markers [56]. This finding suggests that mitochondrial gene expression profiles could capture cell type-specific metabolic signatures and may serve as alternative descriptors of cellular identity. The observed cell type-specific mitochondrial signatures potentially reflect differential energy demands and metabolic status across various cell subsets [26]. Ca^{2+} serves as a key mediator of ion transport and fluid secretion in the salivary gland and regulates the activation of ion channels [57]. Mitochondrial Ca^{2+} uptake is essential for maintaining intracellular Ca^{2+} homeostasis, and sustained dysregulation of Ca^{2+} signalling can induce mitochondrial dysfunction and excessive ROS production [58,59]. Consistently, our immunofluorescence analysis revealed elevated ROS levels in periductal

regions with mitochondrial dysfunction, suggesting potential mechanisms linking dysregulated Ca^{2+} signalling and mitochondrial impairment.

Alterations of mitochondrial functions in cells may initiate inflammatory signalling cascades by activating pattern recognition receptors, followed by the release of pathogen-associated molecular patterns and DAMPs. These events are recognized as critical initiating factors in autoimmune disorders [60–63]. Through scRNA-seq profiling, a distinct $MMP7^+$ SD cell subset exhibiting pronounced transcriptomic alterations in mitochondria were identified in salivary glands from SjD patients. Our CellChat analysis revealed intensive communication networks between $MMP7^+$ SD cells and immune cells, particularly in TLS-positive SjD patients compared with controls. Our integrated multimodal analyses indicate that this specialized epithelial cell subset critically orchestrates glandular immunopathology by mediating crosstalk between epithelial and immune cells.

Based on pseudotime analysis, our study identified a continuous transition of ductal epithelial cells along the trajectory from ED to SD and then to ID under SjD or non-SjD conditions. Although earlier work has supported the presence of continuous transcriptional changes among epithelial cells, it has not explicitly proposed a linear differentiation hierarchy among ductal subpopulations [64]. Other studies have emphasized branching differentiation patterns, suggesting that ductal differentiation may be more complex than a simple linear process [65]. In the disease context, we further observed a marked alteration of this trajectory in SjD-TLS+, characterized by an increased proportion of the SD-C1 subpopulation and a concomitant restriction in differentiation towards ID and then acinar lineages. We also observed a reduction in self-renewal-associated features in ductal cells within SjD-TLS+, which is consistent with previous study [66]. In contrast, prior single-cell studies in SjD have largely focused on the selective damage of acinar cells, with relatively limited attention to differentiation dynamics within the ductal cell types [67]. Our findings therefore provide complementary evidence by highlighting epithelial abnormalities from the perspective of ductal differentiation. These discrepancies may arise from multiple factors. First, developmental tissues and adult tissues differ inherently in lineage organization and cellular plasticity. Second, pseudotime inference is sensitive to the choice of root cell and computational algorithm, which may influence the inferred directionality of differentiation. In addition, the persistent inflammatory microenvironment and the formation of TLS may disrupt normal differentiation.

Lastly, a high-resolution spatial atlas was presented on the microenvironment of SjD salivary gland, revealing salivary gland-specific TLSs in SjD. Beyond the conventional T/B cell components [13], a unique $MMP7^+$ SD subcluster within TLS niches was positioned, which validated our findings through scRNA-seq. This specialized epithelial cell population exhibited upregulated inflammatory cytokine expression levels and extensive interactions with immune cells. Spatial mapping confirmed the colocalization of epithelial cells with inflammatory regulating molecules (CXCL13, TLR4, CD21), suggesting their role as periductal immunopathological epithelial orchestrators. Notably, our data support a reciprocal pathogenic relationship: the inflammatory TLS microenvironment promotes oxidative stress and mitochondrial dysfunction in SD epithelial cells, while epithelial mitochondrial damage in turn fuels immune cell recruitment and TLS maturation. Collectively, these findings delineate a bidirectional, self-reinforcing feedback loop between mitochondrial-impaired ductal epithelium and TLS-associated immunity, which underlies the pathological progression of SjD.

Despite the findings described above, limitations remain to be discussed in this study. First, since this study is based on cross-sectional analysis of human tissues, causality between SD mitochondrial impairment and TLS formation remains to be established, which should be addressed in future studies. Comprehensive validation of our findings will require mechanistic investigation and validation using *in vitro* and *in vivo* disease models, although certain experimental systems remain technically challenging and require further optimization [67,68]. Second, multiomic analysis regarding sample consistency is not achievable so far due to the limited samples of LSG biopsies that are prioritized for diagnostic histopathology [69]. Third, dissociation-induced stress is a well-acknowledged limitation of current single-cell techniques, which may induce changes of mitochondrial transcriptional signatures [70,71]. Fourth, further studies with long-term follow-up are required to investigate the clinical relevance of TLS with the prognosis in SjD patients. Finally, given that LSG biopsy is an invasive diagnostic procedure typically performed in patients with clinical symptoms or serological abnormalities, samples from asymptomatic healthy controls were not included in this study. In future studies, we will pay attention to collecting samples from this cohort for further validating the disease specificity of our observations.

In summary, our multimodal study positions mitochondrial dysfunction within a distinct ductal epithelial subset as a pathological feature intertwined with immune dysregulation and TLS organization in SjD, highlighting a clinically relevant axis for potential therapeutic intervention. These insights offer a microenvironment-based framework for disease stratification and suggest that modulation of mitochondrial function in specific epithelial types may serve as therapeutics in prevention or attenuation of SjD progression.

Competing interests

The authors declare no competing interests.

CRediT authorship contribution statement

Yuan Zong: Writing – original draft, Visualization, Investigation. **Yi Yang:** Writing – original draft, Software, Investigation. **Jiawen Zhao:** Writing – original draft, Visualization. **Shiyi Wen:** Writing – original draft, Software, Investigation. **Lei Li:** Investigation, Data curation. **Na Xiong:** Validation, Investigation, Data curation. **Tong Wu:** Methodology, Investigation. **Xiaoyu Zhao:** Validation, Methodology. **Yiming Gao:** Validation, Methodology. **Ning Li:** Supervision, Project administration, Conceptualization. **Guojun Shi:** Writing – original draft, Project administration, Funding acquisition, Conceptualization. **Liting Jiang:** Writing – review & editing, Supervision, Project administration, Conceptualization.

Acknowledgements

This work was supported by the Core Facility of Basic Medical Sciences, Shanghai Jiao Tong University School of Medicine. We thank Xiaochun Fei (Department of Pathology, Ruijin Hospital, Shanghai Jiao Tong University School of Medicine, Shanghai, China) for histological image reading quality control. We thank Chen Li (Shenzhen Salus BioMed Co. Ltd., Shenzhen, Guangdong, China) for assisting in spatial transcriptomics analysis.

Funding

This work was funded by the National Key R&D program of China (2023YFF0724200 to G.S.); the Guangzhou Municipal Science and Technology Project 906 (202201020497 and 2024A01J6567 to G.S.); and the Guangdong Basic and Applied Basic Research Foundation (2024A1515012501 to G.S.).

Patient consent for publication

Written informed consent was obtained from all participants prior to inclusion.

Ethics approval

The study protocol was reviewed and approved by the Ethics Committee of Ruijin Hospital, Shanghai Jiao Tong University School of Medicine, and was prospectively registered in the Chinese Clinical Trial Registry (ChiCTR2000039820). The animal study was approved by the Institutional Animal Care and Use Committee of Sun Yat-sen University (2022000154 and K2024-01-050-116).

Provenance and peer review

Not commissioned; externally peer reviewed.

Data availability statement

Data are available in a public, open access repository. Raw TEM images and scRNA-seq data are available in OMIX (CNCB-NGDC) under accession codes OMIX015227 and OMIX015237, respectively. Preview links for these entries are provided below:

TEM images: https://ngdc.cncb.ac.cn/omix/release/OMIX015227

Raw scRNA-seq data: https://ngdc.cncb.ac.cn/omix/release/OMIX015237

Other data and code are available upon reasonable request.

Supplementary materials

Supplementary material associated with this article can be found, in the online version, at doi:10.1016/j.ard.2026.05.014.

Orcid

Liting Jiang: http://orcid.org/0000-0002-2342-2017

REFERENCES

[1] Nocturne G, Mariette X. Advances in understanding the pathogenesis of primary Sjögren's syndrome. Nat Rev Rheumatol. 2013;9(9):544–56. doi: 10.1038/nrrheum.2013.110.

[2] Fiorentino DF, Presby M, Baer AN, Petri M, Rieger KE, Soloski M, et al. PUF60: a prominent new target of the autoimmune response in dermatomyositis and Sjögren's syndrome. Ann Rheum Dis. 2016;75(6):1145–51. doi: 10.1136/annrheumdis-2015-207509.

[3] van Luijk P, Pringle S, Deasy JO, Moiseenko VV, Faber H, Hovan A, et al. Sparing the region of the salivary gland containing stem cells preserves saliva production after radiotherapy for head and neck cancer. Sci Transl Med. 2015;7(305):305ra147. doi: 10.1126/scitranslmed.aac4441.

[4] Ramos-Casals M, Brito-Zerón P, Bombardieri S, Bootsma H, De Vita S, Dörner T, et al. EULAR recommendations for the management of Sjögren's syndrome with topical and systemic therapies. Ann Rheum Dis. 2020;79(1):3–18. doi: 10.1136/annrheumdis-2019-216114.

[5] Seror R, Nocturne G, Mariette X. Current and future therapies for primary Sjögren syndrome. Nat Rev Rheumatol. 2021;17(8):475–86. doi: 10.1038/s41584-021-00634-x.

[6] Furman D, Campisi J, Verdin E, Carrera-Bastos P, Targ S, Franceschi C, et al. Chronic inflammation in the etiology of disease across the life span. Nat Med. 2019;25(12):1822–32. doi: 10.1038/s41591-019-0675-0.

[7] Chovatiya R, Medzhitov R. Stress, inflammation, and defense of homeostasis. Mol Cell. 2014;54(2):281–8. doi: 10.1016/j.molcel.2014.03.030.

[8] Davidson S, Coles M, Thomas T, Kollias G, Ludewig B, Turley S, et al. Fibroblasts as immune regulators in infection, inflammation and cancer. Nat Rev Immunol. 2021;21(11):704–17. doi: 10.1038/s41577-021-00540-z.

[9] Xiao F, Lin X, Tian J, Wang X, Chen Q, Rui K, et al. Proteasome inhibition suppresses Th17 cell generation and ameliorates autoimmune development in experimental Sjogren's syndrome. Cell Mol Immunol. 2017;14(11):924–34. doi: 10.1038/cmi.2017.8.

[10] Brito-Zerón P, Baldini C, Bootsma H, Bowman SJ, Jonsson R, Mariette X, et al. Sjogren syndrome. Nat Rev Dis Primers 2016;2:16047. doi: 10.1038/nrdp.2016.47.

[11] Manoussakis MN, Kapsogeorgou EK. The role of intrinsic epithelial activation in the pathogenesis of Sjogren's syndrome. J Autoimmun. 2010;35(3):219–24. doi: 10.1016/j.jaut.2010.06.011.

[12] Verstappen GM, Pringle S, Bootsma H, Kroese FGM. Epithelial-immune cell interplay in primary Sjogren syndrome salivary gland pathogenesis. Nat Rev Rheumatol 2021;17(6):333–48. doi: 10.1038/s41584-021-00605-2.

[13] Bombardieri M, Lewis M, Pitzalis C. Ectopic lymphoid neogenesis in rheumatic autoimmune diseases. Nat Rev Rheumatol. 2017;13(3):141–54. doi: 10.1038/nrrheum.2016.217.

[14] Theander E, Vasaitis L, Baecklund E, Nordmark G, Warfvinge G, Liedholm R, et al. Lymphoid organisation in labial salivary gland biopsies is a possible predictor for the development of malignant lymphoma in primary Sjogren's syndrome. Ann Rheum Dis. 2011;70(8):1363–8. doi: 10.1136/ard.2010.144782.

[15] Zhao L, Jin S, Wang S, Zhang Z, Wang X, Chen Z, et al. Tertiary lymphoid structures in diseases: immune mechanisms and therapeutic advances. Signal Transduct Target Ther. 2024;9(1):225. doi: 10.1038/s41392-024-01947-5.

[16] Aure MH, Symonds JM, Mays JW, Hoffman MP. Epithelial cell lineage and signaling in murine salivary glands. J Dent Res. 2019;98(11):1186–94. doi: 10.1177/0022034519864592.

[17] Barrera MJ, Aguilera S, Castro I, Carvajal P, Jara D, Molina C, et al. Dysfunctional mitochondria as critical players in the inflammation of autoimmune diseases: potential role in Sjögren's syndrome. Autoimmun Rev. 2021;20(8):102867. doi: 10.1016/j.autrev.2021.102867.

[18] Suomalainen A, Nunnari J. Mitochondria at the crossroads of health and disease. Cell 2024;187(11):2601–27. doi: 10.1016/j.cell.2024.04.037.

[19] Nunnari J, Suomalainen A. Mitochondria: in sickness and in health. Cell 2012;148(6):1145–59. doi: 10.1016/j.cell.2012.02.035.

[20] Cogliati S, Frezza C, Soriano ME, Varanita T, Quintana-Cabrera R, Corrado M, et al. Mitochondrial cristae shape determines respiratory chain supercomplexes assembly and respiratory efficiency. Cell 2013;155(1):160–71. doi: 10.1016/j.cell.2013.08.032.

[21] Katsiougiannis S, Stergiopoulos A, Moustaka K, Havaki S, Samiotaki M, Stamatakis G, et al. Salivary gland epithelial cell in Sjögren's syndrome: metabolic shift and altered mitochondrial morphology toward an innate immune cell function. J Autoimmun. 2023;136:103014. doi: 10.1016/j.jaut.2023.103014.

[22] Huang KT, Wagner LE, Takano T, Lin XX, Bagavant H, Deshmukh U, et al. Dysregulated Ca^{2+} signaling, fluid secretion, and mitochondrial function in a mouse model of early Sjögren's disease. eLife. 2024;13:RP97069. doi: 10.7554/eLife.97069.

[23] Li N, Li Y, Hu J, Wu Y, Yang J, Fan H, et al. A link between mitochondrial dysfunction and the immune microenvironment of salivary glands in primary Sjogren's syndrome. Front Immunol. 2022;13:845209. doi: 10.3389/fimmu.2022.845209.

[24] Luo D, Li L, Wu Y, Yang Y, Ye Y, Hu J, et al. Mitochondria-related genes and metabolic profiles of innate and adaptive immune cells in primary Sjögren's syndrome. Front Immunol. 2023;14:1156774. doi: 10.3389/fimmu.2023.1156774.

[25] Zong Y, Yang Y, Zhao J, Li L, Luo D, Hu J, et al. Identification of key mitochondria-related genes and their relevance to the immune system linking Parkinson's disease and primary Sjögren's syndrome through integrated bioinformatics analyses. Comput Biol Med. 2024;175:108511. doi: 10.1016/j.compbiomed.2024.108511.

[26] Wahl AM, Takano T, Su S, Warner BM, Perez P, Sneyd J, et al. Structural and functional analysis of salivary intercalated duct cells reveals a secretory phenotype. J Physiol. 2023;601(20):4539–56. doi: 10.1113/jp285104.

[27] Hall JC, Baer AN, Shah AA, et al. Molecular subsetting of interferon pathways in Sjögren's syndrome. Arthritis Rheumatol. 2015;67(9):2437–46. doi: 10.1002/art.39204.

[28] Shiboski CH, Shiboski SC, Seror R, Criswell LA, Labetoulle M, Lietman TM, et al. 2016 American College of Rheumatology/European League Against Rheumatism classification criteria for primary Sjogren's syndrome: a consensus and data-driven methodology involving three international patient cohorts. Arthritis Rheumatol. 2017;69(1):35–45. doi: 10.1002/art.39859.
[29] Roche JV, Törnroth-Horsefield S. Aquaporin protein-protein interactions. Int J Mol Sci 2017;18(11):2255. doi: 10.3390/ijms18112255.
[30] Pitzalis C, Jones GW, Bombardieri M, Jones SA. Ectopic lymphoid-like structures in infection, cancer and autoimmunity. Nat Rev Immunol. 2014;14(7):447–62. doi: 10.1038/nri3700.
[31] Nayar S, Turner JD, Asam S, Fennell E, Pugh M, Colafrancesco S, et al. Molecular and spatial analysis of tertiary lymphoid structures in Sjogren's syndrome. Nat Commun. 2025;16(1):5. doi: 10.1038/s41467-024-54686-0.
[32] Barone F, Bombardieri M, Manzo A, Blades MC, Morgan PR, Challacombe SJ, et al. Association of CXCL13 and CCL21 expression with the progressive organization of lymphoid-like structures in Sjögren's syndrome. Arthritis Rheum. 2005;52(6):1773–84. doi: 10.1002/art.21062.
[33] Barone F, Bombardieri M, Rosado MM, Morgan PR, Challacombe SJ, De Vita S, et al. CXCL13, CCL21, and CXCL12 expression in salivary glands of patients with Sjogren's syndrome and MALT lymphoma: association with reactive and malignant areas of lymphoid organization. J Immunol. 2008;180(7):5130–40. doi: 10.4049/jimmunol.180.7.5130.
[34] Alunno A, Leone MC, Giacomelli R, Gerli R, Carubbi F. Lymphoma and lymphomagenesis in primary Sjögren's syndrome. Front Med. 2018;5:102. doi: 10.3389/fmed.2018.00102.
[35] Li N, Ye Y, Wu Y, Li L, Hu J, Luo D, et al. Alterations in histology of the aging salivary gland and correlation with the glandular inflammatory microenvironment. iScience. 2023;26(5):106571. doi: 10.1016/j.isci.2023.106571.
[36] Covarrubias AJ, Perrone R, Grozio A, Verdin E. NAD^+ metabolism and its roles in cellular processes during ageing. Nat Rev Mol Cell Biol. 2021;22(2):119–41. doi: 10.1038/s41580-020-00313-x.
[37] Gong B, Pan Y, Vempati P, Zhao W, Knable L, Ho L, et al. Nicotinamide riboside restores cognition through an upregulation of proliferator-activated receptor-γ coactivator 1α regulated β-secretase 1 degradation and mitochondrial gene expression in Alzheimer's mouse models. Neurobiol Aging. 2013;34(6):1581–8. doi: 10.1016/j.neurobiolaging.2012.12.005.
[38] Liang J, Huang F, Hao X, Zhang P, Chen R. Nicotinamide mononucleotide supplementation rescues mitochondrial and energy metabolism functions and ameliorates inflammatory states in the ovaries of aging mice. MedComm (2020). 2024;5(10):e727. doi: 10.1002/mco2.727.
[39] Guo YY, Liang NN, Zhang XY, Ren YH, Wu WZ, Liu ZB, et al. Mitochondrial GPX4 acetylation is involved in cadmium-induced renal cell ferroptosis. Redox Biol. 2024;73:103179. doi: 10.1016/j.redox.2024.103179.
[40] Hänzelmann S, Castelo R, Guinney J. GSVA: gene set variation analysis for microarray and RNA-seq data. BMC Bioinformatics. 2013;14:7. doi: 10.1186/1471-2105-14-7.
[41] Lake NJ, Ma K, Liu W, Battle SL, Laricchia KM, Tiao G, et al. Quantifying constraint in the human mitochondrial genome. Nature. 2024;635(8038):390–7. doi: 10.1038/s41586-024-08048-x.
[42] Jew B, Alvarez M, Rahmani E, Miao Z, Ko A, Garske KM, et al. Accurate estimation of cell composition in bulk expression through robust integration of single-cell information. Nature Commun. 2020;11(1):1971. doi: 10.1038/s41467-020-15816-6.
[43] Hao R, Liu Z, Chou Y, Wang Y, Ren X, Jiang X, et al. Impression cytology and *in vivo* confocal microscopy of lip mucosa compared with labial gland biopsy and classification criteria in patients with clinically suspected primary Sjogren's syndrome. Front Immunol. 2022;13:829320. doi: 10.3389/fimmu.2022.829320.
[44] Venhuizen JH, Jacobs FJC, Span PN, Zegers MM. P120 and E-cadherin: Double-edged swords in tumor metastasis. Semin Cancer Biol. 2020;60:107–20. doi: 10.1016/j.semcancer.2019.07.020.
[45] Sautès-Fridman C, Petitprez F, Calderaro J, Fridman WH. Tertiary lymphoid structures in the era of cancer immunotherapy. Nat Rev Cancer 2019;19(6):307–25. doi: 10.1038/s41568-019-0144-6.
[46] Aure MH, Arany S, Ovitt CE. Salivary glands: stem cells, self-duplication, or both? J Dent Res. 2015;94(11):1502–7. doi: 10.1177/0022034515599770.
[47] Huang N, Pérez P, Kato T, Mikami Y, Okuda K, Gilmore RC, et al. SARS-CoV-2 infection of the oral cavity and saliva. Nat Med. 2021;27(5):892–903. doi: 10.1038/s41591-021-01296-8.
[48] Grillet B, Pereira RVS, Van Damme J, Abu El-Asrar A, Proost P, Opdenakker G. Matrix metalloproteinases in arthritis: towards precision medicine. Nat Rev Rheumatol. 2023;19(6):363–77. doi: 10.1038/s41584-023-00966-w.
[49] Kang I, Bucala R. The immunobiology of MIF: function, genetics and prospects for precision medicine. Nat Rev Rheumatol. 2019;15(7):427–37. doi: 10.1038/s41584-019-0238-2.
[50] Vincent FB, Lang T, Kandane-Rathnayake R, Downie-Doyle S, Morand EF, Rischmueller M. Serum and urinary macrophage migration inhibitory factor (MIF) in primary Sjögren's syndrome. Joint Bone Spine. 2019;86(3):393–5. doi: 10.1016/j.jbspin.2018.07.001.
[51] Maier-Moore JS, Koelsch KA, Smith K, Lessard CJ, Radfar L, Lewis D, et al. Antibody-secreting cell specificity in labial salivary glands reflects the clinical presentation and serology in patients with Sjögren's syndrome. Arthritis Rheumatol. 2014;66(12):3445–56. doi: 10.1002/art.38872.
[52] Weinberg SE, Chandel NS. Mitochondria reactive oxygen species signaling-dependent immune responses in macrophages and T cells. Immunity 2025;58(8):1904–21. doi: 10.1016/j.immuni.2025.07.012.
[53] Kleshchevnikov V, Shmatko A, Dann E, Aivazidis A, King HW, Li T, et al. Cell2location maps fine-grained cell types in spatial transcriptomics. Nat Biotechnol. 2022;40(5):661–71. doi: 10.1038/s41587-021-01139-4.
[54] Zhang Q, Raoof M, Chen Y, Sumi Y, Sursal T, Junger W, et al. Circulating mitochondrial DAMPs cause inflammatory responses to injury. Nature 2010;464(7285):104–7. doi: 10.1038/nature08780.
[55] Kirchweger P, Wolf SG, Varsano N, Dadosh T, Resch GP, Elbaum M. Snapshots of mitochondrial fission imaged by cryo-scanning transmission electron tomography. J Cell Sci. 2025;138(9):jcs263639. doi: 10.1242/jcs.263639.
[56] Gupta S, Yamada E, Nakamura H, Perez P, Pranzatelli TJ, Dominick K, et al. Inhibition of JAK-STAT pathway corrects salivary gland inflammation and interferon driven immune activation in Sjögren's disease. Ann Rheum Dis. 2024;83(8):1034–47. doi: 10.1136/ard-2023-224842.
[57] Takano T, Yule DI. Neuronal and hormonal control of Ca^{2+} signalling in exocrine glands: insight from in vivo studies. J Physiol. 2024;602(14):3341–50. doi: 10.1113/jp285461.
[58] Ambudkar IS. Calcium signalling in salivary gland physiology and dysfunction. J Physiol. 2016;594(11):2813–24. doi: 10.1113/jp271143.
[59] Kopach O, Pivneva T, Fedirko N, Voitenko N. Mitochondrial malfunction mediates impaired cholinergic Ca^{2+} signalling and submandibular salivary gland dysfunction in diabetes. Neuropharmacology. 2024;243:109789. doi: 10.1016/j.neuropharm.2023.109789.
[60] Grazioli S, Pugin J. Mitochondrial damage-associated molecular patterns: from inflammatory signaling to human diseases. Front Immunol. 2018;9:832. doi: 10.3389/fimmu.2018.00832.
[61] Weyand CM, Wu B, Huang T, Hu Z, Goronzy JJ. Mitochondria as disease-relevant organelles in rheumatoid arthritis. Clin Exp Immunol. 2023;211(3):208–23. doi: 10.1093/cei/uxac107.
[62] Alissafi T, Kalafati L, Lazari M, Filia A, Kloukina I, Manifava M, et al. Mitochondrial oxidative damage underlies regulatory T cell defects in autoimmunity. Cell Metab. 2020;32(4):591–604.e7. doi: 10.1016/j.cmet.2020.07.001.
[63] Ye B, Chen B, Guo C, Xiong N, Huang Y, Li M, et al. C5a-C5aR1 axis controls mitochondrial fission to promote podocyte injury in lupus nephritis. Mol Ther. 2024;32(5):1540–60. doi: 10.1016/j.ymthe.2024.03.003.
[64] Ehnes DD, Alghadeer A, Hanson-Drury S, Zhao YT, Tilmes G, Mathieu J, et al. Sci-Seq of human fetal salivary tissue introduces human transcriptional paradigms and a novel cell population. Front Dent Med. 2022;3:887057. doi: 10.3389/fdmed.2022.887057.
[65] Moskwa N, Mahmood A, Nelson DA, Altrieth AL, Forni PE, Larsen M. Single-cell RNA sequencing reveals PDGFRα+ stromal cell subpopulations that promote proacinar cell differentiation in embryonic salivary gland organoids. Development 2022;149(6):dev200167. doi: 10.1242/dev.200167.
[66] Pringle S, Wang X, Verstappen GMPJ, Terpstra JH, Zhang CK, He A, et al. Salivary gland stem cells age prematurely in primary Sjögren's syndrome. Arthritis Rheumatol. 2019;71(1):133–42. doi: 10.1002/art.40659.
[67] Pranzatelli TJF, Perez P, Ku A, Matuck B, Huynh K, Sakai S, et al. $GZMK^+CD8^+$ T cells target a specific acinar cell type in Sjögren's disease. Ann Rheum Dis. 2026;85(5):880–98. doi: 10.1016/j.ard.2025.08.014.
[68] Dezfulian MH, Kula T, Pranzatelli T, Kamitaki N, Meng Q, Khatri B, et al. TScan-II: a genome-scale platform for the de novo identification of $CD4^+$ T cell epitopes. Cell. 2023;186(25):5569–5586.e21. doi: 10.1016/j.cell.2023.10.024.
[69] Clark M, Walsh H, Stephens-Laborde I, Khurram SA. The value of labial gland biopsies as a diagnostic test for Sjögren's syndrome. Head Neck Pathol. 2024;18(1):64. doi: 10.1007/s12105-024-01662-1.
[70] Ilicic T, Kim JK, Kolodziejczyk AA, Bagger FO, McCarthy DJ, Marioni JC, et al. Classification of low quality cells from single-cell RNA-seq data. Genome Biol. 2016;17:29. doi: 10.1186/s13059-016-0888-1.
[71] Neuschulz A, Bakina O, Badillo-Lisakowski V, Olivares-Chauvet P, Conrad T, Gotthardt M, et al. A single-cell RNA labeling strategy for measuring stress response upon tissue dissociation. Mol Syst Biol. 2023;19(2):e11147. doi: 10.15252/msb.202211147.

Ann Rheum Dis 85 (2026) 1800–1810

Contents lists available at ScienceDirect

Annals of the Rheumatic Diseases

journal homepage: https://www.sciencedirect.com/journal/annals-of-the-rheumatic-diseases

Systemic sclerosis

Novel HLA class I and II insights into the pathogenesis of systemic sclerosis–associated interstitial lung disease

Carlos Rosa-Baez[1], Carlos Rangel-Peláez[1], Inmaculada Rodriguez-Martin[1], Gonzalo Borrego-Yaniz[1], Martin Kerick[1], Alfredo Guillen-Del-Castillo[2], Carmen P. Simeón-Aznar[2], José Luis Callejas[3], Alexandre E. Voskuyl[4], Alexander Kreuter[5], Oliver Distler[6], International SSc Group, Susanna M. Proudman[7,8], Mandana Nikpour[9,10], Australian Scleroderma Interest Group, Nicholas Hunzelmann[11], Jeska K. de Vries-Bouwstra[12], Ariane L. Herrick[13,14], Yannick Allanore[15], Lorenzo Beretta[16], Maureen D. Mayes[17], Christopher P. Denton[18], Shervin Assassi[17], Javier Martín[1], Marialbert Acosta-Herrera[1,*]

[1] *Department of Cell Biology and Immunology, Institute of Parasitology and Biomedicine López-Neyra, Consejo Superior de Investigaciones Científicas, Granada, Spain*
[2] *Unit of Systemic Autoimmune Diseases, Department of Internal Medicine, Hospital Universitario Vall d'Hebron, Barcelona, Spain*
[3] *Department of Internal Medicine, Systemic Autoimmune Disease Unit, Hospital Clínico San Cecilio, Instituto de Investigación Biosanitaria Ibs. GRANADA, Granada, Spain*
[4] *Department of Rheumatology and Clinical Immunology, Amsterdam Rheumatology and immunology Center, Amsterdam UMC, Amsterdam, The Netherlands*
[5] *Department of Dermatology, Venereology, and Allergology, Helios St. Elisabeth Klinik Oberhausen, University Witten-Herdecke, Oberhausen, Germany*
[6] *Department of Rheumatology, University Hospital Zurich, University of Zurich, Zurich, Switzerland*
[7] *Department of Rheumatology, Royal Adelaide Hospital, Adelaide, SA, Australia*
[8] *Discipline of Medicine, Adelaide Medical School, University of Adelaide, Adelaide, SA, Australia*
[9] *Department of Medicine, University of Melbourne, Fitzroy, VIC, Australia*
[10] *Department of Rheumatology, The University of Sydney School of Public Health, Sydney, NSW, Australia*
[11] *Department of Dermatology and Venereology, University Hospital Cologne, Cologne, Germany*
[12] *Department of Rheumatology, Leiden University Medical Center, Leiden, The Netherlands*
[13] *Centre for Musculoskeletal Research, The University of Manchester, Northern Care Alliance NHS Foundation Trust, Manchester Academic Health Science Centre, Manchester, UK*
[14] *National Institute for Health and Care Research (NIHR) Manchester Biomedical Research Centre, Manchester, UK*
[15] *Department of Rheumatology, Université Paris Cité UFR de Médecine, Paris, France*
[16] *Scleroderma Unit, Referral Center for Systemic Autoimmune Diseases, Fondazione IRCCS Ca' Granda Ospedale Maggiore Policlinico di Milano, Milan, Italy*
[17] *Division of Rheumatology, Department of Internal Medicine, University of Texas Health, Houston, TX, USA*
[18] *Department of Inflammation and Rare Diseases, Centre for Rheumatology, Royal Free Hospital, University College London, London, UK*

*Correspondence to Dr. Marialbert Acosta-Herrera, Institute of Parasitology and Biomedicine López-Neyra, Consejo Superior de Investigaciones Científicas. Parque Tecnológico de Ciencias de la Salud. Armilla, Granada, Spain.
E-mail address: m.acostaherrera@ipb.csic.es (M. Acosta-Herrera).

Handling editor Josef Smolen

Javier Martin and Marialbert Acosta-Herrera contributed equally to this study and are considered as joint last authors.

https://doi.org/10.1016/j.ard.2026.05.004

0003-4967/© 2026 European Alliance of Associations for Rheumatology (EULAR). Published by Elsevier B.V. All rights are reserved, including those for text and data mining, AI training, and similar technologies.

ARTICLE INFO

Article history:
Received 11 December 2025
Received in revised form 25 March 2026
Accepted 5 May 2026

ABSTRACT

Objectives: Systemic sclerosis–associated interstitial lung disease (SSc-ILD) is the leading cause of mortality in systemic sclerosis (SSc), yet its genetic architecture remains incompletely understood. Therefore, given the key role of the major histocompatibility complex (MHC) in SSc, we aimed to perform a comprehensive MHC-wide association study in the largest SSc-ILD cohort to date.

Methods: We analysed 2412 patients with SSc-ILD$^+$, 3550 patients with SSc-ILD$^-$, and 15,076 controls of European ancestry from 10 international cohorts. After quality control, the MHC region was imputed, and inverse variance weighted meta-analysis was performed. Subsequently, conditional stepwise analyses, adjustment for antitopoisomerase autoantibody (ATA) status, and functional annotation of significant single-nucleotide polymorphisms were performed. Finally, we constructed a composite score combining genetic, clinical, and demographic variables to predict SSc-ILD.

Results: After conditional analysis, we detected 12 significant associations within class I and class II human leukocyte antigen (HLA) genes. ATA adjustment reduced the significance of class II HLA variants, whereas class I HLA variants remained unaffected. Finally, the built composite score had an area under the curve of 0.754, significantly outperforming the models including any of the variables alone.

Conclusions: In this study, we identify genetic mechanisms underlying SSc-ILD that support the potential implication of CD8$^+$ T cells and ATAs in its pathogenesis. Moreover, we also demonstrate the enhanced efficacy of integrating genetic information into predictive models to detect patients at high risk of SSc-ILD. These findings provide new insights into disease pathogenesis and suggest potential biomarkers and therapeutic targets for improved patient management.

WHAT IS ALREADY KNOWN ON THIS TOPIC

- Systemic sclerosis (SSc)–associated interstitial lung disease (ILD) is the leading cause of mortality in SSc.
- The major histocompatibility complex (MHC) region is the strongest genetic risk locus for SSc, but its specific contribution to SSc-ILD has not been clarified and previous genetic studies in this clinical manifestation are often underpowered.

WHAT THIS STUDY ADDS

- This study provides the largest MHC genetic analysis of SSc-ILD to date, identifying 12 specific associations in class I and class II human leukocyte antigen (HLA) genes.
- Class II HLA associations lose significance after adjustment for antitopoisomerase autoantibody (ATA), whereas class I signals remain robust, revealing distinct ATA-dependent and ATA-independent pathogenic pathways.
- Adding genetic information to SSc-ILD risk scores improves its ability to identify patients at high risk of developing SSc-ILD.

HOW THIS STUDY MIGHT AFFECT RESEARCH, PRACTICE OR POLICY

- These findings provide genetic evidence supporting pathogenic mechanisms in SSc-ILD, involving autoantibody-driven processes and CD8$^+$ T cell-mediated pathways.
- Our composite risk score results encourage the inclusion of genetic data in predictive scores for early SSc-ILD screening and monitoring.
- The identified genetic loci and pathways provide potential biomarkers and therapeutic targets relevant to the management of SSc-ILD.

INTRODUCTION

Systemic sclerosis (SSc) is an immune-mediated inflammatory disease characterised by a strong immune imbalance, vasculopathy, and fibrosis affecting skin and internal organs [1]. Although it has low prevalence, SSc exhibits the highest mortality rate of all rheumatic diseases. In fact, pulmonary complications, such as SSc-associated interstitial lung disease (SSc-ILD), are the leading cause of death in these patients [2].

SSc-ILD is present in approximately 50% of patients with SSc, and it exhibits marked heterogeneity, with clinical presentations ranging from mild and stable to rapidly progressive forms [3,4]. Established risk factors for developing SSc-ILD include the presence of antitopoisomerase autoantibodies (ATAs), diffuse cutaneous SSc, and male gender [5,6]. Furthermore, although there are treatments that have been shown to slow the progression of SSc-ILD, there is currently no disease-modifying treatment that improves SSc-ILD or reverses the established pulmonary fibrosis [3].

Both environmental and genetic factors play crucial roles in SSc pathogenesis, and human leukocyte antigen (HLA) genes have consistently proven to be the strongest genetic association for the disease [7–9]. Variants within HLA genes may influence the antigen presentation to CD4$^+$ T-helper cells, leading to autoreactive T-helper and B cells and the production of autoantibodies [8,10]. Although multiple studies have identified genetic associations in SSc [7,8,11–13], few have analysed how genetic risk variants relate to specific clinical manifestations, such as SSc-ILD, and existing studies are often limited by small sample sizes [14–25].

Considering this, we sought to comprehensively analyse the specific contribution of the major histocompatibility complex (MHC) region in SSc-ILD by conducting the largest HLA association analysis to date. We evaluated the association of HLA alleles, single-nucleotide polymorphisms (SNPs) and polymorphic aminoacidic residues with SSc-ILD and functionally assessed its regulatory role in order to identify potential pathogenic mechanisms, biomarkers and/or therapeutic targets.

METHODS

Study population

This study included 10 cohorts comprising 5962 patients with SSc (2412 SSc-ILD$^+$ and 3550 SSc-ILD$^-$) and 15,076

controls. Blood/saliva samples were collected from all individuals, and, after DNA extraction, genome-wide genotyping was carried out using the arrays specified in Supplementary Table S1. All individuals were of European ancestry and recruited from multiple centres across Spain, the United Kingdom, the United States of America, Canada, Australia, Italy, Germany, Switzerland, France, and the Netherlands. All patients with SSc fulfilled the 2013 American College of Rheumatology/the European League Against Rheumatism classification criteria, or the criteria proposed by LeRoy and Medsger for early SSc [26,27]. Clinical characteristics and further information on the 10 cohorts analysed are summarised in Supplementary Table S1.

Presence or absence of SSc-ILD was evaluated using high-resolution computed tomography (HRCT), or by the presence of radiologic findings on chest X-ray, and abnormalities on pulmonary function tests. The study protocol was approved by participating centres and the ethics committee of the Consejo Superior de Investigaciones Científicas, and written informed consent was obtained from all participants in accordance with the principles of the Declaration of Helsinki.

Quality control and MHC imputation

To ensure the high-quality of the genetic data in downstream analysis, we applied stringent quality control (QC) procedures before imputation. Regarding sample filtering, individuals with genotype missingness > 0.05, ambiguous sex annotation based on sex chromosomes, or relatedness were excluded. Relatedness was assessed using identity-by-descent estimation, and 1 individual from each pair of relatives (Pi_Hat > 0.4) or duplicates (Pi_Hat > 0.99) was excluded. Regarding variant filtering, SNPs with low call rate (< 0.98), deviations from Hardy-Weinberg equilibrium (HWE) (P value $< 1 \times 10^{-3}$), or a minor allele frequency (MAF) < 0.01 were excluded. In addition, palindromic SNPs with an A/T or C/G allele frequency > 0.4 were removed to avoid strand ambiguity.

After these QCs, the MHC region variants (SNPs, classical alleles and aminoacidic residues) were imputed using the 4-digit multiethnic HLA v1 (2021) reference panel on the Michigan imputation server with default settings (https://imputationserver.sph.umich.edu/). After imputation, we carried out further QCs, including the exclusion of variants with imputation quality (squared correlation [Rsq]) < 0.9, MAF < 0.01, low call rate (< 0.9), or deviating from HWE (P value $< 1 \times 10^{-6}$). Finally, to control for population structure, we conducted principal component analysis over genome-wide data using PLINK and GCTA64 [28,29] for each of the 10 cohorts. Ten principal components (PC) were calculated for each cohort, and outlier individuals deviating by > 4 SDs from the cluster centroid were excluded.

Statistical analysis

Logistic regression analyses were conducted in PLINK 2.0 for each of the 10 cohorts, adjusting for sex and the first 5 PC. For each cohort, 3 pairwise comparisons were carried out: SSc-ILD$^+$ vs SSc-ILD$^-$, SSc-ILD$^+$ vs controls, and SSc-ILD$^-$ vs controls. Then, inverse variance weighted meta-analyses of the datasets were carried out using Metasoft [30] under a fixed-effect model for nonheterogeneous variants (Cochran's Q P value > .05), whereas for variants showing heterogeneity (Cochran's Q P value < .05), the random effect model (RE2) was used. Statistical significance threshold was declared at 4.6×10^{-6}, and suggestive threshold at 9.2×10^{-5}. These were calculated using the genetic type I error calculator (GEC v0.2) [31], based on the effective number of tests in the imputed data from the MHC region.

In addition, to ensure that our results were specific for SSc-ILD, the associated variants had to meet at least 1 of the 2 following criteria: (i) significant in SSc-ILD$^+$ vs SSc-ILD$^-$ comparison and not reaching suggestive association in the SSc-ILD$^-$ vs controls comparison P value > 9.2×10^{-5}), or (ii) having opposite effects, defined by the odds ratio (OR), associated to SSc-ILD$^+$ and SSc-ILD$^-$ (P value < 4.6×10^{-6} in the 3 comparisons and opposing OR between SSc-ILD$^+$ vs controls and SSc-ILD$^-$ vs controls). This filtering step allowed us to prioritise associations more likely driven by the presence of SSc-ILD rather than by the broader SSc phenotype.

Finally, to detect conditionally independent associations, we performed conditional stepwise analysis with the COJO tool in GCTA 1.92.1 (Yang, J), applied separately to SNPs, classical alleles, and aminoacidic residues. At each step, we selected the most associated variant, re-ran the analysis including it as a covariate, and retained variants that remained significant, iterating until no additional variant reached significance.

Stratification and adjustment of associations by ATA

Given the strong correlation between SSc-ILD and ATA positivity, we performed a stratification of patients with ATA within the SSc-ILD$^+$ subgroup to assess the potential participation of the significant variants in SSc-ILD severity, as well as an ATA-conditioned analysis with the aim of evaluating whether our genetic associations were independent of its effect.

Functional annotation of SSc-ILD specific variants

With the aim to assess the potential regulatory role of our findings, we conducted functional annotation of the significant and SSc-ILD specific SNPs and their proxies ($r^2 > 0.9$), by using the SNP2GENE function of FUMA GWAS (functional mapping and annotation of GWAS) webtool (https://fuma.ctglab.nl/snp2gene) and the GTEx v.8 database. The parameters used for FUMA GWAS are listed in Supplementary Table S2. Specifically, we used FUMA GWAS to annotate relevant genes based on expression quantitative trait loci (eQTL) and chromatin interaction (Chr_Int) mapping. Furthermore, we queried GTEx v.8 database for splicing QTLs (sQTL). We focused this QTL annotation on relevant tissues/cell types for SSc-ILD (whole blood, immune cells, lung, and fibroblasts). In addition, we manually annotated the nearest gene to each of the variants included.

Risk prediction with polygenic risk score

In order to explore a potential clinical application of our results, we built a polygenic risk score (PRS) using the PRSice-2 software (https://choishingwan.github.io/PRSice/) and subsequently integrated the genetic component of this score with clinical and demographical data to generate a composite score of predictors of SSc-ILD. In order to conduct this analysis, the study population for which ATA status information was available was divided into 2 independent datasets: a training cohort comprising 7 of the study cohorts (4081 individuals; 1722 SSc-ILD$^+$ and 2359 SSc-ILD$^-$), used for selecting the SNPs of the model, and a testing cohort including the remaining 3 cohorts (1559 individuals; 553 SSc-ILD$^+$ and 1006 SSc-ILD$^-$), used to assess the predictive capability of the model. Within the training cohort, logistic regressions adjusted by the first 5 PC, sex, and ATA status were performed. Meta-analysis and joint analysis with COJO was carried out to

identify independent variants to be included in the PRS model, resulting in a final set of 10 SNPs. The PRS was then computed in the testing cohort using PRSice-2, including ATA as a covariate. Subsequently, with the aim of constructing the composite score, we quantified the contribution of ATA, anticentromere autoantibody (ACA), disease subtype (limited cutaneous SSc and diffuse cutaneous SSc), and sex variables in the training cohort through a generalised linear model adjusted for the first 5 PCs. Then, the composite score was calculated by combining the genetic PRS and the score derived from the clinical and demographic variables, each weighted by its respective regression coefficient.

Subsequently, the predictive performance of the models was evaluated using the pROC R package (Robin, X). We compared the area under the curve (AUC) across models using DeLong's statistical test, and individuals in the testing cohort were stratified into percentile-based risk categories for which the risk ratio (RR) for developing SSc-ILD was estimated.

Finally, in order to test the replicability/reproducibility of the model, we tested the model in a validation cohort from the UK Biobank using the same parameters optimised in the testing phase. This cohort consisted of 74 patients with SSc-ILD$^+$ and 202 patients with SSc-ILD$^-$ of European ancestry.

RESULTS

MHC associated variants

A total of 1541 MHC genetic variants were significant in the meta-analysis of SSc-ILD$^+$ vs SSc-ILD$^-$ (1399 SNPs, 12 classical alleles, and 130 aminoacidic residues) (Fig 1). After conditional analysis in the region, we found 5 SNPs, 3 classical alleles, and 4 aminoacidic residues jointly significant (Table 1).

Regarding the SNPs, the strongest association corresponded to an intronic protective variant within *HLA-DQB1* gene, chr6:32663912:A:G (OR = 0.52 and 95% CI [0.46-0.60], *P* value = 2.83×10^{-23}), which was in high linkage disequilibrium (LD) with *HLA-DQA1*01:01:01:01* classical allele and the amino acid glutamine in the position 224 of *HLA-DQB1* gene (Fig 2). In addition, we detected another intronic SNP, located in the second intron of *HLA-DPB1* gene and associated with a higher risk of SSc-ILD (chr6:33083222:G:A, OR = 2.53 [1.90-3.36], *P* value = 1.54×10^{-9}). The remaining 3 SNPs significantly associated were intergenic and potentially involved in SSc-ILD through gene regulation.

Concerning classical alleles, *HLA-DQA1*01:01:01:01* was the most strongly associated with the phenotype (OR = 0.54 [0.47-0.61], *P* value = 4.85×10^{-22}). Interestingly, another classical allele of *HLA-DQA1* was also associated, *HLA-DQA1*03:01:01*, conferring protection as well (OR = 0.71 [0.62-0.81], *P* value = 1.97×10^{-10}). Furthermore, we found *HLA-DPB1*13:01:01:01* as a risk variant for SSc-ILD (OR = 2.70 [1.93-3.79], *P* value = 4.4×10^{-8}). It is worth noting that all 3 classical alleles found were in high LD with 3 significant SNPs, and 2 of them also with a significant aminoacidic residue (Fig 2).

With regard to the aminoacidic residues, the most significantly associated with SSc-ILD was the HLA-DQA1 Gln34 (OR = 1.40 [1.28-1.55], *P* value = 4.22×10^{-12}), followed by aminoacidic residues in HLA-DPB1 (Ile76), HLA-DQB1 (Gln224), and HLA-C (Asp9), all of them conferring risk to SSc-ILD. Interestingly, all these residues, except for HLA-DQB1 Gln224, were in the peptide binding groove of the protein, highlighting their potential implication in the recognition of autoantigens by the HLA system.

It is worth mentioning that 2 of the significant risk variants were associated with class I HLA genes, the rs2523558 SNP (near *HLA-B*) and the aminoacidic residue HLA-C Asp9.

Finally, we compared the association of these 12 variants with those reported for SSc vs controls [8]. Interestingly, 8 of the 12 signals were not significantly associated with overall disease, supporting their SSc-ILD specificity. The remaining 4 variants showed smaller effect sizes in overall SSc despite the larger sample size of the study (Supplementary Table S3).

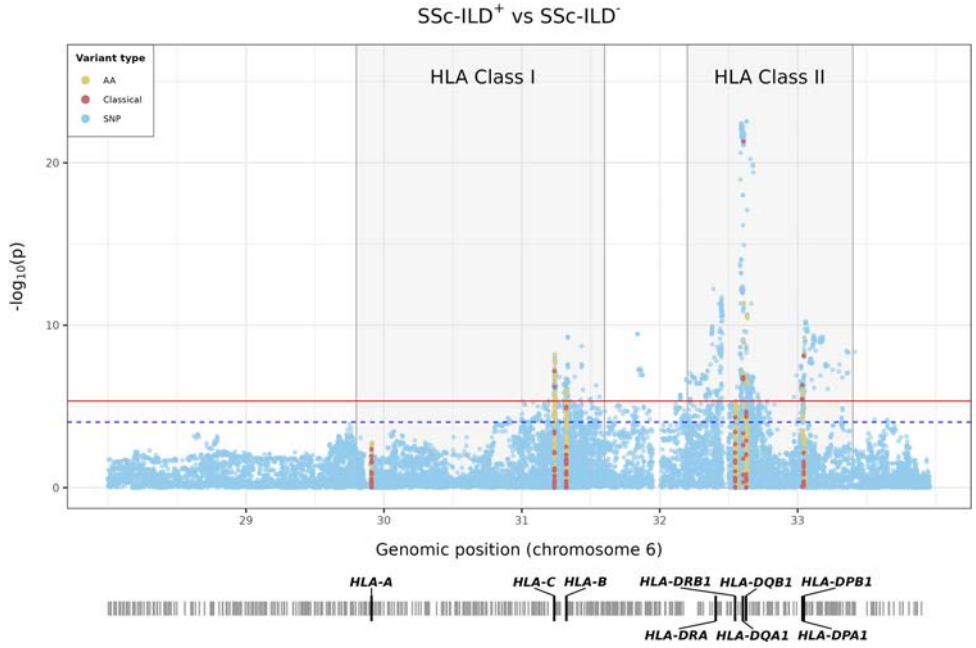

Figure 1. Manhattan plot of the MHC-wide association analysis for SSc-ILD$^+$ vs SSc-ILD$^-$. Association results across the MHC region. Each point represents a variant, plotted according to its genomic position and $-\log_{10}$(*P* value). The colour of the dot indicates the variant type (blue: SNP; red: classical allele; yellow: aminoacidic residue). The red line indicates the significance threshold of 4.6×10^{-6}, and the blue dashed line indicates the suggestive threshold of 9.2×10^{-5}. Relevant HLA genes are plotted into their genomic positions below the x-axis. AA, aminoacidic residue; HLA, human leukocyte antigen; MHC, major histocompatibility complex; SNP, Single-nucleotide polymorphism; SSc-ILD, Systemic sclerosis–associated interstitial lung disease.

Table 1
Summary statistics of the significant and SSc-ILD specific variants after conditional analysis for the comparison of SSc-ILD$^+$ vs SSc-ILD

Gene	Variant	Position (hg38)	EA	OR (95% CI)	*P* value	*P* value cond	SSc-ILD$^+$ freq	SSc-ILD$^-$ freq	SSc-ILD$^+$ vs Controls		SSc-ILD$^-$ vs Controls	
									OR (95% CI)	*P* value	OR (95% CI)	*P* value
Classical alleles												
HLA-DQA1	*HLA-DQA1*01:01:01:01*	32637407	P	0.54 (0.47-0.61)	4.85E-22	–	0.116	0.201	0.72 (0.56-0.92)	5.04E-08	1.41 (1.30-1.53)	8.59E-16
HLA-DQA1	*HLA-DQA1*03:01:01*	32637415	P	0.71 (0.62-0.81)	1.87E-07	1.97E-10	0.131	0.182	0.80 (0.71-0.89)	1.06E-04	1.18 (1.08-1.29)	1.65E-04
HLA-DPB1	*HLA-DPB1*13:01:01:01*	33075955	P	2.70 (1.93-3.79)	7.68E-09	4.40E-08	0.060	0.024	3.80 (3.01-4.79)	3.91E-29	1.33 (0.99-1.78)	5.68E-02
SNPs												
HLA-DQB1	chr6:32663912:A:G	32663912	G	0.52 (0.46-0.60)	2.83E-23	–	0.118	0.205	0.71 (0.55-0.91)	1.17E-08	1.42 (1.31-1.54)	1.55E-16
HLA-DQA1	rs9272353	32636679	C	0.71 (0.62-0.80)	1.39E-07	8.37E-11	0.132	0.183	0.79 (0.71-0.89)	6.82E-05	1.18 (1.08-1.28)	2.41E-04
HLA-DPB1	chr6:33083222:G:A	33083222	A	2.53 (1.90-3.36)	1.72E-10	1.54E-09	0.061	0.025	4.13 (3.32-5.15)	1.71E-36	1.39 (1.06-1.83)	1.74E-02
HLA-B	rs2523558	31363260	G	1.37 (1.24-1.51)	6.01E-10	1.66E-06	0.377	0.297	1.35 (1.24-1.47)	3.15E-12	0.97 (0.86-1.10)	4.58E-01
NCR3	rs3132452	31595463	A	1.42 (1.22-1.64)	2.54E-06	3.60E-06	0.118	0.087	1.33 (1.18-1.50)	2.40E-06	0.97 (0.86-1.09)	6.00E-01
Aminoacidic residues												
HLA-DQA1	HLA-DQA1 Gln34	32641403	P	1.40 (1.28-1.55)	4.22E-12	–	0.630	0.546	1.39 (1.28-1.52)	6.96E-14	0.98 (0.92-1.06)	6.51E-01
HLA-DPB1	HLA-DPB1 Ile76	33080890	P	2.37 (1.81-3.12)	5.69E-10	3.32E-10	0.067	0.029	3.23 (2.63-3.96)	2.74E-29	1.17 (0.92-1.50)	2.07E-01
HLA-DQB1	HLA-DQB1 Gln224	32660998	P	1.95 (1.61-2.38)	2.36E-11	1.18E-07	0.867	0.774	1.48 (1.02-2.14)	2.70E-05	0.78 (0.68-0.89)	2.95E-04
HLA-C	HLA-C Asp9	31271844	P	1.27 (1.17-1.37)	6.36E-09	2.77E-06	0.435	0.372	1.20 (1.12-1.28)	1.59E-07	0.93 (0.88-0.99)	2.78E-02

EA, effect allele; OR, odds ratio; SNP, single-nucleotide polymorphism; SSc-ILD, systemic sclerosis–associated interstitial lung disease.
Variants in this table meet the criteria for significance (*P* value < 4.6E-06) and SSc-ILD specificity (opposing effect or *P* value > 9.2E-05 in SSc-ILD$^-$ vs controls comparison). For classical alleles and aminoacidic residues, the effect allele (P) indicates the presence of the variant.

ATA adjustment maintains class I significance but reduces class II

Given the strong correlation of ATA with SSc-ILD, we decided to perform a complementary analysis including ATA as a covariate in the regression model in order to adjust for its effect. First, in order to check this association, we checked the proportion of ATA/ACA individuals in both SSc-ILD$^+$ and SSc-ILD$^-$ individuals. We found that the majority of patients in the SSc-ILD$^+$ group had ATA antibodies (72.8%), whereas only 21.5% of patients with SSc-ILD$^-$ presented it (Supplementary Fig 1). Subsequently, regarding the ATA adjusted analysis, the results showed that out of the 12 significant variants initially identified, 4 remained significant after adjustment. Two of them are class II HLA variants, and the other 2 are class I. Interestingly, although the class II associations substantially reduced their significance, the class I variants not only retained significance but showed a slight increase in association strength (Table 2).

Stratified analysis reveals potential progression/severity genetic markers

To investigate potential genetic determinants of SSc-ILD progression/severity, we performed a stratified analysis within patients with SSc-ILD using ATA status as a surrogate marker of a more severe clinical phenotype. The stratified meta-analysis identified 3814 variants reaching statistical significance, including 16 classical HLA alleles, 83 aminoacidic residues, and 3715 SNPs. After performing conditional analysis within each variant category, we identified 6 classical alleles, 5 amino acid residues, and 7 SNPs as jointly significant associations (Supplementary Table S4).

Notably, the classical alleles *HLA-DPB1*13:01:01:01* and *HLA-DQA1*03:01:01*, as well as the aminoacidic residue HLA-DPB1 Ile76, were among the jointly significant signals detected, overlapping with the variants identified as lead signals in the main comparison (SSc-ILD$^+$ vs SSc-ILD$^-$).

Functional assessment of SNPs

Since all the significant SNPs we identified were noncoding, we investigated whether they contribute to disease pathogenesis through regulatory roles. In order to assess this, we carried out functional annotation using the FUMA GWAS webtool and GTEx v.8 databases. Two of the SNPs (chr6:32663912:A:G and chr6:33083222:G:A) were not present in the FUMA GWAS database; thus, they could not be included in the analysis. However, all the SNPs that were included showed overlap with at least 1 functional category such as QTLs or Chr_Int, suggesting they influence disease by affecting regulatory elements (Supplementary Fig 2; Fig 3).

In lung tissue, 25 genes showed altered expression associated with at least 1 of the 3 SNPs. These prioritised genes included HLA class I and class II genes, complement genes as *C4A*, or other genes as *MICA* and *MICB*. Notably, we also found that rs2523558 and rs3132452 SNPs, although they are independent in terms of LD (R^2 and D′ < 0.1), contributed jointly to the regulation of 4 genes: *CCHCR1, PSORS1C1, PSORS1C2*, and *MICA*. Finally, regarding sQTL annotation, rs9272353 and rs3132452 variants were associated with the modulation of the isoform proportions of 7 genes, including *HLA-DQA1, HLA-DRB1*, and *NCR3* (Fig 3). In total, our results prioritised 66 genes as potentially relevant for SSc-ILD (Supplementary Fig 2; Fig 3).

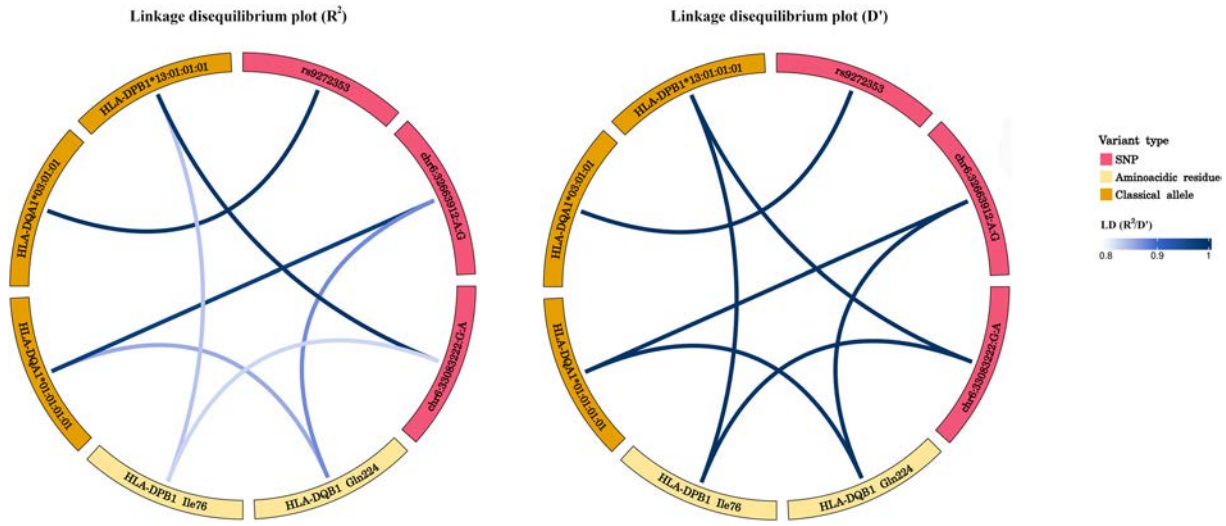

Figure 2. Linkage disequilibrium among significant HLA variant types. Circular plot representing the linkage disequilibrium (LD) structure (R^2 and D') among the significant variants identified in the MHC region. The circle shows all LD interactions detected between SNPs (pink), classical HLA alleles (orange), and amino acid residues (yellow). Lines connecting variants represent pairwise LD, with colour intensity proportional to R^2/D' values. HLA, human leukocyte antigen; LD, linkage disequilibrium; MHC, major histocompatibility complex; SNP, single-nucleotide polymorphism

Integration of genetic and clinical predictors improves SSc-ILD risk stratification

To develop a clinically relevant model, we combined PRS, autoantibody status, SSc subtype, and sex to predict SSc-ILD. Using the training cohort, PRSice-2 identified an optimal model including 6 SNPs of the 10 given as an input (Supplementary Table S5). Application of this PRS, or any of the clinical/demographic scores to the independent testing cohort, resulted in AUCs < 0.7. However, interestingly, the composite score integrating all components achieved an AUC of 0.754 (Fig 4a). Remarkably, DeLong's statistical test for comparing receiver operating characteristic (ROC) curves showed that there was a statistically significant difference between the composite score and each of the individual scores considered (Supplementary Table S6). Furthermore, we tested the difference between this composite score and a score including all variables except the PRS, finding a significant difference (P value $= 8.64 \times 10^{-3}$) and confirming the added value of integrating genetic information into predictive scores.

In addition, to ensure that the risk estimates were consistent in an independent cohort, we ran a validation analysis in an SSc-ILD cohort from UK Biobank. Using the same parameters as in the testing cohort, we were able to validate the predictive capacity of our genetic model. For instance, the AUC in the testing cohort was 0.585, and in the validation cohort 0.589.

Finally, using our composite score, we stratified individuals in the testing cohort into percentile-based risk categories to define a high-risk subgroup for SSc-ILD. The 85th percentile group corresponded to a RR of 3.54 (95% CI: 2.77-4.55) for SSc-ILD development, indicating that patients in this high-risk group present > 3 times higher risk of developing this clinical manifestation (Fig 4b).

DISCUSSION

In this study, we performed the largest MHC-focused genetic analysis of SSc-ILD to date, including 2412 SSc-ILD$^+$, 3550 SSc-ILD$^-$, and 15,076 controls. By analysing classical alleles, aminoacidic residues, and SNPs, we show that the MHC plays a key

Table 2
Summary statistics of the significant and SSc-ILD specific variants and their value after adjusting for the ATA status as a covariate

Gene	Variant	Position (hg38)	Effect allele	OR (95% CI)	*P* value cond	ATA adjustment	
						OR (95% CI)	*P* value
Classical alleles							
HLA-DQA1	***HLA-DQA1*01:01:01:01***	**32637407**	**P**	**0.54 (0.47-0.61)**	**4.85E-22**	**0.64 (0.56-0.73)**	**4.93E-11**
HLA-DQA1	*HLA-DQA1*03:01:01*	32637415	P	0.71 (0.62-0.81)	1.97E-10	0.80 (0.70-0.92)	1.69E-03
HLA-DPB1	*HLA-DPB1*13:01:01:01*	33075955	P	2.70 (1.93-3.79)	4.40E-08	1.40 (0.97-2.04)	7.30E-02
SNPs							
HLA-DQB1	**chr6:32663912:A:G**	**32663912**	**G**	**0.52 (0.46-0.60)**	**2.83E-23**	**0.63 (0.56-0.72)**	**7.90E-12**
HLA-DQA1	rs9272353	32636679	C	0.71 (0.62-0.80)	8.37E-11	0.80 (0.70-0.92)	1.46E-03
HLA-DPB1	chr6:33083222:G:A	33083222	A	2.53 (1.90-3.36)	1.54E-09	1.32 (0.97-1.80)	7.26E-02
HLA-B	**rs2523558**	**31363260**	**G**	**1.37 (1.24-1.51)**	**1.66E-06**	**1.33 (1.20-1.48)**	**1.06E-07**
NCR3	rs3132452	31595463	A	1.42 (1.22-1.64)	3.60E-06	1.29 (1.10-1.52)	1.80E-03
Aminoacidic residues							
HLA-DQA1	HLA-DQA1 Gln34	32641403	P	1.40 (1.28-1.55)	4.22E-12	1.25 (1.13-1.39)	2.22E-05
HLA-DPB1	HLA-DPB1 Ile76	33080890	P	2.37 (1.81-3.12)	3.32E-10	1.32 (0.94-1.84)	1.08E-01
HLA-DQB1	HLA-DQB1 Gln224	32660998	P	1.95 (1.61-2.38)	1.18E-07	1.57 (1.28-1.92)	1.30E-05
HLA-C	**HLA-C Asp9**	**31271844**	**P**	**1.27 (1.17-1.37)**	**2.77E-06**	**1.24 (1.14-1.35)**	**1.32E-06**

ATA, antitopoisomerase autoantibody; OR, odds ratio; SNP, single-nucleotide polymorphism; SSc-ILD, systemic sclerosis–associated interstitial lung disease.
In boldface: variants that remain significant after adjusting for ATA. For classical alleles and aminoacidic residues, the effect allele (P) indicates the presence of the variant.

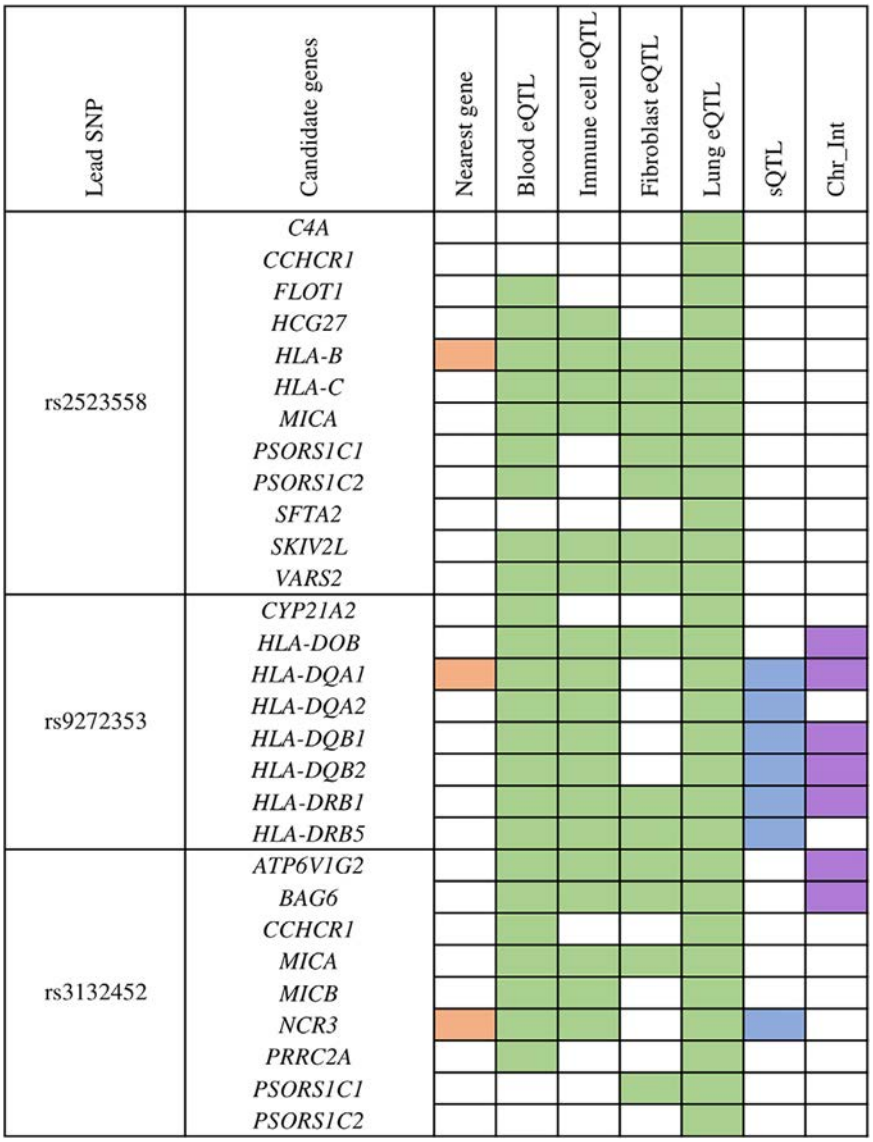

Figure 3. Summary of functional annotation of the significant SNPs. Figure highlighting the functional role of 3 significant SNPs (and/or proxies) identified. Genes were prioritised based on positional mapping (orange), eQTL effects in relevant tissues/cell types (green), sQTL effects (blue), and chromatin interactions (purple). The presence of an annotation in a specific category is indicated by its corresponding colour. eQTL, expression quantitative trait loci; SNP, single-nucleotide polymorphism; sQTL, splicing quantitative trait loci.

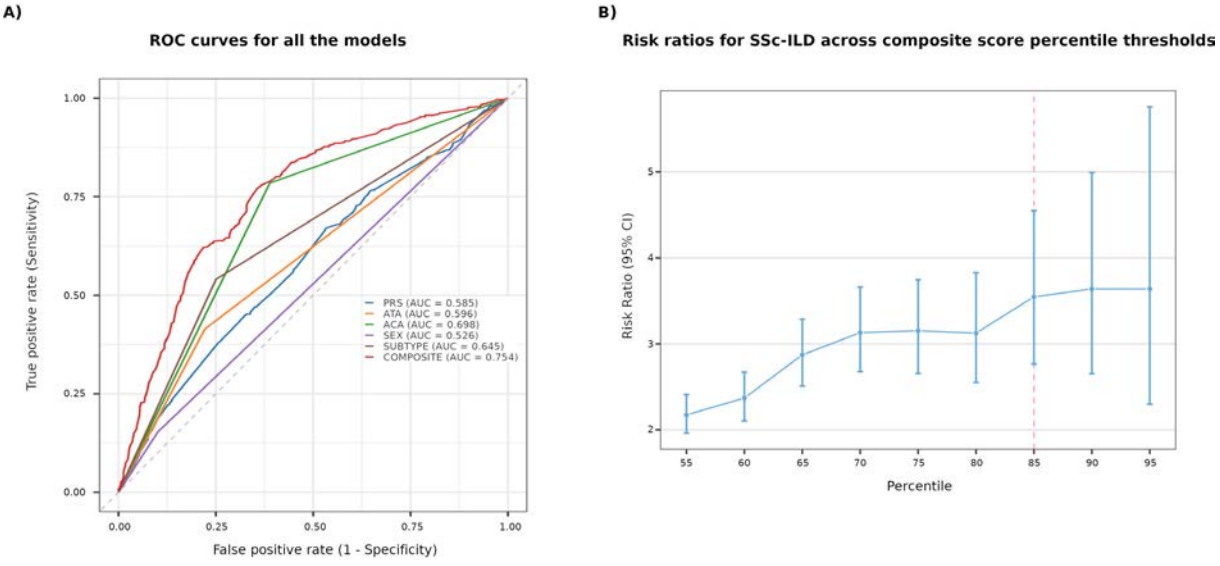

Figure 4. Predictive performance and risk stratification for SSc-ILD. (A) ROC curves and area under the curve (AUC) for the genetic PRS (green), ATA-only (blue), and composite score (red) models. (B) Odds ratios (OR) and 95% CI for SSc-ILD across percentile thresholds of the composite score. The dashed red line indicates the 85th percentile, which was selected as the high-risk cutoff. ACA, anticentromere autoantibody; ATA, antitopoisomerase autoantibody; PRS, polygenic risk score; ROC, receiver operating characteristic; SSc-ILD, systemic sclerosis–associated interstitial lung disease.

role in SSc-ILD susceptibility and identify novel class I and class II signals with potential pathogenic relevance. We also examined the impact of ATA$^+$ status on these associations, functionally annotated the associated SNPs and developed a composite score to identify patients at increased risk of SSc-ILD.

We detected 12 significant variants comparing SSc-ILD$^+$ against SSc-ILD$^-$, 8 of which were not significant in the overall disease [8], with the remaining showing greater effects in SSc-ILD. Nine of the 12 variants localised to HLA class II, including *HLA-DQA1*01:01:01:01* and *HLA-DPB1*13:01:01:01*, which have previously been associated with SSc-related pulmonary fibrosis [19], and ATA positivity [8,11,19,32]. Interestingly, *HLA-DPB1*13:01:01:01, HLA-DQA1*03:01:01*, and the aminoacidic residue HLA-DPB1 Ile76 were also significant in the ATA-stratified analysis within SSc-ILD, supporting a contribution of these variants to disease severity in the SSc-ILD subset. However, because ATA is an imperfect surrogate of progression, longitudinal studies will be needed to determine whether these variants influence fibrotic trajectories. Furthermore, to disentangle direct effects on SSc-ILD from those mediated by ATA, we adjusted the analysis for ATA status. After adjustment, all HLA class II associations were markedly attenuated, whereas HLA class I associations remained significant and became slightly stronger. This pattern is consistent with a model in which HLA class II variation contributes to SSc-ILD mainly through ATA-related mechanisms, whereas HLA class I variation acts through a distinct, ATA-independent pathway. This would also be consistent with ATA autoantibodies participating in the pathogenic processes of SSc-ILD, which would explain why only HLA class II variants lose significance. This interpretation is supported by experimental evidence showing that ATA-containing immune complexes can incorporate nucleic acids and activate Toll-like receptors (TLR) that induce profibrotic programmes [33,34], as well as by clinical evidence linking B-cell activity in patients with ATA$^+$ with pulmonary fibrosis severity [35].

Beyond HLA class II, we detected 2 significant HLA class I signals: rs2523558 near *HLA-B* and Asp9 in HLA-C. As HLA class I molecules present peptides to CD8$^+$ T cells and are expressed on essentially all nucleated cells [36], these associations point to a role for CD8$^+$ T-cell-mediated antigen recognition in SSc-ILD. Variation in HLA class I molecules could affect the self-peptide repertoire, promoting a cytotoxic response. In fact, class I HLA variants have previously been reported for overall SSc [8]. Furthermore, CD8$^+$ T-cell enrichment has been observed in skin from early diffuse patients with SSc [37], together with reduced numbers in peripheral blood [38], suggesting redistribution to affected organs. Single-cell RNA-seq studies further support this mechanism. Shimagami et al [39] reported an enrichment of a CD8$^+$ effector-memory population in peripheral blood and lung from patients with SSc-ILD, characterised by a strong type-II interferon signature, and expression of migration markers as *CXCR3* or *CCR5*. Moreover, Padilla et al [40] found increased CD8$^+$ tissue-resident memory T cells in SSc-ILD lungs showing upregulation of TCR signalling, exhaustion markers, and fibrosis-associated pathways. Altogether, this evidence supports a model linking altered HLA-I presentation of self-peptides to persistent CD8$^+$ T-cell activation leading to fibrotic remodelling.

To give functional insight into the associated noncoding SNPs, we annotated them using FUMA GWAS and GTEx v.8. In total, we prioritised 66 genes, and the expression of 25 of them was regulated in lung tissue by at least 1 of the 3 SNPs included in the analysis. In addition, the expression levels of several genes, including *HLA-DRB1, HLA-DQA1*, and *HLA-DQB1*, were predicted to be regulated across other relevant tissues/cell types considered, such as blood, immune cells, and fibroblasts. Although some prioritised genes have been associated with other ILDs as rheumatoid arthritis-associated ILD and myositis-associated ILD, the specific variants differed, suggesting partly distinct pathogenic mechanisms despite their clinical overlap [41,42]. Furthermore, we found that rs2523558 is a lung eQTL for *C4A*, with the risk allele associated with reduced expression. This result aligns with previous associations of *C4* variation with SSc, systemic lupus erythematosus (SLE) or primary Sjögren's Syndrome [43−46]. Moreover, given the role of C4 in clearing immune complexes [47], this also supports their aforementioned pathogenic role in SSc-ILD. Finally, regulation of *MICA* and *MICB* further supports cytotoxic involvement in SSc-ILD [48]. Both genes have also been associated with SLE and RA [49−53], and a recent study using exome sequencing and machine learning highlighted *MICB* as a genetic risk locus for SSc [54].

Finally, our composite score integrating the effects of 6 HLA SNPs, the presence of ATA/ACA, SSc subtype, and sex achieved an AUC of 0.754, significantly outperforming models based on any single variable. The improvement observed after adding genetic factors to clinical and demographic variables (P value = .0086) further supports the value of combining these dimensions for SSc-ILD risk prediction, which is consistent with previous observations in SSc [55]. Because current guidelines already recommend baseline HRCT screening for all patients with SSc [6], the main clinical utility of this score lies in follow-up. In particular, it could help clinicians identify patients with SSc-ILD$^-$ at high risk of future SSc-ILD development who may benefit from closer surveillance, especially in late-onset SSc-ILD cases [56]. Beyond risk prediction, the distinction between ATA-linked HLA class II associations and ATA-independent HLA class I signals also has potential mechanistic and therapeutic implications. For instance, our ATA-dependent HLA class II associations pointing towards the role of immune complexes support the rationale for B-cell−directed therapies and provide an opportunity for therapies targeting TLR signalling, as currently explored in SLE (NCT05540327, NCT04895696) or plaque psoriasis (NCT01899729). In addition, the ATA-independent HLA class I associations, together with the regulatory signals at *MICA* and *MICB*, point towards CD8$^+$ T cells and natural killer cells, suggesting that modulation of cytotoxic lymphocyte activity may also hold therapeutic promise in SSc-ILD.

Despite its strengths, this study has several limitations. First, < 10% of patients from earlier cohorts were not evaluated by HRCT because imaging was performed selectively according to clinical risk factors. This may have led to some underdiagnosis of SSc-ILD, although the impact on statistical power is likely limited given the small proportion affected. Second, as this study focuses on the MHC region, the derived analyses, including the PRS incorporated into the composite score, only include variants from this locus. Incorporating risk variants from other genomic regions in future studies may further improve predictive performance and provide a broader view of the genetic architecture of this clinical manifestation. Finally, our analyses were restricted to individuals of European ancestry, limiting generalizability. Validation in higher-risk populations, such as African Americans, will be essential [6].

In summary, this comprehensive MHC analysis identifies loci specifically associated with SSc-ILD and supports distinct contributions of HLA class I and class II variation to disease pathogenesis. HLA class I signals point towards CD8$^+$ T-cell participation, whereas HLA class II associations are consistent with a contribution of ATA-related mechanisms. We also developed a composite

score integrating genetic, clinical, and demographic variables to help identify patients at high risk of SSc-ILD. Together, these findings refine the immunogenetic architecture of SSc-ILD and may inform biological stratification and clinical monitoring.

Acknowledgements

We sincerely thank Sofia Vargas and Gema Robledo for their exceptional technical support and to all the patients and control donors for their invaluable participation and cooperation. This research has been conducted using the UK Biobank Resource under Application Number 276785. This research is part of the doctoral degree awarded to CR-B, within the Biomedicine programme from the University of Granada.

Contributors

Conceptualisation: JM, MA-H; Methodology: MA-H; Formal analysis: CR-B, CR-P, IR-M, GB-Y, MK; Resources: AG-D-C, CPS-A, JLC, AEV, AK, OD, SMP, MN, NH, JDV-B, ALH, YA, LB, MM, CPD, SA; Data curation: CR-B, CR-P, IR-M, GB-Y, MK, AG-D-C, CPS-A, JLC, AEV, AK, OD, SMP, MN, NH, JDV-B, ALH, YA, LB, MM, CPD, SA; Writing original draft: CR-B, MA-H; Visualisation: CR-B; Supervision: JM, MA-H; Project Administration: MA-H. All authors have carefully read and approved the final version of the manuscript.

Funding

This work was supported by grant PID2022-139292OB-I00 funded by MICIU/AEI/10.13039/501100011033 and by ERDF/EU, by the Instituto de Salud Carlos III PI22/00092, and by Redes de Investigación Cooperativa Orientadas a Resultados en Salud (RD21/0002/0039, RD24/0007/0016). CR-B was supported by the programme FPU: (FPU22/01652), funded by the Spanish Ministry of Science Innovation and Universities. CR-P was funded by Grant PREP2022-000747 funded by MICIU/AEI/10.13039/501100011033 and by ESF+. IR-M was supported by the programme FPU: [FPU21/02746], funded by the Spanish Ministry of University. GB-Y's contract is part of the grant PREP2022-000712, funded by the MCIN/AEI/10.13039/501100011033 and the FSE+. The Australian Scleroderma Cohort Study is supported by Janssen, Boehringer Ingelheim, Scleroderma Australia, Scleroderma Victoria, Arthritis Australia, Musculoskeletal Australia (muscle, bone, and joint health), Australian Rheumatology Association, and St. Vincent's Hospital Melbourne IT Department and Research Endowment Fund. SA was supported by NIH/NIAMS, R01AR081280 and DoD-W81XWH-22-1-0162.

Competing interests

MDM reports a relationship with Prometheus/Merck, Mitsubishi Tanabe, Boehringer Ingelheim, AstraZeneca, aTYR Pharma, Horizon/Amgen, and BMS Pharma that includes: funding grants; with Cabaletta Pharma and Amgen that includes: consulting or advisory; and with GSK Pharma, AstraZeneca, and Novartis that includes: speaking and lecture fees. OD reports a relationship with 4P-Pharma, AbbVie, AstraZeneca, Boehringer Ingelheim, and Janssen that includes: consulting or advisory, funding grants, and speaking and lecture fees; with Acepodia, Aera, AnaMar, Anaveon, Argenx, BMS, Calluna, Cantargia, CSL Behring, EMD Serono, Galderma, Gossamer, Hemetron, Innovaderm, Kali, Lilly, MSD Merck, Nkarta, Oorja Bio, Orion, Pilan, Quell, Redx Pharma, Sumitomo, Tandem, Topadur, UCB, and Umlaut Bio that includes: consulting or advisory; and with Prometheus and Scleroderma Research Foundation that includes: funding grants. SP reports a relationship with Janssen that includes: consulting or advisory and speaking and lecture fees; and with Boehringer Ingelheim and MSD that includes: consulting or advisory. MN reports a relationship with Janssen, AstraZeneca, GSK, Boehringer Ingelheim, and Bristol-Myers Squibb that includes: consulting or advisory. AG-D-C reports a relationship with Boehringer Ingelheim, Janssen, and MSD Merck that includes: funding grants, consulting or advisory, and speaking and lecture fees. CPS-A reports a relationship with Boehringer Ingelheim, Janssen, and MSD Merck that includes: funding grants, consulting or advisory, and speaking and lecture fees. JdV-B reports a relationship with AbbVie that includes: consulting or advisory; with Janssen and Boehringer Ingelheim that includes: consulting or advisory and speaking and lecture fees; with GSK, Pfizer, and BMS that includes: speaking and lecture fees; and with Roche, Galapagos, Janssen Pharmaceutical Companies, Vifor, NVLE, and ReumaNederland that includes: funding grants. AH reports a relationship with AbbVie, Arena, Merck, Novartis, and ZuraBio that includes: consulting or advisory; and with Boehringer Ingelheim and Janssen that includes: consulting or advisory and speaking and lecture fees. OD has patent #mir-29 for the treatment of systemic sclerosis (US8247389, EP2331143) issued to OD. The other authors declare they have no competing interests.

Patient consent for publication

Not applicable.

Ethics approval

The study protocol was approved by participating centres and the ethics committee of the Consejo Superior de Investigaciones Científicas (CSIC), and written informed consent was obtained from all participants in accordance with the principles of the Declaration of Helsinki.

Provenance and peer review

Not commissioned; externally peer reviewed.

Data availability statement

Summary statistics for the 3 comparisons performed in this study are publicly available in the following Figshare repository: https://doi.org/10.6084/m9.figshare.30773531

Declaration of generative AI and AI-assisted technologies in the manuscript preparation process

During the preparation of this work, the authors used ChatGPT in order to enhance the writing of some sections of the manuscript. After using this tool, the authors reviewed and edited the content as needed and take full responsibility for the content of the publication.

Supplementary materials

Supplementary material associated with this article can be found in the online version at doi:10.1016/j.ard.2026.05.004.

Orcid

Carlos Rosa-Baez: http://orcid.org/0000-0002-1257-3338
Marialbert Acosta-Herrera: http://orcid.org/0000-0002-9868-6535

REFERENCES

[1] Volkmann ER, Andréasson K, Smith V. Systemic sclerosis. Lancet 2023;401:304–18. doi: 10.1016/S0140-6736(22)01692-0.
[2] Perelas A, Silver RM, Arrossi AV, Highland KB. Systemic sclerosis-associated interstitial lung disease. Lancet Respir Med. 2020;8:304–20. doi: 10.1016/S2213-2600(19)30480-1.
[3] Liakouli V, Ciancio A, Del Galdo F, Giacomelli R, Ciccia F. Systemic sclerosis interstitial lung disease: unmet needs and potential solutions. Nat Rev Rheumatol. 2024;20:21–32. doi: 10.1038/S41584-023-01044-X.
[4] Bergamasco A, Hartmann N, Wallace L, Verpillat P. Epidemiology of systemic sclerosis and systemic sclerosis-associated interstitial lung disease. Clin Epidemiol. 2019;11:257–73. doi: 10.2147/CLEP.S191418.
[5] Khanna D, Tashkin DP, Denton CP, Renzoni EA, Desai SR, Varga J. Etiology, risk factors, and biomarkers in systemic sclerosis with interstitial lung disease. Am J Respir Crit Care Med. 2020;201:650–60. doi: 10.1164/RCCM.201903-0563CI.
[6] Antoniou KM, Distler O, Gheorghiu A-M, Moor CC, Vikse J, Bizymi N, et al. ERS/EULAR clinical practice guidelines for connective tissue disease-associated interstitial lung disease developed by the task force for connective tissue disease-associated interstitial lung disease of the European Respiratory Society (ERS) and the European Alliance of Associations for Rheumatology (EULAR) Endorsed by the European Reference Network on rare respiratory diseases (ERN-LUNG). Ann Rheum Dis. 2026;85:22–60. doi: 10.1016/j.ard.2025.08.021.
[7] López-Isac E, Acosta-Herrera M, Kerick M, Assassi S, Satpathy AT, Granja J, et al. GWAS for systemic sclerosis identifies multiple risk loci and highlights fibrotic and vasculopathy pathways. Nat Commun. 2019;10:4955. doi: 10.1038/S41467-019-12760-Y.
[8] Acosta-Herrera M, Kerick M, Lopéz-Isac E, Assassi S, Beretta L, Simeón-Aznar CP, et al. Comprehensive analysis of the major histocompatibility complex in systemic sclerosis identifies differential HLA associations by clinical and serological subtypes. Ann Rheum Dis. 2021;80:1040–7. doi: 10.1136/ANNRHEUMDIS-2021-219884.
[9] Arnett FC, Gourh P, Shete S, Ahn CW, Honey RE, Agarwal SK, et al. Major histocompatibility complex (MHC) class II alleles, haplotypes and epitopes which confer susceptibility or protection in systemic sclerosis: analyses in 1300 Caucasian, African-American and Hispanic cases and 1000 controls. Ann Rheum Dis. 2010;69:822–7. doi: 10.1136/ard.2009.111906.
[10] Ortíz-Fernández L, Martín J, Alarcón-Riquelme ME. A summary on the genetics of systemic lupus erythematosus, rheumatoid arthritis, systemic sclerosis, and Sjögren's syndrome. Clin Rev Allergy Immunol. 2023;64:392–411. doi: 10.1007/S12016-022-08951-Z.
[11] Gourh P, Safran SA, Alexander T, Boyden SE, Morgan ND, Shah AA, et al. HLA and autoantibodies define scleroderma subtypes and risk in African and European Americans and suggest a role for molecular mimicry. Proc Natl Acad Sci U S A. 2020;117:552–62. doi: 10.1073/PNAS.1906593116.
[12] Beretta L, Rueda B, Marchini M, Santaniello A, Simeón CP, Fonollosa V, et al. Analysis of Class II human leucocyte antigens in Italian and Spanish systemic sclerosis. Rheumatology (Oxford). 2012;51:52–9. doi: 10.1093/RHEUMATOLOGY/KER335.
[13] Mayes MD, Bossini-Castillo L, Gorlova O, Martin JE, Zhou X, Chen WV, et al. Immunochip analysis identifies multiple susceptibility loci for systemic sclerosis. Am J Hum Genet. 2014;94:47–61. doi: 10.1016/j.ajhg.2013.12.002.
[14] He D, Wang J, Yi L, Guo X, Guo S, Guo G, et al. Association of the HLA-DRB1 with scleroderma in Chinese population. PLoS One. 2014;9. doi: 10.1371/JOURNAL.PONE.0106939.
[15] Odani T, Yasuda S, Ota Y, Fujieda Y, Kon Y, Horita T, et al. Up-regulated expression of HLA-DRB5 transcripts and high frequency of the HLA-DRB5*01:05 allele in scleroderma patients with interstitial lung disease. Rheumatology (Oxford). 2012;51:1765–74. doi: 10.1093/RHEUMATOLOGY/KES149.
[16] Dieudé P, Guedj M, Truchetet ME, Wipff J, Revillod L, Riemekasten G, et al. Association of the CD226 Ser307 variant with systemic sclerosis: Evidence of a contribution of costimulation pathways in systemic sclerosis pathogenesis. Arthritis Rheum. 2010;63:1097–105. doi: 10.1002/ART.30204.
[17] Dieudé P, Guedj M, Wipff J, Ruiz B, Riemekasten G, Airo P, et al. NLRP1 influences the systemic sclerosis phenotype: a new clue for the contribution of innate immunity in systemic sclerosis-related fibrosing alveolitis pathogenesis. Ann Rheum Dis. 2011;70:668–74. doi: 10.1136/ARD.2010.131243.
[18] Zhou X, Yi L, Guo XJ, Chen E, Zou HJ, Jin L, et al. Association of HLA-DQB1*0501 with scleroderma and its clinical features in Chinese population. Int J Immunopathol Pharmacol. 2013;26:747–51. doi: 10.1177/039463201302600318.
[19] Louthrenoo W, Kasitanon N, Wongthanee A, Okudaira Y, Takeuchi M, Nakajima F, et al. Association of HLA-DRB1*15:02:01, DQB1*05:01:24 and DPB1*13:01:01 in Thai patients with systemic sclerosis. HLA. 2022;100:563–81. doi: 10.1111/TAN.14793.
[20] Simeón CP, Fonollosa V, Tolosa C, Palou E, Selva A, Solans R, et al. Association of HLA class II genes with systemic sclerosis in Spanish patients. J Rheumatol. 2009;36:2733–6. doi: 10.3899/JRHEUM.090377.
[21] Manetti M, Ibba-Manneschi L, Fatini C, Guiducci S, Cuomo G, Bonino C, et al. Association of a functional polymorphism in the matrix metalloproteinase-12 promoter region with systemic sclerosis in an Italian population. J Rheumatol. 2010;37:1852–7. doi: 10.3899/JRHEUM.100237.
[22] Kawaguchi Y, Tochimoto A, Ichikawa N, Harigai M, Hara M, Kotake S, et al. Association of IL1A gene polymorphisms with susceptibility to and severity of systemic sclerosis in the Japanese population. Arthritis Rheum. 2003;48:186–92. doi: 10.1002/ART.10736.
[23] Hoshino K, Satoh T, Kawaguchi Y, Kuwana M. Association of hepatocyte growth factor promoter polymorphism with severity of interstitial lung disease in Japanese patients with systemic sclerosis. Arthritis Rheum. 2011;63:2465–72. doi: 10.1002/ART.30415.
[24] Sumita Y, Sugiura T, Kawaguchi Y, Baba S, Soejima M, Murakawa Y, et al. Genetic polymorphisms in the surfactant proteins in systemic sclerosis in Japanese: T/T genotype at 1580 C/T (Thr131Ile) in the SP-B gene reduces the risk of interstitial lung disease. Rheumatology (Oxford) 2008;47:289–91. doi: 10.1093/RHEUMATOLOGY/KEM355.
[25] David Carmona F, Carmen Cénit M, Diaz-Gallo LM, Broen JC, Simeón CP, Carreira PE, et al. New insight on the Xq28 association with systemic sclerosis. Ann Rheum Dis. 2013;72:2032–8. doi: 10.1136/ANNRHEUMDIS-2012-202742.
[26] LeRoy EC, Medsger TA. Criteria for the classification of early systemic sclerosis - PubMed. J Rheumatol 2001;28:1573–6.
[27] Van Den Hoogen F, Khanna D, Fransen J, Johnson SR, Baron M, Tyndall A, et al. 2013 classification criteria for systemic sclerosis: an American college of rheumatology/European league against rheumatism collaborative initiative. Ann Rheum Dis. 2013;72:1747–55. doi: 10.1136/ANNRHEUMDIS-2013-204424.
[28] Chang CC, Chow CC, Tellier LCAM, Vattikuti S, Purcell SM, Lee JJ. Second-generation PLINK: rising to the challenge of larger and richer datasets. Gigascience. 2015;4:7. doi: 10.1186/S13742-015-0047-8.
[29] Yang J, Lee SH, Goddard ME, Visscher PM. GCTA: a tool for genome-wide complex trait analysis. Am J Hum Genet. 2011;88:76–82. doi: 10.1016/J.AJHG.2010.11.011.
[30] Han B, Eskin E. Random-effects model aimed at discovering associations in meta-analysis of genome-wide association studies. Am J Hum Genet 2011;88:586–98. doi: 10.1016/J.AJHG.2011.04.014.
[31] Li MX, Yeung JMY, Cherny SS, Sham Pak C. Evaluating the effective numbers of independent tests and significant p-value thresholds in commercial genotyping arrays and public imputation reference datasets. Hum Genet. 2012;131:747–56. doi: 10.1007/S00439-011-1118-2.
[32] Wang J, Guo X, Yi L, Guo G, Tu W, Wu W, et al. Association of HLA-DPB1 with scleroderma and its clinical features in Chinese population. PLoS One. 2014;9:e87363. doi: 10.1371/JOURNAL.PONE.0087363.
[33] Raschi E, Privitera D, Bodio C, Lonati PA, Borghi MO, Ingegnoli F, et al. Scleroderma-specific autoantibodies embedded in immune complexes mediate endothelial damage: an early event in the pathogenesis of systemic sclerosis. Arthritis Res Ther. 2020;22:265. doi: 10.1186/S13075-020-02360-3.
[34] Raschi E, Chighizola CB, Cesana L, Privitera D, Ingegnoli F, Mastaglio C, et al. Immune complexes containing scleroderma-specific autoantibodies induce a profibrotic and proinflammatory phenotype in skin fibroblasts. Arthritis Res Ther. 2018;20:187. doi: 10.1186/S13075-018-1689-6.
[35] Wortel CM, Liem SIE, Van Leeuwen NM, Boonstra M, Fehres CM, Stöger L, et al. Anti-topoisomerase, but not anti-centromere B cell responses in systemic sclerosis display active, Ig-secreting cells associated with lung fibrosis. RMD open. 2023;9:e003148. doi: 10.1136/RMDOPEN-2023-003148.
[36] Dendrou CA, Petersen J, Rossjohn J, Fugger L. HLA variation and disease. Nat Rev Immunol. 2018;18:325–39 SUBJMETA. doi: 10.1038/NRI.2017.143.
[37] Skaug B, Khanna D, Swindell WR, Hinchcliff ME, Frech TM, Steen VD, et al. Global skin gene expression analysis of early diffuse cutaneous systemic

sclerosis shows a prominent innate and adaptive inflammatory profile. Ann Rheum Dis. 2020;79:379–86. doi: 10.1136/annrheumdis-2019-215894.
[38] Benyamine A, Magalon J, Sabatier F, Lyonnet L, Robert S, Dumoulin C, et al. Natural killer cells exhibit a peculiar phenotypic profile in systemic sclerosis and are potent inducers of endothelial microparticles release. Front Immunol 2018;9:1665. doi: 10.3389/FIMMU.2018.01665/BIBTEX.
[39] Shimagami H, Nishimura K, Matsushita H, Metsugi S, Kato Y, Kawasaki T, et al. Single-cell analysis reveals immune cell abnormalities underlying the clinical heterogeneity of patients with systemic sclerosis. Nat Commun. 2025;16:4949. doi: 10.1038/S41467-025-60034-7.
[40] Padilla CM, Valenzi E, Tabib T, Nazari B, Sembrat J, Rojas M, et al. Increased CD8+ tissue resident memory T cells, regulatory T cells and activated natural killer cells in systemic sclerosis lungs. Rheumatology (Oxford). 2024;63:837–45. doi: 10.1093/RHEUMATOLOGY/KEAD273.
[41] Bernardinello N, Zen M, Castelli G, Cocconcelli E, Balestro E, Borie R, et al. Navigating interstitial lung disease associated with rheumatoid arthritis (RA-ILD): from genetics to clinical landscape. Front Med. 2025;12:1542400. doi: 10.3389/FMED.2025.1542400/BIBTEX.
[42] Shappley CL, Paik JJ, Saketkoo LA. Myositis-related interstitial lung diseases: diagnostic features, treatment, and complications. Curr Treat Options Rheumatol 2019;5:56–83 2019 51. doi: 10.1007/S40674-018-0110-6.
[43] Kerick M, Acosta-Herrera M, Simeón-Aznar CP, Callejas JL, Assassi S, et al. International SSc Group. Complement component C4 structural variation and quantitative traits contribute to sex-biased vulnerability in systemic sclerosis. NPJ genomic Med. 2022;7:57. doi: 10.1038/S41525-022-00327-8.
[44] Lundtoft C, Sjöwall C, Rantapää-Dahlqvist S, Bengtsson AA, Jönsen A, Pucholt P, et al. Strong association of combined genetic deficiencies in the classical complement pathway with risk of systemic lupus erythematosus and primary Sjögren's syndrome. Arthritis Rheumatol. 2022;74:1842–50. doi: 10.1002/ART.42270/ABSTRACT.
[45] Kamitaki N, Sekar A, Handsaker RE, de Rivera H, Tooley K, Morris DL, et al. Complement genes contribute sex-biased vulnerability in diverse disorders. Nature. 2020;582:577–81. doi: 10.1038/S41586-020-2277-X.
[46] Martínez-López J, Rangel-Peláez C, Rodriguez-Martin I, Guillen-Del-Castillo A, Simeón-Aznar CP, Callejas JL, et al. Distinct effects of complement C4A and C4B copy number in Systemic Sclerosis serological and clinical subtypes. Arthritis Rheumatol. 2026;78:904–13. doi: 10.1002/ART.43433.
[47] Reis ES, Mastellos DC, Hajishengallis G, Lambris JD. New insights into the immune functions of complement. Nat Rev Immunol. 2019;19:503–16 SUBJMETA. doi: 10.1038/S41577-019-0168-X.
[48] Carapito R, Bahram S. Genetics, genomics, and evolutionary biology of NKG2D ligands. Immunol Rev. 2015;267:88–116. doi: 10.1111/IMR.12328.
[49] Morris DL, Taylor KE, Fernando MMA, Nititham J, Alarcón-Riquelme ME, Barcellos LF, et al. Unraveling multiple MHC gene associations with systemic lupus erythematosus: Model choice indicates a role for HLA alleles and non-HLA genes in europeans. Am J Hum Genet. 2012;91:778–93. doi: 10.1016/j.ajhg.2012.08.026.
[50] López-Arbesu R, Ballina-García FJ, Alperi-López M, López-Soto A, Rodríguez-Rodero S, Martínez-Borra J, et al. MHC class I chain-related gene B (MICB) is associated with rheumatoid arthritis susceptibility. Rheumatology (Oxford). 2007;46:426–30. doi: 10.1093/RHEUMATOLOGY/KEL331.
[51] Wang CM, Tan KP, Wu YJJ, Zheng JW, Wu J, Chen JY. Functional MICA variants are differentially associated with immune-mediated inflammatory diseases. Int J Mol Sci. 2024;25:3036. doi: 10.3390/IJMS25053036.
[52] Tangtanatakul P, Thumarat C, Satproedprai N, Kunhapan P, Chaiyasung T, Klinchanhom S, et al. Meta-analysis of genome-wide association study identifies FBN2 as a novel locus associated with systemic lupus erythematosus in Thai population. Arthritis Res Ther. 2020;22:185. doi: 10.1186/S13075-020-02276-Y.
[53] Bossini-Castillo L, De Kovel C, Kallberg H, van't Slot R, Italiaander A, Coenen M, et al. A genome-wide association study of rheumatoid arthritis without antibodies against citrullinated peptides. Ann Rheum Dis. 2015;74:e15. doi: 10.1136/annrheumdis-2013-204591.
[54] Ketkar S, Dai H, Burrage L, Murdock D, Dawson B, Acosta-Herrera M, et al. Integrative exome sequencing and machine learning identify MICB and interferon pathway genes as contributors to SSc risk. Ann Rheum Dis. 2025;84:1363–74. doi: 10.1016/j.ard.2025.05.009.
[55] Bossini-Castillo L, Villanueva-Martin G, Kerick M, Acosta-Herrera M, López-Isac E, Simeón CP, et al. Genomic Risk Score impact on susceptibility to systemic sclerosis. Ann Rheum Dis. 2021;80:118–27. doi: 10.1136/annrheumdis-2020-218558.
[56] Volkmann ER. Understanding late-onset interstitial lung disease in systemic sclerosis: implications for clinical practice and trial design. Arthritis Rheumatol. 2024;77:380–2. doi: 10.1002/ART.43053.

Ann Rheum Dis 85 (2026) 1811–1824

Contents lists available at ScienceDirect

Annals of the Rheumatic Diseases

journal homepage: https://www.sciencedirect.com/journal/annals-of-the-rheumatic-diseases

Systemic sclerosis

Engaging the PD-1 pathway in systemic sclerosis attenuates inflammation-driven fibrosis

Maithri Aspari[1], Voon Ong[2], Klaus Søndergaard[3,4], Esben Næser[3,4], Malene Hvid[1,4], Kim Ravnskjaer[5], Angela Y.Y. Tam[2], Shiwen Xu[2], Xinyue Bian[2], Henry Lopez[2,6], Christopher P. Denton[2], David Abraham[2], Bent Deleuran[1,3], Stinne R. Greisen[1,3,*]

[1] *Department of Biomedicine, Aarhus University, Aarhus, Denmark*
[2] *Department of Inflammation and Rare Diseases, UCL Royal Free Campus, London, UK*
[3] *Department of Rheumatology, Aarhus University, Aarhus, Denmark*
[4] *Department of Clinical Medicine, Aarhus University, Aarhus, Denmark*
[5] *Department of Biochemistry and Molecular Biology, University of Southern Denmark, Odense, Denmark*
[6] *MuriGenics, Vallejo, San Francisco, CA, USA*

ARTICLE INFO

Article history:
Received 8 November 2024
Received in revised form 9 January 2026
Accepted 10 January 2026

ABSTRACT

Objectives: The study elucidates the impact of the programmed cell death protein 1 (PD-1) pathway on immune activation and fibrosis in diffuse cutaneous systemic sclerosis (dcSSc).

Methods: We obtained blood and skin biopsies from patients with dcSSc and healthy controls (HCs). Soluble PD-1 was measured in serum. Human recombinant PD-1 protein (PD-1:Fc) and anti-PD-1 antibodies were used to stimulate peripheral blood mononuclear cells (PBMCs), HC, and systemic sclerosis (SSc) dermal fibroblast cultures, and cocultures. PD-1-positive (PD-1^{pos}) and PD-1-negative (PD-1^{neg}) populations of dcSSc PBMCs were characterised. We used a murine bleomycin model of pulmonary injury to study the effect of PD-1:Fc on pulmonary fibrosis *in vivo*.

Results: Soluble and cellular PD-1 were elevated in dcSSc compared to HC. Naïve fibroblasts differed between HC and dcSSc, but did not respond to PD-1:Fc treatment. Transforming growth factor β (TGF-β)-stimulated fibroblasts from dcSSc displayed a myofibroblast profile with a differential clustering compared to HC fibroblasts. PD-1:Fc downregulated the secretion of extracellular matrix (ECM) proteins, surface markers of fibroblast activation, and the production of inflammatory cytokines in TGF-β-stimulated *in vitro* cultures. PD-1^{pos} SSc T cells had a different and more regulatory transcriptional profile than the PD-1^{neg} T cell population. *In vivo* studies demonstrated that treatment with PD-1:Fc inhibited the development of lung fibrosis and the production of profibrotic cytokines.

Conclusions: Administrating PD-1:Fc attenuated inflammation and ECM protein production in dcSSc *in vitro* models and decreased systemic inflammation and pulmonary fibrosis in the bleomycin-induced fibrosis model in mice. Our data indicate that modulating the PD-1/PD-Ligand 1 axis represents a novel therapeutic avenue in dcSSc.

*Correspondence to Dr. Stinne R Greisen, Department of Biomedicine, Aarhus University, Aarhus, Denmark.
E-mail address: srg@biomed.dk (S.R. Greisen).

Handling editor Josef S. Smolen.

Bent Deleuran and Stinne R Greisen shared last authorship.

https://doi.org/10.1016/j.ard.2026.01.008

0003-4967/© 2026 The Author(s). Published by Elsevier B.V. on behalf of European Alliance of Associations for Rheumatology (EULAR). This is an open access article under the CC BY-NC-ND license (http://creativecommons.org/licenses/by-nc-nd/4.0/)

WHAT IS ALREADY KNOWN ON THIS TOPIC

- There is an imbalance between checkpoint inhibitory and stimulatory receptors in systemic sclerosis.
- The contribution of checkpoint receptors, specifically the programmed cell death protein 1 (PD-1) pathway, to the pathogenesis of systemic sclerosis remains unexplored.
- The PD-1 pathway is associated with the development and progression of lung fibrosis in mouse models.

WHAT THIS STUDY ADDS

- This research provides novel insights into the functionality of PD-1 in systemic sclerosis and critical crosstalk between immune cells and fibroblasts.
- It uncovers the presence of soluble PD-1 in systemic sclerosis and shows the effect of adding PD-1:Fc to reduce fibrosis *in vitro* and in mouse models.
- It provides an increased mechanistic understanding of the cellular sources and targets (fibroblast subpopulations) and temporal dynamics of the PD-1 pathway during the initiation and progression of fibrosis.
- It highlights the role of the PD-1/PD-Ligand 1 axis in influencing inflammation and fibrosis in systemic sclerosis.
- An *in vivo* model validation demonstrates the potential therapeutic impact of targeting PD-1.

HOW THIS STUDY MIGHT AFFECT RESEARCH, PRACTICE OR POLICY

- This study directs research focus onto the PD-1 pathway and its contribution to immune regulation and fibrosis progression in systemic sclerosis.
- This study lays the foundation for pioneering treatment strategies targeting the concurrent challenges of inflammation and fibrosis in systemic sclerosis.
- It emphasises the significance of the PD-1 pathway in systemic sclerosis and provides a strong basis for suggesting this pathway as a future treatment target to limit the development of fibrosis.
- This study promotes further exploration of the immune checkpoint microenvironment in fibrosis in systemic sclerosis.

INTRODUCTION

Systemic sclerosis (SSc) is an autoimmune connective tissue disorder that presents as fibrosis of the skin and internal organs [1]. The disease is caused by a combination of genetic, epigenetic, and environmental factors that result in chronic immune activation [2,3]. Continued exposure to autoantigens is suggested to be the prime factor for continued immune stimulation, leading to SSc [4]. SSc is a heterogeneous disease often described in 2 major subsets, diffuse cutaneous SSc (dcSSc) and limited cutaneous SSc, defined by the extent of skin involvement [5]. A key challenge lies in understanding the mechanisms that drive disease into these different subsets, as well as changes that may be critical to disease pathogenesis. Costimulatory and coinhibitory receptors play a crucial role in maintaining immune homeostasis, and a disruption of their functions or response can result in immune imbalance and activation. Programmed cell death protein 1 (PD-1) is 1 such coinhibitory receptor expressed by activated T and B cells. The PD-1 pathway is the key immunosuppressive pathway maintaining peripheral immune tolerance by inhibiting T cell activation, proliferation, and cytokine secretion and inducing T cell apoptosis. These functions collectively reduce the T cell immune effector function of CD4+ T cells and CD8+ T cells [6,7]. The PD-1 ligand(PD-L1), is mainly expressed by antigen-presenting cells, but can also be found on fibroblasts [8]. The PD-1/PD-L1 axis plays an essential role in modulating T cell immune responses. Both PD-1 and its ligands are present in soluble (s) forms. Soluble PD-1 (sPD-1) can be measured in plasma and is increased in inflammatory conditions [9]. The biological significance of the soluble forms is still unknown, and conflicting data have suggested they exert both antagonistic and agonistic effects on the cellular signalling pathway [10,11].

This multifaceted role of PD-1 in dcSSc has been a subject of scientific interest [12,13], and the PD-1/PD-L1 axis is suggested to be involved in promoting fibrosis [14]. Reverse signalling downstream of PD-L1 has also been recognised and believed to be associated with the development of fibrosis [15]. PD-L1 signalling is proposed to directly promote nascent fibroblasts to differentiate into the profibrotic myofibroblast by promoting the transcription of α-smooth muscle actin (αSMA) independent of transforming growth factor -β (TGF-β1) [16]. It has been further demonstrated in explants from patients with idiopathic pulmonary fibrosis that deletion of PD-L1 from fibroblasts results in reduced invasiveness of these cells and amelioration of fibrosis [17]. The use of antagonistic antibodies towards PD-L1 has also been suggested to decrease lung fibrosis in the bleomycin animal model [18], whereas blocking this pathway with anti-PD-1 increases the burden of interstitial lung disease [19]. The functional role of sPD-1 in the progression of fibrosis and inflammation remains poorly understood.

In the present study, we investigate the role of the PD-1 axis in dcSSc, focusing on both immune activation and the development of fibrosis. By integrating analyses of patient-derived samples, mechanistic *in vitro* systems and an *in vivo* model of fibrosis, we demonstrate that modulation of PD-1 signalling can attenuate inflammatory responses and extracellular matrix (ECM) production, supporting the PD-1/PD-L1 axis as a potential therapeutic strategy in dcSSc.

METHODS

Please refer to the Materials and Methods section in the supplementary file.

RESULTS

Increased levels of soluble and cellular PD-1 in dcSSc

We measured sPD-1 levels in serum from patients with dcSSc and from healthy control (HC). We found that the patients with dcSSc had significantly higher levels of sPD-1 in serum compared to the HC (Fig 1A, $P < .0001$). We also investigated the association between sPD-1 levels and disease activity scores. Here, we found that sPD-1 levels correlated with forced vital capacity (FVC) (spearman r = 0.37, $P = .03$), modified Rodnan skin score (spearman r = 0.37, $P = .04$), erythrocyte sedimentation rate (ESR) (spearman r = 0.35, $P = .04$) but not with C-reactive protein (CRP) (Fig 1B). Having observed increased levels of sPD-1 in patients with dcSSc, we next investigated the cellular expression of PD-1 in unstimulated and anti-CD3/CD28-stimulated dcSSc peripheral blood mononuclear cell (PBMC) cultures and compared these to HC PBMCs. In patients with dcSSc, 43% of unstimulated CD4+ T cells expressed PD-1,

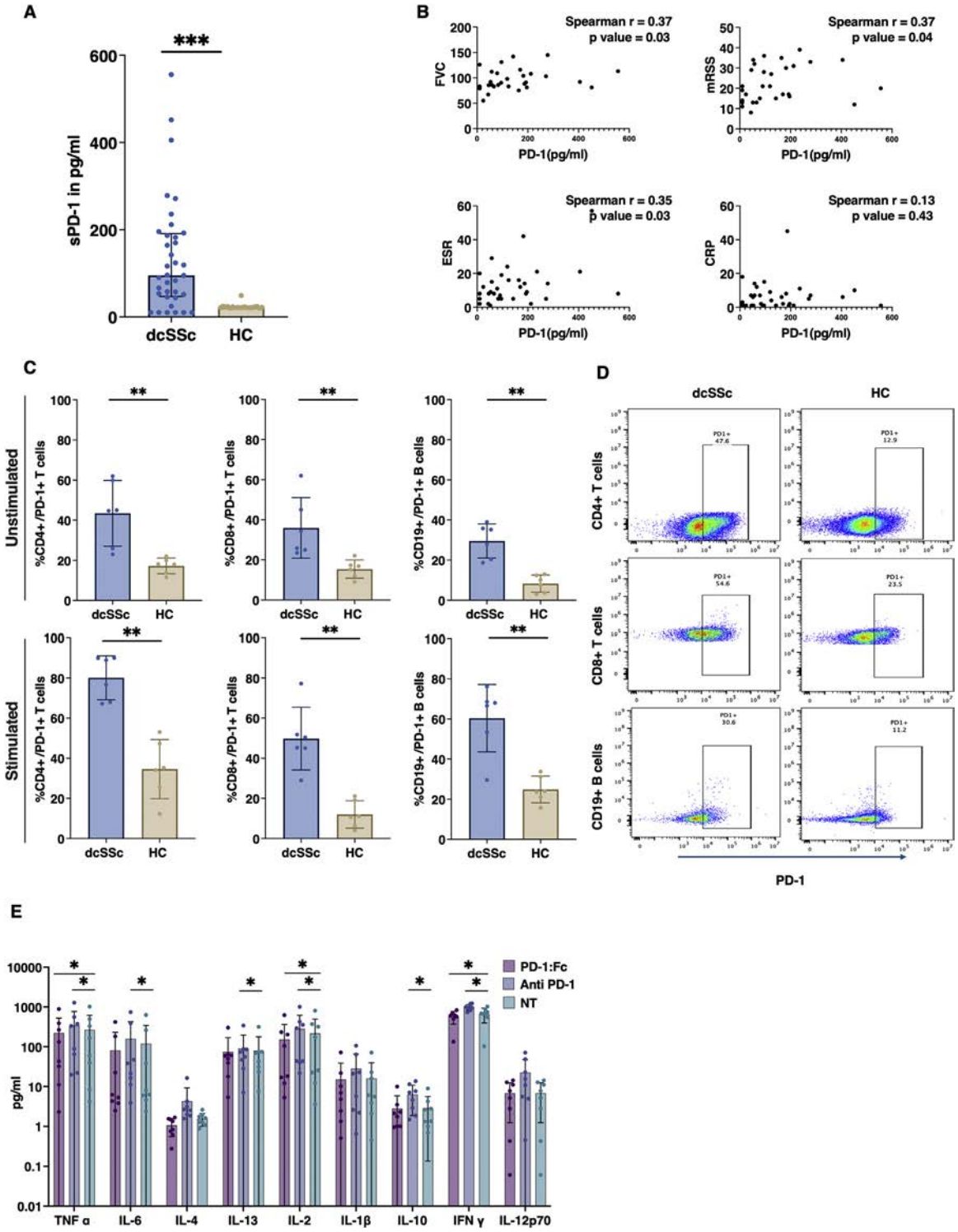

Figure 1. Soluble and cellular expression of PD-1 in systemic sclerosis (dcSSc). (A) Soluble PD-1 (sPD-1) levels measured by enzyme-linked immunoabsorbant assay (ELISA) were significantly elevated in serum from patients with dcSSc in comparison to serum from healthy controls (HCs) (represented as a median with IQR) (n = 36, 20). (B) Assessed by a Spearman's ranked correlation, the levels of sPD-1 in dcSSc serum correlated with forced vital capacity (FVC), modified Rodnan skin score (mRSS), and erythrocyte sedimentation rate (ESR) but not with C-reactive protein (CRP). (C) Surface expression of PD-1 on peripheral blood mononuclear cells (PBMCs) from both dcSSc (n = 6) and HC (n = 5). Top representing unstimulated state and bottom representing cells stimulated with anti-CD3/CD28. The percentage of PD-1 expressing CD4+, CD8+ T cells, and B cells was increased in patients with dcSSc compared to HCs, both in stimulated and unstimulated states. Data represented as mean with SD. (D) Flow cytometric data illustrating the percentages of PD-1 expressing CD4+ T cells, CD8+ T cells, and CD19+ B cells in unstimulated dcSSc and HC PBMCs. (E) Anti-CD3/CD28–stimulated dcSSc PBMC monocultures (n = 8) were treated with PD-1: Fc and pembrolizumab (anti-PD-1 antibody) and compared to non-treated (NT) cultures. PD-1: Fc reduced TNF-α, IL-2, and IFN-γ levels, whereas the addition of pembrolizumab increased the levels of TNF-α, IL-6, IL-13, IL-2, IL-10, and IFN-γ. Data are represented as mean with SD. dcSSc, diffuse cutaneous systemic sclerosis; IFN-γ, interferon gamma; IL, interleukin; ns, nonsignificant; PD-1, programmed cell death protein 1; TNF-α, tumour necrosis factor alpha. Significance levels: $^{*}P < .05$, $^{**}P < .01$, $^{***}P = .001$.

whereas in HCs, only 16% of unstimulated CD4+ T cells expressed PD-1. Evaluating CD8+ T cells and CD19+ B cells, we observed a similar higher PD-1 expression in dcSSc PBMCs compared to HC PBMCs (Fig 1C,top,D). In the stimulated state, we observed a significant increase in PD-1 expression on CD4+ T cells from both dcSSc and HC. PD-1 expression in dcSSc increased from a mean of 43% in unstimulated to a mean of 80% in stimulated CD4+ PBMCs ($P = .0019$). The increase in PD-1 expression on B cells was comparable ($P = .001$), whereas the increased PD-1 expression on CD8+ T cells did not increase significantly compared to unstimulated states ($P = .2775$) (Fig 1C, bottom).

Addition of PD-1: Fc reduces cytokine production in dcSSc PBMC cultures

Based on our findings of increased levels of PD-1 in dcSSc, we employed a recombinant human PD-1:Fc to mimic the function of sPD-1 using *in vitro* cell cultures. As a control, we utilised the Food and Drug Administration (FDA)-approved anti-PD-1 blocking antibody, pembrolizumab. In cultures of anti-CD-3/CD28 activated PBMCs from dcSSc, the addition of PD-1:Fc led to a decrease in the levels of tumour necrosis factor alpha (TNF-α) (220 pg/mL vs 265 pg/mL, $P = .04$), interleukin (IL)-2 (152 pg/mL vs 217 pg/mL, $P = .04$), and interferon gamma (IFN-γ) (571 pg/mL vs 663 pg/mL, $P = .01$) compared with nontreated (NT) samples. Conversely, pembrolizumab increased the production of TNF-α (by approximately 1.2-fold, $P = .04$), IL-6 (by approximately 1.3-fold, $P = .04$), IL-13 (by approximately 1.1-fold, $P = .01$), IL-2 (by approximately 1.3-fold, $P = .04$), IL-10 (by approximately 2.2-fold, $P = .008$), and IFN-γ (by approximately 1.75-fold, $P = .01$) compared to NT samples (Fig 1E).

Collectively, these results indicate that binding the soluble PD-1:Fc reduces immune activation, as indicated by T cell-related cytokine production. Conversely, blocking the PD-1 with pembrolizumab increases immune activation as assessed by increased cytokine production.

The dcSSc fibroblast transcriptome differs from HC fibroblasts

Fibroblasts play an essential role in disease progression and fibrosis in dcSSc. We therefore continued to evaluate the transcriptomic profile in dcSSc fibroblasts and HC fibroblasts. Cultured dcSSc fibroblasts were significantly different compared to cultured HC fibroblasts, with 824 genes differentially expressed. Among these, 405 genes were upregulated in dcSSc fibroblasts, with 4 of the highly upregulated genes being associated with collagen (*COL24A1, COL22A1, COL4A2, COL4A1*; all padj <.05) (Fig 2A). Enrichment analysis supported these findings with 8 gene ontology (GO) terms associated with ECM structure and organisation (Fig 2B and Supplementary Fig S1A). We next treated the fibroblasts with PD-1:Fc or immunoglobolin G (IgG) control for 24 hours. The treatment induced changes in the transcriptomic profile and independent of treatment; the dcSSc fibroblasts continued to cluster largely separately from HC fibroblasts (Fig 2C and Supplementary Fig S1B). PD-1:Fc did not seem to affect dcSSc and HC fibroblasts differently evaluated by the enrichment analysis (Supplementary Fig S1C). However, fewer genes were differentially expressed between dcSSc fibroblasts treated with PD-1:Fc and NT HC fibroblasts compared to NT dcSSc and NT HC fibroblasts (Supplementary Fig S1D). We further observed fewer genes related to collagen, with only *COL4A2* being upregulated ($P_{adj} = .02$). This was also confirmed in the enrichment analysis, with only 4 GO terms associated with ECM and collagen (Fig 2D). We continued to analyse the fibroblasts by flow cytometry for their surface and intracellular expression of fibroblast activation markers. To induce a more activated state, we cultured fibroblasts with TGF-β. When stimulated with TGF-β, dcSSc fibroblasts displayed a 2.3-fold increased expression of podoplanin, a 1.5-fold increased expression of fibroblast activation protein (FAP), a 1.3-fold increased expression of PD-L1 and a 7-fold increased expression of intercellular adhesion molecule-1 (CAM-1) compared to HC fibroblasts. This was further paralleled by a 2-fold higher intracellular expression of αSMA, a hallmark of myofibroblasts (Supplementary Fig S1E). For the nonstimulated fibroblasts, no significant difference between dcSSc and HC was observed, except for αSMA, which was significantly higher in dcSSc fibroblasts (Supplementary Fig S1F). A t-distributed stochatic neighbour embedding (t-SNE) analysis visualised clusters of myofibroblast populations in TGF-β-stimulated dcSSc and HC fibroblasts. Myofibroblast population from dcSSc and HC were PD-L1 positive, podoplanin positive, FAP positive, ICAM-1 positive, along with a positive coexpression of αSMA. Clusters of myofibroblasts were increased in patients with dcSSc and clustered differently compared to HC fibroblasts (Fig 2E). Among the αSMA+ myofibroblasts of patients with dcSSc, 65% expressed FAP, and 85% of these FAP+ fibroblasts expressed PD-L1. Fibroblasts did not express PD-1 (data not shown). To further establish the functions of the HC and dcSSc fibroblasts, we investigated the production of ECM proteins. Here, we observed that when stimulated with TGF-β, dermal fibroblasts from patients with dcSSc produced significantly higher levels of type 1 procollagen α 62 ng/mL vs 30 ng/mL) and fibronectin (39 ng/mL vs 22 ng/mL) compared to HC dermal fibroblasts. Significant differences between dcSSc fibroblasts and HC fibroblast cultures were also observed in unstimulated states (Fig 2F).

Addition of PD-1: Fc reduces ECM protein production in activated dcSSc dermal fibroblasts

Having shown that TGF-β-stimulated fibroblasts dcSSc expressed higher levels of PD-L1, and that treatment with PD-1: Fc reduced collagen transcription, we investigated the influence of PD-1: Fc on type 1 procollagen α and fibronectin secretion from the TGF-β-stimulated dcSSc fibroblasts. We observed that PD-1:Fc treatment resulted in a decreased production of both type 1 procollagen α (45 ng/mL vs 57 ng/mL, $P = .008$) and fibronectin (27 ng/mL vs 33 ng/mL, $P = .01$) compared to its isotype control in TGF-β1-stimulated dcSSc fibroblasts (Fig 3A). There was no difference in the fibronectin production between the PD-1:Fc-treated and NT samples. We continued to further investigate the surface expression of myofibroblast markers in TGF-β-stimulated dcSSc fibroblasts treated with PD-1: Fc or its isotype control. We observed that PD-1:Fc significantly decreased the expression of podoplanin, PD-L1 and ICAM-1 when compared to the isotype control. No difference was observed in the expression of αSMA or FAP (Fig 3B). This led us to further investigate the effect of PD-1:Fc on inducing profibrotic genes in dcSSc fibroblasts. Here, fibroblasts were primed for 4 hours with interferon α and subsequently treated with PD-1:Fc or the isotype control. Here, PD-1:Fc significantly decreased the induction of vascular cell adhesion molecule (*VCAM-1*), *PD-L1, IFN-β1,* and *IL-6* compared to the IgG1 isotype control, whereas both PD-1:Fc and the isotype control decreased the induction of *ICAM-1* (Fig 3C).

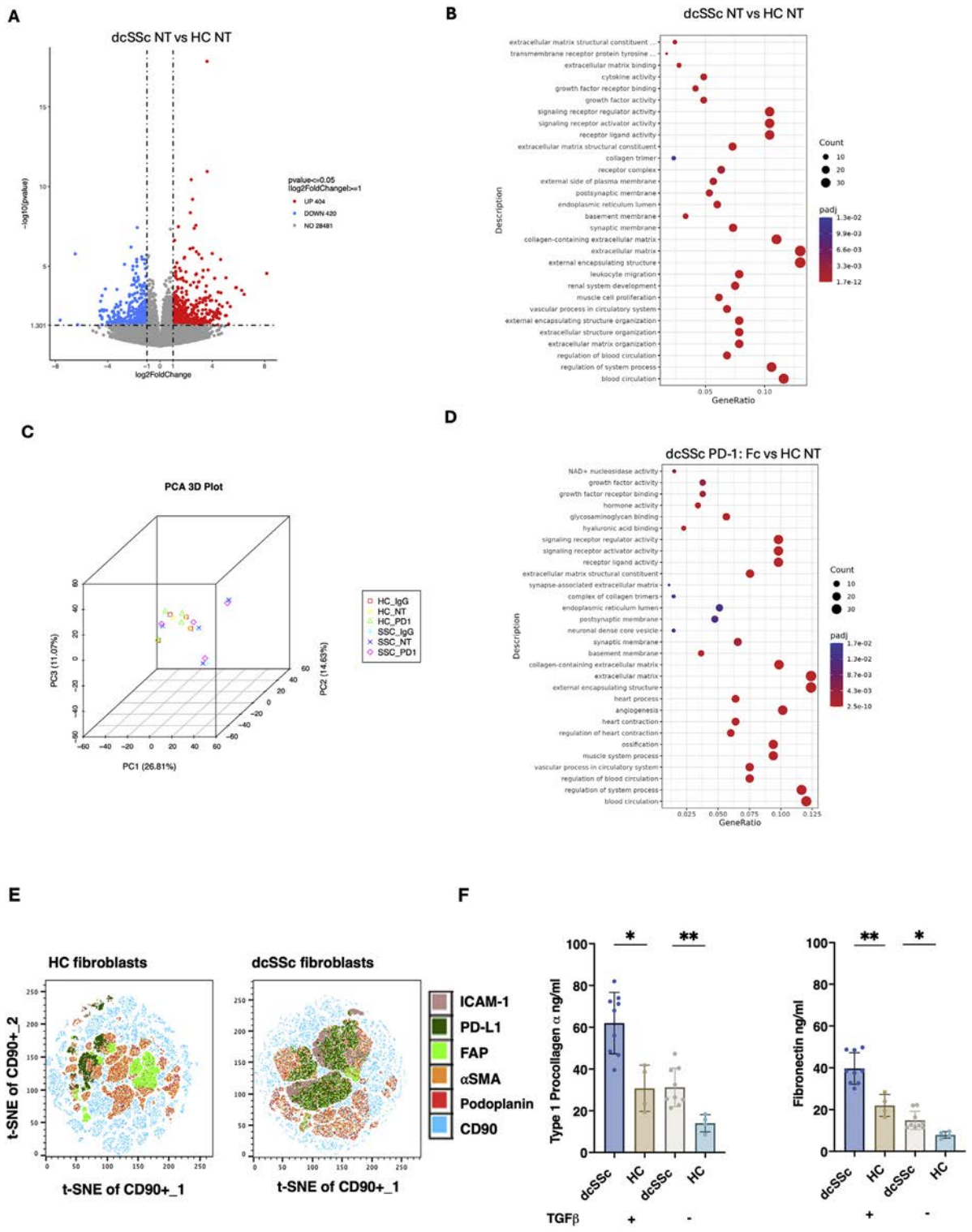

Figure 2. PD-1 mitigates extracellular matrix protein production in activated fibroblasts from patients with systemic sclerosis (dcSSc). (A) Volcano plot representing differentially expressed genes when comparing cultured dcSSc and HC fibroblasts. Blue represents downregulated genes and red represents upregulated genes. (B) Gene ontology (GO) enrichment analysis of upregulated genes between cultured dcSSc and HC fibroblasts. Several pathways associated with the extracellular matrix and collagen were found. (C) 3D PCA plot visualising the clustering of HC fibroblasts and dcSSc fibroblasts cultured for 24 hours with or without the addition of PD-1: Fc (PD-1). Clustering is unaffected by treatment, but fibroblasts cluster dependent on HC or dcSSc origin. (D) GO enrichment analysis of upregulated genes between cultured dcSSc PD-1: Fc-treated and NT HC fibroblasts. Few pathways associated with the extracellular matrix and collagen were found. (E) A t-distributed stochatic neighbour embedding (t-SNE) visualisation of fibroblasts. Left panel HC fibroblasts and right panel dcSSc fibroblasts showing increased clusters of myofibroblasts expressing α smooth muscle acti (αSMA). Both dcSSc and HC fibroblasts were stimulated with transforming growth factor β (TGF-β). (F) Dermal fibroblasts from patients with dcSSc or HC stimulated with TGF-β or left unstimulated for 48 hours. Dermal fibroblasts from dcSSc (n = 9) showed significantly higher production of type-1 procollagen α and fibronectin compared to HCs (n = 4) in unstimulated and TGF-β1 stimulated conditions, respectively. Data are represented as mean with SD. dcSSc, diffuse cutaneous systemic sclerosis; HC, healthy control; NT, nontreated; PCA, principal component analysis; PD-1, programmed cell death protein 1. (For interpretation of the references to colour in this figure legend, the reader is referred to the web version of this article.)

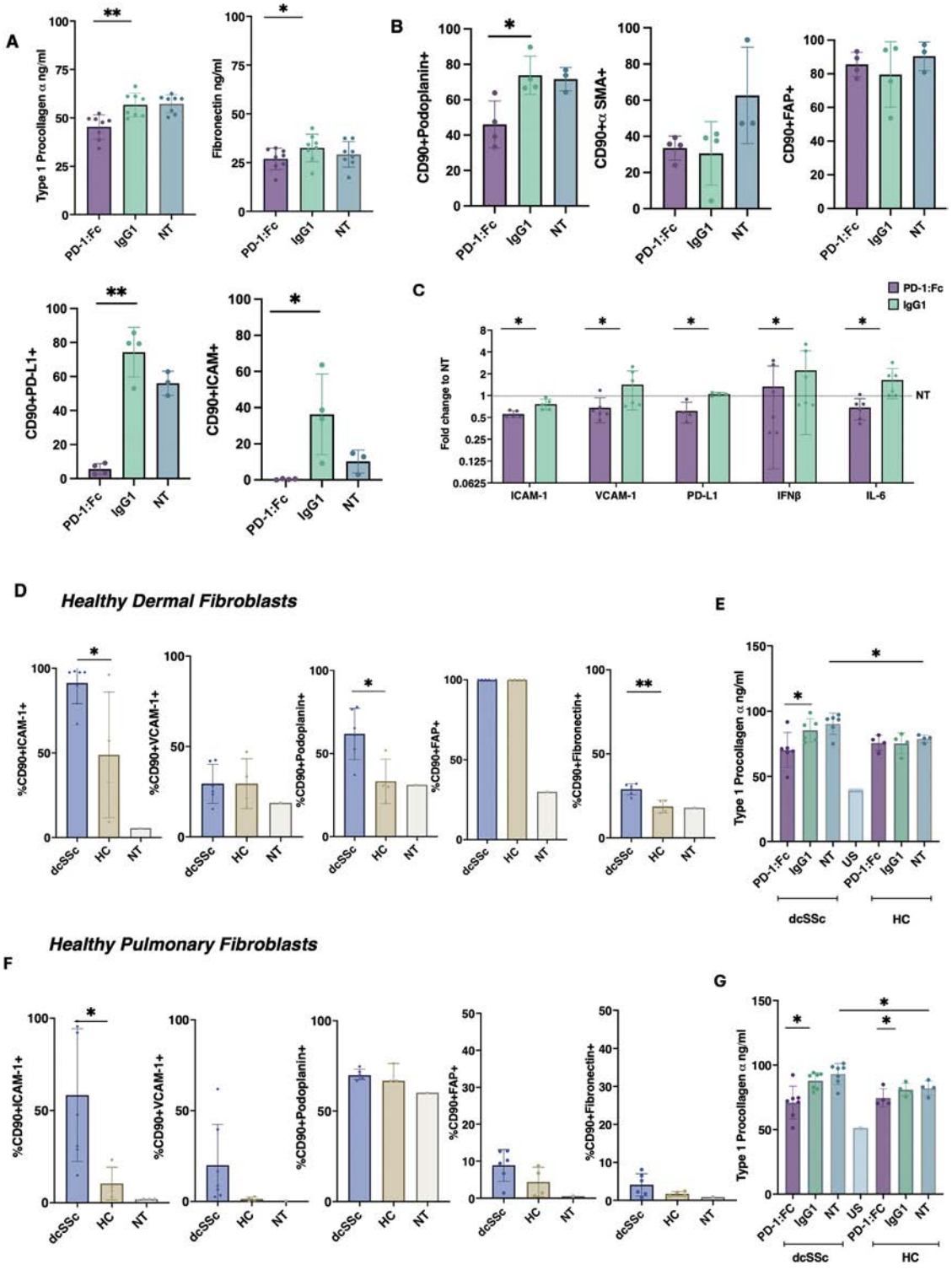

Figure 3. The addition of PD-1: Fc limits the immune activation of healthy fibroblast cocultures with dcSSc PBMCs. (A) DcSSc fibroblasts stimulated with tranforming growth factor β (TGF-β) and subsequently treated with PD-1:Fc for 48 hours produced significantly lower levels of type-1 procollagen α and fibronectin than when cultures were treated with the isotype control (n = 8). Data are represented as mean with SD. (B) dcSSc fibroblasts stimulated with TGF-β and subsequently left nontreated (NT) or treated with PD-1:Fc or isotype control (Immunoglobulin G subclass 1 [IgG1]) for 48 hours. Flow cytometric representation of the percentage expression of podoplanin, α smooth muscle actin (αSMA), fibroblast activation protein (FAP), PD-L1, and intercellular adhesion molecule-1 (ICAM-1) among the CD90+ fibroblasts. Podoplanin, PD-L1, and ICAM expression decreased when fibroblasts were stimulated with PD-1: Fc (n = 4). Data are represented as mean with SD. (C) dcSSc fibroblast monocultures primed with IFN-α for 4 hours and subsequently treated with PD-1: Fc or control for 6 hours. The mRNA levels of *vascular cell adhesion molecule-1 (VCAM-1), PD-L1*, and *IFN* were significantly reduced in dcSSc (n = 6) monocultures treated with PD-1:Fc compared to its isotype control (IgG1). Both PD-1:Fc and the isotype control reduced the mRNA levels of *ICAM-1*. Data are represented as mean with SD. (D) Healthy dermal fibroblasts cocultured with dcSSc PBMCs (n = 6) showed significantly higher expression of ICAM-1, podoplanin, and fibronectin compared to when cultured with HC PBMCs (n = 4). VCAM-1 and FAP expression were not significantly changed. Cells were not stimulated prior to culture. Data represented as mean with SD. (E) PD-1: Fc treatment compared to the isotype control (IgG1) significantly reduced type-1 procollagen α production in the fibroblasts cocultured with dcSSc PBMCs. This was not seen in fibroblasts cocultured with HC PBMC (n = 6). Cells were not subjected to any prestimulation. Data represented as mean with SD. (F) Healthy pulmonary fibroblast cocultured with dcSSc PBMCs (n = 7) showed significantly higher expression of ICAM-1 compared to cocultures

These findings suggest that PD-1:Fc has the potential to decrease the production and induction of ECM proteins as well as markers of myofibroblast activation in TGF-β−treated dcSSc fibroblasts.

The addition of PD-1:Fc limits the activation of healthy dermal fibroblasts by dcSSc PBMCs

Having observed an activated phenotype in immune cells from patients with dcSSc, we proceeded to investigate whether dcSSc PBMCs could drive healthy dermal fibroblasts and healthy pulmonary fibroblasts towards activation, and whether the PD-1 pathway influenced this potential activation. To elucidate this, we cocultured healthy dermal fibroblasts with either dcSSc or HC PBMCs in an unstimulated state. Dermal fibroblasts were seeded at the bottom of the wells, and PBMCs, along with either PD-1:Fc or IgG isotype control, were added to the transwell inserts. All fibroblasts were CD90+. The addition of dcSSc PBMCs, but not HC PBMCs, significantly increased the surface expression of ICAM-1 (97% vs 45%), podoplanin (63% vs 44%), and fibronectin (30% vs 19%) on the healthy dermal CD90+ fibroblasts, whereas no change in expression of FAP or VCAM-1 was observed (Fig 3D).

Having observed an activation of the healthy dermal fibroblasts as evaluated by surface markers, we proceeded to measure ECM protein levels from these cultures. The presence of PBMCs increased the production of type 1 procollagen α, and fibroblast cocultured with dcSSc PBMCs produced significantly higher amounts of type 1 procollagen α compared to those cocultured with HC PBMCs. Additionally, upon addition of PD-1:Fc, cocultures with dcSSc PBMCs, but not HC PBMCs, significantly reduced the type 1 procollagen α production by 1.2-fold compared to the isotype control (70 ng/mL vs 85 ng/mL) (Fig 3E). We observed a similar effect on healthy pulmonary fibroblasts, where dcSSc PBMCs induced significantly higher percentages of fibroblasts expressing ICAM-1 (58 % vs 10 %, $P = .01$) than HC PBMCs. In contrast, no significant changes were seen in the expression of VCAM-1, podoplanin, FAP, or fibronectin when compared to cocultures with HC PBMCs (Fig 3F). From the pulmonary fibroblasts, we also observed that PD-1:Fc significantly reduced the procollagen production compared with the isotype control. This was most pronounced when these were cocultured with dcSSc PBMC, but also present when using HC PBMC (Fig 3G).

PD-1 pathway influences cytokine and ECM production in dcSSc fibroblasts and PBMC cocultures

To explore the importance of immune cell-fibroblast interactions in PD-1 signalling, we progressed our study to investigate the role of PD-1 in dcSSc PBMC and dcSSc fibroblast crosstalk by coculturing autologous dcSSc fibroblasts stimulated with TGF-β and anti-CD3/CD28-stimulated PBMCs. We included both the PD-1:Fc and the anti-PD-1 antibody pembrolizumab, and compared these to NT cultures and the Immunoglobulin G subclass 1 (IgG1) isotype control. We observed no difference between NT and the isotype control (Supplementary Fig S2A,B). Treatment with PD-1:Fc significantly increased the levels of IL-10 (1.5-fold) compared with NT samples and reduced the levels of IL-12p70 (1.5-fold), IL-1β (1.4-fold), IL-2 (1.5-fold), and IL-4 (1.2-fold) compared with NT samples in these cocultures (Fig 4A). Pembrolizumab, on the other hand, significantly increased the production of proinflammatory cytokines such as IL-12p70 (1.5-fold), IL-13 (1.3-fold), IL-1β (1.6-fold), IL-2 (1.4-fold), IL-4 (1.8-fold), and TNF-α (1.8-fold) as compared to NT samples. Pembrolizumab did not affect the production of IL-10 (Fig 4A).

These results demonstrate the importance of the PD-1 pathway in regulating the inflammatory response in dcSSc PBMC-fibroblast cocultures and strongly support our observations from the monocultures. We also evaluated the production of ECM proteins in these cultures. PD-1:Fc significantly reduced both type-1 procollagen α (49.5 ng/mL vs 54.4 ng/mL) and fibronectin (9.0 ng/mL vs 11.9 ng/mL) levels in these cocultures when compared to NT samples (Fig 4B). On the other hand, pembrolizumab increased both type 1 procollagen α and fibronectin (1.2-fold) secretion in these cocultures compared to NT samples (Fig 4B). These findings highlight the central role of PD-1 in immune crosstalk, emphasising its ability to modulate both inflammation and fibrosis in dcSSc. To further evaluate the importance of the immune cross talk, we stained dcSSc skin for the presence of αSMA and PD-1. In the dcSSc skin, αSMA was clearly expressed around the blood vessels and on inflammatory cells. PD-1 expression was also found in and around the blood vessels, supporting infiltration of immune cells. In HC skin, we observed αSMA around the blood vessel, but no infiltrating immune cells were detected (Fig 4C).

PD-1-positive and PD-1-negative CD3 T cells from patients with dcSSc exert differential effects on fibroblast activation and exhibit unique transcriptional signatures

We proceeded to examine the importance of the PD-1 expression in dcSSc by coculturing healthy dermal fibroblasts with either anti-CD3/CD28−stimulated PD-1-positive (PD-1^{pos}) or PD-1-negative (PD-1^{neg}) sorted CD3+ T cells or their supernatants. Both PD-1^{pos} and PD-1^{neg} T cells and supernatants from patients with dcSSc activated the healthy dermal fibroblasts. PD-1^{pos} supernatants significantly upregulated the surface expression of FAP and PD-L1 and downregulated the expression of ICAM-1 on the dermal fibroblasts compared to cultures with PD-1^{neg} supernatants. A similar activation pattern was seen when dermal fibroblasts were cultured with cells from the PD-1^{pos} and PD-1^{neg} cell populations (Fig 5A,B). Next, we evaluated the production of ECM proteins in these cultures. Fibroblasts stimulated with PD-1^{pos} cells produced significantly less type 1 procollagen α than those stimulated with PD-1^{neg} cells. A similar pattern emerged when fibroblasts were stimulated with the supernatant from the PD-1^{pos} or PD-1^{neg} populations (Fig 5C). We observed no difference in cell viability between the cultures (Supplementary Fig S2C). We next analysed differentially expressed genes (DEGs) between nonstimulated PD-1^{pos} and PD-1^{neg} T cells. Nearly 1000 DEGs with an adjusted P value $\leq .05$ and log2 fold change ≤ -1 or ≥ 1 were identified, supporting

with HC PBMCs (n = 4). Cells were not subjected to any prestimulation. No significant changes in the expression of VCAM-1, FAP, podoplanin, or fibronectin were observed. Data represented as mean with SD. (G) Upon treatment with PD 1: Fc, cocultures with either dcSSc PBMCs or HC PBMCs significantly reduced type-1 procollagen α production compared to the isotype control or nontreated (NT) samples. The levels of type-1 procollagen α in cocultures remained higher than in fibroblast cultures without PBMCs (US) (n = 7). Cells were not subjected to any prestimulation. Data are presented as mean with SD. dcSSc, diffuse cutaneous systemic sclerosis; HC, healthy control; IFN, interferon; ns, nonsignificant; PBMC, peripheral blood mononuclear cell; PD-1, programmed cell death protein 1. Significance levels: $^{*}P < .05$, $^{**}P < .01$.

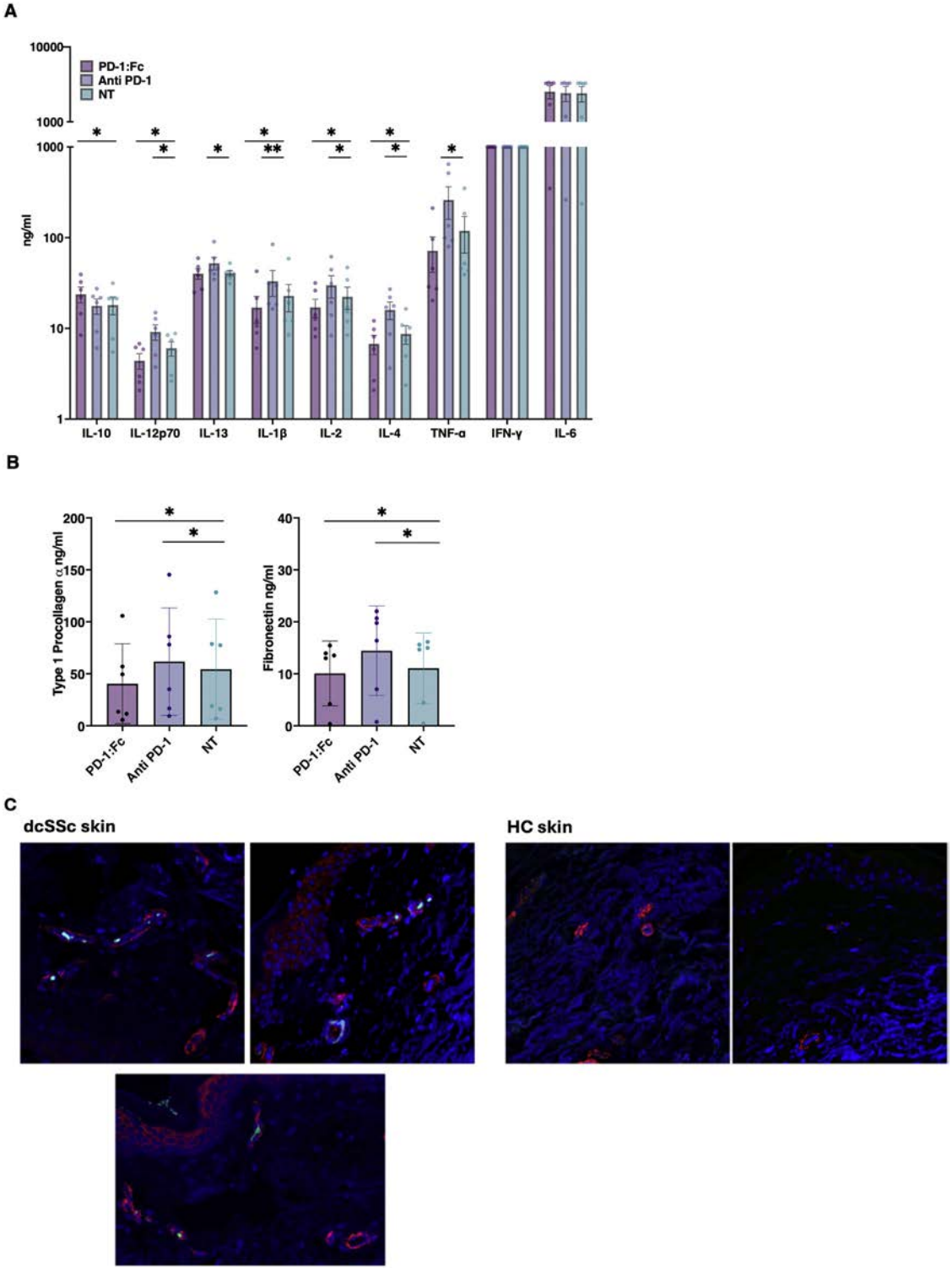

Figure 4. Modulation of the PD-1 pathway significantly differentially influences cytokine and ECM production in dcSSc fibroblasts and PBMC cocultures. (A) In autologous cocultures of anti-CD3/CD28−stimulated dcSSc PBMCs and TGF-β-stimulated fibroblasts (n = 6), PD-1:Fc treatment significantly reduced the levels of IL-12p70, IL-1β, IL-2, IL-4, and IL-10 compared to nontreated (NT) samples. In contrast, adding pembrolizumab (anti-PD-1) significantly increased the production of IL-12p70, IL-13, IL-1β, IL-2, IL-4, and TNF-α. Data are represented as mean with SD. (B) In autologous cocultures of anti-CD3/CD28−stimulated dcSSc PBMCs and TGF-β-stimulated fibroblasts (n = 6), treatment with PD-1:Fc significantly decreased the levels of type-1 procollagen type α and fibronectin compared to NT samples, whereas pembrolizumab (anti-PD-1) increased the levels of these ECM proteins. Data are represented as mean with SD. (C) Representative images showing immunofluorescence staining of dcSSc skin (n = 3) and healthy control (HC) skin (n = 2) stained for nuclear staining; DAPI (blue), αSMA (red), and PD-1 (green). dcSSc images represent 2 different donors. Magnification ×20 (n = 1). αSMA, α smooth muscle actin; DAPI, 4',6-diamidino-2-phenylindole, nuclear staining; dcSSc, diffuse cutaneous systemic sclerosis; ECM, extracellular matrix; IL, interleukin; ns, nonsignificant; PBMC, peripheral blood mononuclear cell PD-1, programmed cell death protein 1; SSc, Systemic sclerosis; TGF-β, transforming growth factor β; TNF-α, tumour necrosis factor alpha. Significance levels: *$P < .05$, **$P < .01$. (For interpretation of the references to colour in this figure legend, the reader is referred to the web version of this article.)

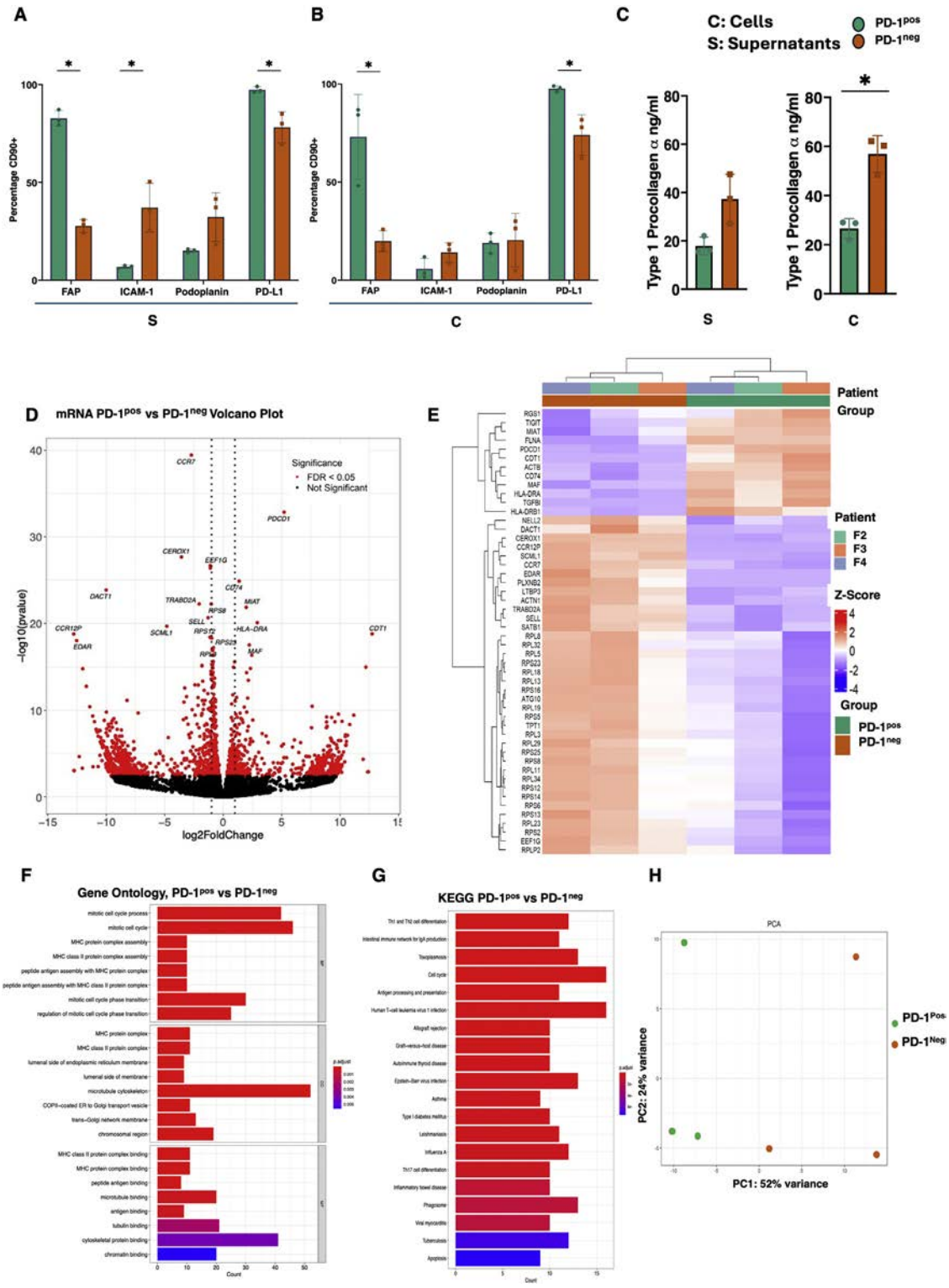

Figure 5. PD-1 ^{pos} and PD-1^{neg} T cells from patients with dSSc exert differential effects on fibroblast activation and exhibit unique immune gene signatures. (A) Expression of fibroblast activation protein (FAP), Intercellular adhesion molecule 1 (ICAM-1), podoplanin and PD-L1 in healthy dermal fibroblasts cultured with anti-CD3/CD28−stimulated dcSSc PD-1^{pos} or PD-1^{neg} T cell supernatants(n = 3). Expression of FAP and PD-L1 was increased when fibroblasts were cultured with PD-1^{pos} cells, whereas expression of ICAM-1 was decreased when fibroblasts were cultured with PD-1^{pos} cells. (B) Expression of FAP, ICAM-1, podoplanin, and PD-L1 in healthy dermal fibroblasts cultured with anti-CD3/CD28−stimulated dcSSc PD-1^{pos} or PD-1^{neg} T cells (n = 3). Expression of FAP and PD-L1 was increased when fibroblasts were cultured with PD-1^{pos} cells. Data represented as median with IQR. (C) Production of type-1 procollagen α by fibroblasts cocultured with anti-CD3/CD28−stimulated PD-1^{pos} or PD-1^{neg} T cells or supernatants. Production of type-1 procollagen α was decreased when fibroblasts were cultured with PD-1^{pos} T cells. (D) Volcano plot comparing differentially expressed genes (DEGs) between PD-1^{pos} and PD-1^{neg} T cells from patients with dcSSc showed a distinct transcriptional profile between PD-1^{pos} and PD-1^{neg} T cells population. The top 10 genes are marked by names. Genes with a log fold change above 2 are indicated in red. Cells were not stimulated prior to RNA sequencing. (E) Heatmap of top 50 DEG between PD-1^{pos} and PD-1^{neg} T cells from patients with dcSSc. (F) Enrichment analysis of gene ontology (GO) and Kyoto Encyclopaedia of Genes and (G) Genomes (KEGG) pathway for differentially expressed genes. Enrichment analysis of GO was divided into biological processes, cellular components, and molecular function. Barplot represented the value of −log10-adjusted *P* value of enrichment significance. Enrichment analysis of KEGG pathway. Different colours represent the value of −log10-adjusted *P* value of enrichment significance. (H)

that the PD-1^{pos} and PD-1^{neg} T cell populations exhibited unique transcriptional profiles (Fig 5D). PD-1^{pos} T cells exhibited a more regulatory profile with upregulated *RGS-1, FLNA, CD74, TGF-β1,* and *TIGIT* compared to PD-1^{neg} T cells (Fig 5E). We carried out a GO enrichment analysis to better understand the significance of the DEG between the PD-1^{pos} and PD-1^{neg} T cell population in dcSSc. In terms of biological processes, we found that the PD-1^{pos} population upregulated genes involved in cell cycle processes and antigen presentation, where genes related to major histocompability complex class presentation were upregulated (Fig 5F). Furthermore, the Kyoto Encyclopaedia of Genes and Genomes pathway analysis revealed that the PD-1^{pos} population had increased gene signalling associated with Th1 and Th2 differentiation, Th17 differentiation, and antigen presentation (Fig 5G). Additionally, the high expression of *TGF-β1* supported the increased expression of FAP and PD-L1 on the fibroblasts seen on flow cytometry. Principal component analysis based on the DEG revealed that the transcriptional profile of PD-1^{pos} clustered together and was distinct from that of PD-1^{neg} for all samples analysed (Fig 5H).

PD-1 attenuates inflammation and fibrosis in the bleomycin-induced pulmonary injury model.

To examine the role of PD-1 in influencing lung inflammation and fibrosis *in vivo*, we analysed the effects of murine recombinant PD-1:Fc injections on the development of lung fibrosis in the bleomycin mouse model. We utilised 2 approaches: 1 involved administering PD-1:Fc on days 1, 3, and 7 after bleomycin inhalation, whereas the other involved injecting PD-1:Fc on days 14 and 17, to ensure that fibrosis was present prior to treatment [20]. These were compared to a control group that received an isotype control at the same time points, days 1, 3, 7, 14, and 21 (Fig 6A).

Early administration of PD-1:Fc (days 1, 3, and 7) significantly decreased the level of lung fibrosis as assessed by the level of collagen in the lungs, whereas delayed administration starting at day 14 exhibited a trend for reduced fibrosis but did not reach significance (Fig 6B). This attenuation in fibrosis was further supported by the modified Ashcroft score for lung fibrosis, which was significantly lower in both early and late-treated PD-1:Fc groups and supported by histological evaluation (Fig 6C,E top). As myofibroblasts expressing αSMA are significant contributors to fibrosis, we stained the lungs for the presence of αSMA-positive cells. αSMA-positive cells were found in all groups, however significantly more abundant in the IgG control treated group. We observed a significant difference between the early PD-1:Fc-treated group and the IgG control treated group, whereas the difference to the PD-1:Fc late-treated group was only numerical (Fig 6D,E bottom). We also evaluated the lung sections for the presence of CD4+ cells; however, no CD4 + cells were found to infiltrate the lungs at this late stage of the disease (Supplementary Fig S3). We examined cytokine levels in the serum after sacrifice, and observed that early and late PD-1 treatments resulted in a significant decrease in several proinflammatory cytokines, including TNF-α, IL-2, IL-6, and IL-1β, compared to the isotype control. Moreover, both early and late initiated PD-1:Fc treatment also led to a reduction in the production of profibrotic cytokines, such as IL-4, IL-13, and monocyte chemoattractent protein-1 (MCP-1) when compared to the control group treated with the isotype control antibody (Fig 6F).

DISCUSSION

SSc is a multifaceted autoimmune disease characterised by inflammation and fibrosis. This complex condition affects the immune system, connective tissue, and the vascular system, resulting in severe clinical manifestations and high mortality rates [21]. Although genetic and epigenetic factors contribute to this disease's initiation and early development, constant immune activation and fibrosis are the primary drivers of progression and severity and are responsible for much of the disease's morbidity and mortality [22,23].

Our study delves into the role of PD-1 in influencing the complex microenvironment of SSc, specifically inflammation and fibrosis. Furthermore, we highlight the importance of the PD-1 pathway in regulating these complex microenvironments.

We demonstrate that PD-1 is upregulated at a cellular and soluble level in dcSSc. On the soluble level, we observe a weak association with FVC, mRodnan skin score, and ESR. We investigate these associations in a cross-sectional study where structural changes have progressed over several years. The measured serum level of sPD-1 may be associated with the current inflammation status, as seen in the correlation to ESR. However, the association with the structural changes may be more complex and does not consider the effect of sPD-1 and PD-1 expressing cells in the microenvironment over time. We see an upregulation of PD-1 on both CD4+ and CD8+ T cells, reflecting the role of PD-1 in regulating acute and long-term inflammatory responses and supporting this pathway to be available for the crosstalk between immune cells and antigen presenting cells to influence fibrosis. When administering the PD-1:Fc to *in vitro* models, we observe a decrease in the production of SSc signature cytokines, including TNF-α, IFN-γ, IL-4, and IL-1β, suggesting a local effect of the PD-1:Fc treatment. The importance of the PD-1 pathway in autoimmunity has previously been demonstrated in mouse models of autoimmune diseases, such as type 1 diabetes, lupus, and multiple sclerosis [24,25]. Blocking PD-1 via antibody blockade or genetic deletion can accelerate or worsen the disease [26]. Similarly, patients with cancer treated with pembrolizumab may experience adverse effects resembling autoimmune diseases such as dcSSc [27,28]. Previous studies have also shown that the PD-1/PD-L1 pathway plays a role in pulmonary fibrosis through a T cell-dependent immune mechanism. Celada et al [29] and Wang et al [30] both reported that although proliferation and differentiation of CD4$^+$ T cells are suppressed in idiopathic pulmonary fibrosis, TGF-β1 secretion, and potentially IL-17A, from PD-1+ CD4+ T cells was increased, which significantly promoted fibrosis in idiopathic pulmonary fibrosis.

Consistent with these previous studies, our data show that PD-1^{pos} T cells from patients with dcSSc may promote fibrosis through upregulation of *TGF-β1*. Because of the upregulation of *TGF-β1* and *HLA-DRA* in the PD-1^{pos} T cells, we expected fibroblasts cocultured with these cells to increase their type 1 procollagen α production, but the opposite was observed. This could be explained by a relatively short incubation time, and a high level proinflammatory cytokines from the PD-1^{neg} cells to predominantly activate the fibroblasts. It has been shown that CD4 + T cells from patients with dcSSc in general have increased expression of genes related to cytokines and effector molecules, supporting these cells to activate fibroblasts [31]. In addition,

Principal component analysis (PCA) of PD-1^{pos} and PD-1^{neg} T cells from patients with dcSSc represents separate clustering of the 2 populations and individual differences. dcSSc, diffuse cutaneous systemic sclerosis; ns, nonsignificant; PD-1, programmed cell death protein 1; PD-1^{neg}, PD-1-negative; PD-1^{pos}, PD-1-positive. Significance levels: *$P < .01$, **$P < .001$. (For interpretation of the references to colour in this figure legend, the reader is referred to the web version of this article.)

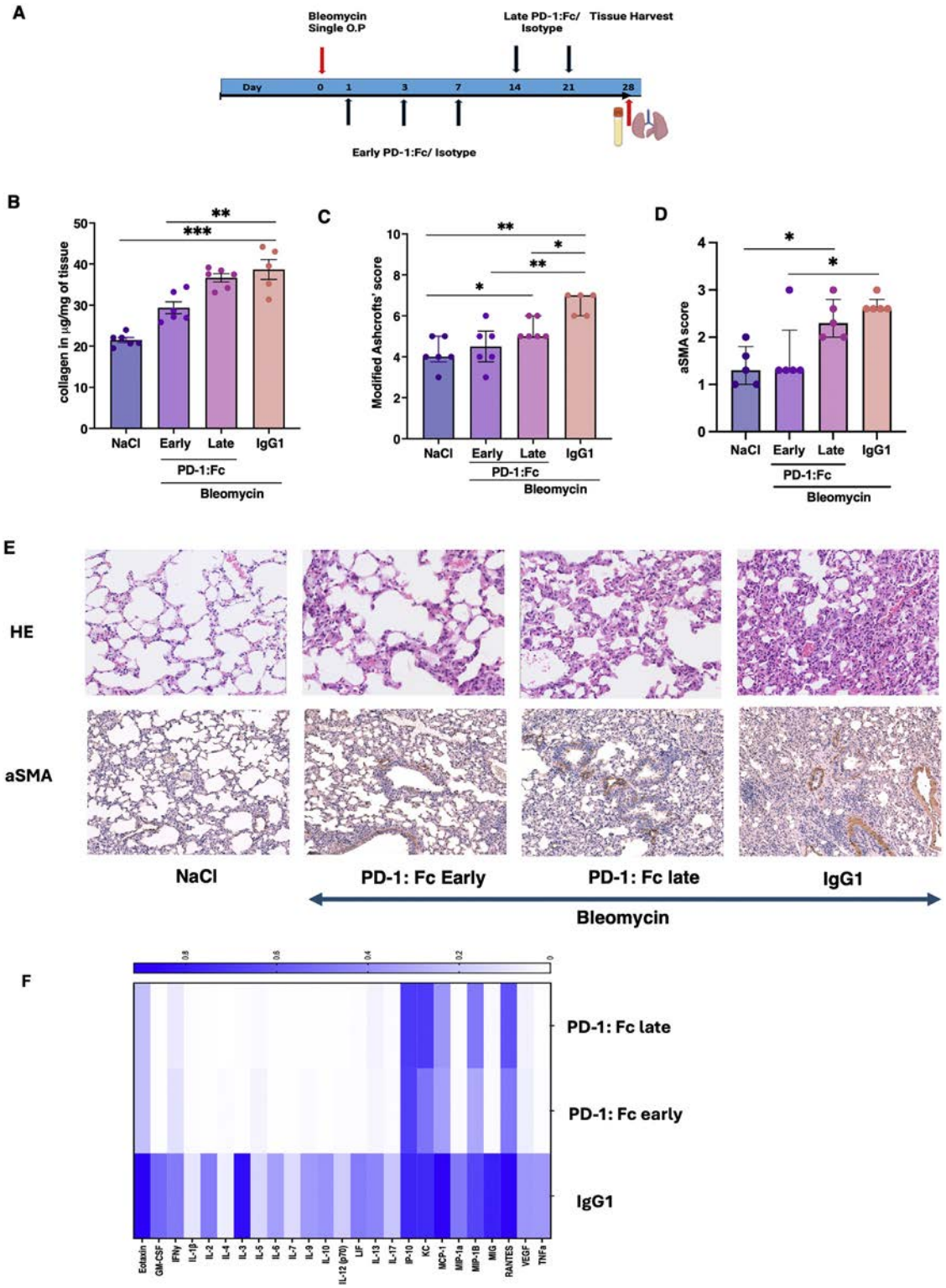

Figure 6. PD-1 attenuates inflammation and fibrosis in the bleomycin-induced pulmonary injury model. (A) Pictorial representation of the timeline for the bleomycin mouse model of lung fibrosis. The mice were treated with saline (n = 6) or bleomycin inhalation in combination with either early PD-1:Fc (n = 6) or late PD-1: Fc (n = 6) or an immunoglobolin G (IgG) isotype control (n = 5). (B) Insoluble collagen measured in mice lung tissue after sacrificed at day 28 was significantly lower in early PD-1:Fc-treated mice as compared to the IgG isotype control group. Data are presented as mean with SD. (C) Modified Ashcroft's score for lung fibrosis showed a significantly lower fibrotic score in mice receiving both early and late PD-1: Fc treatment compared to the Isotype control. Data are presented as median with IQR. (D) The presence of α smooth muscle acti (αSMA)-positive cells was graded from 1 to 3. Scoring was done blinded and repeated 3 times. αSMA-positive cells were present in all groups. The average score for each mouse is depicted in the plot. The early PD-1: Fc treatment group had scores comparable to NaCl, whereas the presence of αSMA was significantly increased in the IgG-treated control group. Data are presented as median with IQR. (E) The decrease in lung fibrosis is represented by images of sections of lungs from each of the treatment groups stained with HE staining (top), magnification ×40 as well as the presence of αSMA-positive cells (bottom), magnification ×20 (F) Heatmap showing early and late PD-1: Fc treatment reducing proinflammatory cytokines as compared to the IgG control in bleomycin-treated groups, represented as a relative expression of mean values of each group compared to the isotype control. IFN, interferon; IL, interleukin; ns, nonsignificant; PD-1, programmed cell death protein 1; TNF, tumour necrosis factor. Significance levels: *$P < .05$; **$P < .01$, ***$P < .001$. Created in BioRender.com.

our analysis of T cell subsets revealed a distinct gene expression signature between PD-1−positive and PD-1−negative T cells in SSc. Notably, several genes previously associated with SSc pathobiology, including *CD74, MAF, CDT1*, and *ACTB* [32–35], were significantly reduced in the PD-1−negative T cell population compared with PD-1−positive cells. This finding supports the concept that diminished PD-1 signalling is associated with attenuation of the SSc-specific transcriptional programme, consistent with a partial reversion of disease-associated gene expression upon modulation of the PD-1 pathway.

We observed an upregulation of PD-L1 on fibroblasts after coculture with PD-1^{pos} cells. This is in line with the observation that we also show that PD-L1 expression is upregulated on dcSSc myofibroblasts after TGF-β 1 stimulation. A high PD-L1 expression is associated with a persistent inflammatory response, and it promotes fibrosis in various autoimmune diseases and cancers through epithelial-mesenchymal transformation [36,37]. We further demonstrate that ECM protein production from TGF-β-stimulated dcSSc fibroblasts is high but can be reduced by the addition of PD-1:Fc. The effect of PD-1:Fc is modest on collagen and fibronectin production; however, combined with a synergistic effect on SSc signature cytokines as also seen in cocultures, the effect becomes pathophysiological relevant as also demonstrated in the mouse model. This supports the idea that PD-L1 signalling is involved in both fibrosis and the regulation of T cell activation, a notion previously explored in dendritic cells [38]. By flow cytometry, we demonstrate that the PD-1:Fc can reduce surface expression of ICAM, PD-L1, and podoplanin on TGF-β-stimulated dcSSc fibroblasts. This confirms a similar pattern with downregulation of *PD-L1, ICAM*, and *VCAM* when evaluating the effect of PD-1:Fc on fibroblasts by quantitative polymerase chain reaction. However, these differences were not pronounced in fibroblasts without TGF-β stimulation, where we observed only modest changes in the transcriptomic profile in dcSSc fibroblasts when treated with PD-1:Fc. This supports the notion that targeting the PD-1 pathway is likely to be especially efficient in an environment with both proinflammatory and profibrotic stimuli. The important interaction between T cells and fibroblasts has also been highlighted in rheumatoid arthritis, where it was recently reported that synovial lining and sublining fibroblasts, in close association with CD45+ cells, had a more activated phenotype [39]. In addition, it is also evident that specific fibroblast subsets are highly relevant for the severity of the disease [40,41]. In the inflamed dcSSc skin, we confirmed the presence of αSMA-positive cells and PD-1-positive cells, supporting that this interaction can take place at the fibrotic site. Continued immune system activation is implicated in driving fibrosis in dcSSc [42]. Our coculture experiments of dcSSc PBMCs with healthy dermal and lung fibroblasts highlight that pathological activated PBMCs, as previously demonstrated in rheumatoid arthritis, [39] can induce fibroblast activation and collagen production. This has also been noted in the context of inflammation-driven heart fibrosis following injury and post-myocardial infarct wound healing [43]. This effect can be attenuated by adding PD-1:Fc, which in the cocultures decrease ECM protein production and SSc signature cytokines.

In our mouse model of lung fibrosis, we observed downregulation of proinflammatory cytokines after treatment with PD-1:Fc. We noted similar effects with early- and late-administered PD-1:Fc, supporting a direct and sustained effect on the production of proinflammatory cytokines such as IL-4, IL-13, and TNF-α. Early treatment with PD-1:Fc decreased both fibrosis and collagen production in the lung. The late PD-1:Fc treatment also decreased the lung fibrosis score but not collagen levels. The presence of αSMA was increased in the more inflammatory state of the disease. In our *in vitro* studies, we did not observe a direct effect PD-1:Fc on αSMA, suggesting that the decreased αSMA expression in mouse lungs after early treatment with PD-1:Fc is a secondary effect caused by decreased inflammation. Our *in vivo* studies underscore that early treatment more efficiently decreases the development of fibrosis and that some degree of fibrosis is irreversible. However, administering a late treatment with PD-1:Fc still led to a reduction in fibrosis. This is a challenge for current antifibrotic drugs [44,45]. Previous findings in the bleomycin model suggest that the absence of PD-L1-expressing fibroblasts leads to reduced fibrosis, reinforcing our findings that treatment with PD-1:Fc has a regulatory effect [46]. Patients with dcSSc have an ongoing interaction between their immune cells and fibroblasts, augmenting the fact that targeting the PD-1 pathway is a sensible approach to lessen both inflammation and fibrosis in dcSSc. Our studies are limited by only evaluating fibroblasts and not also considering dendritic cells and macrophages. We also do not explore the function of PD-L2 in influencing this pathway. Still, our data support the observation that PD-1:Fc binding to PD-L1 reduces the development of lung fibrosis in the bleomycin lung model and reduces ECM proteins, fibroblast activation markers, and SSc signature cytokines *in vitro*. This highlights the PD-1 pathway as a potential new treatment target to reduce fibrosis in dcSSc.

Overall, our findings support the pivotal role of T cell and fibroblast interaction in driving inflammation and fibrosis in SSc. Moreover, our study highlights the crucial role of the PD-1 pathway in controlling this inflammation-induced fibrosis. This insight could pave the way for developing targeted therapeutic strategies to restore immune homeostasis in SSc.

Competing interests

All other authors declare they have no competing interests.

CRediT authorship contribution statement

Maithri Aspari: Writing – review & editing, Writing – original draft, Validation, Software, Resources, Project administration, Methodology, Investigation, Formal analysis, Data curation, Conceptualization. **Voon Ong:** Visualization, Supervision, Resources, Data curation, Conceptualization. **Klaus Søndergaard:** Resources, Data curation. **Esben Næser:** Writing – review & editing, Formal analysis, Data curation. **Malene Hvid:** Writing – review & editing, Validation, Supervision, Data curation. **Kim Ravnskjaer:** Validation, Formal analysis, Data curation. **Angela Y.Y. Tam:** Validation, Supervision, Software, Resources, Methodology, Investigation, Data curation. **Shiwen Xu:** Methodology, Data curation. **Xinyue Bian:** Writing – original draft, Visualization, Methodology, Formal analysis, Data curation. **Henry Lopez:** Software, Formal analysis, Data curation. **Christopher P. Denton:** Writing – review & editing, Supervision, Resources, Conceptualization. **David Abraham:** Writing – review & editing, Validation, Supervision, Resources, Project administration, Funding acquisition, Data curation, Conceptualization. **Bent Deleuran:** Writing – review & editing, Visualization, Validation, Supervision, Resources, Project administration, Funding acquisition, Data curation, Conceptualization. **Stinne R. Greisen:** Writing – review & editing, Validation, Supervision, Project administration, Methodology, Funding acquisition, Data curation, Conceptualization.

Acknowledgements

We would like to acknowledge our laboratory technician, Sulaiman Hussein Kassem, for all his help in the lab. Thanks to the FACS core facility at Aarhus University for assistance with flow cytometry and cell sorting. Thanks to the Histology core facility at Aarhus University for assistance with IHC staining of mouse lung sections.

Funding

This research has been funded by The Danish Rheumatoid Association (Gigtforening) (Grant numbers R211-A7627-B1757 and R186-A6654-B1757) and FOREUM- Foundation for Rheumatology Research and the Lundbeck Foundation (grant R287-2018-1094) and LEO Foundation (grant LF-FE-24-700026).

Ethics approval

The studies were approved by the Regional Ethics Committee (Reference number 700779) and Region Midt's Data Protection Agency (1-16-02-542-20) in DK. In the UK, the studies were approved by the NHS Research and Ethics Committee (number 6398). Patient informed consent covering participation was approved by the London- Hampstead (IRAS 270295) and London-Fulham Research Ethics Committees (IRAS 279682). All subjects' written informed consents were obtained according to the Declaration of Helsinki. For all in vivo mouse experiments, strict adherence to institutional guidelines was practiced, and full local ethics committee approval through the UCL Animal Welfare and Ethical Review Body (AWERB) and appropriate Home Office Project and Personal license were obtained.

Data availability statement

Data have not been uploaded to a data bank as they include sensitive and confidential information linking it to patients. Data are available upon reasonable request to the corresponding author.

Supplementary materials

Supplementary material associated with this article can be found in the online version at doi:10.1016/j.ard.2026.01.008.

Orcid

Maithri Aspari: http://orcid.org/0000-0002-8842-0186
Voon Ong: http://orcid.org/0000-0001-5474-0053
Kim Ravnskjaer: http://orcid.org/0000-0002-5322-3887
Angela Y.Y. Tam: http://orcid.org/0000-0001-8322-180X
Shiwen Xu: http://orcid.org/0000-0002-3624-2410
Xinyue Bian: http://orcid.org/0009-0005-2362-884X
Christopher P. Denton: http://orcid.org/0000-0003-3975-8938
David Abraham: http://orcid.org/0000-0001-8952-6057
Bent Deleuran: http://orcid.org/0000-0002-7079-1587
Stinne R. Greisen: http://orcid.org/0000-0003-2922-3307

REFERENCES

[1] Truchetet ME, Brembilla NC, Chizzolini C. Current concepts on the pathogenesis of systemic sclerosis. Clin Rev Allergy Immunol 2023;64(3):262–83.
[2] Villanueva-Martín G, Martín J, Bossini-Castillo L. Recent advances in elucidating the genetic basis of systemic sclerosis. Curr Opin Rheumatol 2022;34(6):295–301.
[3] Tsou PS, Varga J, O'Reilly S. Advances in epigenetics in systemic sclerosis: molecular mechanisms and therapeutic potential. Nat Rev Rheumatol 2021;17(10):596–607.
[4] Francisco LM, Sage PT, Sharpe AH. The PD-1 pathway in tolerance and autoimmunity. Immunol Rev 2010;236:219–42.
[5] Kowalska-Kępczyńska A. Systemic scleroderma-definition, clinical picture and laboratory diagnostics. J Clin Med 2022;11(9):2299.
[6] Chen RY, Zhu Y, Shen YY, Xu QY, Tang HY, Cui NX, et al. The role of PD-1 signaling in health and immune-related diseases. Front Immunol 2023;14:1163633.
[7] Patsoukis N, Wang Q, Strauss L, Boussiotis VA. Revisiting the PD-1 pathway. Sci Adv 2020;6(38):eabd2712.
[8] Zhang P, Wang Y, Miao Q, Chen Y. The therapeutic potential of PD-1/PD-L1 pathway on immune-related diseases: based on the innate and adaptive immune components. Biomed Pharmacother 2023;167:115569.
[9] Greisen SR, Rasmussen TK, Stengaard-Pedersen K, Hetland ML, Hørslev-Petersen K, Hvid M, et al. Increased soluble programmed death-1 (sPD-1) is associated with disease activity and radiographic progression in early rheumatoid arthritis. Scand J Rheumatol 2014;43(2):101–8.
[10] Curnock AP, Bossi G, Kumaran J, Bawden LJ, Figueiredo R, Tawar R, et al. Cell-targeted PD-1 agonists that mimic PD-L1 are potent T cell inhibitors. JCI Insight 2021;6(20):e152468.
[11] Ohkuma R, Ieguchi K, Watanabe M, Takayanagi D, Goshima T, Onoue R, et al. Increased plasma soluble PD-1 concentration correlates with disease progression in patients with cancer treated with anti-PD-1 antibodies. Biomedicines 2021;9(12):1929.
[12] Niu M, Liu Y, Yi M, Jiao D, Wu K. Biological characteristics and clinical significance of soluble PD-1/PD-l1 and exosomal PD-L1 in cancer. Front Immunol 2022;13:827921.
[13] Terrier B, Humbert S, Preta LH, Delage L, Razanamahery J, Laurent-Roussel S, et al. Risk of scleroderma according to the type of immune checkpoint inhibitors. Autoimmun Rev 2020;19(8):102596.
[14] Zhao Y, Qu Y, Hao C, Yao W. PD-1/PD-L1 axis in organ fibrosis. Front Immunol 2023;14:1145682.
[15] Jalali S, Price-Troska T, Bothun C, Villasboas J, Kim HJ, Yang ZZ, et al. Reverse signaling via PD-L1 supports malignant cell growth and survival in classical Hodgkin lymphoma. Blood Cancer J 2019;9(3):22.
[16] Guo X, Sunil C, Adeyanju O, Parker A, Huang S, Ikebe M, et al. PD-L1 mediates lung fibroblast to myofibroblast transition through Smad3 and β-catenin signaling pathways. Sci Rep 2022;12(1):3053.
[17] Geng Y, Liu X, Liang J, Habiel DM, Kulur V, Coelho AL, et al. PD-L1 on invasive fibroblasts drives fibrosis in a humanized model of idiopathic pulmonary fibrosis. JCI Insight 2019;4(6):e125326.
[18] Lu Y, Zhong W, Liu Y, Chen W, Zhang J, Zeng Z, et al. Anti-PD-L1 antibody alleviates pulmonary fibrosis by inducing autophagy via inhibition of the PI3K/Akt/mTOR pathway. Int Immunopharmacol 2022;104:108504.
[19] Akella P, Loganathan S, Jindal V, Akhtar J, Lal A. Anti PD-1 immunotherapy related interstitial lung disease presenting as respiratory failure—a review with case series. Respir Med Case Rep 2019;26:17–22.
[20] Kolb P, Upagupta C, Vierhout M, Ayaub E, Bellaye PS, Gauldie J, et al. The importance of interventional timing in the bleomycin model of pulmonary fibrosis. Eur Respir J 2020;55(6):1901105.
[21] Pokeerbux MR, Giovannelli J, Dauchet L, Mouthon L, Agard C, Lega JC, et al. Survival and prognosis factors in systemic sclerosis: data of a French multicenter cohort, systematic review, and meta-analysis of the literature. Arthritis Res Ther 2019;21(1):86.
[22] Szabo I, Badii M, Gaál IO, Szabo R, Popp RA, Joosten LAB, et al. Enhanced innate and acquired immune responses in systemic sclerosis primary peripheral blood mononuclear cells (PBMCs). Int J Mol Sci 2023;24(19):14438.
[23] Laurent P, Sisirak V, Lazaro E, Richez C, Duffau P, Blanco P, et al. Innate immunity in systemic sclerosis fibrosis: recent advances. Front Immunol 2018;9:1702.
[24] Deng Y, Huang F, Wang J. A narrative review of PD-1 and autoimmune diseases. Ann Blood 2021;7:31.
[25] Carter LL, Leach MW, Azoitei ML, Cui J, Pelker JW, Jussif J, et al. PD-1/PD-L1, but not PD-1/PD-L2, interactions regulate the severity of experimental autoimmune encephalomyelitis. J Neuroimmunol 2007;182(1-2):124–34.
[26] Riella LV, Paterson AM, Sharpe AH, Chandraker A. Role of the PD-1 pathway in the immune response. Am J Transplant 2012;12(10):2575–87.
[27] Fattore D, Battista T, De Lucia M, Annunziata MC, Fabbrocini G. Scleroderma-like syndrome in the setting of pembrolizumab therapy for non-small cell lung cancer: diagnosis and dermatologic management. Case Rep Dermatol 2022;14(2):225–9.

[28] Ibis B, Aliazis K, Cao C, Yenyuwadee S, Boussiotis VA. Immune-related adverse effects of checkpoint immunotherapy and implications for the treatment of patients with cancer and autoimmune diseases. Front Immunol 2023;14:1197364.
[29] Celada LJ, Kropski JA, Herazo-Maya JD, Luo W, Creecy A, Abad AT, et al. PD-1 up-regulation on $CD4^+$ T cells promotes pulmonary fibrosis through STAT3-mediated IL-17A and TGF-β1 production. Sci Transl Med 2018;10(460):eaar8356.
[30] Wang B, Bai W, Ma H, Li F. Regulatory effect of PD1/PD-ligand 1 (PD-L1) on Treg cells in patients with idiopathic pulmonary fibrosis. Med Sci Monit 2021;27:e927577.
[31] Paleja B, Low AHL, Kumar P, Saidin S, Lajam A, Nur Hazirah S, et al. Systemic sclerosis perturbs the architecture of the immunome. Front Immunol 2020;11:1602.
[32] Corallo C, Paulesu L, Cutolo M, Ietta F, Carotenuto C, Mannelli C, et al. Serum levels, tissue expression and cellular secretion of macrophage migration inhibitory factor in limited and diffuse systemic sclerosis. Clin Exp Rheumatol 2015;33(4):S98–105 Suppl 91.
[33] Baños-Hernández CJ, Bucala R, Hernández-Bello J, Navarro-Zarza JE, Villanueva-Pérez MA, Godínez-Rubí M, et al. Expression of macrophage migration inhibitory factor and its receptor CD74 in systemic sclerosis. Cent Eur J Immunol 2021;46(3):375–83.
[34] Gaydosik AM, Tabib T, Domsic R, Khanna D, Lafyatis R, Fuschiotti P. Single-cell transcriptome analysis identifies skin-specific T-cell responses in systemic sclerosis. Ann Rheum Dis 2021;80(11):1453–60.
[35] Milano A, Pendergrass SA, Sargent JL, George LK, McCalmont TH, Connolly MK, et al. Molecular subsets in the gene expression signatures of scleroderma skin. PLoS One 2008;3(7):e2696.
[36] Zhang Y-C, Zhang YT, Wang Y, Zhao Y, He LJ. What role does PDL1 play in EMT changes in tumors and fibrosis? Front Immunol 2023;14:1226038.
[37] Sun C, Mezzadra R, Schumacher TN. Regulation and function of the PD-L1 checkpoint. Immunity 2018;48(3):434–52.
[38] Lucas ED, Schafer JB, Matsuda J, Kraus M, Burchill MA, Tamburini BAJ. PD-L1 reverse signaling in dermal dendritic cells promotes dendritic cell migration required for skin immunity. Cell Rep 2020;33(2):108258.
[39] Smith MH, Gao VR, Periyakoil PK, Kochen A, DiCarlo EF, Goodman SM, et al. Drivers of heterogeneity in synovial fibroblasts in rheumatoid arthritis. Nat Immunol 2023;24(7):1200–10.
[40] Croft AP, Campos J, Jansen K, Turner JD, Marshall J, Attar M, et al. Distinct fibroblast subsets drive inflammation and damage in arthritis. Nature 2019;570(7760):246–51.
[41] Fullard N, O'Reilly S. Role of innate immune system in systemic sclerosis. Semin Immunopathol 2015;37(5):511–7.
[42] Worrell JC, O'Reilly S. Bi-directional communication: conversations between fibroblasts and immune cells in systemic sclerosis. J Autoimmun 2020;113:102526.
[43] Bradshaw AD, DeLeon-Pennell KY. T-cell regulation of fibroblasts and cardiac fibrosis. Matrix Biol 2020;91-92:167–75.
[44] Pope JE, Denton CP, Johnson SR, Fernandez-Codina A, Hudson M, Nevskaya T. State-of-the-art evidence in the treatment of systemic sclerosis. Nat Rev Rheumatol 2023;19(4):212–26.
[45] Ma J, Li G, Wang H, Mo C. Comprehensive review of potential drugs with anti-pulmonary fibrosis properties. Biomed Pharmacother 2024;173:116282.
[46] Tan J, Xue Q, Hu X, Yang J. Inhibitor of PD-1/PD-L1: a new approach may be beneficial for the treatment of idiopathic pulmonary fibrosis. J Transl Med 2024;22(1):95.

Ann Rheum Dis 85 (2026) 1825–1838

Contents lists available at ScienceDirect

Annals of the Rheumatic Diseases

journal homepage: https://www.sciencedirect.com/journal/annals-of-the-rheumatic-diseases

Vasculitis

Single-cell analysis identifies monocyte signatures of disease activity and clinical subtypes in Behçet's disease

Elio Carmona[1], Rabia Deniz[2,3,4], Cemal Bes[2], Haner Direskeneli[3], Ahmet Gül[4], Amr H. Sawalha[5,*]

[1] *Division of Pediatric Rheumatology, Department of Pediatrics, University of Pittsburgh School of Medicine, Pittsburgh, PA, USA*
[2] *Department of Rheumatology, University of Health Sciences, Başakşehir Çam and Sakura City Hospital, Istanbul, Türkiye*
[3] *Division of Rheumatology, Department of Internal Medicine, Marmara University, Istanbul, Türkiye*
[4] *Division of Rheumatology, Department of Internal Medicine, Istanbul Faculty of Medicine, Istanbul University, Istanbul, Türkiye*
[5] *Departments of Pediatrics, Medicine, and Immunology & Lupus Center of Excellence, University of Pittsburgh School of Medicine, Pittsburgh, PA, USA*

ARTICLE INFO

Article history:
Received 10 December 2025
Received in revised form 26 June 2026
Accepted 27 June 2026

ABSTRACT

Objectives: Behçet's disease (BD) is a multisystem inflammatory disorder with diverse phenotypes and incompletely defined immune mechanisms. This study aimed to map immune dysregulation in BD at high resolution, comparing active vs remission states and identifying pathways linked to clinical phenotypes.

Methods: We performed single-cell RNA sequencing on 247,028 peripheral blood mononuclear cells from 34 patients with BD and 12 healthy controls. Transcriptomic profiling, differential gene expression, pathway enrichment analyses, and phenotype-stratified comparisons were used to delineate immune cell alterations associated with disease activity and clinical subtypes.

Results: All 3 monocyte subsets were markedly expanded in BD and demonstrated dominant interferon (IFN)-γ–associated activation, robust heat-shock responses, and enhanced antigen-presentation programmes. In active disease, monocytes exhibited pronounced type II IFN signatures, which reversed in remission alongside restoration of regulatory and metabolic pathways. Remission was instead characterised by increased expression of type I IFN–regulated genes and activation of serine protease inhibitor (SERPIN)-associated programmes linked to tissue stabilisation. Clinical phenotype stratification revealed distinct transcriptional signatures in peripheral blood monocytes, including enrichment of heat-shock and stress-response pathways in monocytes from patients with vascular BD and tumour necrosis factor/NF-κB–associated programmes in monocytes from patients with ocular BD. Patients without organ involvement demonstrated an increased type I IFN gene signature.

Conclusions: This study provides a high-resolution immune atlas of BD, identifying monocyte-driven dysregulation as a central feature. Our findings map the immune heterogeneity of BD, identify activity- and phenotype-linked peripheral blood monocyte states, and suggest immune pathways suitable for targeted intervention.

*Correspondence to Dr Amr H. Sawalha, Rangos Research Center, Pittsburgh, PA, USA.
E-mail address: asawalha@pitt.edu (A.H. Sawalha).
Handling editor Josef Smolen.

https://doi.org/10.1016/j.ard.2026.06.033

0003-4967/© 2026 The Author(s). Published by Elsevier B.V. on behalf of European Alliance of Associations for Rheumatology (EULAR). This is an open access article under the CC BY-NC-ND license (http://creativecommons.org/licenses/by-nc-nd/4.0/)

WHAT IS ALREADY KNOWN ON THIS TOPIC

- Behçet's disease (BD) is a clinically heterogeneous inflammatory disorder in which monocytes and innate immune pathways are thought to play central pathogenic roles. A comprehensive single-cell map integrating BD disease activity and clinical phenotypes has not previously been available.

WHAT THIS STUDY ADDS

- This study identifies monocyte-driven immune dysregulation as the dominant hallmark of BD, with significant expansion and interferon (IFN)-γ–associated activation across all monocyte subsets.
- We demonstrate distinct transcriptional programmes in active vs remission BD, including reversal of type II IFN signatures and emergence of type I IFN– and serine protease inhibitor (SERPIN)-associated recovery pathways in remission.
- We uncover phenotype-specific signatures in peripheral blood monocytes, such as heat-shock/stress-response pathways in monocytes from patients with vascular BD and tumour necrosis factor/NF-κB–driven inflammation in monocytes from patients with ocular BD.

HOW THIS STUDY MIGHT AFFECT RESEARCH, PRACTICE, OR POLICY

- These findings provide a high-resolution immune atlas that can guide development of phenotype-specific biomarkers and innate-immune–targeted therapies in BD.
- Identifying reversal genes and activity-associated immune states supports the refinement of treatment-response biomarkers and may aid in monitoring disease activity or predicting relapse.
- The phenotype-associated peripheral blood monocyte programmes highlight the importance of clinically stratified approaches in BD research and therapeutic trial design.

INTRODUCTION

Behçet's disease (BD) is a chronic, relapsing, multisystem inflammatory disorder characterised by recurrent oral and genital ulcers, uveitis, and systemic vasculitis that can affect vessels of all sizes and types [1,2]. The disease exhibits substantial clinical heterogeneity, with vascular, ocular, and mucocutaneous involvement representing distinct phenotypic spectrums associated with variable severity and prognosis [2–4]. Although the aetiology of BD remains elusive, converging evidence implicates an aberrant innate immune activation and dysregulated monocyte responses as central drivers of its pathogenesis [5–7].

Monocytes and their derivatives play a key role in bridging innate and adaptive immunity through cytokine secretion, antigen presentation, and crosstalk with endothelial and T cells [8,9]. Aberrant production of proinflammatory mediators, such as tumour necrosis factor (TNF), interleukin (IL)-1β, IL-6, and type I interferons (IFNs), has been reported in BD monocytes and peripheral blood mononuclear cells (PBMCs) [10,11]. Yet, bulk transcriptomic and proteomic analyses have offered limited resolution to disentangle the contribution of individual monocyte subsets, which encompass classical ($CD14^+CD16^-$), intermediate ($CD14^+CD16^+$), and nonclassical ($CD14^{dim}CD16^+$) populations with distinct immunoregulatory and tissue-repair functions [12,13]. Understanding how these subsets are transcriptionally remodelled across disease activity states and clinical phenotypes in BD remains unaddressed.

Single-cell RNA sequencing (scRNA-seq) enables the dissection of immune cell heterogeneity and reveals cellular states driving complex diseases at unprecedented resolution [14]. Recent studies in immune-mediated conditions have uncovered disease-specific reprogramming of monocyte subsets, including IFN-responsive and cytotoxic phenotypes linked to disease flares and phenotype involvement [15–18]. However, a comprehensive single-cell map of BD immune cells, integrating both activity and clinical heterogeneity, is still lacking.

Herein, we performed single-cell transcriptomic profiling of PBMCs from patients with BD and healthy controls to define immune cell alterations associated with disease activity and phenotype. By integrating data from active and remission samples and across vascular, ocular, and mucocutaneous clinical forms, we provide an unbiased atlas of immune dysregulation in BD. Our analyses reveal transcriptional remodelling within the monocyte compartment, including the expansion of distinct monocyte subsets exhibiting chemotactic and IFN-responsive gene programmes. These findings uncover shared and subset-specific molecular signatures underlying disease activity and organ involvement, offering new insight into the mechanisms driving immune heterogeneity in BD.

METHODS

Patient recruitment and clinical characteristics

Peripheral blood samples were collected from 34 patients fulfilling the International Study Group diagnostic criteria for BD [19] and 12 healthy controls. Patient recruitment was conducted at Başakşehir Çam and Sakura City Hospital, Department of Rheumatology, Istanbul, Türkiye, and Istanbul University, Istanbul Faculty of Medicine, Division of Rheumatology, Istanbul, Türkiye. All participants provided written informed consent before sample collection. The study was approved by the Marmara University Clinical Research Ethics Committee (approval no: 09.2021.52) and the Institutional Review Board of the University of Pittsburgh.

Active BD was defined as the presence of at least 1 new or recurrent clinical manifestation (oral or genital ulceration, ocular inflammation, or vascular involvement) within the last 4 weeks. All patients in the active BD group were newly diagnosed and treatment-naïve, having received no colchicine, corticosteroids, or immunosuppressive medications before sample collection. Remission BD was defined as the absence of any active clinical manifestation for at least 4 consecutive weeks after systemic therapy, with complete resolution of clinical signs and normalisation of acute-phase reactants. Because remission samples were obtained after treatment initiation, transcriptional differences between active and remission groups may reflect both clinical disease improvement and direct treatment effects. Among the 34 patients with BD included in the study, 8 had vascular involvement, 4 had ocular involvement, and 19 had only mucocutaneous disease. Clinical characteristics, including age, sex, organ involvement, disease status, and medications used, were recorded at the time of sample collection (Supplementary Table S1). Healthy controls were sex-matched healthy volunteers without a history of autoimmune or inflammatory diseases. Four of the 34 patients provided blood samples before and after disease remission; therefore, in total, 38 patient samples and 12 healthy control samples were evaluated in this study.

PBMC isolation and single-cell RNA-seq protocol

Peripheral blood (20-30 mL) was collected into EDTA-coated tubes and processed within 2 hours of venipuncture. PBMCs

were isolated by Ficoll-Paque density gradient centrifugation and washed twice with phosphate-buffered saline (PBS). No red blood cell lysis step was required. Cells were resuspended in freezing media (90% foetal bovine serum; 10% dimethyl sulfoxide), aliquoted at 5×10^6 cells per vial, and frozen. Cells were thawed, washed, and assessed for viability (>85% required). TotalSeq B hashtag antibodies (BioLegend) were then used for multiplexing samples in groups of 6 [20]. Single-cell suspensions were loaded onto the 10x Genomics Chromium Controller for droplet encapsulation and library construction using the Chromium Next GEM Single Cell 3′ v4 HT kit, following the manufacturer's protocol (10x Genomics). Libraries were sequenced on an Illumina NovaSeq 6000 platform with a mean sequencing depth of over 11,000 reads per cell.

Data preprocessing and quality control

Sequencing reads were aligned to the GRCh38 human reference genome using the Cell Ranger pipeline (v8.0.1, 10x Genomics). Resulting count matrices were imported into Seurat (v5.0) [21] for downstream analysis. Quality control filters included removal of cells with <400 detected genes, cells with >10% mitochondrial reads, and genes detected in <3 cells. Doublets were identified and removed using the DoubletFinder package [22]. Only high-quality cells were retained for further analysis. Raw and processed scRNA-seq data have been deposited in the Gene Expression Omnibus (GEO) under accession number GSE338165.

Clustering and cell-type annotation

Filtered count matrices were normalised and variance-stabilised using SCTransform v2 [23] with regression of mitochondrial content. Dimensionality reduction was performed using principal component analysis, accounting for >90% variation, followed by Uniform Manifold Approximation and Projection (UMAP). Clusters in monocyte subsets were identified with the Louvain algorithm at a resolution of 0.4. Cell types were annotated based on canonical marker expression, supported by reference mapping to the Monaco Immune Database included as SingleR PBMC reference [24,25]. Cell types represented by <200 cells were considered residual or low-confidence populations and excluded from downstream analysis to ensure adequate power and stability of statistical estimates.

Differential gene expression and enrichment analyses

Differential gene expression (DGE) was assessed between BD and healthy controls, as well as between active and remission patient subsets and disease phenotypes, using Seurat's FindMarkers function (Wilcoxon rank-sum test, Bonferroni/false discovery rate [FDR]-adjusted $P < .05$). Enrichment analyses of significant gene sets were performed using EnrichR [26] with the Gene Ontology Biological Process (GO:BP 2025) database. For each differential expression contrast, upregulated and downregulated genes were analysed separately to preserve directionality of regulation. Enriched terms with adjusted P value < .05 were reported and ranked by the EnrichR Combined Score. For active vs remission BD monocyte subset comparisons, we also performed transcription factor target enrichment on differential expression signatures using TF-oriented EnrichR libraries (ChEA_2022, ENCODE and ChEA Consensus TFs from ChIP-X, and TRRUST Transcription Factors 2019) to infer putative upstream regulators.

Compositional analysis of immune cell subsets

Changes in immune cell subset proportions were analysed using the sccomp package [27]. Unlike common proportion tests, sccomp provides probabilistic estimates of differential abundance that integrate uncertainty across subsets, yielding robust inference even in unbalanced designs. Relative frequencies of major PBMC subsets (T cells, B cells, natural killer [NK] cells, monocytes, and dendritic cells) and subclusters were compared across patients with BD and controls, and between disease activity states. Statistical significance was assessed using Bayesian proportion modelling.

Patient and public involvement

Patients or the public were not involved in the design, conduct, or reporting of this research. However, we are committed to ensuring that the findings are shared in formats accessible to nonscientific audiences, including patients and the wider public.

RESULTS

Single-cell atlas of peripheral blood from patients with BD and healthy controls

We generated scRNA-seq profiles from PBMCs of 34 patients with BD and 12 healthy controls to delineate immune cell heterogeneity and disease-related transcriptional changes (Fig 1A). After quality control filtering (removal of doublets and low-quality cells), 227,735 high-quality cells were retained for downstream analyses. For active vs remission disease and longitudinal analysis, we also included 4 posttreatment samples of patients already included in the study, for a total of 247,028 cells. After clustering, cells were annotated into canonical PBMC populations using *SingleR* with *MonacoImmuneData* [25] as a reference dataset and marker gene inspection. These included all major immune cell types (T cells, B cells, NK cells, monocytes, and dendritic cells) that were broken down into 26 subcell types after removing residual populations (Fig 1B, Supplementary Fig S1). The UMAP representation demonstrated clear separation of immune compartments, and integration after SCTransform normalisation and scaling minimised technical variation among sequencing pools effectively (Fig 1C). The resulting dataset thus constitutes a comprehensive single-cell atlas of circulating immune cells in BD.

Immune composition and transcriptional landscape distinguish BD monocytes from healthy controls

We first compared the cellular composition between patients with BD and healthy controls. Monocytes were significantly expanded in BD compared with controls (effect = 0.486, 95% credible interval (CrI) = 0.169-0.8; FDR = 0.0098), corresponding to an ~1.57-fold increase in their predicted proportion relative to healthy controls (Supplementary Table S2, Supplementary Fig S2A). This imbalance in the monocyte compartment led us to further explore its cellular composition and transcriptional activity. Monocytes were subclustered and characterised according to established canonical markers, distinguishing between classical, intermediate, and nonclassical subsets (Fig 2A,B).

Compositional modelling revealed a significant expansion of all 3 monocyte subsets in BD compared with healthy controls. The most significant increase was observed in classical

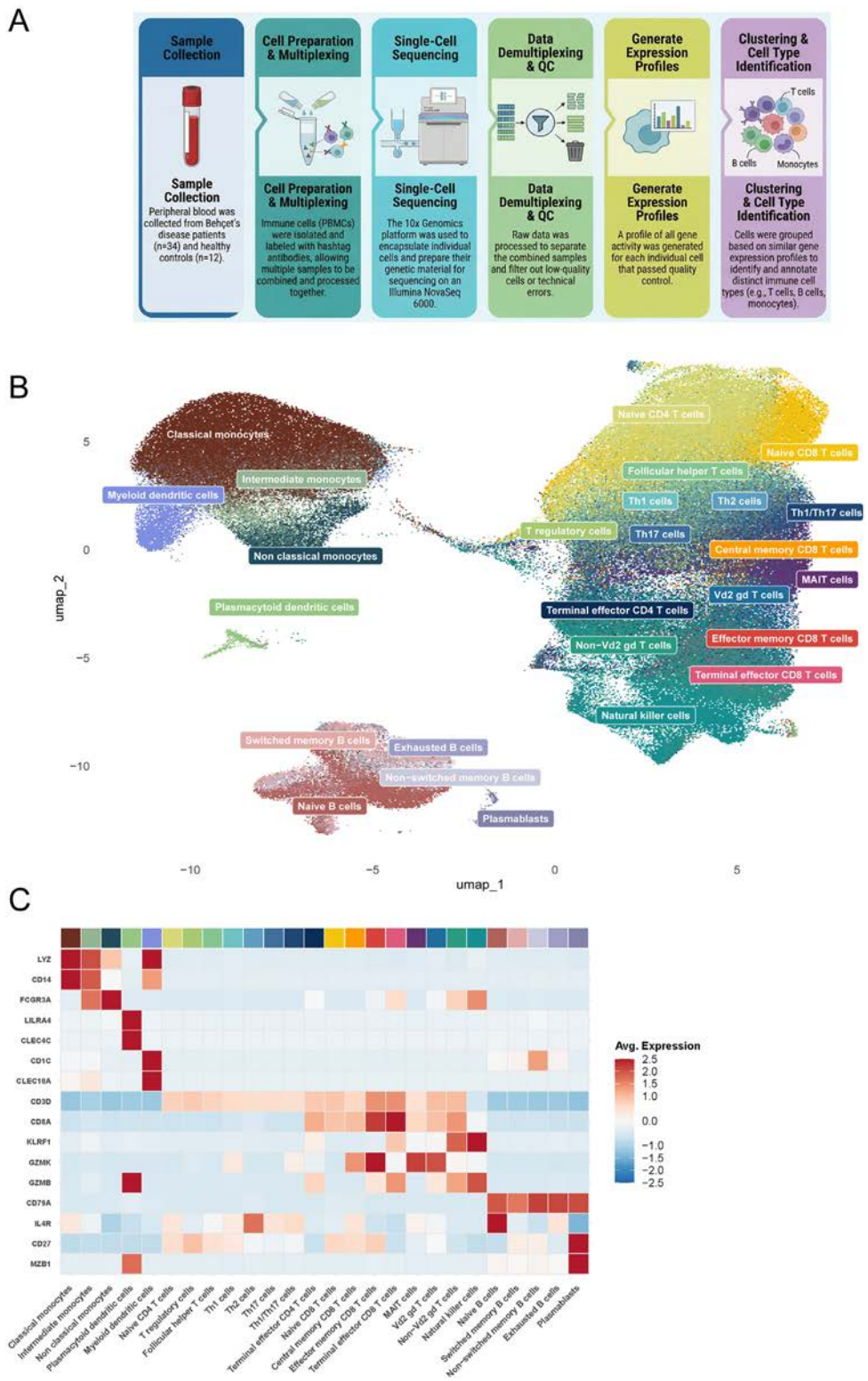

Figure 1. Study design and single-cell atlas of circulating immune cells in Behçet's disease (BD). (A) Overview of the study design. PBMCs were isolated from patients with BD and healthy controls, spanning active and remission disease states and distinct clinical phenotypes, and profiled by single-cell RNA sequencing followed by demultiplexing, quality control, and integration. (B) UMAP projection of 247,028 high-quality PBMCs coloured by annotated immune cell types, illustrating the overall cellular landscape and major compartments, including monocytes; plasmacytoid and myeloid dendritic cells; $CD4^+$ and $CD8^+$ T-cell subsets; natural killer (NK) cells; and B-cell subsets. (C) Heatmap of canonical marker genes demonstrating expression patterns that define each cluster and validate the annotation. PBMC, peripheral blood mononuclear cell; UMAP, uniform manifold approximation and projection; QC, quality control.

monocytes (1.64-fold, effect = 0.53, 95% CrI [0.22-0.83], FDR = 0.0018), followed by nonclassical monocytes (1.49-fold, effect = 0.44, 95% CrI [0.08-0.80], FDR = 0.0116), and a milder yet significant increase in intermediate monocytes (1.35-fold, effect = 0.34, 95% CrI [−0.01 to 0.67], FDR = 0.0447) (Fig 2C). Beyond monocytes, myeloid dendritic cells, and non-Vd2 $\gamma\delta$ T cells also displayed increased relative abundance, whereas naïve T cells, central memory $CD8^+$ T cells, and MAIT cells, as well as nonswitched memory B cells, exhibited decreased proportions in BD compared with healthy controls.

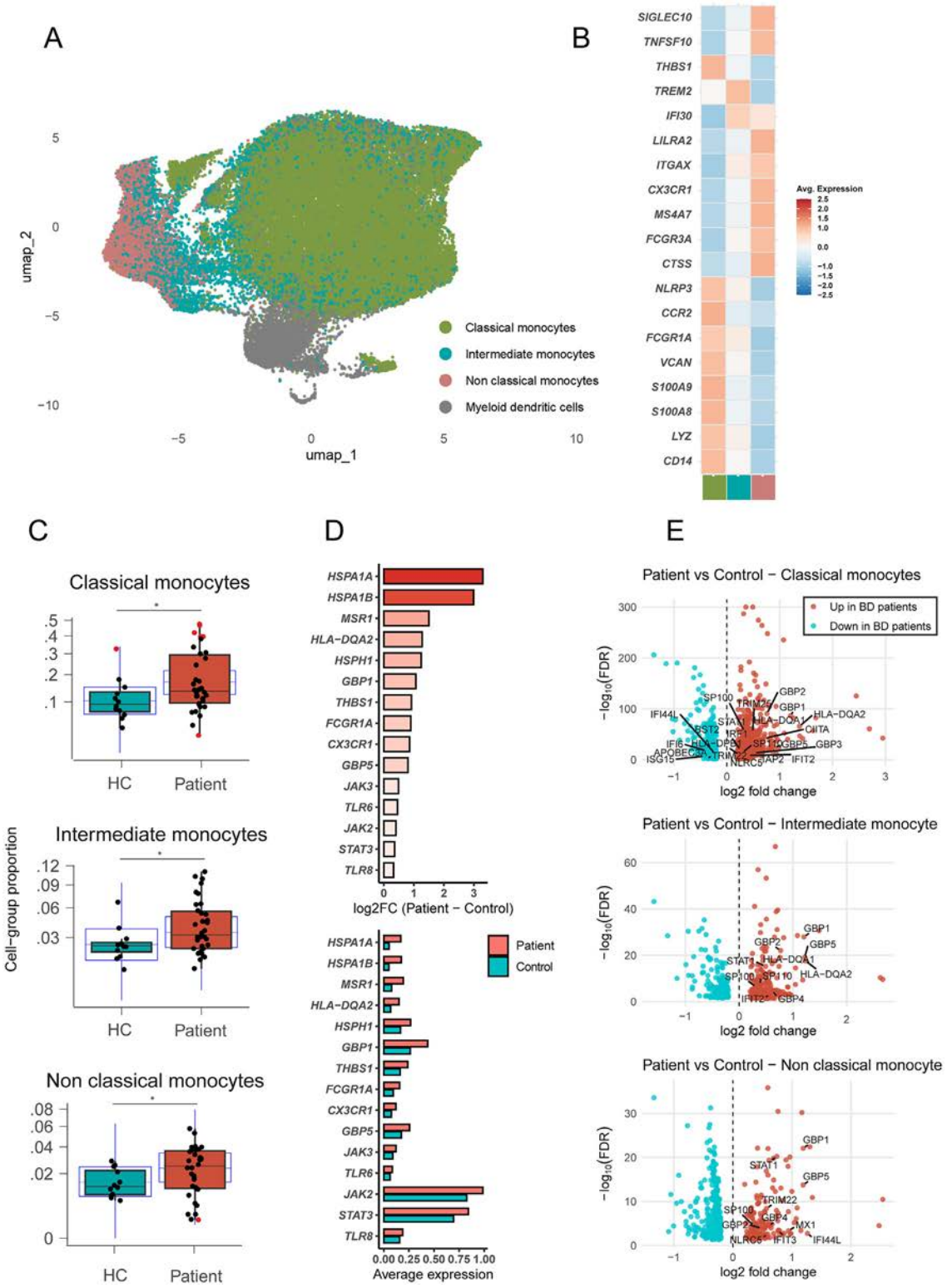

Figure 2. Monocyte subset heterogeneity and disease-associated transcriptional programmes in Behçet's disease (BD). (A) UMAP projection of the monocyte compartment, delineating 3 transcriptionally distinct subsets: classical, intermediate, and nonclassical monocytes. (B) Heatmap showing the top canonical marker genes defining each subset. (C) Cell-type composition analysis comparing the relative abundance of monocyte subsets between patients with BD and healthy controls (HCs), illustrating significant expansion across subsets in BD. (*) indicates an FDR-adjusted *P* value < .05. (D) Barplot showing the top upregulated DEGs in BD monocytes compared with HCs. The upper panel displays $\log_2$ fold-change values (patient −control). The lower panel shows the corresponding average expression levels in each group. (E) Volcano plots of DEGs comparing patients with BD vs HCs across monocyte subsets. Each point represents a gene, red indicating upregulation in BD and blue downregulation. The x-axis denotes the $\log_2$ fold-change, and the y-axis shows the $-\log_{10}$(FDR). Only genes passing the significance threshold (FDR < 0.05) are shown. Canonical type I and type II interferon−stimulated genes (eg, *GBP1, GBP2, GBP5, IFI27*, and *IFI44L*) together with other ISG-related markers are labelled. DEG, differentially expressed gene; FDR, false discovery rate; UMAP, uniform manifold approximation and projection.

These results highlight a coordinated expansion of the innate myeloid compartment alongside contraction of naïve T-cell pools, suggesting a systemic shift towards a proinflammatory immune landscape in BD (Supplementary Table S3, Supplementary Fig S2B).

To identify transcriptional alterations underlying the compositional changes in monocytes, we first examined DGE across the monocyte compartment. BD monocytes displayed top upregulated genes related to inflammatory and IFN-responsive programmes, including increased expression of canonical IFN −regulated genes (eg, *GBP1, GBP5,* and *FCGR1A*), stress-response genes (*HSPA1A, HSPA1B,* and *HSPH1)*, and immune-activation markers (*MSR1, HLA-DQA2, THBS1,* and *CX3CR1*) (Fig 2E, Supplementary Table S4). Pathway enrichment analysis further revealed broad regulation of IL-1 production and response to type II IFN signalling, pinpointing the participation of genes like *JAK2/3, STAT3*, and TLR gene family members (eg, *TLR6, TLR8*) (Supplementary Table S5).

We then analysed each monocyte subset independently. Nonclassical monocytes displayed transcriptional dysregulation characterised by upregulation of IFN-stimulated genes such as *GBP1−5, IFIT3, IFI44L, MX1,* or *STAT1* in BD compared with healthy controls (Fig 2D, Supplementary Table S6). Pathway enrichment analysis revealed overrepresentation of type II IFN response, cytokine-mediated signalling, and antigen processing and presentation as predominant biological processes (Supplementary Table S7).

Intermediate monocytes showed a similar pattern, with increased expression of *GBP1/5, MSR1, HLA-DQA1/2, SLAMF7*, and *GIMAP* family genes, together with enrichment of heat-shock proteins (HSP), immune activation, and response to IFN and interleukin pathways (Supplementary Tables S7 and S8). In classical monocytes, which constitute the majority of monocytes in BD, there was marked upregulation of type II IFN−regulated genes in patients compared with controls, and downregulation of genes associated with the type I IFN signature (*IFI44L, IFI6, BST2, APOBEC3A,* and *ISG15*) (Fig 2D, Supplementary Table S9). Conversely, classical and intermediate subsets displayed reduced expression of *PHLDA2, DHRS3*, and *TMEM* family genes, which function as regulators of cell stress signalling, metabolic homeostasis, and membrane trafficking (Supplementary Tables S8 and S9). Notably, several transcripts were consistently suppressed across all monocyte subsets, including *G0S2, ABTB2, CXXC5,* and *HBEGF*.

We further dissected the myeloid compartment into 11 transcriptionally distinct clusters to characterise disease-associated programmes (Supplementary Fig S3A). Among these, cluster 7 displayed a prominent C1Q-high signature (*C1QA* avg. $\log_2$FC = 8.449; *C1QB* = 6.387; *C1QC* = 8.531; Supplementary Table S10, Supplementary Fig S3B), along with higher *ISG15* and *ISG20*, which is consistent with a C1Q$^+$ IFN-stimulated nonclassical monocyte subset. This population, previously described in BD, represents a proinflammatory monocyte phenotype enriched in complement and type I/II IFN−response genes, and has been associated with disease activity and heightened innate immune activation [28,29]. However, in our dataset, this specific subset was slightly but not significantly expanded in BD compared with healthy controls (Supplementary Table S11).

Transcriptional reprogramming of monocytes differentiates active from remission BD

We next investigated molecular features distinguishing active (n = 27) from remission (n = 11) BD samples. Composition analysis revealed that all 3 monocyte subsets were significantly increased in frequency in active BD compared with healthy controls. The largest effect was observed in classical monocytes (effect = 0.62, 95% CrI = 0.33-0.92; FDR = 0.0005), corresponding to an ∼1.73-fold increase with respect to healthy controls. Nonclassical and intermediate monocytes were similarly expanded (nonclassical: 1.61-fold, effect = 0.55, CrI = 0.18-0.94, FDR = 0.0042; intermediate: 1.38-fold, effect = 0.41, CrI = 0.06-0.78; FDR = 0.0231) (Fig 3A; Supplementary Table S12, Supplementary Fig S4A). In contrast, remission BD showed a significant reduction in all 3 monocyte subsets compared with active disease, indicating restoration towards control-like composition after clinical improvement (Fig 3A; Supplementary Table S13, Supplementary Fig S4B).

To define the transcriptional basis of these compositional changes, we compared gene expression profiles between remission and active BD samples. Remission monocytes displayed a broad shift away from the highly proinflammatory active disease state (Fig 3B, Supplementary Table S14). Type II IFN−associated genes, including *GBP2*, *GBP5*, *TMEM176A/B*, *HLA-DQA2*, and *HRH2*, were markedly reduced in remission compared with active disease, indicating contraction of the IFN-γ−driven inflammatory programme. In contrast, canonical type I IFN −stimulated genes (*IFITM1*, *IFIT1*, *IFIT3*, *IFITM3*, *IFI44L*, *IFI6*, *APOBEC3A*, and *EMP1*) were overexpressed in remission compared with active BD, suggesting an enhanced type I IFN imprint in monocytes during clinical improvement (Fig 3B,C, Supplementary Fig S5, Supplementary Tables S15-S17). Remission was also characterised by the induction of a distinct set of recovery-associated transcripts. Genes including *SERPINA1*, *SERPINB8*, and *SERPINB9* were increased in total monocytes during disease remission, reflecting activation of protease-inhibitory and cytoprotective programmes that may contribute to tissue stabilisation (Fig 3B,C). In classical monocytes, *ADAMTS2* was upregulated, consistent with extracellular matrix remodelling and repair (Supplementary Table S15).

Consistent with these transcriptional changes, GO:BP pathway enrichment analyses revealed that classical and intermediate monocytes in active BD were dominated by type II IFN−driven inflammatory programmes as well as cytokine-mediated pathways when compared with remission BD, underscoring a shared inflammatory core. In contrast, nonclassical monocytes showed fewer and more heterogeneous pathways when comparing active vs remission BD, and lacked the prominent type II IFN and cytokine-response signatures observed in classical and intermediate subsets. Instead, remission nonclassical monocytes were enriched for terms related to pharmacological responses, including cellular response to glucocorticoids. A similar enrichment of glucocorticoid response pathways was observed in intermediate monocytes in remission (Fig 3D, Supplementary Table S18).

To gain additional insight into putative upstream regulators of disease activity−associated transcriptional programmes, we performed a transcription factor target enrichment analysis on differential expression signatures between remission and active monocyte subsets. This analysis revealed enrichment of IRF- and STAT-associated target programmes in genes overexpressed in active compared with remission BD in classical and intermediate monocytes, consistent with an IFN-skewed inflammatory state during active disease. In contrast, remission-associated signatures displayed a more heterogeneous enrichment pattern, including target sets related to NR3C1, NFE2L2, RELB/RELA, and SMAD family regulators, suggestive of more regulatory or stress-adaptive transcriptional states (Supplementary Fig S6, Supplementary Table S19).

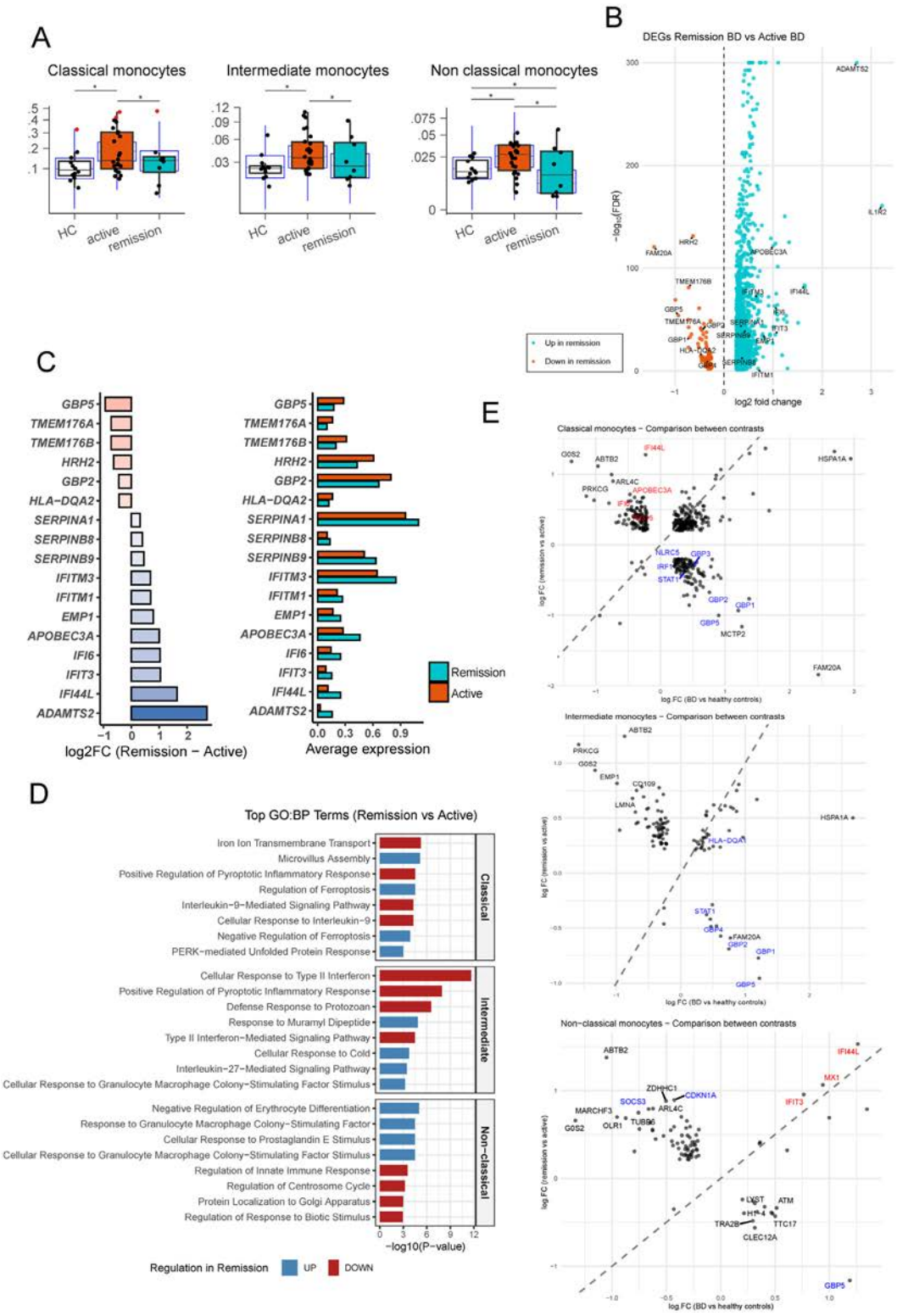

Figure 3. Monocyte subset remodelling across disease activity states in Behçet's disease (BD). (A) Compositional analysis comparing classical, intermediate, and nonclassical monocyte proportions among active BD, remission BD, and healthy controls (HCs). Active BD is characterised by expansion of all 3 subsets, which partially normalise during remission. (*) indicates an FDR-adjusted *P* value < .05. (B) Volcano plot of DEGs comparing remission vs active BD samples within all monocyte subsets. Each point represents a gene, with colour indicating direction of expression change: orange denotes downregulation in remission BD, and blue denotes upregulation. Only points (genes) with an FDR-adjusted *P* value <.05 are shown. (C) Differential expression summary of selected type I and II ISGs and SERPIN family members in remission vs active BD in total monocytes. The left panel presents the $\log_2$ fold-change for each gene, with bar colour and length indicating fold-change magnitude and direction (positive values reflecting higher expression in remission BD; negative values indicating higher expression in active BD). The right panel displays paired average expression values for active and remission samples. All genes showed an FDR-adjusted *P* value < .05. (D) Gene Ontology:Biological Process (GO:BP) analysis of the top 4 upregulated (blue) and downregulated (red) pathways comparing remission vs active BD across monocyte subsets. Significance is shown as $-\log_{10}$(*P* value). (E) Quadrant plots depicting $\log_2$ fold-change relationships between BD vs healthy control (x-axis) and remission vs active BD (y-axis) comparisons in monocyte subsets. DEG, differentially expressed gene; FDR, false discovery rate; ISG, interferon-stimulated gene.

To delineate how disease activity remodels monocyte states in BD, we performed a reversal-gene analysis by jointly contrasting BD cases vs healthy controls and active vs remission BD for each monocyte subset. This 2-dimensional framework identifies genes whose regulation across disease activity opposes their case–control behaviour, highlighting transcriptional programmes that invert with clinical improvement (Fig 3E). Classical monocytes displayed 2 major reversal patterns. Genes in the lower-right quadrant were upregulated in BD compared with healthy controls and downregulated in remission, representing inflammatory programmes that reverse as disease activity resolves. Among the top features, *GBP1, GBP2, GBP3, GBP5*, and *HLA-DQA2* exhibited strong reversal, along with *FAM20A* and *MCTP2*. Together with other ISGs, such as *STAT1, NLRC5*, or *IRF1*, these findings suggest that type II IFN signalling, antigen presentation, and vesicular trafficking dominate the active inflammatory signature in classical monocytes that normalises upon remission. On the other hand, upper-left quadrant genes were downregulated in BD but increased in remission, indicative of recovery of homeostatic and regulatory pathways. Top genes in this quadrant included *G0S2, ABTB2, PRKCG, and ARL4C*, reflecting reactivation of metabolic control, cytoskeletal organisation, and signalling balance lost during inflammation. Importantly, type I IFN–regulated genes, including *APOBEC3A, ISG15, IFI6,* and *IFI44L*, were also downregulated in patients vs controls that became upregulated upon disease remission (Fig 3E, Supplementary Table S20).

Nonclassical monocytes revealed a similar but functionally distinct pattern. Genes in the lower-right quadrant (*GBP5, CLEC12A, H1-4, ATM, TTC17, TRA2B,* and *LYST*) were elevated in BD and downregulated in disease remission. In contrast, genes, including *ABTB2, G0S2, SOCS3, ARL4C, ZDHHC1, MARCHF3,* and *OLR1*, were downregulated in BD but rebounded in remission, whereas the type I IFN markers *IFIT3, MX1,* and *IFI44L* remained out of the reversal genes. These results reflect restoration of regulatory and metabolic programmes in disease remission in nonclassical monocytes, notably JAK–STAT negative feedback (*SOCS3*), lipid metabolism (*G0S2*), and cytoskeletal–adhesion reorganisation (*ARL4C* and *TUBB6*) (Fig 3E, Supplementary Table S21). Intermediate monocytes exhibited a reversal signature in type II IFN–regulated genes similar to classical monocytes, along with a rebound in genes including *G0S2, ABTB2, PRKCG,* and *HSPA1A* upon disease remission (Fig 3E, Supplementary Table S22).

As a donor-level validation of the active vs remission BD comparisons, we performed pseudobulk differential expression analyses in each monocyte subset by aggregating raw RNA counts per donor. Comparison of pseudobulk and cell-level $\log_2$FC estimates demonstrated concordance with cell-level data across monocyte subsets (Supplementary Fig S7). These analyses indicate that the principal transcriptional patterns described in the single-cell analysis are broadly preserved at the donor level.

Longitudinal paired analysis reveals partial normalisation of IFN-driven inflammation after treatment

Among our BD cohort, 4 active patients were resampled in remission after therapy, enabling within-subject (paired) evaluation (Supplementary Tables S23-S25). For classical monocytes, some of the top differentially expressed gene upregulated genes pretreatment, *TMEM176A, TMEM176B, MCTP2,* and *FAM20A*, overlapped with those identified in the full active-versus-remission cohort. A similar trend was also observed in intermediate monocytes. GO:BP enrichment in classical monocytes emphasised bioenergetic/mitochondrial up-shift (eg, *oxidative phosphorylation, electron transport chain, and adenosine triphosphate synthesis*), with concurrent upregulation in type II IFN response and cytokine regulation pretreatment compared with posttreatment in the same patients (Supplementary Table S26). In intermediate monocytes, top pretreatment GO:BP terms when compared with posttreatment samples reflect a strong IFN-γ–induced antigen-presentation signature, coupled with activation of monocyte/macrophage differentiation programmes and concurrent regulatory pathways that modulate T-cell responses and inflammatory magnitude (Supplementary Table S26). In nonclassical monocytes, only 2 upregulated genes, *FMNL2* and *FCGR3A,* reached significance when comparing paired pretreatment to posttreatment samples. These paired pre-/posttreatment samples showed moderate concordance with the full active-remission analysis across monocyte subsets, with consistent overall directionality (Supplementary Fig S8).

Clinical phenotypes exhibit distinct immune signatures and intercellular communication patterns

To dissect clinical heterogeneity, we compared patients with vascular, ocular, and mucocutaneous disease-only subsets. We detected distinct distribution patterns among classical, intermediate, and nonclassical monocytes (Fig 4A, Supplementary Table S27).

In classical monocytes, patients with vascular involvement showed a significant increase in proportion compared with healthy controls (1.86-fold, effect = 0.59 [95% CrI 0.27-0.91], FDR = 0.0045), whereas mucocutaneous BD displayed a milder but still notable expansion (1.42-fold, effect = 0.39 [0.12-0.68], FDR = 0.0485). Cases with ocular BD exhibited a trend towards higher abundance (1.14-fold, effect = 0.40 [−0.09 to 0.91]), though not statistically significant (FDR = 0.083). In contrast, intermediate monocytes showed no significant compositional shifts across phenotypes, with a similar expanded trend in mucocutaneous BD (1.48-fold, effect = 0.44 [−0.08 to 0.79], FDR = 0.063). Finally, nonclassical monocytes demonstrated a marked increase in mucocutaneous BD (1.7-fold, effect = 0.56 [0.19-0.93], FDR = 0.023) but no significant change in vascular (1.18-fold, effect = 0.11 [−0.34 to 0.57], FDR = 0.34) or ocular BD (1.77-fold decrease, effect = −0.28 [−0.88 to 0.31], FDR = 0.20).

We next sought to identify phenotype-specific transcriptional programmes across vascular, ocular, and mucocutaneous involvements. Pairwise differential expression analyses were performed within each cell type to pinpoint genes upregulated in one phenotype relative to the other 2. To ensure these genes reflect features unique to that phenotype in disease, we then required that they also be upregulated in that phenotype compared with healthy controls. This 2-step approach isolated a set of *phenotype-specific, disease-associated signatures* while excluding genes that are common to all cases with BD (Fig 4B). Distinct inflammatory modules were observed. Mucocutaneous BD was characterised by broad upregulation of IFN-stimulated genes (*IFITM1, IFITM2, IFI44, GBP1, GBP4, GBP5, STAT1,* and *STAT2*) across classical, intermediate, and nonclassical monocytes. In contrast, vascular BD, particularly in nonclassical monocytes, showed strong enrichment for heat-shock and stress-response genes (*HSPA1A, HSPA1B, HSP90AA1, HSPH1,* and *HSPD1*), consistent with heightened cellular stress and protein-folding demand under inflammatory or oxidative conditions. Meanwhile, ocular BD displayed prominent expression of TNF/NF-κB–associated cytokines and receptors, including *IL1B, CXCL8,*

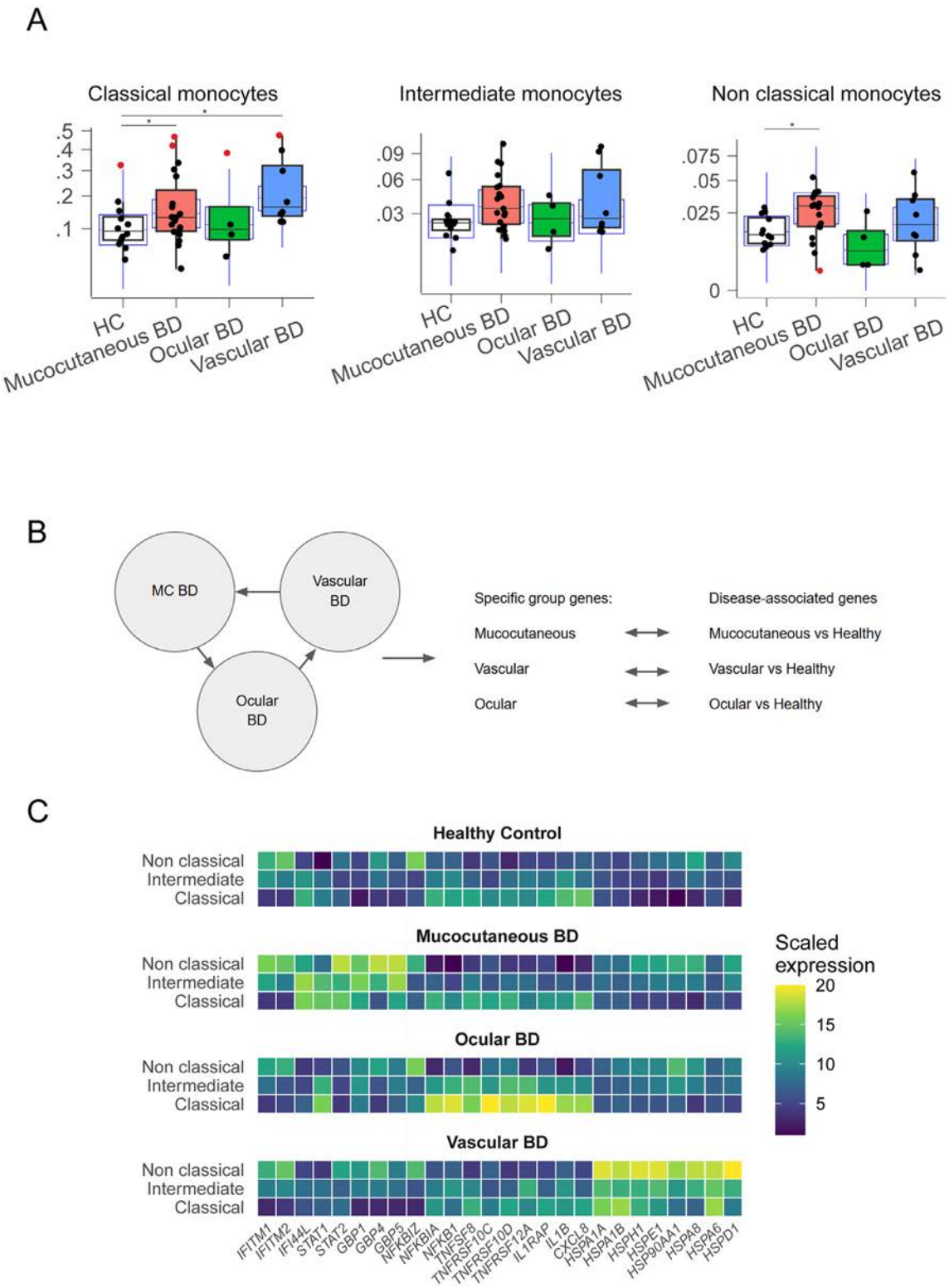

Figure 4. Monocyte compositional and transcriptional diversity across Behçet's disease (BD) clinical phenotypes. (A) Compositional analysis comparing the relative abundance of classical, intermediate, and nonclassical monocytes among BD phenotypes—mucocutaneous, ocular, and vascular—vs healthy controls (HC). Distinct patterns of subset expansion are observed across phenotypes. (*) indicates an FDR-adjusted *P* value < .05. (B) Schematic overview of the 2-step filtering strategy used to define transcriptional signatures unique to each BD phenotype. In the first step, pairwise differential expression analyses were performed among BD phenotypes (mucocutaneous, vascular, and ocular) to identify genes upregulated in each phenotype relative to the other 2. In the second step, these upregulated genes were intersected with those upregulated in the same phenotype vs healthy controls, yielding phenotype-specific, disease-associated gene sets. (C) Tile plots illustrating phenotype-specific transcriptional programmes within each monocyte subset. Interferon-stimulated genes (eg *IFI44, IFITM1/2*, and *GBP1/4/5*), NF-κB and TNF signalling mediators (*NFKB1, TNFRSF10A/D*, and *IL1B*), and stress-response genes (*HSPA1A/B*, and *HSP90AA1*) reveal differential expression signatures across phenotypes, highlighting subset-specific immune programmes. FDR, false discovery rate; TNF, tumour necrosis factor; NF-κB, nuclear factor kappa-light-chain-enhancer of activated B cells.

NFKB1, NFKBIA, NFKBIZ, and *TNFRSF10C/D* (Fig 4C, Supplementary Table S28). These polarised transcriptional programmes were most evident in monocytes but were also partly mirrored in other immune populations (Supplementary Table S28), suggesting that phenotype-specific inflammatory signatures (IFN signalling in mucocutaneous BD, stress-response activation in vascular BD, and TNF/NF-κB–mediated inflammation in ocular BD) extend beyond the myeloid compartment and may underlie the divergent clinical manifestations of the disease.

DISCUSSION

Our study provides a comprehensive single-cell view of circulating immunity in BD across activity states and clinical phenotypes. By profiling 247,028 PBMCs from 34 patients with BD and 12 healthy controls, we delineate a robust atlas in which the monocyte compartment emerges as the principal locus of dysregulation. Compositionally, our data support coordinated expansion of monocyte subsets in BD, while transcriptionally, we resolve subset-specific programmes that differentiate active disease from remission and vary across vascular, ocular, and mucocutaneous phenotypes. Together, these data refine current models of BD pathogenesis by linking clinical heterogeneity to discrete myeloid activation states, and suggest that phenotype-specific targeting of innate pathways may better align with the underlying cellular biology. Although our dataset captured all major PBMC compartments and identified compositional changes beyond monocytes, a comprehensive transcriptional dissection of all 26 annotated immune subsets was beyond the scope of this study; instead, we focused mechanistic interpretation on monocytes as they showed the strongest and most coherent disease-associated expansion and transcriptional remodelling.

BD is increasingly recognised as a monocyte/macrophage–driven vasculitis, with circulating monocytes showing M1-skewed activation, enhanced TLR expression, and elevated production of TNF-α, IL-6, and IL-1 family cytokines [7]. Previous studies have reported an imbalance of CD14/CD16-defined subsets characterised by expansion of intermediate monocytes and contraction of nonclassical monocytes [30], a pattern interpreted as enhanced recruitment of $CD16^+$ monocytes to inflamed tissues. In this context, our findings of an overall expansion of circulating monocytes in BD, driven by significant increases in all subsets compared with healthy controls, indicate that the entire compartment is numerically amplified in BD rather than a single subset being selectively depleted. Although partially divergent from previous reports, these findings still fit within a broader model where monocyte dysregulation and activation are key to BD pathogenesis. In addition, the even stronger expansion of all 3 subsets in active disease and their partial normalisation in remission mirror prior observations of monocyte frequencies declining with effective therapy [28].

Prior transcriptomic and single-cell studies have converged on a prominent type II IFN imprint in BD monocytes. Bulk and tissue-level analyses show that differentially expressed genes in BD are enriched for IFN-γ–response pathways, with upregulation of CXCR3 ligands (*CXCL9* and *CXCL10*) and guanylate-binding proteins (*GBP4* and *GBP5*) [29]. Single-cell profiling of PBMCs further identified an expanded $CD14^+$ $C1Q^{hi}$ monocyte population driven by IFN-γ–JAK–STAT signalling and reversible with tofacitinib, directly linking IFN-γ–dependent monocyte programmes to hyperinflammation *in vivo* [28]. In parallel, functional work has shown that BD monocytes display dysregulated posttranscriptional control of CXCL10, leading to exaggerated secretion of this IFN-γ–inducible chemokine and thereby amplifying Th1-cell recruitment upon IFN-γ stimulation [31]. Together, these studies support a model in which IFN-γ positions monocytes at the core of BD immunopathology, reprogramming them into antigen-presenting, chemokine-producing effectors that sustain Th1-skewed, vasculitic inflammation.

In this context, our data extend previous work by showing how this IFN-γ activation is extended to the broader monocyte compartment. As a whole, BD monocytes upregulated canonical type II IFN and inflammatory genes (eg, *GBP1/5, JAK2/3, FCGR1A, HLA-DQA1/2,* and *CX3CR1*) compared with healthy controls, with enrichment of IL-1 production, and response to type II IFN, indicating that IFN-γ shapes both effector function (phagocytosis and Fc receptor signalling) and tissue-interacting properties (adhesion and chemotaxis). Across classical, intermediate, and nonclassical subsets, we observed consistent induction of IFN-γ–responsive modules, whereas classical monocytes showed a broader type II IFN signature coupled to downregulation of some canonical type I ISGs. In line with prior data, our findings point towards a ubiquitous type II IFN signature across classical, intermediate, and nonclassical monocytes that amplifies IL-1 and JAK–STAT–dependent inflammation and sustains the hyperinflammatory milieu characteristic of BD.

The role of type I IFN in BD, however, appears to be more complex and context-dependent. Exogenous IFN-α has well-established therapeutic efficacy in BD, where it can dampen pathogenic Th17 responses and promote regulatory circuits [32–34]. In this sense, we observed that classical monocytes, which dominate the circulating monocyte pool, showed a clear skewing towards a type II IFN programme in BD, with marked upregulation of IFN-γ–regulated genes and concomitant downregulation of canonical type I ISGs (*IFI44L, IFI6, BST2, APOBEC3A,* and *ISG15)*. By contrast, nonclassical and intermediate monocytes upregulated a more restricted set of ISG-family genes often labelled as type I responsive (such as *IFI44L, IFIT3, IFI16* in nonclassicals and *IFI16, IFIT2* in intermediates) in BD vs controls. This pattern reflects that BD is not a type I interferonopathy in circulating monocytes but rather an IFN-γ/IL-1–dominated activation state in classical monocytes, with selective type I ISG induction in $CD16^+$ subsets (intermediate and nonclassical). Consistent with this idea, we identified a $C1Q^{hi}$/$ISG15^{hi}$ monocyte cluster (Supplementary Table S10) that closely matches the $C1Q^{hi}$ and $ISG15^+$ monocytes described in previous studies, where BD skin lesions show expansion of $ISG15^{hi}$ monocytes with strong expression of ISG15 and other ISGs such as IFI44L together with C1Q genes, consistent with IFN-like stimulation within inflamed lesions [29]. However, the relative abundance of this subset was only modestly increased in BD and did not reach statistical significance in our cohort. Thus, its degree of expansion may vary depending on various factors such as cohort composition, disease spectrum, or technical differences and should therefore be interpreted cautiously. A recent single-cell transcriptomic study further demonstrated mobilisation of inflammatory $C1Q^{hi}$ monocytes in BD blood and their accumulation as $C1Q^+$ and $ISG15^+$ monocytes within the skin, underscoring a direct contribution of activated monocyte subsets to tissue inflammation [28].

Notably, many of the ISGs induced in nonclassical and intermediate monocytes are shared targets of both type I and type II IFNs and can also be driven by other inflammatory factors, particularly in patrolling cells engaged in antiviral and endothelial surveillance [35]. In this sense, an unexpected finding was the differential behaviour of some type I vs type II IFN genes across

disease activity. Although IFN-γ–associated signatures (*GBP1/5, FCGR1A, CCL4, IL15RA,* and *TMEM176A/B*) showed marked reduction in patients with remission BD, previously mentioned type I ISGs (*ABTB2, ISG15, IFI6, IFI44L,* and *APOBEC3A*) remained elevated or were even more prominent in remission monocytes. This decoupling explains how current therapies may effectively suppress the most defined IFN-γ–driven inflammatory circuits while leaving behind a persistent type I IFN imprint.

When examined, clinical activity at subset level revealed that IFN modules likewise did not behave uniformly across disease states. In active BD, monocytes were dominated by a type II IFN–driven programme, with strong induction of GBP genes and antigen-presentation pathways. By contrast, in remission, these GBP-associated, IFN-γ–linked signatures declined, whereas canonical type I ISGs (eg, *IFI44L, IFI6, IFIT3, IFITM1/2/3,* and *APOBEC3A*) were consistently upregulated across all monocyte subsets and particularly in classical monocytes. Together with the observation that this canonical type I ISG module is selectively downregulated in BD vs controls in classical monocytes, the re-emergence of type I ISG expression in remission is consistent with a shift in the IFN landscape away from the dominant IFN-γ–skewed inflammatory programme observed in active disease. However, without additional functional studies, these data do not establish whether this remission-associated type I IFN signature is protective, treatment-related, or otherwise context-dependent. These data support previous literature, where Th1/Th17 cytokines (IFN-γ, IL-12, IL-23, and IL-17) are repeatedly implicated as pathogenic in BD [36]. The recovery of *APOBEC3A* in classical monocytes, a type I ISG recently shown to limit STAT1-dependent ISG expression, is consistent with re-establishment of a feedback-regulated type I IFN network in remission rather than ongoing uncontrolled IFN activation [37]. Similarly, *SOCS3*, a JAK–STAT feedback inhibitor [38], was decreased in intermediate and nonclassical monocytes from patients with BD yet selectively increased in remission in nonclassicals, consistent with re-engagement of negative-feedback circuits that restrain IL-6–family and IFN signalling in this patrolling subset. Such *SOCS3* induction in remission BD would be expected to limit residual type I and II IFN signals, potentially protecting against relapse of Th1/Th17-driven inflammation, while also raising the possibility that homeostatic type I IFN–mediated antiviral and endothelial-surveillance programmes are attenuated in nonclassical monocytes. Although exploratory, these signals raise the possibility that disrupted negative regulators contribute to the reshaped IFN landscape in BD and ask for a functional follow-up. Transcription factor target enrichment analysis of differential expression signatures further supported an IRF/STAT–centred inflammatory regulatory landscape in active BD monocytes, particularly in the classical and intermediate subsets. In contrast, remission-associated signatures showed a more heterogeneous enrichment pattern, including regulators linked to glucocorticoid response, oxidative stress adaptation, and broader regulatory programmes, consistent with a less inflammatory transcriptional state.

Based on our data, monocyte activation in active BD is dominated by a type II IFN– and IL-1–skewed programme, marked by GBP and human leukocyte antigen (HLA) upregulation, whereas canonical type I IFN–stimulated genes are relatively attenuated in this state and rebound in remission. Thus, this pattern supports therapeutic strategies like ustekinumab and JAK inhibitors that dampen IFN-γ/IL-12/23–JAK–STAT signalling [39,40]. By contrast, the partial re-emergence of a canonical type I ISG module in remission, together with prior clinical experience showing efficacy of IFN-α in refractory Behçet uveitis [41], is consistent with the notion that type I IFN can exert net immunomodulatory rather than pathogenic effects in BD. Definitive conclusions regarding type I IFN agonism vs antagonism, however, will require dedicated mechanistic studies. The remission-associated increase in canonical type I IFN–related transcripts should be interpreted cautiously, as remission samples were obtained after treatment initiation and may therefore reflect a combination of disease quiescence and therapy-induced transcriptional remodelling rather than a purely intrinsic IFN–mediated protective state.

In addition, remission BD monocytes were also characterised by a SERPIN-enriched, tissue-preserving programme. The observed increase in *SERPINB2, SERPINB9*, and *SERPINA1* expression suggests that remission in BD involves more than simple suppression of inflammation. SERPINB2 (plasminogen activator inhibitor type 2) has been implicated in the regulation of fibrinolytic pathways and pericellular proteolysis, whereas *SERPINA1* encodes α-1 antitrypsin, a major antiprotease with anti-inflammatory and tissue-protective functions, and SERPINB9 (protease inhibitor 9) protects cells from granzyme B-mediated apoptosis, conferring resistance to NK and $CD8^+$ T-cell cytotoxicity [42]. Previous studies have reported abnormalities in fibrinolytic regulation and plasminogen-activation pathways in BD, including altered tissue-type plasminogen activator/ plasminogen activator inhibitor-1–related parameters and impaired fibrinolytic activity, with some studies linking these changes to vascular manifestations or thrombosis [43,44]. In this context, the SERPIN-enriched remission programme observed here may reflect a broader protease-regulatory state relevant to vascular stabilisation and restoration of immune homeostasis, although this interpretation remains hypothetical. An exploratory analysis comparing SERPIN family gene expression in vascular BD to other BD subsets did not reveal significant differences (Supplementary Fig S9).

By looking at the phenotype distribution of cells, the expansion of circulating monocytes observed in patients with BD compared with controls was largely driven by the mucocutaneous and vascular phenotypes, where classical and nonclassical subsets, showed the most pronounced increases. In contrast, intermediate monocytes exhibited a more uniform distribution across phenotypes, suggesting a less disease-specific modulation. Interestingly, ocular BD showed a trend towards reduced monocyte abundance, which, although not statistically significant, could reflect compartmentalisation of these cells to inflamed ocular tissues, as previously described in uveitis [45,46]. Such tissue recruitment may deplete circulating monocytes while contributing to local myeloid activation within the eye, consistent with the highly localised inflammatory pattern characteristic of ocular BD.

The HSP-enriched programme we observe in nonclassical monocytes from vascular BD is biologically coherent with stress-induced endothelial HSP expression acting as danger signals via TLR2/4, amplifying myeloid activation and leukocyte–endothelial interactions [47]. HSPs have been recognised as important drivers of inflammation in BD, particularly in monocytes, where they can act as an autoantigen linking microbial triggers to autoreactive T-cell responses and also induce cytokine production via TLR signalling [7]. Patients with BD show elevated serum levels of HSP60 and HSP70 families [48], and HSP60-reactive T cells are thought to contribute to vasculitis and endothelial injury [49]. This further supports a model in which HSP-driven immune activation participates in vascular inflammation and thrombotic events.

Consistent with this literature, our data identify *HSPA1A* and *HSPA1B* (HSP70 family) among the top differentially expressed genes in BD monocytes, and reveal a phenotype-specific HSP70 transcriptional signature in patients with vascular BD, involving multiple HSP family members (*HSPA1A/B, HSPA8, HSPH1,* and *HSPE1*). This vascular-skewed HSP70 programme, to our knowledge, not previously reported in BD, suggests that monocytes from patients with vascular BD engage a heightened stress-response/chaperone network, potentially reflecting chronic exposure to inflammatory and endothelial stress signals along the vasculature.

In line with prior work demonstrating constitutive NF-κB activation and M1-skewed monocyte/macrophage polarisation in BD, our ocular BD subgroup showed a classical-monocyte programme heavily wired into the TNF/IL-1/NF-κB axis (Fig 4C). Specifically, upregulation of *NFKB1* together with the feedback inhibitor *NFKBIA* is consistent with chronic NF-κB engagement previously described in BD phagocytes and T cells, supporting persistent inflammatory signalling and apoptosis resistance [50,51]. Concurrent overexpression of TNF superfamily members and receptors (ie, *TNFSF8, TNFRSF10C/D,* and *TNFRSF12A*) suggests that classical monocytes in ocular BD are equipped to resist death signals and participate in vascular inflammation and remodelling [36,52,53]. The concomitant induction of *IL1B*, the IL-1 coreceptor *IL1RAP*, and the neutrophil-attracting chemokine *CXCL8* further supports an IL-1−NF-κB−neutrophil loop that mirrors the high intraocular levels of TNF-α, IL-6, and IL-8 reported in BD uveitis [54]. In light of these data, ocular BD classical monocytes might be circulating effectors of a TNF/IL-1/NF-κB−dominated programme that can sustain neutrophil-rich retinal vasculitis, providing a mechanistic substrate for the previously documented efficacy of TNF-α blockade with infliximab or adalimumab in achieving rapid and sustained control of BD-associated uveitis [41,55,56]. Together, these results indicate that different clinical manifestations of BD may arise from distinct but overlapping myeloid activation states, emphasising the importance of considering disease phenotypes when targeting innate immune pathways therapeutically.

This study has some limitations that should be considered when interpreting the findings. First, although the total number of cells analysed was large and enabled high-resolution characterisation of immune heterogeneity in BD, the number of patients within individual clinical subgroups remained modest, particularly for the phenotype-stratified analyses of vascular, ocular, and mucocutaneous disease. As a result, phenotype-specific transcriptional signatures should be interpreted with caution, and these findings are best considered exploratory and hypothesis-generating until validated in larger independent cohorts. In addition, because the analyses were conducted in PBMCs, the results may not fully represent the immunological alterations occurring within affected tissues, such as vascular or ocular lesions, where key pathogenic mechanisms of BD likely take place. Therefore, phenotype-associated circulating signatures should not be interpreted as direct surrogates of tissue-level pathology and will require validation in tissue-based or spatially resolved studies. It is important to note that remission samples were collected after systemic therapy, whereas active patients were treatment-naïve. Therefore, the observed transcriptional differences likely reflect a combination of clinical disease improvement and direct treatment effects, which cannot be fully disentangled in the current study. Finally, the study is based primarily on transcriptional data, and functional validation at the protein level or through mechanistic assays will be necessary to confirm the biological relevance of the identified genes and pathways.

CONCLUSION

In summary, by generating a comprehensive single-cell atlas of PBMCs from patients with active and remission BD and healthy controls, we provide a robust transcriptomic characterisation of immune cell alterations in BD. Resolving cell-type−specific and subset-specific transcriptional programmes highlights the central role of the monocyte compartment in this vasculitis, reveals phenotype-linked myeloid states and activity-dependent plasticity, and identifies pathways likely involved in disease activity and immune dysregulation. The inclusion of clinically defined subgroups and data integration strengthens the robustness and generalisability of these findings and yields a reference resource for future studies of treatment-specific immune mechanisms in BD. Finally, the identification of reversal genes across monocyte subsets supports a model of dynamic regulatory rebalancing and suggests phenotype-aware biomarkers and therapeutic targets, motivating protein level and tissue-based follow-up to test whether these signatures underlie clinical heterogeneity and treatment response.

Competing interests

The authors declare no conflict of interest.

Contributors

EC contributed to experimental design, participated in sample processing, performed analyses, and wrote the manuscript. RD collected and processed the samples and clinical data. CB contributed to patient recruitment and sample collection. HD and AG contributed to study design, patient recruitment, and sample collection. AHS supervised the study, and contributed to study design, methodology, data interpretation, and manuscript preperation. All authors discussed the results, reviewed, and approved the final version of the manuscript.

Patient consent for publication

All participants provided written infromed consent.

Ethics approval

The study was approved by the Marmara University Clinical Research Ethics Committee (approval no: 09.2021.52) and the Institutional Review Board of the University of Pittsburgh.

Provenance and peer review

Not commissioned; externally peer reviewed.

Supplementary materials

Supplementary material associated with this article can be found in the online version at doi:10.1016/j.ard.2026.06.033.

Orcid

Amr H. Sawalha: http://orcid.org/0000-0002-3884-962X

REFERENCES

[1] Yazici Y, Hatemi G, Bodaghi B, Cheon JH, Suzuki N, Ambrose N, et al. Behçet syndrome. Nat Rev Dis Primers 2021;7:67.
[2] Emmi G, Bettiol A, Hatemi G, Prisco D. Behçet's syndrome. Lancet 2024;403:1093–108.
[3] Bettiol A, Hatemi G, Vannozzi L, Barilaro A, Prisco D, Emmi G. Treating the different phenotypes of behçet's syndrome. Front Immunol. 2019;10: 2830.
[4] Talarico R, Di Cianni F, Sulis A, Marinello D, Lorenzoni V, Mosca M. Assessing disease phenotypes in Behçet's syndrome: insights from a multiple correspondence analysis. Front Immunol. 2025;16:1605714.
[5] Mege JL, Dilsen N, Sanguedolce V, Gul A, Bongrand P, Roux H, et al. Overproduction of monocyte derived tumor necrosis factor alpha, interleukin (IL) 6, IL-8 and increased neutrophil superoxide generation in Behcet's disease. A comparative study with familial Mediterranean fever and healthy subjects. J Rheumatol. 1993;20:1544–9.
[6] Perazzio SF, Andrade LEC, de Souza AWS. Understanding Behçet's disease in the context of innate immunity activation. Front Immunol. 2020; 11:586558.
[7] Hirahara L, Takase-Minegishi K, Kirino Y, Iizuka-Iribe Y, Soejima Y, Yoshimi R, et al. The roles of monocytes and macrophages in Behçet's disease with focus on M1 and M2 polarization. Front Immunol. 2022;13:852297.
[8] Guilliams M, Mildner A, Yona S. Developmental and functional heterogeneity of monocytes. Immunity 2018;49:595–613.
[9] Patel AA, Ginhoux F, Yona S. Monocytes, macrophages, dendritic cells and neutrophils: an update on lifespan kinetics in health and disease. Immunology 2021;163:250–61.
[10] Gholijani N, Ataollahi MR, Samiei A, Aflaki E, Shenavandeh S, Kamali-Sarvestani E. An elevated pro-inflammatory cytokines profile in Behcet's disease: a multiplex analysis. Immunol Lett. 2017;186:46–51.
[11] Lopalco G, Lucherini OM, Vitale A, Talarico R, Lopalco A, Galeazzi M, et al. Putative role of serum amyloid-A and proinflammatory cytokines as biomarkers for Behcet's disease. Medicine (Baltimore). 2015;94:e1858.
[12] Ziegler-Heitbrock L, Ancuta P, Crowe S, Dalod M, Grau V, Hart DN, et al. Nomenclature of monocytes and dendritic cells in blood. Blood. 2010;116: e74–80.
[13] Wong KL, Tai JJ-Y, Wong W-C, Han H, Sem X, Yeap W-H, et al. Gene expression profiling reveals the defining features of the classical, intermediate, and nonclassical human monocyte subsets. Blood. 2011;118:e16–31.
[14] Papalexi E, Satija R. Single-cell RNA sequencing to explore immune cell heterogeneity. Nat Rev Immunol. 2018;18:35–45.
[15] Nehar-Belaid D, Hong S, Marches R, Chen G, Bolisetty M, Baisch J, et al. Mapping systemic lupus erythematosus heterogeneity at the single-cell level. Nat Immunol. 2020;21:1094–106.
[16] Nishide M, Nishimura K, Matsushita H, Edahiro R, Inukai S, Shimagami H, et al. Single-cell multi-omics analysis identifies two distinct phenotypes of newly-onset microscopic polyangiitis. Nat Commun. 2023;14:5789.
[17] Villanueva-Martin G, Acosta-Herrera M, Carmona EG, Kerick M, Ortego-Centeno N, Callejas-Rubio JL, et al. Non-classical circulating monocytes expressing high levels of microsomal prostaglandin E2 synthase-1 tag an aberrant IFN-response in systemic sclerosis. J Autoimmun. 2023;140:103097.
[18] Wu X, Liu Y, Jin S, Wang M, Jiao Y, Yang B, et al. Single-cell sequencing of immune cells from anticitrullinated peptide antibody positive and negative rheumatoid arthritis. Nat Commun. 2021;12:4977.
[19] Criteria for diagnosis of Behcet's disease International Study Group for Behcet's Disease Lancet. 1990;335:1078–80.
[20] Stoeckius M, Zheng S, Houck-Loomis B, Hao S, Yeung BZ, Mauck WM, et al. Cell Hashing with barcoded antibodies enables multiplexing and doublet detection for single cell genomics. Genome Biol. 2018;19:224.
[21] Hao Y, Stuart T, Kowalski MH, Choudhary S, Hoffman P, Hartman A, et al. Dictionary learning for integrative, multimodal and scalable single-cell analysis. Nat Biotechnol. 2023;42:293–304.
[22] McGinnis CS, Murrow LM, Gartner ZJ. DoubletFinder: doublet detection in single-cell RNA sequencing data using artificial nearest neighbors. Cell Syst. 2019;8 329-7.e4.
[23] Choudhary S, Satija R. Comparison and evaluation of statistical error models for scRNA-seq. Genome Biol. 2022;23:27.
[24] Aran D, Looney AP, Liu L, Wu E, Fong V, Hsu A, et al. Reference-based analysis of lung single-cell sequencing reveals a transitional profibrotic macrophage. Nat Immunol. 2019;20:163–72.
[25] Monaco G, Lee B, Xu W, Mustafah S, Hwang YY, Carré C, et al. RNA-Seq signatures normalized by mRNA abundance allow absolute deconvolution of human immune cell types. Cell Rep. 2019;26 1627-40.e7.
[26] Xie Z, Bailey A, Kuleshov MV, Clarke DJB, Evangelista JE, Jenkins SL, et al. Gene set knowledge discovery with enrichr. Curr Protoc. 2021;1:e90.
[27] Mangiola S, Roth-Schulze AJ, Trussart M, Zozaya-Valdés E, Ma M, Gao Z, et al. sccomp. Robust differential composition and variability analysis for single-cell data. Proc Natl Acad Sci U S A 2023;120(33):e2203828120. doi: 10.1073/pnas.2203828120.
[28] Zheng W, Wang X, Liu J, Yu X, Li L, Wang H, et al. Single-cell analyses highlight the proinflammatory contribution of C1q-high monocytes to Behçet's disease. Proc Natl Acad Sci U S A. 2022;119:e2204289119.
[29] Liu Y, Bao D, Meng M, Lu L, Zhu H. The proportion of C1q-high and ISG15-high monocytes in the skin of patients with Behçet disease. Front Pharmacol. 2023;14:1110741.
[30] Tsou PS, Palisoc PJ, Ali M, Khanna D, Sawalha AH. Genome-wide reduction in chromatin accessibility and unique transcription factor footprints in endothelial cells and fibroblasts in scleroderma skin. Arthritis Rheumatol. 2021;73:1501–13.
[31] Ambrose N, Khan E, Ravindran R, Lightstone L, Abraham S, Botto M, et al. The exaggerated inflammatory response in Behcet's syndrome: identification of dysfunctional post-transcriptional regulation of the IFN-gamma/CXCL10 IP-10 pathway. Clin Exp Immunol. 2015;181:427–33.
[32] Qian Y, Qu Y, Gao F, Pei M, Liang A, Xiao J, et al. Comparison of the safety and efficacy of interferon alpha-2a and cyclosporine-A when combined with glucocorticoid in the treatment of refractory Behcet's uveitis: a randomized controlled prospective study. Front Pharmacol. 2021;12:699903.
[33] Lee JH, Lee CS, Lee SC. Interferon alpha-2a treatment for refractory Behcet uveitis in Korean patients. BMC Ophthalmol 2018;18:52.
[34] Onal S, Kazokoglu H, Koc A, Akman M, Bavbek T, Direskeneli H, et al. Long-term efficacy and safety of low-dose and dose-escalating interferon alfa-2a therapy in refractory Behçet uveitis. Arch Ophthal. 2011;129:288–94.
[35] Smiljanovic B, Grun JR, Biesen R, Schulte-Wrede U, Baumgrass R, Stuhlmuller B, et al. The multifaceted balance of TNF-alpha and type I/II interferon responses in SLE and RA: how monocytes manage the impact of cytokines. J Mol Med (Berl). 2012;90:1295–309.
[36] Tong B, Liu X, Xiao J, Su G. Immunopathogenesis of Behcet's disease. Front Immunol. 2019;10:665.
[37] Taura M, Frank JA, Takahashi T, Kong Y, Kudo E, Song E, et al. APOBEC3A regulates transcription from interferon-stimulated response elements. Proc Natl Acad Sci U S A. 2022;119:e2011665119.
[38] Tsai MH, Pai LM, Lee CK. Fine-tuning of type I interferon response by STAT3. Front Immunol 2019;10:1448.
[39] Mirouse A, Barete S, Monfort JB, Resche-Rigon M, Bouyer AS, Comarmond C, et al. Ustekinumab for Behcet's disease. J Autoimmun 2017;82:41–6.
[40] Tulunay A, Dozmorov MG, Ture-Ozdemir F, Yilmaz V, Eksioglu-Demiralp E, Alibaz-Oner F, et al. Activation of the JAK/STAT pathway in Behcet's disease. Genes Immun. 2015;16:170–5.
[41] Calvo-Rio V, Blanco R, Beltran E, Sanchez-Burson J, Mesquida M, Adan A, et al. Anti-TNF-alpha therapy in patients with refractory uveitis due to Behcet's disease: a 1-year follow-up study of 124 patients. Rheumatology (Oxford). 2014;53:2223–31.
[42] Schroder WA, Hirata TD, Le TT, Gardner J, Boyle GM, Ellis J, et al. SerpinB2 inhibits migration and promotes a resolution phase signature in large peritoneal macrophages. Sci Rep. 2019;9:124241.
[43] Hampton KK, Chamberlain MA, Menon DK, Davies JA. Coagulation and fibrinolytic activity in Behcet's disease. Thromb Haemost. 1991;66:292–4.
[44] Oztürk MA, Ertenli I, Kiraz S, C Haznedaroğlu I, Celik I, Kirazli S, et al. Plasminogen activator inhibitor-1 as a link between pathological fibrinolysis and arthritis of Behcet's disease. Rheumatol Int. 2004;24:98–102.
[45] Sterling JK, Rajesh A, Droho S, Gong J, Wang AL, Voigt AP, et al. Retinal perivascular macrophages regulate immune cell infiltration during neuroinflammation in mouse models of ocular disease. J Clin Invest. 2024;134:e180904.
[46] Xiao J, Zhao C, Cheng G, Song H, Zhang Y, Zhang M. Multiple cytokine analysis of aqueous humor in uveitis with or without secondary glaucoma. BMC Ophthalmol. 2024;24:451.
[47] Direskeneli H. Innate and adaptive responses to heat shock proteins in Behcet's disease. Genet Res Int. 2013;2013:249157.
[48] Sahebari M, Hashemzadeh K, Mahmoudi M, Saremi Z, Mirfeizi Z. Diagnostic yield of heat shock protein 70 (HSP-70) and anti-HSP-70 in Behcet-induced uveitis. Scand J Immunol. 2013;77:476–81.
[49] Shaker O, Ay El-Deen MA, El Hadidi H, Grace BD, El Sherif H, Abdel Halim A. The role of heat shock protein 60, vascular endothelial growth factor and antiphospholipid antibodies in Behcet disease. Br J Dermatol. 2007;156:32–7.
[50] Wu X, Wang Z, Shi J, Yu X, Li C, Liu J, et al. Macrophage polarization toward M1 phenotype through NF-kappaB signaling in patients with Behcet's disease. Arthritis Res Ther. 2022;24:249.
[51] Hu D, Guan JL. The roles of immune cells in Behcet's disease. Adv Rheumatol. 2023;63:49.
[52] Winkles JA. The TWEAK-Fn14 cytokine-receptor axis: discovery, biology and therapeutic targeting. Nat Rev Drug Discov. 2008;7:411–25.

[53] Rossin A, Miloro G, Hueber AO. TRAIL and FasL functions in cancer and autoimmune diseases: towards an increasing complexity. Cancers (Basel) 2019;11:639.
[54] Bonacini M, Soriano A, Cimino L, De Simone L, Bolletta E, Gozzi F, et al. Cytokine profiling in aqueous humor samples from patients with non-infectious uveitis associated with systemic inflammatory diseases. Front Immunol. 2020;11:358.
[55] Hu Y, Huang Z, Yang S, Chen X, Su W, Liang D. Effectiveness and safety of anti-tumor necrosis factor-alpha agents treatment in Behcets' disease-associated uveitis: a systematic review and meta-analysis. Front Pharmacol. 2020;11:941.
[56] van der Houwen TB, Humer B, Missotten TO, Thiadens AAHJ, van Hagen PM, van Laar JAM. Long-term data on efficacy and safety of adalimumab in Behcet's disease. Clin Immunol. 2023;247:109242.

Ann Rheum Dis 85 (2026) 1839–1853

Contents lists available at ScienceDirect

Annals of the Rheumatic Diseases

journal homepage: https://www.sciencedirect.com/journal/annals-of-the-rheumatic-diseases

Vasculitis

Single-cell multiomics reveals activation of the STAT3–PIM1 axis in T-cell subsets in proteinase 3-ANCA–positive granulomatosis with polyangiitis

Nanthicha Inrueangsri[1], Carlo G. Bonasia[2], Kevin P. Mennega[1], Matthew A. Jackson-Wood[3], Samuel J. Bullers[3], Oliver Wood[3], Malte Borggrewe[4], Petya D. Marinova[1], Rindert R. Venema[1], Theo Bijma[1], Rosanne D. Reitsema[2], Wayel H. Abdulahad[1,2,5], Jan-Stephan F. Sanders[6], Abraham Rutgers[2], Peter Heeringa[1,*]

[1] *Department of Pathology and Medical Biology, University Medical Center Groningen, University of Groningen, Groningen, The Netherlands*
[2] *Department of Rheumatology and Clinical Immunology, University Medical Center Groningen, University of Groningen, Groningen, The Netherlands*
[3] *Gilead Sciences, Oxford, United Kingdom*
[4] *Independent Bioinformatics Consultant, Hamburg, Germany*
[5] *Department of Clinical Sciences, College of Medicine, University of Sharjah, Sharjah, United Arab Emirates*
[6] *Division of Nephrology, Department of Internal Medicine, University Medical Center Groningen, University of Groningen, Groningen, The Netherlands*

ARTICLE INFO

Article history:
Received 17 October 2025
Received in revised form 30 April 2026
Accepted 4 May 2026

ABSTRACT

Objectives: Granulomatosis with polyangiitis (GPA) is an autoimmune disease marked by relapses and treatment-related morbidity. CD4⁺ T cells play a central role in GPA pathogenesis, but their molecular profile remains incompletely defined. This study aimed to characterise CD4⁺ T cells in patients with proteinase 3-antineutrophil cytoplasmic antibody (ANCA)–positive GPA (PR3-GPA) using single-cell multiomics to identify molecular signatures associated with disease activity.

Methods: Peripheral blood mononuclear cells were obtained from patients with PR3-GPA during active disease, remission, and healthy controls. Single-cell RNA sequencing (scRNA-seq) and Cellular Indexing of Transcriptomes and Epitopes by sequencing (CITE-seq) were used to define transcriptional and protein expression profiles of CD4⁺ T cell subsets. Findings were validated using reverse transcription quantitative polymerase chain reaction (RT-qPCR) and flow cytometry–based assays, including phospho-flow cytometry. Serum cytokines were measured by a Luminex assay, and CD4⁺ T-cell responses to Pim kinase inhibition were assessed. Spatial transcriptomics data from kidney biopsies from patients with PR3-ANCA-positive-associated crescentic glomerulonephritis were analysed.

Results: scRNA-seq and CITE-seq revealed upregulated *PIM1* expression in CD4⁺ T-cell subsets in active GPA compared with controls. RT-qPCR and flow cytometry–based analyses confirmed elevated expression of *PIM1*, *SOCS3*, and *STAT3* in CD4⁺ T cells from patients with active disease. STAT3 phosphorylation and serum interleukin-6 (IL-6) were increased in active GPA. Pim kinase inhibition reduced CD4⁺ T-cell activation, proliferation, and cytokine production. Spatial

*Correspondence to Dr Peter Heeringa, Department of Pathology and Medical Biology, University Medical Center Groningen, University of Groningen, Groningen, 9713 GZ, The Netherlands.

E-mail address: p.heeringa@umcg.nl (P. Heeringa).

Handling editor Josef Smolen

https://doi.org/10.1016/j.ard.2026.05.003

0003-4967/© 2026 The Author(s). Published by Elsevier B.V. on behalf of European Alliance of Associations for Rheumatology (EULAR). This is an open access article under the CC BY license (http://creativecommons.org/licenses/by/4.0/)

transcriptomics showed upregulated *STAT3* and *PIM* kinase expression in inflamed regions of PR3-ANCA–associated glomerulonephritis biopsies.
Conclusions: These findings indicate that circulating CD4$^+$ T cells in active PR3-GPA are characterised by activation of the STAT3–PIM1 axis, potentially driven by upstream IL-6 signalling. This supports further investigation of Pim kinase inhibition and Janus kinase–signal transducer and activator of transcription (JAK–STAT) pathway modulation as potential therapeutic strategies in PR3-GPA.

WHAT IS ALREADY KNOWN ON THIS TOPIC

- Granulomatosis with polyangiitis (GPA) is a relapsing autoimmune vasculitis in which aberrant CD4$^+$ T cells contribute to disease pathogenesis and remain activated even during remission. The molecular mechanisms sustaining this dysregulation and their association with disease activity remain poorly defined, and single-cell multiomics data in antineutrophil cytoplasmic antibody (ANCA)–associated vasculitis are limited.

WHAT THIS STUDY ADDS

- This is the first study to identify activation of the STAT3–PIM1 signalling axis as a defining molecular feature of circulating CD4$^+$ T cells in active PR3-ANCA–positive GPA.
- Through single-cell multiomics and functional assays, it demonstrates coordinated upregulation of *PIM1* and *STAT3* expression in circulating CD4$^+$ T cells.
- Elevated interleukin-6 (IL-6) serum levels and increased STAT3 phosphorylation in circulating CD4$^+$ T cells support a mechanistic link between IL-6–JAK–STAT3 signalling and *PIM1* induction during active disease.

HOW THIS STUDY MIGHT AFFECT RESEARCH, PRACTICE OR POLICY

- Supports exploration of Pim kinase inhibitors and IL-6–JAK–STAT pathway modulators as potential therapeutic strategies to control inflammation and prevent relapse.
- Provides a single-cell multiomics and validation framework for dissecting immune dysregulation and pathogenic signalling pathways in ANCA-associated vasculitis.

INTRODUCTION

Antineutrophil cytoplasmic antibody (ANCA)–associated vasculitides (AAV) are severe systemic autoimmune disorders comprising granulomatosis with polyangiitis (GPA), microscopic polyangiitis (MPA), and eosinophilic granulomatosis with polyangiitis (EGPA) [1]. They are characterised by the presence of pathogenic autoantibodies (ie, ANCAs) specific for neutrophil granule proteins, mainly proteinase 3 (PR3) and myeloperoxidase (MPO), which mediate microvascular inflammation in various tissues [1,2]. GPA is typically associated with PR3-ANCAs and primarily features necrotising granulomatous inflammation of the respiratory tract and kidneys [1]. PR3-ANCA-positive GPA (PR3-GPA) has a notably high relapse rate, exceeding that of MPA and EGPA, leading to cumulative tissue damage and increased risk of organ failure [1]. Although glucocorticoids and rituximab [3] are effective, their use carries substantial adverse effects, including increased infection risk. Thus, improved understanding of GPA pathogenesis and identification of biomarkers and therapeutic targets are needed.

T cells are significantly involved in the pathogenesis of GPA, as supported by multiple studies. Patients with GPA exhibit an increased frequency of circulating activated CD4$^+$ T cells compared with healthy controls (HCs), with activation persisting during remission [4]. Numerical and functional abnormalities in T-cell subsets have been reported in GPA, including expansion of circulating effector memory T cells, skewed differentiation towards T helper 17 (Th17) and follicular helper T (Tfh) cells, and impaired regulatory T-cell (Treg) function [5–8]. Furthermore, T-cell infiltration is a hallmark of inflammatory lesions and granulomas in GPA [9,10]. Moreover, the predominance of isotype-switched affinity-matured PR3-ANCAs in GPA suggests T-cell involvement in autoantibody formation [11].

High-throughput single-cell RNA sequencing (scRNA-seq) has emerged as a tool for uncovering cellular heterogeneity, functionality, and the molecular mechanisms driving biological processes [12]. Complementing this, Cellular Indexing of Transcriptomes and Epitopes by sequencing (CITE-seq) integrates oligonucleotide-barcoded antibodies to measure cell-surface proteins alongside mRNA at single-cell resolution [13]. Recent single-cell transcriptomic studies have revealed distinct transcriptional signatures and identified potential novel therapeutic targets in autoimmune diseases, such as rheumatoid arthritis (RA), systemic lupus erythematosus, and MPA [14–16]. In AAV, single-cell and spatial transcriptomic studies have provided insights into neutrophils [17,18], monocytes [19], and inflamed kidney tissue [20], highlighting dysregulated immune responses and tissue-specific inflammatory niches. However, single-cell characterisation of circulating CD4$^+$ T cells in PR3-ANCA–positive GPA remains limited, particularly in studies integrating multiomics profiling with complementary functional validation.

In this study, we aimed to characterise the molecular signatures of CD4$^+$ T cells in PR3-GPA during both active disease and remission, using single-cell multiomics, including scRNA-seq and CITE-seq of peripheral blood mononuclear cells (PBMCs). These analyses were complemented by validation in bulk-sorted CD4$^+$ T-cell subsets from patients with PR3-GPA and functional assays to delineate molecular pathways associated with T-cell activation.

METHODS

Study population

An overview of the study design is presented in Figure 1. The characteristics of patients with GPA and HC included in this study are detailed in Supplementary Tables S1 to S3 and S4. Peripheral blood samples were collected from patients with active PR3-GPA, patients with PR3-GPA in clinical remission, and HC using lithium heparin–coated vacutainers, EDTA-coated vacutainers, and nonanticoagulant vacutainers (BD Biosciences). A comprehensive overview of all samples used in each experiment is provided in Supplementary Tables S6 and S7. The diagnosis of GPA was established based on the Chapel Hill Consensus Conference definitions [21]. The study protocol was approved by the Institutional Review

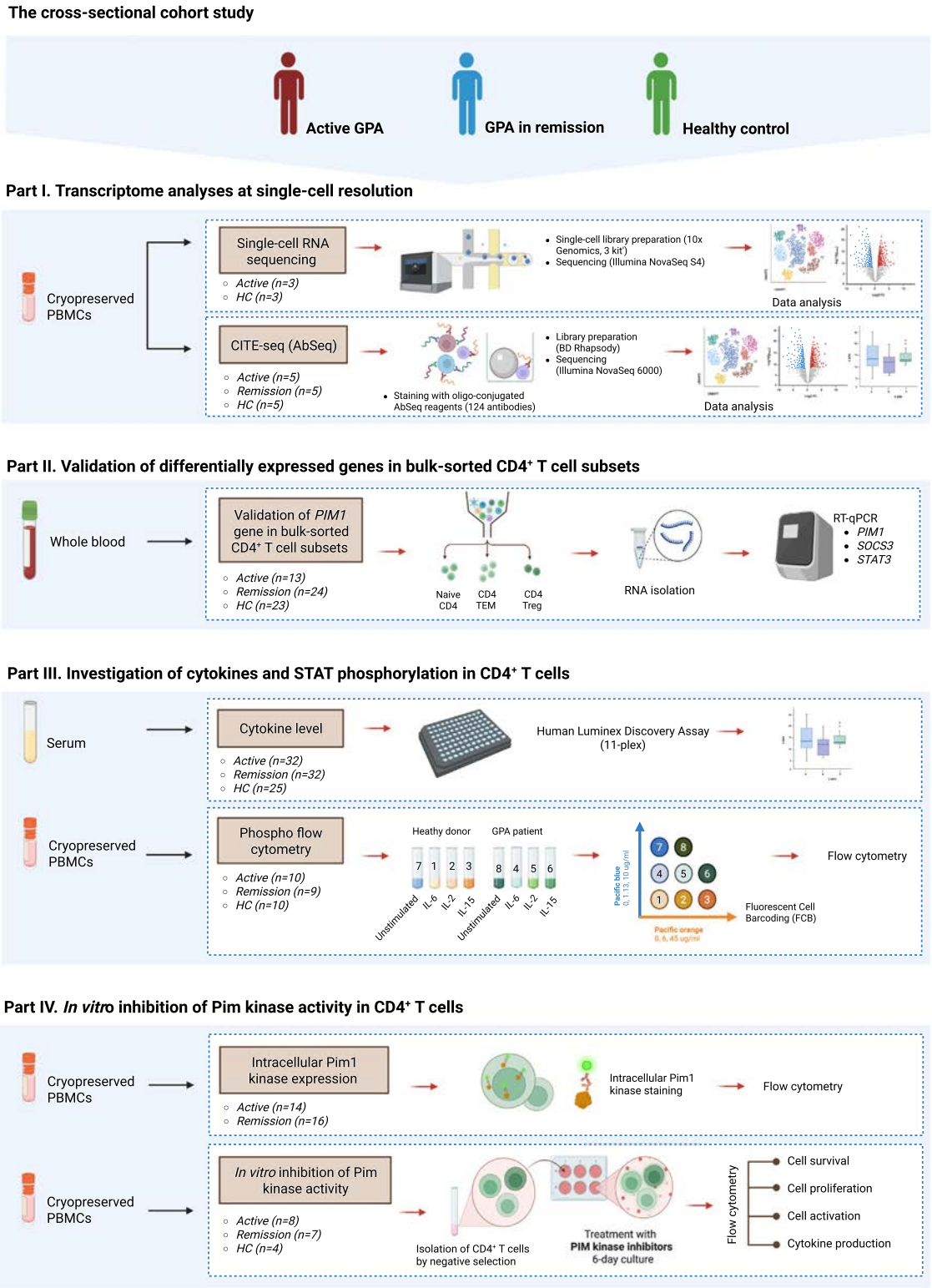

Figure 1. Schematic overview of the study. This cross-sectional study integrated single-cell transcriptomics and functional assays to investigate transcriptional signatures of CD4$^+$ T cells in PR3-GPA. Peripheral blood samples were collected from patients with active PR3-GPA, patients with PR3-GPA in remission, and HC. In Part I, transcriptomic profiling of cryopreserved PBMCs was performed using single-cell RNA sequencing (10x Genomics) and AbSeq profiling (BD Rhapsody). In Part II, differentially expressed genes identified by scRNA-seq and AbSeq were validated by RT-qPCR in bulk-sorted CD4$^+$ T cell subsets (naive, TEM, and Treg) from whole blood. In Part III, the IL-6–pSTAT3–PIM1 axis in CD4$^+$ T cells was investigated using serum cytokine profiling and phospho-flow cytometry of PBMCs. In Part IV, Pim-1 protein expression levels in CD4$^+$ T cell subsets were validated using intracellular flow cytometry. *In vitro* functional studies were conducted by treating isolated CD4$^+$ T cells with Pim kinase inhibitors, followed by flow cytometry analysis of survival, proliferation, activation, and cytokine production. GPA, granulomatosis with polyangiitis; HC, healthy control; IL, interleukin; PBMC, peripheral blood mononuclear cell; PR3-GPA, proteinase 3-ANCA-positive granulomatosis with polyangiitis; PIM, proviral integration site for Moloney murine leukemia virus kinase; RT-qPCR, reverse transcription quantitative polymerase chain reaction; scRNA-seq, single-cell RNA sequencing; STAT, signal transducer and activator of transcription; TEM, effector memory T cell; Treg, regulatory T cell.

Board of the University Medical Center Groningen (METc no. 2012/151 and 2020/007), and all participants provided written informed consent.

Isolation of PBMCs

PBMCs were isolated from lithium heparin-treated blood by density gradient centrifugation using Lymphoprep (STEMCELL Technologies). Following isolation, PBMCs were resuspended in Roswell Park Memorial Institute 1640 medium (Lonza), supplemented with 10% fetal bovine serum, 10% dimethyl sulfoxide (DMSO), and 50 μg/mL gentamicin (Lonza). Cells were cryopreserved and stored in liquid nitrogen for long-term preservation.

Single-cell RNA sequencing

Cryopreserved PBMCs were used from 3 patients with PR3-GPA with active disease and 3 age- and sex-matched HC. In this study, sex refers to biological classification as male or female, as recorded in the study data. The samples were provided to Single Cell Discoveries for scRNA-seq, including single-cell processing, DNA library construction, and sequencing using 10x Genomics' Chromium Single Cell 3′ Reagent Kits (V3.1), following the manufacturer's instructions. DNA libraries were sequenced on an Illumina NovaSeq S4 system with a paired-end 2 × 150 bp kit. A detailed description of scRNA-seq data analyses is provided in the Supplementary Methods.

CITE-seq

Cryopreserved PBMCs were obtained from 5 patients with active PR3-GPA, 5 patients with PR3-GPA in remission, and 5 age- and sex-matched HC. The samples were processed for CITE-seq (AbSeq, BD Biosciences). Cells were barcoded, sorted, and stained with a panel of 124 antibodies (30 from the BD Immune Discovery Panel and 93 custom-conjugated; Supplementary Table S8), and processed using the BD Rhapsody system following the manufacturer's instructions. Sequencing libraries for sample tags, AbSeq oligos, and mRNAs were prepared using the BD AbSeq Amplification Kit. A custom mRNA primer panel targeting 529 immune-related genes was used for transcript enrichment (Supplementary Data; Excel 1). Libraries were sequenced on an Illumina NovaSeq 6000, using 150bp paired-end reads. A detailed description of experimental protocols and data analyses is provided in the Supplementary Methods.

Reverse transcription quantitative polymerase chain reaction for gene expression validation

Total RNA from bulk-sorted naive $CD4^+$ T cells ($CD4^+CD8^-CD45RO^-CCR7^+$), effector memory $CD4^+$ T (TEM $CD4^+$) cells ($CD4^+CD8^-CD45RO^+CCR7^-$), and Tregs ($CD4^+$CD8-$CD45RO^+CD127^-$ $CD25^{high}$) were used to validate gene expression, as described by Dekkema et al [22]. Total RNA was reverse transcribed into complementary DNA (cDNA) using the High-Capacity cDNA Reverse Transcription Kit (Thermo Fisher). Real-time RT-qPCR was performed on a ViiA7 Real-time PCR System using TaqMan probes, as specified in Supplementary Table S9. Amplification data were analysed with QuantStudio Real-time PCR Software v1.3 (Applied Biosystems). Cycle threshold (CT) values were averaged and normalised to *RPL13A*.

Profiling of cytokines by Luminex assay

Serum or plasma samples from patients and HC were collected following centrifugation of coagulated peripheral blood samples or EDTA-treated blood samples and stored at −20°C. Cytokine levels, as listed in Supplementary Table S10, were quantified using a custom 11-plex human Luminex discovery kit (R&D Systems), following the guidelines provided by the manufacturer. A Luminex 200 system was used for plate reading, and the analysis was conducted using xPONENT software version 4.2 (DiaSorin) together with GraphPad Prism version 10.

Phospho-flow cytometry

Cryopreserved PBMCs from patients with PR3-GPA and HC were thawed, counted, and divided into 4 aliquots per sample. To assess STAT protein phosphorylation, cells were stimulated with interleukin (IL)-2, IL-6, IL-15, or left unstimulated. After fixation and permeabilisation, fluorescent cell barcoding was performed, and samples were pooled and stained with antibody panels (Supplementary Table S11) as outlined in Supplementary Figure S1. Data were acquired on a BD FACSymphony A5 flow cytometer and analysed using Kaluza software (Beckman Coulter) and GraphPad Prism v10. Experimental details are provided in the Supplementary Methods.

In vitro *suppression of Pim kinase activity*

Cryopreserved PBMCs from patients with PR3-GPA and HC were thawed and used for $CD4^+$ T-cell isolation by negative selection (EasySep Human $CD4^+$ T-Cell Isolation Kit, STEMCELL Technologies). Cell purity (92%-98%) was verified by flow cytometry (Supplementary Table S11). Purified $CD4^+$ T cells were cultured at 1 × 10^6 cells/mL in serum-free X-Vivo 15 medium supplemented with 5% heat-inactivated human serum and stimulated with plate-bound anti-CD3 (0.5 μg/mL) and soluble anti-CD28/49d (1 μg/mL) for 6 days at 37°C and 5% CO_2.

For *in vitro* inhibition assays, $CD4^+$ T cells were labelled with Cell Proliferation Dye eFluor 670 and treated with either 20 μM Pim-1 inhibitor (TCS PIM-1 1; Tocris) or 10 μM pan-Pim inhibitor AZD1208 (BioVision); DMSO served as a control. Cells were harvested on days 0 and 6 to assess cell activation, proliferation, cytokine production (interferon-gamma (IFNγ), IL-4, IL-17A, and IL-21), and Treg frequencies using flow cytometry. Data were acquired on a BD FACSymphony A5 and analysed with Kaluza software and FCS Express v7 (De Novo Software). Detailed protocols for culture conditions and antibody staining are provided in the Supplementary Methods.

Spatial and single-cell transcriptomics analyses of public datasets

AnnData objects from publicly available spatial transcriptomics data of patients with PR3-ANCA–associated glomerulonephritis (PR3-ANCA-GN) and control samples (healthy tissue from tumour nephrectomies) [20] were accessed through the National Center for Biotechnology Information Gene Expression Omnibus (NCBI GEO) (accession number GSE250138) and analysed using Scanpy (v.1.9.8) [23]. Data were subset to patients with PR3-ANCA-GN and control samples, followed by visualisation of normalised expression levels of genes of interest across niches. The original annotation of spatial niches provided in the study [20] was retained. To assess differences in gene expression between patients with PR3-ANCA-GN and control samples of selected genes, the average gene expression per sample was determined (pseudobulk), and differential expression was assessed using the Wilcoxon rank-sum test. For single-cell transcriptomic analysis of renal T cells, data were obtained from NCBI GEO (accession number GSE253633) and analysed using Scanpy. The dataset was subsetted to kidney samples from

patients with PR3-ANCA-GN (n = 8). Gene expression was assessed, and cluster markers of T-cell subsets were identified using a Wilcoxon rank-sum test (sc.tl.rank_genes_groups). Genes with an adjusted P-value (Benjamin Hochberg) of less than .05 were regarded as significant.

Statistical analyses

Group comparisons among active GPA, GPA in remission, and HC were performed using the nonparametric Kruskal-Wallis test followed by Dunn's multiple comparisons test. For the *in vitro* experiments, comparisons among the DMSO, PIM1i, and PanPIMi conditions were analysed using the 2-sided Wilcoxon signed-rank test. Statistical significance was defined as $P < .05$. Correlations between the Birmingham Vasculitis Activity Score (BVAS) and gene expression level were assessed using Spearman's rank correlation coefficient. The strength of the correlation coefficient was categorised as weak (<0.4), moderate (0.4-<0.6), strong (0.6-0.8), or excellent (>0.8). Statistical methods for single-cell analyses are described in the Supplementary Methods.

RESULTS

Single-cell transcriptomics reveals upregulated PIM1 *expression in circulating CD4$^+$ T cells in active PR3-GPA*

To characterise the transcriptional profile of circulating CD4$^+$ T-cell subsets in active PR3-GPA, we performed scRNA-seq on PBMCs from 3 patients with active PR3-GPA and 3 HC. A combined dataset of 30,809 cells in total was used to generate a Uniform Manifold Approximation and Projection (UMAP) for cell subset visualisation (Fig 2A,B; Supplementary Fig S2A,B). Subclustering of total T cells (CD4$^+$ and CD8$^+$ subsets, 19.090 cells in total) revealed 9 distinct T-cell subsets, including naive CD4$^+$, CD4$^+$ TEM, regulatory T, CD4$^+$/CD8$^+$ TCM, naive CD8$^+$, CD8$^+$ TEM, CD8$^+$ TEMRA, $\gamma\delta$ T, and mucosal-associated invariant T cell (MAIT) cells (Fig 2C-E; Supplementary Fig S3A). Differential expression analysis showed significant gene expression changes across CD4$^+$ T-cell subsets between the groups (Fig 2F). Interestingly, *PIM1* (Pim-1 Proto-Oncogene, Serine/Threonine Kinase) was the most prominently upregulated gene in naive CD4$^+$, TEM CD4$^+$, and Tregs in active GPA compared with HC (Fig 2F-I; Supplementary Fig 3B). *PIM1* encodes a serine/threonine kinase involved in cell survival, proliferation, and immune regulation, acting downstream of Janus kinase–signal transducer and activator of transcription (JAK–STAT) signalling and implicated in inflammatory processes and autoimmunity [24]. Pim1 belongs to the Pim kinase family, which consists of 3 isoforms: Pim1, Pim2, and Pim3. Of note, *PIM2* was also upregulated in the same CD4$^+$ subsets in active GPA (Fig 2G,H; Supplementary Figure S2C; Supplementary Data; Excel 2). In addition, *SOCS3* (Suppressor Of Cytokine Signalling 3), a negative feedback regulator of the JAK–STAT pathway [25], was also upregulated in these subsets in active GPA (Fig 2F-H,J, Supplementary Data; Excel 2).

To validate and extend these findings, we used CITE-seq on PBMCs from 5 patients with active PR3-GPA, 5 in remission, and 5 HC. A UMAP was generated from 31,767 PBMCs, resulting in 22 cell populations (Fig 3A,B; Supplementary Fig S3C-E). As our focus was on CD4$^+$ T cells, 4 CD4$^+$ subsets were identified and visualised: naive T, TEM, T regulatory, and cytotoxic T cells (Fig 3A-C). *PIM1* expression was elevated in active GPA, particularly in naive and TEM CD4$^+$ cells (Fig 3D,E, and Supplementary Fig S4), and remained elevated in TEM CD4$^+$ cells during remission (Fig 3F). Correlation analysis across all groups showed weak to moderate positive correlations between *PIM1* transcript levels and activation markers (CCR7, CD27, and CD38), and weak but significant negative correlations with inhibitory markers (PD-1, FAS, SLAMF5, and SLAMF4) (Figure 3G).

Together, these findings demonstrate consistent upregulation of *PIM1* in circulating CD4$^+$ T cells in active PR3-GPA, with sustained expression in TEM cells during remission.

RT-qPCR validates elevated PIM1, SOCS3, *and* STAT3 *expression in CD4$^+$ T-cell subsets in PR3-GPA*

To validate the upregulation of *PIM1* and *SOCS3* expression in circulating CD4$^+$ T-cell subsets from patients with active GPA, we performed RT-qPCR on bulk-sorted CD4$^+$ naive, CD4$^+$ TEM, and Tregs from whole blood of patients with PR3-GPA during active disease and remission, as well as from HC. We also assessed *STAT3* expression, an upstream positive regulator of *PIM1* and *SOCS3*. All 3 genes, *PIM1, SOCS3,* and *STAT3,* were upregulated in CD4$^+$ naive and CD4$^+$ TEM cells in active disease compared with HC (Fig 4A-C). In addition, *PIM1* expression was elevated in Tregs during active disease relative to both remission and HC. Compared with remission, CD4$^+$ naive T cells showed higher expression of *PIM1, SOCS3*, and *STAT3* during active disease. In Tregs, *PIM1* and *SOCS3* were also upregulated, whereas *SOCS3* was elevated in CD4$^+$ TEM cells during active disease relative to remission. Interestingly, *PIM1* expression in CD4$^+$ TEM cells was higher in remission than in HC. Moreover, expression levels of *PIM1, SOCS3*, and *STAT3* correlated moderately to strongly with BVAS in active GPA, particularly within the CD4$^+$ TEM subset (Supplementary Fig S5). In an exploratory analysis of patients with MPO-ANCA–positive MPA (Supplementary Table S5), *PIM1* and *STAT3* expression were comparable to PR3-GPA across CD4$^+$ T-cell subsets, with the exception of higher *PIM1* expression in naive CD4$^+$ T cells in PR3-GPA (Supplementary Fig S6).

Collectively, RT-qPCR analysis confirmed increased expression of *PIM1, SOCS3*, and *STAT3* in CD4$^+$ T-cell subsets during active PR3-GPA. These results are consistent with our scRNA-seq and CITE-seq findings and further support the involvement of the *PIM1*-centred JAK–STAT signalling pathway in T-cell activation during GPA pathogenesis.

Circulating IL-6 and CD4$^+$ T-cell STAT3 phosphorylation are increased in active PR3-GPA

To identify upstream signals potentially driving *PIM1* upregulation in CD4$^+$ T cells (Fig 5A), serum cytokine concentrations implicated in JAK–STAT-mediated regulation of *PIM1* expression [26] were quantified using an 11-plex Luminex assay in the same cohort of patients with GPA and HC. The panel included cytokines predominantly activating STAT3 (IL-6 and G-CSF), STAT5 (IL-7, IL-15, and GM-CSF), and STAT1 (IFNγ).

IL-6 levels were higher in patients with active disease than in both those in remission and HC (Fig 5B). G-CSF, IL-7, IL-15, and IFNγ were also elevated in active GPA compared with HC, whereas GM-CSF was increased in active GPA relative to remission (Supplementary Fig S7).

To extend these findings, we next assessed intracellular phosphorylated STAT proteins (pSTAT1, pSTAT3, and pSTAT5) in circulating CD4$^+$ T-cell subsets using phospho-flow cytometry (Supplementary Fig S8). At baseline, the proportion of pSTAT3-

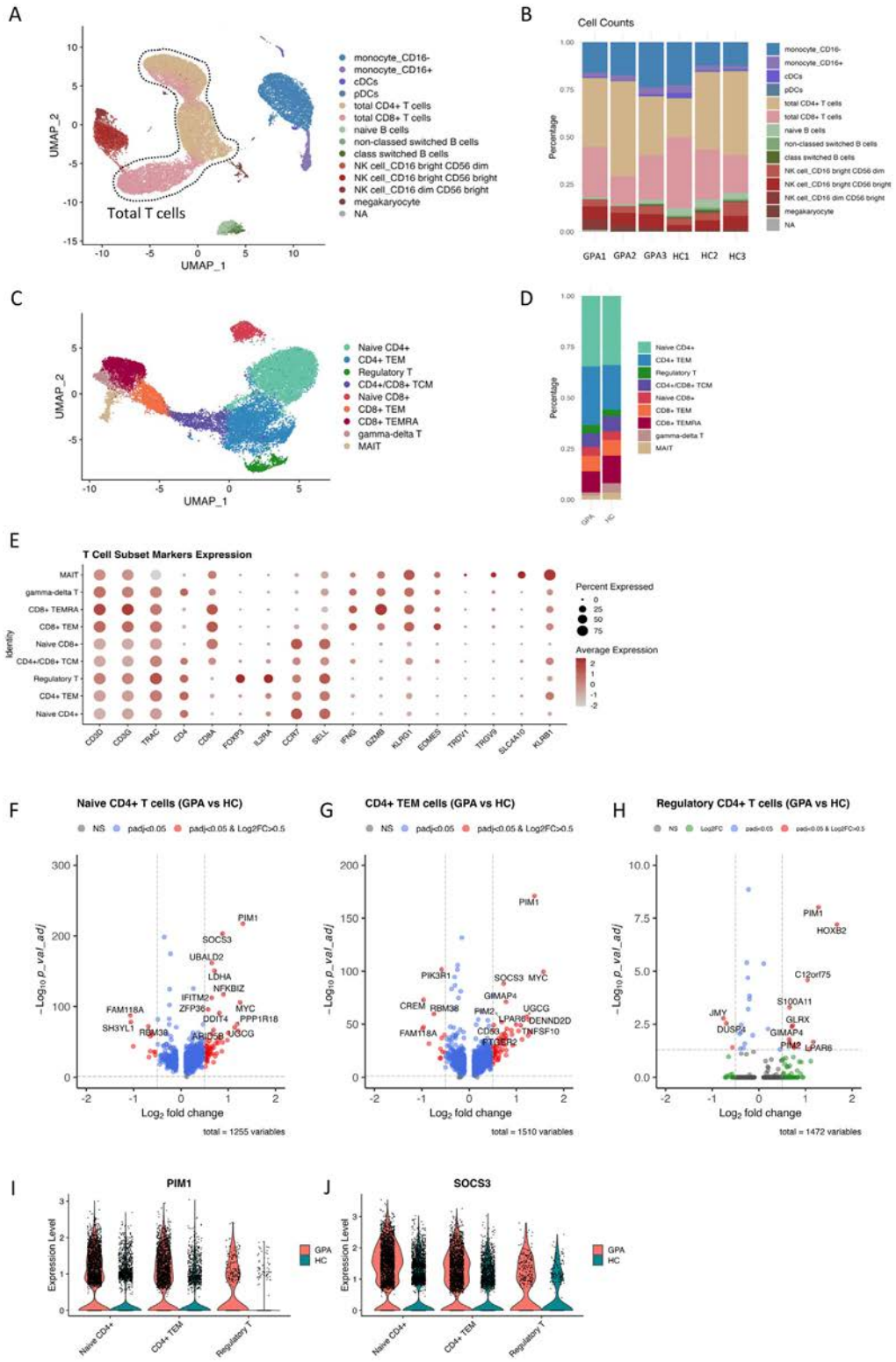

Figure 2. Single-cell transcriptome analysis of T cells from patients with active PR3-GPA and HC. (A) UMAP plot of PBMCs coloured by immune cell types identified from scRNA-seq data of patients with active GPA ($n = 3$) and HC ($n = 3$). (B) Proportions of immune cell types across individual samples. (C) UMAP plot of T-cell subset clusters generated by subclustering total T cells shown in (A). (D) Distribution of T cell subsets per sample group. (E) Dot plot showing the expression of marker genes across T-cell subsets. (F-H) Volcano plots of differentially expressed genes (DEGs) in naive CD4$^+$ T cells, CD4$^+$ TEM cells, and regulatory T cells from patients with active GPA vs HC. DEGs are highlighted in red, with the top 15 regulated genes labelled. (I,J) Violin plots showing *PIM1* and *SOCS3* expression across CD4$^+$ T-cell subsets in patients with GPA and HC. cDC, conventional dendritic cell; GPA, granulomatosis with polyangiitis; HC, healthy control; MAIT, mucosal-associated invariant T cell; NS, not statistically significant; NK, natural killer cell; pDC, plasmacytoid dendritic cell; PBMC, peripheral blood mononuclear cell; PR3-GPA, proteinase 3-ANCA-positive granulomatosis with polyangiitis; scRNA-seq, single-cell RNA sequencing; TEM, effector memory T cell; TEMRA, terminally differentiated effector memory T cell; SOCS3, suppressor of cytokine signaling 3; UMAP, Uniform Manifold Approximation and Projection.

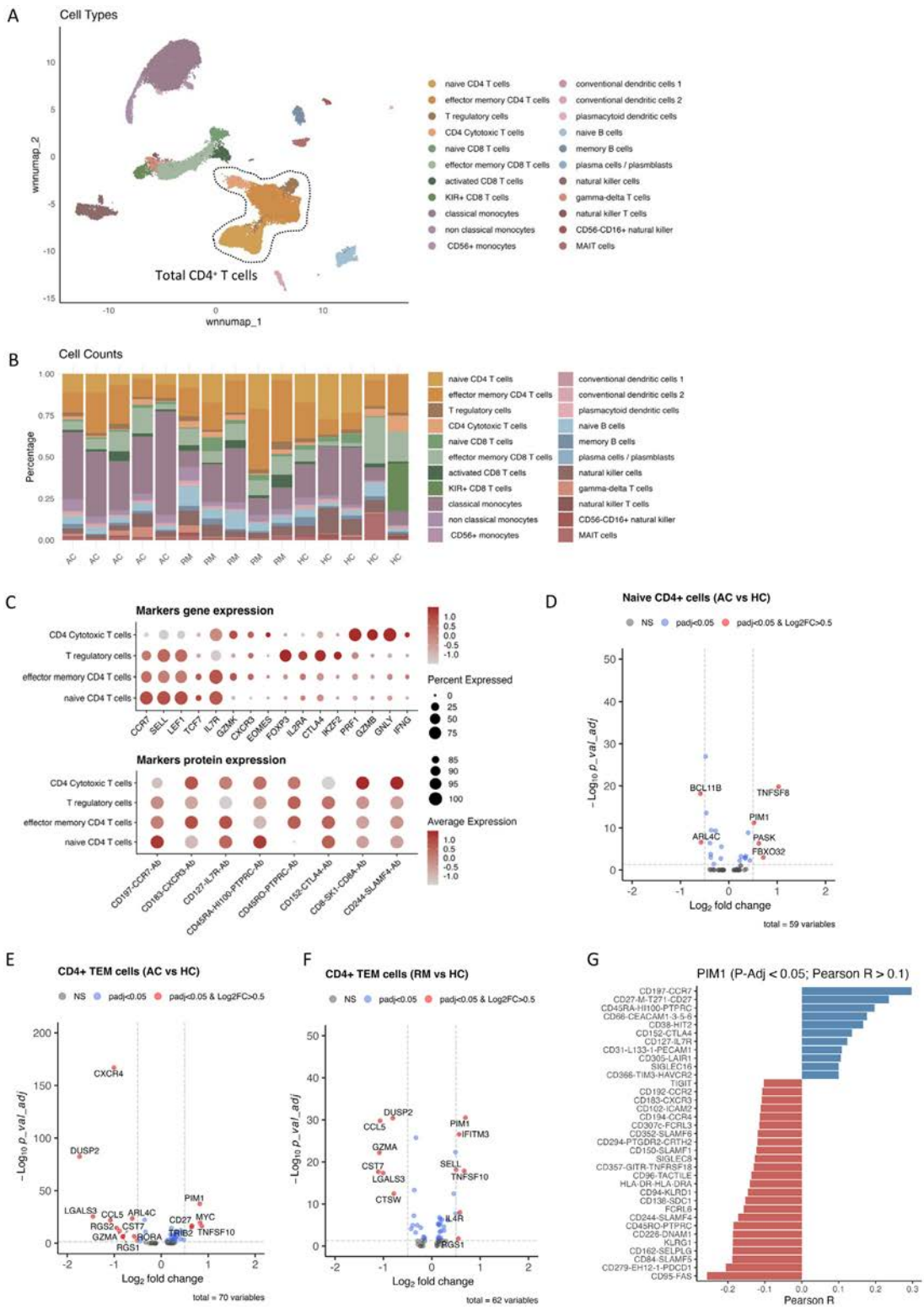

Figure 3. CITE-seq profiling of CD4⁺ T cells in patients with PR3-GPA (active and remission) and HC. (A) UMAP plot of PBMCs profiled by AbSeq identified CD4⁺ T-cell subsets in active PR3-GPA (n = 5), PR3-GPA in remission (n = 5), and HC (n = 5), including naive, central memory, effector memory, regulatory, and cytotoxic T cells. (B) A bar plot showing the relative proportions of these subsets across individual samples. (C) Dot plots representing gene marker expression (top) and surface protein marker expression (bottom) were used to define subsets of CD4+ T cells, with dot size indicating the percentage of expressing cells and colour intensity representing average expression levels. (D,E) Volcano plots showing differentially expressed genes in naive CD4⁺ T cells and CD4⁺ TEM cells from patients with active GPA vs HC, as well as (F) in CD4⁺ TEM cells from patients with GPA in remission vs HC, with significant genes labelled, including *PIM1*. (G) Correlation analysis between PIM1 and surface protein expression across CD4⁺ T cells (Pearson R > 0.1 and *P*adj < .05). GPA, granulomatosis with polyangiitis; HC, healthy control; CITE-seq, Cellular Indexing of Transcriptomes and Epitopes by sequencing; PBMC, peripheral blood mononuclear cell; PR3-GPA, proteinase 3-ANCA-positive granulomatosis with polyangiitis; UMAP, Uniform Manifold Approximation and Projection; TEM, effector memory T cell; KIR, killer cell immunoglobulin-like receptor; MAIT, mucosal-associated invariant T cell; AC, active; RM, remission; NS, not statistically significant.

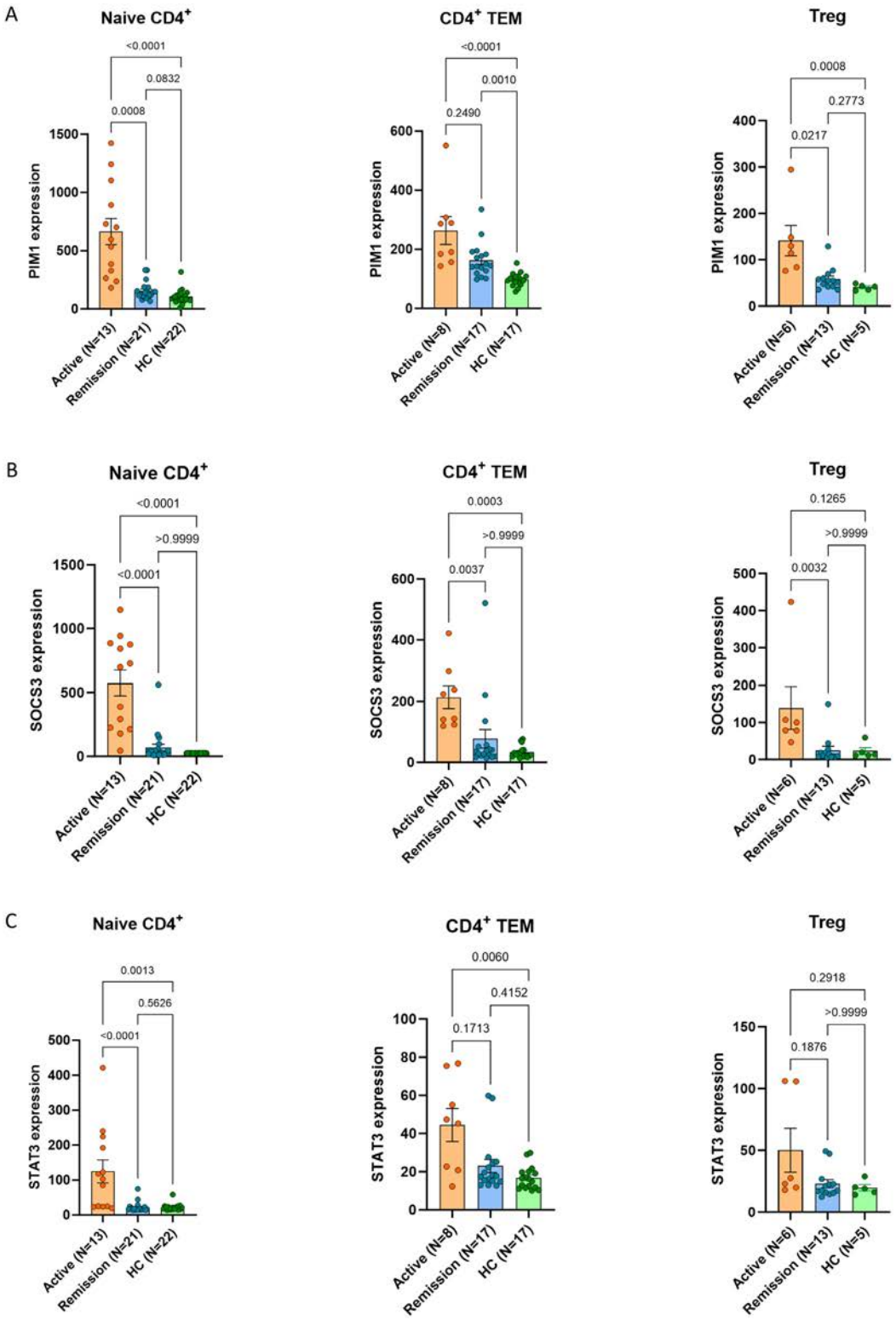

Figure 4. RT-qPCR validates elevated *PIM1, SOCS3,* and *STAT3* expression in CD4$^+$ T-cell subsets in PR3-GPA. (A) *PIM1,* (B) *SOCS3,* and (C) *STAT3* expression in naive CD4$^+$ T cells, effector memory CD4$^+$ (TEM) cells, and regulatory T cells (Tregs). Expression was measured by RT-qPCR in sorted CD4$^+$ T-cell subsets from the whole blood of patients with active PR3-GPA, patients with PR3-GPA in remission, and HC. Expression was quantified as $2^{-\Delta Ct}$ values relative to the reference gene *RPL13A*. Data are shown as mean ± SEM. Statistical analysis was performed using the Kruskal-Wallis test followed by Dunn's multiple comparisons test, with significance defined as $P < .05$. HC, healthy control; PR3-GPA, proteinase 3-ANCA-positive granulomatosis with polyangiitis; RT-qPCR, reverse transcription quantitative polymerase chain reaction; TEM, effector memory T cell; Treg, regulatory T cell.

positive cells and median fluorescence intensity (MFI) of pSTAT3 were significantly higher in total CD4$^+$, naive CD4$^+$, and CD4$^+$ TEM cells from patients with active GPA compared with HC (Fig 5C,D). The MFI of pSTAT3 in Tregs was also upregulated in active disease when compared with HC. Based on prior reports, linking IL-6 to PR3-GPA pathogenesis [27] and its elevation in our cohort, IL-6 was selected for functional follow-up analysis of downstream STAT signalling. Following *ex vivo* IL-6 stimulation, pSTAT3-positive cell frequencies increased significantly across all groups relative to baseline; however, no differences in response were observed between the 3 groups and across any CD4$^+$ T-cell subset (Fig 5E). No differences among

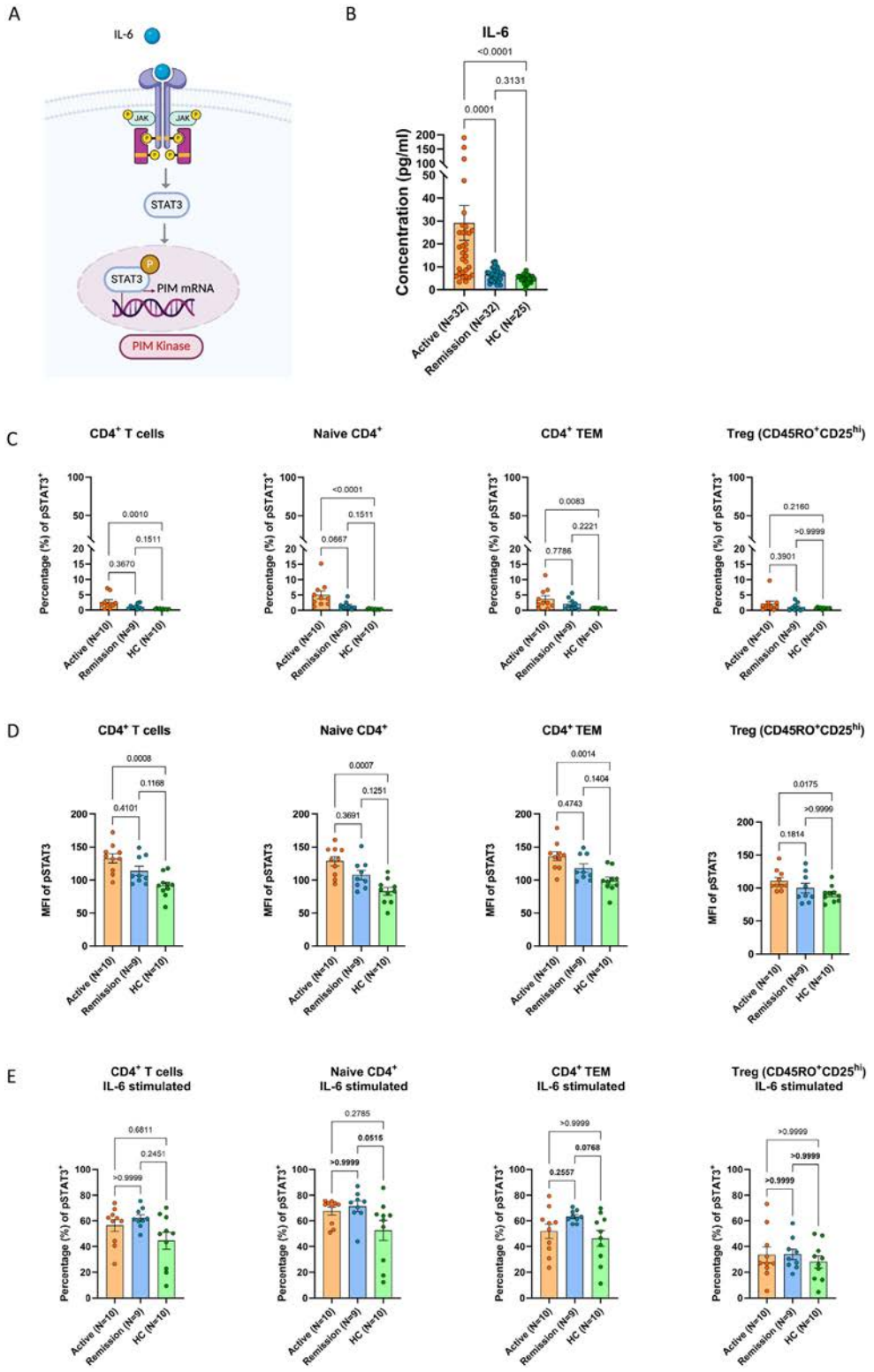

Figure 5. Circulating IL-6 and baseline STAT3 phosphorylation are increased in active PR3-GPA. (A) Schematic overview of the IL-6–pSTAT3–PIM1 signalling axis. IL-6 stimulation induces STAT3 phosphorylation, which promotes transcriptional upregulation of downstream targets, including *PIM1*. (B) Serum IL-6 concentrations measured by Luminex assay in patients with active PR3-GPA (n = 32), PR3-GPA in remission (n = 32), and HC (n = 25). (C,D) Baseline pSTAT3 expression in CD4$^+$ T-cell subsets (naive CD4$^+$, CD4$^+$ TEM, and regulatory T cells) in active GPA (n = 10), GPA in remission (n = 9), and HC (n = 10), assessed by phospho-flow cytometry. (D) pSTAT3 expression in the same CD4$^+$ T-cell subsets following IL-6 stimulation. Data are shown as mean ± SEM. Statistical analysis was performed using the Kruskal-Wallis test followed by Dunn's multiple comparisons test, with significance defined as $P < .05$. GPA, granulomatosis with polyangiitis; HC, healthy control; PR3-GPA, proteinase 3-ANCA-positive granulomatosis with polyangiitis; PIM, proviral integration site for Moloney murine leukemia virus; IL-6, interleukin-6; TEM, effector memory T cell; Treg, regulatory T cell.

the groups were observed in baseline pSTAT5 expression, whereas the proportions of pSTAT1-positive naive CD4$^+$ and CD4$^+$ TEM cells were elevated in patients with active GPA compared with HC (Supplementary Fig S9). In addition, analysis of MFI showed no differences in pSTAT1 and pSTAT5 expression between groups (Supplementary Fig S9).

Collectively, these data show increased circulating concentrations of cytokines acting through STAT3-, STAT5-, and STAT1-mediated pathways, including IL-6, G-CSF, IL-7, IL-15, and IFNγ in patients with active PR3-GPA. In parallel, circulating CD4$^+$ T cells from patients with active PR3-GPA are characterised by enhanced basal STAT3 phosphorylation. Integrated with our transcriptomic and RT-qPCR findings, these results delineate activation of a STAT3–PIM1 signalling axis as a defining feature of active PR3-GPA, potentially influenced by elevated IL-6.

Pim kinase inhibitors reduce CD4$^+$ T-cell activation, proliferation, and proinflammatory cytokine production

We next examined whether direct inhibition of Pim kinases with either the Pim-1-specific inhibitor (TCS PIM-1 1; PIM1i) or the pan-Pim inhibitor (AZD1208; PanPIMi) could modulate CD4$^+$ T-cell responses in GPA. Purified CD4$^+$ T cells from cryopreserved PBMCs of patients with PR3-GPA (active disease and remission) were stimulated with anti-CD3/CD28/49d and cultured with each inhibitor as described previously [28].

Intracellular Pim-1 protein expression in all CD4$^+$ T-cell subsets was higher in active GPA compared with remission, except for CD4$^+$ TEM, which showed a trend towards increased expression (Fig 6A). Treatment with either PIM1i or PanPIMi reduced the frequency of activated (CD25$^+$) CD4$^+$ T cells in active GPA (Fig 6B,C; Supplementary Fig S10-12) and significantly decreased proliferation in both active disease and remission, without affecting cell viability. PanPIMi also lowered the proportion of divided CD4$^+$ T cells in both groups. Regarding cytokine production, PanPIMi consistently reduced the proportion of IL-21$^+$ and IFNγ^+ CD4$^+$ T cells in active GPA and remission, whereas PIM1i showed a nonsignificant trend towards reduced IL-21$^+$ CD4$^+$ T cells in active GPA. Both inhibitors reduced the frequency of IL-17A$^+$ CD4$^+$ T cells in remission.

Together, these findings indicate that Pim kinase inhibition suppresses activation, proliferation, and proinflammatory cytokine production of circulating CD4$^+$ T cells from PR3-GPA during both active disease and remission.

STAT3 *and* PIM *kinase expression is upregulated in inflamed glomeruli of patients with PR3-ANCA-GN*

To extend our peripheral blood findings to the tissue level, we analysed a publicly available spatial transcriptomics dataset of PR3-ANCA-GN kidney biopsies [20] including 6 patients and 8 control samples (healthy tissue from tumour nephrectomies). UMAP projections and niche annotations from the original study (Fig 7A,B) demonstrated a higher prevalence of inflamed glomeruli and tubulointerstitial regions in PR3-ANCA-GN (Fig 7C). Expression of selected genes (*PIM1, PIM2, PIM3, STAT3, SOCS3, and IL6*) was increased in both inflamed compartments (Supplementary Fig S13). To quantify differential expression between PR3-ANCA-GN and control samples, average gene expression per sample was calculated. *PIM1, PIM2*, and *STAT3* were upregulated in inflamed glomeruli, whereas only *PIM2* showed increased expression in the inflamed tubulointerstitium (Fig 7D, E). To further assess the expression of these genes in renal (in-tissue) T cells, we analysed a scRNA-seq dataset from the same study [20] comprising 8 patients with PR3-ANCA-GN. UMAP analysis identified 15 renal T/Natural killer (T/NK) cell clusters (Fig 7F), with CD4$^+$ effector T cells representing the most abundant population, followed by CD8$^+$ effector T cells (Fig 7G). Among renal T-cell subsets, *PIM1, PIM2, PIM3, STAT3*, and *SOCS3* expression was highest in CD4$^+$ effector T cells (Fig 7H).

These spatial and single-cell transcriptomics findings provide tissue-level evidence for elevated *STAT3* and *PIM* kinase expression in the inflamed glomerular and renal CD4$^+$ effector T cells in PR3-ANCA-GN.

DISCUSSION

In this study, we characterised the transcriptional landscape of circulating CD4$^+$ T cells in PR3-GPA using an integrated single-cell and functional multiomics approach. Our data identify, for the first time, activation of the STAT3–PIM1 signalling axis in CD4$^+$ T-cell subsets during active disease, with IL-6 emerging as a key upstream cytokine potentially driving this pathway. *In vitro* inhibition of Pim kinases attenuated CD4$^+$ T-cell activation, proliferation, and proinflammatory cytokine production. Complementary analysis of spatial transcriptomics data from PR3-ANCA-GN biopsies further demonstrated upregulation of *STAT3* and *PIM* kinase (*PIM1* and *PIM2*) expression within inflamed glomerular niches. Collectively, these findings implicate the STAT3–PIM1 axis as a mediator of CD4$^+$ T-cell–driven inflammation in PR3-GPA and highlight this pathway as a potential therapeutic target.

Pim kinases (Pim-1, Pim-2, and Pim-3) are well studied in oncology [29], but their immunological roles in humans have only recently gained attention [24,30,31]. Emerging evidence implicates Pim kinases in immune dysregulation across several autoimmune diseases, including psoriasis [32], inflammatory bowel disease [33], lupus nephritis [34], and RA [35]. Here, we demonstrate that *PIM1* mRNA is upregulated in circulating CD4$^+$ T-cell subsets from patients with PR3-GPA with active disease, as revealed by single-cell transcriptomic analyses and confirmed by RT-qPCR in bulk-sorted subsets, and at the protein level by increased intracellular Pim-1 expression. This aligns with reports of elevated *PIM1* expression in CD4$^+$ T cells from treatment-naive patients with early RA [28] and Vogt-Koyanagi–Harada disease [36].

Pim-1 promotes human Th1 differentiation by enhancing TBX21 (T-bet) and IFNγ expression [37] and modulates early Th17 differentiation [38], thereby promoting effector T-cell responses. Conversely, Pim-1 negatively regulates FOXP3$^+$ Tregs [39]. Given that skewed T-cell subset distribution, heightened T-cell activation, and impaired Treg function are hallmarks of PR3-GPA, the observed upregulation of *PIM1* in CD4$^+$ T-cell subsets, together with its association with activated T-cell phenotypes, supports a potential pathogenic role for Pim-1 in PR3-GPA. Interestingly, *PIM1* expression remained elevated during remission with both CITE-seq and RT-qPCR confirming sustained expression in effector memory CD4$^+$ T cells in clinically quiescent disease, suggesting incomplete normalisation. This aligns with prior reports of persistent T-cell activation during remission [4], suggesting that sustained *PIM1* expression may reflect ongoing immune activity. Longitudinal studies are warranted to determine whether *PIM1* may serve as a biomarker of immune persistence or relapse risk.

Although Pim kinases are downstream of multiple signalling cascades [40], Pim-1 is primarily induced by JAK–STAT signalling [29,38]. *PIM1* expression is regulated by STAT3 and STAT5

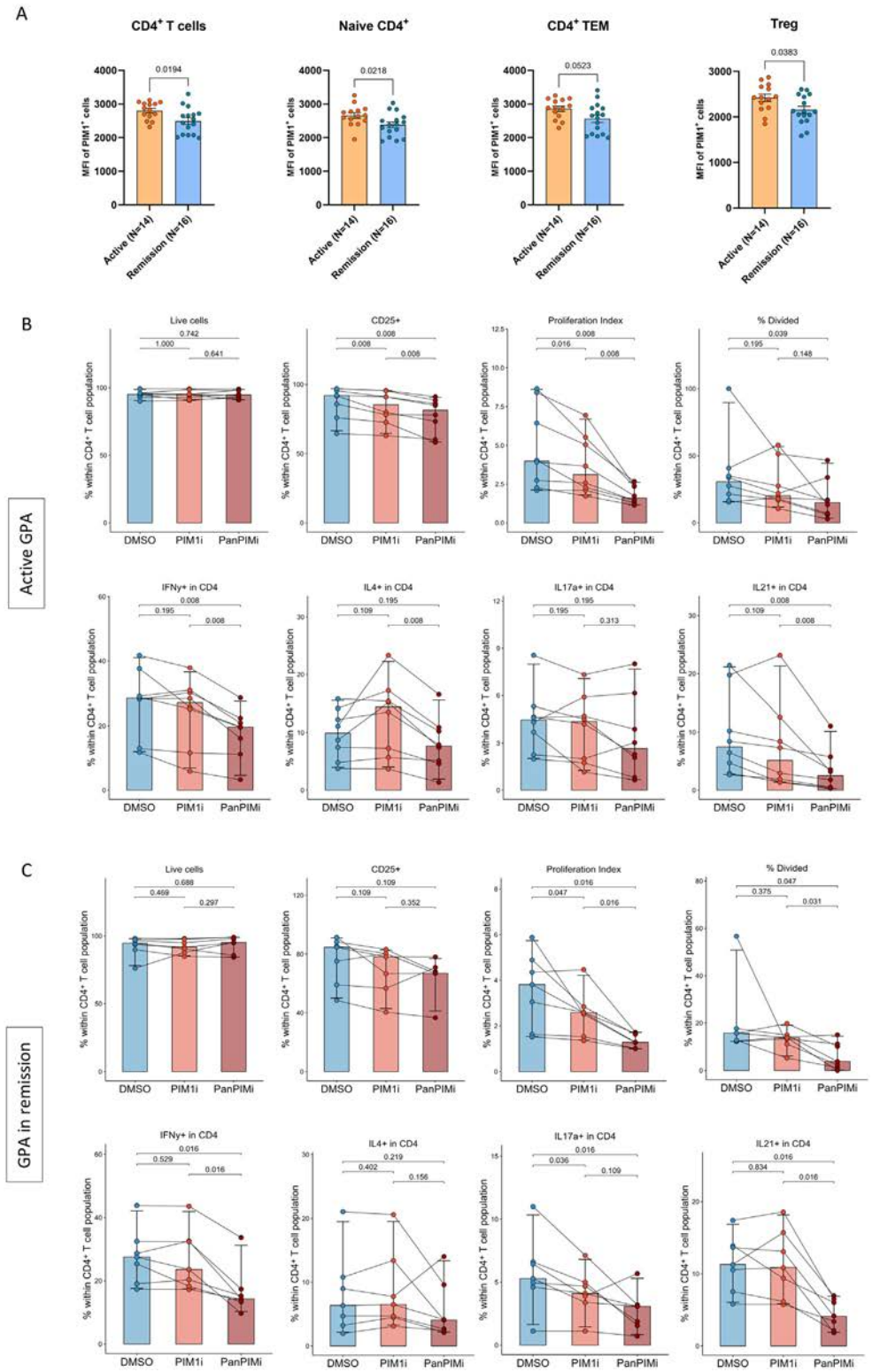

Figure 6. Pim kinase inhibitors reduce CD4⁺ T-cell activation, proliferation, and proinflammatory cytokine production. (A) Pim-1 protein expression level was assessed in CD4$^+$ T-cell subsets using intracellular flow cytometry. Data are presented as median fluorescence intensity (MFI). Statistical analysis was performed using a Mann-Whitney U test with significance defined as P <.05. For *in vitro* Pim kinase inhibition assays, CD4⁺ T cells were isolated from PBMCs of patients with active PR3-GPA (n = 8) and patients with PR3-GPA in remission (n = 7). Purified CD4⁺ T cells (92%-98% purity) were cultured for 6 days under T-cell receptor stimulation (anti-CD3, 0.5 μg/mL; anti-CD28/49d, 1 μg/mL) in the presence of DMSO (control), a Pim-1 −selective inhibitor (PIM1i, 20 μM), or a pan-Pim inhibitor (PanPIMi, 10 μM). Results from active GPA are shown in panel (B) and from remission in panel (C). Panels display the frequency of live CD4⁺ T cells, CD25 expression as a marker of T-cell activation, proliferation index (refers to the average number of cells that an initial cell became) and percentage of divided cells (refers to the percentage of the original cells that divided) assessed by cell proliferation dye staining and analysed using FCS Express software (De Novo Software) and production of intracellular IFNγ, IL-4, IL-17a, and IL-21 following restimulation on day 6 with phorbol 12-myristate 13-acetate (PMA)/calcium ionophore (CaI)/brefeldin A (BFA). Data are presented as median with the 2.5th and 97.5th percentiles and paired individual values. Statistical analysis was performed using the 2-sided Wilcoxon rank-sum test, with significance defined as P < .05. DMSO, dimethyl sulfoxide; GPA, granulomatosis with polyangiitis; PBMC, peripheral blood mononuclear cell; PR3-GPA, proteinase 3-ANCA-positive granulomatosis with polyangiitis; IFNγ, interferon-gamma; IL, interleukin.

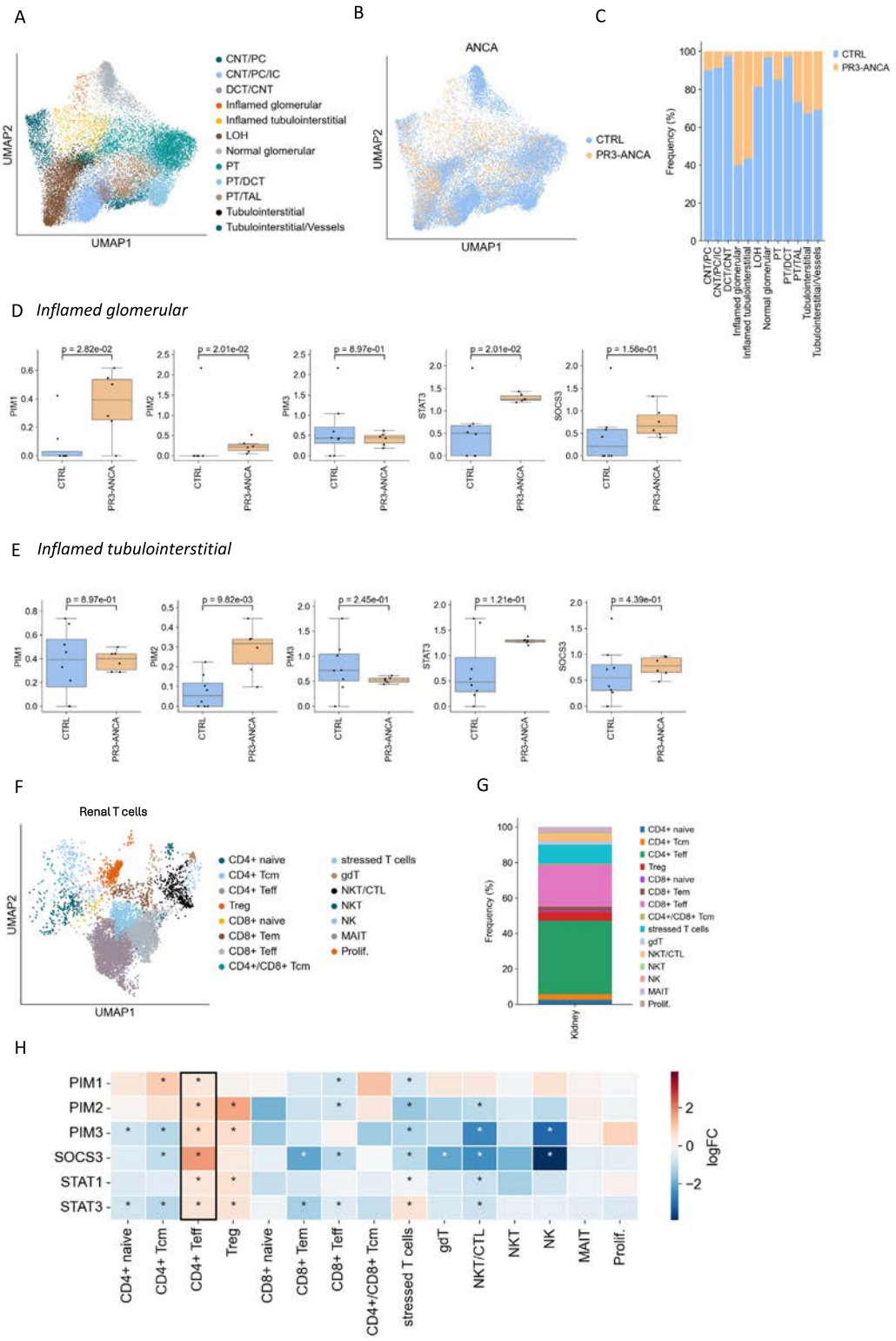

Figure 7. Spatial and single-cell transcriptomic profiling identifies *STAT3* and *PIM* kinase expression in inflamed renal niches and infiltrating CD4$^+$ T cells of PR3-ANCA–associated glomerulonephritis (PR3-ANCA-GN). Spatial and single-cell transcriptomics data were obtained from publicly available datasets (Engesser et al [20], 2024; NCBI GEO accession numbers GSE250138 and GSE253633, respectively). Biopsies of the patient with PR3-ANCA-GN (n = 6) and control samples from healthy tissue of tumour nephrectomies (n = 8) were analysed, and the original spatial niche annotation was retained. (A) UMAP of annotated spatial niches comprising 12 clusters. (B) UMAP showing distribution of niches between controls (CTRL) and PR3-ANCA-GN groups. (C) Relative distribution of annotated spatial niches per group. (D) Differential gene expression analysis based on sample-level averaged expression in the inflamed glomerular niche. (E) Differential gene expression analysis based on sample-level averaged expression in the inflamed tubulointerstitial niche. Differential expression was assessed using the Wilcoxon rank-sum test. Single-cell transcriptomic analysis of renal T cells was performed using PR3-ANCA-GN samples (n = 8). (F) UMAP representation of renal T/NK cell subsets comprising 15 clusters. (G) Relative abundance of renal T/NK cell subsets. (H) Heatmap depicting differential expression of PIM family kinases and STAT signalling-related genes across renal T-cell populations, shown as log fold change (logFC). Asterisks indicate statistically significant differential expression (*P*adj < .05). UMAP, Uniform Manifold Approximation and Projection; MAIT, mucosal-associated invariant T cell; T/NK, T cell/natural killer cell; NKT, natural killer T cell, CNT, connecting tubule; CTRL, controls; DCT, distal convoluted tubule; IC, intercalated cell; LOH, loop of Henle; PC, principal cell; PR3-ANCA-GN, proteinase 3-anti-neutrophil cytoplasmic antibody-positive–associated glomerulonephritis; PT, proximal tubule; TAL, thick ascending limb of Henle's loop.

phosphorylation. Cytokines such as IL-6, IL-10, IL-21, IL-23, and G-CSF predominantly signal through STAT3 [41], whereas IL-2, IL-7, IL-15, and GM-CSF act primarily via STAT5 [42], and IFNγ signals through STAT1; all of which can induce *PIM1* expression [40]. Among these, IL-6 and IL-15 have been strongly linked to PR3-GPA [7,27]. As IL-6 is a central driver of chronic autoimmune inflammation, this directed our attention to its potential role as an upstream regulator of Pim-1. In line with this, a recent plasma proteomics study [43] identified enrichment of STAT3 signalling pathways in PR3-ANCA–positive compared with MPO-ANCA–positive vasculitis. In our cohort, IL-6 was elevated during active disease, accompanied by increased baseline proportions of pSTAT3-positive cells and higher pSTAT3 expression levels, together with induction of *STAT3* and *SOCS3* mRNA in $CD4^+$ T-cell subsets. Together, these observations demonstrate involvement of IL-6–JAK–STAT3 signalling in *PIM1* upregulation. However, our data do not indicate that this pathway is exclusively responsible, and other cytokines and signalling pathways, including STAT5-mediated mechanisms, may also contribute. Interestingly, proportions of pSTAT3-positive $CD4^+$ T cells following IL-6 stimulation did not differ between patients and controls, suggesting that T cells may have already reached their activation plateau. Although IL-15 was also elevated during active disease, baseline proportions and expression levels of pSTAT5 remained unchanged. These findings identify upregulation of the IL-6–STAT3–PIM1 axis in active PR3-GPA and suggest it may represent a common inflammatory mechanism similar to those previously described in other autoimmune diseases, including RA [44]. Consistent with this, patients with MPO-ANCA–positive MPA showed largely comparable *PIM1* and *STAT3* expression across $CD4^+$ T-cell subsets. However, we did not comprehensively assess other cytokines capable of activating STAT3–PIM1 signalling, and further studies are required to define the full spectrum of cytokines that can induce or modulate this pathway in PR3-GPA.

In vitro inhibition of Pim kinases, using either a selective Pim-1 inhibitor or a pan-Pim inhibitor, reduced $CD4^+$ T-cell proliferation and suppressed IFNγ and IL-21 production in both active and remission patients with PR3-GPA. The decrease in IFNγ^+ $CD4^+$ T cells aligns with findings in RA using similar inhibitors [28]. In the same study, Pim-1 inhibition led to a reduction in IL-17A$^+$ $CD4^+$ T cells, whereas in our cohort, this effect was observed only during remission and not in active disease. IL-4$^+$ $CD4^+$ T cells showed no significant changes, except that in active disease, PanPIMi treatment reduced IL-4$^+$ $CD4^+$ T cells in active disease compared with PIM1i. These discrepancies may reflect interindividual variability in inhibitor responses. Notably, a decrease in IL-21$^+$ $CD4^+$ T cells was observed, suggesting that Pim kinases may influence Tfh cells, a subset implicated in PR3-ANCA generation [6]. Previous studies have demonstrated Tfh expansion in GPA [6]. Further studies will be required to define the precise contribution of Pim kinases to Tfh biology in this context. Pim inhibition did not lead to an increase in $CD25^{hi}$-FOXP3$^+$ Treg cells, in contrast to previous reports [28]. One possible explanation may lie in the disease context: patients with PR3-GPA exhibit both numerical and functional Treg impairments [22,45], and the inflammatory milieu may override Pim-dependent regulation. Alternatively, discrepancies could stem from differences in assay conditions or selective effects on memory/effector vs naive T-cell subsets. Future studies should therefore aim to dissect isoform- and subset-specific roles of Pim kinases in $CD4^+$ T cells.

The relevance of the STAT3–PIM axis was further supported by analysis of a publicly available spatial transcriptomics dataset from PR3-ANCA-GN kidney biopsies [20]. This revealed significant upregulation of *STAT3, PIM1*, and *PIM2* expression within inflamed glomeruli and only *PIM2* expression within inflamed tubulointerstitium compared with controls. Although these niches were not exclusively composed of $CD4^+$ T cells, the original dataset demonstrated localisation of $CD4^+$ Th1 and Th17 cells within these regions [20]. Consistently, complementary single-cell RNA-seq analysis from the same study showed higher expression of *PIM1, PIM2, PIM3, STAT3*, and *SOCS3* in renal $CD4^+$ effector T cells, supporting activation of the STAT3–PIM axis in infiltrating renal T cells. Importantly, drug prediction analysis from the same dataset identified tocilizumab, an IL-6 receptor antagonist, as a potential therapeutic targeting these inflamed compartments [20], further supporting the clinical relevance of targeting this pathway in PR3-GPA.

From a translational perspective, several therapeutic strategies could be considered to target this signalling axis. IL-6 receptor inhibition with tocilizumab, approved for RA [46] and giant cell arteritis [47], remains a plausible therapeutic approach. Small studies and case reports have also indicated potential benefit in ANCA-associated vasculitis, particularly in MPA [48,49]. Similarly, JAK–STAT inhibitors are being investigated across multiple autoimmune diseases [50], with a pilot study of tofacitinib, an oral JAK1/3 inhibitor, suggesting potential efficacy in refractory GPA [51,52]. PIM kinase inhibitors, primarily explored in oncology, have also entered clinical trials [53], including pan-Pim inhibitors such as AZD1208 (AstraZeneca), PIM447 (Novartis), and INCB053914 (Incyte), though none have achieved approval yet [29]. More recently, efforts have shifted towards PIM1-selective inhibitors, such as Nuvisertib (TP-3654) [54], which has shown early signs of benefit in cancer. Notably, a subanalysis of the PROTECT-V (PROphylaxis for paTiEnts at risk of COVID-19 infecTion) randomised, placebo-controlled trial evaluating intranasal niclosamide (which inhibits STAT3 phosphorylation) in AAV reported reduced ear, nose, and throat manifestations during treatment, particularly in PR3-ANCA–positive patients. These findings are consistent with a potential role for IL-6–STAT3–related signalling in AAV and suggest that this pathway may represent a therapeutic target, although they remain preliminary and require confirmation [55].

Our study has several limitations that should be acknowledged. Our single-cell analyses were conducted in a limited number of samples, although findings were validated by independent RT-qPCR, protein-level analyses, and functional assays. Although *in vitro* inhibition demonstrated effects of Pim kinase blockade, confirmation in larger cohorts and ultimately *in vivo* studies will be required to establish safety and efficacy. Although Pim-1 emerged as the dominant isoform, Pim-2 was also upregulated in our data, and the relative contributions of individual isoforms remain to be clarified. Finally, whether persistent *PIM1* expression during remission can reliably predict relapse will need to be addressed in longitudinal studies.

In conclusion, our single-cell multiomics investigation revealed the STAT3–PIM1 axis, possibly driven by IL-6, as a defining feature of activated circulating $CD4^+$ T cells in PR3-GPA. By integrating data from peripheral blood and kidney tissue, these findings highlight Pim kinases and upstream IL-6–JAK–STAT signalling as potential therapeutic targets warranting further exploration in PR3-GPA.

Competing interests

The authors declare no conflicts of interest.

Acknowledgements

We would like to thank the patients and healthy controls for their participation in this study. We also thank Single Cell Discoveries for their support with project design, single-cell sequencing services, and data analysis. In addition, we extend our appreciation to Irene Sanz Fernández and Anouk Bouwmeester for their contribution to this work. Part of this work was presented at the 21st International Vasculitis Workshop, and the abstract was published.

Contributors

NI contributed in performance of the experiments, data analysis, and writing – original draft preparation. CGB contributed in data analysis and writing – original draft preparation. KPM, MAJ-W, SJB, OW, PDM, and RRV contributed in performance of the experiments and writing – review & editing. MB, TB, and RDR contributed in data analysis and writing – review & editing. WHA, J-SFS, AR, and PH contributed in conceptualisation and writing – review & editing.

Funding

This project was supported by the Development and Promotion of Science and Technology Talents Project (Royal Government of Thailand scholarship awarded to NI) and by funding from the De Cock-Hadders Foundation. The project also received funding from the Dutch Ministry of Economic Affairs and Climate Policy through the Public-Private Partnership (PPP)-allowance made available by the Top Sector Life Sciences & Health to stimulate public-private partnerships (Project: UMCG PPP-2021-02). Single-cell RNA sequencing was supported by a grant from the Dutch Vasculitis Foundation.

Patient consent for publication

Not applicable.

Ethics approval

The study protocol was approved by the Institutional Review Board of the University Medical Center Groningen (METc no. 2012/151 and 2020/007) was conducted according to Declaration of Helsinki principles. All participants provided written informed consent.

Provenance and peer review

Not commissioned; externally peer reviewed.

Data availability statement

Single-cell RNA sequencing and Cellular Indexing of Transcriptomes and Epitopes by sequencing data generated in this study are available in the NCBI GEO database under accession number GSE331351 (active GPA, n = 3) and GSE330573, respectively. Healthy control scRNA-seq data (n = 3) were previously deposited under GSE198891. Other data supporting the findings of this study are available from the corresponding author upon request.

Declaration of generative AI and AI-assisted technologies in the writing process

During the preparation of this work, the authors used ChatGPT (GPT-5, OpenAI) in order to check grammar and improve language clarity. After using this tool, the authors reviewed and edited the content as needed and take full responsibility for the content of the publication. The AI tool did not contribute to the conceptual development, data interpretation, or conclusions of the study.

Supplementary materials

Supplementary material associated with this article can be found in the online version at doi:10.1016/j.ard.2026.05.003.

Orcid

Nanthicha Inrueangsri: http://orcid.org/0009-0008-1028-8403

REFERENCES

[1] Kitching AR, Anders HJ, Basu N, Brouwer E, Gordon J, Jayne DR, et al. ANCA-associated vasculitis. Nat Rev Dis Primers 2020 Aug 27;6(1):71. doi: 10.1038/s41572-020-0204-y.

[2] Falde SD, Fussner LA, Tazelaar HD, O'Brien EK, Lamprecht P, Konig MF, et al. Proteinase 3-specific antineutrophil cytoplasmic antibody-associated vasculitis. Lancet Rheumatol. 2024 May;6(5):e314–27. doi: 10.1016/S2665-9913(24)00035-3.

[3] Hellmich B, Sanchez-Alamo B, Schirmer JH, Berti A, Blockmans D, Cid MC, et al. EULAR recommendations for the management of ANCA-associated vasculitis: 2022 update. Ann Rheum Dis. 2024 Jan;83(1):30–47. doi: 10.1136/ard-2022-223764.

[4] Marinaki S, Kälsch AI, Grimminger P, Breedijk A, Birck R, Schmitt WH, et al. Persistent T-cell activation and clinical correlations in patients with ANCA-associated systemic vasculitis. Nephrol Dial Transplant. 2006 Jul;21(7):1825–32. doi: 10.1093/ndt/gfl097.

[5] Abdulahad WH, Stegeman CA, Limburg PC, Kallenberg CG. Skewed distribution of Th17 lymphocytes in patients with Wegener's granulomatosis in remission. Arthritis Rheum. 2008 Jul;58(7):2196–205. doi: 10.1002/art.23557.

[6] Abdulahad WH, Lepse N, Stegeman CA, Huitema MG, Doornbos-van der Meer B, Tadema H, et al. Increased frequency of circulating IL-21 producing Th-cells in patients with granulomatosis with polyangiitis (GPA). Arthritis Res Ther. 2013;15(3):R70. doi: 10.1186/ar4247.

[7] Bonasia CG, Inrueangsri N, Bijma T, Mennega KP, Wilbrink R, Arends S, et al. Circulating immune profile in granulomatosis with polyangiitis reveals distinct patterns related to disease activity. J Autoimmun. 2024 Jun;146:103236. doi: 10.1016/j.jaut.2024.103236.

[8] Abdulahad WH, van der Geld YM, Stegeman CA, Kallenberg CG. Persistent expansion of CD4+ effector memory T cells in Wegener's granulomatosis. Kidney Int. 2006 Sep;70(5):938–47. doi: 10.1038/sj.ki.5001670.

[9] Wilde B, Thewissen M, Damoiseaux J, van Paassen P, Witzke O, Tervaert JW. T cells in ANCA-associated vasculitis: what can we learn from lesional versus circulating T cells? Arthritis Res Ther. 2010;12(1):204. doi: 10.1186/ar2923.

[10] Komocsi A, Lamprecht P, Csernok E, Mueller A, Holl-Ulrich K, Seitzer U, et al. Peripheral blood and granuloma CD4(+)CD28(-) T cells are a major source of interferon-gamma and tumor necrosis factor-alpha in Wegener's granulomatosis. Am J Pathol. 2002 May;160(5):1717–24. doi: 10.1016/s0002-9440(10)61118-2.

[11] Brouwer E, Tervaert JW, Horst G, Huitema MG, van der Giessen M, Limburg PC, et al. Predominance of IgG1 and IgG4 subclasses of anti-neutrophil cytoplasmic autoantibodies (ANCA) in patients with Wegener's granulomatosis and clinically related disorders. Clin Exp Immunol. 1991 Mar;83(3):379–86. doi: 10.1111/j.1365-2249.1991.tb05647.x.

[12] Haque A, Engel J, Teichmann SA, Lönnberg T. A practical guide to single-cell RNA-sequencing for biomedical research and clinical applications. Genome Med. 2017 Aug 18;9(1):75. doi: 10.1186/s13073-017-0467-4.

[13] Shahi P, Kim SC, Haliburton JR, Gartner ZJ, Abate AR. Abseq: Ultrahigh-throughput single cell protein profiling with droplet microfluidic barcoding. Sci Rep. 2017 Mar;7:44447. doi: 10.1038/srep44447.

[14] Nishide M, Shimagami H, Kumanogoh A. Single-cell analysis in rheumatic and allergic diseases: insights for clinical practice. Nat Rev Immunol. 2024 Nov;24(11):781–97. doi: 10.1038/s41577-024-01043-3.
[15] Zhang F, Wei K, Slowikowski K, Fonseka CY, Rao DA, Kelly S, et al. Defining inflammatory cell states in rheumatoid arthritis joint synovial tissues by integrating single-cell transcriptomics and mass cytometry. Nat Immunol. 2019 Jul;20(7):928–42. doi: 10.1038/s41590-019-0378-1.
[16] Perez RK, Gordon MG, Subramaniam M, Kim MC, Hartoularos GC, Targ S, et al. Single-cell RNA-seq reveals cell type-specific molecular and genetic associations to lupus. Science. 2022 Apr;376(6589):eabf1970. doi: 10.1126/science.abf1970.
[17] Nishide M, Nishimura K, Matsushita H, Kawada S, Shimagami H, Metsugi S, et al. Neutrophil single-cell analysis identifies a type II interferon-related subset for predicting relapse of autoimmune small vessel vasculitis. Nat Commun. 2025 Apr;16(1):3581. doi: 10.1038/s41467-025-58550-7.
[18] Wei S, Tan L, Tang L, Xiong HY, Yang Q, Jiao J, et al. Single-cell RNA-sequencing of peripheral blood reveals neutrophil heterogeneity in childhood ANCA-associated vasculitis. J Inflamm Res. 2026 Jan 15;19:545080. doi: 10.2147/JIR.S545080.
[19] Nishide M, Nishimura K, Matsushita H, Edahiro R, Inukai S, Shimagami H, et al. Single-cell multi-omics analysis identifies two distinct phenotypes of newly-onset microscopic polyangiitis. Nat Commun. 2023 Oct;14(1):5789. doi: 10.1038/s41467-023-41328-0.
[20] Engesser J, Khatri R, Schaub DP, Zhao Y, Paust HJ, Sultana Z, et al. Immune profiling-based targeting of pathogenic T cells with ustekinumab in ANCA-associated glomerulonephritis. Nat Commun. 2024 Sep;15(1):8220. doi: 10.1038/s41467-024-52525-w.
[21] Jennette JC, Falk RJ, Bacon PA, Basu N, Cid MC, Ferrario F, et al. 2012 Revised International Chapel Hill Consensus Conference Nomenclature of Vasculitides. Arthritis Rheum. 2013 Jan;65(1):1–11. doi: 10.1002/art.37715.
[22] Dekkema GJ, Bijma T, Jellema PG, Van Den Berg A, Kroesen BJ, Stegeman CA, et al. Increased miR-142-3p expression might explain reduced regulatory T cell function in granulomatosis with polyangiitis. Front Immunol. 2019 Sep;10:2170. doi: 10.3389/fimmu.2019.02170.
[23] Wolf FA, Angerer P, Theis FJ. SCANPY: large-scale single-cell gene expression data analysis. Genome Biol. 2018 Feb;19(1):15. doi: 10.1186/s13059-017-1382-0.
[24] Yang X, Liu C, Lei Y, Liu Z, Zhu B, Zhao D. PIM1 signaling in immunoinflammatory diseases: an emerging therapeutic target. Front Immunol. 2024 Sep;15:1443784. doi: 10.3389/fimmu.2024.1443784.
[25] Kershaw NJ, Murphy JM, Liau NP, Varghese LN, Laktyushin A, Whitlock EL, et al. SOCS3 binds specific receptor-JAK complexes to control cytokine signaling by direct kinase inhibition. Nat Struct Mol Biol. 2013 Apr;20(4):469–76. doi: 10.1038/nsmb.2519.
[26] Narlik-Grassow M, Blanco-Aparicio C, Carnero A. The PIM family of serine/threonine kinases in cancer. Med Res Rev. 2014 Jan;34(1):136–59. doi: 10.1002/med.21284.
[27] Berti A, Warner R, Johnson K, Cornec D, Schroeder D, Kabat B, et al. Brief Report: circulating cytokine profiles and antineutrophil cytoplasmic antibody specificity in patients with antineutrophil cytoplasmic antibody-associated vasculitis. Arthritis Rheumatol. 2018 Jul;70(7):1114–21. doi: 10.1002/art.40471.
[28] Maney NJ, Lemos H, Barron-Millar B, Carey C, Herron I, Anderson AE, et al. Pim kinases as therapeutic targets in early rheumatoid arthritis. Arthritis Rheumatol. 2021 Oct;73(10):1820–30. doi: 10.1002/art.41744.
[29] Bellon M, Nicot C. Targeting Pim kinases in hematological cancers: molecular and clinical review. Mol Cancer. 2023 Jan;22(1):18. doi: 10.1186/s12943-023-01721-1.
[30] Liu Z, Han M, Ding K, Fu R. The role of Pim kinase in immunomodulation. Am J Cancer Res. 2020 Dec;10(12):4085–97.
[31] Assirelli E, Ciaffi J, Scorcu V, Naldi S, Brusi V, Mancarella L, et al. PIM kinases as potential biomarkers and therapeutic targets in inflammatory arthritides. Int J Mol Sci. 2024 Mar;25(6):3123. doi: 10.3390/ijms25063123.
[32] Perera GK, Ainali C, Semenova E, Hundhausen C, Barinaga G, Kassen D, et al. Integrative biology approach identifies cytokine targeting strategies for psoriasis. Sci Transl Med. 2014 Feb;6(223):223ra22. doi: 10.1126/scitranslmed.3007217.
[33] Jackson LJ, Pheneger JA, Pheneger TJ, Davis G, Wright AD, Robinson JE, et al. The role of PIM kinases in human and mouse CD4+ T cell activation and inflammatory bowel disease. Cell Immunol. 2012;272(2):200–13. doi: 10.1016/j.cellimm.2011.10.011.
[34] Fu R, Xia Y, Li M, Mao R, Guo C, Zhou M, et al. Pim-1 as a therapeutic target in lupus nephritis. Arthritis Rheumatol. 2019 Aug;71(8):1308–18. doi: 10.1002/art.40863.
[35] Ha YJ, Choi YS, Han DW, Kang EH, Yoo IS, Kim JH, et al. PIM-1 kinase is a novel regulator of proinflammatory cytokine-mediated responses in rheumatoid arthritis fibroblast-like synoviocytes. Rheumatology (Oxford). 2019 Jan;58(1):154–64. doi: 10.1093/rheumatology/key261.
[36] Li H, Xie L, Zhu L, Li Z, Wang R, Liu X, et al. Multicellular immune dynamics implicate PIM1 as a potential therapeutic target for uveitis. Nat Commun. 2022 Oct;13(1):5866. doi: 10.1038/s41467-022-33502-7.
[37] Tahvanainen J, Kyläniemi MK, Kanduri K, Gupta B, Lähteenmäki H, Kallonen T, et al. Proviral integration site for Moloney murine leukemia virus (PIM) kinases promote human T helper 1 cell differentiation. J Biol Chem. 2013 Feb;288(5):3048–58. doi: 10.1074/jbc.M112.361709.
[38] Buchacher T, Shetty A, Koskela SA, Smolander J, Kaukonen R, Sousa AGG, et al. PIM kinases regulate early human Th17 cell differentiation. Cell Rep. 2023 Dec;42(12):113469. doi: 10.1016/j.celrep.2023.113469.
[39] Li Z, Lin F, Zhuo C, Deng G, Chen Z, Yin S, et al. PIM1 kinase phosphorylates the human transcription factor FOXP3 at serine 422 to negatively regulate its activity under inflammation. J Biol Chem. 2014 Sep;289(39):26872–81. doi: 10.1074/jbc.M114.586651.
[40] Tursynbay Y, Zhang J, Li Z, Tokay T, Zhumadilov Z, Wu D, et al. Pim-1 kinase as cancer drug target: an update. Biomed Rep. 2016 Feb;4(2):140–6. doi: 10.3892/br.2015.561.
[41] Egwuagu CE. STAT3 in CD4+ T helper cell differentiation and inflammatory diseases. Cytokine 2009 Sep;47(3):149–56. doi: 10.1016/j.cyto.2009.07.003.
[42] Read KA, Powell MD, McDonald PW, Oestreich KJ. IL-2, IL-7, and IL-15: multistage regulators of CD4(+) T helper cell differentiation. Exp Hematol. 2016 Sep;44(9):799–808. doi: 10.1016/j.exphem.2016.06.003.
[43] Hellbacher E, van Hoef V, Johansson A, Knight A, Gunnarsson I, Bruchfeld A, et al. The plasma proteome reveals distinct signaling pathways associated with PR3-ANCA positive and MPO-ANCA positive vasculitis. Front Immunol. 2025 Jun;16:1600754. doi: 10.3389/fimmu.2025.1600754.
[44] Anderson AE, Pratt AG, Sedhom MA, Doran JP, Routledge C, Hargreaves B, et al. IL-6-driven STAT signalling in circulating CD4+ lymphocytes is a marker for early anticitrullinated peptide antibody-negative rheumatoid arthritis. Ann Rheum Dis. 2016 Feb;75(2):466–73. doi: 10.1136/annrheumdis-2014-205850.
[45] Abdulahad WH, Stegeman CA, van der Geld YM, Doornbos-van der Meer B, Limburg PC, Kallenberg CG. Functional defect of circulating regulatory CD4 + T cells in patients with Wegener's granulomatosis in remission. Arthritis Rheum. 2007 Jun;56(6):2080–91. doi: 10.1002/art.22692.
[46] Parisi S, Ditto MC, Ghellere F, Panaro S, Piccione F, Borrelli R, et al. Update on tocilizumab in rheumatoid arthritis: a narrative review. Front Immunol. 2025 Feb;16:1470488. doi: 10.3389/fimmu.2025.1470488.
[47] Conway R, Putman MS, Mackie SL. Benchmarking tocilizumab use for giant cell arteritis. Rheumatol Adv Pract. 2022 May;6(2):rkac037. doi: 10.1093/rap/rkac037.
[48] Sakai R, Kondo T, Kurasawa T, Nishi E, Okuyama A, Chino K, et al. Current clinical evidence of tocilizumab for the treatment of ANCA-associated vasculitis: a prospective case series for microscopic polyangiitis in a combination with corticosteroids and literature review. Clin Rheumatol. 2017 Oct;36(10):2383–92. doi: 10.1007/s10067-017-3752-0.
[49] Berti A, Cavalli G, Campochiaro C, Guglielmi B, Baldissera E, Cappio S, et al. Interleukin-6 in ANCA-associated vasculitis: rationale for successful treatment with tocilizumab. Semin Arthritis Rheum. 2015 Aug;45(1):48–54. doi: 10.1016/j.semarthrit.2015.02.002.
[50] Banerjee S, Biehl A, Gadina M, Hasni S, Schwartz DM. JAK-STAT signaling as a target for inflammatory and autoimmune diseases: current and future prospects. Drugs. 2017 Apr;77(5):521–46. doi: 10.1007/s40265-017-0701-9.
[51] Linde L, Faurschou M, Krintel SB, Baslund B. Response to treatment with tofacitinib in 11 patients with refractory granulomatosis with polyangiitis. J Rheumatol 2023 Aug;50(8):1088–9. doi: 10.3899/jrheum.221219.
[52] Liu Y, Ji Z, Yu W, Wu S, Chen H, Ma L, et al. Tofacitinib for the treatment of antineutrophil cytoplasm antibody-associated vasculitis: a pilot study. Ann Rheum Dis. 2021 Dec;80(12):1631–3. doi: 10.1136/annrheumdis-2021-220484.
[53] Asati V, Mahapatra DK, Bharti SK. PIM kinase inhibitors: structural and pharmacological perspectives. Eur J Med Chem. 2019 Jun;172:95–s108. doi: 10.1016/j.ejmech.2019.03.050.
[54] El Chaer F, Rein LAM, Yuda J, Shimoda K, Takami A, Ichii M, et al. Nuvisertib (TP-3654), an investigational selective PIM1 kinase inhibitor, showed durable clinical response and sustained hematological improvement in relapsed/refractory myelofibrosis patients. Blood. 2024;144:655. doi: 10.1182/blood-2024-200312.
[55] Lim B, Qian W, Dowling F, Salama A, Smith RM. The effect of intranasal niclosamide on nasal symptoms in patients with antineutrophil cytoplasmic antibody-associated vasculitis. Arthritis Rheumatol. 2026 Apr;78(4):970–5. doi: 10.1002/art.70061.

Ann Rheum Dis 85 (2026) 1854–1865

Contents lists available at ScienceDirect

Annals of the Rheumatic Diseases

journal homepage: https://www.sciencedirect.com/journal/annals-of-the-rheumatic-diseases

Paediatric rheumatology

Impact of tofacitinib on growth in patients with juvenile idiopathic arthritis

Hermine I. Brunner[1,*], Mittermayer Santiago[2], Beth Gottlieb[3], Sheila K. Oliveira[4], Pooja Patel[5], Viviane Angelina De Souza[6], Kristin Houghton[7], Clovis A. Silva[8], Maria Teresa Terreri[9], Ruben Cuttica[10], Muammer Hakan Poyrazoglu[11], Halley M. Wasserman[12], Michelle Saul[13], Catherine I. Soderstrom[14], Annette Diehl[15], Ivana Vranic[16], Arne Yndestad[17], Mahta Mortezavi[18], Daniel J. Lovell[1], Alberto Martini[19], Nicolino Ruperto[20,21], for the Paediatric Rheumatology International Trials Organisation (PRINTO) and the Pediatric Rheumatology Collaborative Study Group (PRCSG)

[1] *Division of Rheumatology, Department of Pediatrics, Cincinnati Children's Hospital Medical Center, Cincinnati, Ohio, USA*
[2] *Serviços Especializados em Reumatologia da Bahia, Salvador, Bahia, Brazil*
[3] *Pediatric Rheumatology, Cohen Children's Medical Center, Northwell, New Hyde Park, New York, USA*
[4] *Instituto de Puericultura e Pediatria Martagao Gesteira, Universidade Federal do Rio de Janeiro, Rio de Janeiro, Brazil*
[5] *Division of Rheumatology, Ann & Robert H. Lurie Children's Hospital of Chicago, Chicago, Illinois, USA*
[6] *CMIP-Centro Mineiro de Pesquisa Ltda/Reumatocenter Rua Delfim Moreira, Faculdade de Medicina da Universidade Federal de Juiz De Fora, Juiz de Fora, Brazil*
[7] *Division of Rheumatology, Department of Pediatrics, British Columbia Children's Hospital and University of British Columbia, Vancouver, British Columbia, Canada*
[8] *Pediatric Rheumatology Unit, Instituto da Criança e do Adolescente, Hospital das Clinicas da FMUSP, São Paulo, Brazil*
[9] *Rheumatology Division, Pediatrics Department, Federal University of Sao Paulo, Sao Paulo, Brazil*
[10] *Pediatric Rheumatology, Hospital Britanico de Buenos Aires, Buenos Aires, Argentina*
[11] *Division of Pediatric Rheumatology, Department of Pediatrics, Erciyes University Faculty of Medicine, Kayseri, Turkey*
[12] *Division of Pediatrics, Department of Endocrinology, Cincinnati Children's Hospital Medical Center and University of Cincinnati College of Medicine, Cincinnati, Ohio, USA*
[13] *Pfizer Inc, Biomarker Statistics, La Jolla, California, USA*
[14] *Pfizer Inc, Translational Clinical Sciences, Groton, Connecticut, USA*
[15] *Pfizer Inc, Inflammation and Immunology, Collegeville, Pennsylvania, USA*
[16] *Pfizer Ltd, Safety Surveillance and Risk Management, Tadworth, Surrey, UK*
[17] *Pfizer Inc, Inflammation and Immunology, Oslo, Norway*
[18] *Pfizer Inc, Inflammation and Immunology, New York, New York, USA*
[19] *University of Genova, Genova, Italy*
[20] *Dipartimento di Medicina e Chirurgia, Università Milano Bicocca, Monza, Italy*
[21] *Fondazione IRCCS San Gerardo dei Tintori, Reumatologia Pediatrica, PRINTO, Monza Italy*

*Correspondence to Dr. Hermine I. Brunner, Division of Rheumatology, Cincinnati Children's Hospital Medical Center, 3333 Burnet Avenue, Cincinnati, OH, USA.
E-mail address: hermine.brunner@cchmc.org (H.I. Brunner).
Handling editor Josef S. Smolen.

https://doi.org/10.1016/j.ard.2026.03.030

0003-4967/© 2026 The Author(s). Published by Elsevier B.V. on behalf of European Alliance of Associations for Rheumatology (EULAR). This is an open access article under the CC BY-NC-ND license (http://creativecommons.org/licenses/by-nc-nd/4.0/)

ARTICLE INFO

Article history:
Received 28 November 2025
Received in revised form 26 March 2026
Accepted 27 March 2026

ABSTRACT

Objectives: Tofacitinib is a Janus kinase inhibitor studied in different categories of juvenile idiopathic arthritis (JIA). This *post hoc* analysis evaluated the impact of tofacitinib on the growth of patients with JIA and on biomarkers of growth hormone (GH) function and bone metabolism.
Methods: The analysis included 225 patients, primarily with polyarticular-course JIA, receiving long-term tofacitinib (median [IQR] follow-up 3.6 [1.9-4.6] years). Height velocities (cm/y) and height Z-scores (based on age- and sex-matched reference data) were calculated. Biomarkers were measured in serum from 137 patients with JIA completing 18 weeks of open-label treatment with tofacitinib.
Results: This population of patients with JIA had a baseline height distribution similar to the general population. During treatment with tofacitinib, patients experienced height velocities that appeared greater (patients ≤12 years) or as expected (patients >12 years) relative to the reference for their ages. Height Z-scores were largely stable during treatment with tofacitinib. In patients in puberty and a height Z-score less than −−1.0 at baseline, an increase in height Z-score ($P < .05$) was detected after 24 months of treatment. Tofacitinib treatment did not impact levels of insulin-like growth factor (IGF)-1, IGF binding protein 3 and osteocalcin in the overall population, but in patients aged 6 to 12 years, IGF-1 levels increased with tofacitinib from baseline to 18 weeks.
Conclusions: This *post hoc* analysis of patients with JIA indicated normal or higher than expected growth velocity during long-term treatment, with tofacitinib with catch-up growth during puberty and, overall, no concerning changes in biomarkers of GH signalling.

WHAT IS ALREADY KNOWN ON THIS TOPIC

- Growth failure is a well-known complication in children and adolescents with chronic inflammatory conditions such as juvenile idiopathic arthritis (JIA).
- Tofacitinib is an oral Janus kinase inhibitor used in different categories of JIA, particularly in those with polyarticular-course JIA.

WHAT THIS STUDY ADDS

- This *post hoc* analysis of the tofacitinib JIA development programme found that patients with JIA receiving long-term treatment with tofacitinib (median follow-up 3.6 years) had normal height Z-scores.
- In younger patients with JIA (≤12 years of age), height velocities during tofacitinib treatment were higher than expected from a reference population, and catch-up growth was observed in patients in puberty or 6 to 12 years of age and low baseline height Z-scores.
- No concerning changes in biomarkers of growth hormone function were seen after 18 weeks of treatment with tofacitinib.

HOW THIS STUDY MIGHT AFFECT RESEARCH, PRACTICE OR POLICY

- These results support the safety of long-term use of tofacitinib in children with JIA and inform the impact of treatment on growth.

INTRODUCTION

Growth failure is a complication in children and adolescents with chronic inflammatory conditions such as juvenile idiopathic arthritis (JIA), childhood-onset systemic lupus erythematosus, juvenile dermatomyositis, and inflammatory bowel disease [1–6]. The impact on growth has been attributed to uncontrolled disease activity, active systemic and local inflammation, and the prolonged use of glucocorticoids [6]. Common for these factors is a negative impact on the growth hormone (GH)-insulin-like growth factor (IGF) axis and the growth plate directly [6]. IGF-1, IGF binding protein 3 (IGFBP3), and osteocalcin are all produced in response to GH and their levels peak at the time of the adolescent growth spurt and are low when GH production or activity is impaired [6–10].

Tofacitinib is an oral Janus kinase (JAK) inhibitor used in different categories of JIA, particularly in those with polyarticular-course JIA (pcJIA) [11,12]. The weight-based dosing regimen of tofacitinib tablets and oral solution for children with JIA aged ≥2 years was determined in a phase 1 study [13], and a phase 3 withdrawal study assessed the safety and efficacy of tofacitinib in patients with pcJIA, juvenile psoriatic arthritis (jPsA), and enthesitis-related arthritis (ERA) [14]. A recent interim analysis of an open-label long-term extension (LTE) study, enrolling patients who completed the phase 1 or phase 3 study, did not observe any safety findings unique to the JIA population treated with tofacitinib or new to the tofacitinib safety profile [15].

The primary mechanism of action of tofacitinib is through inhibition of JAK1 and JAK3 [16]. To a much lesser extent, it can also inhibit JAK2; however, the JAK2 inhibition at clinically approved concentrations for JIA (5 mg twice daily or weight-based equivalent for patients <40 kg) is thought to be minimal [16,17]. The latter is of particular importance since JAK2 is a part of the receptor mechanism for GH, leading to the production of IGF-1 [6]. Importantly, existing data from preclinical studies in juvenile rats treated with tofacitinib have not identified evidence of any direct effect of tofacitinib on bone growth and development [18].

In this *post hoc* analysis, we investigated the long-term impact of tofacitinib use in patients with JIA on height and height velocity. We also assessed the impact of open-label treatment with tofacitinib on biomarkers of GH function (IGF-1 and IGFBP3), and bone turnover (osteocalcin).

METHODS

Patients and study design

This analysis was designed to evaluate the impact of tofacitinib on height in patients who were aged 2 to <18 years at inclusion

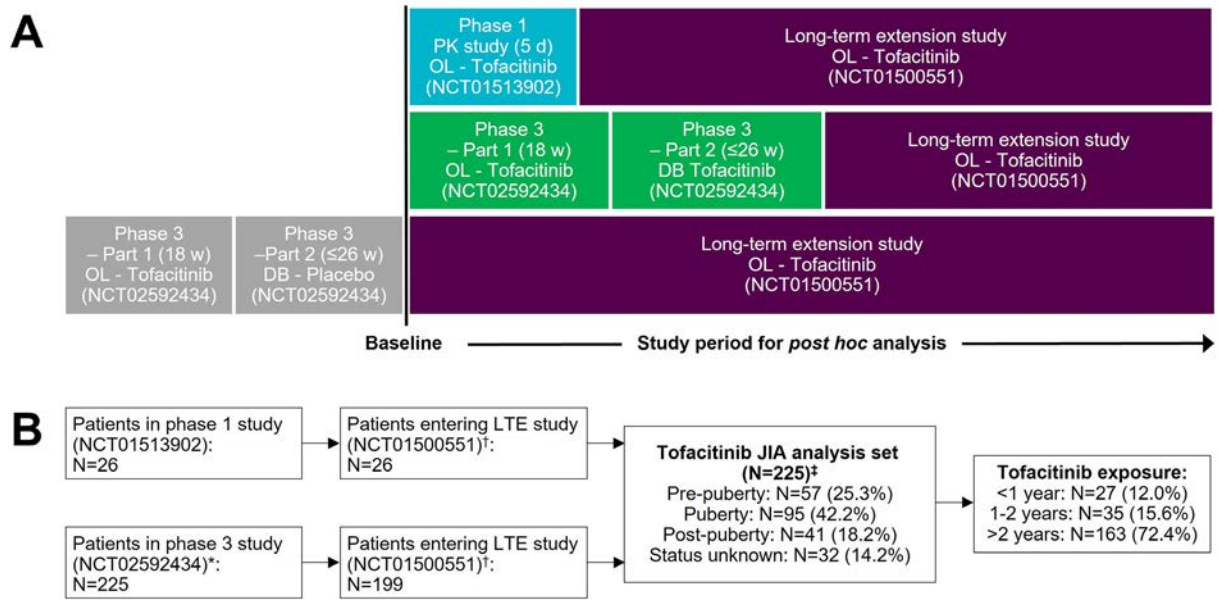

Figure 1. Analysis, design, and patient disposition. (A) The analysis was designed to include patients who received tofacitinib continuously (unless temporarily withheld) in the JIA development programme. All patients treated with tofacitinib in a phase 1 PK study (NCT01513902) or a phase 3 placebo-controlled study (NCT02592434) and subsequently enrolled in an open-label long-term extension study (NCT01500551; data cut-off date was July 11, 2022) were included. For patients randomised to receive placebo during Study 2 (phase 3 study), tofacitinib treatment start was defined as entry into the LTE study. (B) *For patients randomised to placebo in the phase 3 study (N = 80), assessments at entry in the LTE study were set as baseline. †Data cut-off date was July 11, 2022. ‡Tofacitinib analysis set included 185 patients with polyarticular-course JIA (extended oligoarthritis, N = 27; rheumatoid factor-positive polyarthritis, N = 36; rheumatoid factor-negative polyarthritis, N = 111; systemic JIA without active systemic features in the 6 months before enrolment, N = 11), 19 patients with juvenile psoriatic arthritis, and 21 patients with enthesitis-related arthritis. Pubertal status was based on the baseline Tanner stage, where prepuberty = Tanner stage 1, puberty = Tanner stage 2 to 4, and postpuberty = Tanner stage 5. D, days; DB, double blind; JIA, juvenile idiopathic arthritis; LTE, long-term extension; N, number of patients; OL, open-label; PK, pharmacokinetic; w, weeks.

and received continuous tofacitinib treatment (unless temporarily withheld) in 3 studies of the JIA development programme (Fig 1A). Study 1 was a phase 1 pharmacokinetics study (NCT01513902) [13]. Study 2 was a phase 3 placebo-controlled study (NCT02592434) that enrolled patients with pcJIA (ie, extended oligoarthritis [EO], rheumatoid factor (RF)-positive and RF-negative polyarthritis, and systemic JIA (sJIA) without active systemic features in the 6 months before enrolment), jPsA, and ERA [14]. Study 3 was an open-label LTE study (NCT01500551; data cut-off date was 11 July 2022) and enrolled patients who had completed study 1 or 2 (the index studies) or had discontinued 1 of the studies for reasons other than treatment-related serious adverse events [15]. For patients randomly assigned to receive placebo during study 2 (phase 3 study), tofacitinib treatment start was defined as entry into the LTE study (Fig 1A). Patients from a recently completed phase 3 placebo-controlled study of tofacitinib in sJIA (NCT03000439) [19] were not included in this analysis.

All patients received open-label tofacitinib 5 mg twice daily or an equivalent weight-based lower dose. Maximum dosages of allowable background JIA therapies in the qualifying studies included methotrexate (≤25 mg/wk or ≤20 mg/m^2/wk, whichever was lower), leflunomide (10 mg every other day, 10 mg/d or 20 mg/d, in patients weighing <20 kg, 20-40 kg or >40 kg, respectively) and oral glucocorticoids (≤0.2 mg/kg/d or 10 mg/d of prednisone or equivalent, whichever was lower). Dosages of background JIA therapy could be changed by the treating physician during the LTE study only. Adherence was monitored during the study by accounting for returned trial medication. Continued nonadherence led to withdrawal from the study.

All studies were conducted across 22 countries at centres of either the Paediatric Rheumatology INternational Trials Organisation (www.printo.it) [20], or the Pediatric Rheumatology Collaborative Study Group (www.prcsg.org) [21], and in accordance with the Guidelines for Good Clinical Practice, the Declaration of Helsinki, and local regulatory requirements and laws, and was approved by institutional review boards or ethics committees at all sites. Written informed consent/assent was provided by parents/legal guardians/patients. Parents/legal guardians/patients were not involved in the design or dissemination of this analysis.

Assessments

Height

Height was recorded on the day of the first administration of tofacitinib (baseline), month 1, month 3, and then every third month throughout the study. Height velocities (cm/y) were calculated for all patients from baseline to year 1 and from baseline to year 2. Height Z-scores were determined for patients at baseline and during follow-up using 2007 World Health Organization (WHO) age- and sex-matched reference data [22,23]. Missing height measurements were imputed using last observation carried forward (LOCF).

Pubertal status

Tanner stage rating was assigned at baseline and yearly in the LTE study by the clinician/physician based on examination of physical and sexual maturation or based on the subject's self-assessment (using photographs or line drawings corresponding to the Tanner stages) [24]. Participants at Tanner stage 1 were categorised *ad hoc* as prepubertal, Tanner stage 2 to 4 defined a pubertal phase, and participants at Tanner stage 5 were categorised as postpubertal.

Biomarkers

Immunoassays for IGF-1 (R&D Systems), IGFBP3 and osteocalcin (both: Mesoscale Discovery) were used to determine biomarker quantities in serum, collected in a fasting state, from patients with JIA who completed 18 weeks of open-label treatment with tofacitinib in study NCT02592434. These assays are validated for precision, but not vs a reference population.

Statistical analyses

All statistical analyses were performed using R (version 4.3.1; The R foundation). Height Z-score and IGF-1 change from baseline, least square means were estimated using a mixed model repeated measures (MMRMs) analysis. Associated *P* values and 95% confidence intervals (CIs) for contrasts between cohorts were derived from *t*-tests within the MMRM framework [25].

For categorical variables, summary statistics were compared using the Kruskal-Wallis rank sum test, while numeric data were analysed using the Wilcoxon rank sum test. Scatter plot data were visualised with locally estimated scatterplot smoothing regression lines to illustrate trends.

Data (as observed) and from all participants were included in the analysis until participants either completed the study or discontinued for any reason. To identify potential outlier height measurements, residuals and fitted values were extracted from the MMRM model. Standardised residuals were computed, and observations with absolute values >6.5 were flagged as potential outliers. Flagged data points were visually assessed to ensure consistency with the overall longitudinal trend. Specifically, timepoints were examined to determine whether deviations were likely due to data entry errors rather than true biological variation. Outliers were removed only at specific timepoints without excluding entire subjects from the analysis.

All tests were 2-sided, with statistical significance set at $P < .05$ unless otherwise specified. No adjustments for multiple comparisons were applied unless explicitly stated.

RESULTS

Patients

The analysis included 225 patients with JIA who were enrolled in the tofacitinib open-label LTE study after completion of qualifying/index studies or discontinuation of the studies for reasons other than treatment-related serious adverse events (Fig 1) [15]. Most patients (N = 185) had pcJIA (EO, N = 27; RF-positive polyarthritis [RF + PA], N = 36; RF-negative polyarthritis [RF − PA], N = 111; sJIA without active systemic features in the 6 months before enrolment, N = 11), and there were 19 patients with jPsA and 21 patients with ERA. Twenty-six patients were from the phase 1 study [13] and 199 patients from the tofacitinib phase 3 study [14].

Of the 225 patients, 57 (25.3%) were in a prepubertal phase (Tanner stage 1), 95 (42.2%) were in puberty (Tanner stage 2-4), and 41 (18.2%) were in a postpubertal phase (Tanner stage 5) (Fig 1B). Tanner stage was unknown in 32 patients (14.2%; Fig 1B). Median duration of tofacitinib treatment was 3.6 years (interquartile range, 1.9-4.6 years), and 72.4% (163/225) of patients were treated for more than 2 years (Fig 1B). Patient demographics and baseline (day of the first administration of tofacitinib) disease characteristics are summarised in Table 1.

Table 1
Demographic and baseline disease characteristics

	Tofacitinib (n = 225)
Female sex, n (%)	169 (75.1)
Age (y)	13.0 (9.0-16.0)
Disease duration (y)	3.0 (1.7-5.7)
JIA category, n (%)	
pcJIA	185 (82.2)
Extended oligoarthritis	27 (12.0)
RF-positive polyarthritis	36 (16.0)
RF-negative polyarthritis	111 (49.3)
sJIA[a]	11 (4.9)
jPsA	19 (8.4)
ERA	21 (9.3)
Tanner stage, n (%)	
Stage 1	57 (25.3)
Stage 2	23 (10.2)
Stage 3	31 (13.8)
Stage 4	41 (18.2)
Stage 5	41 (18.2)
Not available	32 (14.2)
JADAS-27 CRP Score at baseline, n (%)	
High disease activity	201 (89.3)
Moderate disease activity	4 (1.8)
Low disease activity	1 (0.4)
Not available	19 (8.4)
CRP above normal range (>2.87 mg/L), n (%)	101 (44.9)
Prior medication use, n (%)	
csDMARDs	199 (88.4)
bDMARDs	69 (30.7)
Concomitant medication use, n (%)	
Methotrexate	148 (65.8)
Corticosteroids	101 (44.9)

bDMARD, biological disease-modifying antirheumatic drug; CRP, C-reactive protein; csDMARD, conventional synthetic disease-modifying antirheumatic drug; ERA, enthesitis-related arthritis; JADAS, juvenile arthritis disease activity score; JIA, juvenile idiopathic arthritis; jPsA, juvenile psoriatic arthritis; pcJIA, polyarticular-course juvenile idiopathic arthritis; RF, rheumatoid factor; sJIA, systemic JIA.
Data are median (IQR) or n (%).
[a] sJIA without active systemic features in the 6 months before enrolment.

Height Z-scores at baseline

Based on height Z-scores, the study population had a baseline height distribution that resembled that of the general, healthy population, with a median height Z-score of −0.13 (IQR, −1.0 to 0.52) (Fig 2A). Short stature at baseline (ie, height Z-score < −2.0) was, however, observed in 8.4% (19/225) of patients (2.5% expected in a normally distributed reference population). A baseline height Z-score < −1.0 was observed in 25.3% (57/225) of patients.

There was no statistical association between baseline height Z-score and age group, sex, or race (Fig 2B; Supplementary Table S1). However, there was a notable trend ($P = .06$) between disease duration and lower baseline height Z-score (Fig 2B), and patients with disease duration ≥6 years had the lowest height Z-scores. Across the 5 Tanner stages, there was no association with baseline height Z-scores, but the numerically lowest baseline height Z-scores were seen in patients in Tanner stage 5 (ie, postpuberty) (Fig 2B). Although there was no significant association between JIA category (EO, RF+ PA, RF − PA, sJIA, jPsA, and ERA) and baseline height Z-score ($P = .09$; Fig 2B), patients with sJIA (without active systemic features) had the lowest height Z-scores.

Patients with baseline C-reactive protein (CRP) levels above the normal range (ie, >2.87 mg/L) had lower height Z-scores ($P = .01$) than patients with normal baseline CRP levels (ie, ≤2.87 mg/L) (Fig 2B). Patients with concomitant use of glucocorticoids had lower height Z-scores ($P<.01$) than patients not using glucocorticoids at the time of enrolment (Fig 2B).

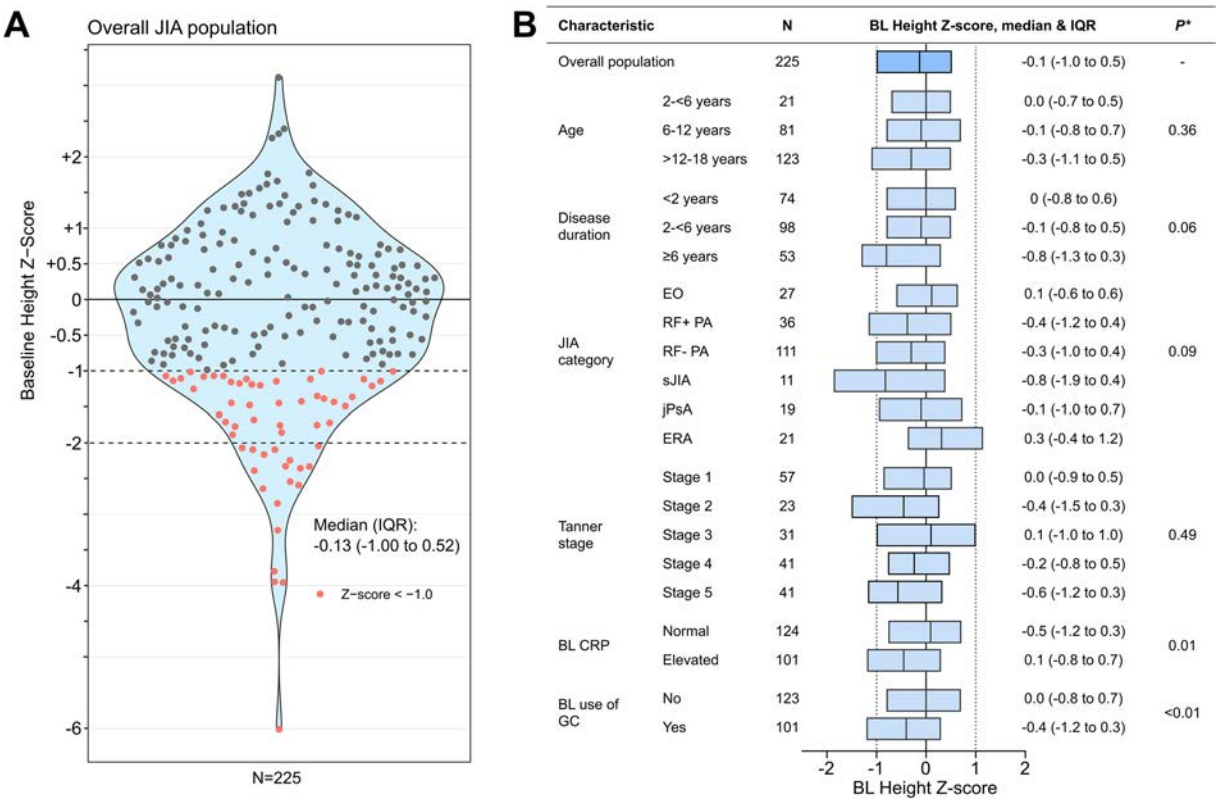

Figure 2. Baseline height Z-scores. (A) Baseline height Z-scores in patients included in the analysis. The Z-score represents the number of standard deviations below or above the mean height of an age and sex-matched reference population. (B) Baseline height Z-score by demographics and clinical characteristics. *Analysed using the Kruskal-Wallis rank sum test. †sJIA without active systemic features in the 6 months before enrolment. BL, baseline; CRP, C-reactive protein; EO, extended oligoarthritis; ERA, enthesitis-related arthritis; GC, glucocorticoid; JIA, juvenile idiopathic arthritis; jPsA, juvenile psoriatic arthritis; N, number of patients; PA, polyarthritis; RF, rheumatoid factor; sJIA, systemic JIA.

Height velocity in patients with JIA during treatment with tofacitinib

During observed treatment with tofacitinib, the height velocities for patients who were ≤12 years of age appeared greater than expected, and patients aged >12 years had height velocities that were at the expected rate, when compared with the WHO age-appropriate norms (Fig 3). Among patients not in Tanner stage 1 to 4 at baseline, the 2-year height velocity was higher than the WHO norm in 66.3% (63/95) of the overall population and 86.0% (43/50) of patients aged ≤12 years (Table 2 and Fig 3). Results were generally similar in female and male patients.

Among patients aged ≤12 years and not in Tanner stage 1 to 4 at baseline, 32 were on glucocorticoids at baseline and 18 were not. Among those receiving glucocorticoids, 18.8% (6/32) had a 2-year height velocity lower than the WHO norm, compared with 5.6% (1/18) among patients not using glucocorticoids (Fig 3A and Table 2). No association between JIA category and 2-year height velocity was apparent, but the number of patients in the different categories was low (Fig 3B).

Results were similar when assessing 1-year height velocities in the overall population and in patients who were aged ≤12 or >12 years (Supplementary Fig S1 and Table S2).

Change from baseline in height Z-score in patients with JIA during treatment with tofacitinib

In the prepubertal group of patients, an increase in mean height Z-scores was observed after 42 months of treatment ($P < .05$), whereas height Z-scores were stable in patients in puberty (ie, Tanner stage 2-4) at baseline (Fig 2; Supplementary Fig S2 shows data per baseline Tanner stage). When assessed by Tanner stages, there was a minor, but statistically significant, reduction in height Z-scores observed from month 6 in patients with baseline Tanner stage 3 (Supplementary Fig S2). However, in the subgroup of patients going through puberty at baseline and with a height Z-score <−1.0, an increase in height Z-score vs baseline ($P < .05$) was detected after 24 months of treatment with tofacitinib (Fig 4B). The increase in height Z-scores was most prominent in patients at Tanner stage 2 at baseline (Supplementary Fig S3).

Similar trends were observed when grouping patients by their age at baseline (Fig 5A). In patients 6 to 12 years at baseline, height Z-scores tended to increase during tofacitinib treatment. This was also true in those with height Z-score < −1 at baseline (Fig 5B).

A total of 6 single time point height measurements in 5 patients were considered outlier measurements and excluded due to biological implausibility (Supplementary Fig S4). For these outlier measurements, LOCF was applied.

Impact of treatment with tofacitinib on biomarkers of GH function and bone turnover

Serum levels of IGF-1 were measured in participants in the tofacitinib phase 3 JIA study [14]. IGF-1 levels were low in patients aged <10 years, and peaked at approximately 14 years of age (Fig 6A). In Supplementary Figure S5, baseline log IGF-1 values of the study participants are shown vs reference values by puberty stage [26]. Younger age, disease duration between 2 to <6 years, lower Tanner stage, and CRP above normal were all associated with lower baseline IGF-1 levels ($P < .05$; Supplementary Fig S6).

Tofacitinib treatment for 18 weeks did not appear to have an impact on IGF-1 levels in the overall population (Supplementary

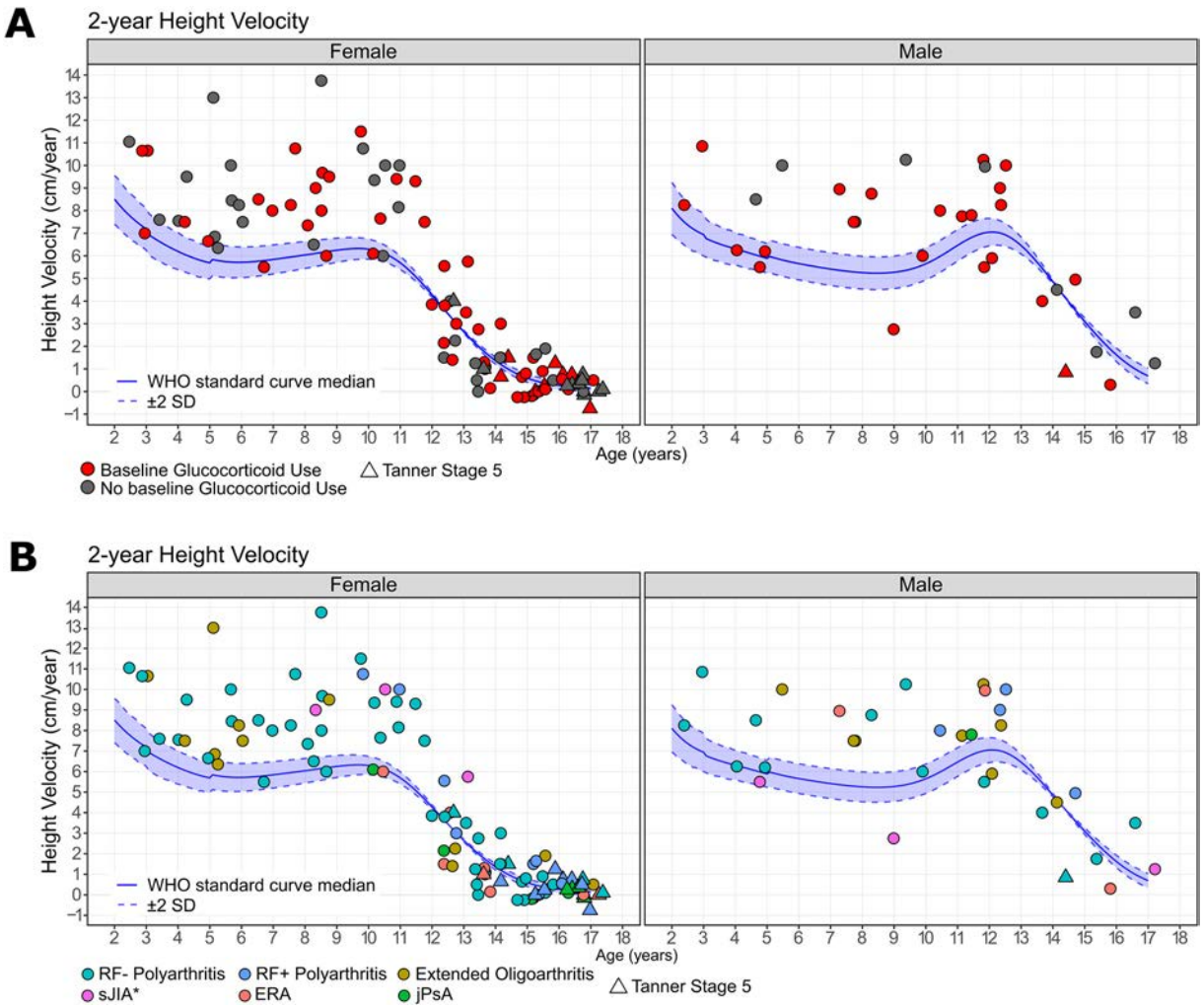

Figure 3. Annualised height velocity determined after 2 years of continuous treatment with tofacitinib by (A) concomitant glucocorticoid use and (B) JIA disease category. Height velocity (2-year average) vs baseline age in female and male patients. Height velocities (cm/y) were calculated for all patients from baseline to year 2. Panel A shows data by concomitant baseline use of glucocorticoids, and panel B, data by JIA categories. The blue line represents the expected height velocities based on World Health Organization (WHO) norms, and the dashed blue lines reflect + or −2 SD. Triangles indicate patients who were at Tanner stage 5 at baseline. *sJIA without active systemic features in the 6 months before enrolment. ERA, enthesitis-related arthritis; JIA, juvenile idiopathic arthritis; jPsA, juvenile psoriatic arthritis; RF, rheumatoid factor; sJIA, systemic JIA.

Fig S7). However, in patients aged 6 to 12 years, IGF-1 levels increased from baseline to 18 weeks (P = .032; Fig 6). In patients aged <6 years or >12 years, there was no difference in serum levels of IGF-1 after 18 weeks of treatment with tofacitinib (Fig 6B).

Serum levels of IGFBP3 did not appear to be different across the age subgroups assessed in the analysis (Supplementary Fig S8). similar. For osteocalcin, the lowest serum levels were observed in patients who were aged >12 years at baseline (Supplementary Fig S9). There were no differences in serum levels of IGFBP3 and osteocalcin during treatment with tofacitinib either in the overall population or as assessed by age subgroups (Supplementary Figs S8 and S9).

DISCUSSION

Growth impairment is a well-known complication of JIA [2]. Although tofacitinib primarily inhibits JAK1 and JAK3, it has the theoretical potential to impair growth, given its moderate

Table 2

Proportions of patients (excluding those in Tanner stage 5 at baseline) with 2-year height velocity ≥ or < WHO norm by age and baseline concomitant use of glucocorticoids

		Overall population		Female		Male	
		≥WHO Norm	<WHO Norm	≥WHO Norm	<WHO Norm	≥WHO Norm	<WHO Norm
Overall population		66.3% (63/95)	33.7% (32/95)	63.8% (44/69)	36.2% (25/69)	73.1% (19/26)	26.9% (7/26)
≤12 y		86.0% (43/50)	14.0% (7/50)	87.9% (29/33)	12.1% (4/33)	82.4% (14/17)	17.6% (3/17)
>12 y		44.4% (20/45)	55.6% (25/45)	41.7% (15/36)	58.3% (21/36)	55.6% (5/9)	44.4% (4/9)
≤12 y	No BL GC	94.4% (17/18)	5.6% (1/18)	92.9% (13/14)	7.1% (1/14)	100% (4/4)	0% (0/4)
	BL GC	81.2% (26/32)	18.8% (6/32)	84.2% (16/19)	15.8% (3/19)	76.9% (10/13)	23.1% (3/13)
>12 y	No BL GC	40.0% (6/15)	60.0% (9/15)	36.4% (4/11)	63.6% (7/11)	50.0% (2/4)	50% (2/4)
	BL GC	46.7% (14/30)	53.3% (16/30)	44% (11/25)	56% (14/25)	60.0% (3/5)	40.0% (2/5)

BL, baseline; GC, glucocorticoids; WHO, World Health Organization.

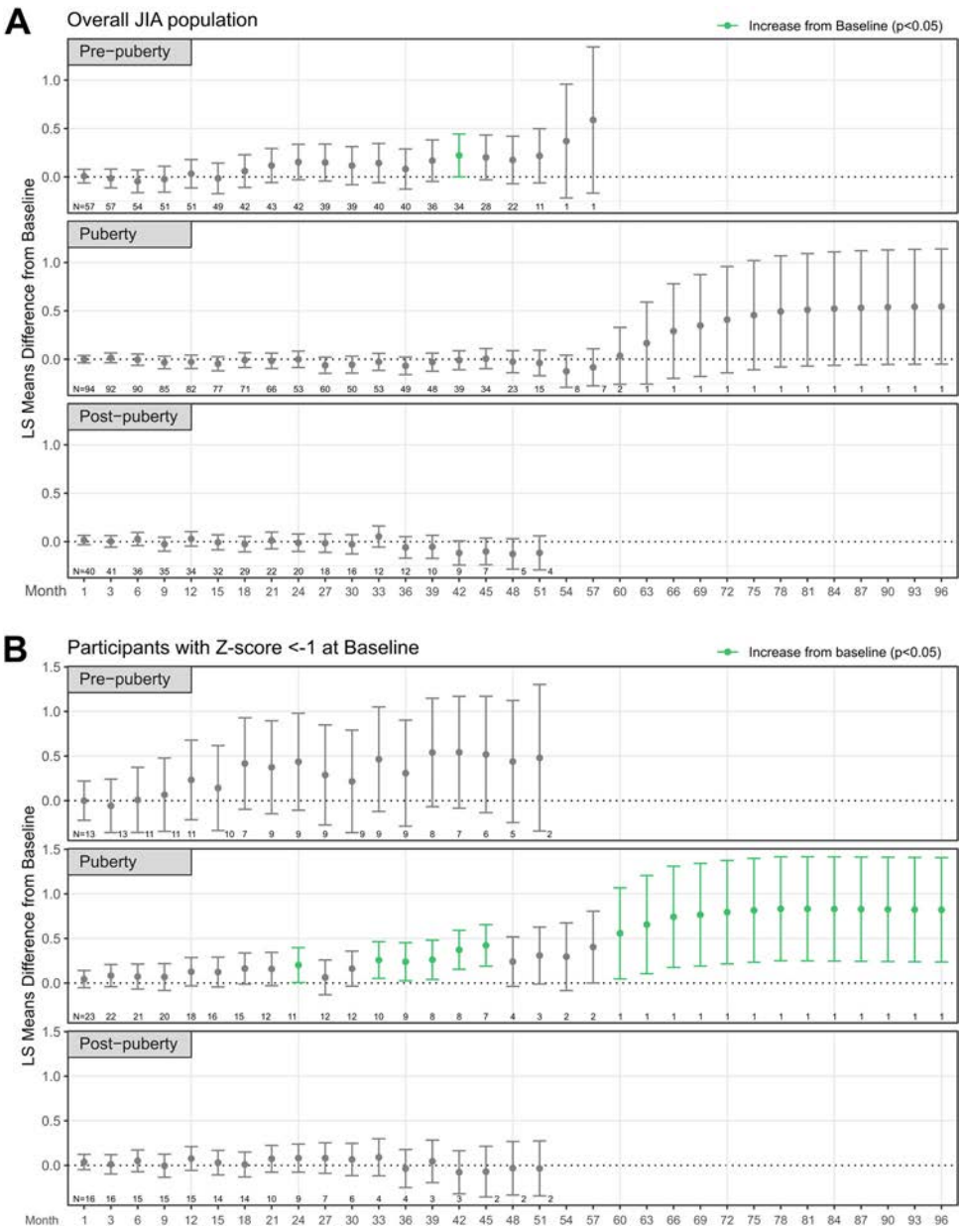

Figure 4. Change from baseline in height Z-score by baseline puberty status in (A) overall JIA population and (B) participants with baseline height Z-score <-1. Pubertal status was based on the baseline Tanner stage where prepuberty = Tanner stage 1, puberty = Tanner stage 2 to 4, and postpuberty = Tanner stage 5. Height Z-score change from baseline, least square (*LS*) means were estimated using a mixed model repeated measures (MMRMs) analysis. Associated *P* values and 95% CIs for contrasts between cohorts were derived from *t*-tests within the MMRM framework. JIA, juvenile idiopathic arthritis.

JAK2 inhibition. In this analysis of patients from the tofacitinib JIA development programme, treatment with tofacitinib was associated with growth, as measured by height velocities that were greater (patients ≤12 years) or as expected (patients >12 years) vs a reference population. In patients in puberty at baseline and a low height Z-score (ie, <−1.0), results indicated catch-up of growth during long-term (ie, ≥24 months) treatment with tofacitinib.

A notable observation in this analysis was that the patients with JIA enrolled in this study had near-normal heights at study entry. Short stature (height Z-score less than −2 compared with reference data) was observed in 8.4% of patients, and 25.3% had a baseline height Z-score of less than −1. This could be a reflection of overall improved treatments for JIA than in the past. Categories of JIA differ in terms of severity and likelihood of long-term complications [1,27], and patients with pcJIA, jPsA, and ERA have a lower risk of experiencing growth failure than patients with sJIA with active systemic features [2]. Importantly, the latter group of patients was excluded from the studies considered in our analyses. However, among the patients with pcJIA, there were a few patients with sJIA but without systemic features for at least 6 months before study enrolment; notably, these patients had nominally lower baseline height Z-scores than patients within the other JIA categories. Further, our observation is consistent with the current understanding of mechanisms of growth restriction in JIA [2], where elevated CRP levels and prolonged glucocorticoid use are associated with growth reduction. Patients in this study with baseline CRP levels above normal, reflecting active systemic inflammation, and patients with baseline use of glucocorticoids had lower baseline height Z-scores. However, given that few patients had low baseline height Z-scores, it was not feasible to evaluate catch-up growth in these important subgroups.

The introduction of advanced forms of treatment for patients with JIA, ie, inhibitors of tumour necrosis factor (TNFi), interleukin-6 (tocilizumab), and CTLA4 (abatacept), has improved

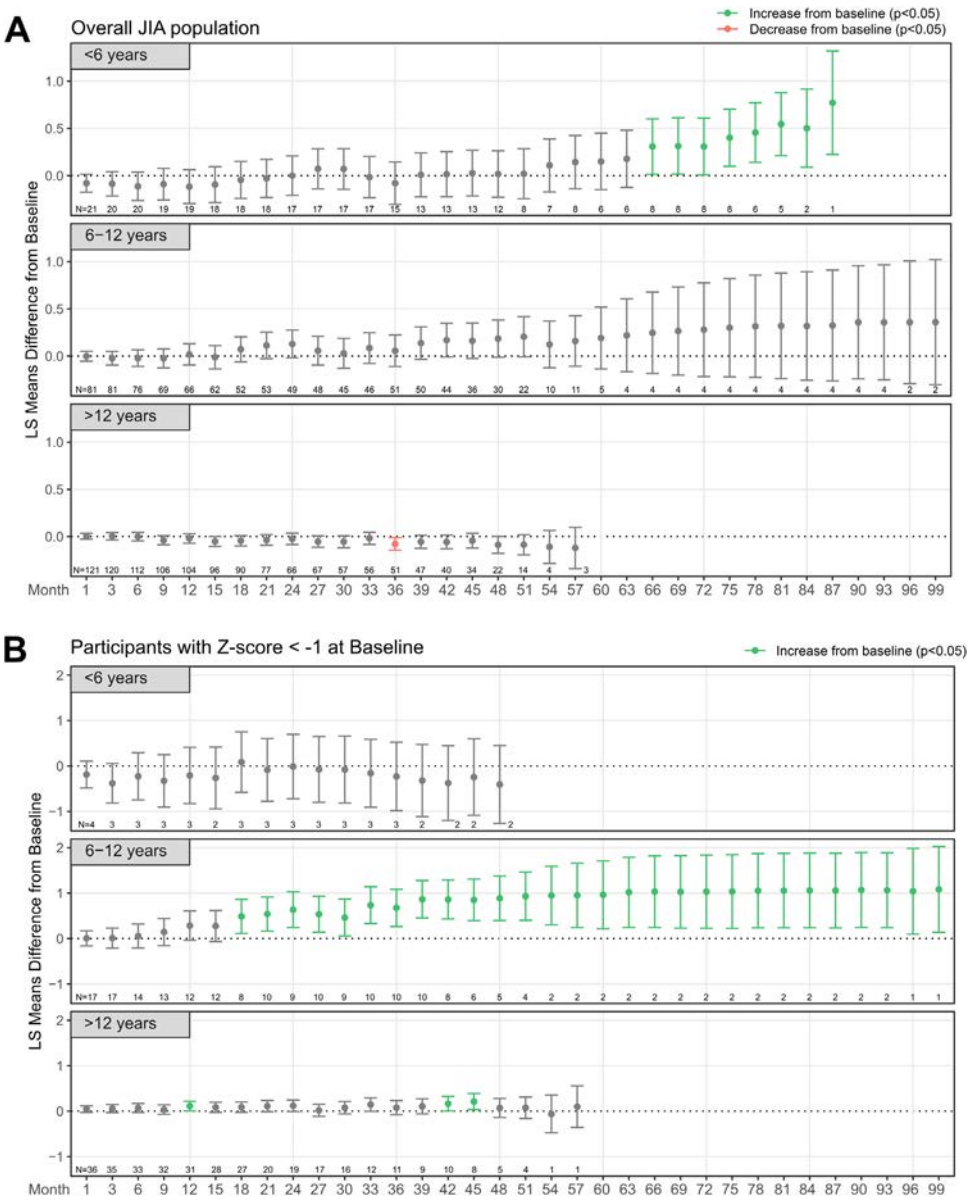

Figure 5. Change from baseline in height Z-score by baseline age in (A) overall JIA population and (B) participants with baseline height Z-score <-1. Height Z-score change from baseline, least square (LS) means were estimated using a mixed model repeated measures (MMRMs) analysis. Associated *P* values and 95% CIs for contrasts between cohorts were derived from *t*-tests within the MMRM framework. JIA, juvenile idiopathic arthritis.

the likelihood of achieving disease control and allowed for reduced use of glucocorticoids [28–30]. The use of these treatments has also been shown to have a positive impact on growth [30–36]. A key observation in our analysis was that height velocities during treatment with tofacitinib over 1 or 2 years appeared to be higher than expected in patients ≤12 years and, as expected, in patients >12 years at baseline. Importantly, this was determined in a clinical trial setting where adherence to study treatment was monitored. This supports the finding that growth appears to be normal during tofacitinib treatment and suggests that there may be even catch-up growth. Our results are consistent with height velocities in analyses of growth over 2 years in a phase 3 study on tocilizumab in patients with pcJIA [31]. A formal comparison of the relative impact of approved medications for pcJIA on growth that considers Tanner staging, differences in JIA-associated inflammation and background treatments, is, however, beyond the scope of this analysis.

It was observed that among the patients aged ≤12 years, baseline concomitant use of glucocorticoids was associated with a higher likelihood of height velocities lower than the WHO norm. The analysis did not consider total glucocorticoid exposure among the 44.9% (101/225) of patients on glucocorticoids during the study. This might have impacted the precision with which we can document the growth impact of tofacitinib during the later period of tofacitinib use, given the known detrimental effects of long-term systemic glucocorticoids on growth [37].

Catch-up growth in those with residual growth potential, ie, higher than expected growth velocity in patients with delayed growth, has been observed in patients with sJIA treated with tocilizumab [33], and with TNFi in patients with pcJIA or sJIA [34,35]. In this study, it was found that among patients with JIA with low baseline height Z-scores (ie, < −1), of which 69% (36/52) had residual growth potential, an increase in height Z-scores vs baseline was observed after approximately 1.5 to 2 years in patients in a pubertal phase and in patients who were aged 6 to 12 years at inclusion.

The main regulator of height growth is the GH/IGF-1 axis [2,6]. Current evidence indicates that GH resistance, occurring

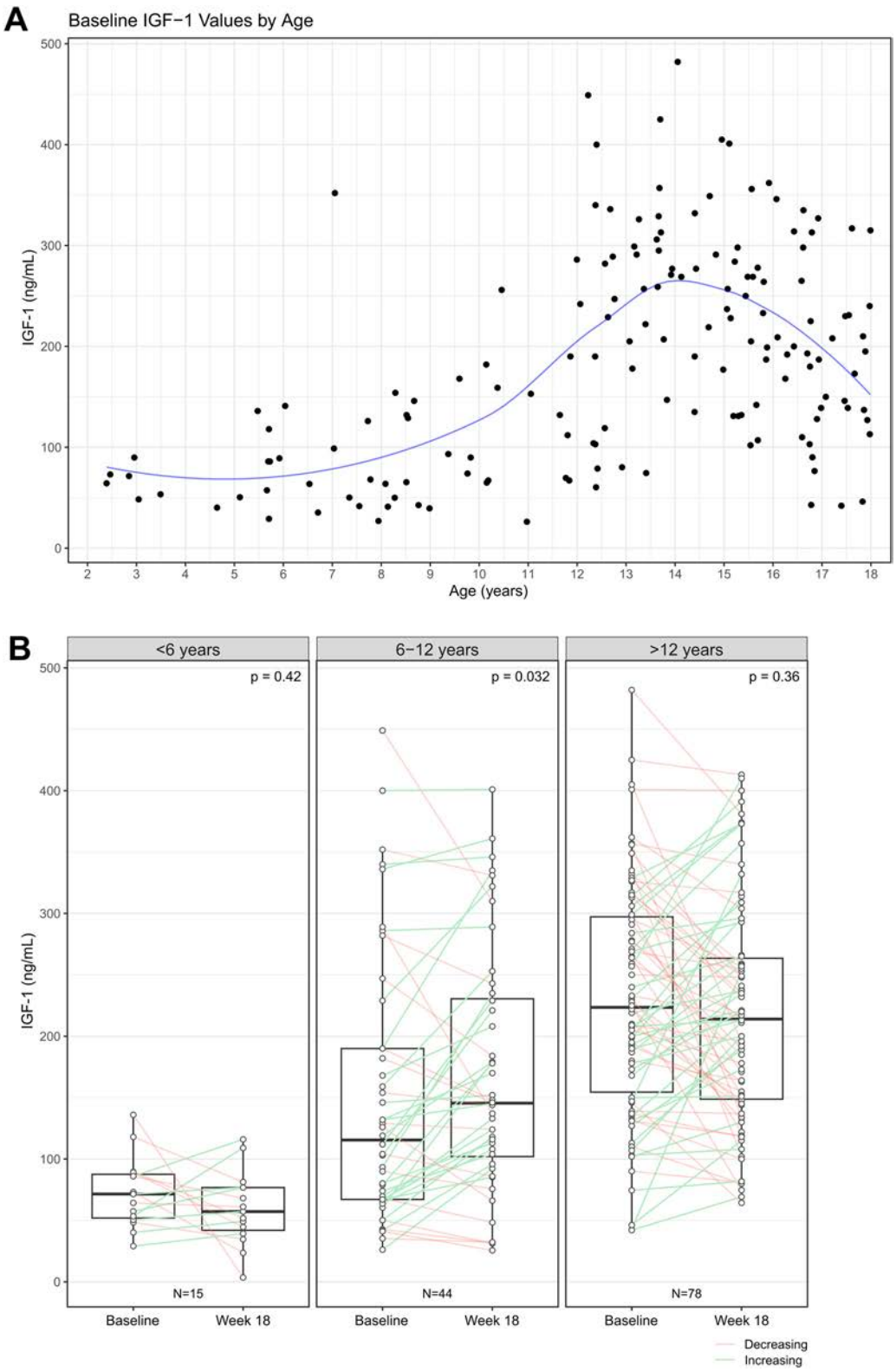

Figure 6. Serum levels of IGF-1 at (A) baseline by age and (B) before and after open-label tofacitinib treatment for 18 weeks. (A) Baseline serum IGF-1 levels vs age. The blue line illustrates trend as determined with locally estimated scatterplot smoothing regression. (B) Data were analysed using the paired Wilcoxon rank sum test. IGF-1, insulin-like growth factor-1; N, number of patients with samples available for analysis at baseline and Week 18.

at the pituitary, systemic, or growth plate levels, is the main mechanism in cases of restricted growth in children with JIA [6]. Treatment with a JAK inhibitor such as tofacitinib could potentially alleviate GH resistance through reducing local (ie, articular) and systemic inflammation [2]. Tofacitinib inhibits the signalling of a wide range of inflammatory cytokines [38]. This includes IL-6, a cytokine believed to be a central mediator of GH resistance in JIA [2]. Tofacitinib has also been shown to reduce IL-6 levels in patients with rheumatoid arthritis [39]. GH signals through a homodimer of JAK2, raising the question as to whether JAK inhibitors, such as tofacitinib, could inhibit GH signalling and thus increase GH resistance. The results presented in this analysis do not indicate that tofacitinib 5 mg twice daily or similar weight-based dosing has a negative impact on GH

function. This is aligned with expectations based on *in vitro* cytokine receptor inhibition with tofacitinib [16]. IGF-1 may be considered the most common biomarker for growth [40], and a direct target of GH through JAK2 [6], and this analysis demonstrates that 18 weeks of open-label treatment with tofacitinib was not associated with a change in circulating levels of IGF-1 in the overall population. Similarly, other biomarkers of GH function and bone metabolism such as the levels of IGFBP3 and osteocalcin were not different before and with treatment with tofacitinib. Importantly, in patients aged 6 to 12 years at baseline, tofacitinib treatment was associated with an increase in levels of IGF-1. This increase is consistent with the observation of higher than expected height velocities and recapture of growth with tofacitinib in patients with JIA younger than 12 years of age.

The most important limitations of this analysis are its *post hoc* nature and the relatively low number of patients studied. Accordingly, the results need to be interpreted with caution. The protocol indicated that height during the study should be measured preferentially using a Harpenden stadiometer. This was, however, not a requirement and could have resulted in lower accuracy measurements of height. Ideally, this analysis would also have included an assessment of the impact of tofacitinib on pubertal development. However, due to relatively few patients included, the length of follow-up, and the pubertal status of patients at baseline, this was not feasible. In analogy with similar studies [3,31,33], analyses only considered baseline Tanner stages and participants at Tanner stage 5 (postpuberty without growth potential) were excluded or indicated separately in our analyses. The potential impact of change in pubertal status during the study on growth was not considered in our analyses. Lastly, WHO growth standards were developed for population assessments; however, growth in the individual child is also influenced by environmental, nutritional, and genetic factors, including parental height, which are not accounted for in the WHO standards and in this analysis [41]. This might have impacted the precision of our estimates of the effects of tofacitinib treatment in pcJIA, but it is unlikely that it influenced the overall results of this study.

CONCLUSION

In this *post hoc* analysis, patients with JIA began with near-normal height Z-scores and during long-term treatment (ie, ≥24 months) with tofacitinib, growth appeared normal. In younger patients with JIA, height velocities during tofacitinib treatment were higher than expected from a reference population. Consistent with this, catch-up growth was observed in patients in puberty or 6 to 12 years of age and low baseline height Z-scores. During treatment with tofacitinib, no concerning changes in biomarkers of GH signalling were observed.

Acknowledgements

We thank the PRCSG and PRINTO investigators for the collection of serum samples and data used. We also thank Tiffany Hidalgo and Jessica Anderson, both employees of Pfizer Inc, for their contribution to the biomarker analyses.

Contributors

HIB, AY, MM, DJL, AM, and NR conceptualised the study and data analyses. MS, CIS, and AY analysed the data. All authors had access to the data, made substantial contributions to the interpretation of data, and reviewed and approved the manuscript's content before submission.

Funding

This study was sponsored by Pfizer Inc. The study was designed jointly by Pfizer and the PRINTO/PRCSG officers (HIB, DJL, AM, and NR). Pfizer was responsible for the overall management of the study and the data analysis. Publication of this article was not contingent upon approval by Pfizer.

Competing interests

HIB has received research grants from Bristol Myers Squibb, Novartis, and Pfizer; is an employee of Cincinnati Children's Hospital Medical Center; has received consulting fees or other remuneration from AbbVie, AstraZeneca/MedImmune, Bayer, Biocon, Boehringer Ingelheim, Bristol Myers Squibb, Cerecor, Eli Lilly, EMD Serono, Janssen, Novartis, Pfizer, Roche, R-Pharm, and Sobi; and is a member of speaker bureaus for Novartis and Pfizer. CAS has received research grants from Fundação de Amparo à Pesquisa do Estado de São Paulo (FAPESP) (#2022/12925-8), Conselho Nacional de Desenvolvimento Científico e Tecnológico (CNPq 304984/2020-5), and by Núcleo de Apoio à Pesquisa "Saúde da Criança e do Adolescente" da USP (NAP-CriAd). HMW has received consulting fees from Kyowa Kirin and Viiv Healthcare, and receives research support from Ultragenyx and Calcilytix. MS, AD, IV, and AY are employees and stockholders of Pfizer Inc. CIS and MM were employees and stockholders of Pfizer Inc at the time of the analysis, and MM is a current employee and stockholder of Kymera Therapeutics Inc. DJL's institution, the Cincinnati Children's Hospital Medical Center, has received research grants from Bristol Myers Squibb, Janssen, Novartis, Pfizer, Roche and UBC; and has received consulting fees or other remuneration from AstraZeneca, Boehringer Ingelheim, GSK, Roche, Novartis, Pfizer, Takeda, and UBC. DJL is also a data safety and monitoring board member or chairperson for the National Institutes of Health and the Canadian Arthritis Society. AM has received consulting fees or other remuneration from Aurinia, Bristol Myers Squibb, Eli Lilly, EMD Serono, Janssen, and Pfizer. NR has received honoraria for consultancies or speaker bureaus in the past 2 years from: Abbvie, AClaris, AlfaSigma, Amgen, AstraZeneca, Aurinia, Boehringer Ingelheim, Bristol Myers and Squibb, Eli Lilly, Galapagos, Genentech Roche, Guidepoint, Idorsia, Janssen, Novartis, Pfizer, Sanofi, and Takeda. All the other authors declare they have no competing interests.

Patient consent for publication

Not applicable.

Ethics approval

Studies included in the analysis (NCT01513902, NCT02592434, and NCT01500551) were all conducted in accordance with the Guidelines for Good Clinical Practice, the Declaration of Helsinki, and local regulatory requirements and laws, and was approved by institutional review boards or ethics committees at all sites. Written informed consent/assent was provided by parents/legal guardians/patients.

Provenance and peer review

Not commissioned; externally peer reviewed.

Data availability statement

Upon request, and subject to review, Pfizer will provide the data that support the findings of this study. Subject to certain criteria, conditions, and exceptions, Pfizer may also provide access to the related individual deidentified participant data. See https://www.pfizer.com/science/clinical-trials/trial-data-and-results for more information.

Supplementary materials

Supplementary material associated with this article can be found in the online version at doi:10.1016/j.ard.2026.03.030.

Orcid

Hermine I. Brunner: http://orcid.org/0000-0001-9478-2987

REFERENCES

[1] Martini A, Lovell DJ, Albani S, runner HI, Hyrich KL, Thompson SD, et al. Juvenile idiopathic arthritis. Nat Rev Dis Primers 2022;8(1):5.
[2] d'Angelo DM, Di Donato G, Breda L, Chiarelli F. Growth and puberty in children with juvenile idiopathic arthritis. Pediatr Rheumatol Online J 2021;19(1):28.
[3] Nordal E, Pistorio A, Rygg M, Giancane G, Maghnie M, Di Iorgi N, et al. Growth and puberty in juvenile dermatomyositis: a longitudinal cohort study. Arthritis Care Res (Hoboken) 2020;72(2):265–73.
[4] Rygg M, Pistorio A, Ravelli A, Maghnie M, Di Iorgi N, Bader-Meunier B, et al. A longitudinal PRINTO study on growth and puberty in juvenile systemic lupus erythematosus. Ann Rheum Dis 2012;71(4):511–7.
[5] Parra RS, da Rocha JJR, Feres O. Growth delay in inflammatory bowel diseases: the importance of surgery. Dig Dis Sci 2021;66(8):2840–1.
[6] Wong SC, Dobie R, Altowati MA, Werther GA, Farquharson C, Ahmed SF. Growth and the growth hormone-insulin like growth factor 1 axis in children with chronic inflammation: current evidence, gaps in knowledge, and future directions. Endocr Rev 2016;37(1):62–110.
[7] Moser SC, van der Eerden BCJ. Osteocalcin-a versatile bone-derived hormone. Front Endocrinol (Lausanne) 2019;9:794.
[8] Seydewitz HH, Henschen M, Kuhnel W, Brandis M. Pediatric reference ranges for osteocalcin measured by the Immulite analyzer. Clin Chem Lab Med 2001;39(10):980–2.
[9] Kanbur NO, Derman O, Kinik E. The relationships between pubertal development, IGF-1 axis, and bone formation in healthy adolescents. J Bone Miner Metab 2005;23(1):76–83.
[10] Li W, Wang Y, Dong J, Di R, Liu X, Liu S. Age- and sex-specific differences in the association of serum osteocalcin and cardiometabolic risk factors in type 2 diabetes. Diabetol Metab Syndr 2023;15(1):48.
[11] European Medicines Agency. Xeljanz® (tofacitinib): summary of product characteristics [Internet]. 2024. Available from: https://www.ema.europa.eu/en/documents/product-information/xeljanz-epar-product-information_en.pdf; Accessed 13 Feb 2025.
[12] US Food and Drug Administration. XELJANZ® (tofacitinib): highlights of prescribing information [Internet]. 2024. Available from: http://labeling.pfizer.com/ShowLabeling.aspx?id=959; Accessed 13 Feb 2025.
[13] Ruperto N, Brunner HI, Zuber Z, Tzaribachev N, Kingsbury DJ, Foeldvari I, et al. Pharmacokinetic and safety profile of tofacitinib in children with polyarticular course juvenile idiopathic arthritis: results of a phase 1, open-label, multicenter study. Pediatr Rheumatol Online J 2017;15(1):86.
[14] Ruperto N, Brunner HI, Synoverska O, Ting TV, Mendoza CA, Spindler A, et al. Tofacitinib in juvenile idiopathic arthritis: a double-blind, placebo-controlled, withdrawal phase 3 randomised trial. Lancet 2021;398(10315):1984–96.
[15] Brunner HI, Akikusa JD, Al-Abadi E, Bohnsack JF, Boteanu AL, Chedeville G, et al. Safety and efficacy of tofacitinib for the treatment of patients with juvenile idiopathic arthritis: preliminary results of an open-label, long-term extension study. Ann Rheum Dis. 2024;83(11):1561–71.
[16] Dowty ME, Lin TH, Jesson MI, Hegen M, Martin DA, Katkade V, et al. Janus kinase inhibitors for the treatment of rheumatoid arthritis demonstrate similar profiles of in vitro cytokine receptor inhibition. Pharmacol Res Perspect 2019;7(6):e00537.
[17] Traves PG, Murray B, Campigotto F, Galien R, Meng A, Di Paolo JA. JAK selectivity and the implications for clinical inhibition of pharmacodynamic cytokine signalling by filgotinib, upadacitinib, tofacitinib and baricitinib. Ann Rheum Dis 2021;80(7):865–75.
[18] Campion SN, Potter DM, Bowman CJ, Catlin NR, Davis S, Millard C, et al. Lack of direct bone effect of tofacitinib, a JAK inhibitor, in juvenile rats and evaluation of the association between offspring growth and femur length. Reprod Toxicol 2022;113:35–41.
[19] Brunner H, Li C, Chinniah K, Uziel Y, Synoverska O, Swahney S, et al. Efficacy and safety of tofacitinib in patients with active systemic juvenile idiopathic arthritis [abstract]. Arthritis Rheumatol 2024;76.
[20] N Ruperto, A Martini. Networking in paediatrics: the example of the Paediatric Rheumatology International Trials Organisation (PRINTO). Arch Dis Child 2011;96(6):596–601.
[21] Brunner HI, Rider LG, Kingsbury DJ, Co D, Schneider R, Goldmuntz E, et al. Pediatric Rheumatology Collaborative Study Group - over four decades of pivotal clinical drug research in pediatric rheumatology. Pediatr Rheumatol Online J 2018;16(1):45.
[22] World Health Organization. Length/height-for-age [Internet]. Available from: https://www.who.int/tools/child-growth-standards/standards/length-height-for-age. Accessed 26 Feb 2025.
[23] de Onis M, Onyango AW, Borghi E, Siyam A, Nishida C, Siekmann J. Development of a WHO growth reference for school-aged children and adolescents. Bull World Health Organ 2007;85(9):660–7.
[24] Tanner JM. Normal growth and techniques of growth assessment. Clin Endocrinol Metab 1986;15(3):411–51.
[25] Cnaan A, Laird NM, Slasor P. Using the general linear mixed model to analyse unbalanced repeated measures and longitudinal data. Stat Med 1997;16(20):2349–80.
[26] Lofqvist C, Andersson E, Gelander L, Rosberg S, Blum WF, Albertsson Wikland K. Reference values for IGF-I throughout childhood and adolescence: a model that accounts simultaneously for the effect of gender, age, and puberty. J Clin Endocrinol Metab 2001;86(12):5870–6.
[27] Petty RE, Southwood TR, Manners P, Baum J, Glass DN, Goldenberg J, et al. International League of Associations for Rheumatology classification of juvenile idiopathic arthritis: second revision, Edmonton, 2001. J Rheumatol 2004;31(2):390–2.
[28] Ringold S, Angeles-Han ST, Beukelman T, Lovell D, Cuello CA, Becker ML, et al. 2019 American College of Rheumatology/Arthritis Foundation Guideline for the Treatment of Juvenile Idiopathic Arthritis: therapeutic approaches for non-systemic polyarthritis, sacroiliitis, and enthesitis. Arthritis Care Res (Hoboken) 2019;71(6):717–34.
[29] Shenoi S, Horneff G, Aggarwal A, Ravelli A. Treatment of non-systemic juvenile idiopathic arthritis. Nat Rev Rheumatol 2024;20(3):170–81.
[30] Makhlouf Y, Ayed HB, Miladi S, Boussaa H, Abdelghani KB, Fazaa A, et al. Effect of biologic treatments on growth in children with juvenile idiopathic arthritis: a systematic review. PLoS One 2025;20(5):e0324440.
[31] Bharucha KN, Brunner HI, Calvo Penades I, Nikishina I, Rubio-Pérez N, Oliveira S, et al. Growth during tocilizumab therapy for polyarticular-course juvenile idiopathic arthritis: 2-year data from a phase III clinical trial. J Rheumatol 2018;45(8):1173–9.
[32] Kearsley-Fleet L, Hyrich KL, Davies R, Lunt M, Southwood TR, British Society for Paediatric and Adolescent Rheumatology Etanercept Cohort Study. Growth in children and adolescents with juvenile idiopathic arthritis over 2 years of treatment with etanercept: results from the British Society for Paediatric and Adolescent Rheumatology Etanercept Cohort Study. Rheumatology (Oxford) 2015;54(7):1279–85.
[33] De Benedetti F, Brunner H, Ruperto N, Schneider R, Xavier R, Allen R, et al. Catch-up growth during tocilizumab therapy for systemic juvenile idiopathic arthritis: results from a phase III trial. Arthritis Rheumatol 2015;67:840–8.
[34] Tynjala P, Lahdenne P, Vahasalo P, Kautiainen H, Honkanen V, et al. Impact of anti-TNF treatment on growth in severe juvenile idiopathic arthritis. Ann Rheum Dis 2006;65(8):1044–9.
[35] Giannini EH, Ilowite NT, Lovell DJ, Wallace CA, Rabinovich CE, Reiff A, et al. Effects of long-term etanercept treatment on growth in children with selected categories of juvenile idiopathic arthritis. Arthritis Rheum 2010;62(11):3259–64.
[36] Hsu JL, Huang CC, Huang BH, Huang Hsin-Yi, Huang JL, Wu CY. Biologics promote catch-up growth in young Juvenile idiopathic arthritis patients with lower body height. Pediatr Neonatol 2025;66(5):454–61.

[37] Ravelli A, Consolaro A, Horneff G, Laxer RM, Lovell DJ, Wulffraat NM, et al. Treating juvenile idiopathic arthritis to target: recommendations of an international task force. Ann Rheum Dis 2018;77(6):819–28.
[38] Veale DJ, McGonagle D, McInnes IB, Krueger JG, Ritchlin CT, Elewaut D, et al. The rationale for Janus kinase inhibitors for the treatment of spondyloarthritis. Rheumatology (Oxford) 2019;58(2):197–205.
[39] Migita K, Izumi Y, Jiuchi Y, Kozuru H, Kawahara C, Izumi M, et al. Effects of Janus kinase inhibitor tofacitinib on circulating serum amyloid A and interleukin-6 during treatment for rheumatoid arthritis. Clin Exp Immunol 2014;175(2):208–14.
[40] Mastromauro C, Giannini C, Chiarelli F. Short stature related to Growth Hormone Insensitivity (GHI) in childhood. Front Endocrinol (Lausanne) 2023;14:1141039.
[41] Fenton TR, Gilbert N, Elmrayed S, Fenton CJ, Boctor DL. What is normal growth? Principles, practicalities and pitfalls of growth assessments in infants and children. Ann Nutr Metab 2024;80(Suppl 1):7–17.

Ann Rheum Dis 85 (2026) 1866–1878

Contents lists available at ScienceDirect

Annals of the Rheumatic Diseases

journal homepage: https://www.sciencedirect.com/journal/annals-of-the-rheumatic-diseases

Paediatric rheumatology

Shared genetic architecture and therapeutic targets across paediatric immune-mediated diseases

Jin Li[1,2,*], Hui-Qi Qu[3], Michael E. March[3], Joseph T. Glessner[3,4,5], Yuqiao Fu[1], Jiayue Chen[1], Yang Xu[1], Hao Chen[1], Yun R. Li[6], Qianghua Xia[1], Frank D. Mentch[3], Leila Youssefian[7], Hassan Vahidnezhad[3,4,5], Amir H. Saeidian[8], Xiao Chang[3], Wei Liu[9,10], Wei Wei[2], Hakon Hakonarson[3,4,5,**]

[1] *Department of Cell Biology, Department of Bioinformatics, The Province and Ministry Co-sponsored Collaborative Innovation Center for Medical Epigenetics, State Key Laboratory of Experimental Hematology, Tianjin Key Laboratory of Medical Epigenetics, Key Laboratory of Immune Microenvironment and Disease (Ministry of Education), School of Basic Medical Sciences, Tianjin Medical University, Tianjin, China*
[2] *Department of Rheumatology and Immunology, Tianjin Medical University General Hospital, Tianjin, China*
[3] *Center for Applied Genomics, Children's Hospital of Philadelphia, Philadelphia, PA, USA*
[4] *Division of Human Genetics, Children's Hospital of Philadelphia, Philadelphia, PA, USA*
[5] *Department of Pediatrics, Perelman School of Medicine, University of Pennsylvania, Philadelphia, PA, USA*
[6] *Department of Radiation Oncology and Department of Cancer Genetics and Epigenetics, City of Hope, Duarte, CA, USA*
[7] *Department of Pathology, Cytogenetics Laboratory, City of Hope National Medical Center, Irwindale, CA, USA*
[8] *Department of Molecular and Human Genetics, Baylor College of Medicine, Houston, TX, USA*
[9] *Children's Hospital, Tianjin University, Tianjin, China*
[10] *Tianjin Key Laboratory of Birth Defects for Prevention and Treatment, Tianjin, China*

ARTICLE INFO

Article history:
Received 26 August 2025
Received in revised form 18 June 2026
Accepted 11 July 2026

ABSTRACT

Objectives: Paediatric-onset immune-mediated inflammatory diseases (IMIDs), including juvenile idiopathic arthritis and related rheumatic diseases, remain genetically undercharacterised. We aimed to define shared and category-specific genetic architecture across paediatric IMIDs, compare signals with adult IMIDs, and identify therapeutic opportunities.

Methods: We analysed 24 paediatric IMIDs classified as autoimmune, polygenic-autoinflammatory, mixed-pattern, or allergic. Genome-wide association analyses included 18,086 cases and 131,019 controls of European ancestry. We estimated single nucleotide polymorphism (SNP)-based heritability, genetic correlations, and polygenic overlap; performed subset-based meta-analysis; and conducted functional annotation, gene prioritisation, pathway and protein network analyses, adult-IMID comparison, and drug-target prioritisation.

Results: SNP-based heritability ranged from 28.9% for allergic IMIDs to 61.9% for autoimmune IMIDs. Genetic correlation and polygenic modelling supported partial sharing across categories with category-specific components. Meta-analysis identified 39 genome-wide significant loci outside the Major Histocompatibility Complex (MHC) region, including 15 previously unreported loci; 19 loci were shared between categories. Gene-prioritisation and protein interaction analyses identified a core MHC-centred antigen-presentation network, with category-enriched modules involving complement, innate/barrier pathways, epithelial biology, and type 2

*Correspondence to Dr. Jin Li, Department of Cell Biology, Tianjin Medical University, Tianjin, China.
**Correspondence to Dr Hakon Hakonarson, Center for Applied Genomics, Children's Hospital of Philadelphia, Philadelphia, PA, USA.
E-mail addresses: jli01@tmu.edu.cn (J. Li), hakonarson@chop.edu (H. Hakonarson).

Handling editor Josef Smolen.

https://doi.org/10.1016/j.ard.2026.07.007

0003-4967/© 2026 The Authors. Published by Elsevier B.V. on behalf of European Alliance of Associations for Rheumatology (EULAR). This is an open access article under the CC BY-NC-ND license (http://creativecommons.org/licenses/by-nc-nd/4.0/)

immunity. Enriched pathways included nuclear factor κB signalling, T helper 17 related pathways, Janus kinase-signal transducer and activator of transcription signalling, programmed cell death protein 1/programmed death-ligand 1, cytotoxic T-lymphocyte associated protein 4 regulation, and osteoclast differentiation, several of which are relevant to rheumatic diseases. Paediatric IMIDs shared broad polygenic architecture with adult IMIDs, whereas top-ranked genes converged strongly with adult rheumatic diseases. Priority Index analysis identified 178 high-scoring genes, including 43 approved or investigational IMID drug targets.

Conclusions: Paediatric-onset IMIDs share core pathways with adult forms but exhibit distinct genetic architecture shaped by age-specific immune and neurodevelopmental biology. These findings provide a genomic framework for paediatric precision medicine, guiding classification, risk prediction, and therapeutic development.

WHAT IS ALREADY KNOWN ON THIS TOPIC

- The genetic architecture of adult-onset immune-mediated inflammatory diseases (IMIDs) has been extensively characterised, leading to improved disease classification and targeted therapies.
- Paediatric-onset IMIDs, including juvenile idiopathic arthritis and other paediatric rheumatic diseases, remain underexplored at the genomic level, with uncertain overlap between paediatric and adult forms.

WHAT THIS STUDY ADDS

- This large-scale genome-wide meta-analysis maps the genetic architecture of paediatric-onset IMIDs, identifying shared susceptibility signals and 15 novel loci.
- Prioritised genes implicate immune regulation, epigenetic remodelling, neuroimmune communication, and immunometabolic pathways, highlighting developmentally relevant mechanisms in paediatric disease.
- Paediatric IMIDs show substantial gene-level overlap with adult rheumatic diseases and nominate high-priority therapeutic targets, supporting a genetic continuum from childhood immune dysregulation to adult rheumatologic disease.

HOW THIS STUDY MIGHT AFFECT RESEARCH, PRACTICE OR POLICY

- The findings challenge the assumption that paediatric-onset rheumatic and other immune disorders are simply early manifestations of adult diseases, underscoring the need for further research on the interaction between genetic factors and developmental context in disease pathogenesis.
- The genomic framework generated here may inform precision approaches in paediatric rheumatology, including early risk stratification, mechanistic disease subclassification, and prioritisation of therapeutic targets for childhood-onset immune disorders.

INTRODUCTION

Immune-mediated inflammatory diseases (IMIDs) comprise a broad spectrum of disorders driven by dysregulated innate and/or adaptive immune responses, resulting in chronic or recurrent tissue inflammation. This spectrum includes autoimmune diseases, polygenic autoinflammatory diseases, mixed-pattern inflammatory conditions, and allergic diseases [1,2]. Autoimmune diseases are typically characterised by loss of immune tolerance and prominent adaptive immune responses against self-antigens, whereas autoinflammatory diseases are more strongly associated with innate immune and barrier-inflammatory mechanisms, although adaptive immunity may also contribute [3]. Mixed-pattern IMIDs include disease subtypes that exhibit features of both autoimmune and autoinflammatory mechanisms [4]. Allergic diseases are characterised by hypersensitivity to environmental antigens and type 2–polarised immune responses, particularly at epithelial barrier tissues [5]. With the exception of classic monogenic disorders, most IMIDs arise through interactions between polygenic susceptibility and environmental exposures.

Although historically classified as distinct entities, IMIDs exhibit substantial genetic, clinical, and therapeutic overlap. These conditions share varying combinations of genetic susceptibility, immune dysregulation, and inflammatory tissue injury, often without a single identifiable external trigger. Increasing evidence suggests that many IMIDs lie along a continuum, with differing contributions from innate, adaptive, and barrier-associated immune mechanisms [4,6]. Therapeutically, multiple IMIDs respond to cytokine-targeted and other immunomodulatory interventions [7], further supporting shared inflammatory pathways across disease categories.

Rheumatic diseases represent a prominent subgroup of IMIDs and exemplify the complex interplay between innate and adaptive immunity. Diseases such as autoimmune arthritis and systemic lupus erythematosus (SLE) may occur in both children and adults, but disease onset during childhood can differ from adult-onset disease in clinical presentation, disease course, and underlying biology [8–10]. These differences underscore the importance of studying and understanding paediatric IMIDs directly rather than extrapolating entirely from adult cohorts.

Advances in genomic technologies have transformed our understanding of the genetic architecture of IMIDs. Genome-wide association studies (GWAS) in adults have identified hundreds of susceptibility loci for IMIDs, particularly rheumatoid arthritis (RA) and SLE [11]. However, the genetic basis of paediatric-onset IMIDs remains far less characterised, in part due to the smaller size and greater heterogeneity of paediatric cohorts. This has limited biologically informed disease classification, risk prediction, and therapeutic stratification in paediatric populations.

Paediatric IMIDs may also reflect distinct developmental contexts, as observed in juvenile idiopathic arthritis (JIA) [9,12,13]. Emerging evidence suggests that some genetic risk loci are shared between paediatric- and adult-onset disease, whereas others show age-specific effects or even opposite directions of association. For example, the T allele of rs17457484, which likely regulates expression of Tumor necrosis factor ligand superfamily member 11 (*TNFSF11*), confers increased risk for 3 adult rheumatic diseases but is protective in JIA [14]. These findings highlight the need for genomic studies specifically focused on paediatric populations.

A systematic investigation of the genetic basis of paediatric IMIDs spanning autoimmune, polygenic autoinflammatory, mixed-type, and allergic subclasses may therefore provide insight into shared and distinct genetic architecture across disease categories and may help to identify genetic factors relevant to paediatric disease classification, risk stratification, and therapeutic prioritisation.

METHODS

Ethics statement

The study was approved by the Institutional Review Boards at the Children's Hospital of Philadelphia and conducted according to the Declaration of Helsinki. Written informed consent was obtained from all the study participants or their legal guardians. Patients and/or the public were not involved in the design, conduct, or reporting of this research.

Study subjects and phenotype description

All subjects in the biobank of the Center for Applied Genomics (CAG), the Children's Hospital of Philadelphia, with both phenotypic and genotypic data available, were screened for cases and controls in this study. Case status was defined based on the diagnosis history in the electronic medical records. The diseases were classified into 4 categories of IMIDs: autoimmune, polygenic-autoinflammatory/barrier-dysfunction, mixed-pattern, and allergic/type 2–predominant type (Supplementary Table S1) based on prior literature and established immunopathogenic features [4]. Genotyped individuals in the CAG database with no diagnostic history of immune-mediated diseases were defined as controls and allocated proportionally to each IMID category according to sex, age, and genotyping platform.

Genotyping and quality control (QC) filtering

The samples were genotyped on Illumina single nucleotide polymorphism (SNP) arrays with at least 500K SNPs. Standardised and uniform QC was performed on all genotyped subjects included in the study using PLINK2.0 [15]. Any sample with a call rate <98% was excluded. SNPs with call rate <98% or with minor allele frequency (MAF) <0.01 or with Hardy–Weinberg equilibrium P values $<10^{-5}$ were excluded. Kinship estimation was performed with a threshold of 0.177 to remove 1st-degree relations. Principal component analysis (PCA) was conducted with the implemented –pca option on a set of linkage disequilibrium (LD) pruned independent SNPs, and subjects of non-European ancestry were excluded from further study. PCA was performed again in the remaining samples, and the resulting principal components were used as covariates for the association analysis.

Imputation

After QC filtering, the genotype data from different versions of arrays were merged together on their common variants. The genotyped data were converted to variant call format (VCF) using PLINK2.0, keeping the A1 and A2 assignments made by the HRC-1000G-check-bim.pl script. The VCF files were then uploaded for imputation to the TopMed Imputation Server. The imputation was carried out using Genotype Imputation (Minimac4 [16]) 1.3.3, with the TopMed R2 reference panel [17] as the reference panel, and QC frequency was checked against the TopMed panel. The imputed data were QC filtered using bcftools v1.6 based on a combination matrix of MAF and the estimated R2. SNPs with MAF ≥0.05 and R2 ≥0.3, or with MAF <0.05 but R2 ≥0.5, were retained.

Estimation of heritability and genetic correlation

The estimation of heritability and genetic correlation of paediatric IMIDs based on individual genotype and phenotype data was carried out using the tool for Genome-wide Complex Trait Analysis [18] method.

Association analysis

The imputed data were converted into PLINK 2.0 pgen files, and QC filtering was performed again. Association testing was performed using imputed allele dosages. SNPs with P value $<1 \times 10^{-5}$ in the missingness test between cases and controls were removed from further analyses. Genome-wide association analyses were subsequently performed separately for each of the 4 paediatric disease groups using PLINK 2.0 –glm firth-residualise framework, adjusting for sex, age, genotyping platform (modelled as dummy variables), and the first 9 principal components. Genomic inflation factors (λ) were computed to evaluate potential inflation of the test statistics. As λ is influenced by sample size, the standardised λ_{1000}, which is corrected for an equivalent sample size of 1000 cases and 1000 controls, was also calculated.

Chromosome X-wide association analyses

Sex-stratified analyses of the X chromosome were performed using PLINK 2.0 with the default chrX model, in which male hemizygous variants outside the pseudoautosomal regions (PARs) are coded on a 0 to 2 dosage scale. Association models were adjusted for age, genotyping arrays, and the first 9 principal components.

Meta-analysis

A heterogeneity-sensitive meta-analysis approach, association analysis based on SubSETs (ASSET) [19], was used to identify genomic loci conferring shared effects to ≥2 categories of immune disorders. The 1-sided test with the 'h.traits' methods implemented in ASSET was adopted, which exhaustively searches for combinations of immune disorder categories yielding the best association statistics with the same direction of effects. ASSET allows and accounts for sample overlap between subtypes. The Discrete Local Maximum method was employed for multiple testing adjustment over all the possible disease combinations. Meta-analysis was similarly performed for chromosome X SNPs among males and females separately.

Post-GWAS analyses

We conducted comprehensive post-GWAS analyses, including polygenic overlap analysis using MiXeR [20]; decoding shared associations across immune disorders using METASOFT [21]; and functional enrichment analysis using GARFIELD [22]. Priority index analysis for drug-target potential [23].

Gene prioritisation within each significant locus was conducted through 8 approaches, including positional mapping, Functional Mapping and Annotation (FUMA) [24] high-throughput chromosome conformation capture (HiC) and expression quantitative trait locus (eQTL) mapping, MAGMA (Multi-marker Analysis of GenoMic Annotation) [25], DEPICT (Data-driven Expression-Prioritised Integration for Complex Traits) [26], FUSION TWAS (transcriptome-wide association studies) [27] algorithm, SMR (Summary data–based Mendelian randomisation) [28], and PoPS (Polygenic Priority Score) [29].

Protein-protein interaction (PPI) analysis of the top 1% genes from MAGMA analysis was performed using the STRING web portal (https://string-db.org/).

Methodological details are described in the Supplementary Methods.

RESULTS

We identified 24 paediatric IMIDs, grouped them into 4 biologically informed categories, and performed category-specific GWAS among participants of European ancestry (Supplementary Table S1): autoimmune IMIDs (2242 cases; 15,663 controls), polygenic autoinflammatory/barrier-dysfunction IMIDs (2916 cases; 20,449 controls), mixed-pattern IMIDs with both innate and adaptive immune features (5136 cases; 36,142 controls), and allergic/type 2–predominant IMIDs (7792 cases; 58,765 controls) (Supplementary Table S2, Supplementary Figs S1, S2). The standardised genomic inflation factor (λ_{GC1000}) of each GWAS was <1.02 (Supplementary Table S2).

We extracted reported genome-wide significant SNPs for the 24 immune disorders from the GWAS catalogue and compared their replication rates across our 4 GWAS cohorts using a 1-sided exact McNemar test. Autoimmune GWAS-catalogue SNPs (N_{SNP} = 1197) had a significantly higher replication rate (P < 0.05) in our autoimmune cohort (30.4%) compared with the poly-autoinflammatory (22.1%; $P = 1.1 \times 10^{-6}$), allergic (11.6%; $P = 1.8 \times 10^{-31}$), or mixed-pattern (15.6%; $P = 2.0 \times 10^{-21}$) cohorts. The poly-autoinflammatory set (N_{SNP} = 735) showed an even stronger matched-cohort enrichment, with a 61.9% replication rate in our autoinflammatory cohort versus only 8.3% to 15.4% in the other 3 cohorts (all $P < 1.4 \times 10^{-67}$). The allergic GWAS-catalogue SNPs (N_{SNP} = 1776) were modestly enriched in the matched allergic cohort (20.1%) relative to the autoimmune (15.6%; $P = 2.1 \times 10^{-4}$) and mixed-pattern (11.1%; $P = 2.5 \times 10^{-13}$) cohorts, but were in fact more frequently significant in the poly-autoinflammatory cohort (28.3%), suggesting similarity in underlying barrier-inflammatory mechanism. For the mixed-pattern set (N_{SNP} = 1226), the matched cohort did not show enrichment over any other (13.1% vs 12.9%-31.8%), likely reflecting differences in statistical power and the heterogeneous nature of this category (Supplementary Figs S3 and S4).

SNP-based heritability estimates indicated substantial common-variant contributions across the 4 paediatric IMID categories, ranging from 28.9% for allergic IMIDs to 61.9% for autoimmune IMIDs. Estimates for mixed-pattern and polygenic autoinflammatory IMIDs were intermediate at 32.8% and 49.0%, respectively (Fig 1; Supplementary Table S2). The lower heritability observed for allergic and mixed-pattern IMIDs suggests a relatively greater contribution from environmental exposures, disease heterogeneity, or other non–common-variant factors in these categories.

The 4 IMID categories showed positive but variable genetic correlations (Fig 1A; Supplementary Table S3). Consistent with this, MiXeR analyses indicated partial polygenic overlap across categories together with substantial trait-specific components. Allergic and mixed-pattern IMIDs showed greater polygenicity than autoimmune and polygenic autoinflammatory IMIDs, likely reflecting greater clinical and biological heterogeneity (Fig 1B).

Based on the observed genetic correlations and polygenic overlap, we next performed a fixed-effect subset-based meta-analysis across the 4 paediatric IMID categories. The analysis included 6,601,385 SNPs shared across imputed GWAS datasets and comprised 18,086 cases and 131,019 controls (λ_{GC} = 1.135, λ_{GC1000} = 1.004; Supplementary Fig S1). Excluding the extended Major Histocompatibility Complex (MHC) region (chr6:25-34Mb), we identified 39 genome-wide significant loci, including 15 previously unreported loci (Fig 2A, Supplementary Fig S5, Table 1, Supplementary Table S4). Using Metasoft, we found 19 loci with pleiotropic effects across more than 1 IMID category (m-value >0.9; Supplementary Table S5, Supplementary Fig S6). Representative examples in Figure 2C illustrate distinct cross-category patterns, including shared associations across multiple IMID categories for rs597808 and rs7992283, and a more restricted mixed-pattern IMID signal for rs4862110 (Fig 2C).

As an external validation step, we evaluated the lead variant from each genome-wide significant locus in FinnGen [30] for immune-mediated or inflammatory endpoints. All lead variants showed nominal association with at least 1 relevant FinnGen phenotype at P < 0.01 (Supplementary Table S6), spanning rheumatologic, gastrointestinal, respiratory, and dermatologic conditions. Notably, 11 of the 15 lead variants were associated with rheumatologic conditions.

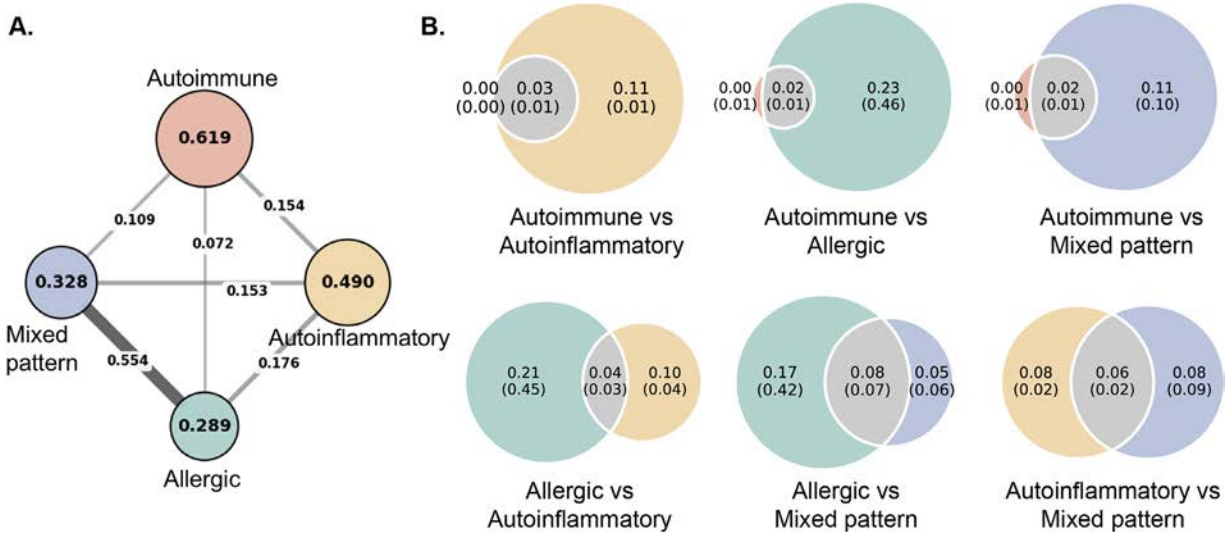

Figure 1. Genetic overlap among 4 categories of paediatric immune-mediated inflammatory diseases (IMIDs). The 4 paediatric IMID categories included autoimmune, polygenic autoinflammatory/barrier-dysfunction, mixed-pattern, and allergic/type 2–predominant IMIDs. (A) SNP-based heritability estimates and pairwise genetic correlations across IMID categories. Each circle represents 1 IMID category, with the SNP-based heritability estimate displayed within the circle. Connecting lines indicate pairwise genetic correlations, with greater line thickness and darker shading representing stronger correlations. (B) Pairwise polygenic overlap among the 4 paediatric IMID categories estimated using MiXeR. IMID, immune-mediated inflammatory disease; SNP, single nucleotide polymorphism.

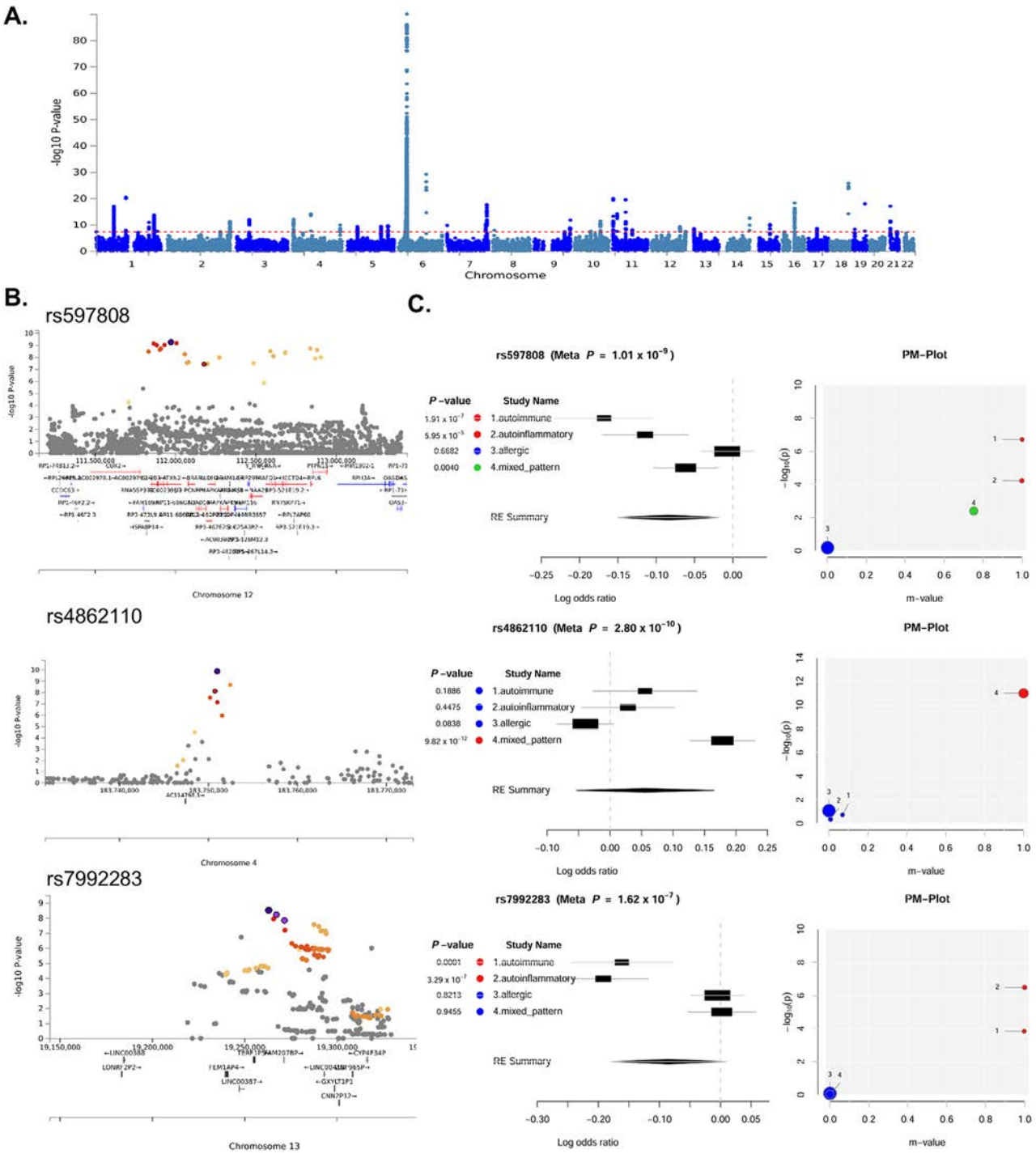

Figure 2. Meta-analysis identifies genome-wide significant loci across paediatric IMID categories. Meta-analysis was performed across autoimmune, polygenic autoinflammatory/barrier-dysfunction, mixed-pattern, and allergic/type 2–predominant IMIDs. (A) Manhattan plot of the meta-analysis across the 4 paediatric IMID GWAS cohorts. (B) Regional association plots showing representative genome-wide significant loci identified in the meta-analysis, illustrating loci with either restricted or shared associations across IMID categories. (C) Forest plots and PM-plots summarising category-specific effects for representative loci. Forest plots show *P* values, log odds ratios, and standard errors for each IMID category. PM-plots show Metasoft m-values for each category, with the y-axis representing category-specific association strength as $-\log_{10}(P \text{ value})$ and point size proportional to the GWAS sample size. Categories with m-values ≥0.9 are highlighted in red, indicating strong evidence for SNP association with this IMID category. GWAS, genome-wide association studies; IMID, immune-mediated inflammatory disease; PM, P-value vs. m-value; RE, random effects; SNP, single nucleotide polymorphism.

Functional annotation of the meta-analysis loci, including those at a sub-genome-wide threshold ($P < 1E\text{-}7$), revealed that enrichments spanned 9 tissue types and 33 cell types, but were dominated by blood-related annotations (151/174). The signal was driven primarily by chromatin accessibility peaks (92) and hotspots (57), with additional enrichment in histone-mark annotations (17), including active regulatory marks such as H3K27ac and H3K4me1. The frequently enriched cell types were CD34+, CD8+, CD3+, CD4+, and CD19+ cells. Enrichments were also observed in foetal thymus and foetal intestine (Supplementary Fig S7). Similar patterns were observed at the more stringent threshold of GWAS *P* value $<1 \times 10^{-8}$ (Supplementary Table S7).

To identify target genes, we employed locus-based and similarity-based approaches linking genome-wide significant loci to genes based on proximity, eQTLs, and chromatin interactions

Table 1

Genome-wide significant non-MHC loci from ASSET analyses of the 4 categories of immune-mediated inflammatory diseases

SNP	Chr	Pos	A1	A1_freq	Beta	*P*	Disorders	Annotation	Positional	HiC	eQTL	SMR	TWAS	PoPS	MAGMA	DEPICT
rs113935720	1	67713346	C	0.067	−0.656	1.19E-17	2	Intronic	*IL23R*	*TCTEX1D1;IL23R; SERBP1;GADD45A*	*TCTEX1D1;MIER1;C1orf141; IL23R;SERBP1;GADD45A*	/	/	*IL23R*	/	*IL23R*
rs6679677	1	114303808	A	0.095	0.468	3.92E-21	1	Downstream	*RSBN1*	*ST7L;MAGI3; CAPZA1;PHTF1; DCLRE1B;PTPN22; AP4B1;BCL2L15; NRAS*	*MAGI3;PHTF1;PTPN22; BCL2L15;AP4B1;DCLRE1B*	/	/	*RSBN1;MAGI3; DCLRE1B*	*RSBN1;PHTF1*	*PTPN22*
rs13303363	**1**	**203494379**	**T**	**0.466**	**−0.152**	**1.44E-11**	**1, 2**	**Downstream**	***OPTC***	/	***CHI3L1;ZBED6;SNRPE***	/	/	/	/	/
rs35835288	**1**	**222982059**	**C**	**0.218**	**−0.216**	**2.14E-14**	**1, 2**	**Upstream**	***DISP1***	***HHIPL2;DISP1; BROX;AIDA***	***HHIPL2;TAF1A;MIA3;AIDA; BROX;DISP1;SUSD4***	/	/	***MIA3;AIDA; FAM177B***	***MIA3;BROX; AIDA; FAM177B***	***TAF1A***
rs10910476	1	234734956	C	0.462	−0.172	2.83E-08	2	Downstream	*IRF2BP2*	*TARBP1;B3GALNT2; TOMM20*	*TARBP1;IRF2BP2*	/	/	/	/	/
rs11571316	2	204731089	A	0.417	−0.109	4.43E-08	1, 3	Upstream	*CTLA4*	*CARF;RAPH1*	*RAPH1;ICOS*	/	/	*CTLA4*	/	/
rs34236350	2	241568326	T	0.175	0.262	6.32E-12	2	Intronic	*GPR35*	/	*GPC1;DUSP28;CAPN10;GPR35*	/	/	*GPR35*	/	*PDCD1;NEU4*
rs7371228	2	242627097	C	0.388	−0.160	6.95E-12	1, 2	Upstream	*DTYMK*	/	*HDLBP;FARP2;STK25;BOK; THAP4;ATG4B;DTYMK;ING5; D2HGDH;GAL3ST2;NEU4; PDCD1;AC131097.4*	*ING5*	*ING5*	*ATG4B; D2HGDH; ING5*	*D2HGDH*	
rs11712569	3	49540152	G	0.313	0.218	1.16E-12	- 2	Intronic	*DAG1*	*BSN;APEH;USP19; QARS;QRICH1*	*WDR6;DALRD3;NDUFAF3; IMPDH2;QRICH1;CCDC71; CCDC36;RP11-B7.1;C3orf62; USP4;GPX1;RHOA;TCTA; AMT;NICN1;DAG1;BSN; APEH;MST1;RNF123; AMIGO3;GMPPB;IP6K1; CDHR4;FAM212A;CAMKV; MST1R;MON1A;RBM6*	*AMT*	*APEH;DAG1; MST1;AMT*	*RHOA; TCTA; RNF123*	*AMT;TCTA; NICN1;DAG1*	*BSN-AS2*
rs12506405	4	4057590	C	0.095	0.251	1.02E-12	1, 2	Intergenic	/	*ADRA2C*	*LYAR;ZBTB49;NSG1*	/	/	/	/	/
rs3775782	**4**	**70465153**	**T**	**0.422**	**−0.177**	**8.84E-15**	**1, 2**	**Intronic**	***UGT2A1***	/	***UGT2B11;UGT2B28;UGT2B4; UGT2A1;CSN1S1***	/	/	/	/	/
rs4862110	**4**	**183751029**	**C**	**0.175**	**0.178**	**1.37E-10**	**3**	**Downstream**	***ODZ3***	/	***DCTD***	/	/	/	/	/
rs9283753	5	40490609	C	0.426	−0.192	6.29E-10	2	Upstream	*PTGER4*	*PTGER4*	*PTGER4;TTC33;RPL37;C7*	/	/	/	/	/
rs2248116	5	131804347	C	0.415	0.189	4.41E-10	2	Intronic	*C5orf56*	*AFF4;IL4;RAD50;IL5; IRF1;PDLIM4; KIF3A;ZCCHC10; CDC42SE2;RAP-GEF6;ACSL6;IL3; CSF2;SEPT8; SHROOM1;GDF9; UQCRQ;LEAP2; IL13;HINT1; HSPA4;LYRM7; SLC22A5;C5orf56; SOWAHA;CCNI2*	*IL3;P4HA2;PDLIM4;SLC22A4; SLC22A5;C5orf56;IRF1;IL5; RAD50;IL13;IL4;KIF3A; CCNI2;SEPT8;SHROOM1; LEAP2*	/	/	*CSF2;IRF1; FNIP1*	*P4HA2;PDLIM4; IL3; CSF2; SLC22A4; SLC22A5*	*IL3;RAPGEF6; SLC22A4; CSF2*
rs10043720	5	158767333	A	0.314	−0.213	2.43E-10	2	Intronic	*LOC285626*	*TTC1;RNF145; UBLCP1;ADRA1B; C5orf54*	*RNF145;UBLCP1*	/	/	/	/	/
rs12529070	**6**	**107456170**	**C**	**0.218**	**0.425**	**7.73E-30**	**1**	**Downstream**	***PDSS2***	/	***PDSS2***	/	/	/	/	/
rs6970378	**7**	**714906**	**C**	**0.101**	**−0.256**	**1.99E-10**	**1, 2**	**Intronic**	***PRKAR1B***	/	***PRKAR1B;HEATR2;SUN1; GET4;ADAP1;COX19; C7orf50;GPR146;ZFAND2A***	/	/	/	/	/
rs6976464	7	149797718	T	0.447	−0.149	6.30E-11	1, 2	Downstream	*ACTR3C*	/	*ZNF862;ATP6V0E2;ACTR3C; ZBED6CL;GIMAP8*	/	/	/	/	/
rs2622165	**7**	**153487022**	**C**	**0.451**	**−0.288**	**2.85E-18**	**1**	**Upstream**	***DPP6***	/	***DPP6***	/	/	/	/	/
rs4372078	9	117563687	T	0.281	−0.194	4.96E-08	2	Intronic	*TNFSF15*	/	*ORM1;ATP6V1G1;C9orf91; TNFSF15;TNC*	/	/	/	/	/
rs4078099	9	139267533	A	0.406	0.184	1.74E-09	2	Intronic	*CARD9*	/	*UBAC1;QSOX2;GPSM1;DNLZ; CARD9;SNAPC4;C9orf163; NOTCH1;LCN15*	/	/	*SNAPC4;CARD9*	/	/
rs224125	10	64454089	A	0.405	0.130	2.58E-08	1, 2	Downstream	*ZNF365*	*NRBF2;ADO*	*ZNF365;ADO;EGR2;NRBF2*	/	/	/	/	/
rs10748781	10	101283330	C	0.439	0.206	4.57E-12	2	Upstream	*NKX2-3*	/	*NKX2-3;SLC25A28;COX15; DNMBP*	/	/	/	/	/
rs689	11	2182224	A	0.272	−0.366	1.37E-20	1	Intronic	*INS*	/	*MRPL23;IGF2;TH;ASCL2; C11orf21;TSPAN32;CD81*	/	/	/	/	/

(*continued on next page*)

Table 1 (*Continued*)

SNP	Chr	Pos	A1	A1_freq	Beta	*P*	Disorders	Annotation	Positional	HiC	eQTL	SMR	TWAS	PoPS	MAGMA	DEPICT
rs2237968	**11**	**17491386**	**T**	**0.370**	**−0.183**	**7.68E-15**	**1, 2**	**Intronic**	***ABCC8***	/	***PIK3C2A;NCR3LG1;KCNJ11; ABCC8***	/	/	/	/	/
rs76091727	**11**	**50094998**	**A**	**0.059**	**0.383**	**3.26E-20**	**1, 2**	**Upstream**	***OR4C12***	***OR4C5;OR4C46; OR4C12;OR4A47***	***OR4C12***	/	/	/	***OR4C46; OR4A5***	/
rs61893460	11	76291154	A	0.463	0.174	1.14E-08	2	Downstream	*C11orf30*	*LRRC32*	*RP11-111M22.2;LRRC32;ACER3*	/	/	/	/	/
rs597808	12	111973358	G	0.495	−0.100	5.76E-10	1, 2, 3	Intronic	*ATXN2*	*MAPKAPK5;BRAP; ACAD10;ALDH2; TRAFD1;PPP1CC; RP11-162P23.2*	*FAM109A;SH2B3;ACAD10; RP11-162P23.2;ALDH2;MAP-KAPK5;TMEM116;ERP29; NAA25*	/	/	*TRAFD1;RPL6; SH2B3*	*MAPKAPK5; BRAP;ERP29; SH2B3; ACAD10; ALDH2; NAA25; TMEM116; FAM109A; ATXN2; RP11-162P23.2*	*TRAFD1*
rs28437244	**12**	**132934696**	**A**	**0.156**	**−0.187**	**3.39E-08**	**1, 2**	**Upstream**	***GALNT9***	/	***GALNT9;PGAM5;ANKLE2***	/	/	/	/	/
rs7992283	**13**	**19263109**	**A**	**0.192**	**−0.179**	**3.10E-09**	**1, 2**	**Downstream**	***ANKRD20A9P***	/	/	/	/	/	/	/
rs5000577	**14**	**107067117**	**G**	**0.097**	**0.253**	**2.83E-13**	**1, 2**	**Downstream**	***IGHV1-58***	/	/	***IGHV3-53***	***IGHV4-61***	/	/	***IGHV3-72; IGHV1-69***
rs72743482	15	67466599	G	0.213	0.225	1.01E-10	2	Intronic	*SMAD3*	*SMAD3;RP11-342M21.2*	*SMAD3;RP11-342M21.2; AAGAB;IQCH;C15orf61; MAP2K5*	/	/	/	/	/
rs2066845	16	50756540	C	0.015	0.736	5.93E-19	2	Intronic	*NOD2*	*CYLD;PAPD5;ADCY7; NKD1;HEATR3; CHD9;CNEP1R1*	*ADCY7;BRD7;NKD1;CYLD*	*NOD2;CYLD*	*NKD1; SNK20;NOD2*	*NOD2;CYLD; SNK20*	*NOD2;CYLD; SNK20;NKD1*	*NOD2;SNX20; CYLD*
rs12949100	17	38057189	A	0.451	−0.112	2.61E-09	4	Downstream	*GSDMB*	*GSDMB;PSMD3; NR1D1;GRB7; MIEN1;IKZF3; ZPBP2;MSL1*	*MED1;CDK12;PPP1R1B; STARD3;PNMT;PGAP3; ERBB2;MIEN1;GRB7;IKZF3; ZPBP2;GSDMB;ORMDL3; LRRC3C;GSDMA;PSMD3; CSF3;MED24;THRA;NR1D1; MSL1;CASC3;WIPF2;CDC6*	*IKZF3;GSDMB; ORMDL3*	*GSDMB; ORMDL3; IKZF3; PGAP3*	*GSDMB; ORMDL3; IKZF3*	*ZPBP2*	/
rs7232266	**18**	**70488712**	**G**	**0.395**	**0.147**	**2.00E-26**	**3, 4**	**Intronic**	***NETO1***	/	/	/	/	/	/	/
rs74956615	19	10427721	A	0.047	−0.243	6.10E-09	1, 2, 3	Intronic	*RAVER1*	*ICAM3;KEAP1; OLFM2;MRPL4; ICAM4;TYK2; KRI1;CDKN2D; ATG4D;PPAN; EIF3G;ANGPTL6; RAVER1;S1PR5; PPAN-P2RY11; P2RY11*	*OLFM2;C19orf66;ANGPTL6; P2RY11;ICAM4;ICAM5;TYK2; CDC37;PDE4A;KEAP1;KRI1*	/	/	*ICAM3;TYK2; PDE4A*	*TYK2;CDC37*	*ICAM1;ICAM3*
rs556052	**19**	**49377436**	**C**	**0.371**	**−0.207**	**1.30E-18**	**1, 2**	**Intronic**	***PPP1R15A***	/	***GRWD1;LMTK3;RPL18;DBP; BCAT2;HSD17B14;PLE-KHA4;PPP1R15A;TULP2; NUCB1;DHDH;BAX;FTL; GYS1;CGB2;SNRNP70; TEAD2***	/	/	***PPP1R15A***	/	***TULP2; PPP1R15A***
rs9975691	**21**	**14928355**	**G**	**0.434**	**0.186**	**1.09E-17**	**1, 2**	**Upstream**	***POTED***	/	/	/	/	/	/	/
rs2836883	21	40466744	A	0.276	−0.199	4.34E-08	2	Downstream	*PSMG1*	*ETS2*	*ETS2;PSMG1;HMGN1;WRB*	/	*LINC02940*	/	/	/

A1, effect allele; A1_freq, effect allele frequency; ASSET, association analysis based on SubSETs; Chr, chromosome; DEPICT, Data-driven Expression-Prioritised Integration for Complex Traits; eQTL, expression quantitative trait locus; Hi-C, high-throughput chromosome conformation capture; MAGMA, Multi-marker Analysis of GenoMic Annotation; MHC, major histocompatibility complex; PoPS, Polygenic Priority Score; Pos, genomic position based on genome build hg19; *P* value, meta-analysis *P* value; SMR, summary data–based Mendelian randomisation; SNP, single nucleotide polymorphism; TWAS, transcriptome-wide association study.

Novel loci are highlighted in bold.

SNP denotes the lead SNP at each genome-wide significant locus. Disorder indicates the contributing disorder(s) in the ASSET meta-analysis. Disorder categories are coded as follows: 1, autoimmune; 2, polygenic autoinflammatory; 3, mixed pattern; and 4, allergic. Prioritised genes were identified using multiple complementary approaches, including positional proximity, Hi-C and eQTL gene mapping annotated by the FUMA platform, MAGMA, TWAS, SMR, PoPS, and DEPICT.

(Table 1). We uncovered genes with well-recognised roles in immune and inflammatory disease at the established loci (Supplementary Table S8). Among the newly identified loci, prioritised genes fell into several broad functional categories (Supplementary Table S9), highlighting potentially novel biology for paediatric IMIDs. These included immune- and cell-surface–related genes (eg, the immunoglobulin heavy chain variable region (IGHV) near *IGHV1-58, IGHV3-53*, and *IGHV4-61*, as well as *NCR3LG1*, a ligand involved in natural killer cell –mediated immune recognition, and *CHI3L1*, an extracellular inflammatory and tissue-remodelling mediator). The second group comprised genes involved in protein processing, trafficking, secretion, extracellular matrix organisation, and posttranslational modification, including *melanoma inhibitory activity protein 3* (*MIA3), polypeptide N-acetylgalactosaminyltransferase 9* (*GALNT9),* and dispatched RND transporter family member 1 (*DISP1*). Additional prioritised genes pointed to cellular stress responses, mitochondrial function, and metabolic regulation, including *decaprenyl diphosphate synthase subunit 2* (*PDSS2), protein phosphatase 1 regulatory subunit 15A* (*PPP1R15A), phosphoglycerate mutase family member 5* (*PGAM5), ATP-binding cassette subfamily C member 8* (*ABCC8) and potassium inwardly rectifying channel subfamily J member 11* (*KCNJ11)*. Several loci prioritised genes with predominantly neural or neurodevelopmental functions, such as *dipeptidyl peptidase-like 6* (*DPP6), neuropilin and tolloid-like protein 1* (*NETO1)*, and *teneurin transmembrane protein 3* (*TENM3*)*/Odd Oz/Ten-M Homolog 3*(*ODZ3*), suggesting that some paediatric IMID associations may involve broader developmental or neuroimmune pathways (Supplementary Table S9).

We next performed X-chromosome-wide association analyses separately in females and males across the 4 IMID subtypes (Supplementary Tables S10 and S11), followed by cross-subtype meta-analysis. In females, the ASSET analysis identified a genome-wide significant locus at Xp22.33, with the lead signal mapping to a region containing genes *glycogenin-2* (*GYG2), arylsulfatase D* (*ARSD), arylsulfatase H* (*ARSH*), and *Xg glycoprotein* (*XG)* (Supplementary Figs S8–S10). XG has been implicated in the regulation of neutrophil and T-cell extravasation and homotypic cell–cell adhesion [31]. A second locus at Xp11.4, encompassing *ubiquitin specific peptidase 9 X-linked* (*USP9X)* and *mediator complex subunit 14* (*MED14*), showed suggestive evidence of association and approached genome-wide significance. In males, a genome-wide significant signal was also observed at Xp22.33, indicating a shared association at this locus across sexes. In addition, we identified a male-specific genome-wide significant locus at Xq26.3 (Supplementary Figs S8-S10), a region previously reported by our group [32]. Collectively, these findings highlight both shared and sex-dependent chromosome X association signals contributing to IMID susceptibility.

MAGMA tissue enrichment analysis of the meta-analysis results identified significant enrichment in immune- and barrier-related tissues, with the strong signals observed in spleen, whole blood, lung, and small intestine, consistent with clinical observations of disease-affected organs (Supplementary Fig S11).

We applied the top 1% of genes identified by MAGMA (Supplementary Table S12) to PPI network analysis (Supplementary Fig S12). The resulting connected protein network was dominated by a human leukocyte antigen (HLA)/MHC-centred subnetwork, indicating that antigen processing and presentation constitute a major shared feature across the 4 IMID groups. Additional interconnected subnetworks included genes involved in inflammatory cytokine signalling, complement activation, and innate immune responses, such as *nucleotide-binding oligomerization domain-containing protein 2* (*NOD2), interleukin-23 receptor* (*IL23R), complement component 2* (*C2)*, and *complement factor B* (*CFB)*; genes related to epithelial/barrier and mucosal biology; and more peripheral sets of stress-response and regulatory genes, including heat-shock proteins, *tripartite motif* (*TRIM*) family members, and chromatin-associated genes.

Pathway analyses of MAGMA- and PoPS-prioritised genes (Supplementary Tables S12 and S13) showed concordant enrichment of immune regulatory pathways, including T-cell receptor signalling, TNF signalling, nuclear factor kappa-light-chain-enhancer of activated B cells (NF-κB) signalling, T helper 17 (Th17) cell differentiation, and Janus kinase - signal transducer and activator of transcription (JAK–STAT) signalling (Supplementary Tables S14-S17). Additional enrichment for complement activation, ubiquitin-dependent processing, DNA methylation, and other posttranslational or epigenetic regulatory processes suggests broader mechanisms linking immune activation, inflammatory regulation, and tissue remodelling across paediatric IMIDs. In addition, enrichment of osteoclast differentiation may also be of interest in the context of inflammatory tissue remodelling; pathways involving programmed cell death protein 1 (PD-1)/programmed death-ligand 1 (PD-L1) and cytotoxic T-lymphocyte-associated protein 4 (CTLA4) related T-cell regulation point to potentially relevant translational signals (Supplementary Figs S13 and S14, Supplementary Tables S14-S17).

Similar analyses on the top 150 MAGMA genes (Supplementary Table S12) associated with each class of immune disorders also revealed distinct network architectures across the 4 IMID categories. Autoimmune disorders showed the most densely interconnected network, dominated by an HLA-centred antigen-presentation module with additional links to proteasome, complement, and lymphocyte signalling genes, consistent with a strong adaptive immune signature (Supplementary Fig S15). The polygenic autoinflammatory/barrier-inflammatory IMID group showed a less HLA-dominant but still well-connected network enriched for innate and inflammatory signalling hubs, including *NOD2*, *interleukin-12 subunit beta* (*IL12B*), *interferon gamma* (*IFNG*), *interleukin 18 receptor 1* (*IL18R1*), *caspase recruitment domain-containing protein 9* (*CARD9*), and *tumor necrosis factor receptor superfamily member 6B* (*TNFRSF6B*) (Supplementary Fig S16). In contrast, the allergic IMID network was more heterogeneous, with smaller subnetworks involving genes related to epithelial regulation, type 2 immunity, and immune modulation, including *interleukin 4 receptor* (*IL4R*), *thymic stromal lymphopoietin* (*TSLP*), *orosomucoid like 3* (*ORMDL3*), *gasdermin A* (*GSDMA*), and *gasdermin B* (*GSDMB*) (Supplementary Fig S17). The JIA-representative mixed-pattern IMID network shared features with autoimmune IMID, including a visible HLA-related core, but also showed broader peripheral connectivity suggestive of additional regulatory and tissue-related processes (Supplementary Fig S18). These findings support both shared immune connectivity across IMIDs and category-specific differences in the dominant interacting biological modules.

We compared the shared genetic architecture of paediatric IMIDs with IMIDs that commonly occur in adolescents and adults (Supplementary Table S18) using 2 complementary approaches. Comparator traits included RA, SLE, systemic sclerosis (SSc), ankylosing spondylitis (AS), adult asthma, ulcerative colitis (UC), Crohn's disease (CD), and inflammatory bowel disease (IBD). First, MiXeR analysis of the paediatric IMID meta-analysis demonstrated substantial polygenic overlap with adolescent- and adult-onset IMIDs. The extent of overlap was greater for adult asthma, UC, CD, and IBD than for adult rheumatic diseases, likely reflecting the broader genome-wide polygenicity of these comparator traits (Fig 3A). Second, we

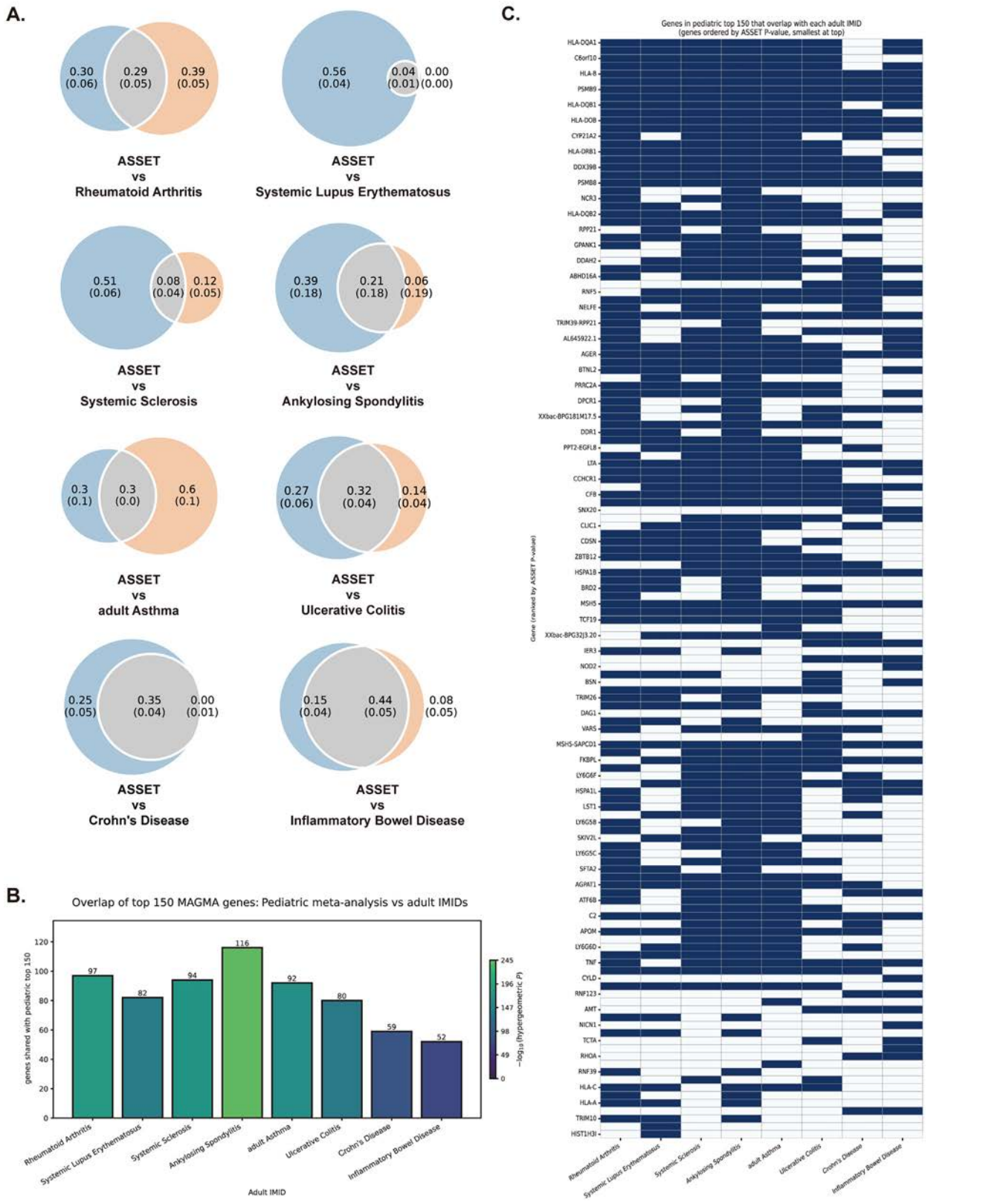

Figure 3. Genetic overlap between paediatric IMIDs and adolescent- or adult-onset IMIDs. Genetic overlap between the meta-analysis across the 4 paediatric IMID categories and IMIDs commonly occurring in adolescents or adults, as reported in the GWAS Catalogue. Comparator traits included rheumatoid arthritis, systemic lupus erythematosus, systemic sclerosis, ankylosing spondylitis, adult-onset asthma, ulcerative colitis, Crohn's disease, and inflammatory bowel disease. (A) Pairwise MiXeR analyses showing the estimated number of shared and trait-specific polygenic components between the paediatric IMID meta-analysis and each comparator IMID. Blue circles represent the paediatric IMID meta-analysis, orange circles represent comparator IMIDs, and grey overlap indicates shared polygenic components. (B) Number of overlapping genes between the top 150 MAGMA-prioritised genes from the paediatric IMID meta-analysis and the top 150 MAGMA-prioritised genes from each adolescent- or adult-onset IMID GWAS. (C) Gene-level overlap matrix showing the presence or absence of the top 150 paediatric IMID MAGMA genes across the comparator IMIDs. Genes are ordered by MAGMA gene-based association *P* value in the paediatric IMID meta-analysis, with the most significant genes shown at the top. ASSET, association analysis based on SubSETs; GWAS, genome-wide association studies; IMID, immune-mediated inflammatory disease; MAGMA, Multi-marker Analysis of GenoMic Annotation.

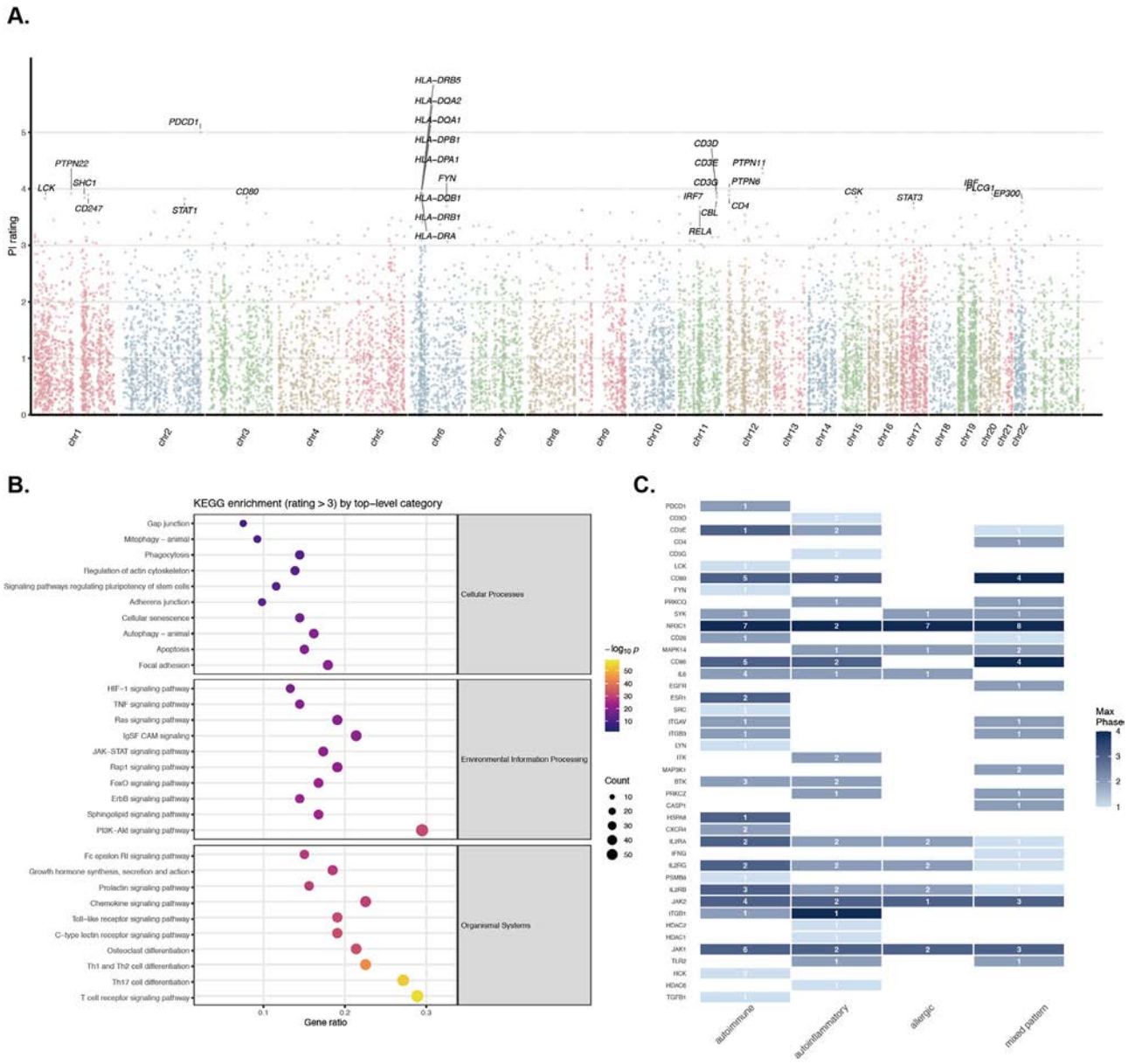

Figure 4. Priority Index–based gene prioritisation and drug-target potential across paediatric IMID categories. (A) Genome-wide distribution of Priority Index scores for genes mapped to immune disorder GWAS loci. The x-axis indicates chromosomal position, and the y-axis indicates the Priority Index score. Each point represents 1 gene, and the top-ranked genes are labelled. (B) KEGG pathway enrichment among genes with Priority Index score >3.0. Enriched pathways are grouped by top-level KEGG categories, including cellular processes, environmental information processing, and organismal systems. Dot size represents the number of genes contributing to each pathway, and colour indicates enrichment significance as $-\log_{10}(P)$. (C) Drug-target evidence among genes with Priority Index score >3.0 across the 4 IMID categories. Rows represent prioritised genes targeted by drugs in clinical trials for immune disorders, and columns represent IMID categories. Cell colour indicates the maximum clinical trial phase, and numbers indicate the number of drugs targeting each gene within the corresponding IMID category. GWAS, genome-wide association studies; IMID, immune-mediated inflammatory disease; KEGG, kyoto encyclopedia of genes and genomes.

compared the top 150 MAGMA-prioritised genes from the paediatric IMID meta-analysis (Supplementary Table S12) with those derived from adult-IMID GWAS summary statistics (Supplementary Table S19). This analysis showed substantial gene-level overlap between paediatric IMIDs and adult-IMID comparator traits, with highly significant enrichment across all comparisons by hypergeometric testing (Fig 3B, Supplementary Table S20). The overlap was particularly pronounced for adult rheumatic diseases, suggesting convergence of leading disease-associated genes between paediatric IMIDs and adult rheumatic disease biology (Fig 3C). Among the 9 genes that were absent from the top 150 gene lists of all 8 adult-IMID comparator traits (Supplementary Figs S19, S20), 6 were annotated to metabolic processes and 3 encoded histone proteins.

We further compared each paediatric IMID category with adult IMIDs. Polygenicity analyses revealed that the overlapping polygenic signal varies substantially by comparator trait (Supplementary Fig S21). Autoimmune IMID showed the most prominent correlation with SLE and positive correlations with RA, SSc, and AS, consistent with shared adaptive immune mechanisms. Autoinflammatory IMID showed stronger correlations with IBD-related traits and AS. Allergic and mixed-pattern IMIDs showed broader but less disease-specific sharing, including moderate correlations with AS and RA (Supplementary Fig S22).

We further compared the top 150 MAGMA-prioritised genes from each paediatric IMID category with those from adolescent- or adult-onset IMIDs (Supplementary Fig S23). Paediatric autoimmune IMIDs showed the strongest and highly significant

overlap with all 4 adult rheumatic diseases included in the study. Paediatric mixed-pattern IMIDs showed a similar but weaker pattern, with prominent overlap with AS and RA. In contrast, paediatric autoinflammatory IMIDs overlapped more strongly with IBD-related traits, whereas paediatric allergic IMIDs showed limited overlap across comparator traits. These results further support shared gene-level architecture between paediatric IMIDs, especially autoimmune and mixed-pattern categories, and adult rheumatic disease biology. Top-ranking MAGMA genes unique to paediatric IMIDs (Supplementary Figs S19 and S20) were significantly enriched for growth hormone-receptor signalling pathway by both Gene Ontology (GO) and Kyoto Encyclopedia of Genes and Genomes (KEGG) analyses (Supplementary Fig S24).

We used the Priority Index pipeline to prioritise genes with potential relevance as therapeutic targets. In total, 178 genes had a Priority Index score >3.0, including established rheumatic disease susceptibility genes such as *PTPN22* and *CD247* (Fig. 4A, Supplementary Table S21), with prominent enrichment of immune-related pathways, along with additional signals involving osteoclast differentiation, growth hormone synthesis, secretion and action, autophagy, and other cellular processes (Fig. 4B). Among these prioritised genes, 43 were approved or investigational drug targets for at least 1 IMID (Fig. 4C, Supplementary Table S21). Twelve of these genes were targeted by drugs that had reached clinical phase ≥3 across 20 IMIDs, including rheumatic diseases such as JIA, Sjögren syndrome, SLE, SSc, and lupus nephritis (Supplementary Table S22). Together, these findings highlight both established and less-characterised genes with potential relevance for drug repurposing or therapeutic target prioritisation in paediatric IMIDs, particularly paediatric rheumatic disorders, although disease- and age-specific validation will be required to assess direct clinical applicability.

DISCUSSION

To address the limited genomic data in paediatric-onset immune diseases, we conducted a meta-analysis across 4 IMID categories. This strategy enabled identification of loci distinct from those in adult cohorts, likely reflecting age-related differences in disease development [33,34]. The novel loci identified in this study include *DISP1, Hedgehog interacting protein-like 2* (*HHIPL2)* (Hedgehog signalling in the developing thymus), *Axin interactor dorsalization-associated protein* (*AIDA*) (Wnt-pathway modulation) [35], *MIA3* (central to cartilage, bone and dentin development), *IGHV1-58/IGLV7-46* (early B-cell repertoire) [36], *NETO1*, *DPP6*, and *TENM3/ODZ3* (neuroimmune and synaptic maturation) [37], and *GALNT9*, *UDP-glucuronosyltransferase 2A1* (*UGT2A1*), and *ABCC8* (age-specific glycosylation, glucuronidation and β-cell biology) [38]. These genes underscore contributions of developmental and growth-phase programmes to paediatric IMID risk. These processes are especially active or regulated in childhood but wane or are compensated in adults. By pooling data across diseases, we increased statistical power and uncovered shared risk loci within each immunological category, revealing genetic factors often missed in single-disease studies.

Interactions between the immune and neural systems, as well as the shared genetic basis of immune and neurodevelopmental disorders, have similarly been highlighted in previous studies [39]. In addition, the emerging field of immunometabolism emphasises how metabolic changes driven by glycolysis, the Krebs cycle, lipids, amino acids, and polyamines affect protein modification, localisation, and transport. These changes influence immune cell phenotypes and functions, particularly in macrophages and T cells, impacting immunity and inflammation [40]. Thus, with the increased statistical power driven by the large sample size and the strong genetic contribution of paediatric diseases, we uncovered additional players with pleiotropic function in immune disorders, as well as in neurodevelopmental disorders and metabolic processes.

The molecular drivers for different IMID categories frequently overlap. Our findings refine this view by showing that a shared HLA-anchored adaptive immune scaffold underlies all 4 paediatric IMID categories, while distinct peripheral modules—proteasomal and complement machinery in autoimmune disease, a NOD2/CARD9/IL-12-IFN-γ innate hub in autoinflammatory disease, an epithelial-type 2 axis in allergic disease, and hybrid regulatory connections in mixed-pattern IMID—may contribute to category-specific phenotypes. Several of the recurrently implicated pathways, including JAK–STAT, TNF, IL-23/Th17, and PD-1/CTLA-4 co-stimulation, are already actionable in adults [41–44], supporting the rationale for paediatric repurposing while underscoring the need for age-specific efficacy and safety evaluation [45–47]. The concurrent enrichment of osteoclast differentiation pathways further provides a plausible molecular link between chronic immune activation and the growth impairment and osteopenia that complicate paediatric JIA and IBD [48], which is also in line with our previous report that JIA and bone mineral density share genomic loci [49].

Comparative analyses of paediatric IMID genetics with adolescent- or adult-onset immune-mediated diseases revealed both shared and distinct genetic architectures. The top-ranked risk genes showed the strongest convergence with adult rheumatic diseases, which extended our previous observation of substantial genetic overlap between JIA and SLE, SSc, and RA [14] from a single paediatric entity to the IMID categories as a whole. Together with the association of paediatric IMID lead SNPs with rheumatic diseases in the independent FinnGen cohort, these results support a genetic continuum between paediatric immune dysregulation and adult rheumatologic disease, consistent with clinical evidence that a subset of paediatric IMID patients later develop rheumatic manifestations or diagnoses [50]. The enrichment of paediatric unique genes in hormone-receptor binding suggests that paediatric-specific IMID risk may partly reflect developmental and metabolic programmes active during childhood, while immune maturation and environmental exposures are dynamically shaping disease susceptibility.

Overall, our study delineates shared and paediatric-specific genetic components of IMIDs and highlights the potential value of genetically informed early risk stratification. Such approaches may ultimately help identify children at increased risk for persistent or evolving immune-mediated disease, including progression towards adult rheumatic disorders.

Competing interests

All authors declare they have no competing interests.

Acknowledgements

We thank all the participants in this study. We also acknowledge the High-Performance Computing Platform at the Children's Hospital of Philadelphia, the High-Performance Computing Platform at Tianjin Medical University for technical support.

Contributors

JL, YRL, and HH conceptualised and designed the project. FDM was responsible for database management. MEM performed genome-wide imputation and quality control filtering. JL, H-QQ, and JTG carried out data analyses. YF, JC, YX, and HC conducted functional annotation and downstream analyses. QX, AHS, LY, HV, WL, and WW contributed to data interpretation. HH supervised and coordinated the project. JL, H-QQ, and QX drafted the manuscript. All authors reviewed and approved the submitted version of the manuscript.

Funding

This study was supported by the Institutional Development Funds from the Children's Hospital of Philadelphia, the fund of the Children's Hospital of Philadelphia Endowed Chair in Genomic Research, National Natural Science Foundation of China (No. 82572080). Dr Wei Liu was funded by the Tianjin Key Medical Discipline (Specialty) Construction Project (TJYXZDXK-040A), Tianjin Outstanding Health Professional Selection and Training Program (TJSJMYXYC-D2-031).

Patient consent for publication

Not required.

Ethics approval

The study was approved by the Institutional Review Board at the Children's Hospital of Philadelphia and conducted according to the Declaration of Helsinki. The written informed consent was obtained from all the study participants or their legal guardian. Patients and/or the public were not involved in the design, conduct or reporting of this research.

Provenance and peer review

Not commissioned, externally peer reviewed.

Data availability statement

The full summary statistics of the ASSET analysis can be downloaded from https://github.com/CAG-CNV/Autoimmune_Autoinflammatory_GWAS_meta-analysis_summary_statistics.

Supplementary materials

Supplementary material associated with this article can be found in the online version at doi:10.1016/j.ard.2026.07.007.

REFERENCES

[1] Szekanecz Z, McInnes IB, Schett G, Szamosi S, Benko S, Szucs G. Autoinflammation and autoimmunity across rheumatic and musculoskeletal diseases. Nat Rev Rheumatol 2021 Oct;17(10):585–95.
[2] Kim YD. Systemic autoinflammatory disorders: autoinflammatory and autoimmune disorders. Clin Exp Pediatr. 2023 Oct;66(10):439–40.
[3] de Jesus AA, Canna SW, Liu Y, Goldbach-Mansky R. Molecular mechanisms in genetically defined autoinflammatory diseases: disorders of amplified danger signaling. Annu Rev Immunol. 2015;33:823–74.
[4] Pathak S, McDermott MF, Savic S. Autoinflammatory diseases: update on classification diagnosis and management. J Clin Pathol. 2017 Jan;70(1):1–8.
[5] Lopez Espinoza A, Christopher T, Tait Wojno ED. Epithelial-immune interactions govern type 2 immunity at barrier surfaces. Curr Opin Immunol 2024 Dec;91:102501.
[6] Betrains A, Staels F, Schrijvers R, Meyts I, Humblet-Baron S, De Langhe E, et al. Systemic autoinflammatory disease in adults. Autoimmun Rev. 2021 Apr;20(4):102774.
[7] Song Y, Li J, Wu Y. Evolving understanding of autoimmune mechanisms and new therapeutic strategies of autoimmune disorders. Signal Transduct Target Ther. 2024 Oct 4;9(1):263.
[8] Martini A, Lovell DJ, Albani S, Brunner HI, Hyrich KL, Thompson SD, et al. Juvenile idiopathic arthritis. Nat Rev Dis Primers 2022 Jan 27;8(1):5.
[9] Degboe Y, Vastert SJ, Prakken BJ, McInnes IB. How does age determine the development of human immune-mediated arthritis? Nat Rev Rheumatol. 2022 Sep;18(9):501–12.
[10] Wang Q, Zhu H, Sun X, Zhang C, Ma S, Jin Y, et al. Loss-of-function mutations in PLD4 lead to systemic lupus erythematosus. Nature. 2025 Nov;647(8089):498–505.
[11] Ishigaki K, Sakaue S, Terao C, Luo Y, Sonehara K, Yamaguchi K, et al. Multi-ancestry genome-wide association analyses identify novel genetic mechanisms in rheumatoid arthritis. Nat Genet. 2022 Nov;54(11):1640–51.
[12] Bolton C, Mahony CB, Clay E, Nisa PR, Lomholt S, Hackland A, et al. Synovial tissue atlas in juvenile idiopathic arthritis reveals pathogenic niches associated with disease severity. Sci Transl Med. 2025 Jul;17(805):eadt6050.
[13] Amador-Patarroyo MJ, Rodriguez-Rodriguez A, Montoya-Ortiz G. How does age at onset influence the outcome of autoimmune diseases? Autoimmune Dis. 2012;2012:251730.
[14] Fan J, Hao J, Fu Y, Liu X, Qu HQ, Glessner JT, et al. Genetic association of juvenile idiopathic arthritis with adult rheumatic disease. JAMA Netw Open. 2024 Dec;7(12):e2451341.
[15] Chang CC, Chow CC, Tellier LC, Vattikuti S, Purcell SM, Lee JJ. Second-generation PLINK: rising to the challenge of larger and richer datasets. Gigascience. 2015;4:7.
[16] Fuchsberger C, Abecasis GR, Hinds DA. minimac2: faster genotype imputation. Bioinformatics 2015 Mar;31(5):782–4.
[17] Taliun D, Harris DN, Kessler MD, Carlson J, Szpiech ZA, Torres R, et al. Sequencing of 53,831 diverse genomes from the NHLBI TOPMed Program. Nature. 2021 Feb;590(7845):290–9.
[18] Yang J, Lee SH, Goddard ME, Visscher PM. GCTA: a tool for genome-wide complex trait analysis. Am J Hum Genet. 2011 Jan;88(1):76–82.
[19] Bhattacharjee S, Rajaraman P, Jacobs KB, Wheeler WA, Melin BS, Hartge P, et al. A subset-based approach improves power and interpretation for the combined analysis of genetic association studies of heterogeneous traits. Am J Hum Genet. 2012 May;90(5):821–35.
[20] Frei O, Holland D, Smeland OB, Shadrin AA, Fan CC, Maeland S, et al. Bivariate causal mixture model quantifies polygenic overlap between complex traits beyond genetic correlation. Nat Commun. 2019 Jun;10(1):2417.
[21] Han B, Eskin E. Random-effects model aimed at discovering associations in meta-analysis of genome-wide association studies. Am J Hum Genet. 2011 May;88:586–98.
[22] Iotchkova V, Ritchie GRS, Geihs M, Morganella S, Min JL, Walter K, et al. GARFIELD classifies disease-relevant genomic features through integration of functional annotations with association signals. Nat Genet. 2019 Feb;51(2):343–53.
[23] Fang H, ULTRA-DD Consortium, De Wolf H, Knezevic B, Burnham KL, Osgood J, et al. A genetics-led approach defines the drug target landscape of 30 immune-related traits. Nat Genet. 2019 Jul;51(7):1082–91.
[24] Watanabe K, Taskesen E, van Bochoven A, Posthuma D. Functional mapping and annotation of genetic associations with FUMA. Nat Commun. 2017 Nov;8(1):1826.
[25] de Leeuw CA, Mooij JM, Heskes T, Posthuma D. MAGMA: generalized gene-set analysis of GWAS data. PLOS Comput Biol 2015 Apr;11(4):e1004219.
[26] Pers TH, Karjalainen JM, Chan Y, Westra HJ, Wood AR, Yang J, et al. Biological interpretation of genome-wide association studies using predicted gene functions. Nat Commun. 2015 Jan;6:5890.
[27] Gusev A, Ko A, Shi H, Bhatia G, Chung W, Penninx BW, et al. Integrative approaches for large-scale transcriptome-wide association studies. Nat Genet. 2016 Mar;48(3):245–52.
[28] Zhu Z, Zhang F, Hu H, Bakshi A, Robinson MR, Powell JE, et al. Integration of summary data from GWAS and eQTL studies predicts complex trait gene targets. Nat Genet. 2016 May;48(5):481–7.
[29] Weeks EM, Ulirsch JC, Cheng NY, Trippe BL, Fine RS, Miao J, et al. Leveraging polygenic enrichments of gene features to predict genes underlying complex traits and diseases. Nat Genet. 2023 Aug;55(8):1267–76.
[30] Kurki MI, Karjalainen J, Palta P, Sipila TP, Kristiansson K, Donner KM, et al. FinnGen provides genetic insights from a well-phenotyped isolated population. Nature. 2023 Jan;613(7944):508–18.
[31] Lee YQ, Storry JR, Olsson ML. The Xg blood group system: no longer forgotten. Immunohematology. 2020 Jan;36(1):4–6.
[32] Li YR, Li J, Zhao SD, Bradfield JP, Mentch FD, Maggadottir SM, et al. Meta-analysis of shared genetic architecture across ten pediatric autoimmune diseases. Nat Med. 2015 Sep;21(9):1018–27.

[33] Hinks A, Bowes J, Cobb J, Ainsworth HC, Marion MC, Comeau ME, et al. Fine-mapping the MHC locus in juvenile idiopathic arthritis (JIA) reveals genetic heterogeneity corresponding to distinct adult inflammatory arthritic diseases. Ann Rheum Dis. 2017 Apr;76(4):765–72.
[34] Okada Y, Wu D, Trynka G, Raj T, Terao C, Ikari K, et al. Genetics of rheumatoid arthritis contributes to biology and drug discovery. Nature. 2014 Feb;506(7488):376–81.
[35] Hernandez JB, Newton RH, Walsh CM. Life and death in the thymus—cell death signaling during T cell development. Curr Opin Cell Biol. 2010;22(6):865–71.
[36] Nielsen SCA, Roskin KM, Jackson KJL, Joshi SA, Nejad P, Lee JY, et al. Shaping of infant B cell receptor repertoires by environmental factors and infectious disease. Sci Transl Med. 2019 Feb;11(481):eaat2004.
[37] Dantzer R. Neuroimmune interactions: from the brain to the immune system and vice versa. Physiol Rev. 2018 Jan;98(1):477–504.
[38] Lyons JJ, Milner JD, Rosenzweig SD. Glycans instructing immunity: the emerging role of altered glycosylation in clinical immunology. Front Pediatr. 2015;3:54.
[39] Xiu Z, Sun L, Liu K, Cao H, Qu HQ, Glessner JT, et al. Shared molecular mechanisms and transdiagnostic potential of neurodevelopmental disorders and immune disorders. Brain Behav Immun. 2024 Jul;119:767–80.
[40] Diskin C, Ryan TAJ, O'Neill LAJ. Modification of proteins by metabolites in immunity. Immunity. 2021 Jan;54(1):19–31.
[41] Benucci M, Bernardini P, Coccia C, De Luca R, Levani J, Economou A, et al. JAK inhibitors and autoimmune rheumatic diseases. Autoimmun Rev. 2023 Apr;22(4):103276.
[42] Croft M, Salek-Ardakani S, Ware CF. Targeting the TNF and TNFR superfamilies in autoimmune disease and cancer. Nat Rev Drug Discov. 2024 Dec;23(12):939–61.
[43] Veerasubramanian PK, Wynn TA, Quan J, Karlsson FJ. Targeting TNF/TNFR superfamilies in immune-mediated inflammatory diseases. J Exp Med. 2024 Nov;221(11):e20240806.
[44] Bonelli M, Kerschbaumer A, Kastrati K, Ghoreschi K, Gadina M, Heinz LX, et al. Selectivity, efficacy and safety of JAKinibs: new evidence for a still evolving story. Ann Rheum Dis. 2024 Jan;83(2):139–60.
[45] Kingsmore KM, Grammer AC, Lipsky PE. Drug repurposing to improve treatment of rheumatic autoimmune inflammatory diseases. Nat Rev Rheumatol 2020 Jan;16(1):32–52.
[46] Reiff DD, Stoll ML, Cron RQ. Precision medicine in juvenile idiopathic arthritis-has the time arrived? Lancet Rheumatol. 2021 Nov;3(11):e808–17.
[47] Wedderburn LR, Ramanan AV, Croft AP, Hyrich KL, Dick AD, Consortium C. Towards molecular-pathology informed clinical trials in childhood arthritis to achieve precision medicine in juvenile idiopathic arthritis. Ann Rheum Dis. 2023 Apr;82(4):449–56.
[48] van Bodegraven AA, Bravenboer N. Perspective on skeletal health in inflammatory bowel disease. Osteoporos Int. 2020 Apr;31(4):637–46.
[49] Fan J, Li X, Yang J, Zhang S, Qu HQ, Ji D, et al. Revealing novel genomic insights and therapeutic targets for juvenile idiopathic arthritis through omics. Rheumatology (Oxford). 2024 Sep;63(SI2):SI249–59.
[50] Hersh A, von Scheven E, Yelin E. Adult outcomes of childhood-onset rheumatic diseases. Nat Rev Rheumatol 2011 May;7(5):290–5.

Ann Rheum Dis 85 (2026) 1879–1889

Contents lists available at ScienceDirect

Annals of the Rheumatic Diseases

journal homepage: https://www.sciencedirect.com/journal/annals-of-the-rheumatic-diseases

Inflammatory arthritis

Oral glucocorticoid treatment for checkpoint inhibitor-associated inflammatory arthritis does not affect cancer progression-free survival: a RADIOS Registry study

Deanna P Jannat-Khah[1,2,*], Pankti Reid[3], Laura C Cappelli[4], Maria E Suarez-Almazor[5], Noha Abdel-Wahab[6,7,8], Jeffrey A Sparks[9], Tawnie J Braaten[10], Alexa Meara[11], Minerva Nong[1,12], Kyle Ge[1], Tamiko R Katsumoto[13], Cassandra Calabrese[14], Alice Tison[1,15,16], Karmela Chan[1,2], Nilasha Ghosh[1,2], Ami A Shah[4], Clifton Bingham[4], Anne R Bass[1,2]

[1] *Division of Rheumatology, Department of Medicine, Hospital for Special Surgery, New York, NY, USA*
[2] *Division of Rheumatology, Department of Medicine, Weill Cornell Medicine, New York, NY, USA*
[3] *Department of Medicine, Section of Rheumatology, Committee on Clinical Pharmacology and Pharmacogenomics, University of Chicago, Chicago, IL, USA*
[4] *Division of Rheumatology, Department of Medicine, Johns Hopkins University School of Medicine, Baltimore, MD, USA*
[5] *MD Anderson Cancer Center, Section of Rheumatology & Clinical Immunology, University of Texas, Houston, TX, USA*
[6] *Department of Rheumatology & Rehabilitation, Assiut University Faculty of Medicine, Assiut, Egypt*
[7] *Department of Cancer Sciences, Global Center for Immunotherapy and Precision Immuno-Oncology, Cleveland Clinic, OH, USA*
[8] *Cancer Institute, Cleveland Clinic, Abu Dhabi, UAE*
[9] *Division of Rheumatology, Inflammation, and Immunity, Brigham and Women's Hospital and Harvard Medical School, Boston, MA, USA*
[10] *University of Utah, Salt Lake City, UT, USA*
[11] *Division of Oncology and Hematology, Department of Internal Medicine, The Ohio State University Comprehensive Cancer Center, Columbus, OH, USA*
[12] *Columbia College of Physicians & Surgeons, Columbia University, New York, NY, USA*
[13] *Department of Medicine-Immunology & Rheumatology, Stanford University, Stanford, CA, USA*
[14] *Department of Rheumatologic and Immunologic Disease, Cleveland Clinic Foundation, Cleveland Heights, OH, USA*
[15] *Department of Rheumatology, CHRU Brest, Brest, France*
[16] *LBAI UMR1227, Université de Bretagne Occidentale, Inserm, Brest, France*

ARTICLE INFO

Article history:
Received 11 November 2025
Received in revised form 22 January 2026
Accepted 17 February 2026

ABSTRACT

Objectives: Glucocorticoids are the first-line treatment for immune checkpoint inhibitor-associated inflammatory arthritis (ICI-IA). However, glucocorticoids may negatively impact cancer progression-free survival (PFS). We investigated the association between glucocorticoids and PFS among patients with cancer with ICI-IA.

Methods: Data from the prospective multicentre rheumatic adverse events due to Immunotherapy Observational Study registry were used. Kaplan-Meier plots and multivariable Cox regression

*Correspondence to Dr Deanna P. Jannat-Khah.
E-mail address: jannatkhahd@hss.edu (D.P. Jannat-Khah).
Handling editor Josef S. Smolen.

https://doi.org/10.1016/j.ard.2026.02.017

0003-4967/© 2026 European Alliance of Associations for Rheumatology (EULAR). Published by Elsevier B.V. All rights are reserved, including those for text and data mining, AI training, and similar technologies.

models (time-varying and landmark) assessed glucocorticoid dose and its association with PFS. Participants who progressed before glucocorticoid initiation were excluded from the landmark analysis.
Results: Participants with ICI-IA (N = 269) had a mean age of 64.85 years (SD: 12.87), 48.3% were female, 87% were White, 32% had melanoma, and most were stage IV (56.4%). In the first month of treatment, the median glucocorticoid dose (prednisone equivalent) was 13 mg daily and 7.8% of participants received an immunomodulatory disease-modifying antirheumatic drug. Cancer progression occurred in 67 participants (24.9%). In a time-varying Cox model, glucocorticoids were not associated with PFS (adjusted hazard ratio [aHR]: 2.64 [95% CI: 0.36-19.61]). Glucocorticoid doses above the median compared with below the median in the first month of ICI-IA treatment were not associated with worse PFS in adjusted Cox models (aHR: 1.15 [95% CI: 0.59-2.25]).
Conclusions: In this prospective ICI-IA cohort, low doses of glucocorticoids (median dose 13 mg [IQR: 7.5, 25] in the first month of treatment) did not adversely affect PFS.

WHAT IS ALREADY KNOWN ON THIS TOPIC

- Oncology and rheumatology guidelines provide mixed advice on the treatment of immune checkpoint inhibitor-associated inflammatory arthritis (ICI-IA) including the recommended dosages of glucocorticoids for treatment.
- Glucocorticoids are first-line treatment for ICI-IA, but standardisation in dosing, tapering, and duration is lacking.
- Several studies have reported mixed results regarding the effect of oral glucocorticoids on cancer progression-free survival (PFS) among immune checkpoint inhibitor-treated participants.

WHAT THIS STUDY ADDS

- Results from the largest prospective cohort of ICI-IA participants (n = 269) worldwide demonstrate no association between glucocorticoid treatment and PFS.
- Median glucocorticoid dose (prednisone equivalent) in the first month of treatment was 13 mg (IQR: 7.5, 25) daily among patients with ICI-IA treated by a rheumatologist. This dose is lower than that used for other immune-related adverse events, such as colitis.
- In a sensitivity analysis of melanoma patients with ICI-IA only, there was no association between glucocorticoid treatment and PFS.

HOW THIS STUDY MIGHT AFFECT RESEARCH, PRACTICE OR POLICY

- Rheumatologists can feel comfortable prescribing low-dose glucocorticoids to cancer patients with ICI-IA.

INTRODUCTION

Immune checkpoint inhibitors (ICIs) are monoclonal antibodies that work by blocking immune checkpoints, such as cytotoxic T lymphocyte-associated protein 4 or programmed cell death protein-1 (PD-1)/programmed cell death protein ligand-1 (PDL-1), allowing the immune system to target cancer cells [1]. However, their use can cause side effects termed immune-related adverse events (irAEs). IrAEs can affect any organ system and range in severity from mild to life-threatening [2]. One study found that among 12,030 patients who received ICIs, 40% experienced an irAE within 90 days of an ICI dose [3]. Severe irAEs can lead to significant morbidity, hospitalisation, and mortality [4,5]. However, irAEs may be associated with better cancer survival, serving as a proxy for immune activation [6–8]. Several studies have found ICI-associated inflammatory arthritis (ICI-IA) to be associated with better tumour response and a longer progression-free survival (PFS) [8–10].

Glucocorticoids are a cornerstone of treatment for many cases of ICI-IA, but standardisation in dosing, tapering, and duration is lacking. Oncology and rheumatologic guidelines provide mixed advice on the treatment of ICI-IA including the recommended dosages of glucocorticoids for treatment. For example, the National Comprehensive Cancer Network recommends starting at 10 to 20 mg prednisone per day for mild and 20 to 30 mg prednisone per day for higher severity ICI-IA [11] and the American Society of Clinical Oncology recommends glucocorticoids, for grade 3 dosed up to 1 mg/kg for ICI-IA treatment (0.5-1 mg/kg depending on the severity) [12]. Alternatively, the European Alliance of Associations for Rheumatology recommended against high-dose steroids in the absence of life-threatening irAEs such as ICI-IA and recommended tapering down to prednisone 10 mg per day when possible [13].

Mixed results have been reported regarding the effect of oral glucocorticoids on cancer PFS among ICI-treated participants. Some studies have found no association between glucocorticoid use and PFS or overall survival (OS) [14]. In contrast, some studies have found that higher glucocorticoid doses were associated with worse PFS in adjusted models [15] and that longer durations of high-dose glucocorticoids were associated with worse outcomes [16]. Others have reported that the timing of glucocorticoid administration, rather than duration of glucocorticoid use, might be associated with survival [17–19]. Several studies have found worse survival outcomes with glucocorticoid treatment given in the first 30 to 90 days [15,20].

Given these mixed results, we investigated oral glucocorticoid use and its association with PFS among participants with ICI-IA in a large multicentred irAE cohort in the United States.

METHODS

Rheumatology Adverse Events Due to Immunotherapy Observational Study Registry

The Rheumatology Adverse Events Due to Immunotherapy Observational Study (RADIOS) registry is a prospective, multicentre registry of 12 academic centres within the United States. The registry includes participants diagnosed with cancer and treated with an ICI who develop a rheumatologic irAE as well as participants with antecedent rheumatic diseases who are initiating ICI for cancer. Participating centres include Johns Hopkins University (JHU), The Ohio State University, Cleveland Clinic, Brigham and Women's Hospital, MD Anderson, University of Chicago, Stanford University, University of Utah, and Hospital

for Special Surgery (HSS), with expansion to the University of Washington, Yale, and Massachusetts General Hospital in 2025. Clinical data are entered into a dedicated research electronic data capture database housed at JHU. Participants were enrolled on RADIOS at JHU starting in 2018, while the other sites joined the registry in 2023. Some participants prospectively enrolled into a pre-existing irAE registry at HSS were rolled over into RADIOS in January 2023. Patients are assessed during routine clinical follow-up. Data are collected prospectively, and some data were collected retrospectively for record completeness. Institutional review boards at each institution reviewed and approved participation in RADIOS including HSS (HSS IRB 2020-2572), and all participants provided informed consent. At the time of the data pull for the current analysis (April 2025), 9 sites were actively enrolling participants.

ICI-associated inflammatory arthritis

ICI-IA was defined in this study as inflammatory arthritis, inflammatory arthralgia and/or polymyalgia rheumatic (PMR) that developed after ICI initiation, as determined by the treating rheumatologist.

Study inclusion criteria

Participants with ICI-IA, as defined above, were enrolled in RADIOS before April 2025 (date of the data pull for this analysis). In addition, details of the patient's cumulative glucocorticoid doses had to be entered into a dedicated registry form.

Exclusion

Participants with a history of inflammatory arthritis or PMR before ICI initiation.

Primary exposure of interest

Oral glucocorticoid dose was the primary exposure of interest. The index date (baseline) was defined as the date of initiation of glucocorticoids for ICI-IA, as noted on the glucocorticoid form. Glucocorticoid dosages were converted to prednisone equivalents. Cumulative glucocorticoid exposure was documented at several timepoints (0-2 weeks postglucocorticoid initiation, 3-4 weeks, month 2, and months 3-5). Those cumulative doses were divided by the number of days to calculate individual average daily doses. Group medians (and IQRs) for these average daily doses were calculated and reported. The average daily glucocorticoid dose over the first month was calculated by combining the cumulative doses for weeks 1 to 2 plus 3 to 4 and then dividing by 30 days for the 30-day landmark Cox model and, similarly, combining weeks 1 to 2, 3 to 4, and month 2 for the 60-day landmark models. The 30- and 60-day landmarks were chosen based on the results of the box plot, which showed when the glucocorticoid doses were highest. For the multivariable Cox regression models, glucocorticoid use was dichotomised as above and below the median, and, separately, into quartiles.

Primary outcome of interest

PFS, defined as radiographic cancer progression or death, was the primary outcome of interest. Cancer progression was based on imaging reports and the oncologist's impression of the reports. In the survival analysis, we excluded participants whose cancer progressed before glucocorticoid initiation.

Covariates

Demographics, cancer characteristics/treatment, and disease-modifying antirheumatic drugs (DMARDs) were collected. Demographic variables included age, sex, race, ethnicity, and study site. Cancer covariates included baseline ICI-IA, as determined by common terminology criteria for adverse events grade [21], cancer type, ICI type, concomitant chemotherapy, and if ICI was discontinued. ICI duration was defined as the time from ICI initiation to ICI discontinuation or ICI switch or progression/death. DMARD treatment was defined as use around the time of glucocorticoid initiation (as recorded on the glucocorticoid form) and ever use of hydroxychloroquine, methotrexate, sulfasalazine, leflunomide, rituximab, tumour necrosis factor (TNF) inhibitor, and interleukin 6 (IL-6) receptor inhibitor. Immunosuppressive DMARDs included all of these except for hydroxychloroquine.

Statistical analyses

Descriptive statistics were reported. A box plot was created to visualise the cumulative glucocorticoid dose. A time-varying survival model was performed to assess glucocorticoid use (yes/no) among the entire population. Glucocorticoid use was allowed to vary, and survival was measured from the time of ICI initiation. In this model, glucocorticoid use was defined as yes/no during 5 lagged time segments: 90 days before ICI initiation to ICI initiation, 0 to 90 days after ICI initiation, 91 to 180 days, 181 to 270 days, 271 to 365 days, and was allowed to vary over time. Glucocorticoid use in the previous 90 days was included in the model as a dichotomous variable (yes/no).

Among glucocorticoid users, 30-day landmark Kaplan-Meier plots assessed glucocorticoid exposure and its association with PFS, measured from glucocorticoid initiation to radiographic cancer progression or death. In addition, 60-day landmark plots were also performed.

Immortal time bias was addressed using multivariable time-varying and separately, landmark Cox regression models [22,23]. Models were adjusted for age, irAE grade at baseline, cancer type (melanoma, nonsmall cell lung cancer [NSCLC], renal cell carcinoma [RCC]), cancer stage, ICI combination therapy, time from ICI initiation to glucocorticoid initiation, and immunosuppressive DMARD use in the first month of glucocorticoid treatment. Proportional hazard assumptions were tested using Schoenfeld residuals. Follow-up started at ICI initiation for the time-varying models and separately at glucocorticoid initiation for the landmark models, and censoring variables were radiographic cancer progression, death, or last follow-up (whichever came first) for both types of models.

Two sensitivity analyses were performed. The first sensitivity analysis excluded participants who began glucocorticoids before January 3, 2023. The rationale for this analysis was to minimise survival bias among participants who had been enrolled in a prospective registry before the formation of RADIOS and then rolled over into RADIOS, since this influenced survival time. A second sensitivity analysis was performed in the subset of participants who were diagnosed with melanoma, which was the most frequent cancer among RADIOS participants.

A two-sided P value $<.05$ was considered statistically significant. All analyses were performed using Stata version 18.0 (Stata, StataCorp LLC).

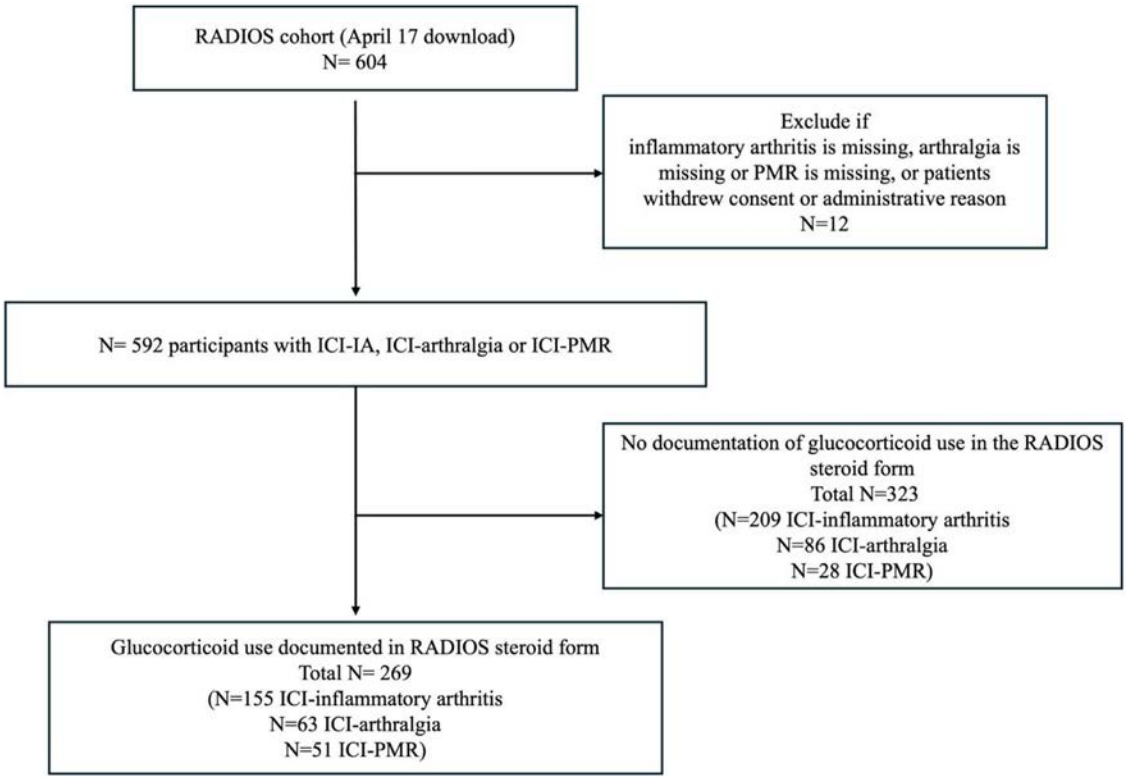

Figure 1. Analytic cohort with N = 592 participants of which N = 269 had detailed glucocorticoid documentation in a dedicated RADIOS registry form. ICI, immune checkpoint inhibitor; ICI-IA, immune checkpoint inhibitor-associated inflammatory arthritis; ICI-PMR, immune checkpoint inhibitor-associated polymyalgia rheumatic; PMR, polymyalgia rheumatic; RADIOS, Rheumatology Adverse Events Due to Immunotherapy Observational Study.

Patient and public involvement statement

Patients and/or the public were not involved in the design, conduct, reporting, or dissemination of this research.

RESULTS

Study sample and baseline characteristics

As of April 2025, 592 participants with a diagnosis of ICI-IA, ICI-PMR, or ICI-arthralgia were enrolled in RADIOS, of whom n = 269 (45.4%) patients had detailed glucocorticoid treatment documentation in the dedicated glucocorticoid form and were included in the study (Fig 1). A comparison of included and excluded participants is shown in Supplementary Table S1. Statistically significant differences between included and excluded participants included age, prevalence of NSCLC, RCC, breast cancer, and per cent with ICI pause or discontinuation. There were no other statistically significant differences between included and excluded patients.

Among the n = 269 included patients with ICI-IA, the mean (SD) age was 64.85 (12.87), 48.3% were female, and a majority identified as White race (87.0%) (Table 1). A majority were diagnosed with ICI-inflammatory arthritis (N = 155 [57.6%]), whereas N = 63 (23.4%) had ICI-arthralgia, and N = 51 (19%) had ICI-PMR. Thirty-two percent had melanoma, 11.2% had NSCLC, and 17.5% had RCC. A majority had stage IV cancer (56.4%) followed by stage III (24.5%). Time from ICI initiation to ICI-IA diagnosis was a median of 4.1 months (0.93, 9.1). Anti-PD-1/PDL-1 monotherapy was the most common ICI treatment (58.7%) followed by anticytotoxic T lymphocyte-associated protein-4/PD-1 combination treatment (29.7%). Use of methotrexate ever was 26.4%, TNF inhibitor use ever was 12.6%, and IL-6 inhibitor use ever was 20.8%. DMARD use around the time of glucocorticoid treatment (defined as treatment occurring 90 days before to 30 days after glucocorticoid initiation) was low (N = 21, 7.8%), specifically, 13 (4.8%) participants were treated with methotrexate, 2 (0.7%) TNF inhibitors, and 6 (2.2%) IL-6 inhibitors (Table 1). Prescription nonsteroidal anti-inflammatory drugs (NSAIDs) were used by N = 21 (7.8%); over the counter NSAIDs were used by 23 people (8.6%), and 4 people (1.5%) used topical NSAIDs.

The median (IQR) of the mean daily glucocorticoid dose over weeks 0 to 2 of glucocorticoid treatment was 15 mg daily (IQR 10, 28.57); for weeks 3 to 4, 12.5 mg daily (IQR 7.5, 25); for month 2, 9.67 mg daily (IQR 4.67, 18); and for months 3 to 5, 4.5 mg daily (IQR 1.25, 7.96) (Fig 2). Supplementary Table S2 compares characteristics of the cohort by the 1-month median dose.

PFS by glucocorticoid use (yes/no)

A multivariable time-varying Cox proportional hazard model was performed to assess if glucocorticoid use vs nonuse was associated with PFS. Time was measured from the time of ICI initiation. Glucocorticoid use was not statistically significantly associated with PFS (adjusted hazard ratio [aHR]: 2.64 [95% CI: 0.36-19.61]) (Supplementary Table S3). A diagnosis of melanoma was associated with better PFS than other cancers (aHR: 0.50 [95% CI: 0.25-0.97]). None of the other covariates was associated with PFS.

PFS by median glucocorticoid dose

Characteristics of patients taking an average daily glucocorticoid dose in the first month of treatment above vs below the

Table 1
Demographics and clinical characteristics among glucocorticoid users

Factor	Glucocorticoid use N (%)
N	269 (45.44)
Age, mean (SD)	64.85 (12.87)
Female	130 (48.3)
Missing	0 (0.0)
Race	
Asian	5 (1.9)
Black or African American	13 (4.8)
Native Hawaiian or Pacific Islander	1 (0.4)
Other race	7 (2.6)
White	234 (87.0)
Prefer not to answer	12 (4.5)
Ethnicity	
Prefer not to answer	14 (5.2)
Hispanic	13 (4.8)
Missing	1 (0.4)
ICI-inflammatory arthritis	155 (57.6)
ICI-PMR	51 (19.0)
ICI-arthralgia	63 (23.4)
Baseline irAE grade	
1	83 (30.9)
2	96 (35.7)
3+	31 (11.5)
Missing	59 (21.9)
Cancer type	
Melanoma	86 (32.0)
Nonsmall cell lung cancer	30 (11.2)
Renal cell carcinoma	47 (17.5)
Bladder cancer	10 (3.7)
Breast cancer	18 (6.7)
Other cancers	34 (12.6)
Cancer stage	
Stage 1	6 (2.2)
Stage 2	15 (5.6)
Stage 3	68 (25.3)
Stage 4	151 (56.1)
Missing	29 (10.8)
Time from ICI initiation to arthritis onset in months, median (IQR)	4.1 (0.93, 9.1)
Time from arthritis onset (diagnosis date) to glucocorticoid initiation (from the glucocorticoid form) in months, median (IQR)	5.5 (1.96, 10.93)
Time from ICI initiation to glucocorticoid initiation (from the glucocorticoid form) in months, median (IQR)	6.9 (2.8, 14.43)
Cancer Treatment	
ICI + chemotherapy	91 (33.8)
ICI regimen preceding ICI-IA onset	
PD-1/PDL-1 monotherapy	158 (58.7)
CTLA4 monotherapy	3 (1.1)
LAG3 monotherapy	1 (0.4)
CTLA4/ LAG3 combination therapy	3 (1.1)
CTLA4/PD-1 combination therapy	80 (29.7)
Other	24 (8.9)
Any DMARD use (methotrexate, TNF inhibitor or IL-6 inhibitor) within 30 d of glucocorticoid initiation[a]	21 (7.8)
Methotrexate within 30 d of glucocorticoid initiation[a]	13 (4.8)
Methotrexate within 6 mo of glucocorticoid initiation	36 (13.4)
TNFi within 30 d of glucocorticoid initiation[a]	2 (0.7)
TNFi within 6 mo of glucocorticoid initiation	13 (4.8)
IL-6i within 30 d of glucocorticoid initiation[a]	6 (2.2)
IL-6i within 6 mo of glucocorticoid initiation	23 (8.6)
Time from ICI-IA onset to DMARD initiation in months, median (IQR)	11.02 (5.9, 18.65)
ICI discontinuation due to irAE at follow-up	
Yes	56 (20.8)
Missing	64 (23.8)
Nonsteroidal anti-inflammatory drugs	
Prescription	21 (7.8)
Over the counter	23 (8.6)
Topical	4 (1.5)
ICI held for rheumatic irAE at any point since ICI start	
Yes	122 (45.4)
Missing	73 (27.1)
ICI duration, in months, median (IQR)	8.5 (3.5, 17.3)
ICI duration from ICI closest to ICI-IA onset in months, median (IQR)	7.27 (2.8, 13.4)
Study site	
Johns Hopkins University	15 (5.6)
Utah	21 (7.8)
Brigham Women's Hospital	37 (13.8)
Cleveland Clinic	14 (5.2)
Hospital for Special Surgery	81 (30.1)
Stanford	4 (1.5)
University of Chicago	41 (15.2)
MD Anderson	54 (20.1)
Ohio	2 (0.7)
Cancer progression	67 (24.9)
Death	26 (9.7)
Time from ICI initiation to cancer progression, in months median (IQR)	17.1 (8.62, 29.53)
Time from glucocorticoid initiation to cancer progression/or last follow-up in months, median (IQR)	7.3 (2.78, 15.1)
Glucocorticoid treatment duration (d), median (IQR)	183 (60,183)

CTLA-4, cytotoxic T lymphocyte-associated protein-4; DMARD, disease-modifying antirheumatic drug; ICI, immune checkpoint inhibitor; ICI-IA, immune checkpoint inhibitor-associated inflammatory arthritis; IL-6, interleukin-6; IL-6i, interleukin-6 inhibitor; irAE, immune-related adverse event; LAG-3, lymphocyte activation gene-3; PDL-1, programmed cell death protein ligand-1; PD-1, programmed cell death protein-1; PMR, polymyalgia rheumatica; TNF, tumour necrosis factor; TNFi, tumour necrosis factor inhibitor.
[a] Defined as treatment that occurred within −90 days to +30 days of glucocorticoid initiation.

median (13.08 mg daily) are shown in Supplementary Table S2. The 30-day landmark Kaplan-Meier curve for PFS comparing those with a dose above vs below the median is displayed in Figure 3 (log rank *P* value .73). A 30-day landmark Kaplan-Meier curve that excluded n = 84 participants who initiated glucocorticoids before 3 January 2023 (sensitivity analysis) showed similar results (log rank *P* value = .46, Supplementary Fig S1). A multivariable Cox regression model demonstrated no significant association between glucocorticoid doses above vs below the median in the first month, with PFS aHR 1.15 (95% CI: 0.59-2.25) (Table 2). In addition, other covariates, including age, cancer type, cancer stage, or concomitant chemotherapy, were also not associated with PFS. Melanoma was associated with better PFS compared with other cancer types (aHR: 0.28 [95% CI: 0.11-0.74]). Furthermore, a longer time from ICI initiation to glucocorticoid treatment was associated with better PFS (aHR: 0.91 [95% CI: 0.87-0.96]) (Table 2). A 60-day landmark model gave similar results (Supplementary Table S4).

A separate set of models was performed that adjusted for DMARD use in the first month of glucocorticoid treatment, and glucocorticoid dose was still not significantly associated with PFS (Supplementary Tables S5 and S6). Due to the low number of DMARD users at the time of corticosteroid initiation (2 [0.7%] on TNF inhibitors, and 6 [2.2%] on IL-6 inhibitors), the point estimates were inflated, and the CIs were wide for the TNF and IL-6 inhibitor variables; thus, we decided to focus on the models that did not control for DMARDs.

PFS by glucocorticoid dose quartile

Quartiles of the average daily glucocorticoid dose in the first month were used to construct a 30-day landmark Kaplan-Meier

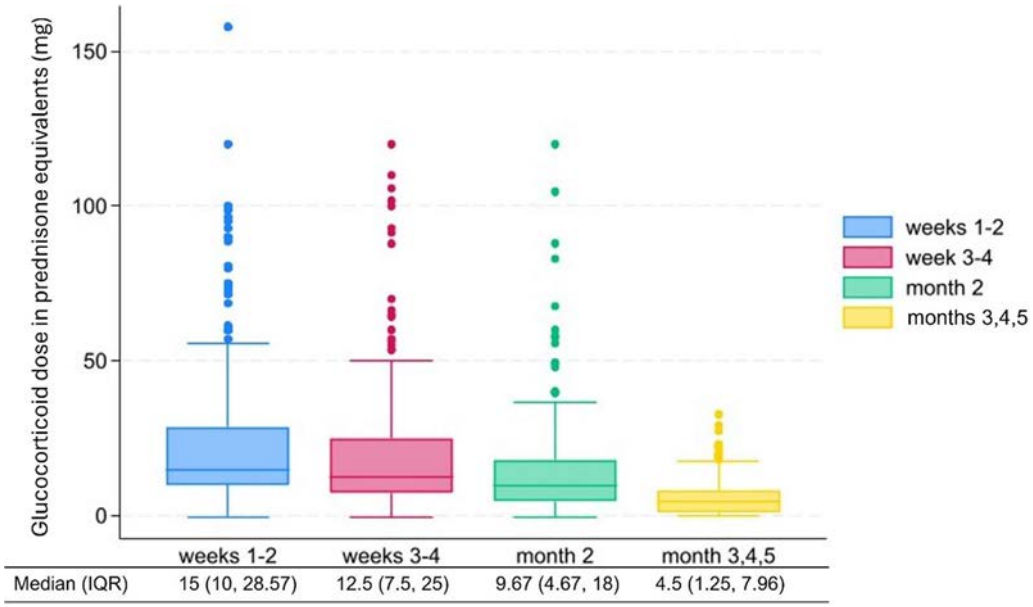

Figure 2. Box plot of the distribution of mean daily glucocorticoid doses (in prednisone equivalents, milligram) for various time periods.

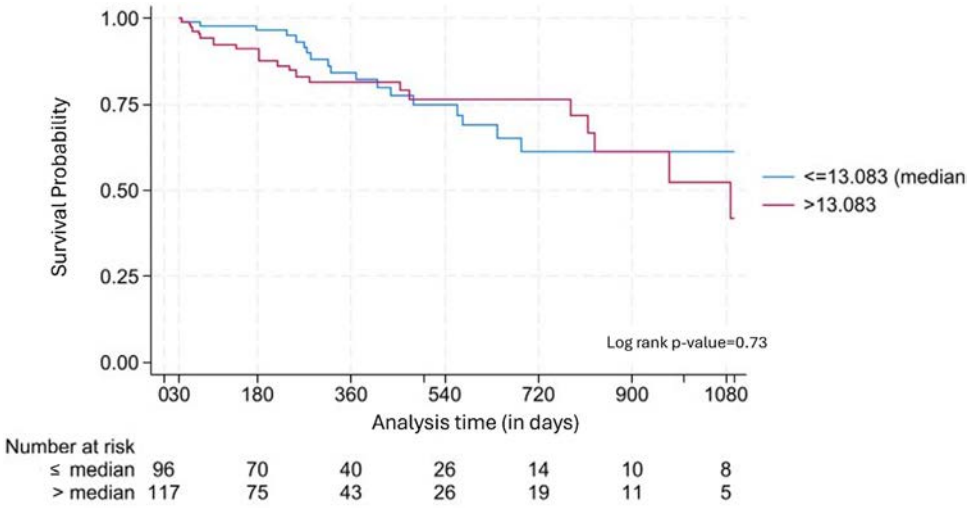

Figure 3. Thirty-day landmark Kaplan-Meier curve for cancer progression-free survival by median dose of glucocorticoids in the first month. People who progressed before glucocorticoid initiation were excluded from the Kaplan-Meier curve.

curve for PFS (log rank *P* value = .45) (Fig 4). Similar results were obtained from the 30-day adjusted landmark Cox proportional hazards models for quartiles (Table 3). None of the quartiles was associated with PFS. Compared with the lowest quartile for glucocorticoid dose, quartile 2 had an aHR of 0.97 (95% CI: 0.37-2.53), quartile 3 an aHR of 1.59 (95% CI: 0.60-4.21), and quartile 4 had an aHR of 0.92 (95% CI: 0.35-2.44). A 60-day landmark model by quartiles of glucocorticoid dose gave similar results (Supplementary Table S7).

Sensitivity analysis among participants with melanoma

A sensitivity analysis was performed among participants with melanoma (N = 88). A landmark Kaplan-Meier curve (log rank *P* value = .62) for this subcohort is displayed in Supplementary Figure S2. Two separate adjusted landmark models were performed; 1 using the median 1-month glucocorticoid dose (Supplementary Table S8) and the other using the quartiles of glucocorticoid dose in the first month (Supplementary Table S9). Given the small sample size, the models were only adjusted for glucocorticoid dose, age, cancer stage, and concomitant chemotherapy. There was no significant relationship between median steroid dose and PFS (aHR: 1.28 [95% CI: 0.19-8.54]), or quartiles of glucocorticoid dose in the first month and PFS (quartile 2 aHR: 0.42 [95% CI: 0.02-7.63], quartile 3 aHR: 0.89 [95% CI: 0.079-11.93], and quartile 4 aHR: 0.64 [95% CI: 0.05-8.06]).

DISCUSSION

This study takes advantage of the largest prospective cohort of ICI-IA participants worldwide. The dataset is unique in having detailed documentation of glucocorticoid dosing, which enabled us to evaluate the relationship between glucocorticoid dose and PFS. Although other studies have suggested that higher doses of glucocorticoids are associated with worse survival in ICI-treated participants with irAEs [15,16], we found that the use of glucocorticoids above the median average daily dose of the entire cohort was not associated with worse PFS compared with doses below the median, even after adjusting for demographic and

Table 2
Multivariable hazard ratios for cancer progression-free survival in a 32 landmark analysis for median glucocorticoid dose over the first month and other baseline factors

Variable	Landmark 30 d Hazard ratio (95% CI)
≤1 mo median glucocorticoid dose	referent
>1 mo median[a] glucocorticoid dose	1.15 (0.59, 2.25)
Age (per y)	1.00 (0.98, 1.02)
Other cancers except melanoma	referent
Melanoma	**0.28 (0.11, 0.74)**
Other cancers except nonsmall cell lung cancer	referent
Nonsmall cell lung cancer	0.99 (0.35, 2.76)
Other cancers except renal cell carcinoma	referent
Renal cell carcinoma	1.21 (0.49, 2.94)
Cancer stage ≤2	referent
Cancer stage 3 +	4.54 (0.61, 33.88)
ICI monotherapy	referent
ICI + chemotherapy	1.11 (0.50, 2.47)
Time from ICI initiation to glucocorticoid start (mo)	**0.91 (0.87, 0.96)**

ICI, immune checkpoint inhibitor.
Bold values indicate statistically significant results.
[a] Median daily glucocorticoid dose over the first month was 13.08 mg.

cancer-related factors. These results were confirmed in the subset of participants with a single cancer, melanoma.

One reason for the discrepancy between our results and those of other investigators is that the glucocorticoid dosages prescribed by rheumatologists are much lower than those prescribed by oncologists [24]. In our study, the median (IQR) prednisone dose was 13 mg during the first month of ICI-IA treatment. This finding is supported by other studies, eg, 1 in which the mean daily prednisolone dose prescribed by rheumatologists was 14 mg compared with 53.3 mg by oncologists, which is comparable to the median we report for this cohort [24]. Although most glucocorticoid dosages prescribed in our study were under 50 mg, a small number of participants had dosages reported above 50 mg (N = 15). Several studies reported an inverse effect of glucocorticoid dosage and PFS, with worse survival experienced as glucocorticoid dosage increases [20,25,26]. Verheijden et al [26] found that higher glucocorticoid doses were associated with worse PFS in adjusted models (aHR: 1.14 [95% CI: 1.01-1.29 for 80 vs 40 mg] and aHR: 1.42 [95% CI: 1.03-1.95 for 160 vs 40 mg]). However, results from our analysis using quartiles of glucocorticoid dosing showed no association with PFS even among those in the higher dose quartiles of glucocorticoid dose (>26.67 mg).

The association of high-dose glucocorticoids with PFS can be confounded by concomitant DMARD use. However, within our cohort, few participants took DMARDs (N = 21 ever and N = 8 during the first month of treatment). When we controlled for DMARD use in the first month in the models, the glucocorticoid point estimates were not significant.

Some have shown that the timing of glucocorticoid treatment is associated with worse OS. One study found that participants who received glucocorticoids for an irAE within the first 6 weeks of ICI initiation had worse OS than those who received it later (aHR: 2.47 [95% CI: 1.49-4.09]) [15]. Another found that treatment with glucocorticoids within 30 or 90 days after ICI initiation was associated with a lower overall response rate; however, those who initiated glucocorticoid treatment 6 months or more after ICI initiation did not have worse PFS [20]. Of note, ICI-IA onset in our study was 123 (median, IQR: 30, 278) days after ICI initiation, and glucocorticoids were initiated a median of 6.9 (2.8, 14.5) months after ICI initiation, much later than is typical for common irAE such as colitis [27]. In our study, the variable 'time from ICI initiation to glucocorticoid initiation' was in fact associated with PFS in our models (aHR: 0.91 [95% CI: 0.87-0.96]). This suggests that earlier onset and/or earlier treatment of ICI-IA is associated with worse cancer outcomes. This could be due to patients' stopping or pausing ICI treatment prematurely, or a more deleterious impact of glucocorticoid treatment earlier in the course.

Some investigators have posited that the indication for glucocorticoid treatment, cancer palliation vs irAE treatment, influences its relationship to cancer survival. In some studies, particularly in participants with lung cancer, glucocorticoids prescribed for irAEs were not associated with worse survival [25,28,29], whereas glucocorticoids prescribed for cancer palliation (eg, dexamethasone) were associated with worse survival [17,25,30]. However, another study did find that high doses of glucocorticoids for irAE treatment (eg, 160 mg vs 40 mg) were associated with worse OS [31]. Attention is needed while

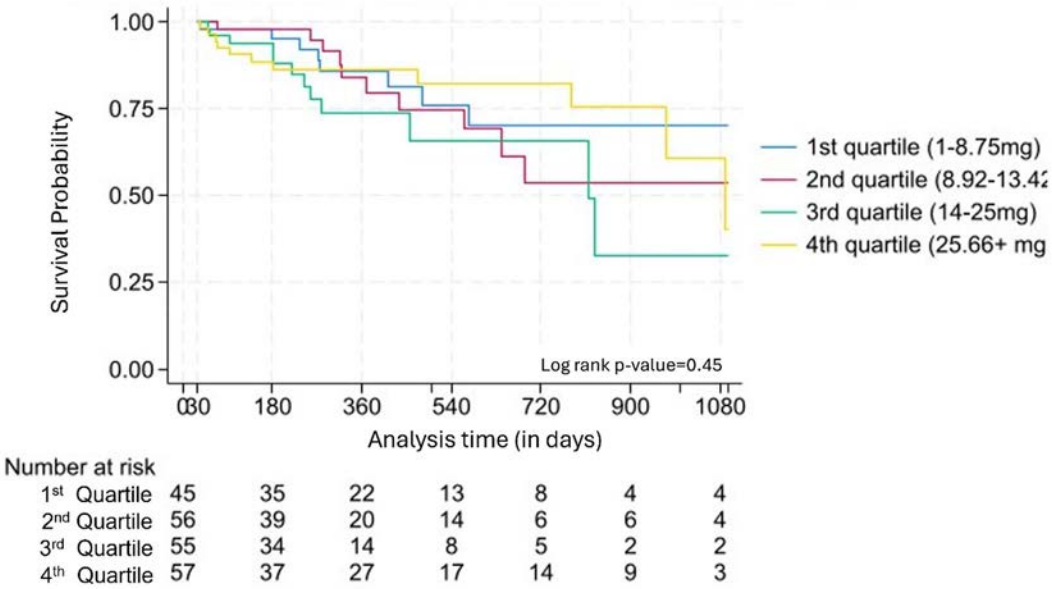

Figure 4. Thirty-day landmark Kaplan-Meier curve for cancer progression-free survival by quartile doses of glucocorticoids in the first month. People who progressed prior to glucocorticoid initiation were excluded from the Kaplan-Meier curve.

Table 3
Multivariable hazard ratios for cancer progression-free survival from a 32 landmark adjusted Cox proportional hazard model for quartile glucocorticoid dose over the first month

Variable	Landmark 30 d Hazard ratio (95% CI)
Glucocorticoid quartiles	
1st	Referent
2nd	0.97 (0.37, 2.53)
3rd	1.59 (0.60, 4.21)
4th	0.92 (0.35, 2.44)
Age	1.00 (0.98, 1.02)
Other cancers except melanoma	Referent
Melanoma	**0.25 (0.09, 0.70)**
Other cancers except nonsmall cell lung cancer	Referent
Nonsmall cell lung cancer	0.96 (0.34, 2.73)
Other cancers except renal cell carcinoma	Referent
Renal cell carcinoma	1.14 (0.47, 2.74)
Cancer stage ≤2	Referent
Cancer stage 3+	5.22 (0.68, 39.77)
ICI monotherapy	Referent
ICI +Chemotherapy	1.02 (0.46, 2.30)
Time from ICI initiation to Glucocorticoid start (mo)	**0.91 (0.87,0.96)**

ICI, immune checkpoint inhibitor.
Bold values indicate statistically significant results.

interpreting studies analysing the association between glucocorticoids and survival, as some do not account for immortal time bias [32–34]. Perhaps the combination of timing, dosage, and reason for glucocorticoid treatment all contribute to survival.

Cancer stage could influence the likelihood of cancer progression, but across all the models in our study, the variable cancer stage had wide CIs. This could be due to the large percentage with stage 3 and 4 cancer (N = 224, 81.5%). One hundred seventy-nine people in our cohort had melanoma, and of these patients, 95.2% had stage 3 or 4 cancer. Participants with advanced melanoma treated with ICI are known to do especially well [35]. ICI-treated melanoma participants are often younger and have fewer comorbidities than those with other cancers [36–38].

Our study has several strengths including the use of the RADIOS registry, a large multicentre national prospective cohort which continues to expand to additional sites. This registry includes participants with multiple cancer types and treatments. Data on glucocorticoid use are captured using a form specifically developed to capture glucocorticoid dose and timing, which is lacking in many other registries and datasets. However, our study also has several limitations. Participants with ICI-IA, ICI-PMR, and ICI-arthralgia had to survive long enough to develop these irAEs and then be referred to and treated by a rheumatologist, which could introduce survivor bias. ICI-IA typically occurs later than some other irAEs so these participants may reflect a cohort that is responding well to ICI treatment. This could result in some confounding by indication and or inherent survival bias. We mitigated this in our survival analysis by having our survival start time correspond to the time when glucocorticoid treatment began. Although these participants required specialised treatment by a rheumatologist, this should not have biased our findings regarding glucocorticoid exposure. Another limitation is missing data. Certain variables, such as Clinical Disease Activity Index, had considerable missing data and could not be included in the analysis. Lastly, the heterogeneity of the participants (different cancers, variations in ICI-IA presentation, and co-occurrence with other irAEs) is a limitation.

In summary, we demonstrated that a low dose of glucocorticoids (median dose: 13 mg [IQR: 7.5, 25]) does not adversely affect PFS in this very large cohort of participants with ICI-IA.

Competing interests

DPJ-K reports a relationship with AstraZeneca that includes equity or stocks. DPJ-K reports a relationship with CytoDyn Inc that includes equity or stocks. DPJ-K reports a relationship with American College of Rheumatology that includes board membership and travel reimbursement. PR reports a relationship with AbbVie that includes consulting or advisory and speaking and lecture fees and board membership. PR reports a relationship with UCB that includes consulting or advisory and speaking and lecture fees and board membership. PR reports a relationship with Padcev that includes consulting or advisory and speaking and lecture fees and board membership. PR reports a relationship with Amgen that includes consulting or advisory and speaking and lecture fees and board membership. PR reports a relationship with the University of Chicago Institute of Translational Medicine that includes funding grants. PR reports having a patent pending regarding the use of interleukin 6 axis inhibitors for viral infection-associated pneumonitis. LCC reports a relationship with Bristol-Myers Squibb Company that includes consulting or advisory. LCC reports a relationship with AbbVie Inc that includes consulting or advisory. LCC reports a relationship with Amgen Inc that includes consulting or advisory. LCC reports a relationship with Sanofi that includes consulting or advisory. LCC reports fundings from the National Institute of Arthritis and Musculoskeletal and Skin Diseases (NIAMS) R03AR081997 and P30AR070254. MES-A reports a relationship with Novartis that includes funding grants. MES-A reports a relationship with Syneos Health Inc that includes consulting or advisory. MES-A reports a relationship with Set Point Medical that includes consulting or advisory. NA-W is supported in part by the National Institutes of Health/National Institute of Allergy and Infectious Diseases (NIH/NIAID) Career Development Award (K01AI163412, 2021–2026). NA-W previously received institutional support from The University of Texas MD Anderson Cancer Center (2018-July 2025), including the Cancer Survivorship Seed Fund, Institutional Research Grant, Prioritizing Research Innovation & Mentoring Excellence (PRIME) Award, Division of Internal Medicine Development & Translational Science Award, Bridge Funding Award, Cyrus Scholar Award for Outstanding Clinical Research, Melanoma SPORE Career Enhancement Program Award, and the Melanoma Boat Walk Seed Fund, for research around the subject matter. NA-W reports a relationship with ChemoCentryx Inc that includes consulting or advisory and speaking and lecture fees. NA-W reports a relationship with Alliance for Clinical Trials in Oncology Immuno-Oncology Toxicity (IOTOX) Working Group that includes board membership. NA-W reports a relationship with Alliance for Support and Prevention of Immune-Related adverse Events (ASPIRE) that includes board membership. JAS reports a relationship with the National Institute of Allergy and Infectious Diseases that includes funding grants. JAS reports a relationship with the National Heart Lung and Blood Institute that includes funding grants. JAS reports a relationship with the Rheumatology Research Foundation that includes funding grants. JAS reports a relationship with the Arthritis Foundation that includes funding grants. JAS reports a relationship with R. Bruce and Joan M. Mickey Research Scholar Fund that includes funding grants. JAS reports a relationship with Gordon and Llura Gund Foundation that includes funding grants. JAS reports a

relationship with Bristol-Myers Squibb Company that includes consulting or advisory and funding grants. JAS reports a relationship with Boehringer Ingelheim that includes consulting or advisory and funding grants. JAS reports a relationship with Johnson & Johnson that includes consulting or advisory and funding grants. JAS reports a relationship with Sonoma Biotherapeutics Inc that includes funding grants. JAS reports a relationship with AbbVie that includes consulting or advisory. JAS reports a relationship with Amgen that includes consulting or advisory. JAS reports a relationship with Anaptys that includes consulting or advisory. JAS reports a relationship with AstraZeneca that includes consulting or advisory. JAS reports a relationship with Fresenius Kabi that includes consulting or advisory. JAS reports a relationship with Gilead Sciences Inc that includes consulting or advisory. JAS reports a relationship with INOVA Diagnostics Inc that includes consulting or advisory. JAS reports a relationship with Invivvd that includes consulting or advisory. JAS reports a relationship with Merck & Co Inc that includes consulting or advisory. JAS reports a relationship with MustangBio that includes consulting or advisory. JAS reports a relationship with Novartis that includes consulting or advisory. JAS reports a relationship with Optum that includes consulting or advisory. JAS reports a relationship with Pfizer that includes consulting or advisory. JAS reports a relationship with ReCor that includes consulting or advisory. JAS reports a relationship with Sana that includes consulting or advisory. JAS reports a relationship with Sobi that includes consulting or advisory. JAS reports a relationship with UCB that includes consulting or advisory. AM reports a relationship with AbbVie that includes consulting or advisory and travel reimbursement. AM reports a relationship with Sanofi that includes consulting or advisory and travel reimbursement. AM reports a relationship with AstraZeneca that includes consulting or advisory. AM reports a relationship with Amgen that includes consulting or advisory and travel reimbursement. AM reports a relationship with Foundation for Autoimmune Cancer Support that includes board membership. AM reports a relationship with Yes, Davis, Levin, and Livingston that includes paid expert testimony. TRK reports a relationship with Sanofi that includes funding grants. TRK reports a relationship with Genentech that includes equity or stocks. TRK reports a relationship with Roche that includes equity or stocks. CC reports a relationship with Sanofi that includes consulting or advisory and speaking and lecture fees. CC reports a relationship with Regeneron that includes consulting or advisory and speaking and lecture fees. AT reports financial support was provided by the French Society of Rheumatology, the French network of University Hospitals HUGO (Hôpitaux Universitaires du Grand Ouest), the Brest University Hospital endowment fund (Innoveo), and Philippe Foundation. AT reports a relationship with Bristol-Myers Squibb that includes speaking and lecture fees. AT reports a relationship with Sandoz that includes speaking and lecture fees. AT reports a relationship with Galapagos that includes consulting or advisory. AT reports a relationship with Lilly that includes travel reimbursement. AAS reports a relationship with National Institutes of Health that includes funding grants. CB reports a relationship with AbbVie that includes consulting or advisory. CB reports a relationship with Avalo that includes consulting or advisory. CB reports a relationship with Bristol-Myers Squibb Company that includes consulting or advisory. CB reports a relationship with Eli Lilly that includes board membership and consulting or advisory. CB reports a relationship with Janssen that includes consulting or advisory. CB reports a relationship with Pfizer that includes consulting or advisory. CB reports a relationship with Sanofi that includes consulting or advisory. CB reports a relationship with Tonix that includes consulting or advisory. CB reports a relationship with PROMIS Health Organization that includes board membership. ARB reports a relationship with American College of Rheumatology that includes board membership. ARB reports a relationship with National Institutes of Health that includes funding grants. All other authors declare they have no competing interests.

CRediT authorship contribution statement

Deanna P Jannat-Khah: Writing – review & editing, Writing – original draft, Visualization, Software, Methodology, Investigation, Formal analysis. **Pankti Reid:** Writing – review & editing, Data curation. **Laura C Cappelli:** Writing – review & editing, Project administration, Data curation. **Maria E Suarez-Almazor:** Writing – review & editing, Methodology, Data curation. **Noha Abdel-Wahab:** Writing – review & editing, Methodology, Data curation, Conceptualization. **Jeffrey A Sparks:** Writing – review & editing, Data curation. **Tawnie J Braaten:** Writing – review & editing, Data curation. **Alexa Meara:** Writing – review & editing, Data curation. **Minerva Nong:** Writing – review & editing, Data curation. **Kyle Ge:** Writing – review & editing, Data curation. **Tamiko R Katsumoto:** Writing – review & editing, Data curation. **Cassandra Calabrese:** Writing – review & editing, Data curation. **Alice Tison:** Writing – review & editing, Data curation. **Karmela Chan:** Writing – review & editing, Data curation. **Nilasha Ghosh:** Writing – review & editing, Data curation. **Ami A Shah:** Writing – review & editing, Resources, Project administration, Data curation. **Clifton Bingham:** Writing – review & editing, Resources, Project administration, Funding acquisition, Data curation. **Anne R Bass:** Writing – review & editing, Supervision, Resources, Project administration, Methodology, Investigation, Funding acquisition, Data curation, Conceptualization.

Acknowledgements

We would like to thank Hospital for Special Surgery, Johns Hopkins University and the National Institutes of Health (NIH/NIAID K01AI163412 [NAH] and NIH/NIAMS K24AR08217 [AAS]), which provided support for this research. Additional support was provided by the French Society of Rheumatology, the French network of University Hospitals HUGO (Hôpitaux Universitaires du Grand Ouest), the Brest University Hospital endowment fund (Innoveo), and the Philippe Foundation.

Funding

The RADIOS registry is supported by Johns Hopkins University. This research did not receive any specific grant from funding agencies in the public, commercial, or not-for-profit sectors.

Patient consent for publication

Not Applicable.

Ethics approval

Institutional review boards at each institution reviewed and approved participation in RADIOS including HSS (HSS IRB 2020-2572), and all participants provided informed consent.

Provenance and peer review

Not commissioned; externally peer reviewed.

Supplementary materials

Supplementary material associated with this article can be found in the online version at doi:10.1016/j.ard.2026.02.017.

Orcid

Deanna P Jannat-Khah: http://orcid.org/0000-0002-1091-379X

REFERENCES

[1] Angelopoulou F, Bogdanos D, Dimitroulas T, Sakkas L, Daoussis D. Immune checkpoint inhibitor-induced musculoskeletal manifestations. Rheumatol Int 2021;41:33–42. doi: 10.1007/s00296-020-04665-7.

[2] Postow MA, Sidlow R, Hellmann MD. Immune-related adverse events associated with immune checkpoint blockade. N Engl J Med 2018;378:158–68. doi: 10.1056/NEJMra1703481.

[3] Zheng Y, Kim R, Yu T, Gayle JA, Wassel CL, Dreyfus J, et al. Real-world clinical and economic outcomes in selected immune-related adverse events among patients with cancer receiving immune checkpoint inhibitors. Oncologist 2021;26:e2002–12. doi: 10.1002/onco.13918.

[4] Postow MA, Callahan MK, Wolchok JD. Immune checkpoint blockade in cancer therapy. J Clin Oncol 2015;33:1974–82.

[5] Chan KK, Bass AR. Autoimmune complications of immunotherapy: pathophysiology and management. BMJ 2020;369:m736. doi: 10.1136/bmj.m736.

[6] Liew DFL, Leung JLY, Liu B, Cebon J, Frauman AG, Buchanan RRC. Association of good oncological response to therapy with the development of rheumatic immune-related adverse events following PD-1 inhibitor therapy. Int J Rheum Dis 2019;22:297–302. doi: 10.1111/1756-185X.13444.

[7] Hussaini S, Chehade R, Boldt RG, Raphael J, Blanchette P, Maleki Vareki S, et al. Association between immune-related side effects and efficacy and benefit of immune checkpoint inhibitors - a systematic review and meta-analysis. Cancer Treat Rev 2021;92:102134. doi: 10.1016/j.ctrv.2020.102134.

[8] Kostine M, Rouxel L, Barnetche T, Veillon R, Martin F, Dutriaux C, et al. Rheumatic disorders associated with immune checkpoint inhibitors in patients with cancer-clinical aspects and relationship with tumour response: a single-centre prospective cohort study. Ann Rheum Dis 2018;77:393–8. doi: 10.1136/annrheumdis-2017-212257.

[9] Verspohl SH, Holderried T, Behning C, Brossart P, Schäfer VS. Prevalence, therapy and tumour response in patients with rheumatic immune-related adverse events following immune checkpoint inhibitor therapy: a single-centre analysis. Ther Adv Musculoskelet Dis 2021;13 1759720 × 211006963. doi: 10.1177/1759720×211006963.

[10] Gonzalez-Mazón I, Sánchez-Bilbao L, Martín-Varillas JL, García-Castaño A, Delgado-Ruiz M, Bernat Piña I, et al. Immune-related adverse events in patients with solid-organ tumours treated with immunotherapy: a 3-year study of 102 cases from a single centre. Clin Exp Rheumatol 2021;39:612–20. doi: 10.55563/clinexprheumatol/o5nvgv.

[11] NCCN Guidelines Insights: Management of Immunotherapy-Related Toxicities, Version 2.2024. In: Journal of the National Comprehensive Cancer Network. Vol. 22, Issue 9. 2024 [updated 2026 Mar 18; cited 2025 Sep 3]. Available from: https://jnccn.org/view/journals/jnccn/22/9/article-p582.xml

[12] Schneider BJ, Naidoo J, Santomasso BD, Lacchetti C, Adkins S, Anadkat M, et al. Management of immune-related adverse events in patients treated with immune checkpoint inhibitor therapy: ASCO guideline update. J Clin Oncol 2021;39:4073–126. doi: 10.1200/JCO.21.01440.

[13] Kostine M, Finckh A, Bingham CO, Visser K, Leipe J, Schulze-Koops H, et al. EULAR points to consider for the diagnosis and management of rheumatic immune-related adverse events due to cancer immunotherapy with checkpoint inhibitors. Ann Rheum Dis 2021;80:36–48. doi: 10.1136/annrheumdis-2020-217139.

[14] Costa Svedman F, Liapi M, Mansson-Broberg A, Chatzidionysiou K, Egyhazi Brage S. Effect of glucocorticoids for the management of immune-related adverse events on outcome in melanoma patients treated with immunotherapy-a retrospective and biomarker study. Immunooncol Technol 2024;22:100713. doi: 10.1016/j.iotech.2024.100713.

[15] Verheijden RJ, May AM, Blank CU, Aarts MJB, van den Berkmortel FWPJ, van den Eertwegh AJM, et al. Association of anti-TNF with decreased survival in steroid refractory ipilimumab and anti-PD1-treated patients in the Dutch Melanoma Treatment Registry. Clin Cancer Res 2020;26:2268–74. doi: 10.1158/1078-0432.CCR-19-3322.

[16] Pan EY, Merl MY, Lin K. The impact of corticosteroid use during anti-PD1 treatment. J Oncol Pharm Pract 2020;26:814–22. doi: 10.1177/1078155219872786.

[17] Passiglia F, Cetoretta V, De Filippis M, Napoli V, Novello S. Exploring the immune-checkpoint inhibitors' efficacy/tolerability in special non-small cell lung cancer (NSCLC) populations: focus on steroids and autoimmune disease. Transl Lung Cancer Res 2021;10:2876–89. doi: 10.21037/tlcr-20-635.

[18] Ricciuti B, Dahlberg SE, Adeni A, Sholl LM, Nishino M, Awad MM. Immune checkpoint inhibitor outcomes for patients with non-small-cell lung cancer receiving baseline corticosteroids for palliative versus nonpalliative indications. J Clin Oncol 2019;37:1927–34.

[19] Fucà G, Galli G, Poggi M, Lo Russo G, Proto C, Imbimbo M, et al. Modulation of peripheral blood immune cells by early use of steroids and its association with clinical outcomes in patients with metastatic non-small cell lung cancer treated with immune checkpoint inhibitors. ESMO Open 2019;4:e000457. doi: 10.1136/esmoopen-2018-000457.

[20] Albarrán V, Guerrero P, de Quevedo CG, González C, Chamorro J, Rosero DI, et al. Negative association of steroids with immunotherapy efficacy in a multi-tumor cohort: time and dose-dependent. Cancer Immunol Immunother 2024;73:186. doi: 10.1007/s00262-024-03772-9.

[21] National Cancer Institute. CTCAE and adverse event Reporting [Internet]. 2025 [updated 2026 Mar 18; cited 2025 Sep 3]. Available from: https://dctd.cancer.gov/research/ctep-trials/for-sites/adverse-events

[22] Kfoury M, Najean M, Lappara A, Voisin A-L, Champiat S, Michot J-M, et al. Analysis of the association between prospectively collected immune-related adverse events and survival in patients with solid tumor treated with immune-checkpoint blockers, taking into account immortal-time bias. Cancer Treat Rev 2022;110:102452. doi: 10.1016/j.ctrv.2022.102452.

[23] Giobbie-Hurder A, Gelber RD, Regan MM. Challenges of guarantee-time bias. J Clin Oncol 2013;31:2963–9. doi: 10.1200/JCO.2013.49.5283.

[24] Yoon JS, Zhao F, Masood H, De Silva R, Binns J, Atkinson V, et al. Comparative study of management strategies for immune checkpoint inhibitor-induced inflammatory arthritis: rheumatologists versus oncologists. Intern Med J 2025;55:426–34. doi: 10.1111/imj.16629.

[25] Curkovic NB, Irlmeier R, Bai X, Cui C, Ye F, Burnette HR, et al. Impact of steroid dose and timing on efficacy of combination PD-1/CTLA-4 blockade. Oncoimmunology 2025;14:2494433. doi: 10.1080/2162402X.2025.2494433.

[26] Verheijden RJ, de Groot JS, Fabriek BO, Hew MN, May AM, Suijkerbuijk KPM. Corticosteroids for immune-related adverse events and checkpoint inhibitor efficacy: analysis of six clinical trials. J Clin Oncol 2024;42:3713–24. doi: 10.1200/JCO.24.00191.

[27] Weber JS, Hodi FS, Wolchok JD, Topalian SL, Schadendorf D, Larkin J, et al. Safety profile of nivolumab monotherapy: a pooled analysis of patients with advanced melanoma. J Clin Oncol 2017;35:785–92. doi: 10.1200/JCO.2015.66.1389.

[28] Schwarzlmueller P, Triebig A, Assié G, Jouinot A, Theurich S, Maier T, et al. Steroid hormones as modulators of anti-tumoural immunity. Nat Rev Endocrinol 2025;21:331–43. doi: 10.1038/s41574-025-01102-2.

[29] Skribek M, Rounis K, Afshar S, Grundberg O, Friesland S, Tsakonas G, et al. Effect of corticosteroids on the outcome of patients with advanced non-small cell lung cancer treated with immune-checkpoint inhibitors. Eur J Cancer 2021;145:245–54. doi: 10.1016/j.ejca.2020.12.012.

[30] Arbour KC, Mezquita L, Long N, Rizvi H, Auclin E, Ni A, et al. Impact of baseline steroids on efficacy of programmed cell death-1 and programmed death-ligand 1 blockade in patients with non-small-cell lung cancer. J Clin Oncol 2018;36:2872–8. doi: 10.1200/JCO.2018.79.0006.

[31] Verheijden RJ, Burgers FH, Janssen JC, Putker AE, Veenstra SPGR, Hospers GAP, et al. Corticosteroids and other immunosuppressants for immune-related adverse events and checkpoint inhibitor effectiveness in melanoma. Eur J Cancer 2024;207:114172. doi: 10.1016/j.ejca.2024.114172.

[32] Dall'Olio FG, Rizzo A, Mollica V, Massucci M, Maggio I, Massari F. Immortal time bias in the association between toxicity and response for immune checkpoint inhibitors: a meta-analysis. Immunotherapy 2021;13:257–70. doi: 10.2217/imt-2020-0179.

[33] Duchesneau ED, Jackson BE, Webster-Clark M, Lund JL, Reeder-Hayes KE, Nápoles AM, et al. The timing, the treatment, the question: comparison of epidemiologic approaches to minimize immortal time bias in real-world data using a surgical oncology example. Cancer Epidemiol Biomarkers Prev 2022;31:2079–86. doi: 10.1158/1055-9965.EPI-22-0495.

[34] Quandt Z, Lucas A, Liang SI, Yang E, Stone S, Fadlullah MZH, et al. Associations between immune checkpoint inhibitor response, immune-related adverse events, and steroid use in RADIOHEAD: a prospective pan-tumor cohort study. J Immunother Cancer 2025;13:e011545. doi: 10.1136/jitc-2025-011545.

[35] Carlino MS, Larkin J, Long GV. Immune checkpoint inhibitors in melanoma. Lancet 2021;398:1002–14. doi: 10.1016/S0140-6736(21)01206-X.

[36] Paulson KG, Gupta D, Kim TS, Veatch JR, Byrd DR, Bhatia S, et al. Age-specific incidence of melanoma in the United States. JAMA Dermatol 2020;156:57–64. doi: 10.1001/jamadermatol.2019.3353.

[37] American Cancer Society. Cancer facts & figures 2025 [Internet]. [updated 2026 Mar 18; cited 2025 Mar 2]. Available from: https://www.cancer.org/research/cancer-facts-statistics/all-cancer-facts-figures/2025-cancer-facts-figures.html

[38] Grann AF, Frøslev T, Olesen AB, Schmidt H, Lash TL. The impact of comorbidity and stage on prognosis of Danish melanoma patients, 1987-2009: a registry-based cohort study. Br J Cancer 2013;109:265–71. doi: 10.1038/bjc.2013.246.

Ann Rheum Dis 85 (2026) 1890–1893

Contents lists available at ScienceDirect

Annals of the Rheumatic Diseases

journal homepage: https://www.sciencedirect.com/journal/annals-of-the-rheumatic-diseases

Letter

Bilirubin regulating the onset of rheumatoid arthritis

Bilirubin, a tetrapyrrolic bile pigment and the end product of heme catabolism, is primarily generated through haemoglobin degradation. Once considered a mere waste metabolite, it is now recognised for its antioxidant and immunomodulatory properties. At the molecular level, binding to nuclear receptors such as Peroxisome proliferator-activated receptor alpha (PPARα) [1] and the aryl hydrocarbon receptor [2] is thought to confer these properties. An inverse correlation between bilirubin levels and several diseases, including Crohn's disease [3] and metabolic syndrome [4], has been reported. In accordance with this, patients with Gilbert's syndrome who experience hyperbilirubinemia appear to be protected from cardiovascular diseases [5]. In patients with rheumatoid arthritis (RA), correlations between disease activity and bilirubin levels were first reported in 2017 [6]. More recent untargeted metabolomic studies have consistently shown decreased bilirubin levels in patients with RA [7], extending to anticitrullinated protein antibody (ACPA)-positive high-risk RA cohorts [8]. However, whether bilirubin can serve as an early biomarker for RA or possess therapeutic potential remains unclear.

Notably, bilirubin-based nanomedicine has demonstrated efficacy in alleviating intestinal inflammation [9]. Given that intestinal inflammation is an early event in RA pathogenesis [10], these findings suggest that reduced bilirubin levels may serve as both a complementary predictive biomarker and a novel therapeutic strategy to delay or prevent progression to clinical disease.

Here, untargeted serum metabolomics by liquid chromatography-mass spectrometry (LC-MS) was performed in 82 ACPA-positive individuals with musculoskeletal pain but no clinical arthritis [11] and in 50 healthy controls (blood donors) (Fig, A). Baseline characteristics are shown in the Table. At a median follow-up of 72 months, 39 patients (48%) developed clinical arthritis after a median of 6 months. In total, 417 identified metabolites were found to be differentially abundant in baseline serum samples across at least 2 groups, as determined by one-way analysis of variance with Fisher's post hoc test (Supplementary Fig, A and Supplementary Table S1). As shown in Figure B, the metabolic profile of healthy subjects differed significantly between progressors and nonprogressors. Nevertheless, partial least squares discriminant analysis (PLS-DA) demonstrated the presence of discriminatory metabolites that distinguished progressors from nonprogressors (Fig, C). Enrichment analysis of all metabolites identified to be differentially abundant in progressors compared with nonprogressors revealed changes in pathways of key branches of human metabolism, including amino acid, lipid, carbohydrate, energy, and cofactor/vitamin metabolism (Fig, D). Notably, porphyrin metabolism was identified as the most significantly altered among all identified enrichment terms. Our analyses revealed that both bilirubin and biliverdin, constituents of porphyrin metabolism, were significantly less abundant in nonprogressors than in progressors, but not in healthy individuals vs nonprogressors, suggesting their potential as biomarkers and therapeutics (Fig, E and Supplementary Fig, B). Additionally, Cox regression and Kaplan-Meier analysis highlighted the predictive capacity of bilirubin for progression to clinical arthritis (Supplementary Tables S2 and S3 and Fig, F).

Based on these findings, 2 bilirubin-based nanomedicines—SPION-APTES (S-A^{BN}; Fig, G) and hyaluronic acid (HA-BN; Fig, J)—were administered prophylactically during the asymptomatic phase of collagen-induced arthritis (CIA) (experimental design in Supplementary Fig, E). Both S-A^{BN} and HA-BN significantly reduced arthritis severity relative to controls, as evidenced by lower mean paw swelling (shown in mm; Fig, H and K). Bray-Curtis analysis of 16S rRNA sequencing of intestinal contents revealed distinct gut microbiome profiles in treated mice (Fig, I and L). Notably, in the S-A^{BN} treatment group, the microbiota composition shifted predominantly towards a physiological profile (Fig, I).

In summary, our findings identify bilirubin as a promising biomarker for progression to RA in ACPA-positive at-risk individuals and demonstrate that prophylactic bilirubin nanomedicine can reduce arthritis severity while partially restoring a healthy gut microbiota. Given that both platforms, S-A^{BN} and HA-BN, have been widely explored for clinical applications with minimal toxicity and intestinal barrier-healing properties, these results support a translational approach in which low serum bilirubin could guide early treatment strategies to modulate disease progression, highlighting a combined biomarker-therapeutic-microbiota axis for intervention.

https://doi.org/10.1016/j.ard.2026.03.014
Received 31 October 2025; Revised 19 February 2026; Accepted 12 March 2026

0003-4967/© 2026 European Alliance of Associations for Rheumatology (EULAR). Published by Elsevier B.V. All rights are reserved, including those for text and data mining, AI training, and similar technologies.

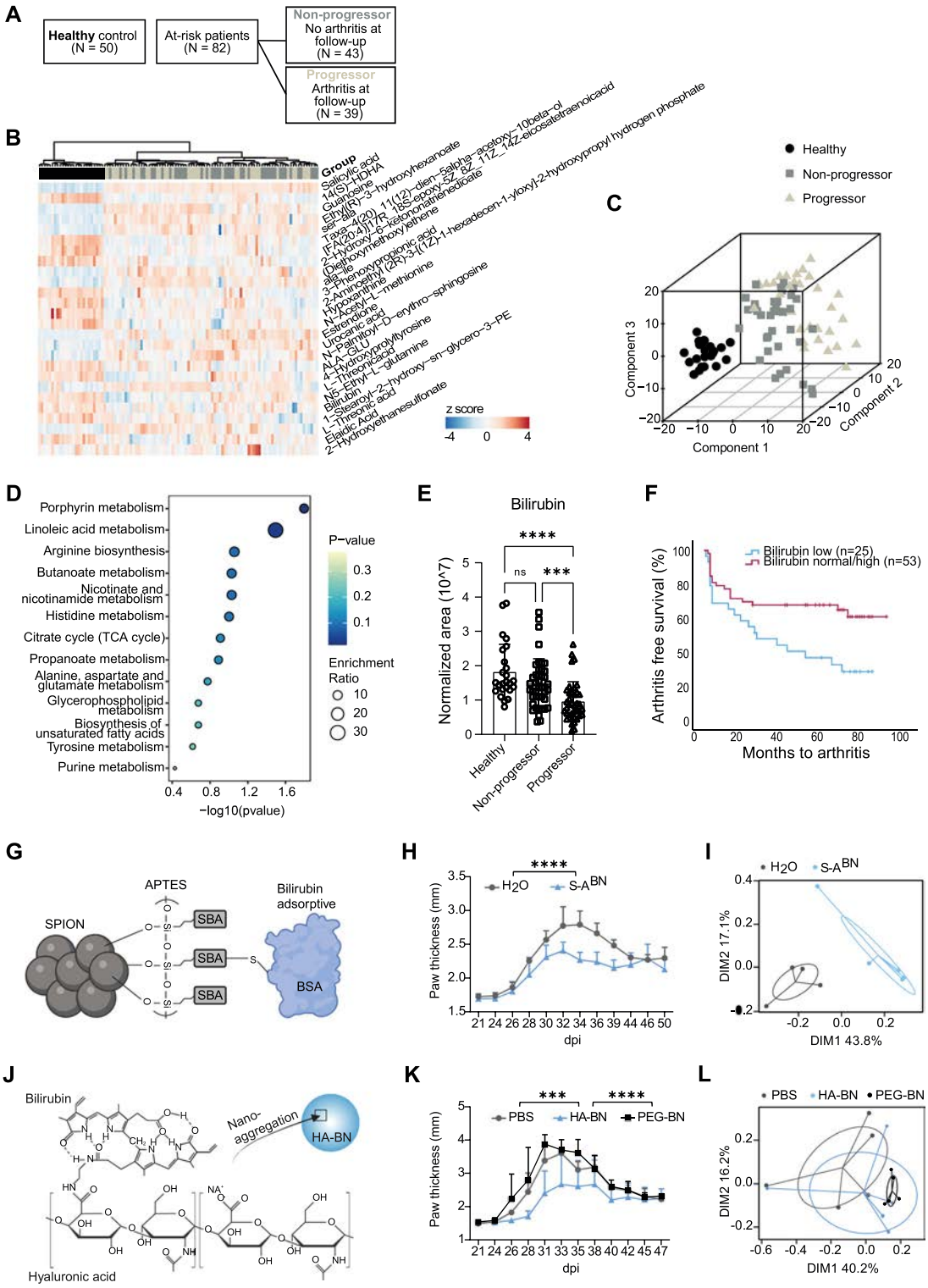

Figure. Distinct serum metabolome profile and decreased serum bilirubin levels in patients at risk of developing rheumatoid arthritis (RA) and reduced symptom severity in bilirubin nanoparticle (BN)-treated collagen-induced arthritis (CIA) mice. A, Trial profile of the TIRx study cohort (Swedish acronym for 'xtra early rheumatology follow-up') and healthy controls, with baseline serum metabolomics analysed. For healthy controls, pools of 2 sera were always analysed. B, Heatmap of differentially abundant metabolites in reverse-phase liquid chromatography negative ionisation (RP_{neg}) mode, as measured by one-way analysis of variance (ANOVA) in baseline serum samples. C, Partial least squares discriminant analysis (PLS-DA) 3-dimensional plot of baseline serum samples analysed in RP_{neg} mode. D, Enrichment analysis of metabolites identified as differentially abundant in baseline serum samples of progressors compared with nonprogressors. E, Normalised area of bilirubin (RP_{neg} mode) in baseline serum samples. F, Kaplan-Meier graph of arthritis-free survival in patients at risk stratified by bilirubin status (low vs normal/high). G, Schematic representation of SPION-APTES bilirubin nanomedicine (S-A^{BN}). H, Clinical arthritis score of CIA mice ± treatment with S-A^{BN}. I, Spider plot of Bray-Curtis principal coordinate analysis of CIA ± S-A^{BN} mice caecal content 50 days post immunisation (dpi). J, Schematic representation of hyaluronic acid bilirubin nanoparticle (HA-BN). K, Clinical arthritis score of CIA mice ± treatment with HA-BN or polyethylene glycol bilirubin nanomedicine (PEG-BN). L, Spider plot of Bray-Curtis principal coordinate analysis of CIA ± HA-BN or PEG-BN mice colon content 47 dpi. Data are presented as mean ± SD. Statistical differences were determined by the (E) Kruskal-Wallis test with Dunn's post hoc correction and (H, K) the Welch's *t*-test of the area under the curve (AUC); ***$P < .001$, ****$P < .0001$. APTES, 3-aminopropyl triethoxysilane; DIM, dimension; ns, not significant; PBS, phosphate-buffered saline.

Table
Clinical characteristics of research individuals and bilirubin-treated mice

	Healthy (N = 50)	Nonprogressors (n = 43)	Progressors (n = 39)	p^f	p^g	p^h	p^i
Age (y)	51 ± 13	49 ± 15	55 ± 12	.209[b]	.501[b]	.224[b]	.090[b]
Female	32 (64)	34 (79)	32 (82)	.105[d]	.169[e]	.090[e]	.786[e]
Months to arthritis	-	-	6 (3-24)	-	-	-	-
Symptom duration, mo							
0-6	-	7 (16)	8 (21)	-	-	-	.514[d]
6-18	-	22 (51)	15 (39)				
>18	-	14 (33)	16 (41)				
IgG ACPA							
Low	-	20 (47)	14 (36)	-	-	-	.375[e]
High	-	23 (54)	25 (64)				
RF							
Positive	-	8 (19)	16 (41)	-	-	-	.031[e]
Negative	-	35 (81)	23 (59)				
CRP (mg/L)	-	5 ± 0	8 ± 9	-	-	-	.008[b]
ESR (mm/h)	-	10 ± 7[j]	14 ± 12	-	-	-	.240[b]
Smoking							
Nonsmoker	-	23 (54)	20 (51)	-	-	-	.884[d]
Ex-smoker	-	14 (33)	12 (31)				
Current smoker	-	6 (14)	7 (18)				
Bilirubin RP_{neg}	$1.51*10^7$ ($1.51*10^7$-$2.28*10^7$)	$1.36*10^7$ ($1.02*10^7$-$1.84*10^7$)	$8.39*10^6$ ($5.68*10^6$-$1.22*10^7$)	<.001[a]	.273[a]	<.001[a]	<.001[a]
Biliverdin RP_{pos}	$8.0*10^6$ ($6.5*10^6$-$1.4*10^7$)	$6.9*10^6$ ($4.4*10^6$-$1.0*10^7$)	$3.74*10^6$ ($2.4*10^6$-$5.95*10^6$)	<.001[a]	.402[a]	<.001[a]	<.001[a]
	Control H_2O (n = 5)	**S-A^{BN} (n = 5)**		**p^k**			
AUC MCS	25.79 [0.31]	23.39 [0.37]		<.001[c]			
	Control PBS (n = 5)	**HA-BN (n = 5)**	**PEG-BN (n = 5)**	**p^l**	**p^m**	**p^n**	
AUC MCS_{hind}	28.47 [0.64]	23.9 [1.21]	30.27 [1.02]	.178[a]	<.001[c]	<.001[c]	
BV/TV (%)	50.8 (41.29-50.98)	55.91 (51.14-63.57)	54.99 (37.37-61.58)	.163[a]	.047[b]	.054[b]	

Data are presented as n (%), mean ± SD, median (IQR), or AUC [SE].
ACPA, anticitrullinated protein antibody; AUC, area under the curve; BV, bone volume; CRP, C-reactive protein; ESR, erythrocyte sedimentation rate; HA-BN, hyaluronic acid bilirubin nanoparticle; Ig, immunoglobulin; MCS, mean calliper score; MCS_{hind}, mean calliper score hind limbs; PBS, phosphate-buffered saline; PEG-BN, polyethylene glycol bilirubin nanomedicine; RF, rheumatoid factor; RP_{neg}, reverse-phase liquid chromatography negative ionisation mode; RP_{pos}, reverse-phase liquid chromatography positive ionisation mode; S-A^{BN}, SPION-APTES bilirubin nanomedicine; TV, total volume.
[a] Kruskal-Wallis test with Dunn's post hoc correction.
[b] Mann-Whitney U test.
[c] Welch's *t*-test.
[d] Pearson chi-square test.
[e] Fisher's exact test.
[f] Comparison between 3 groups (healthy vs nonprogressors vs progressors).
[g] Comparison between 2 groups (healthy vs nonprogressors).
[h] Comparison between 2 groups (healthy vs progressors).
[i] Comparison between 2 groups (nonprogressors vs progressors).
[j] n = 42.
[k] Comparison between 2 groups (control H_2O vs S-A^{BN}).
[l] Comparison between 3 groups (control PBS vs HA-BN vs PEG-BN).
[m] Comparison between 2 groups (control PBS vs HA-BN).
[n] Comparison between 2 groups (PEG-BN vs HA-BN).

Competing interests

None declared.

CRediT authorship contribution statement

Nadine Otterbein: Writing – original draft, Visualization, Formal analysis, Data curation. **Klara Martinsson:** Data curation, Conceptualization. **Eva Schmid:** Writing – original draft, Investigation. **Lukas Heinen:** Investigation. **Nayoon Park:** Investigation. **Heike Danzer:** Investigation. **Kerstin Dürholz:** Investigation. **Agnus Monica Davis:** Investigation, Data curation. **Yubin Luo:** Data curation. **Georg Schett:** Writing – original draft. **Rainer Tietze:** Investigation. **Yonghyun Lee:** Investigation. **Alf Kastbom:** Writing – original draft, Data curation, Conceptualization. **Mario M. Zaiss:** Writing – original draft, Conceptualization.

Acknowledgements

We thank Prof Martin Fromm, head of the Core Unit Metabolomics at the FAU Medical Faculty, and Dr Arne Gessner, for the serum untargeted metabolomics analysis. We thank Dr Wirtz, head of the Microbiome Analysis Core Unit, Erlangen, for the 16S rRNA sequencing.

Contributors

All authors had access to the data. KM, GS, AK, and MMZ contributed to the study conception and design. AK was responsible for patient recruitment and characterisation. Sample

preparation was done by ES, HD, KD, and AMD. Data was collected by NO, AMD, and Y Luo. Statistical analyses were performed by NO and KM. LH, NP, RT, and Y Lee generated the nanoparticles. NO and MMZ wrote the first draft of the manuscript, and all authors commented on subsequent versions and approved the final manuscript.

Funding

The Orbitrap mass spectrometer used for untargeted metabolomics was supported by funding from the German Research Foundation (DFG), grant number INST 90/1048-1 FUGG. AK is funded by the King Gustaf V's 80-year Foundation, the Swedish Research Council, the Swedish Rheumatism Association, and ALF grants from Region Östergötland. NO, ES, HD, KD, and MMZ are funded by the Deutsche Forschungsgemeinschaft (DFG) (TRRR369 DIONE-501752319-A01 and DFG-CRC1755 CASCAID-550296805-10), and within the Research Training Group 'Immunomicrotope,' GRK 2740/447268119-B04. This research was also supported by a grant from the Korea Health Technology R&D Project through the Korea Health Industry Development Institute (KHIDI), funded by the Ministry of Health & Welfare, Republic of Korea (RS-2023-00265981).

Patient consent for publication

Not required.

Ethics approval

We declare that this study was approved by the Swedish Ethical Review Authority (2020-06162) and conducted in accordance with the ethical standards outlined in the Declaration of Helsinki and its subsequent amendments. All study subjects provided written informed consent before inclusion in the TIRx cohort. All animal experiments were approved by the Regierung von Unterfranken in Würzburg (approval ID: 55.2-2532-2-1835).

Provenance and peer review

Not commissioned; externally peer reviewed.

Supplementary materials

Supplementary material associated with this article can be found in the online version at doi:10.1016/j.ard.2026.03.014.

Orcid

Mario M. Zaiss: http://orcid.org/0000-0003-3844-1664

REFERENCES

[1] Stec DE, John K, Trabbic CJ, Luniwal A, Hankins MW, Baum J, et al. Bilirubin binding to PPARα inhibits lipid accumulation. PLoS One 2016;11(4):e0153427.
[2] Longhi MS, Vuerich M, Kalbasi A, Kenison JE, Yeste A, Csizmadia E, et al. Bilirubin suppresses Th17 immunity in colitis by upregulating CD39. JCI Insight 2017;2(9):e92791.
[3] Su Q, Li X, Mo W, Yang Z. Low serum bilirubin, albumin, and uric acid levels in patients with Crohn's disease. Medicine (Baltimore) 2019;98(19):e15664.
[4] Novák P, Jackson AO, Zhao GJ, Yin K. Bilirubin in metabolic syndrome and associated inflammatory diseases: new perspectives. Life Sci 2020;257:118032.
[5] Bulmer AC, Bakrania B, Du Toit EF, Boon AC, Clark PJ, Powell LW, et al. Bilirubin acts as a multipotent guardian of cardiovascular integrity: more than just a radical idea. Am J Physiol Heart Circ Physiol 2018;315(3):H429–47.
[6] Peng YF, Wang JL, Pan GG. The correlation of serum bilirubin levels with disease activity in patients with rheumatoid arthritis. Clin Chim Acta 2017;469:187–90.
[7] Hur B, Gupta VK, Huang H, Wright KA, Warrington KJ, Taneja V, et al. Plasma metabolomic profiling in patients with rheumatoid arthritis identifies biochemical features predictive of quantitative disease activity. Arthritis Res Ther 2021;23(1):164.
[8] Luo Y, Tong Y, Wu L, Niu H, Li Y, Su LC, et al. Alteration of gut microbiota in individuals at high-risk for rheumatoid arthritis associated with disturbed metabolome and the initiation of arthritis through the triggering of mucosal immunity imbalance. Arthritis Rheumatol 2023;75(10):1736–48.
[9] Lee Y, Sugihara K, Gillilland 3rd MG, Jon S, Kamada N, Moon JJ. Hyaluronic acid-bilirubin nanomedicine for targeted modulation of dysregulated intestinal barrier, microbiome and immune responses in colitis. Nat Mater 2020;19(1):118–26.
[10] Tajik N, Frech M, Schulz O, Schälter F, Lucas S, Azizov V, et al. Targeting zonulin and intestinal epithelial barrier function to prevent onset of arthritis. Nat Commun 2020;11(1):1995.
[11] Eloff E, Martinsson K, Ziegelasch M, Cedergren J, Reckner Å, Skogh T, et al. Autoantibodies are major predictors of arthritis development in patients with anti-citrullinated protein antibodies and musculoskeletal pain. Scand J Rheumatol 2021;50(3):189–97.

Nadine Otterbein[1,2], Klara Martinsson[3], Eva Schmid[1,2], Lukas Heinen[4], Nayoon Park[5], Heike Danzer[1,2], Kerstin Dürholz[1,2], Agnus Monica Davis[1,2], Yubin Luo[6], Georg Schett[1,2], Rainer Tietze[4], Yonghyun Lee[5,7], Alf Kastbom[3,8], Mario M. Zaiss[1,2,*]

[1] *Department of Internal Medicine 3, Rheumatology and Immunology, Universitätsklinikum Erlangen, Friedrich-Alexander-Universität Erlangen-Nürnberg, Erlangen, Germany*
[2] *Deutsches Zentrum für Immuntherapie, Friedrich-Alexander-University Erlangen-Nürnberg, Universitätsklinikum Erlangen, Erlangen, Germany*
[3] *Department of Biomedical and Clinical Sciences, Linköping University, Linköping, Sweden*
[4] *Section of Experimental Oncology and Nanomedicine (SEON), Department of Otorhinolaryngology, Head and Neck Surgery, Else Kröner-Fresenius-Stiftung-Professorship, Universitätsklinikum Erlangen, Erlangen, Germany*
[5] *College of Pharmacy, Ewha Womans University, Seoul, South Korea*
[6] *Department of Rheumatology and Immunology, Sports Medicine Center, Department of Orthopedics, and Laboratory of Rheumatology and Immunology, West China Hospital, Sichuan University, Chengdu, Sichuan, China*
[7] *Graduate Program in Innovative Biomaterials Convergence, Ewha Womans University, Seoul, South Korea*
[8] *Clinical Department of Rheumatology in Östergötland, Region Östergötland, Linköping, Sweden*

*Correspondence to Dr Mario M. Zaiss, Department of Internal Medicine 3, Universitätsklinikum Erlangen, Erlangen, Germany.
E-mail address: mario.zaiss@uk-erlangen.de (M.M. Zaiss).

Ann Rheum Dis 85 (2026) 1894–1896

Contents lists available at ScienceDirect

Annals of the Rheumatic Diseases

journal homepage: https://www.sciencedirect.com/journal/annals-of-the-rheumatic-diseases

Letter

Proinflammatory autoantibodies enhancing tumor necrosis factor and RANKL signaling in axial spondyloarthritis associate with hyperphosphorylated progranulin and osteoprotegerin

Axial spondyloarthritis (axSpA) is a chronic, seronegative inflammatory disease of the axial skeleton, with extra-articular manifestations such as arthritis, uveitis, psoriasis and inflammatory bowel disease . Diagnosis relies on clinical features (eg, nocturnal back pain), inflammatory markers, human leukocyte antigen (HLA)-B27 positivity and imaging (magnetic resonance imaging/radiographic sacroiliitis), with advanced cases classified as ankylosing spondylitis [1]. Although termed 'seronegative', autoantibodies, including anti-CD74, have been reported in axSpA [2].

In several rheumatic inflammatory diseases, we and others have identified proinflammatory autoantibodies neutralising endogenous anti-inflammatory mediators such as progranulin (PGRN), interleukin (IL)-36Ra and IL-1Ra [3–6]. Given the dual features of chronic inflammation and aberrant bone remodelling in axSpA, likely due to dysregulated receptor activator of nuclear factor-κB ligand (RANKL)-RANK signalling, we aimed to investigate whether autoantibodies that either neutralise anti-inflammatory antagonists or directly target proinflammatory receptors such as RANK or its decoy receptor osteoprotegerin (OPG) could be involved in disease, as suggested by 1 previous report [7].

To assess this, we screened sera from axSpA patients (Supplementary Table S1), disease controls (Supplementary Table S2), and healthy individuals for autoantibodies against IL-1Ra, PGRN, IL-36Ra, IL-18BP, RANK, and OPG using our previously established methodological platform [3–5]. Functional and biochemical analyses included immune complex detection, antigen neutralisation, atypical isoform identification, and RANKL-signalling reporter assays.

Anti-PGRN and anti-OPG autoantibodies were detected in 8 of 46 (17.4%) and 4 of 46 (8.7%) of axSpA patients, respectively (Fig. 1A and Supplementary Fig. S1). No patient tested double-positive for these autoantibodies, and no antibodies to IL-1Ra, IL-36Ra, IL-18BP, IL-17R, or CD74 were found (Fig. 1A). Both OPG- and PGRN-directed autoantibodies belonged to the immunoglobulin (Ig)G1 subclass, with titers ranging from 1:800 to 1:1600 (Supplementary Fig. S2). Western blot analysis and gel filtration confirmed the presence of OPG-IgG immune complexes in anti-OPG-positive samples (Fig. 1B and Supplementary Fig. S3). Anti-OPG and anti-PGRN autoantibodies were associated with reduced circulating levels of their respective antigen as observed from native gradient PAGE and Western blot (OPG; Fig. 1B and Supplementary Fig. S4) and commercial enzyme-linked immunosorbent assay (ELISA) (PGRN, OPG; Fig. 1C).

When tested in an in vitro RANKL-signalling reporter assay, plasma from anti-OPG seropositive patients enhanced RANKL-signalling, which was not observed with plasma from antibody-negative individuals (Fig. 1D). The addition of a therapeutic anti-RANKL monoclonal antibody (denosumab biosimilar) reversed enhanced RANKL-signalling in the presence of seropositive plasma in a dose-dependent manner (Fig. 1D).

Isoelectric focusing revealed a hyperphosphorylated OPG isoform in seropositive patients, characterized by a more negatively charged protein band profile than observed in seronegative axSpA patients or healthy controls (Fig. 1E). Alkaline phosphatase treatment abrogated this pattern (Fig. 1F).

Mutagenesis of phosphorylation sites and subsequent expression in lymphoblastoid cell lines (LCLs) identified tyrosine 92 (Y92) as a differential phosphorylation site specific to anti-OPG-seropositive patients (Fig. 1G). In PGRN-autoantibody-positive axSpA patients, we detected a previously reported hyperphosphorylated pSer81 isoform of PGRN using an already established phospho-specific ELISA (Supplementary Fig. S4) [5].

Collectively, our present data confirm and extend previous observations on autoantibodies targeting anti-inflammatory mediators in axSpA. Strikingly, the prevalence of anti-OPG antibodies in our cohort (8.7%) matches an earlier report (8.2%) [7]. Using an alternative RANKL-reporter assay compared with a previous study [8], we independently validated their proinflammatory, RANKL-enhancing activity and demonstrated that this effect is reversible with therapeutic RANKL blockade. Unlike earlier studies [2], we did not detect CD74-targeting autoantibodies.

Consistent with prior findings in other autoimmune conditions [3–5], autoantibodies in axSpA were associated with atypical, hyperphosphorylated isoforms of their target antigens. For PGRN, this corresponds to pSer81 [5], whereas for OPG, we identified phosphorylation at Y92 unique to seropositive patients. These modifications may promote breaking of tolerance and autoantibody generation, but longitudinal sampling is required to confirm temporal relationships.

Thus, using independent methodology and cohorts, our data not only provide the first validation regarding presence and

Christoph Kessel and Lorenz Thurner shared last authorship of this study.

https://doi.org/10.1016/j.ard.2026.04.008
Received 30 September 2025; Revised 19 April 2026; Accepted 20 April 2026

0003-4967/© 2026 European Alliance of Associations for Rheumatology (EULAR). Published by Elsevier B.V. All rights are reserved, including those for text and data mining, AI training, and similar technologies.

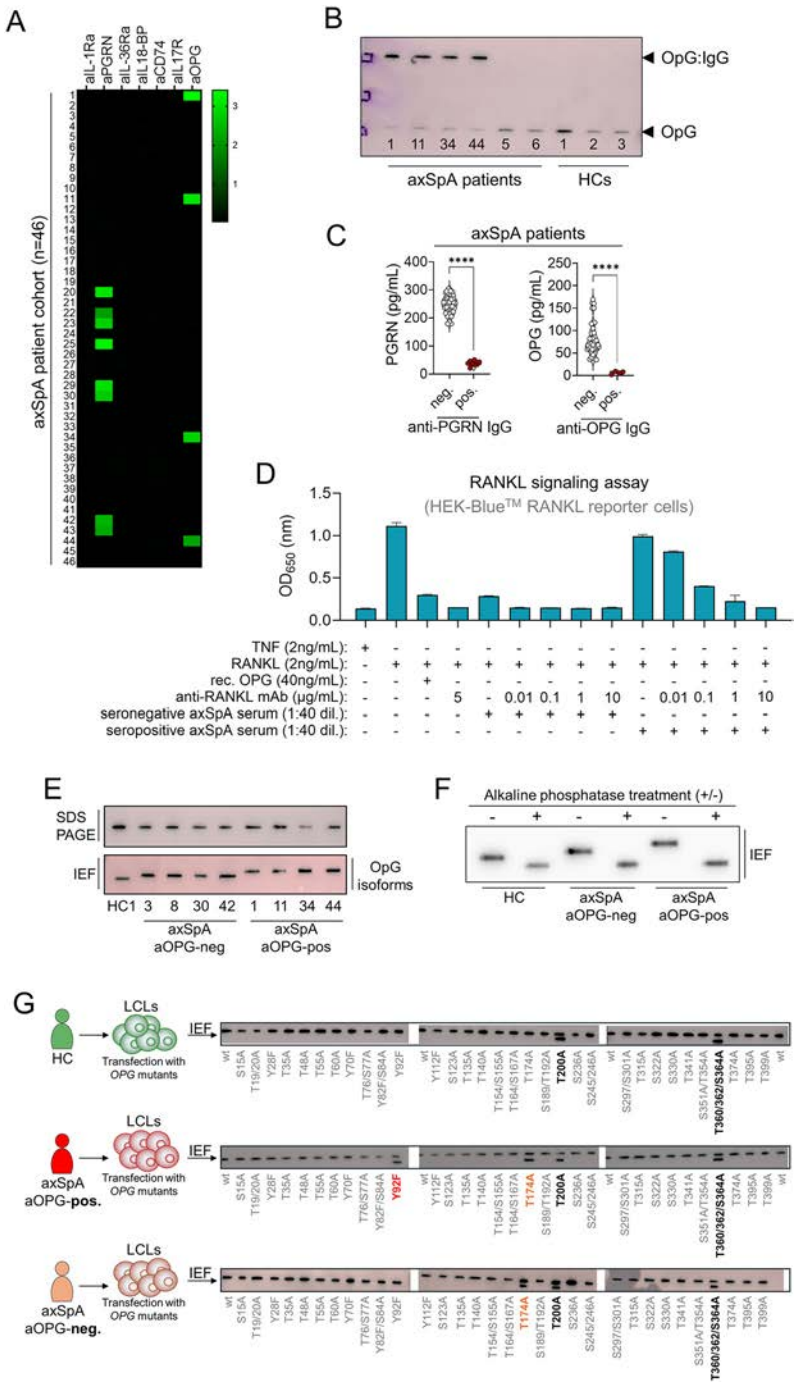

Figure 1. Neutralising autoantibodies targeting OPG and other anti-inflammatory mediators in axSpA. A, Autoantibodies targeting the indicated antigens in axSpA patients (n = 46) were detected by in-house ELISA. Colorimetric data (OD_{490} nm) are presented as a heatmap. B, Western blot of native gradient PAGE for OPG:IgG immune complexes. C, Plasma levels of PGRN (left) and OPG (right) as determined by respective commercial ELISA are depicted according to respective autoantibody status in patients with axSpA (n = 46). D, RANKL-signalling assay using HEK-Blue RANKL-reporter cells. A Denusomab biosimilar was used as a recombinant monoclonal anti-RANKL antibody. E, SDS-PAGE and isoelectric focusing (IEF) analysis followed by Western blotting of plasma from indicated donors, with or without anti-OPG autoantibodies. F, IEF and Western blot of plasma from indicated donors following no treatment or pretreatment with alkaline phosphatase. G, LCLs were derived from 1 healthy donor (upper panels) as well as 1 axSpA patient who tested positive (center panels) and 1 axSpA patient testing negative for anti-OPG autoantibodies (lower panels). LCLs were transfected with C-terminally FLAG-tagged mutants of OPG. Amino acid exchanges affecting OPG isoform-formation are given health controls, and axSpA patients are given in black. Amino acid exchanges affecting OPG isoform-formation only in axSpA patients are given in orange, and the one (Y92) specific to axSpA patients seropositive for anti-OPG autoantibodies in red font. axSpA, axial spondyloarthritis; ELISA, enzyme-linked immunosorbent assay; FLAG, polypeptide (DYKDDDDK) recombinant protein tag; HC, healthy control; IgG, immunoglobulin G; LCLs, lymphoblastoid cell lines; OPG, osteoprotegerin; PAGE, polyacrylamide gel electrophoresis; PGRN, progranulin; RANKL, receptor activator of nuclear factor κB ligand; SDS, sodium dodecyl sulfate.

functional impact of anti-OPG autoantibodies in axSpA but also add novel molecular details. Together, this reinforces the antibodies' role in depleting OPG and enhancing in vitro RANKL signalling. Together with anti-PGRN antibodies, these findings highlight a subgroup of axSpA patients in whom proinflammatory autoantibodies may contribute to disease, which requires to be tested in further studies. Importantly, the pathogenic effect of anti-OPG antibodies could be countered by a therapeutic anti-RANKL mAb, suggesting a potential stratified therapeutic approach for seropositive individuals.

CRediT authorship contribution statement

Zanir Abdi: Writing – review & editing, Methodology, Investigation, Data curation. **Natalie Fadle:** Writing – review & editing, Validation, Supervision, Project administration, Methodology, Formal analysis. **Evi Regitz:** Writing – review & editing, Methodology, Formal analysis. **Igor Age Kos:** Writing – review & editing, Data curation. **Onur Cetin:** Writing – review & editing, Data curation. **Klaus-Dieter Preuss:** Methodology. **Marina Zaks:** Writing – review & editing, Data curation. **Philipp Klemm:** Writing – review & editing, Data curation. **Frank Neumann:** Writing – review & editing, Data curation, Resources. **Moritz Bewarder:** Writing – review & editing, Resources. **Philipp B Staber:** Resources. **Bernhard Thurner:** Writing – review & editing, Conceptualization. **Christoph Kessel:** Writing – review & editing, Project administration, Methodology, Formal analysis, Data curation, Writing – original draft, Visualization, Software. **Lorenz Thurner:** Validation, Supervision, Project administration, Methodology, Formal analysis, Data curation, Conceptualization, Writing – original draft, Visualization, Investigation, Funding acquisition.

Funding

This study was funded by a grant of the Schwiete-Stiftung to LTh and CK. CK also receives support from the German Research Foundation (DFG, grant number KE 2026/3-1).

Competing interests

CK has received consulting fees from Novartis and Swedish Orphan Biovitrum (SOBI) (<$10,000 each) and received research support from Novartis (>$10,000). No other disclosures relevant to this article were reported. University of Saarland with LT among other researchers filed a patent regarding progranulin as a marker for autoimmune diseases. LT and CK reports financial support was provided by Dr Rolf M Schwiete Foundation. CK reports financial support was provided by German Research Foundation, reports a relationship with Novartis that includes consulting or advisory, reports a relationship with SOBI that includes consulting or advisory, and reports a relationship with Novartis that includes funding grants. LT has patent progranulin as marker for autoimmune disorders licensed to Universitaet des Saarlandes. The other authors have no competing interests to declare.

Patient consent for publication

Not applicable.

Ethics approval

This study was approved by the local Ethics Committee (Ärztekammer des Saarlandes; approval number 215/24).

Provenance and peer review

Not commissioned; externally peer reviewed.

Supplementary materials

Supplementary material associated with this article can be found in the online version at doi:10.1016/j.ard.2026.04.008.

REFERENCES

[1] Ramiro S, Nikiphorou E, Sepriano A, Ortolan A, Webers C, Baraliakos X, et al. ASAS-EULAR recommendations for the management of axial spondyloarthritis: 2022 update. Ann Rheum Dis. 2023;82(1):19–34.
[2] Steimer A, Gotschi A, Witte T, Scherer A, Brandli J, Nissen MJ, et al. Anti-CD74 autoantibodies in axial spondyloarthritis as biomarkers for activity and severity of disease but not for tumour necrosis factor inhibitor retention: data from the Swiss Clinical Quality Management in rheumatic diseases cohort. Clin Rheumatol. 2025;44(4):1589–96.
[3] Hoffmann MC, Cavalli G, Fadle N, Cantoni E, Regitz E, Fleser O, et al. Autoantibody-mediated depletion of IL-1RA in Still's disease and potential impact of IL-1 targeting therapies. J Clin Immunol. 2024;44(2):45.
[4] Hoffmann MC, Fadle N, Regitz E, Kos IA, Cetin O, Lesan V, et al. Autoantibody mediated deficiency of IL-36-receptor antagonist in a subset of patients with psoriasis and psoriatic arthritis. Immunol Lett. 2024;270:106926.
[5] Thurner L, Preuss KD, Fadle N, Regitz E, Klemm P, Zaks M, et al. Progranulin antibodies in autoimmune diseases. J Autoimmun. 2013;42:29–38.
[6] Jarrell JA, Baker MC, Perugino CA, Liu H, Bloom MS, Maehara T, et al. Neutralizing anti-IL-1 receptor antagonist autoantibodies induce inflammatory and fibrotic mediators in IgG4-related disease. J Allergy Clin Immunol. 2022;149(1):358–68.
[7] Hauser B, Zhao S, Visconti MR, Riches PL, Fraser WD, Piec I, et al. Autoantibodies to osteoprotegerin are associated with low hip bone mineral density and history of fractures in axial spondyloarthritis: a cross-sectional observational study. Calcif Tissue Int. 2017;101(4):375–83.
[8] Riches PL, McRorie E, Fraser WD, Determann C, van't Hof R, Ralston SH. Osteoporosis associated with neutralizing autoantibodies against osteoprotegerin. N Engl J Med. 2009;361(15):1459–65.

Zanir Abdi, Natalie Fadle, Evi Regitz, Igor Age Kos, Onur Cetin, Klaus-Dieter Preuss
José Carreras Center for Immuno- and Gene Therapy, Department of Internal Medicine I, Saarland University Medical School, Homburg/Saar, Germany

Marina Zaks
Department of Nephrology and Medical Intensive Care, Charité - Universitätsmedizin Berlin, corporate member of Freie Universität Berlin and Humboldt-Universität zu Berlin, Berlin, Germany

Philipp Klemm
Department of Rheumatology, Clinical Immunology, Osteology and Physical Medicine, Justus Liebig University Giessen, Campus Kerckhoff, Bad Nauheim, Germany

Frank Neumann
José Carreras Center for Immuno- and Gene Therapy, Department of Internal Medicine I, Saarland University Medical School, Homburg/Saar, Germany

Moritz Bewarder
José Carreras Center for Immuno- and Gene Therapy, Department of Internal Medicine I, Saarland University Medical School, Homburg/Saar, Germany
Agaplesion Bethanien Hospital, Department of Hematology and Oncology, Frankfurt a.M., Germany

Philipp B Staber
José Carreras Center for Immuno- and Gene Therapy, Department of Internal Medicine I, Saarland University Medical School, Homburg/Saar, Germany

Bernhard Thurner
Department of Pediatrics, Klinikum Kempten, Kempten, Germany

Christoph Kessel
Department of Pediatric Rheumatology and Immunology, University Children's Hospital Münster, Münster, Germany

Lorenz Thurner*
José Carreras Center for Immuno- and Gene Therapy, Department of Internal Medicine I, Saarland University Medical School, Homburg/Saar, Germany

*Correspondence to Dr Lorenz Thurner, José Carreras Center for Immuno- and Gene Therapy, Department of Internal Medicine I, Saarland University Medical School, Homburg/Saar, Germany.
E-mail address: Lorenz.thurner@uks.eu (L. Thurner).

Ann Rheum Dis 85 (2026) e89–e90

Contents lists available at ScienceDirect

Annals of the Rheumatic Diseases

journal homepage: https://www.sciencedirect.com/journal/annals-of-the-rheumatic-diseases

Correspondence

Correspondence on 'Upadacitinib vs adalimumab in patients with rheumatoid arthritis and a prior inadequate response or intolerance to a tumour necrosis factor inhibitor: 12-week results from the randomised, double-blind, SELECT-SWITCH study' by Mysler et al

The SELECT-SWITCH (A Study of Upadacitinib Compared With Adalimumab in Subjects With Rheumatoid Arthritis Who Have Inadequate Response or Intolerance to a TNF Inhibitor) trial by Mysler et al [1] addresses a clinically relevant question: after failure of a first tumour necrosis factor inhibitor (TNFi), should patients switch mechanisms or cycle to another TNFi? The authors conclude that upadacitinib is superior to adalimumab. This conclusion, however, is not supported by the data because the primary endpoint (Disease Activity Score 28-joints C-reactive protein (DAS28-CRP) ≤ 3.2) is systematically biased in favour of upadacitinib, and the control arm does not reflect true TNFi cycling.

Firstly, the primary endpoint (DAS28-CRP ≤ 3.2) is inherently biased in favour of Upadacitinib (UPA). Janus kinase (JAK) inhibitors directly suppress hepatic CRP synthesis, independent of their anti-inflammatory effects [2]. Figure 5H [1] shows a greater reduction in High-sensitivity C-reactive protein with UPA (least squares mean change: −13.5 vs −8.3 mg/L; nominal $P < .001$). Because DAS28-CRP assigns 30% of its weight to CRP, pharmacologic CRP-lowering artificially inflates response rates with UPA. Critically, CRP-independent remission endpoints, ie, Disease Activity Score 28-joints Erythrocyte Sedimentation Rate < 2.6 (15.9% vs 10.2%; Fig 3B [1]) and Clinical Disease Activity Index ≤ 2.8 (8.6% vs 4.5%; Fig 3C [1]), showed no statistically significant differences (both nominal $P > .05$). The authors acknowledge this limitation but did not prespecify a CRP-independent coprimary endpoint, rendering the claim of 'superiority' unsubstantiated for truly disease-driven outcomes.

Secondly, the study population does not reflect real-world 'cycling' to a second TNFi. Patients with prior Adalimumab (ADA) failure were excluded (Table 1 shows that only 1 patient had prior ADA [1]). Yet the control arm received ADA, and the conclusion advocates 'cycling to a second TNFi' after a first TNFi failure. In clinical practice, patients who cycle to a second TNFi have typically failed the first TNFi, and the second TNFi often shows reduced efficacy due to class-level nonresponse [3]. By excluding ADA-experienced patients, the study tests ADA in a population that is essentially ADA-naïve, thereby overestimating the expected response to TNFi cycling. The reported ADA response rate (22.4% for DAS28-CRP ≤ 3.2) is therefore not generalisable to true cycling scenarios.

Thirdly, the statistical interpretation of secondary endpoints violates multiplicity control. The step-down procedure was applied only to the 5 ranked secondary endpoints (American College of Rheumatology (ACR)50, DAS28-CRP < 2.6, DAS28-CRP change, pain, and Health Assessment Questionnaire Disability Index). However, the paper repeatedly cites nominal P values for unranked endpoints (eg, ACR20: 67.7% vs 55.4%, nominal $P = .005$; ACR70: 18.8% vs 9.3%, nominal $P = .0025$; Fig 4A,C [1]). With more than 20 secondary comparisons, the probability of at least 1 false-positive finding exceeds 0.64. The authors provide no adjustment for these, nor do they label them as exploratory.

Finally, the 12-week duration is insufficient to claim comparable safety for events with known delayed onset. No Major Adverse Cardiovascular Events or Venous Thromboembolism occurred, but JAK inhibitors carry boxed warnings for these events that may occur after 6 to 12 months [4]. The statement that 'safety was generally comparable' (abstract) is misleading without a longer follow-up, especially given that 72.1% of patients had ≥1 cardiovascular risk factor.

Competing interests

The authors declare no competing interests.

CRediT authorship contribution statement

Wenpeng Zhang: Conceptualization, Data curation, Writing – original draft, Writing – review & editing. **Yiwen Ding:** Conceptualization, Data curation, Writing – original draft, Writing – review & editing. **Xiaowei Zhang:** Conceptualization, Data curation, Writing – original draft, Writing – review & editing. **Meng Dong:** Conceptualization, Data curation, Writing – original draft, Writing – review & editing.

Funding

No funding was received for this study.

https://doi.org/10.1016/j.ard.2026.04.014
Received 24 April 2026; Accepted 28 April 2026

0003-4967/© 2026 European Alliance of Associations for Rheumatology (EULAR). Published by Elsevier B.V. All rights are reserved, including those for text and data mining, AI training, and similar technologies.

Patient consent for publication

No patient consent was required for this publication.

Ethics approval

Ethics approval was not required for this study.

Provenance and peer review

Not commissioned; externally peer reviewed.

REFERENCES

[1] Mysler E, Sidiropoulos PI, Balanescu A, Detert J, Xavier RM, Charles-Schoeman C, et al. Upadacitinib vs adalimumab in patients with rheumatoid arthritis and a prior inadequate response or intolerance to a tumour necrosis factor inhibitor: 12-week results from the randomised, double-blind, SELECT-SWITCH study. Ann Rheum Dis 2026;85(Suppl 2):A123–4. doi: 10.1136/ard-2026-228976.

[2] Schwartz DM, Kanno Y, Villarino A, Ward M, Gadina M, O'Shea JJ. JAK inhibition as a therapeutic strategy for immune and inflammatory diseases. Nat Rev Drug Discov. 2017;16(12):843–62. doi: 10.1038/nrd.2017.201.

[3] Johnson KJ, Sanchez HN, Schoenbrunner N. Defining response to TNF-inhibitors in rheumatoid arthritis: the negative impact of anti-TNF cycling and the need for a personalized medicine approach to identify primary non-responders. Clin Rheumatol. 2019;38(11):2967–76. doi: 10.1007/s10067-019-04684-1.

[4] Ytterberg SR, Bhatt DL, Mikuls TR, Koch GG, Fleischmann R, Rivas JL, et al. Cardiovascular and cancer risk with tofacitinib in rheumatoid arthritis. N Engl J Med 2022;386(4):316–26. doi: 10.1056/NEJMoa2109927.

Wenpeng Zhang[1,a], Yiwen Ding[2,a], Xiaowei Zhang[1], Meng Dong[1,*]

[1] *Department of Orthopedics, Zibo Central Hospital, Zibo, Shandong, China*

[2] *Department Of Ultrasound, Zibo Central Hospital, No 54, Zibo, China*

*Correspondence to Dr Meng Dong, Department of Orthopedics, Zibo Central Hospital, Zibo, Shandong, China.

E-mail address: liondmqn@163.com (M. Dong).

[a]Wenpeng Zhang and Yiwen Ding are cofirst authors.

Ann Rheum Dis 85 (2026) e91–e93

Contents lists available at ScienceDirect

Annals of the Rheumatic Diseases

journal homepage: https://www.sciencedirect.com/journal/annals-of-the-rheumatic-diseases

Response

Response to correspondence on 'Upadacitinib vs adalimumab in patients with rheumatoid arthritis and a prior inadequate response or intolerance to a tumour necrosis factor inhibitor: 12-week results from the randomised, double-blind, SELECT-SWITCH study' by Mysler et al

We thank Zhang et al [1] for their comments on our recently published phase 3 study evaluating upadacitinib (UPA) vs adalimumab (ADA) for the treatment of rheumatoid arthritis in patients with a prior inadequate response or intolerance to a tumour necrosis factor inhibitor (TNFi; SELECT-SWITCH, NCT05814627) [2], which provides us with an opportunity to clarify key findings from this trial.

The authors raised the following 4 concerns: (1) the primary endpoint of disease activity score 28-joint count C-reactive protein (DAS28-CRP) <3.2 is biased in favour of UPA; (2) the study population did not reflect a real-world scenario, as patients with prior ADA use were not allowed to be enrolled; (3) inappropriate interpretation of secondary endpoints, which were not multiplicity-controlled; and (4) one cannot state comparable safety after a 12-week observation duration.

With respect to their first point, we agree that the use of DAS28-CRP favours UPA because of the direct effect of Janus kinase inhibition on C-reactive protein (CRP) compared with TNFi, as we discussed in the limitations section of our manuscript [2]. We also acknowledge that DAS28-CRP has been shown to capture deeper clinical response rates than the DAS28-erythrocyte sedimentation rate (ESR), the Clinical Disease Activity Index (CDAI), and the Simplified Disease Activity Index [3]. However, we explained that DAS28-CRP < 3.2 was selected as the primary endpoint because: (1) it is an endpoint favoured by the European Medicines Agency [4]; (2) CRP is a consistent central laboratory metric rather than one that introduces a high likelihood of variable results (for instance, ESR must be performed locally); and (3) the primary endpoint for SELECT-SWITCH was consistent with the design of the previous SELECT-BEYOND study of UPA in biologic-inadequate responders, which was comprised predominantly of TNFi-inadequate responders, representing approximately 90% of the population [5]. It should also be noted that DAS28-CRP is commonly used in real-world clinical practice, where treatment decisions are often made based on this assessment.

Given the limitations of DAS28-CRP described above, we selected additional endpoints for analysis that were non−CRP-dependent. These included DAS28-ESR and CDAI, which served as internal barometers of the accuracy of our results. Both DAS28-ESR $\leq$ 3.2 and CDAI $\leq$ 10 showed numerical improvement in UPA over ADA at week 12, with nominal *P* value of <.0001 [2]. As anticipated, assessment of DAS28-ESR < 2.6 and CDAI < 2.8 yielded low responses in all treatment arms, and while response rates numerically favoured UPA, with an approximate doubling of responses relative to ADA, these low absolute response rates and the available sample size limited the ability to detect clear treatment differences for these endpoints. For these reasons, we maintain that the superiority of UPA over ADA was demonstrated using the validated DAS28-CRP metric and confirmed by additional non−CRP-dependent endpoints, DAS28-ESR and CDAI, both of which are validated composite scores. In addition, the clinical efficacy observed in both the ADA and UPA treatment arms in SELECT-SWITCH is consistent with that reported in previous studies of similar patient populations [5,6]. The ADA arm is consistent with the EXXELERATE trial in a similar TNFi nonresponder population, supporting the reproducibility and validity of our findings on ADA's efficacy [6], while the efficacy outcomes for UPA are consistent with those reported in the aforementioned SELECT-BEYOND study [5].

The second concern expressed by Zhang et al [1] is that the study population did not reflect 'real-world' cycling to a second TNFi, as prior use of ADA was not allowed. In clinical practice, reinitiating the same treatment after prior failure or intolerance is uncommon and does not align with clinical recommendations (eg, the European Alliance of Associations for Rheumatology [EULAR] [7] or American College of Rheumatology [ACR] guidelines [8]). Indeed, if a patient is not responding to their current treatment, retreatment with the same medication is unlikely to yield a better response and would therefore be against treat-to-target principles, potentially raising medical and ethical concerns. In addition, if we had allowed prior failure of ADA for study entry, this would have biased the results in favour of UPA; as above, a patient who failed ADA and was randomised to ADA would be unlikely to respond to or continue ADA. For these

DOI of original article: http://dx.doi.org/10.1016/j.ard.2026.04.014.

https://doi.org/10.1016/j.ard.2026.05.026
Received 14 May 2026; Accepted 16 May 2026

0003-4967/© 2026 European Alliance of Associations for Rheumatology (EULAR). Published by Elsevier B.V. All rights are reserved, including those for text and data mining, AI training, and similar technologies.

reasons, patients with prior exposure to a planned control treatment in a randomised clinical trial are typically excluded.

Regarding the third point on the statistical interpretation of nonranked additional endpoints, the statistical methodology of SELECT-SWITCH included a prespecified hierarchical step-down procedure applied only to the 5 ranked secondary endpoints. The unranked endpoints, such as ACR20 and ACR70, were not part of the formal multiplicity-controlled testing strategy; they were included as additional and not secondary endpoints. Furthermore, the corresponding *P* values are nominal (raw), unadjusted values and should not be interpreted as multiplicity-adjusted inferential claims.

Finally, we are not entirely clear what Zhang et al [1] are questioning regarding the comparability of the week 12 safety results for UPA and ADA. As described in the article, the safety profile of UPA was generally comparable across SELECT-SWITCH and other SELECT clinical trials at 12 weeks [2,5,9]. While adverse events of special interest, including major adverse cardiovascular events (MACEs), venous thromboembolism (VTE), and malignancy, were assessed, no analysis was performed relating them to baseline cardiovascular (CV) risk factors not just because the 12-week duration was too short to observe these events but more importantly, because the study population was too small to detect clinically meaningful differences in these events, which occur relatively rarely. As such, we did not make any claims or conclusions regarding the risk of these events in this patient population. However, the long-term CV safety of UPA in patients with rheumatoid arthritis has been previously characterised in multiple studies with larger populations and longer treatment durations, including analyses of >12,000 patient-years of exposure and analyses of patients with baseline CV risk [10,11]. The ongoing SELECT-SWITCH study will continue to evaluate safety data up to 48 weeks; however, it is important to note again that the study is not powered to detect statistical differences between UPA and ADA for adverse events, particularly rare safety events such as MACE, VTE, and malignancy.

Contributors

RF and EM drafted the manuscript, and medical writing support was provided by Karen B Chien, PhD, of AbbVie.

Competing Interests

RF is a consultant for AbbVie, Almirall, AnaptysBio, Artiva Biotherapeutics, Atomwise, Biohaven Pharmaceuticals, Bristol Myers Squibb, Cyxone, DeepCure, Dren Bio, Ecor, Eisai, Eli Lilly, Galvani Bioelectronics, Gates Biomanufacturing Facility, Genentech, Gilead Sciences, GSK, Halia Therapeutics, Immunovant, ImmuneMed, InventisBio, Istesso, Janssen, Janux Therapeutics, MSD, Monte Rosa Therapeutics, Overland Pharmaceuticals, Novartis, Pfizer, Roche, R-Pharm, SynAct Pharma, TPG, UCB, VYNE Therapeutics, and Xencor. ON and JR are employees of AbbVie and may hold stock or options. EM has received or has pending grants from AbbVie, Bristol Myers Squibb, Eli Lilly, Novartis, Pfizer, and Roche; he has received honoraria from AbbVie, AnaptysBio, AstraZeneca, Biogen, Eli Lilly, GSK, MSD, Pfizer, Roche, Sandoz, and Sanofi; has provided writing assistance, medicines, equipment, or administrative support to AbbVie, Pfizer, and Roche; and has received payment for lectures, including service on speaker's bureaus, from AbbVie, Alpine Immune Sciences, Amgen, AstraZeneca, GSK, Eli Lilly, Hi-Bio, Janssen, Novartis, Pfizer, Roche, Sandoz, and Sanofi.

Funding

The sponsor (AbbVie) designed the trial, and the investigators and sponsor jointly gathered data. The sponsor analysed the data and provided medical writing support; the sponsor and authors interpreted the data. All authors reviewed and approved the manuscript, had access to the data, and decided to submit the manuscript for publication.

Patient consent for publication

Not applicable.

Ethics approval

Not applicable.

Provenance and peer review

Commissioned; internally peer reviewed.

Orcid

Eduardo Mysler: http://orcid.org/0000-0002-8993-0313

REFERENCES

[1] Zhang W, Ding Y, Zhang X, Dong M. Correspondence on 'Upadacitinib vs adalimumab in patients with rheumatoid arthritis and a prior inadequate response or intolerance to a tumour necrosis factor inhibitor: 12-week results from the randomised, double-blind, SELECT-SWITCH study' by Mysler et al. Ann Rheum Dis 2026. doi: 10.1016/j.ard.2026.04.014.

[2] Mysler E, Sidiropoulos PI, Balanescu A, Detert J, Xavier RM, Charles-Schoeman C, et al. Upadacitinib vs adalimumab in patients with rheumatoid arthritis and a prior inadequate response or intolerance to a tumour necrosis factor inhibitor: 12-week results from the randomised, double-blind, SELECT-SWITCH study. Ann Rheum Dis. 2026 in press. doi: 10.1016/j.ard.2026.03.013.

[3] Fleischmann R, Haraoui B, Buch MH, Gold D, Sawyerr G, Shi H, et al. Analysis of disease activity metrics in a methotrexate withdrawal study among patients with rheumatoid arthritis treated with tofacitinib plus methotrexate. Rheumatol Ther. 2023;10(2):375–86. doi: 10.1007/s40744-022-00511-3.

[4] European Medicines Agency. Guideline on clinical investigation of medicinal products for the treatment of rheumatoid arthritis [Internet]. [cited 2026 Apr 26]. Available from: https://www.ema.europa.eu/en/documents/scientific-guideline/guideline-clinical-investigation-medicinal-products-treatment-rheumatoid-arthritis_en.pdf.

[5] Genovese MC, Fleischmann R, Combe B, Hall S, Rubbert-Roth A, Zhang Y, et al. Safety and efficacy of upadacitinib in patients with active rheumatoid arthritis refractory to biologic disease-modifying anti-rheumatic drugs (SELECT-BEYOND): a double-blind, randomised controlled phase 3 trial. Lancet. 2018;391(10139):2513–24. doi: 10.1016/S0140-6736(18)31116-4.

[6] Smolen JS, Burmester GR, Combe B, Curtis JR, Hall S, Haraoui B, et al. Head-to-head comparison of certolizumab pegol versus adalimumab in rheumatoid arthritis: 2-year efficacy and safety results from the randomised EXXELERATE study. Lancet. 2016;388(10061):2763–74. doi: 10.1016/S0140-6736(16)31651-8.

[7] Smolen JS, Edwards CJ, Konzett V, Laskou F, Aletaha D, Caporali R, et al. EULAR recommendations for the management of rheumatoid arthritis with synthetic and biologic disease-modifying antirheumatic drugs: 2025 update. Ann Rheum Dis 2026;85(6):991–1009. doi: 10.1016/j.ard.2026.01.023.

[8] Fraenkel L, Bathon JM, England BR, St Clair EW, Arayssi T, Carandang K, et al. 2021 American College of Rheumatology guideline for the treatment of rheumatoid arthritis. Arthritis Care Res (Hoboken). 2021;73(7):924–39. doi: 10.1002/acr.24596.

[9] Fleischmann RM, Blanco R, Hall S, Thomson GTD, Van den Bosch FE, Zerbini C, et al. Switching between Janus kinase inhibitor upadacitinib and adalimumab following insufficient response: efficacy and safety in patients with rheumatoid arthritis. Ann Rheum Dis. 2021;80(4):432–9. doi: 10.1136/annrheumdis-2020-218412.

[10] Burmester GR, Deodhar A, Irvine AD, Panaccione R, Winthrop KL, Vleugels RA, et al. Safety profile of upadacitinib: descriptive analysis in over 27,000 patient-years across rheumatoid arthritis, psoriatic arthritis, axial spondyloarthritis, atopic dermatitis, and inflammatory bowel disease. Adv Ther. 2025;42(10):5215–37. doi: 10.1007/s12325-025-03328-y.
[11] Fleischmann R, Curtis JR, Charles-Schoeman C, Mysler E, Yamaoka K, Richez C, et al. Safety profile of upadacitinib in patients at risk of cardiovascular disease: integrated post hoc analysis of the SELECT phase III rheumatoid arthritis clinical programme. Ann Rheum Dis. 2023;82(9):1130–41. doi: 10.1136/ard-2023-223916.

Roy Fleischmann
Metroplex Clinical Research Center, University of Texas Southwestern Medical Center, Dallas, TX, USA

Orsolya Nagy
AbbVie Ltd, Budapest, Hungary

Jingchen Ren
AbbVie Inc, North Chicago, IL, USA

Eduardo Mysler *

*Correspondence to Dr Eduardo Mysler, Department of Rheumatology, Organización Medica de Investigación, Buenos Aires, Argentina.
E-mail address: e.mysler@omiargentina.com.ar (E. Mysler).

Ann Rheum Dis 85 (2026) e94–e95

Contents lists available at ScienceDirect

Annals of the Rheumatic Diseases

journal homepage: https://www.sciencedirect.com/journal/annals-of-the-rheumatic-diseases

Correspondence

Correspondence on 'Results of a 1-year randomised double-blind placebo-controlled trial with methotrexate 25 mg/week in recently diagnosed polymyalgia rheumatica' by Bolhuis *et al*

Dear Editor,

Evidence on methotrexate (MTX) efficacy as a glucocorticoid (GC)-sparing agent in polymyalgia rheumatica (PMR) is conflicting, likely due to low-dose treatment (<10 mg/wk). In their study, Bolhuis et al [1] showed that early use of higher-dose MTX (25 mg/wk) in patients with recently diagnosed PMR is associated with a significantly lower incidence of relapse and a faster time to GC-free remission. Interestingly, a similar previous study showed that low-dose MTX is associated with shorter prednisone treatment, steroid sparing, and fewer flares [2]. To avoid misleading conclusions, adjustment between groups is needed for factors that affect the required dose of steroids and steroid-sparing drugs, such as evidence of arthritis.

Patient characteristics indicate that about 1 in 5 participants on placebo and 7% of those on MTX had peripheral arthritis (Table 1) [1]. Additionally, the total number of flares over 52 weeks was 31 in the MTX group, compared with 45 in the placebo group (Table 2) [1]. It is unclear whether the flares are due to the PMR disease itself or to underlying associated arthritis.

Relapse was defined in the study based on the treating physician's clinical judgment, without clear criteria. However, remission was well defined using the Polymyalgia Rheumatica-Activity Score (PMR-AS), calculated as follows: C-reactive protein (mg/dL) + (duration of morning stiffness [in minutes] × 0.1) + elevation of upper limbs (ranging 0-3) + visual analogue score (VAS) for pain (ranging 0-10) + VAS physician's global (ranging 0-10) [1,2] Relapses could be disease-related when there is a sudden increase in clinical complaints of pain and stiffness and in inflammatory markers. However, they could be non–disease-related when the increase in global complaints is due to GC withdrawal symptoms or partial adrenal insufficiency. So, counting relapse episodes without a clear definition of a flare could be misleading.

Moreover, PMR-AS values <1.5 indicate remission, <7 low disease activity, 7 to 17 moderate disease activity, and >17 high disease activity [3]. Currently, there is no consensus in the literature on the optimal cut-off for differentiating active from inactive disease, but PMR-AS <10 is an acceptable threshold [3]. In their study, Bolhuis and coauthors used a cut-off of <10 and no GC use to define remission (Table 2) [1]. Surprisingly, the median PMR-AS at baseline in both groups and during the trial (Fig 3) was around 6 to 7 (Table 1), indicating that study participants at trial entry had only modest disease activity or even remission [1]. All PMR-AS values were below the remission cut-off throughout the 1-year study duration, with outcomes ranging from on-GCs to off-GCs [1]. I wonder why the study's inclusion criteria were designed to include patients with such a low level of active PMR.

In their trial, MTX at appropriate doses significantly increased the likelihood of achieving GC-free remission, reduced the incidence of relapse, and shortened the time to GC-free remission in patients with recently diagnosed PMR [1]. However, no significant GC-sparing effect was observed [1]. GC-sparing remains the most crucial factor and is clinically relevant in elderly patients with PMR, in whom biological therapy, eg, interleukin-6 receptor inhibitors, is used to minimize GC exposure and its associated adverse effects, especially in the elderly with frequent comorbidities [1,4].

In conclusion, the work by Bolhuis and coauthors did not clarify MTX's role in the evolving treatment landscape for PMR, and further research is needed. To minimize conflicting results, research should incorporate clinical clustering of PMR by subtyping PMR into 4 groups: the classical inflammatory, the soft-tissue rheumatism with extra-articular tendinitis and bursitis, the arthritic and seronegative, and the vasculitic with subclinical large-vessel vasculitis [4,5]. Such subtyping in research and clinical practice could aid in tailoring GC-based treatment and in determining when to add MTX or biologics.

Competing interests

The author reports no conflicts of interest.

CRediT authorship contribution statement

Suhail Aamar: Conceptualization, Data curation, Investigation, Resources, Validation, Visualization, Writing – original draft, Writing – review & editing.

Handling editor Josef S. Smolen.

https://doi.org/10.1016/j.ard.2026.04.015
Received 25 April 2026; Accepted 28 April 2026

0003-4967/© 2026 European Alliance of Associations for Rheumatology (EULAR). Published by Elsevier B.V. All rights are reserved, including those for text and data mining, AI training, and similar technologies.

Funding

None. No financial support.

Patient consent for publication

Not applicable.

Ethics approval

This Letter to the Editor is based exclusively on previously published literature and contains no original data, human subjects research, or identifiable patient information. Therefore, ethics committee/IRB approval was not required.

Provenance and peer review

Not commissioned; externally peer reviewed

Orcid

Suhail Aamar: http://orcid.org/0000-0003-1671-8220

REFERENCES

[1] Bolhuis TE, Kooijman NESEP, Marsman DE, Snijders GF, den Broeder AA, et al. Results of a 1-year randomised double-blind placebo-controlled trial with methotrexate 25 mg/week in recently diagnosed polymyalgia rheumatica. Ann Rheum Dis. 2026;85(4):761–70. doi: 10.1016/j.ard.2025.11.025.

[2] Caporali R, Cimmino MA, Ferraccioli G, Gerli R, Klersy C, Salvarani C, et al. Prednisone plus methotrexate for polymyalgia rheumatica: a randomized, double-blind, placebo-controlled trial. Ann Intern Med. 2004;141(7):493–500. doi: 10.7326/0003-4819-141-7-200410050-00005.

[3] Moreel L, Doumen M, Betrains A, De Langhe E, Blockmans D, Vanderschueren S. Validation of the polymyalgia rheumatica-activity score: a prospective cohort study. Semin Arthritis Rheum 2025;72:152695. doi: 10.1016/j.semarthrit.2025.152695.

[4] Dejaco C, Matteson EL. Polymyalgia Rheumatica. N Engl J Med. 2026;394(11):1097–9. doi: 10.1056/NEJMcp2506817.

[5] Buttgereit F, Boyadzhieva Z, Reisch M, Schneider M, Brabant T, Daikeler T, et al. Recommendations of the German, Austrian and Swiss rheumatology and other medical societies for the management of polymyalgia rheumatica. Rheumatology (Oxford) 2026;65(2):keaf646. doi: 10.1093/rheumatology/keaf646.

Suhail Aamar, MD, MSc [1,2,*]

[1] *Rheumatology Clinic, Hadassah-Hebrew University Medical Center, Mount Scopus Hospital, Jerusalem, Israel*

[2] *Rheumatology Unit, Assuta-Ashdod University Hospital; Faculty of Health Sciences, Ben-Gurion University of the Negev, Beer-Sheva, Israel*

*__Correspondence to__ Dr. Suhail Aamar, Rheumatology Clinic, Hadassah Mount Scopus, Churchill Avn., 8, Jerusalem, Israel.
E-mail address: suhail_aamar@hotmail.com

Ann Rheum Dis 85 (2026) e96–e97

Contents lists available at ScienceDirect

Annals of the Rheumatic Diseases

journal homepage: https://www.sciencedirect.com/journal/annals-of-the-rheumatic-diseases

Correspondence

Response to 'Correspondence on "Results of a 1-year randomized double-blind placebo-controlled trial with methotrexate 25 mg/week in recently diagnosed polymyalgia rheumatica" by Bolhuis TE et al'

To the Editor,

We would like to respond to the 'Correspondence on "Results of a 1-year randomized double-blind placebo-controlled trial with methotrexate 25 mg/week in recently diagnosed polymyalgia rheumatica" by Bolhuis TE et al' [1,2]. First of all, we would like to thank Dr Aamar for the interest in our study and for the opportunity to clarify several aspects of its interpretation. We address the points raised below.

With regard to the distribution of peripheral arthritis, we acknowledge that a numerical imbalance was observed between treatment groups at baseline. This is an inherent feature of randomisation in relatively small sample sizes and does not necessarily induce bias. Confounding in this context seems very unlikely. First, the overall number of patients with peripheral arthritis was limited. Second, peripheral arthritis is recognised within the clinical spectrum of polymyalgia rheumatica, rather than representing a separate disease entity. Finally, the suggestion that peripheral arthritis may be associated with increased glucocorticoid requirements has not been consistently identified as a prognostic factor in the literature, with the majority of studies failing to demonstrate a clear association [3].

Regarding the definition of relapse, we acknowledge that relapse was based on the treating physician's clinical judgment, reflecting the current lack of validated and universally accepted relapse criteria in polymyalgia rheumatica. Although the Polymyalgia Rheumatica Activity Score (PMR-AS) has been applied in defining remission, no validated or widely accepted PMR-AS threshold exists for defining relapse, nor is there evidence to support such PMR-AS guided treat-to-target. However, as shown in the Table, the mean PMR-AS was markedly higher in those judged to have relapsed. Therefore, although the use of clinical judgment for relapse assessment reflects current clinical practice and methodological limitations in the field, it seems unlikely that this has resulted in overly high estimates of relapse rates.

The relatively low PMR-AS values at baseline reflect the inclusion of patients who had already initiated glucocorticoid therapy a few weeks prior to enrolment, as specified in the study design. Baseline disease activity should therefore be interpreted in the context of treated disease rather than untreated polymyalgia rheumatica. In addition, all patients were treated according to a predefined glucocorticoid tapering protocol with close monitoring and treatment adjustments in case of insufficient response or relapse. Therefore, the relatively low PMR-AS values observed during follow-up are as expected with the treatment strategy and do not indicate absence of clinically relevant disease activity.

Although cumulative glucocorticoid exposure did not differ significantly between groups within 52 weeks, this outcome should be interpreted in the context of the study design, including a 24-week predefined tapering regimen and a total follow-up period of 52 weeks. Within this timeframe, cumulative glucocorticoid exposure is largely determined by the tapering protocol and may not fully capture differences in treatment effect. In contrast, glucocorticoid-free remission more directly reflects the ability to successfully discontinue treatment and is therefore expected to be observed earlier. The higher rates of glucocorticoid-free remission in the methotrexate group therefore, in our view, indicate a clinically relevant treatment effect; however, this study does not allow conclusions regarding longer-term glucocorticoid-sparing effects. In addition, it remains possible that this effect is limited, as also discussed in our original manuscript.

Finally, we agree that further research is needed to better define disease heterogeneity and optimize treatment strategies in polymyalgia rheumatica, including the role of methotrexate and its potential glucocorticoid-sparing effects (or its ability to prevent the need for targeted therapy) over longer-term follow-up.

Table
PMR-AS at visits judged as relapse or remission

Physician judgement	Mean PMR-AS (SD)	Median PMR-AS (IQR)
Remission (n = 240)[a]	4.8 (5.4)	3.0 (1.5-6.1)
Relapse (n = 74) [a]	16.8 (11.6)	14.0 (9.6-20.3)

[a] Only scheduled visits with a complete PMR-AS were included in this analysis. PMR-AS were missing or incomplete in 34 of 348 visits.

IQR, interquartile range; PMR-AS, Polymyalgia Rheumatica Activity Score; SD, standard deviation.

DOI of original article: http://dx.doi.org/10.1016/j.ard.2026.04.015.

https://doi.org/10.1016/j.ard.2026.05.027
Received 8 May 2026; Revised 17 May 2026; Accepted 18 May 2026

0003-4967/© 2026 European Alliance of Associations for Rheumatology (EULAR). Published by Elsevier B.V. All rights are reserved, including those for text and data mining, AI training, and similar technologies.

Competing interests

The Sint Maartens hospital received financial support from Dutch Arthritis Foundation (ReumaNederland). Alfons A den Broeder has received grants to the institution for quality of care projects and research outside the current study from AbbVie, Alfasigma, UCB, Galapagos, Pfizer, Novartis, Lilly, Sanofi, Gilead, and Celltrion. Aatke van der Maas received travel and conference reimbursement from AbbVie in 2025. The other authors declare that they have no known competing financial interests or personal relationships.

CRediT authorship contribution statement

Noortje E.S.E.P. Kooijman: Writing – original draft. **Nathan den Broeder:** Writing – review & editing. **Alfons A. den Broeder:** Writing – review & editing. **Aatke van der Maas:** Writing – review & editing.

Funding

The original study was funded by Dutch Arthritis Foundation (ReumaNederland).

Patient consent for publication

Not applicable.

Ethics approval

The original PMR MODE study was approved by the medical ethics committee (NL69979.091.19).

Provenance and peer review

Not commissioned; externally reviewed.

Orcid

Noortje E.S.E.P. Kooijman: http://orcid.org/0000-0001-9125-1187
Nathan den Broeder: http://orcid.org/0000-0001-7126-2209
Alfons A. den Broeder: http://orcid.org/0000-0002-9012-4079
Aatke van der Maas: http://orcid.org/0000-0002-3855-6763

REFERENCES

[1] Aamar S. Correspondence on "Results of a 1-year randomized double-blind placebo-controlled trial with methotrexate 25 mg/week in recently diagnosed polymyalgia rheumatica" by Bolhuis TE et al. Ann Rheum Dis. 2026.
[2] Bolhuis TE, Kooijman NESEP, Marsman DE, Snijders GF, den Broeder AA, den Broeder, et al., et al. Results of a 1-year randomised double-blind placebo-controlled trial with methotrexate 25 mg/week in recently diagnosed polymyalgia rheumatica. Ann Rheum Dis. 2026;85(4):761–70.
[3] Floris A, Piga M, Chessa E, Congia M, Erre GL, Angioni MM, et al. Long-term glucocorticoid treatment and high relapse rate remain unresolved issues in the real-life management of polymyalgia rheumatica: a systematic literature review and meta-analysis. Clin Rheumatol. 2022;41(1):19–31.

Noortje E.S.E.P. Kooijman [1], Nathan den Broeder [1], Alfons A. den Broeder [2,3], Aatke van der Maas [2,*]
[1] *Department of Research, Sint Maartenskliniek, Ubbergen, The Netherlands*
[2] *Department of Rheumatology, Sint Maartenskliniek, Ubbergen, The Netherlands*
[3] *Department of Rheumatology, Radboudumc, Nijmegen, The Netherlands*

*__Correspondence to__ Dr Aatke van der Maas, Department of Rheumatology, Sint Maartenskliniek, Hengstdal 3, 6574 NA, Ubbergen, The Netherlands
E-mail address: a.vandermaas@maartenskliniek.nl (A. van der Maas).

Ann Rheum Dis 85 (2026) e98–e99

Contents lists available at ScienceDirect

Annals of the Rheumatic Diseases

journal homepage: https://www.sciencedirect.com/journal/annals-of-the-rheumatic-diseases

Correspondence

Correspondence on 'EULAR recommendations for the management of rheumatoid arthritis with synthetic and biologic disease–modifying antirheumatic drugs: 2025 update' by Smolen et al and 'Spacing of a TNF inhibitor or dose reduction of methotrexate vs continued treatment in patients with rheumatoid arthritis in remission or low disease activity: a randomised, controlled trial (SORAIRO trial)' by Imai et al

Dear Editor,

In line with 2 recent and interesting articles [1,2] published in Annals of the Rheumatic Diseases, the 2025 European Alliance of Associations for Rheumatology (EULAR) recommendations [1], and the spacing of a TNF inhibitor or dose reduction of methotrexate vs continued treatment in patients with rheumatoid arthritis in remission or low disease activity (the SORAIRO) trial for managing rheumatoid arthritis (RA) [2], I wish to address their significance and highlight some key points. One main issue is the role of conventional synthetic disease–modifying antirheumatic drugs (cs-DMARDs), especially methotrexate (MTX), in maintaining remission, and whether MTX alone is sufficient.

The 2025 EULAR recommendations for managing RA **do not** clarify whether, after achieving sustained remission (for 6-12 months) with combination therapy of MTX and a biological disease–modifying antirheumatic drug (b-DMARD), MTX can be used to maintain remission while tapering the b-DMARD [1]. They state that with sustained remission, disease-modifying antirheumatic drugs (DMARDs) may be tapered, but it is not mentioned in what sequence or which DMARD first. Caution on taper is advised, as discontinuation often leads to flares [1]. The 2021 American College of Rheumatology (ACR) guidelines conditionally recommend continuing DMARDs at a stable dose rather than tapering, and favour discontinuing MTX over stopping a b-DMARD or a targeted synthetic DMARD (ts-DMARD), as the latter is more likely to sustain disease control [3]. This is **an unmet** need to clarify in the 2025 EULAR recommendations, as cost-effectiveness and the sequencing of therapies should be considered in clinical decision-making.

The etanercept and MTX in combination or as monotherapy in subjects with RA (SEAM-RA) trial [4] showed that biologic monotherapy is superior to MTX monotherapy for maintaining remission in RA patients who achieved sustained remission with combination therapy, with a lower risk of flares. However, the intriguing SORAIRO study offered additional insights [2]. It demonstrated that MTX, as the primary DMARD, effectively maintains remission in RA patients and, surprisingly, even in those with aggressive or refractory disease [2]. MTX was given at a relatively low dose (≈8.7 mg weekly) while tumour necrosis factor inhibitors (TNFi) were being tapered, and it was still comparable with maintaining remission when TNFi was the main DMARD and MTX was tapered [2].

One **commentary** on the SORAIRO trial [2] concerns the need for better harmonisation and adjustments to enable a feasible comparison and to avoid misleading interpretations of the results. In the study [2], the ongoing double-treatment arm (TNFi plus MTX) differs from both the spaced TNFi (TNFi-taper) and MTX-reduction (MTX-taper) groups. It seems that the taper groups have more refractory, resistant RA than the continued combined treatment group. First, about half of the participants in the taper groups had prior biologic exposure, likely with an inadequate response, whereas only about a quarter in the continued group [2]. Second, seropositivity for rheumatoid factor and anticyclic citrullinated peptide (CCP) antibodies was higher in the taper groups than in the continued group [2]. Additionally, the latter group used higher doses of concomitant glucocorticoids, which may influence clinical response [2]. Nonetheless, the SORAIRO study emphasises the important role of MTX, even at low doses, after remission induction with combination therapy that includes b-DMARDs, in maintaining remission [2].

The Pan American League of Associations for Rheumatology (PANLAR) 2025 update guidelines recommend that, during tapering in sustained remission (>6-12 months), the b/ts-

DOI of original article: http://dx.doi.org/10.1016/j.ard.2026.06.026.

Handling editor David Pisetsky.

https://doi.org/10.1016/j.ard.2026.05.034
Received 7 April 2026; Accepted 25 May 2026

0003-4967/© 2026 European Alliance of Associations for Rheumatology (EULAR). Published by Elsevier B.V. All rights are reserved, including those for text and data mining, AI training, and similar technologies.

DMARD dose should be reduced first, followed by cs-DMARDs, towards drug-free remission, as costs are significantly reduced [5]. In Latin America and other regions, the economic impact of advanced treatments is particularly significant and may affect drug supply and availability and, consequently, real-world outcomes, resulting in lower treatment retention, increased switching of b/ts-DMARDs, higher rates of refractoriness, and the development of difficult-to-treat (D2T) states.

In line with the 2025 EULAR recommendations suggesting that DMARDs can be tapered once sustained remission is achieved [1,5], the SORAIRO study [2] supports the potential use of MTX to maintain long-term remission, enabling scheduled tapering of double therapy or b-DMARDs. These findings require further validation.

Competing interests

The author reports no conflicts of interest.

CRediT authorship contribution statement

Suhail Aamar: Conceptualization, Data curation, Investigation, Resources, Validation, Writing – original draft, Writing – review & editing.

Funding

None.

Patient consent for publication

Not applicable.

Ethics approval

The manuscript is based exclusively on previously published literature and contains no original data, human subjects research, or identifiable patient information. Therefore, ethics committee/IRB approval was not required.

Provenance and peer review

The manuscript is original, and not considered in an other journal.

Orcid

Suhail Aamar: http://orcid.org/0000-0003-1671-8220

REFERENCES

[1] Smolen JS, Edwards CJ, Konzett V, Laskou F, Aletaha D, Caporali R, et al. EULAR recommendations for the management of rheumatoid arthritis with synthetic and biologic disease-modifying antirheumatic drugs: 2025 update. Ann Rheum Dis. 2026;85(6):991–1009. doi: 10.1016/j.ard.2026.01.023.

[2] Imai Y, Kono M, Ishii T, Kojima T, Hirata S, Tanaka Y, et al. Spacing of a TNF inhibitor or dose reduction of methotrexate vs continued treatment in patients with rheumatoid arthritis in remission or low disease activity: a randomised, controlled trial (SORAIRO trial). Ann Rheum Dis. 2026;85(4):609–19. doi: 10.1016/j.ard.2026.02.004.

[3] Fraenkel L, Bathon JM, England BR, St Clair EW, Arayssi T, Carandang K, et al. 2021 American College of Rheumatology guideline for the treatment of rheumatoid arthritis. Arthritis Care Res (Hoboken). 2021;73(7):924–39. doi: 10.1002/acr.24596.

[4] Curtis JR, Emery P, Karis E, Haraoui B, Bykerk V, Yen PK, et al. Etanercept or methotrexate withdrawal in rheumatoid arthritis patients in sustained remission. Arthritis Rheumatol. 2021;73(5):759–68. doi: 10.1002/art.41589.

[5] Santos Moreno P, García Salinas R, Caballero Uribe CV, Brance ML, Marín Zúcaro NM, Arrieta Vega D, et al. Pan American League of Associations for Rheumatology (PANLAR). Pan American League of Associations for Rheumatology recommendations for the management of rheumatoid arthritis. Lancet Rheumatol. 2026;8(1):e53–65. doi: 10.1016/S2665-9913(25)00259-0.

Suhail Aamar [1,2,3,*]

[1] *Rheumatology Clinic, Hadassah-Hebrew University Medical Center, Mount Scopus Hospital, Jerusalem, Israel*

[2] *Rheumatology Unit, Assuta Ashdod University Hospital, Ashdod, Israel*

[3] *Faculty of Health Sciences, Ben-Gurion University of the Negev, Beer-Sheva, Israel*

*__Correspondence to__ Dr. Suhail Aamar, Rheumatology Clinic, Hadassah Mount Scopus, Churchill Avenue 8, Jerusalem, Israel.
E-mail address: suhail_aamar@hotmail.com

Ann Rheum Dis 85 (2026) e100–e101

Contents lists available at ScienceDirect

Annals of the Rheumatic Diseases

journal homepage: https://www.sciencedirect.com/journal/annals-of-the-rheumatic-diseases

Response

Response to correspondence by Dr Aamar on 'EULAR recommendations for the management of rheumatoid arthritis with synthetic and biologic disease-modifying antirheumatic drugs: 2025 update'

We thank Dr Aamar for their comments on the 2025 update of the European Alliance of Associations for Rheumatology (EULAR) rheumatoid arthritis management recommendations [1]. The main criticism raised relates to the question of tapering disease-modifying antirheumatic drugs (DMARDs) in sustained remission and whether to maintain biological DMARDs (bDMARDs) or conventional synthetic DMARDs (csDMARDs) like methotrexate (MTX) during the tapering process. To this end, Dr Aamar cites the old Study of Etanercept and Methotrexate in Combination or as Monotherapy in Subjects With Rheumatoid Arthritis (SEAM-RA) trial [2] and the SORAIRO study [3], which was recently published in *ARD*, and suggests that MTX alone can sustain treatment effects if bDMARDs have been tapered.

We would like to remind Dr Aamar that the EULAR recommendations do not specify whether bDMARDs should be maintained and MTX tapered or vice versa. Indeed, it is worth bearing in mind that the text of the recommendations and the new systematic literature reviews (SLRs; this time on safety and efficacy), as well as the details of previous recommendations and the SLRs informing them, are part of every update, unless amended. So first, the 2 SLRs performed for the 2025 update focused on papers published between 2022 and January 2025 [4,5] and, therefore, neither covered the SEAM-RA trial published in 2021, which was addressed in the previous efficacy SLR [6], nor the SORAIRO trial, since that was only published in 2026. Dr Aamar may also be interested in considering the TApering strategies in Rheumatoid Arthritis (TARA) trial from 2019, which evaluated a similar question [7].

Thus, we refer Dr Aamar to the 2022 update of EULAR's rheumatoid arthritis management recommendations, where the following statement can be found: 'Evidence has emerged indicating that there was no difference in clinical outcome when either a bDMARD or csDMARD was tapered first. It had previously been suggested that a reduction of bDMARDs should come first because of the costs involved. However, an economic analysis has revealed that the total costs of tapering csDMARDs first vs tapering antitumor necrosis factors first did not differ. Consequently, the Task Force was of the opinion that there is no preferred tapering sequence, and this can be left to the discretion of patients and rheumatologists in a shared decision, but still with an open eye on costs, since prices of bDMARDs may vary significantly within and between countries' [8].

This statement was not reversed during the deliberations for the 2025 recommendations and, therefore, remains fully in place. Indeed, it is supported by the data of the SORAIRO trial, which, however, did not include an economic analysis.

Finally, readers should be reminded that unless specifically amended or reversed, past EULAR recommendations and the information related to them remain in place, because it is not fruitful to repeat all discussion items of previous recommendation papers in addition to new aspects of the process.

Competing interests

The authors declare no conflicts of interest related to the work under consideration for publication.

Funding

The project was funded by EULAR.

Patient consent for publication

Not applicable.

Ethics approval

Not applicable.

Provenance and peer review

Requested as response to a correspondence and internally reviewed.

REFERENCES

[1] Smolen JS, Edwards CJ, Konzett V, Laskou F, Aletaha D, Caporali R, et al. EULAR recommendations for the management of rheumatoid arthritis with

DOI of original article: http://dx.doi.org/10.1016/j.ard.2026.05.034.

Handling editor David Pisetsky

https://doi.org/10.1016/j.ard.2026.06.026
Received 18 June 2026; Accepted 22 June 2026

0003-4967/© 2026 European Alliance of Associations for Rheumatology (EULAR). Published by Elsevier B.V. All rights are reserved, including those for text and data mining, AI training, and similar technologies.

synthetic and biologic disease modifying antirheumatic drugs: 2025 update. Ann Rheum Dis. 2026;85(6):991–1009. doi: 10.1016/j.ard.2026.01.023.

[2] Curtis JR, Emery P, Karis E, Haraoui B, Bykerk V, Yen PK, et al. Etanercept or methotrexate withdrawal in rheumatoid arthritis patients in sustained remission. Arthritis Rheumatol. 2021;73(5):759–68. doi: 10.1002/art.41589.

[3] Imai Y, Kono M, Ishii T, Kojima T, Hirata S, Tanaka Y, et al. Spacing of a TNF inhibitor or dose reduction of methotrexate vs continued treatment in patients with rheumatoid arthritis in remission or low disease activity: a randomised, controlled trial (SORAIRO trial). Ann Rheum Dis. 2026;85(4):609–19 [published Online First: 20260228]. doi: 10.1016/j.ard.2026.02.004.

[4] Konzett V, Laskou F, Smolen JS, Edwards CJ, Aletaha D, van der Heijde D, et al. Efficacy of synthetic and biological DMARDs: a systematic literature review informing the 2025 update of the EULAR recommendations for the management of rheumatoid arthritis. Ann Rheum Dis. 2026;85(6):1039–54. doi: 10.1016/j.ard.2026.03.020.

[5] Laskou F, Konzett V, Smolen JS, Edwards CJ, Aletaha D, van der Heijde D, et al. Safety of synthetic and biological DMARDs: a systematic literature review informing the 2025 update of the EULAR recommendations for the management of rheumatoid arthritis. Ann Rheum Dis. 2026;85(6):1055–72. doi: 10.1016/j.ard.2026.02.024.

[6] Kerschbaumer A, Sepriano A, Bergstra SA, Smolen JS, van der Heijde D, Caporali R, et al. Efficacy of synthetic and biological DMARDs: a systematic literature review informing the 2022 update of the EULAR recommendations for the management of rheumatoid arthritis. Ann Rheum Dis. 2023;82(1):95–106. doi: 10.1136/ard-2022-223365.

[7] van Mulligen E, de Jong P, Kuijper TM, van der Ven M, Appels C, Bijkerk C, et al. Gradual tapering TNF inhibitors versus conventional synthetic DMARDs after achieving controlled disease in patients with rheumatoid arthritis: first-year results of the randomised controlled TARA study. Ann Rheum Dis. 2019;78(6):746–53 annrheumdis-2018-214970 [pii]. doi: 10.1136/annrheumdis-2018-214970.

[8] Smolen JS, Landewé RBM, Bergstra SA, Kerschbaumer A, Sepriano A, Aletaha D, et al. EULAR recommendations for the management of rheumatoid arthritis with synthetic and biological disease-modifying antirheumatic drugs: 2022 update. Ann Rheum Dis. 2023;82(1):3–18. doi: 10.1136/ard-2022-223356.

Josef S. Smolen[1,*], Christopher J. Edwards[2], Victoria Konzett[1], Faidra Laskou[3], Robert Landewe[4], Andreas Kerschbaumer[1]

[1] *Division of Rheumatology, Department of Medicine 3, Medical University of Vienna, Austria*

[2] *NIHR Southampton Clinical Research Facility, University Hospital Southampton NHS Foundation Trust, Southampton, UK*

[3] *MRC Lifecourse Epidemiology Centre, Southampton, UK*

[4] *Amsterdam University Medical Center, Amsterdam and Zuyderland MC, Heerlen, the Netherlands*

*__Correspondence to__ Dr Josef Smolen, Division of Rheumatology, Department of Medicine 3, Medical University of Vienna, Austria.
E-mail address: josef.smolen@meduniwien.ac.at (J.S. Smolen).

Ann Rheum Dis 85 (2026) e102–e103

Contents lists available at ScienceDirect

Annals of the Rheumatic Diseases

journal homepage: https://www.sciencedirect.com/journal/annals-of-the-rheumatic-diseases

Response

Response to correspondence on 'Spacing of a TNF inhibitor or dose reduction of methotrexate vs continued treatment in patients with rheumatoid arthritis in remission or low disease activity (SORAIRO trial)'

We appreciate the thoughtful comments on the SORAIRO trial [1]. We acknowledge that previous exposure to biological disease-modifying antirheumatic drugs (bDMARDs), seropositivity, and concomitant glucocorticoid use were numerically imbalanced among the treatment groups. Although randomisation reduces systematic treatment-selection bias, these imbalances can still occur in a trial of this sample size. In addition, a history of bDMARD use does not necessarily indicate a difficult-to-treat phenotype. Our study was not designed to determine whether these baseline factors predict successful tapering, and this issue warrants further investigation.

We agree that cost and access to advanced therapies should be considered when selecting a tapering strategy. The Pan American League of Associations for Rheumatology (PANLAR) recommendations prioritise the reduction of b/ts-DMARDs before cs-DMARDs in patients with sustained remission, particularly in healthcare settings where the economic burden of advanced therapies substantially affects treatment access [2]. Although this is an important strategy, the SORAIRO trial was not designed to establish a universal tapering sequence or to evaluate cost-effectiveness. Evidence regarding which DMARD to taper first remains unestablished. The 2021 American College of Rheumatology guideline conditionally recommends gradual discontinuation of methotrexate over discontinuation of a b/ts-DMARD in patients receiving both methotrexate and b/ts-DMARDs, although this recommendation is based on very low-certainty evidence [3]. Furthermore, the TApering strategies in Rheumatoid Arthritis (TARA) trial found that the order of tapering a cs-DMARD or a tumour necrosis factor inhibitor (TNFi) did not yield significant differences in clinical outcomes, and its cost-utility analysis demonstrated similar overall cost-effectiveness between these strategies [4,5].

The SORAIRO trial suggested that methotrexate dose reduction, as well as spacing of TNFi dosing, may be associated with a loss of disease control after achieving low disease activity, even among methotrexate-inadequate responders. However, it has also been demonstrated that nearly half of the patients assigned to the methotrexate dose-reduction group successfully discontinued methotrexate. Thus, there may be significant individual differences in the feasibility of methotrexate tapering. Further evaluation to determine which patients can tolerate medication tapering is warranted.

In conclusion, the SORAIRO trial does not establish a single preferred order of tapering. Treatment reduction should be individualised according to the depth and duration of disease control, adverse events, treatment burden, patient preference, drug access and cost, and the feasibility of prompt re-escalation of treatment in the event of a flare.

Competing interests

YK reports financial support was provided by Taisho Pharmaceutical Co., Ltd. MK reports a relationship with AbbVie, Asahi-Kasei, Astellas, AstraZeneca, Ayumi, Bristol, Chugai, Daiichi Sankyo, Eisai, Eli Lilly, Gilead, GlaxoSmithKline, Janssen, Kowa, Kyocera, Lotte, Boehringer Ingelheim, Nippon Shinyaku, Mitsubishi Tanabe, Mochida, Pfizer, and Sandoz that includes: funding grants and speaking and lecture fees. TI reports a relationship with Asahi-Kasei, Chugai, Eli Lilly, GSK, Pfizer, Boehringer Ingelheim, and AstraZeneca that includes: speaking and lecture fees. SH reports a relationship with AbbVie, Asahi-Kasei, Astellas, AstraZeneca, Ayumi, Bristol, Boehringer Ingelheim, Chugai, Daiichi-Sankyo, Eisai, Eli Lilly, Gilead Sciences, Glaxo SmithKline, Janssen, Nihon-Shinyaku, Novartis, Otsuka, Pfizer, Sandoz, Taisho, Tanabe-Mitsubishi, and UCB that includes: consulting or advisory, funding grants, and speaking and lecture fees. YT reports a relationship with Chugai, UCB, AbbVie, AstraZeneca, Eli Lilly, Behringer Ingelheim, GlaxoSmithKline, Eisai, IQVIA, Daiichi-Sankyo, Otsuka, Taisho, Gilead Sciences, and Bristol-Myers that includes: consulting or advisory and speaking and lecture fees. ET reports a relationship with AbbVie, Asahi Kasei, Astellas, Ayumi, Boehringer Ingelheim, Bristol-Myers, Chugai, Eisai, Eli Lilly, Gilead Sciences, GlaxoSmithKline, Mikasa Seiyaku, Nichi-Iko, Nippon Kayaku, Pfizer, Sandoz, Taisho, Takeda, Towa, Mitsubishi-Tanabe, UCB Japan, and Viatris that includes: consulting or advisory, funding grants, and speaking and lecture fees. KO reports a relationship with AbbVie, Asahi KASEI, Astellas Pharma, AstraZeneca, Ayumi, Boehringer Ingelheim, Bristol-Myers, Chugai, Eisai, Eli Lilly, Gilead Sciences, GlaxoSmithKline, Mitsubishi-Tanabe, Novartis Pharma, Otsuka, Taisho, Janssen, and UCB that includes: funding grants and speaking and lecture fees. SO reports a relationship with Taisho Pharmaceutical Co Ltd that includes: employment. RM reports a relationship with Taisho Pharmaceutical Co Ltd that includes: employment. YS reports a relationship with Taisho Pharmaceutical Co Ltd that includes: employment.

https://doi.org/10.1016/j.ard.2026.06.003
Received 29 May 2026; Accepted 2 June 2026

0003-4967/© 2026 European Alliance of Associations for Rheumatology (EULAR). Published by Elsevier B.V. All rights are reserved, including those for text and data mining, AI training, and similar technologies.

TY reports a relationship with Taisho Pharmaceutical Co Ltd that includes: employment. TT reports a relationship with AbbVie, Chugai, Eli Lilly, Eisai, Gilead Sciences, Pfizer, Taisho, and has received consultant fees from AbbVie, Eli Lilly, Gilead Sciences, Mitsubishi-Tanabe, and Taisho that includes: speaking and lecture fees. YK reports a relationship with AbbVie, Asahi-Kasei, Astellas, Ayumi, Boehringer Ingelheim, Bristol-Myers, Chugai, Eisai, Eli Lilly, GlaxoSmithKline, Janssen, Novartis, Pfizer, UCB, Sanofi, Mitsubishi-Tanabe, Gilead Sciences, and Taisho that includes: funding grants and speaking and lecture fees. MK reports a relationship with Taiju Life Social Welfare, Taisho, Takeda, Terumo, UCB, and Yamazaki Baking that includes: funding grants and speaking and lecture fees.

CRediT authorship contribution statement

Yuki Imai: Writing – original draft, Writing – review & editing. **Michihito Kono:** Writing – review & editing. **Tomonori Ishii:** Writing – review & editing. **Toshihisa Kojima:** Writing – review & editing. **Shintaro Hirata:** Writing – review & editing. **Yoshiya Tanaka:** Writing – review & editing. **Eiichi Tanaka:** Writing – review & editing. **Koichiro Ohmura:** Writing – review & editing. **Shunsuke Okamoto:** Writing – review & editing. **Rumiko Matsumoto:** Writing – review & editing. **Yuri Sato:** Writing – review & editing. **Takashi Yamamura:** Writing – review & editing. **Tsutomu Takeuchi:** Writing – review & editing. **Yuko Kaneko:** Writing – review & editing.

Funding

Not applicable.

Patient consent for publication

Not applicable.

Ethics approval

Not applicable.

Provenance and peer review

Not commissioned; internally peer reviewed.

Orcid

Yuki Imai: http://orcid.org/0000-0003-0729-9810

REFERENCES

[1] Imai Y, Kono M, Ishii T, Kojima T, Hirata S, Tanaka Y, et al. Spacing of a TNF inhibitor or dose reduction of methotrexate vs continued treatment in patients with rheumatoid arthritis in remission or low disease activity: a randomised, controlled trial (SORAIRO trial). Ann Rheum Dis. 2026;85(4):609–19.

[2] Santos Moreno P, García Salinas R, Caballero Uribe CV, Brance ML, Marín Zúcaro NM, Arrieta Vega D, et al. Pan American League of Associations for Rheumatology recommendations for the management of rheumatoid arthritis. Lancet Rheumatol. 2026;8(1):e53–65.

[3] Fraenkel L, Bathon JM, England BR, St Clair EW, Arayssi T, Carandang K, et al. 2021 American College of Rheumatology guideline for the treatment of rheumatoid arthritis. Arthritis Care Res (Hoboken). 2021;73(7):924–39.

[4] van Mulligen E, Weel AE, Hazes JM, van der Helm-van Mil A, de Jong PHP. Tapering towards DMARD-free remission in established rheumatoid arthritis: 2-year results of the TARA trial. Ann Rheum Dis. 2020;79(9):1174–81.

[5] van Mulligen E, Weel AE, Kuijper TM, Denissen NHAM, Gerards AH, de Jager MK, et al. Two-year cost effectiveness between two gradual tapering strategies in rheumatoid arthritis: cost-utility analysis of the TARA trial. Ann Rheum Dis. 2020;79(12):1550–6.

Yuki Imai[1], Michihito Kono[2], Tomonori Ishii[3], Toshihisa Kojima[4], Shintaro Hirata[5], Yoshiya Tanaka[6,7], Eiichi Tanaka[8], Koichiro Ohmura[9], Shunsuke Okamoto[10], Rumiko Matsumoto[10], Yuri Sato[10], Takashi Yamamura[10], Tsutomu Takeuchi[1,11], Yuko Kaneko[1,*]

[1] *Division of Rheumatology, Department of Internal Medicine, Keio University School of Medicine, Tokyo, Japan*
[2] *Department of Rheumatology, Endocrinology and Nephrology, Faculty of Medicine and Graduate School of Medicine, Hokkaido University, Sapporo, Japan*
[3] *Department of Haematology and Rheumatology, Tohoku Medical and Pharmaceutical University Hospital, Sendai, Japan*
[4] *Department of Orthopaedic Surgery, National Hospital Organization Nagoya Medical Centre, Nagoya, Japan*
[5] *Department of Clinical Immunology and Rheumatology, Hiroshima University Hospital, Hiroshima, Japan*
[6] *The First Department of Internal Medicine, University of Occupational and Environmental Health, Kitakyushu, Japan*
[7] *Department of Molecular Targeted Therapeutics, School of Medicine, University of Occupational and Environmental Health, Kitakyushu, Japan*
[8] *Department of Rheumatology, Tokyo Women's Medical University School of Medicine, Tokyo, Japan*
[9] *Department of Rheumatology, Kobe City Medical Centre General Hospital, Kobe, Japan*
[10] *Taisho Pharmaceutical Co, Ltd, Tokyo, Japan*
[11] *Saitama Medical University, Saitama, Japan*

*Correspondence to Dr Yuko Kaneko, Division of Rheumatology, Department of Internal Medicine, Keio University School of Medicine, 35 Shinanomachi, Shinjuku-ku, Tokyo, Japan.
E-mail address: ykaneko.z6@keio.jp (Y. Kaneko).